

Pattern formation outside of equilibrium

M. C. Cross

Department of Physics, California Institute of Technology 114-36, Pasadena, California 91125

P. C. Hohenberg

AT&T Bell Laboratories, MH 1D-268, Murray Hill, New Jersey 07974

A comprehensive review of spatiotemporal pattern formation in systems driven away from equilibrium is presented, with emphasis on comparisons between theory and quantitative experiments. Examples include patterns in hydrodynamic systems such as thermal convection in pure fluids and binary mixtures, Taylor-Couette flow, parametric-wave instabilities, as well as patterns in solidification fronts, nonlinear optics, oscillatory chemical reactions and excitable biological media. The theoretical starting point is usually a set of deterministic equations of motion, typically in the form of nonlinear partial differential equations. These are sometimes supplemented by stochastic terms representing thermal or instrumental noise, but for macroscopic systems and carefully designed experiments the stochastic forces are often negligible. An aim of theory is to describe solutions of the deterministic equations that are likely to be reached starting from typical initial conditions and to persist at long times. A unified description is developed, based on the linear instabilities of a homogeneous state, which leads naturally to a classification of patterns in terms of the characteristic wave vector q_0 and frequency ω_0 of the instability. Type I_s systems ($\omega_0=0$, $q_0\neq 0$) are stationary in time and periodic in space; type III_o systems ($\omega_0\neq 0$, $q_0=0$) are periodic in time and uniform in space; and type I_o systems ($\omega_0\neq 0$, $q_0\neq 0$) are periodic in both space and time. Near a continuous (or supercritical) instability, the dynamics may be accurately described via "amplitude equations," whose form is universal for each type of instability. The specifics of each system enter only through the nonuniversal coefficients. Far from the instability threshold a different universal description known as the "phase equation" may be derived, but it is restricted to slow distortions of an ideal pattern. For many systems appropriate starting equations are either not known or too complicated to analyze conveniently. It is thus useful to introduce phenomenological order-parameter models, which lead to the correct amplitude equations near threshold, and which may be solved analytically or numerically in the nonlinear regime away from the instability. The above theoretical methods are useful in analyzing "real pattern effects" such as the influence of external boundaries, or the formation and dynamics of defects in ideal structures. An important element in nonequilibrium systems is the appearance of deterministic chaos. A great deal is known about systems with a small number of degrees of freedom displaying "temporal chaos," where the structure of the phase space can be analyzed in detail. For spatially extended systems with many degrees of freedom, on the other hand, one is dealing with spatiotemporal chaos and appropriate methods of analysis need to be developed. In addition to the general features of nonequilibrium pattern formation discussed above, detailed reviews of theoretical and experimental work on many specific systems are presented. These include Rayleigh-Bénard convection in a pure fluid, convection in binary-fluid mixtures, electrohydrodynamic convection in nematic liquid crystals, Taylor-Couette flow between rotating cylinders, parametric surface waves, patterns in certain open flow systems, oscillatory chemical reactions, static and dynamic patterns in biological media, crystallization fronts, and patterns in nonlinear optics. A concluding section summarizes what has and has not been accomplished, and attempts to assess the prospects for the future.

CONTENTS

I. Introduction	854	III. General Features of Pattern Formation	866
A. General remarks	854	A. Dynamics and stability	866
B. Phenomena	855	1. Dissipative dynamics and attractors	866
C. Theoretical methods	857	2. Stability and bifurcations	866
D. Experimental systems	858	3. Potential motion and Lyapunov functions	868
II. Basic Phenomenology	859	4. Deterministic versus stochastic dynamics	868
A. Rayleigh-Bénard convection	859	5. Bifurcations versus phase transitions	869
B. Other convecting systems	862	B. Linear instabilities and basic nonlinear states	869
1. Convection in fluid mixtures	862	1. Linear instabilities	869
2. Electrohydrodynamic instabilities in nematic		2. Ideal patterns	870
liquid crystals	862	a. Saturation of the linear instability	870
3. Bénard-Marangoni convection	862	b. Stability balloons	870
C. Taylor-Couette flow	863	C. Model Equations	871
D. Parametric waves	864	1. Motivation	872
E. Reaction-diffusion systems	864	2. Partial differential equations	872
F. Solidification patterns	865	a. The Swift-Hohenberg (SH) equation and its	872
G. Nonlinear optics	865	variants	
		b. The Kuramoto-Sivashinsky equation	872
		c. Reaction-diffusion equations	873
		d. Ginzburg-Landau models	873
		3. Discrete models	874

a. Systems of ordinary differential equations	874	(ii) The generalized Ginzburg-Landau model	900
b. Coupled maps	874	(α) The dynamical system	900
c. Cellular automata	874	(β) Coherent structures	901
IV. Theoretical Approaches	874	(iii) Multiplicity of solutions	901
A. Perturbative methods	874	(α) Fronts	901
1. Amplitude equations	875	(β) Pulses	903
a. Type I_s : Stationary periodic	875	(γ) Sources and sinks	903
(i) General form of the amplitude equation	875	(iv) Fronts and pulses in the nonlinear diffusion	904
(ii) Spatially periodic solutions and their stability	876	equation	904
(iii) Superposition of plane-wave solutions: Squares and hexagons	877	(v) Exact solutions	905
(iv) Chiral symmetry; Hamiltonian versus dissipative systems	879	(α) Symmetries, conservation laws, and “integrable” systems	906
b. Type II_s : Stationary instability with $q_0 = 0$	879	(β) Perturbing around exact solutions	906
c. Type III_o : Oscillatory uniform	880	(γ) Particular solutions of the complex	907
(i) Simple solutions	880	Ginzburg-Landau equation	907
(ii) Stability of plane-wave solutions	880	(vi) Other one-dimensional defects	907
d. Type I_o : Oscillatory periodic	881	(α) Weak sources and sinks in the phase equation	907
(i) Superposition of solutions: Traveling versus standing waves	881	(β) The Swift-Hohenberg model; nonadiabatic effects	908
(ii) Stability of plane-wave solutions	882	(γ) Grain boundaries	909
2. Phase equations	882	c. Point defects in two dimensions	909
a. Stationary systems (type I_s)	882	(i) Dislocations in type I_s systems	909
(i) Near threshold	882	(ii) Disclinations	911
(ii) Far from threshold	882	(iii) Target patterns	912
(iii) More complicated situations	883	(iv) Spiral patterns	913
b. Oscillatory systems (types I_o and III_o)	884	d. Three-dimensional defects	915
c. Higher-order phase equations	885	(i) The Swift-Hohenberg model	915
d. Control-parameter ramps	886	(ii) Scroll waves	916
3. Secondary instabilities	886	3. Defect dynamics	916
4. Nonadiabatic effects	887	a. Calculation methods	916
5. Rotationally invariant order parameter equations	887	(i) Perturbative calculations	916
B. Qualitative methods	888	(ii) Potential systems	917
1. Formal methods of bifurcation theory	888	b. Examples	917
a. Normal forms and nondegenerate bifurcations	888	(i) Dislocations	917
b. Bifurcations with symmetry	889	(α) Climb	917
c. Degenerate bifurcations	890	(β) Glide	918
2. Phase variables and topological defects	891	(ii) Interaction of pulses	919
V. Elements of Real Patterns	891	(iii) Interaction of dislocations and spirals in the complex Ginzburg-Landau model	919
A. Effects of boundaries	892	(iv) Scroll waves in three dimensions	922
1. Type I_s : Stationary periodic	892	VI. Pattern Selection	922
a. Threshold effects	892	A. Type I_s : Stationary patterns	923
(i) Periodic boundary conditions	892	1. Selection via constraints	923
(ii) Inhomogeneous boundary conditions	892	a. One dimension: Wave-vector selection	923
(iii) Rigid boundary conditions	892	(i) Rigid sidewalls	923
b. Constraints on nonlinear solutions: Rigid boundaries	893	(ii) Control parameter ramps	923
(i) Mode expansion	894	(iii) Concentric rolls with focus singularity	923
(ii) Wave number selection in one dimension	894	(iv) Dislocations	924
(iii) Orientational effects in two dimensions	896	(v) Grain boundaries	924
2. Type III_o : Oscillatory uniform	897	(vi) Competing selection mechanisms	924
3. Type I_o : Oscillatory periodic	897	b. Two dimensions: general considerations	925
B. Defects and coherent structures	898	(i) Near threshold	925
1. Introduction	898	(ii) Away from threshold	927
2. Structure of defects	898	2. Selection via dynamics	927
a. Calculation methods	898	a. External forcing	927
(i) Far-field calculations	898	(i) Boundary forcing	928
(ii) Phase-space methods	899	(ii) Stochastic forcing or stochastic initial conditions	928
(iii) Special solutions	899	b. Threshold protocol	928
(iv) Perturbation methods	899	c. Front propagation	928
b. One-dimensional defects	899	B. Front and pulse selection	928
(i) Classification of defect solutions: Coherent structures	899	1. The nonlinear diffusion equation	928
		2. General remarks	929
		3. Linear front selection	929
		4. Nonlinear front selection	931
		5. Selection below threshold: Pulses and fronts	932

6. Examples	932	b. Phase equation	971
a. Complex Ginzburg-Landau model	932	c. Forced phase drift by mean flows	972
b. The Swift-Hohenberg equation	933	2. Wave-vector selection	973
C. Type I _o : Oscillatory periodic	934	a. Axisymmetric convection	973
1. Convective versus absolute instability	934	b. Selection by sidewalls	974
2. Effects of boundaries	934	c. Dislocation climb	974
3. External forcing	936	d. Grain boundaries	975
D. Effects of external noise	937	e. Ramps	975
1. Thermal versus nonthermal noise	937	f. Front propagation	976
2. Effects of noise on bifurcations	938	g. Competing mechanisms	976
a. The Swift-Hohenberg model	938	D. Two-dimensional patterns	976
b. Single-mode amplitude equation	939	1. Simple versus natural patterns: The effects of	976
VII. Chaos	940	forcing	976
A. General features	940	a. Imperfect bifurcations and static forcing	977
1. The characteristic lengths	940	b. Transient forcing	977
2. Small versus large systems	941	c. Stochastic forcing	978
B. Small systems	941	d. Experimental investigations	978
1. Characterization of chaos	941	2. Simple two-dimensional patterns	980
2. Reconstructing the attractor from time series	943	3. Natural two-dimensional patterns	983
3. Onset of chaos	945	E. Chaotic convection	985
4. Continuum models and real systems	945	1. Small systems	986
C. Infinite systems: Extensive chaos	945	2. Intermediate systems: Defect mediated chaos	986
1. Characterizing spatiotemporal chaos	945	a. Large Prandtl number: $\sigma \gtrsim 1$	987
a. Correlation length	945	b. Low Prandtl number: $\sigma \lesssim 1$	987
(i) Decay of correlation function	945	3. Large systems: Extensive chaos	988
(ii) Statistics of fluctuations	946	4. Large Rayleigh numbers	988
(iii) Other definitions	946	F. Special topics	990
b. Exponents and dimensions	947	1. Convection between poor conductors	990
2. Response and transport	948	2. Oscillatory instability	991
3. Chaos and turbulence	949	3. Non-Boussinesq effects	992
4. Open systems: Convective instability	950	4. Effect of surface tension: Bénard-Marangoni	995
D. Examples of spatiotemporal chaos	950	convection	995
1. The complex Ginzburg-Landau equation	950	5. Modulated convection	996
2. The Kuramoto-Sivashinsky equation and its ex-	951	a. Threshold shift	996
tensions	952	b. Hexagonal patterns	997
3. Coupled map lattices	952	6. Rotating convection	998
E. Theoretical approaches	953	IX. Other Fluid Systems	998
1. Stochastic models	953	A. Convection in fluid mixtures	998
a. Stochastic dynamics	953	1. Theory	999
b. Quenched randomness	954	a. Basic hydrodynamic equations	999
2. Critical points	954	b. Linear instability	1000
a. Spatiotemporal intermittency	954	c. Nonlinear states	1000
b. Self-organized criticality	955	d. Amplitude equations	1001
(i) Definition	955	e. Other theoretical methods	1001
(ii) Models and mechanisms	955	(i) Lorenz models	1002
(iii) Natural phenomena	957	(ii) Expansion about the pure fluid	1002
c. Correlation-length inequalities	957	(iii) Expansion about the codimension-two	1003
3. Defect-mediated turbulence	958	point	1003
4. Mean-field dynamics	958	(iv) Order-parameter equations	1003
5. Strong turbulence	959	(v) Numerical work	1004
6. Spatial chaos	960	2. Experiment	1005
F. Experimental studies	961	a. One-dimensional patterns	1005
VIII. Rayleigh-Bénard Convection	962	(i) Summary of experimental facts	1005
A. General features	962	(ii) Experiments interpretable by the complex	1005
1. Basic equations	962	amplitude equation	1005
2. Linear instability and ideal solutions	964	(α) Rectangular cells	1005
3. Stability balloon	964	(β) Annular geometry	1006
4. Amplitude equations	965	(iii) Other one-dimensional experiments	1009
5. Phase equations	966	b. Two-dimensional patterns	1009
B. Convection models	968	(i) Traveling rolls for $\psi < 0$	1009
1. Order-parameter models	968	(ii) Squares and rolls for $\psi > 0$	1010
2. Free-slip convection	970	3. Chaos and noise	1011
3. The Lorenz model	970	a. Theory	1011
C. One-dimensional patterns	971	b. Experiments	1011
1. Verification of the amplitude and phase equa-	971	B. Taylor - Couette flow	1011
tions	971	1. General discussion	1011
a. Amplitude equation	971	2. One-dimensional patterns	1014

a. General considerations	1014	B. Time-dependent patterns: Nonlinear waves	1063
b. Short cylinders	1014	1. Pulse propagation in nerves	1063
c. Long cylinders	1016	2. Excitations of heart muscle	1063
d. Ramped boundaries	1017	3. Slime-mold aggregation	1065
e. Front propagation	1018	XII. Other Systems	1065
C. Electrohydrodynamic instabilities in nematic liquid crystals	1018	A. Solidification patterns	1065
1. General features	1018	1. Solidification of a pure supercooled liquid	1066
2. Linear instability mechanism	1019	a. Propagating interface	1066
3. Nonlinear states	1020	b. Linear instability	1066
a. Normal rolls	1020	c. Nonlinear state: The dendrite problem	1067
b. Oblique rolls and the Lifshitz point	1020	2. Directional solidification	1069
4. Convection with spatially periodic forcing	1021	a. Propagating interface	1069
5. Motion of dislocations	1022	b. Linear instability	1070
6. Fluctuations and chaos	1023	c. Nonlinear states	1071
D. Parametric surface waves	1023	3. Eutectic solidification	1072
1. Theory	1023	B. Nonlinear optics	1072
a. Basic equations	1023	1. Basic equations	1072
b. Boundary conditions, real fluid effects	1024	2. Pulse propagation in a dispersive medium	1073
c. Amplitude equations	1025	3. Laser equations	1073
2. Experimental studies	1027	4. Optical bistability	1074
a. One-dimensional systems	1027	5. Self-induced transparency	1074
b. Two-dimensional patterns	1027	C. Parametric spin-wave instabilities	1074
c. Large systems: Spatiotemporal chaos	1028	D. Further pattern forming systems	1076
d. Defects	1028	XIII. Conclusion	1076
E. Open-flow systems	1029	A. What has been accomplished	1076
1. General remarks	1029	B. What has not been accomplished	1077
2. Plane Poiseuille flow	1030	C. Prospects for the future	1078
3. von Karman vortices	1031	Acknowledgements	1080
4. Type-I _s fluid systems with an imposed flow	1031	Appendix A. Derivation of the Amplitude Equation	1080
X. Patterns in Chemical Reactions	1032	1. The Swift-Hohenberg equation	1080
A. The Belousov-Zhabotinsky reaction and the Oregonator model	1032	2. The Kuramoto-Sivashinsky equation	1081
1. Basic experimental facts	1032	3. Rayleigh-Bénard convection	1081
2. The Oregonator model	1033	Appendix B. Derivation of the Phase Equation	1085
3. Oscillatory, bistable, and excitable dynamics	1034	References	1086
4. Front and pulse propagation	1035		
5. Periodic wave trains	1037		
6. Higher-dimensional patterns	1040		
a. Target patterns	1040		
b. Spiral waves	1041		
c. Three-dimensional patterns	1043		
B. Comparisons with experiment	1043		
1. Stirred dynamics	1043		
2. Pulse propagation	1043		
3. Wave trains and target patterns	1044		
4. Spirals and the effects of curvature	1045		
5. Further experiments on chemical reactions	1045		
6. Nonlinear dissipative waves in other systems	1047		
XI. Biological Patterns	1047		
A. Morphogenesis	1050		
1. General features	1050		
2. Theoretical concepts	1051		
a. Positional information	1051		
b. Length scales	1051		
c. Boundary effects	1051		
d. Initial conditions and transient evolution	1052		
3. Modeling the phenomena	1052		
4. Transplantation and regeneration in hydra	1052		
5. Other phenomena	1056		
a. Two-dimensional patterns	1056		
b. Compartment formation in Drosophila	1057		
c. Mammalian coat markings: The variety of patterns	1058		
d. Pigment patterns on mollusk shells	1060		
e. Visual hallucination patterns	1061		
f. Mechanical models	1063		

I. INTRODUCTION

A. General remarks

This article reviews recent progress in our understanding of spatial pattern formation in nonequilibrium fluid systems such as Rayleigh-Bénard convection or Taylor-Couette flow, and seeks to compare and contrast these with other pattern forming systems encountered in solid-state physics, nonlinear optics, chemistry, and biology. The study of pattern formation in fluids has greatly benefited from recent careful and controlled experiments as well as the development of new concepts and new analytic and numerical tools. This shifted focus was inspired by developments in the mathematical study of dynamical systems on the one hand, and by recent progress in statistical mechanics of condensed matter on the other. Our aim is to review the work in fluid dynamics in such a way as to make it accessible to a broad audience of both specialists and nonspecialists. In addition, we discuss pattern formation in chemical and biological systems, in order to display the well-known analogies with patterns in fluid systems in some detail, and in order to provide an introduction accessible for physical scientists to the vast literature in these fields. Finally, we also touch on a topic that does not concern pattern formation per se, but rather the destruction of patterns, namely spatiotemporal

chaos, since it manifests itself in all the systems under study.

Our basic point of view is that nonequilibrium spatial patterns may be *classified* according to the *linear instabilities*^{1,1} of an infinite spatially uniform system. These instabilities arise when the system is brought away from thermal equilibrium by increasing a *control parameter*. The interesting linear instabilities are divided into three broad classes according to the values of the *characteristic wave vector* q_0 , and/or the *characteristic frequency* ω_0 which appear at the instability threshold.

Patterns with wave vectors and/or frequencies centered around these values grow beyond threshold and are in general found to saturate to finite amplitude. Near the instability the system may often be described theoretically by simple equations having a universal form, which go under the name of *amplitude equations* (Newell and Whitehead, 1969; Newell, 1974). Further above threshold, in the strongly nonlinear domain, it is sometimes possible to derive simple *phase equations* by perturbing about an ideal periodic structure (Pomeau and Manneville, 1979; Cross and Newell, 1984). It is also often useful to describe the system using *phenomenological model equations* (Swift and Hohenberg, 1977; Greenside and Cross, 1985; Haken, 1987) that have the same linear instabilities as the experimental system, but are analytically or numerically more tractable than the starting equations. The focus on linear instabilities, on amplitude and phase equations and on simple models illustrates the similarity between pattern formation in widely different systems. The degree of universality of the phenomena is more or less the degree to which they are adequately described by such simple theoretical models.

Throughout our article, we will emphasize the role of *quantitative experiments* which serve to guide the theorist in choosing models and approximations, as well as to test the theoretical results obtained. The experimental interest in pattern formation shown by fluid dynamicists has certainly been a key contributor to the recent progress in that field.

In the rest of this Introduction we wish to highlight some of the concepts we will encounter in the subsequent sections.

B. Phenomena

We will primarily concern ourselves with systems under constant nonequilibrium external conditions. In such systems it is possible to have macroscopic spatial structure in steady state, a phenomenon that goes under the

names of dissipative structures^{1,2} (Nicolis and Prigogine, 1977), synergetics (Haken, 1983), and self-organization (Krisnky, 1984). From a theoretical point of view, since we are not near equilibrium there is no *a priori* reason to suppose that we have a Gibbs ensemble or a free energy functional whose minima yield the patterns obtained under given external conditions. We must therefore discuss the system in terms of some appropriate set of starting equations which we term "microscopic." By this we do not mean that the equations necessarily involve atomic degrees of freedom, just that they represent the elementary building blocks from which our analysis starts. For fluid systems these are generally the Navier-Stokes and other equations of fluid dynamics; for chemical systems they are appropriate reaction laws.

Since "microscopic" equations are typically nonlinear partial differential equations, the reliable information we can extract from them theoretically is quite limited. We place ourselves under conditions that are natural from a theoretical physics perspective though somewhat artificial in many practical cases; namely we consider a spatially infinite^{1,3} uniform system near equilibrium. We then increase a parameter R , called the control parameter, that takes the system further from equilibrium. Suppose that at some threshold value $R = R_c$ the system becomes *unstable* to infinitesimal perturbations with wave vector q_0 and frequency ω_0 (either of which may be zero). For $R > R_c$ we expect a pattern centered around q_0 and ω_0 to grow and in many cases to saturate to a macroscopic amplitude proportional to some power of $R - R_c$. When $\omega_0 = 0$ we speak of *stationary* patterns and when $\omega_0 \neq 0$ we have *oscillatory* patterns.

The mechanism of the instability is expressed in the starting equations and depends on details of the system. Nevertheless, since spatial pattern formation usually arises due to the existence of a *nonzero* q_0 , it is useful to identify generic mechanisms for finite wave vector instabilities. One class of mechanisms arises from the existence of *constraints* and *conservation laws*. It is best illustrated by the example of Rayleigh-Bénard convection of a fluid placed between horizontal plates, where the buoyancy force attempts to lift the whole mass of the fluid (conservation of mass) and the top plate provides a constraint against this motion. Then the most unstable mode turns out to be on a spatial scale $q_0^{-1} \simeq d$, where d is the plate separation. Another mechanism for finite wavelength instabilities is provided by *competing interactions* between elementary units. This mechanism, well

^{1,1}The general connection between spatiotemporal pattern formation in macroscopic systems and linear instabilities was to our knowledge first emphasized in the seminal paper of Turing (1952).

^{1,2}We shall consider almost exclusively systems where dissipation is important.

^{1,3}The system need not be infinite in all three dimensions. When we speak of the dimensionality of a system, or of spatial extension, we refer only to those dimensions in which the system is large. In practice, a system is d -dimensional if it has linear dimension $Lq_0 \gg 1$ in d directions, where q_0^{-1} is the characteristic instability length (see below).

known in magnetic materials where it leads to antiferromagnetism, is also ubiquitous in chemical and biological systems where it is referred to as "local excitation combined with lateral inhibition" (Oster, 1988).

A detailed understanding of the instability mechanism and of its dependence on system parameters can only be achieved if the system is well characterized by the microscopic equations. Sometimes the phenomena are not well enough understood to allow a prediction of the exact location and parameters of the instability, but the characteristic wave vector q_0 and/or frequency ω_0 can nevertheless be estimated and related to properties of the system. It is then useful to classify the patterns that grow beyond threshold in terms of the values of q_0 and ω_0 . We distinguish three types of instabilities:

- Type I_s ($q_0 \neq 0, \omega_0 = 0$) instabilities are periodic in space and stationary in time. Because of the richness of periodic structures in two or three-dimensional space, many different ideal patterns may appear above threshold, the simplest one being the so-called roll state characterized by a single wave vector q . Other regular patterns, such as squares or hexagons in two dimensions or cubes in three dimensions can be formed by superposition of elementary rolls. The different structures can be analyzed with respect to their linear stability, and it usually turns out that only one type of structure is stable, but a continuous band of wave vectors q near q_0 is permitted. The region in the (R, q) plane where stable patterns exist is known as the "stability balloon."

- Type III_o ($q_0 = 0, \omega_0 \neq 0$) instabilities are uniform in space and oscillatory in time. The ideal state does not display any spatial pattern, just a uniform periodic oscillation whose frequency ω varies with R and is equal to ω_0 at threshold. States with spatial dependence can also appear, but we consider them as *defects* of the ideal structure (see below).

- Type I_o ($q_0 \neq 0, \omega_0 \neq 0$) instabilities are periodic in space and oscillatory in time. The simplest ideal pattern in this case involves a *traveling wave* train with a dispersion relation $\omega(q)$. These nonlinear waves are sustained by a competition between the drive (i.e. $R - R_c$), the dispersion and nonlinearity in the medium, and the dissipation. A subclass of such waves occurring in nondissipative (Hamiltonian) systems is the so-called solitary waves where nonlinearity balances dispersion and the waves propagate in the absence of a drive. In the general case, however, effects of driving and dissipation are just as important. Nonlinear waves (also called "autowaves" in the Soviet literature, see, e.g., Krinsky, 1984a) have many distinctive properties. For example, unlike the linear case, when two wave trains collide they do not interfere. They form a domain boundary, or shock which may remain stationary or may consume one or the other wave. Another possibility that occurs even in one-dimensional systems, is a superposition of right- and left-traveling waves to form a standing wave. The relative stability of standing and traveling waves depends on the

parameters of the system. In two and higher dimensions all the richness of the type I_s systems (different structures, stability balloons) is added to the basic dynamics of nonlinear waves, and a complete analysis of even the ideal structures becomes quite involved.

In attempting to apply these ideas to real patterns (either experimental or computational) it is important to understand the limitations inherent in considering an ideal pattern, that is, an infinite spatially periodic structure. The two most important "real pattern" effects we consider are *boundaries* and *defects*. Although finite systems are often thought to be simpler than infinite ones from the point of view of bifurcation theory, our focus is on large systems with many degrees of freedom, and we consider the boundaries^{1,4} to be a perturbation. The most important effect of boundaries is to render discrete the previously continuous band of wave vectors inside the stability balloon. There are, however, more subtle effects such as further restrictions of the allowed wave vector band or preferential orientation of degenerate patterns. Defects can be defined as any departure from the ideal pattern, but the most useful limit is to consider a *localized structure*, embedded in an otherwise ideal pattern. Defects may be stationary or they may move, and their structure often reflects topological characteristics of the ideal patterns in which they are immersed. They play an essential role in pattern dynamics, either in *selecting* a particular regular pattern or in the steady-state evolution of an irregular or chaotic pattern.

The problem of pattern selection arises because under given external conditions there often exist many stable solutions of the equations of motion, for example all states in the wave vector band defined by the stability balloon at a given R . From a mathematical point of view we know that for autonomous deterministic equations the state found at long times depends uniquely on the initial conditions. Experimentally it is found that often the state observed is insensitive to the preparation conditions, so we would like to know if one can formulate rules or criteria for predicting which state will be observed. Traditionally, a rule of thumb has been that one should select the state that grows fastest near the (linear) instability. Although this rule may work under certain conditions, on closer inspection it is found to be too simple-minded. Instead, we define various mechanisms for pattern selection that restrict the available states. Examples of static mechanisms are boundaries (as stated above), parameter inhomogeneities, or distortions of the ideal pattern. Dynamic mechanisms may arise either from external noise or from the dynamics of the creation of the pattern itself. For example it is found that if a roll state

^{1,4}Just as we consider a system to be d -dimensional if it is large in d directions, "boundaries" and "finite size" here refer to the directions in which the system is large.

grows via a front advancing into an unstable uniform state, then it has a unique wave vector and velocity independent of initial conditions, rather than a continuous band. Generally speaking, a primary mechanism for pattern selection is through the motion and interaction of defects, since these provide a way for a region of space with an “unfavorable” pattern to give way to a more favorable one. Notice that near thermal equilibrium the above discussion could be greatly simplified by considering a coarse-grained free energy and selecting the pattern which minimizes this quantity. In general no such free energy (or other so-called Lyapunov potential) can be defined for nonequilibrium systems, though there are notable exceptions.

A characteristic feature of the systems we are considering is the possibility of *chaotic* states, namely irregular behavior that persists to long times even under constant external conditions. This irregularity is a manifestation of instability in a deterministic system, not of the presence of external noise. In studying chaotic behavior we have found it useful to distinguish various regimes depending on the relationship between the size of the system L and a characteristic *correlation length* ξ for chaotic fluctuations. For small systems, with $\xi \gtrsim L$ the fluctuations are spatially correlated in the system and the dynamics may be described by a model with few modes. In the opposite case, $L \gg \xi$, the system is “large” and it may be thought of crudely as consisting of cells of volume ξ^d , whose number $(L/\xi)^d$, is a measure of the number of effective degrees of freedom for the dynamics. For large systems we may hope to use a statistical description of the chaotic states, borrowing concepts from equilibrium statistical mechanics, e.g. defining different phases by the long-distance properties of their correlation functions. In this way we may find phase transitions as a function of external parameters, and in particular critical points where correlations have power-law fall-off. A typical size of the correlation length away from critical points would be the basic instability length q_0^{-1} , or perhaps a characteristic dimension of a dynamically significant defect. Systems that are neither small ($\xi \gtrsim L$) nor large ($\xi \ll L$) are generally the most difficult to analyze. There is some hope of describing them using collective coordinates defined on the scale ξ , but little concrete progress has been made in developing this idea.

C. Theoretical methods

As stated above, our approach begins by assuming a set of equations of motion, the so-called “microscopic” equations, for which we assume that a uniform solution exists, and an instability to a spatially dependent solution arises for certain parameter values. We will consider as microscopic equations either more or less realistic descriptions of the phenomena, or mathematical models chosen so that their linear instabilities and long-time solutions mimic those of the system under study. The instability of the uniform state is established by a *linear*

analysis, which can be carried out even for complicated starting equations, and reveals the basic physical mechanism leading to pattern formation. Immediately above the linear threshold perturbation theory in the nonlinearity typically leads to a simplified description in terms of an *amplitude equation* (Newell and Whitehead, 1969; Segel, 1969), whose form is universal and whose numerical parameters reflect the details of each physical system. Here we use the word “universal” more or less in its technical meaning in critical phenomena, i.e. that there are classes of systems all of which lead to the same equation (see, e.g., Privman *et al.*, 1991, and references therein). An interesting point is that the simplified microscopic models mentioned above lead to the *same* amplitude equations as the realistic equations they are meant to mimic. Further away from threshold a different type of perturbation expansion is sometimes useful, namely an expansion in small and slow distortions of a fully nonlinear ideal periodic solution. This type of expansion leads to *phase equations* (Pomeau and Manneville, 1979; Kuramoto, 1984a,b; Cross and Newell, 1984), which also possess an element of universality, though their form reflects the starting periodic state somewhat more closely.

Another general method of analysis uses the qualitative theory of differential equations to find general features of the solutions. This approach is geometrical and topological and it can be applied either at the level of the microscopic description, or to analyze the amplitude and phase equations that are themselves difficult to solve.

Apart from perturbation theory and qualitative methods it is sometimes possible to find restricted classes of nontrivial exact solutions, especially in the case of model microscopic equations. These solutions can be very revealing, as they provide firm examples of specific types of behavior where otherwise only approximate results are known. We caution, however, that usually the full dynamical significance of the exact solutions is not known, e.g. their stability or their basin of attraction, so their physical interpretation remains a difficult task.

Finally, in reviewing the different theoretical methods available, we mention *numerical calculations*, which one turns to inevitably in the study of nonlinear equations. Although there have been many improvements in numerical work on the fundamental equations of fluid dynamics, optics, or chemistry, the types of questions we are asking involve long times and large distances, and are therefore particularly demanding in computer time. Thus far, few questions involving patterns in large aspect ratio convection cells, for example, have been reliably answered by direct simulation of the Navier-Stokes and heat equations. This is one reason why we introduce *model* systems whose pattern formation properties are designed to be as close as possible to those of the original system, but which are significantly easier to simulate numerically.

Another advantage of model systems is that they allow us to examine difficulties one at a time, so to speak. For example, as we shall see below convection patterns in a

large Rayleigh-Bénard cell at $R - R_c = 3R_c$, say, are influenced (i) by the two-dimensional degeneracy of the orientation of the local roll wave vector, a source of defects in the periodic structure; (ii) by the absence of an exact Lyapunov function whose minimization controls the dynamics (though an approximate one can be defined); (iii) by the possibility of disparate time scales for certain parameter values (e.g. if the Prandtl number $\sigma \ll 1$; see below); (iv) by subtle boundary effects, such as heated sidewalls or slightly nonparallel horizontal plates. Each one of these effects can be either inserted or taken out by appropriate choice of "microscopic" model, and their relative importance for different physical situations can be assessed more easily and reliably in this way than by attempts at brute force simulations of the correct hydrodynamic equations for this system.

D. Experimental systems

The prototypical experiment we wish to start from is that of a large system in d dimensions^{1,3} with control parameter R that can be varied through the first threshold R_c , where the uniform state becomes unstable. Such a situation can be approximated more or less well experimentally in the different areas we discuss, typically best of all in simple hydrodynamic experiments. Then the effects of dimensionality and finite size on regular and chaotic patterns can be studied systematically.

As mentioned earlier, the bulk of our review will be focused on hydrodynamic systems which have significant advantages: the basic equations and parameter values are well understood, controlled quantitative experiments can be carried out, and a body of intuition about fluid flow has been built up over the years. We shall see, however, that some of this traditional "fluid dynamics" intuition can be usefully supplemented by bringing in concepts from condensed matter and statistical physics. By far the most attention will be devoted to thermal convection in what follows, since this is the system where a large part of the recent progress in understanding non-equilibrium patterns has occurred, and also since both of the authors have worked primarily in this area. Besides pure-fluid (Rayleigh-Bénard) convection, interesting variants involve binary-fluid convection, surface-tension driven (Bénard-Marangoni) convection, and electrohydrodynamic convection in nematic liquid crystals. Convection is historically the system in which many of our basic notions of pattern formation were developed, e.g. the stability balloon, the different mechanisms for wave vector selection, classification and dynamics of defects, and small versus large chaotic systems. For all these topics important information came to us from carefully designed experiments, which motivated and in turn were influenced by the theoretical developments.

Another hydrodynamic system that played an important historical role is Taylor-Couette flow between concentric rotating cylinders. Both experiment and theory have exploited the analogies with convection, as well as

the simplifications arising from the axial geometry. Besides convection and Taylor-Couette flow we also discuss parametric surface waves, since this system provides a rich field for study of large nonequilibrium patterns, though so far most experiments have been on small systems, and it is not clear how well the external conditions can be controlled in extended geometries. There are many other hydrodynamic systems where regular patterns arise from linear instabilities, such as flow between adjacent rotating cylinders, flow down an inclined plane, and various magnetohydrodynamic and geostrophic flows. Only our lack of knowledge of the work in these fields and the necessity to stop somewhere has led to their exclusion from this review.

Turning now to nonhydrodynamic systems, we have chosen to discuss patterns in chemistry, biology, and nonlinear optics, as well as crystallization patterns in solids, but to leave out for somewhat arbitrary reasons patterns in flame fronts, in semiconductors, or in colloidal aggregates, to cite only a few of the possible areas we might have included.

Instabilities and patterns in nonlinear optics are central to the study of lasers and many other optical devices, but the main emphasis of fundamental studies has traditionally been on temporal chaos in systems where a few spatial modes are excited, an understandable bias in view of the above mentioned device applications. Apart from the nonlinear Schrödinger equations used to describe pulse propagation in optical fibers, most of the models employed in studies of chaos and instability were variants of the famous Lorenz model, where only three modes interact. It is only relatively recently that experimentalists and theoreticians have turned their attention to systems with many degrees of freedom, by relaxing transverse constraints, and bringing in additional modes of a given cavity. It appears that many of the phenomena that have been studied in hydrodynamic systems, e.g. pattern selection, defects, and spatiotemporal chaos, will also appear in this physical context.

The chemical system we discuss almost exclusively is the Belousov-Zhabotinsky (BZ) oscillatory reaction, since this system has been intensively studied experimentally as well as theoretically, and it bears the closest analogy to oscillatory hydrodynamic systems. The BZ reaction presents an additional theoretical difficulty, however, namely the presence of two vastly different time scales for the principal pattern-forming constituents. As a consequence the amplitude equation approach has no domain of quantitative applicability, and alternative methods of analysis are necessary. Interestingly, the qualitative properties of the observed patterns, particularly the behavior of the characteristic target and spiral defects in two dimensions, are very similar to those deduced from the corresponding amplitude formalism. This is an example of "qualitative universality," a notion that is difficult to make precise, but that operates here in a concrete way. We also briefly mention the recent success in the long-sought goal of finding stationary Turing patterns in a chemical reaction.

The biological patterns we discuss are of two types: those arising in morphogenesis, i.e. during the growth of an organism (Turing, 1952), and patterns created by the dynamics of living systems (Murray, 1989). Our purpose in including these topics in our review is not to claim that the vast and supremely difficult problems of biological pattern formation can be *reduced* to the corresponding questions in hydrodynamics or chemistry. The fact is, however, that most of the literature on biological pattern formation employs the same mathematical models and concepts that we have considered in the rest of this review! Under these circumstances it seems to us appropriate to place the mathematical analysis of these models into a broader context, and to see which of the advances brought about by recent developments in hydrodynamics or chemistry might elucidate the behavior of the biological models, if not the biological systems. The main difficulties with this program are that (i) the models often lack a secure phenomenological base since the systems they are supposed to describe are highly complicated, and (ii) controlled, quantitative experiments are extremely difficult to perform, especially in our "physicist's limit" of a large system under constant external conditions, which might indeed be quite absurd in some cases. Nevertheless, we believe that the perspective we bring to the problems of biological pattern formation may be useful in further developments of the field. In a sense we attempt to solve the easy problems, understanding the basic pattern forming properties of the *models* used in the field, and how these fit into a broader theoretical context. In this way the biologists can concentrate on the difficult problems of elucidating the pattern forming *mechanisms* and choosing appropriate models. It is fair to say that the distinction we are making here between the "easy" and the "hard" problems have not always been appreciated by workers in the field.

The literature on nonequilibrium patterns is so vast that it is difficult for us to give a general list of articles or books related to ours. For each topic discussed we have attempted to give references to the pertinent literature. We do not assume any prior knowledge of pattern formation on the part of the reader, though our paper is not meant to be strictly introductory. The reader may wish to consult Swinney and Gollub (1981), Manneville (1990), Haken (1977, 1983a, 1987), Mikhailov (1991), Mikhailov and Loskutov (1991), Gaponov-Grekov and Rabinovich (1990, 1991), Kuramoto (1984b), Winfree (1987), and Murray (1989), for general discussions of the topics, some of them from a different point of view than ours. There are also innumerable conference proceedings related to the topics we cover, which the reader may wish to consult. The following is a partial list: Ben Amar *et al.* (1991), Bishop *et al.* (1986), Busse and Kramer (1990), Coron *et al.* (1991), Coullet and Huerre (1990), Engelbrecht (1989), Frehland (1984), Gaponov-Grekov *et al.* (1989), Graham and Wunderlin (1987), Güttinger and Dangelmayr (1987), Haken (1980, 1981a,b, 1985), Holden *et al.* (1990), Kai (1992), Krinsky (1984a), Lam and Morris (1990), Markus *et al.* (1988), Meinköhn (1990),

Pacault and Vidal (1979), Perez-Garcia (1992) Sirovich (1991), Stein (1989), Tirapegui and Villarroël (1987, 1989), Walgraef (1987), Walgraef and Ghoniem (1990), Wesfreid and Zaleski (1984), Wesfreid *et al.* (1988).

An early bibliography of nonequilibrium phenomena was assembled by Hohenberg and Langer (1982). A more recent bibliography, going far beyond the subject of chaos in its title, may be found in Zhang (1991).

II. BASIC PHENOMENOLOGY

A. Rayleigh-Bénard convection

In its idealized form Rayleigh-Bénard convection involves a fluid placed between flat horizontal plates that are infinite in extent and are perfect heat conductors. The fluid is driven by maintaining the lower plate at a temperature ΔT above the upper plate temperature. For small driving the fluid remains at rest, and a linear temperature profile is set up interpolating between the upper and lower plate temperatures. This is the "conducting" or "uniform" solution. Due to the thermal expansion, however, the fluid near the lower plate is less dense; an intrinsically unstable situation in the gravitational field. Of course the fluid cannot rise as a whole since there would be no place for the fluid above it to go. Thus, due to a conservation law (mass in this case), we encounter an instability at a finite wavelength — a fundamental precursor of pattern formation. This instability occurs when the driving ΔT is strong enough to overcome the dissipative effects of thermal conduction and viscosity. The control parameter describing the instability, the Rayleigh number R , is the dimensionless ratio of the destabilizing buoyancy force $\rho_0 \alpha g \Delta T$ to the stabilizing dissipative force $\nu \kappa \rho_0 / d^3$

$$R = \frac{\alpha g \Delta T d^3}{\kappa \nu}, \quad (2.1)$$

where ρ_0 is the average mass density, α the thermal expansion coefficient, g the acceleration of gravity, ν the kinematic viscosity, κ the thermal diffusivity and d the plate separation. The instability occurs at the value $R = R_c \approx 1708$, independent of the fluid under consideration (see Chandrasekhar, 1961). The wave vector q_0 of the instability is of order d^{-1} , since d is the only length scale available in the ideal problem. We thus arrive at the picture of an instability toward a pattern in which the fluid rises in some regions and falls in others with a characteristic horizontal length scale d . For Rayleigh number R slightly above R_c the growth of this pattern is limited because convective flow transports part of the heat applied, thus decreasing the temperature gradient and the buoyancy force. At some point there is a balance between the applied temperature gradient and the reduction due to convective motion, and in general the fluid settles down to a stationary flow regime near threshold. The simplest example of such a flow is the familiar convective roll pattern shown schematically in Fig. 1, but su-

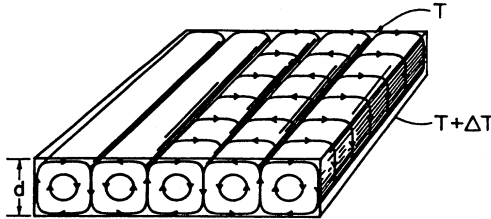


FIG. 1. Schematic picture of Rayleigh-Bénard convection showing fluid streamlines in an ideal roll state.

perpositions of rolls forming hexagons or squares are also possible.

The critical Rayleigh number R_c is the minimum value of R at which the conducting state becomes unstable to disturbance of the velocity v of the form

$$\delta v \sim \exp(i\mathbf{q} \cdot \mathbf{x}),$$

for some wave vector \mathbf{q} in the horizontal plane. As mentioned above, the value $|\mathbf{q}| = q = q_0$ at which the instability at R_c occurs is of order of the inverse plate separation (specifically, $q_0 = 3.117/d$). The instability of the conducting state to disturbances with $q \neq q_0$ occurs for larger R . Indeed, when $q < q_0$ the rolls are flat and involve excess horizontal motion with a dissipative contribution to $R_c(q)$ proportional to q^{-2} at small q . For $q > q_0$, the rolls are tall and thin and the excess vertical shear and horizontal temperature gradient lead to a critical Rayleigh number $R_c(q)$ growing as q^4 . It is useful to represent the domain of stability of the conducting state in terms of the function $R_c(q)$ as in Fig. 2 (dashed curve). For $R > R_c(q)$ a convecting solution grows, and it turns

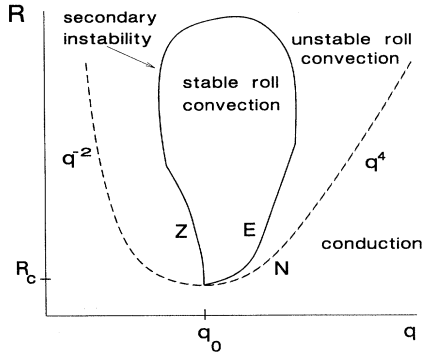


FIG. 2. Schematic stability diagram for Rayleigh-Bénard convection showing the Rayleigh number R vs the wave vector q . Dashed line: instability of uniform conducting state to growth of convecting solution with wave vector q (neutral stability, N). Solid lines: various secondary instabilities of the nonlinear convecting state. Near threshold the Eckhaus (E) and zig-zag (Z) instabilities are common to many systems. The solid line bounds the domain of stable spatially periodic ideal nonlinear solutions. For a more accurate representation see Fig. 32 below.

out that stationary solutions exist in general for R not too large. The existence of stationary convecting states does not, however, guarantee their physical relevance; they must also themselves be *stable* to infinitesimal disturbances. Under rather general physical conditions it may be shown (see Busse, 1978) that near threshold hexagons and squares are unstable to rolls, and periodic roll solutions remain stable inside a smaller domain, delimited by the solid curve in Fig. 2. The region of stable roll convection is often referred to as the “Busse balloon,” named after F. Busse who identified the many *secondary instabilities*, beyond which different types of convecting states are seen; either more complicated stationary roll patterns or *time-dependent* states which may be periodic or nonperiodic. A simple example of a secondary instability occurs when the convective flow reduces the temperature gradient in the central portion of the cell, leaving boundary layers near the top and bottom plate which experience a strong gradient. The thinner layers may themselves be the source of an instability to convective rolls at a shorter wavelength, which are generally oriented perpendicular to the original ones.

Figure 2 refers to a laterally infinite system in which a continuum of periodic states, labelled by the wave vector q , can be defined. For a finite system, of lateral width L , the solutions must satisfy specific lateral boundary conditions which greatly complicate any concrete calculation. Roughly speaking, however, we can say that the effect of the lateral boundaries is to quantize the wave vectors in units of π/L , i.e., the continuum of solutions is reduced to a discrete set.

The spatially periodic stationary roll states we have discussed up to now are of particular interest because of their relative theoretical simplicity. Experimentally, ordered states are only obtained under special conditions, e.g. for R just above threshold, or in containers of prescribed shape. In particular, rolls tend to align perpendicular to the sidewalls, so parallel rolls are most easily obtained in cells which are long and thin. A system which avoids even the small distortion due to the short sidewalls is an annular geometry, which is well represented by a one-dimensional model. In contrast to the above cases, “natural” patterns which arise spontaneously when R is suddenly raised above R_c are spatially disordered. In Fig. 3 we show examples of such structures obtained in experiments and in numerical simulations. Some of these patterns can be thought of as being made up of domains of periodic structures pieced together by different kinds of interfaces or defects. Other cases are so disordered that they bear very little resemblance to a periodic roll structure. We will see in subsequent sections that defects play a crucial role in determining both the dynamics of pattern formation and the structure of the patterns which are obtained at large times under steady external conditions.

From a physical point of view, an appealing feature of hydrodynamic instabilities in general, and convective flow in particular, is that once quantities are expressed in terms of dimensionless numbers, such as the Rayleigh

number R for example, the results obtained are valid for any fluid obeying the Navier-Stokes equations, which includes such disparate substances as water, oil, mercury, air, and liquid or gaseous helium. The most important way in which the specific fluid properties enter thermal convection is in the dimensionless parameter called the Prandtl number

$$\sigma = \nu/\kappa , \quad (2.2)$$

which represents the ratio of the two damping mecha-

nisms acting on the fluid, the kinematic viscosity ν and the thermal diffusivity κ . Fluids with low Prandtl number ($\sigma \lesssim 3$) have a smaller stability balloon for stationary convection and a larger domain of dynamic behavior. Since the size of a convective roll is determined by the plate separation, the only other important parameters controlling the pattern are the so-called aspect ratios

$$L_i = \tilde{L}_i/d , \quad (2.3)$$

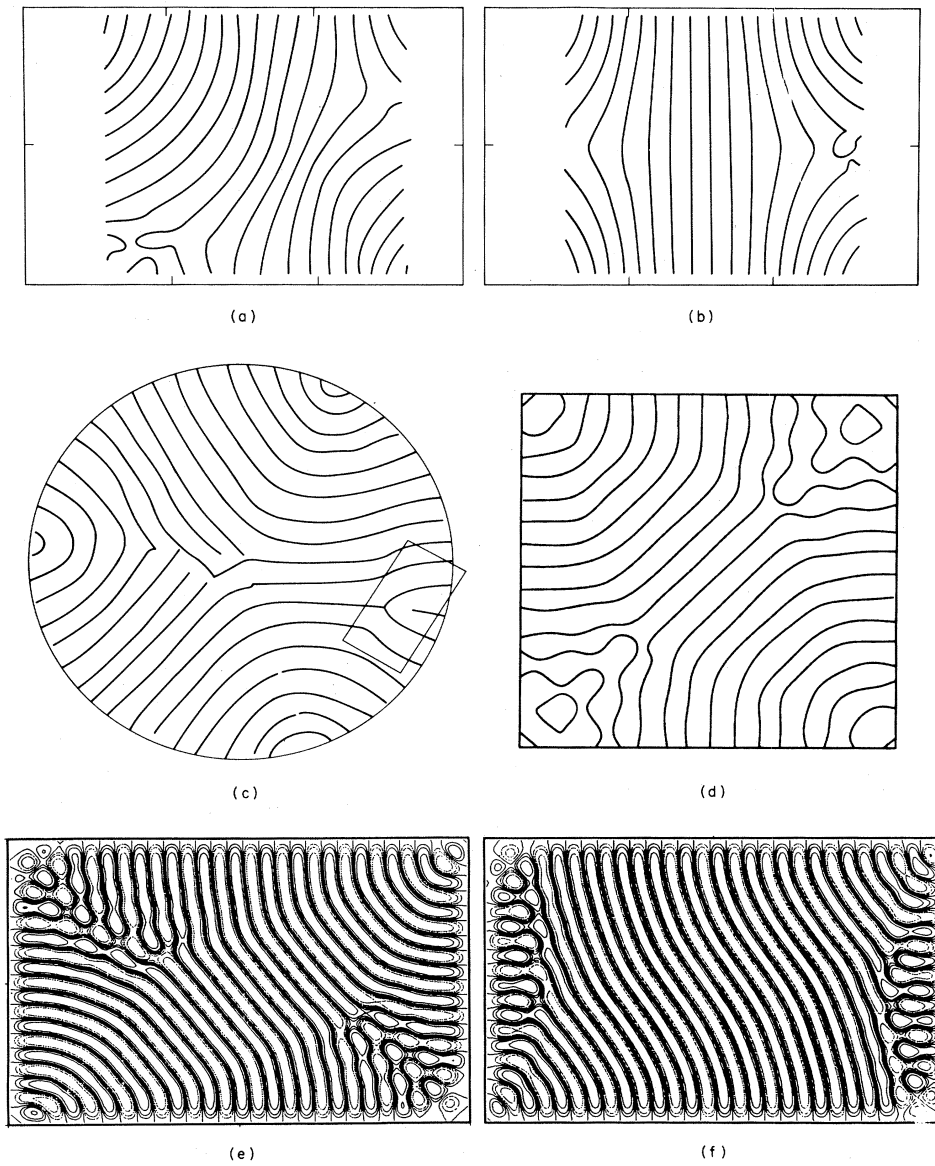


FIG. 3. Horizontal spatial patterns in convection with lateral boundaries; (a) and (b) are from experiments of Gollub *et al.* (1982); (c) from experiments of Croquette *et al.* (1983); and (d)–(f) from numerical simulations of the Swift-Hohenberg model equation (3.27) by Greenside and Coughran (1984).

where \tilde{L}_i is a lateral dimension^{2.1} (e.g. the radius for a cylindrical cell). Roughly speaking the largest aspect ratio L is equal to the number of rolls in the pattern. An important distinction exists between *small* and *large* systems, according to the number of rolls they contain (generally a system with $L \lesssim 3 - 5$ is defined as small). The distinction is relevant in considering the dynamics of convection outside the region of stable rolls, namely chaotic dynamics. For small L one can model the system in terms of a discrete number of degrees of freedom interacting among one another, a situation which is known to lead to a variety of chaotic scenarios which have been well studied in recent years (see, e.g. Bergé *et al.*, 1987; Manneville, 1990). For large systems, on the other hand, the continuum of states available above threshold must be taken into account, and the dynamics involves a large number of active degrees of freedom. The chaotic behavior of such spatially extended systems is not well understood at present, but Rayleigh-Bénard convection is an attractive physical example in which to investigate this problem (see Secs. VII and VIII.E below).

If the horizontal plates are made of poor thermal conductors (with conductivity K_p small compared to the conductivity K_f of the fluid) the critical Rayleigh number curve $R_c(q)$ is modified (Busse and Riahi, 1980). Its minimum becomes $R_c^{ins} = 720$ for $K_p \ll K_f$, and the critical wave vector behaves as

$$q_0 = c_1 (K_p / K_f)^{1/3}, \quad (2.4)$$

($c_1 \approx 3$) in the thick-plate limit, leading to a pattern with a single flat roll (see Sec. VIII.F.1 below).

B. Other convecting systems

1. Convection in fluid mixtures

In a mixture, concentration changes are coupled to density variations via the quantity $\rho^{-1}(\partial\rho/\partial c)_T$, which is analogous to the thermal expansion $\rho^{-1}(\partial\rho/\partial T)_P$, but can have either positive or negative sign. There is thus an additional mechanism which can either favor or suppress convection. Since the dynamics of the concentration variable is associated with an independent time scale governed by the diffusivity D_c , or the Lewis number $\mathcal{L} = D_c/\kappa$, the behavior of convective mixtures can be quite rich indeed (Platten and Legros, 1984). The most interesting new aspect is the appearance, for certain parameter values, of temporal oscillations *at* the convective threshold. This time dependence combines with the spa-

tial periodicity to create traveling wave states whose nonlinear behavior shows remarkable properties. Among these we cite interactions between traveling and standing waves, spatial confinement, and interesting defect structures involving waves of different velocities. Moreover, the existence of time dependence near the onset of convection means that this system offers the possibility of studying chaotic dynamics in a region where nonlinear effects might be small enough to be calculable analytically (see Sec. IX.A).

2. Electrohydrodynamic instabilities in nematic liquid crystals

It is possible to destabilize a nematic liquid crystal by applying an electric field, the electric force ρE acting in a manner similar to the buoyancy force in thermal convection (see Dubois-Violette, *et al.*, 1978). The charge ρ is coupled to fluctuations in the curvature $K = \partial_x n_z$ of the director, with the flow velocity following adiabatically in typical regimes. In order to prevent static charge build-up at the electrodes an a.c. field is usually applied, and depending on the amplitude and frequency of this field different regimes of convection are found. The main advantages of electrohydrodynamic convection are the ability to control the flow by electromagnetic means, and the small spatial scale of the rolls which makes it easier to study large systems, with 1000 rolls, say. This system is discussed further in Sec. IX.C.

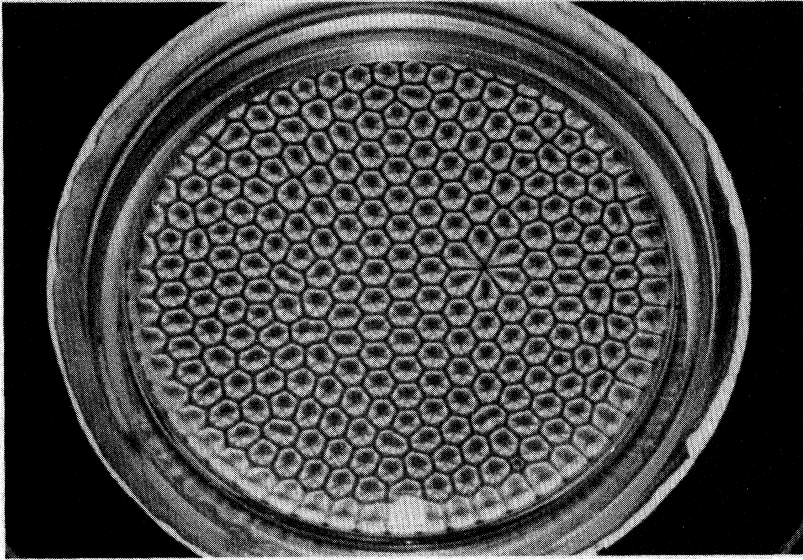
3. Bénard-Marangoni convection

The original experiment of Bénard (1900) was carried out in an open dish, and the flow pattern he found was a regular tesselation of hexagons with fluid rising at the center and falling along the sides as in Fig. 4. The theory developed by Rayleigh (1916) to explain this phenomenon involved a driving force due to differential buoyancy in the bulk of the fluid, but it was later discovered (Pearson, 1958) that the hexagon pattern resulted from a surface instability caused by a temperature dependent surface tension. Indeed, if we imagine a fluid heated from below, and a horizontal temperature fluctuation δT at the surface, there is an induced change $\delta\Sigma$ in the surface tension Σ which causes fluid to flow along the surface toward the point where the fluctuation occurred, and to sink into the bulk at that point. To compensate this flow, warm fluid must rise in adjacent portions of the cell, thus increasing the temperature difference and causing instability. The driving force is now $-(\Delta T/d^2)(\partial\Sigma/\partial T) > 0$, and the control parameter is the Marangoni number

$$M = \frac{\Delta T(d/\rho_0)(-\partial\Sigma/\partial T)}{\kappa\nu}, \quad (2.5)$$

which does not involve the acceleration of gravity g . Comparing the Marangoni and Rayleigh numbers, Eqs. (2.5) and (2.1), we see that for a given ΔT the Marangoni

^{2.1}Since we usually express all lengths in units of the plate separation we do not distinguish between the aspect ratios and the lateral dimensions, and will henceforth use the same symbol L for both.



instability at $M = M_{c0} \approx 80$ is reached before the Rayleigh instability at $R = R_c \approx 1708$ for thin layers, since $(\Delta T)_M \sim 1/d$ whereas $(\Delta T)_R \sim 1/d^3$.

It turns out that for convection with a free surface even the buoyancy driven instability leads to a hexagonal pattern, so the appearance of hexagons does not guarantee a surface tension driven instability. A more careful analysis of the response of the surface reveals that in the case of a buoyancy driven instability the rising fluid at the center of the hexagons is associated with a bump, whereas it leads to a trough in the Marangoni case. In practice both mechanisms are operative, and the surface remains flat when they exactly compensate, which occurs for $d = [4(-\partial\Sigma/\partial T)/\alpha\rho_0 g]^{1/2}$ (see Sec. VIII.F).

C. Taylor-Couette flow

The Taylor-Couette system is another hydrodynamical example analogous to Rayleigh-Bénard convection, except that the buoyancy force is replaced by the centrifugal force due to rotation (see DiPrima and Swinney, 1981). The apparatus consists of two concentric circular cylinders with fluid confined to the gap between the cylinders. If the outer cylinder alone is rotated, an azimuthal shear flow is set up that is stable. If the inner cylinder is rotated instead, however, the larger centrifugal force near the rotating cylinder leads to an instability above a critical rotation rate, towards circulating rolls (called Taylor vortices) perpendicular to the axis of the cylinder (Fig. 5). The radial coordinate is analogous to the vertical coordinate in convection, and the azimuthal and axial directions correspond to the horizontal directions in the Rayleigh-Bénard system. Note, however, that there is no symmetry between these two directions in the Taylor-Couette case: the first instability is to a state of azimuthal rolls, with no spatial variation around the cylinders. Until this azimuthal invariance is destroyed,

FIG. 4. Early experiment showing convection cells in silicone oil under an air surface. Visualization with aluminum powder. Dark lines indicate vertical motion. Bright areas indicate predominantly horizontal motion. (Koschmieder, 1974).

Taylor-Couette flow provides another good laboratory example for studying “one-dimensional” pattern formation. Eventually, as the rotation rate is increased, a secondary instability occurs to a time-dependent flow in which first one and then a second wavy modulation of the

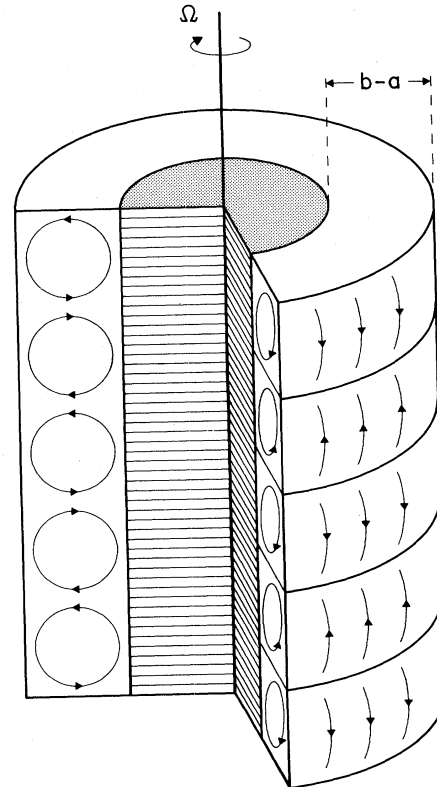


FIG. 5. Schematic picture of the Taylor-Couette system, showing fluid streamlines in the Taylor-vortex state when the inner cylinder is rotated at a rate $\Omega > \Omega_c$.

Taylor vortices travel around the cylinder at independent velocities. The behavior is even richer if the outer cylinder is rotated in the reverse direction to the inner cylinder: now the first transition may be to a spiral (barber's pole) pattern with the rolls simultaneously traveling up (or down) and around the cylinder, analogous to the waves in binary-fluid convection (see Sec. IX.B).

D. Parametric waves

The excitation of waves via nonlinear processes provides another class of pattern forming systems. Again a spatially uniform driving — now time dependent — leads via the nonlinear interaction between the wave excitations of the system to an instability toward states with spatial structure. The simplest situation is where external driving at a frequency ω excites waves at wave vector \mathbf{q} , given approximately by the resonance condition

$$\omega_s(\mathbf{q}) = \frac{1}{2}\omega, \quad (2.6)$$

with $\omega_s(\mathbf{q})$ the spectrum of the waves in the linear approximation. For experiments on finite systems we replace the plane waves by the linear eigenmodes of the system consistent with the boundary conditions. The mathematics of these parametric instabilities is simply displayed in the much studied Mathieu equation.

One simple experimental realization is known as “Faraday’s crisscrosses,” after the early experiments (Faraday, 1831). A shallow disc of liquid is rigidly oscillated in the vertical direction. The acceleration periodically modulates the effective gravity (i.e. one of the parameters of the wave equation). At sufficiently large driving a surface wave instability occurs with frequency one half the driving frequency. The spatial pattern which is usually seen initially corresponds to the linear mode most closely resonant with this subharmonic frequency. (The details depend on the strength of the coupling to the uniform driving, on damping effects, and on geometry.) Interesting pattern competition effects occur close to the frequency at which two modes simultaneously go unstable.

This type of parametric wave instability has a number of attractive features for studies of pattern formation; for example the length scale of the pattern is easily tuned by varying the drive frequency and may often be made small compared with the system size, so that a great many spatial periods may be investigated. On the other hand dissipative effects play a secondary role in these systems except very near threshold, so that the attraction in phase space to simple dynamical behavior is relatively weak, and complicated dynamical effects often occur (see Sec. IX.D).

An analogous system is the parametric excitation of magnetization waves in ferromagnetic bodies (often yttrium-iron garnet spheres) by the spatially uniform pumping of an oscillating magnetic field. However, the

spatial structure of the resulting state is hard to detect experimentally, and attention has mainly focused on the sequence of dynamic phenomena (see L’vov and Prozorova, 1988). This system is treated briefly in Sec. XII.C.

E. Reaction-diffusion systems

Forces and flows are central to fluid systems; chemical systems are dominated by reaction and diffusion. In a remarkable paper Turing (1952) showed that these two simple ingredients could lead to a wide range of pattern forming instabilities. This paper opened up an enormous range of study spanning the fields of developmental biology (Turing’s main interest), laboratory chemistry, applied mathematics, and engineering.

The important feature of these systems for our purposes is the competition between different temporal growth rates and spatial ranges of diffusion for the different chemicals in the system. For example the very simple linear equations for the concentrations $u_1(x, t)$ and $u_2(x, t)$ of two reacting and diffusing chemicals in one dimension,

$$\partial_t u_1 = D_1 \partial_x^2 u_1 + a_1 u_1 - b_1 u_2, \quad (2.7a)$$

$$\partial_t u_2 = D_2 \partial_x^2 u_2 - a_2 u_2 + b_2 u_1, \quad (2.7b)$$

lead to an instability toward a time-independent state with a wave number

$$q_0 = \left[\frac{1}{2} \left(\frac{a_1}{D_1} - \frac{a_2}{D_2} \right) \right]^{1/2}. \quad (2.8)$$

In chemical and biological systems the above expressions have been interpreted in terms of the interaction of an *activator* u_1 and an *inhibitor* u_2 , since for positive a_i and b_i the growth of u_1 stimulates further growth of u_1 and u_2 , whereas the growth of u_2 leads to decay of u_1 and u_2 (see for example Murray, 1989). The diffusion constant D_1 defines a decay length $\ell_1 = (D_1/a_1)^{1/2}$, and similarly for D_2 . The criterion for the existence of a finite-wavenumber instability of the uniform state $u_1 = u_2 = 0$ is seen from Eq. (2.8) to be $\ell_1 < \ell_2$, which means that the inhibitor has a longer range than the activator. This condition has been expressed as the “principle of local activation with lateral inhibition” (Oster, 1988) which is found to occur in many models studied by theoretical biologists (see Sec. XI).

For other parameter values the reaction diffusion equations (2.7) have an instability to a time-periodic state [$\omega_0 \neq 0$] which is spatially uniform ($q_0 = 0$). The oscillatory instability occurs when there is a large cross coupling between activator and inhibitor [$b_1 b_2 > \frac{1}{4}(a_1 + a_2)^2$], and when the activator growth exceeds the decay of the inhibitor ($a_1 > a_2$). Such an instability occurs in the oscillatory chemical reaction discovered by Belousov and Zhabotinsky (see, for example, Winfree, 1974; Ross *et al.*, 1988). The simplest state immediately above threshold consists of a uniform oscil-

lation with no spatial structure. Experimentally, interesting patterns are seen in this system, and they may be understood as *defects* in the uniform medium, which are nucleated by imperfections or externally imposed sources.

For chemical and biological systems, the reaction-diffusion equations (2.7) represent some sort of superficial description of a complicated set of reactions. For example, we have not discussed the mechanism for the production of u_1 and u_2 . Moreover, a closed chemical system, just as a closed fluid system, ultimately must come to equilibrium. Nonequilibrium phenomena of interest to us either occur as a transient — maybe over long times — or in response to some external chemical pumping. We discuss oscillatory chemical reactions in Sec. X.

F. Solidification patterns

The regularity of the shapes produced by crystals growing into a supercooled or supersaturated environment is a well known phenomenon. The beautiful feathery patterns with the hexagonal symmetry of ice, photographed in selected snowflakes, are one example; another is the disordered pattern of metallic alloys formed from the melt, whose microstructure is the determining factor in the resulting material properties.

The tendency towards pattern formation in solidification is demonstrated by the instability of a plane front of the solid phase growing into the supercooled liquid. This instability, known as the Mullins-Sekerka instability, can be understood from the enhanced diffusion in front of a bulge of the surface into the diffusion field of temperature or impurity concentration that limits the growth rate. This enhanced diffusion results in a local increase in the growth velocity and in turn to further growth of the perturbation. In the case of the free growth of an interface into a supercooled region the instability does not saturate at small amplitudes, so that an analysis based on the Mullins-Sekerka instability is only qualitatively useful, for example in identifying characteristic lengthscales. Instead, the resulting state often consists of needles, known as dendrites, moving out along crystal symmetry directions. The growth velocity, the size of the needles (e.g. the tip radius) and the shape of the dendrites, including question of sidebranching, have been the focus of much study. In this situation the surface tension serves to control the instability at short length scales so that regular patterns are observed. On the other hand in growth processes where the only short-scale cutoff is the discrete size of the particles, the random arrival sequence is important and much more irregular structures are observed. These may be fractal in nature, at least at intermediate length and time scales. Such growth processes are modelled by the numerical procedure of “diffusion limited aggregation” or DLA. We will restrict our attention to regular patterns, and refer the reader to Vicsek (1989) for a review of DLA type processes.

An experimental geometry in which the growth of the

Mullins-Sekerka instability is controlled, known as directional solidification, was developed by Jackson and Hunt (1965). In this system the growth rate of solid from a liquid mixture is limited by the diffusion of the impurity species away from the interface. The position of the interface is in addition controlled by an imposed temperature gradient \mathcal{G} , and the growth velocity is determined by physically advancing the solid-liquid system at a fixed velocity v between hot and cold thermal reservoirs. The values of v and \mathcal{G} provide additional control parameters, and may be used to saturate the instability at small amplitudes (in some cases as small as desired). The resulting cellular pattern across the interface is analogous to the periodic roll pattern in convection, and many of the same theoretical ideas can be applied in this case and studied experimentally.

The literature on solidification and other growth processes is vast and we shall only touch on a corner of this field in order to illustrate the analogies with the other pattern forming systems which are the focus of this review and to mention some differences. There are in turn other fluid systems that show strong analogies with solidification, for example the invasion of a viscous fluid by a less viscous one, which may be systematically studied in the Saffman-Taylor geometry. We will not review this work.

G. Nonlinear optics

Intense electromagnetic waves propagating in various types of media can have interesting instabilities, the most famous of which is the lasing instability occurring for example in a cavity containing a gas of two-level atoms. Typically, the laser is operated in such a way that only one spatial mode of the electromagnetic field is excited in the cavity, so the interesting variation is in time rather than in space. Nevertheless, under some circumstances parameters can be adjusted so that more spatial modes come into play and spatial patterns also appear.

Besides a laser cavity, one can also consider intense electromagnetic fields propagating along a glass fiber, whose nonlinear response leads to a cubic propagation equation for the envelope of the wave, in the form of a “nonlinear Schrödinger” equation. This system is known to possess localized propagating pulse solutions called solitons in the ideal dissipationless case. Such solitons are a prototype for many other localized solutions found in nonlinear optics as well as other systems to be considered below. The coupling of electromagnetic waves to atomic degrees of freedom via the Maxwell-Bloch equations offers many examples of nonequilibrium instabilities and patterns, which will be briefly discussed in Sec. XII.B below.

III. GENERAL FEATURES OF PATTERN FORMATION

A. Dynamics and stability

1. Dissipative dynamics and attractors

We will consider *dynamical systems*, defined by a time evolution equation for the system variables (see Guckenheimer and Holmes, 1983). A typical example is a set of nonlinear ordinary differential equations (*ode's*)^{3.1}

$$\partial_t U(t) = f(U; R), \quad (3.1)$$

for the n components of the state vector

$$U(t) = \{u_i(t)\} = u_1(t), \dots, u_n(t), \quad (3.2)$$

where in general $f(U; R)$ is a set of nonlinear functions of all the variables (3.2), depending on a *control parameter* R , which could be a set of parameters $R = R_1, \dots, R_p$. The instantaneous state of the system at fixed values of R can be represented by a point in the n -dimensional *phase space* with coordinates given by (3.2), and the time evolution by a trajectory in that space.^{3.2} It is sometimes useful to consider in place of the continuous time evolution (3.1), discrete dynamics given by

$$U(m+1) = f[U(m); R], \quad (3.3)$$

with m an integer. Such *mappings* often arise as approximations to the continuous dynamics in (3.1). A natural extension of (3.1), which incorporates the notion of spatial dependence and leads to spatial patterns, is to consider a continuous set of state variables that depend on a *spatial coordinate* x ,^{3.3} in addition to the time t . Then (3.1) becomes a set of partial differential equations (*pde's*)

$$\partial_t U(x, t) = G[U, \partial_x U, \dots; R], \quad (3.4)$$

where the right-hand side of (3.4) depends on the gradients and higher spatial derivatives of U . The phase space is then infinite dimensional, though the trajectory is still a curve in this space.

An important class of dynamical equations consists of *conservative* or Hamiltonian systems that have the property of preserving volume in phase space (Guckenheimer and Holmes, 1983). This means that if one follows the

trajectories of all the points in a subvolume δV of phase space, then δV will in general be distorted as time progresses, but its volume will remain constant. Another type of dynamical system, the so-called *dissipative* ones, are of particular relevance to the macroscopic description of physical phenomena. These systems have the property that arbitrary subvolumes in phase space shrink to zero at long times. This means that points eventually end up on a lower-dimensional set called an *attractor*, which has zero volume in the original phase space. Not all points will necessarily end up on the same attractor, of course. If the system has different attractors then each one has its own *basin of attraction*, which is the set of initial points whose trajectories eventually end up on the attractor in question. As we discuss further in Sec. VII below, attractors come essentially in two types: regular attractors correspond to laminar motion and possess a simple geometrical shape such as a fixed point, a closed curve (limit cycle), or a torus; the second class of attractors, the so-called irregular or "strange" attractors, correspond to *chaotic* motion and possess unusual geometrical properties. It may be noted that even regular attractors can have basins with very complicated geometrical structure.

2. Stability and bifurcations

Given a solution $U_0(t)$ of the equations of motion (3.1), we can examine the stability properties of that solution. We will distinguish three types of stability (or instability). To define *linear stability* we consider a solution $U_0(t)$ and apply a small perturbation

$$U(t) = U_0(t) + \delta U(t). \quad (3.5)$$

Inserting (3.5) into (3.1), and linearizing the equation with respect to δU we find

$$\partial_t \delta U = \underset{\approx}{Df} \cdot \delta U, \quad (3.6)$$

where $\underset{\approx}{Df}$ is the Jacobian derivative of f evaluated at U_0 .

$$(Df)_{ij} = \underset{\approx}{\delta f_i / \delta u_j} \Big|_{U=U_0}. \quad (3.7)$$

Then if all the eigenvalues of the matrix Df are negative $\delta U(t)$ decays at long times and U_0 is said to be linearly stable. The linearization leading to (3.6) is appropriate for infinitesimal initial disturbances δU . For finite δU we are dealing with *nonlinear* stability, which involves more complex issues (see for example Sec. II of Normand *et al.*, 1977). The solution $U_0(t)$ is (nonlinearly) stable if any solution that starts sufficiently close to U_0 remains in a finite neighborhood of U_0 for all time. Thus U_0 can be stable by this definition without being on an attractor. If at long times $U(t)$ tends back to $U_0(t)$ then the fixed point is said to be *asymptotically stable* and $U_0(t)$ is an attractor. Generally speaking understanding the nonlinear stability of a solution involves characterizing its

^{3.1}For notational convenience we shall use the symbol ∂ for all derivatives, both partial and total. In cases where a confusion is likely we will write the derivatives out explicitly, e.g. $\partial U / \partial t$ or dU / dt .

^{3.2}For a pictorial introduction to phase space dynamics see Abraham and Shaw (1983).

^{3.3}In the present section we write x in ordinary type though it is in general a vector in d -dimensional space. In later sections, when the distinction is important, we will use boldface type for spatial vectors.

basin of attraction. For complicated time dependence (e.g. chaotic motion) the linear stability properties are most easily summarized by the *Lyapunov exponents*, which will be discussed in Sec. VII.

For spatially extended systems the same concepts apply if we consider linear disturbances satisfying the same physical boundary conditions in the finite region. Often we might want to consider an ideal infinite region, to remove complications of arbitrarily shaped boundaries. In a translationally invariant system it is then natural to consider the stability of Fourier modes^{3,3}

$$\delta U(x, t) \sim \delta U_q(t) e^{iqx}, \quad (3.8)$$

which represent delocalized disturbances. It is also instructive to consider infinitesimal disturbances $U_0(x)$ which are *localized* in space. If such a solution, initially localized around x_0 , say, grows large at x_0 then $U_0(x)$ is said to be *absolutely unstable*. If, on the other hand, the solution grows in amplitude but moves away from x_0 , such that its value at any fixed spatial position eventually decays to zero, we say that the system is *convectively unstable* (see Landau and Lifshitz, 1959, p. 111).

The above concepts of stability and instability have been discussed here in a qualitative way to give the reader an intuitive grasp of the richness of behavior which occurs in dynamical systems. Standard texts on differential equations should be consulted for precise definitions of stable and unstable manifolds (Arnol'd, 1988; Guckenheimer and Holmes, 1983) and of different stability criteria.

As the control parameter R is varied, changes may occur in the qualitative structure of the solutions for certain parameter values. These changes are called *bifurcations* and they involve changes in the number of solutions as well as their stability. The simplest bifurcations of fixed-point solutions which depend on a single control parameter R are of four types, exemplified by the following equations (Guckenheimer and Holmes, 1983):

$$\text{saddle-node: } \partial_t u = R - u^2, \quad (3.9a)$$

$$\text{transcritical: } \partial_t u = Ru - u^2, \quad (3.9b)$$

$$\text{pitchfork: } \partial_t u = Ru - gu^3, \quad (3.9c)$$

$$\text{Hopf: } \begin{aligned} \partial_t u_1 &= -u_2 + Ru_1 - (u_1^2 + u_2^2)u_1, \\ \partial_t u_2 &= u_1 + Ru_2 - (u_1^2 + u_2^2)u_2. \end{aligned} \quad (3.9d)$$

$$\quad (3.9e)$$

The first three examples involve fixed points only. The Hopf bifurcation has a fixed point which loses stability for $R > 0$, and a limit cycle (periodic solution) which appears at $R = 0$ and is stable for $R > 0$. The stability properties of the solutions to Eqs. (3.9) are illustrated in Fig. 6.

The differences between the various bifurcations arise because of differences in the *symmetry* of the equations. The pitchfork bifurcation [Figs. 6(c) and 6(d)] is ubiquitous in physical systems, but it depends on the absence of a quadratic term on the rhs of (3.9c), or more generally

on the symmetry

$$f(-U) = -f(U). \quad (3.10)$$

If, as the control parameter varies, one goes continuously from one stable branch to the other then one speaks of a *supercritical bifurcation*. If there is a loss of stability the bifurcation is *subcritical*. The pitchfork bifurcation is supercritical for $g > 0$ and subcritical for $g < 0$ [see Figs. 6(c) and (d)]. In the language of phase transitions these correspond to second-order or continuous transitions as opposed to first-order or discontinuous transitions, respectively.^{3,4}

Certain perturbations of the equations will change the bifurcation from one type to another. To the extent that the perturbation is small, the original bifurcation is still

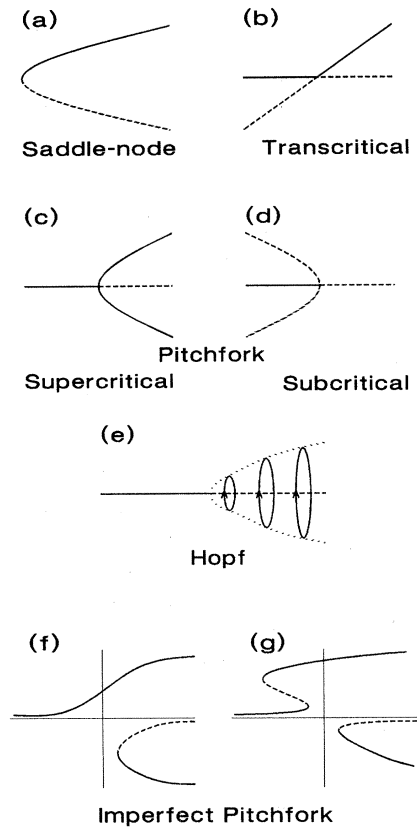


FIG. 6. Simple bifurcations from a time independent state. Curves show how the solution evolves as a control parameter (varying along the abscissa) is changed. Solid lines denote stable solutions, dashed lines unstable solutions. The dotted line in (e) shows the continuous growth of the amplitude of the limit cycle.

^{3,4}Supercritical and subcritical bifurcations are also sometimes referred to as "forward" and "backward".

approximately present, and one speaks of an “imperfect” bifurcation. For example, generic perturbations of the pitchfork bifurcation change Eq. (3.9c) to

$$\partial_t u = h + Ru + pu^2 - g \quad (3.11)$$

which has two characteristic forms, shown in Figs. 6(f) and 6(g). In the first case [for example for $p=0, h > 0$, Fig. 6(f)] one is left with a smooth transition (no bifurcation), plus a saddle-node. In the second case [for example $h > 0, p > 0, p > h^3/27$, Fig. 6(g)] one is left with three saddle nodes and hysteresis, i.e. a subcritical bifurcation.

3. Potential motion and Lyapunov functions

A certain subclass of dynamical systems, namely *potential* or *gradient* systems, are of particular interest because their behavior is simpler than the general case, and because they are frequently encountered in approximate treatments of physical systems. For a gradient^{3.5} system Eq. (3.1) takes the form

$$\partial_t u_i(t) = -\frac{\delta \mathcal{J}}{\delta u_i}, \quad (3.12)$$

where $\mathcal{J}[U]$ is a (scalar) function of the vector U . [Hirsch and Smale, 1974, pp. 199ff]. More generally, a system with an attractor U_0 is said to have a Lyapunov function \mathcal{V} for this attractor if this function satisfies the conditions

$$\mathcal{V}(U_0) = 0, \quad (3.13)$$

$$\frac{d\mathcal{V}}{dt} \leq 0 \text{ for } U \neq U_0, \quad (3.14)$$

and \mathcal{V} is a smooth function of U in some neighborhood of U_0 (Hirsch and Smale, 1974). A gradient system, satisfying (3.12), has a global Lyapunov function if \mathcal{J} is bounded below. For gradient systems the dynamics consists of relaxation toward the minimum in \mathcal{J} . This means that such functions are strictly only defined when the corresponding attractors are fixed points and there is no chaos, nor even any periodic motion at long times. As discussed further below, Eq. (3.12) can be generalized to spatially continuous systems and it provides important examples of pattern forming systems.

Graham and co-workers have introduced a “nonequilibrium potential” that is formally similar to a Lyapunov function but can be defined for an arbitrary dynamical system of the form (3.4) (Graham, 1989; Graham and

Tel, 1986, 1990a,b). It is a single-valued functional in phase space $\Phi[U]$ that is constant on any attractor and decreases in any dynamics away from the attractors. It is defined formally as the solution of a complicated Hamiltonian-Jacobi equation and has an interesting interpretation in terms of the probability distribution of the system under the influence of weak external noise (see subsection III.A.4 below). The main differences between the potential Φ and the functions \mathcal{V} and \mathcal{J} defined above are that (i) Φ is a highly singular function (only piecewise differentiable), and (ii) Φ does not determine the dynamics. On the contrary, it is usually necessary to know the solutions $U(t)$ in order to construct $\Phi[U]$.

4. Deterministic versus stochastic dynamics

In the foregoing we have considered *deterministic* equations such as (3.1) and (3.4), where in principle the solution is uniquely specified by the initial conditions. Physical systems, on the other hand, are often best represented by *stochastic* equations, where the dynamical variables U are coupled to a set of random variables ζ that are specified by their probability distribution rather than by their equations of motion (see Van Kampen, 1981; Gardiner, 1983; Moss and McClintock, 1989). The random force represents a bath of degrees of freedom which are not controlled in the experiment. These could involve either noise on a molecular scale, or various forms of macroscopic noise associated with the apparatus. The prototype equation has the form

$$\partial_t U = f(U; R) + \zeta(t), \quad (3.15)$$

where $\zeta(t)$ represents a set of n random variables. A similar set of equations apply for the continuum system (3.4). More general forms have also been introduced, in which the noise ζ depends on the variable U , but we shall not consider them further here (see Hortschhemke and Lefever, 1984).

The presence of a stochastic force greatly complicates the mathematical problem of finding solutions to (3.15), but we shall primarily be concerned with the qualitative effects of noise. First of all, we can cite the consequences for the geometry of attractors, both in smearing out the singular structure of strange attractors (Graham, 1989), and in providing an ergodic probability measure as discussed in Sec. VII.B below. Another important effect of noise occurs in the case where the deterministic part has the gradient form (3.12), and the stochastic force can cause the system to surmount potential barriers and to move from one local minimum to a lower one. Such processes are ubiquitous in systems near equilibrium under the influence of thermal noise (see Hohenberg and Halperin, 1977). Although considerable theoretical work has been devoted to the effects of noise on nonequilibrium systems (see Hortschhemke and Lefever, 1984; Moss and McClintock, 1989) the problems are difficult both mathematically and physically. In particular, the form and magnitude of the noise in Eq. (3.15) depend on the

^{3.5}In the mathematical literature systems defined by Eq. (3.12) are called “gradient” systems, but we shall follow the practice among physicists and use the terms “gradient” and “potential” interchangeably. Gradient systems are also sometimes referred to as “variational”.

details of each system under study, and they are difficult to determine reliably. We shall discuss the effects of external noise on pattern selection in Sec. VI.D below, and the connection between such extrinsic stochasticity and chaos in Sec. VII.E.

5. Bifurcations versus phase transitions

Sharp bifurcations occur for ordinary differential equations (*ode*'s) or partial differential equations (*pde*'s) on finite spatial domains when parameters in these equations are varied. If a constant term, such as h in Eq. (3.11), is added to the right-hand side the bifurcation is rendered imperfect, i.e. the transition is smeared over a region determined by the magnitude of h . Thermodynamic systems, on the other hand, are known to display sharp phase transitions only in the *thermodynamic limit* of an infinite volume $V \rightarrow \infty$. For finite V the free energy is an *analytic* function of the thermodynamic fields T, H , etc.

In order to reconcile the two different situations let us consider a simple thermodynamic system such as an Ising model. From the point of view of dynamics the Gibbs ensemble can be obtained as the stationary probability measure of a stochastic equation of the form

$$\partial_t u_i = \frac{\delta \mathcal{F}}{\delta u_i} + \xi_i , \quad (3.16)$$

where $\mathcal{F}[\{u_i\}]$ is a free energy functional and ξ is a thermal noise term with $\langle \xi^2 \rangle \sim T$ (see Hohenberg and Halperin, 1977). This system has an imperfect bifurcation for any finite volume, due to the smearing caused by ξ . A sharp phase transition [$\langle u \rangle = 0$ for $T \geq T_c$, $\langle u \rangle \neq 0$ for $T < T_c$] occurs only in the limit $V \rightarrow \infty$, where the thermal noise ξ does not lead to an imperfect bifurcation. The mean-field approximation replaces the system (3.16) by a homogeneous deterministic equation for a single degree of freedom, which has a sharp bifurcation (Binder, 1973). Besides finite-size effects coupled to thermal fluctuations, phase transitions can also be smeared by imperfections. For macroscopic bifurcation phenomena, on the other hand, thermal noise is usually negligible (see Sec. VI.D below), so transitions are of the mean-field type, i.e. they remain sharp in finite systems and smearing is only caused by imperfections in that case. This distinction has not always been appreciated by workers in the field.

B. Linear instabilities and basic nonlinear states

1. Linear instabilities

We start from a system consisting of n partial differential equations (*pde*'s)

$$\partial_t U = G[U, \partial_x U, \dots, R] , \quad (3.17)$$

for the functions $U = u_1(x, t), \dots, u_n(x, t)$. We suppose that the uniform state $U=0$ is a solution for all values of

the control parameter R . In order to define the problem mathematically we must also specify boundary conditions on the domain of definition $x \in V$ of (3.17) and initial values at $t=0$, say. We will classify systems in terms of the response to single Fourier mode disturbances in the ideal infinite system. The basic instability of (3.17) is found by linearizing $G[U]$ about $U=0$ and studying the evolution of modes of given wave vector (see footnote 3.3)

q ,

$$u_j(x, t) = u_{j0} e^{iqx + \sigma t} . \quad (3.18)$$

The ensuing *linear* equations

$$\partial_t U \underset{\approx}{=} D \cdot U , \quad (3.19)$$

with

$$D_{ij} = \delta G_i / \delta u_j , \quad (3.20)$$

have a set of eigenvalues $\sigma_\alpha(q)$, and we choose to focus on the one with the largest real part, which we denote as $\sigma(q)$. It is interesting to remark that in most pattern forming systems the wave vector q lies in a space of restricted dimension (1 or 2). For example in convection the periodicity is in the horizontal plane: the vertical structure is completely determined by the boundary conditions at the plates. Similarly in biology, pattern formation largely seems to occur on surfaces or membranes.

Now suppose that the dependence of G on the *control parameter* R is such that for $R < R_c$, $\text{Re}\sigma(q) < 0$, and for $R = R_c$, $\text{Re}\sigma(q=q_0) = 0$ for some q_0 . We introduce the *reduced* control parameter

$$\varepsilon = (R - R_c) / R_c , \quad (3.21)$$

(assuming $R_c \neq 0$), and show in Fig. 7 the dependence of $\text{Re}\sigma(q)$ on q and ε . For $\varepsilon < 0$ the uniform state is stable and $\text{Re}\sigma < 0$, whereas for $\varepsilon = 0$ the instability sets in ($\text{Re}\sigma = 0$) at a wave vector $q = q_0$. For $\varepsilon > 0$ there is a *band* of wave vectors $q_- < q < q_+$ (in the infinite systems we are considering), for which the uniform state is unstable. The instability of Fig. 7 I can be of two types: either *stationary* if $\text{Im}\sigma(q_0) = 0$, or *oscillatory* if $\text{Im}\sigma(q_0) \equiv \omega_0 \neq 0$ for $\varepsilon = 0$.

Another class of instability occurs if for some reason (usually a conservation law) $\text{Re}\sigma(q=0) = 0$ for all ε . We then have the situation depicted in Fig. 7 II. The critical wave vector is $q_0 = 0$, and the unstable band for $\varepsilon > 0$ is $0 \leq q \leq q_+$, with $q_+ \sim \varepsilon^{1/2}$ or ε , so that the pattern occurs on a long length scale near threshold. Once again there are two possible cases, steady [$\text{Im}\sigma(q=0) = 0$] or oscillatory [$\text{Im}\sigma(q=0) = \omega_0 \neq 0$].

In the case depicted in Fig. 7 III both the instability and the maximum growth rate occur at $q_0 = 0$. Here there is no intrinsic length scale. The structure will presumably occur on a scale defined by the system size, or by the dynamics. As in the other two cases, this situation can correspond to either a steady [$\text{Im}\sigma = 0$] or an oscillatory [$\text{Im}\sigma \neq 0$] instability.

We may thus divide pattern forming systems into

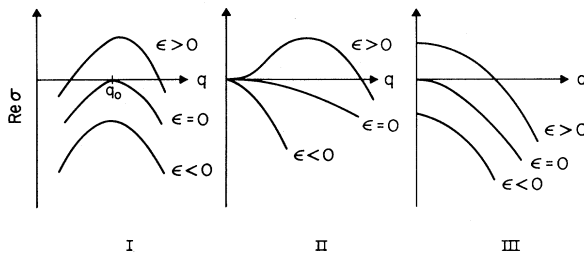


FIG. 7. Schematic representation of the linear growth rate $\text{Re } \sigma$ as a function of the wave vector q , for various values of the reduced control parameter ϵ , showing the classification into types I, II, and III.

different classes according to the nature of the linear instability of the spatially uniform state. There are three types, depending on the value of the most unstable wave vector q_0 near threshold: type I is spatially periodic with $q_0 = O(1)$, type III is uniform with $q_0 = 0$, and type II is intermediate with an unstable band $0 < q < q_+$, $q_+ \sim \epsilon^{1/2}$ or ϵ . For each type there are two subtypes depending on the *temporal* instability: stationary if $\omega_0 = 0$ and oscillatory if $\omega_0 = O(1)$. Since type II can often be scaled to resemble type I we will concentrate on three subclasses:

- Type I_s, stationary periodic ($\omega_0 = 0$, $q_0 \neq 0$),
- Type I_o, oscillatory periodic ($\omega_0 \neq 0$, $q_0 \neq 0$),
- Type III_o, oscillatory uniform ($\omega_0 \neq 0$, $q_0 = 0$).

The case III_s ($\omega_0 = 0$, $q_0 = 0$) does not involve pattern formation in an essential way and will not be considered in what follows.

2. Ideal patterns

In this section we give a qualitative discussion of the basic nonlinear states, i.e. those characterized by certain simple symmetries reflecting the nature of the transition in the laterally infinite system. In Sec. IV we discuss perturbation methods to calculate the properties of these simple states, and in Secs. V and VI we study the more complicated patterns encountered in realistic situations.

Since we are interested in pattern forming systems i.e. systems that spontaneously form spatial structure not imposed by external constraints, we will assume the system to have *translational symmetry*, in one, two, or rarely three dimensions. The patterns breaking this symmetry beyond the instability will then be characterized by a spatial periodicity with a wave vector q . Other symmetries may also be present depending on the system. There may be a continuous spatial rotational symmetry, in two or three dimensions, as in ideal Rayleigh-Bénard convection, which has rotational symmetry in the plane. The Taylor-Couette system has two translational symmetries (axial and azimuthal) but these are not related to each other by a rotational symmetry. In addition, there may be discrete symmetries such as parity $x \rightarrow -x$, or invariance of the equations under “inversion”, i.e. under a

change of sign of the field variables, $U \rightarrow -U$.

We refer to patterns as “ideal” if they retain certain symmetry elements of the full system, in particular at least discrete translational symmetries. Ideal patterns are fundamental to a qualitative understanding of more complicated states. They may be analyzed by group-theoretic methods, and are identified as being isotropic under some subgroup of the full symmetry group of the system, as is found in the Landau theory of phase transitions (Landau and Lifshitz, 1958). We will briefly describe these methods in Sec. IV.B below, but for now we proceed heuristically, describing the ideal patterns which appear at the various types of instabilities.

a. Saturation of the linear instability

A basic role of nonlinearity is to saturate the exponential growth of the unstable mode proportional to $\exp(iqx)$. In addition, since the principle of superposition no longer holds, the nonlinearity may select between different combinations of symmetry-related states which grow equally rapidly in the linear regime. For stationary instabilities the unstable mode may saturate into a state which is spatially periodic (see footnote 3.3)

$$U_q(x, t) = U_\infty(qx). \quad (3.22)$$

This state has a discrete translational symmetry which can be represented by a phase variable $\phi = qx$,

$$U_\infty(\phi) = U_\infty(\phi + 2\pi). \quad (3.23)$$

The ideal convective roll state or the Taylor vortex state are canonical examples of periodicity in one direction. If rotational symmetry is present in the system, we may construct a saturated nonlinear state from the growth of superimposed small amplitude roll solutions with equal wave numbers but different directions. Spatially periodic patterns in the form of squares or hexagons, which may develop from the growth of equal amplitudes of rolls at angles of $\pi/2$ or $2\pi/3$, are commonly discussed [see Fig. 8]. Rhomboid states, with two sets of rolls that are not perpendicular seem possible, but have not received much attention. The hexagonal pattern is particularly interesting since several different possible local structures may be formed with complicated cellular organization. In addition, unlike the roll or square solutions, there is a breaking of inversion symmetry ($U \rightarrow -U$), and the maximum positive values at the center points are larger than the most negative values around the edges of the cell. (The alternate pattern reversing the result is of course also possible.) Small symmetry breaking perturbations in the system may strongly favor one or the other of these patterns, changing the transition from pitchfork to transcritical and making hexagons the preferred state (over rolls, squares, etc.) near threshold. Thus the hexagonal pattern is commonly observed in many systems lacking inversion symmetry, for example convection in non-Boussinesq fluids or under time-dependent heating (see Sec. VIII.F).

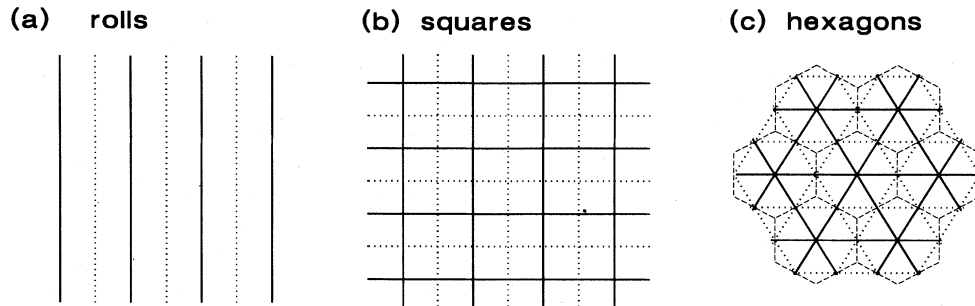


FIG. 8. Ideal states of type I systems, with solid lines denoting positive maxima (e.g. fluid upflow) and dotted lines negative maxima (e.g. fluid downflow): (a) roll state; (b) square state formed from nonlinear saturation of two superimposed roll states at angle $\pi/2$; (c) hexagon state formed from three sets of rolls at angles $\pm \pi/3$. Maximum downflows in hexagon state occur along the dashed line which delineates the boundaries of the hexagonal cells.

For oscillatory instabilities the simplest saturated state is the traveling wave train (or rotating wave)

$$U_{\omega,q}(x,t) = U_\infty(qx - \omega t). \quad (3.24)$$

[Type III_o systems admit the special case of a spatially uniform oscillation $U_\omega(x,t) = U_\infty(\omega t)$.] Note that a time delay Δt is equivalent to a spatial translation $|\Delta x| = v_{ph} \Delta t$, with v_{ph} the phase speed ω/q . This means that as well as maintaining a discrete spatial translational symmetry, the system continues to show a continuous symmetry under a combined space-time translation. One consequence is that spatial averages will be time independent in the ideal infinite system. The wave trains are characterized by a dispersion relation $\omega(q)$, which will in general depend on the nonlinearity.

If the q and $-q$ instabilities occur together, then standing waves may develop at threshold and continue to exist for stronger driving. Standing-wave solutions which are of the general form

$$U(x,t) = U_\infty(qx, \omega t) \quad (3.25)$$

have only discrete translational symmetries along the direction of the wave vector and in time,

$$x \rightarrow x + 2\pi/q, \quad t \rightarrow t + 2\pi/\omega. \quad (3.26)$$

In addition, standing waves possess the discrete symmetries of parity ($x \rightarrow -x$), and the combined symmetry of time translation through half a period ($t \rightarrow t + \pi/\omega$), and inversion ($U \rightarrow -U$). Note that in general there will not be any x and t for which all U are zero simultaneously. For example, in binary-fluid convection equal-phase wave fronts oscillate up and down in the z direction, and the fluid velocity is never simultaneously zero at all z for any x or t .

The selection between the various nonlinear states in both stationary and oscillatory situations is determined in part by stability considerations, but there often exist regions of *multiple stability*. Near threshold the calculations are easily carried out using the amplitude equations developed below. Away from threshold further transi-

tions may occur to states of lower symmetry, e.g. quasi-periodically modulated states.

b. Stability balloons

We can also ask about the magnitude of the wave vector q in the states that exist beyond the instability, for example in the simple roll or wave states. Near threshold, spatially periodic nonlinear states can typically be found over the whole band of wave vectors inside the curve $R_c(q)$ of instability of the uniform state, as may be argued from general principles of bifurcation theory. However, the band of observable or useful wave vectors is further restricted by the *stability* of the corresponding states. For the example of stationary convection, the linear stability analysis of the nonlinear steady states has been carried out in some detail (Busse, 1967a, 1978). Away from threshold, where numerical methods are needed, Busse and co-workers have found a large number of characteristic instabilities, leaving however a finite band of stable wave vectors for Rayleigh numbers not too far away from threshold (Fig. 2). Two instabilities are quite generally seen in such systems, and survive to limit the band near threshold (Newell and Whitehead, 1969). These are the Eckhaus instability, a long-wavelength longitudinal (compressional) instability, and the zigzag instability, a long-wavelength transverse instability. Long wavelength here means that the instability first occurs as a distortion over arbitrarily long length scales. Further from threshold the instabilities found by Busse (knot, oscillatory, etc.) have short wavelengths and are specific to the physics of the fluid system (see Sec. VIII.A below).

C. Model Equations

1. Motivation

The physical, chemical, and biological systems described in Sec. II which we wish to study are often quite

complicated and the equations and boundary conditions describing them are not always known precisely. Even when they are known, as is the case for many hydrodynamic instabilities, a linear analysis already requires numerical evaluation and a direct analytic approach is impossible beyond threshold. The perturbation methods described below are a partial response to this situation, though calculation of the appropriate coefficients can be difficult even if the starting equations are known precisely.

It turns out, however, that full solutions of realistic equations are not usually needed to gain an understanding of the spatial patterns displayed in these systems. Indeed, many different systems show similar patterns, so it is reasonable to attempt to extract from each system those features which control pattern formation, and to incorporate them into *model equations* which will be simpler than the more realistic starting equations. We might, for example, attempt to reproduce the stability balloon of the ideal nonlinear solutions. One way to accomplish this is to find a simpler "microscopic" model^{3,6} which reduces to the same amplitude and phase equations (see below) as the original model. In this way the long-wavelength stability properties will be preserved. Another way to construct a model is by some modifications of the original *U* system, for example replacing realistic boundary conditions by artificial, simpler ones to yield a separable system. The models thus obtained are easier to study both analytically and numerically, and they display interesting pattern-forming properties, e.g. defects, boundary effects, slow relaxation and chaos. Such properties are thought to be independent of the detailed mechanisms leading to the instability, and are therefore shared between realistic equations and appropriately chosen models. In the field of thermodynamic critical points the careful study of simple models to predict certain properties of real systems is an application of the concept of *universality*. By this we do not mean that all systems behave in the same way, but that certain properties, in particular those involving long-range effects, are common to a class of systems, and can therefore be understood by studying a simple member of that (universality) class. For critical-point phenomena this notion is highly quantitative (see, e.g., Privman *et al.*, 1991 and references therein), whereas it is unclear as yet how far the concept may be pushed to study nonequilibrium pattern formation.

^{3,6}As mentioned in the Introduction, we refer to starting equations such as (3.4) as "microscopic" equations to denote the fact that all length and time scales of interest are included in the description. This is in contrast to simpler equations such as amplitude or phase equations, obtained from the original ones by a coarse-graining procedure. Of course the term microscopic is relative, since the *U*-model may itself be the result of averaging some more basic description. We merely use the word to indicate that all length and time scales have been defined by the model.

The models that have been studied in recent years fall into two classes which we consider in turn: the first consists of partial differential equations (*pde's*) which are similar to the realistic field equations of physics and chemistry; the other class comprises various discretizations of field equations, in which one can discretize either space (coupled *ode's*), or space and time (coupled maps), or space, time, and the field (cellular automata). Of course any numerical solution of a partial differential equation involves discretization, but this is only a calculational tool and it is necessary to verify that all results are independent of the discretization to the accuracy claimed for the calculation. For discrete *models* on the other hand, only the universal properties are supposed to be insensitive to the particular discretization, and even this insensitivity may be qualitative rather than quantitative. Clearly, the choice of models and their interpretation require insight and experience in order to determine which are the essential features and which are expendable.

2. Partial differential equations

Here we list some of the simple models whose pattern forming properties are frequently studied. Many other models have been considered for special applications and some of these will be mentioned in later sections.

a. The Swift-Hohenberg (SH) equation and its variants

This model is of the form (Swift and Hohenberg, 1977; Pomeau and Manneville, 1980)

$$\partial_t u = \epsilon u - (\nabla^2 + 1)^2 u - u^3, \quad (3.27)$$

where $u(\mathbf{x}, t)$ is in general a real field in d -dimensional space. Complex generalizations are sometimes considered, as well as asymmetric variants (with addition of a quadratic term on the right-hand side). The model is potential [see Eq. (3.12)] with the potential

$$\mathcal{J} = \int d^d x \left\{ -\frac{1}{2} \epsilon u^2 + \frac{1}{2} [(\nabla^2 + 1)u]^2 + \frac{1}{4} u^4 \right\}. \quad (3.28)$$

An interesting nonpotential variant is the model introduced by Pismen (1986)

$$\partial_t u = \epsilon u - (\nabla^2 + 1)^2 u + 3(\nabla u)^2 \nabla^2 u, \quad (3.29)$$

which has the same type I_s linear instability as (3.27) and many similar nonlinear properties.

b. The Kuramoto-Sivashinsky equation

Another equation which was motivated by the study of amplitude and phase expansions, but which is now studied in its own right as a "microscopic" model, is the Kuramoto-Sivashinsky (KS) system (Kuramoto and Tsuzuki, 1976; Sivashinsky, 1977)

$$\partial_t \phi = -\nabla^2 \phi - \nabla^4 \phi - \frac{1}{2} (\nabla \phi)^2. \quad (3.30)$$

This equation is often generalized to include a linear term and written (in one dimension) as an equation for $u = \partial_x \phi$ in the form

$$\partial_t u = -\eta u - \partial_x^2 u - \partial_x^4 u - u \partial_x u . \quad (3.31)$$

The original (nongeneralized) KS equation has $\eta=0$, which implies a “Galilean symmetry” [$u \rightarrow x-vt$, $u \rightarrow u+v$]. This nonpotential model displays a type I_s instability at $\eta=1/4$, and interesting chaotic behavior which we discuss in Sec. VII.D below, for $\eta < 1/4$. Although present interest focuses on the chaotic properties of Eq. (3.31), it had been studied many years earlier as a model for nonlinear waves (see the references in Greene and Kim, 1988).

c. Reaction-diffusion equations

The reaction-diffusion equations introduced in Sec. II above as a description of chemical reactions can be considered as abstract models of pattern formation. The general form is (Murray, 1977; Fife, 1979)

$$\partial_t U = f(U) + D \nabla^2 U , \quad (3.32)$$

for various functions f and constant matrix D . Of course Eq. (3.32) does not restrict the behavior significantly, and examples of all the types of instability we have considered can easily be found by suitable choices of f and D . If we generalize Eq. (3.32) to

$$\tau \partial_t U = f(U) + D \nabla^2 U , \quad (3.33)$$

with a constant matrix τ then the SH model (3.27) is obtained from a two-component equation of form (3.33) with $\tau_{11}=1$, $\tau_{12}=\tau_{21}=\tau_{22}=0$, $f_1=(\varepsilon-1)u_1-u_1^3-2u_2$, $f_2=u_2$, $D_{12}=-1$, $D_{21}=-1$, $D_{11}=D_{22}=0$.

A reaction-diffusion system which has received considerable attention is the so-called “ $\lambda-\omega$ model” (Howard and Kopell, 1977),

$$\partial_t u_1 = \lambda(u^2)u_1 - \omega(u^2)u_2 + \nabla^2 u_1 , \quad (3.34a)$$

$$\partial_t u_2 = \omega(u^2)u_1 + \lambda(u^2)u_2 + \nabla^2 u_2 , \quad (3.34b)$$

where $u^2 \equiv u_1^2 + u_2^2$, and $\omega(u^2)$ and $\lambda(u^2)$ are smooth functions. If $\omega(0) \neq 0$, the model has a type III_s instability when $\lambda(0)$ goes through zero. The amplitude equation discussed in Eq. (4.49) below, for type III_s instabilities, is a special case of the $\lambda-\omega$ model for which $\lambda(u^2)=\varepsilon-g_0u^2$ and $\omega(u^2)=-c_3u^2$. On the other hand (3.34) corresponds to (4.49) with $c_1 \equiv 0$, so in a sense the $\lambda-\omega$ model is also a special case of the amplitude equation, since (3.34) has a diagonal diffusion matrix.

d. Ginzburg-Landau models

In perturbative analyses of the microscopic equations for various systems one encounters complex pde’s which

go under the name of “amplitude equations”. Considered in their own right as *model* dynamical systems we will refer to them as Ginzburg-Landau models,^{3,7} a prototype of which is

$$\partial_t A = (b_1 + i c_1) \nabla^2 A + f_1(|A|^2) A , \quad (3.35)$$

where

$$f_1 = f_{1r} + i f_{1i} \quad (3.36)$$

is an arbitrary complex function of its argument $|A|^2$, and b_1 and c_1 are real constants. In one dimension we will also consider the generalized equation

$$\begin{aligned} \partial_t A = & (b_1 + i c_1) \partial_x^2 A + f_1(|A|^2) A \\ & + \partial_x [f_2(|A|^2) A] + [\partial_x f_3(|A|^2)] A , \end{aligned} \quad (3.37)$$

where f_2 and f_3 are complex functions. There are clearly many variants of the above equations, with anisotropic derivatives in higher dimensions, or with other fields coupled to A . Some of these will be encountered in what follows.

A frequently encountered one-dimensional example of the complex Ginzburg-Landau model (3.37) is (see, for example, van Saarloos and Hohenberg, 1992)

$$f_1(y) = \varepsilon - (b_3 - i c_3)y - (b_5 - i c_5)y^2, \quad f_2 = f_3 = 0 , \quad (3.38)$$

$$\begin{aligned} \partial_t A = & (b_1 + i c_1) \partial_x^2 A + \varepsilon A \\ & - (b_3 - i c_3)|A|^2 A - (b_5 - i c_5)|A|^4 A . \end{aligned} \quad (3.39)$$

[Often the quintic term is not present, i.e. $b_5 = c_5 = 0$.] When $b_3 > 0$, the model (3.39) has a supercritical bifurcation at $\varepsilon=0$, and when $b_3 < 0$ it has a subcritical bifurcation (when $b_3 < 0$ we assume $b_5 > 0$ for stability). The special case $b_1 = \varepsilon = b_3 = b_5 = c_5 = 0$, is the nonlinear Schrödinger equation

$$\partial_t A = i c_1 \partial_x^2 A + i c_3 |A|^2 A , \quad (3.40)$$

and the case with $c_5 \neq 0$ we will call the quintic-cubic Schrödinger equation

$$\partial_t A = i c_1 \partial_x^2 A + i c_3 |A|^2 A + i c_5 |A|^5 A . \quad (3.41)$$

A model that has been studied in the plasma literature is the “derivative nonlinear Schrödinger” equation

$$b_1 = f_1 = f_3 = 0 , \quad f_2(|A|^2) = s_0 + s_1 |A|^2 , \quad (3.42)$$

$$\partial_t A = i c_1 \partial_x^2 A + \partial_x [(s_0 + s_1 |A|^2) A] . \quad (3.43)$$

^{3,7}The name derives from the formal similarity with the Ginzburg-Landau (1950) theory of superconductivity, though the latter did not concern itself with dynamics. The earliest amplitude equation in space and time with complex coefficients seems to be that of Stewartson and Stuart (1971).

We also can define a case we call the “generalized derivative Schrödinger” equation, obtained from (3.37) by assuming

$$b_1 = f_{1r} = f_{2i} = f_{3i} = 0, \quad (3.44)$$

namely

$$\begin{aligned} \partial_t A &= i c_1 \partial_x^2 A + i f_{1i}(|A|^2) A \\ &\quad + \partial_x [f_{2r}(|A|^2) A] + [\partial_x f_{3r}(|A|^2)] A. \end{aligned} \quad (3.45)$$

It is important to note the role of these Ginzburg-Landau equations as *model* equations. It is true that many properties of nonequilibrium systems are encountered in these equations, and indeed many hard problems, such as the existence and interaction of defects and coherent structures (Sec. V), or the appearance of chaos (Sec. VII), may profitably be addressed in the simple framework provided by these equations. However, it is only as a perturbative expansion valid in a small region near threshold that they provide a quantitative description of real experimental systems, and results may be even qualitatively misleading if applied far from threshold. More technically (as will become clearer below) we may say that far from threshold only the phase of the complex A survives as a slow degree of freedom, since it describes a symmetry of the system. The magnitude $|A|$, on the other hand, only becomes slow near threshold, and far away it is just one of many fast degrees of freedom so there is no reason to expect a simple description in terms of a Ginzburg-Landau model to be quantitatively valid.

3. Discrete models

a. Systems of ordinary differential equations

Systems consisting of a small number of coupled nonlinear *ode*'s have been of central importance in the study of temporal chaos, since the seminal work of Lorenz (1963). If a large or even infinite number of modes are coupled together with short-range coupling, then we have a discretized form of a *pde* which can display interesting spatial patterns. Although such models have been considered in the literature (see, e.g., Aranson *et al.*, 1986), the usual practice is to discretize time as well, and study coupled maps (Kaneko, 1985; Crutchfield and Kaneko, 1987).

b. Coupled maps

A single nonlinear mapping such as the logistic map

$$u_{n+1} = R u_n (1 - u_n) = f(u_n), \quad (3.46)$$

has nontrivial bifurcations and dynamics (see Collet and Eckmann, 1980). When a set of such modes is coupled

together there can be an interplay between the local dynamics of a single map and possible instabilities which arise from the coupling. A system analogous to reaction-diffusion models which has been studied widely in recent years takes the form

$$u_{n+1}(i) = f(u_n(i)) + \frac{1}{2} g \left\{ \sum_{\ell} u_n(i + \ell) - 2d u_n(i) \right\}, \quad (3.47)$$

where g is a coupling constant, i ranges over a d -dimensional hypercubic lattice and $(i + \ell)$ denotes a nearest neighbor of i . A linear stability analysis can be carried out for this model in analogy to the one described in Eq. (3.19), and the different types of instabilities found there can be recovered (see Oppo and Kapral, 1986).

c. Cellular automata

The main appeal of coupled lattices is the relative ease with which their behavior can be simulated numerically. The same holds to an even greater degree for cellular automata, for which also the dynamical variable $u_n(i)$ takes on only a discrete set of values (see Wolfram, 1986). In addition to their numerical convenience cellular automata are simple enough so that a rather complete classification of their dynamical behavior can be given. These systems are therefore potentially useful as simple models with nontrivial dynamics, for which exact results could be proven.

IV. THEORETICAL APPROACHES

In this section we wish to describe some general analytic approaches to the problem of pattern formation, concentrating on general methods of solution that are applicable to most of the systems under consideration.

A. Perturbative methods

Since finding analytic solutions to nonlinear *pde*'s is impossible in general, it is important to devise shortcuts to some understanding of the behavior. One such shortcut is to go to a limit where the solutions may be calculated perturbatively. There are two main situations which have some generality for a diverse range of systems, and we will emphasize these situations here.

- Near threshold. Here the nonlinearities are weak and the spatial and temporal modulations of the basic pattern become slow. The balance between these effects is described by “amplitude equations” for the envelope function of the basic state. These equations come in a small number of universal forms, largely dictated by the linear instability classification of Sec. III.B, and they serve to carry this classification into the weakly nonlinear regime. The approach has been rediscovered in many different contexts (Landau, 1944; Stuart, 1960; Newell

and Whitehead, 1969; Segel, 1969; Stewartson and Stuart, 1971; Newell, 1974; Haken, 1977) and bears a strong resemblance to the mean-field Landau theory of equilibrium phase transitions (Landau and Lifshitz, 1958).

• Weak distortions. Even arbitrarily far from threshold, weak distortions of a regular pattern, involving spatial modulations over distances large compared to the basic period, can be treated perturbatively yielding “phase equations” (Pomeau and Manneville, 1979; Cross and Newell, 1984; Kuramoto, 1978, 1984a,b; Pismen, 1989; Brand, 1988; Bernoff, 1988). Again there is a similarity of form and general behavior among the phase equations for different systems displaying a particular type of instability, but as might be expected there is more freedom in functional dependences, reflecting the detailed nonlinear behavior which must be calculated separately for each system. Whatever universality is left from the broad classification scheme at onset is reflected in the form of the phase equation.

These methods share the common philosophy of eliminating fast modes, which adiabatically follow the slow modes of interest (a procedure referred to as “slaving” by Haken, 1977). Near threshold the slow modes include the magnitudes of the marginally unstable band of solutions, as well as symmetry modes described by phases. Further away from threshold the magnitude and “shape” of the ideal nonlinear solutions join the other fast modes, and we are only left with slow phase modes. A recent review emphasizing fluid dynamical applications has been presented by Newell *et al.* (1993).

1. Amplitude equations

a. Type I_s: Stationary periodic

(i) General form of the amplitude equation

Let us consider the plane-wave growing solution above threshold for a type I_s, stationary-periodic instability [$q_0 \neq 0$, $\omega_0 = 0$]. For concreteness we consider a two-dimensional system and represent the most unstable mode as

$$U(\mathbf{x}, t) = U_0 e^{i\mathbf{q}_0 \cdot \mathbf{x} + \sigma t}. \quad (4.1)$$

For values of the control parameter close to threshold ($|\varepsilon| \ll 1$), the structure on short length scales will be insensitive to ε , but a slow modulation in space and time is possible making use of the band of unstable solutions, and the linear growth is likely to saturate due to nonlinear effects. This behavior can be analyzed by writing

$$U(\mathbf{x}, t) = [U_0 A(\mathbf{x}, y, t) e^{i\mathbf{q}_0 \cdot \mathbf{x}} + \text{c.c.}] + O(\varepsilon), \quad (4.2)$$

where we have assumed a two-dimensional pattern ($\mathbf{x} = (x, y)$) consisting of one-dimensional rolls perpendicular to the x direction, with any dependence on the third spatial dimension being included in U_0 , and c.c. denotes

the complex conjugate. A *complex* amplitude is chosen since a phase change then corresponds to a spatial translation of the unstable mode. For an isotropic system the function $A(x, y, t)$ satisfies the equation

$$\begin{aligned} \tau_0 \partial_t A &= \varepsilon A + \xi_0^2 [\partial_x - (i/2q_0)\partial_y]^2 A \\ &\quad - g_0 |A|^2 A. \end{aligned} \quad (4.3)$$

There are several ways of deriving Eq. (4.3) from particular microscopic equations. These include the introduction of multiple scales to formally separate the fast and slow dependences (Newell and Whitehead, 1969; Segel, 1969), or the use of mode projection techniques (Cross, 1980; Haken, 1977), which emphasizes the slaving idea. However the *form* of the equation is quite general, reflecting the *symmetries* of the type I_s instability. The detailed properties of the individual systems are entirely contained in the real constants τ_0 , ξ_0 , q_0 , and g_0 which set the scales of variation in time, space, and amplitude.

In fact the form of Eq. (4.3) can be written down by inspection. The linear terms are prescribed by the growth rate of the linear instability, and represent the real space form needed to reproduce the growth rate $\sigma(q)$ of a plane-wave disturbance at wave vector $\mathbf{q} = q_0 \hat{\mathbf{x}} + \mathbf{k}$

$$\begin{aligned} \sigma(q) &= \tau_0^{-1} [\varepsilon - \xi_0^2 (q - q_0)^2] \\ &\simeq \tau_0^{-1} [\varepsilon - \xi_0^2 (k_x + k_y^2/2q_0)^2], \end{aligned} \quad (4.4)$$

where we have kept the lowest order terms in each of k_x and k_y in expanding $|q_0 \hat{\mathbf{x}} + \mathbf{k}| - q_0$ for small $|\mathbf{k}|$. Note that the difference in scaling in the two directions reflects the inherent symmetry breaking of the instability, which was here chosen with wave vector in the x direction. Equation (4.3) is recovered by the substitution $\sigma \rightarrow \partial_t$, $k_x \rightarrow -i\partial_x$, and $k_y \rightarrow -i\partial_y$. The constants τ_0 and ξ_0 are directly given from the linear instability spectrum through Eq. (4.4)

$$\tau_0^{-1} = \frac{\partial \sigma(q)}{\partial \varepsilon} \Big|_{q=q_0, \varepsilon=0}, \quad (4.5a)$$

$$\tau_0^{-1} \xi_0^2 = -\frac{1}{2} \frac{\partial^2 \sigma(q)}{\partial q^2} \Big|_{q=q_0, \varepsilon=0}. \quad (4.5b)$$

Newell (1974) has presented a derivation of amplitude equations in various situations incorporating this idea more formally.

The nonlinear terms may again be obtained by inspection: the cubic term is the first one that feeds back on the unstable mode, and this is the only term that preserves the invariance of the equation under a phase change $A \rightarrow A e^{i\phi}$, which simply corresponds to a spatial shift of the pattern. (Derivative nonlinear terms would be of higher order in the expansion parameter $|\varepsilon|^{1/2}$.) Sometimes other symmetry properties (e.g., $A \rightarrow -A$), can be used to eliminate certain hypothetical nonlinearities. In more complicated situations, such as degenerate bifurcations, the method of “normal forms” provides a systematic way of generating the complete set of nonlinear

terms (see subsection IV.B below).

Equation (4.3) correctly describes the variations of the pattern on the slow time scale ϵt , and slow spatial scales $\epsilon^{1/2}x$ perpendicular to the rolls and $\epsilon^{1/4}y$ parallel to the rolls. To emphasize these scales, and the common form of the equation we can rescale coordinates and amplitudes, assuming $g_0 > 0$,

$$X = |\epsilon|^{1/2} x / \xi_0 , \quad (4.6a)$$

$$Y = |\epsilon|^{1/4} y (q_0 / \xi_0)^{1/2} , \quad (4.6b)$$

$$T = |\epsilon| t / \tau_0 , \quad (4.6c)$$

$$\bar{A} = (|g_0| / |\epsilon|)^{1/2} A , \quad (4.6d)$$

to give a universal form

$$\partial_T \bar{A} = \pm \bar{A} + (\partial_X - \frac{1}{2} i \partial_Y^2)^2 \bar{A} - |\bar{A}|^2 \bar{A} , \quad (4.7)$$

where \pm refers to $\epsilon \geq 0$. When $g_0 < 0$, the sign in front of the cubic term is positive and a quintic term in the expansion leading to (4.3) must be added, as well as other possible terms (see Sec. V.B).

An important property of Eq. (4.3) is that the time evolution has the gradient form [see Eq. (3.12)],

$$\tau_0 \partial_t A = - \frac{\delta \mathcal{J}}{\delta A^*} , \quad (4.8)$$

with the potential functional $\mathcal{J}\{A, A^*\}$ given by

$$\begin{aligned} \mathcal{J} = \int \int dx dy [-\epsilon |A|^2 + (g_0/2) |A|^4 \\ + |\xi_0(\partial_x - (i/2q_0)\partial_y^2)A|^2] . \end{aligned} \quad (4.9)$$

The equation of motion (4.3) then implies that

$$\partial_t \mathcal{J} = -2\tau_0 \int \int dx dy |\partial_t A|^2 \leq 0 , \quad (4.10)$$

so that \mathcal{J} is a Lyapunov function, as discussed in Sec. III.A. This considerably aids in the analysis of Eq. (4.3). On the other hand the validity of the amplitude equation is clearly seen to be restricted to the range of driving for which persistent motion is absent.

Another important limitation of the amplitude equation is that it only describes situations in which the rolls are everywhere almost normal to a particular direction, labeled the x direction [more precisely, the roll orientation may only vary by an angle of $O(\epsilon^{1/4})$]. The slow re-orientation of the rolls over large angles commonly observed in experiments and numerical simulations cannot be accounted for by the present theory. We may however use the amplitude equation to describe many properties near threshold, such as the stability and competition of ideal patterns, as well as more complicated states involving boundary effects, defects, etc. We will discuss the application to ideal patterns here, and will defer the more complicated situations to Sec. V.

We finally remark that if the system is not invariant under rotations in the plane the amplitude equation takes the form

$$\tau_0 \partial_t A = \epsilon A + \xi_x^2 \partial_x^2 A + \xi_y^2 \partial_y^2 A - g_0 |A|^2 A , \quad (4.11)$$

instead of (4.3), with different coherence lengths ξ_x and ξ_y in x and y directions (we have chosen coordinate axes along the principal directions to eliminate $\partial_x \partial_y$ terms). This situation occurs in electrohydrodynamic instabilities in nematics (Sec. IX.C), where the nematic director provides the microscopic anisotropy, and in the Taylor-Couette system (Sec. IX.B), where axial and azimuthal directions are clearly not equivalent. Equation (4.11) may be rescaled and put into the isotropic form

$$\partial_T \bar{A} = \pm \bar{A} + (\partial_X^2 + \partial_Y^2) \bar{A} - |\bar{A}|^2 \bar{A} . \quad (4.12)$$

We thus have the somewhat paradoxical situation that the amplitude equation (4.3) for the isotropic system is anisotropic, whereas for the anisotropic system it can take on an isotropic form. The reason for this is that the roll pattern breaks the rotational symmetry in the isotropic system so transverse and longitudinal variations are qualitatively different, whereas in the anisotropic system they can be made the same by a simple scale change.

(ii) Spatially periodic solutions and their stability

In the rest of this section we shall assume $g_0 > 0$ and rescale x, t and A , ($x \rightarrow x/\xi_0$, $q_0 \rightarrow q_0 \xi_0$, $t \rightarrow t/\tau_0$, $A \rightarrow g_0^{1/2} A$) in order to eliminate the constants ξ_0, τ_0 , and g_0 , so that Eq. (4.3) reads^{4.1}

$$\partial_t A = \epsilon A + (\partial_x - (i/2q_0)\partial_y^2)^2 A - |A|^2 A . \quad (4.13)$$

[Unless otherwise noted we adopt the units of Eq. (4.13) as our standard scaling.] Then a simple nonlinear steady state solution of the amplitude equation for $\epsilon > 0$ is

$$A_k(x) = a_k e^{ikx} , \quad (4.14)$$

with amplitude

$$a_k = (\epsilon - k^2)^{1/2} , \quad (4.15)$$

which corresponds to a spatially periodic solution of the original problem with a modified wave number $q = q \hat{x}$ of magnitude

$$q = q_0 + k . \quad (4.16)$$

Note that adding a y component to the vector k would yield a rotation of the pattern wave vector q away from $q_0 \hat{x}$ by an angle proportional to k_y , as well as a change in magnitude proportional to k_y^2 , for small k_y . We choose our reference state along the x direction, so that $k_y = 0$. It is a straightforward matter to calculate the *linear stability* of Eq. (4.14) by inserting the solution

$$A(\mathbf{x}, t) = A_k(\mathbf{x}) + \delta A(\mathbf{x}, t) , \quad (4.17)$$

$$\delta A(\mathbf{x}, t) = e^{ikx} [\delta a_+(t) e^{iQ \cdot \mathbf{x}} + \delta a_-^*(t) e^{-iQ \cdot \mathbf{x}}] , \quad (4.18)$$

^{4.1}To return to dimensional variables in the formulas below, rescale all wave vectors by $k \rightarrow k \xi_0$ and all growth rates by $\sigma \rightarrow \sigma \tau_0$.

with $\mathbf{k} = k \hat{\mathbf{x}}$, and linearizing in $\delta a_{\pm}(t)$ to obtain

$$\partial_t \delta a_+ = -(p^2 + U_+) \delta a_+ - p^2 \delta a_-, \quad (4.19a)$$

$$\partial_t \delta a_- = -p^2 \delta a_+ - (p^2 + U_-) \delta a_-, \quad (4.19b)$$

with

$$p^2 = \varepsilon - k^2 \quad (4.20)$$

and

$$U_{\pm} = [(k \pm Q_x)^2 + Q_y^2 / 2q_0] - k^2. \quad (4.21)$$

The growth rate $\sigma_k(Q)$ defined by $\delta a_{\pm} \sim \exp[\sigma_k(Q)t]$ is then

$$\begin{aligned} \sigma_k(Q) = & -p^2 - \frac{1}{2} (U_+ + U_-) \\ & \pm \left[p^4 + \frac{1}{4} (U_+ - U_-)^2 \right]^{1/2}. \end{aligned} \quad (4.22)$$

The ensuing "stability balloon," given for each k by the condition $\sigma_k(Q) < 0$ for all Q is shown in Fig. 9 with its three stability boundaries.

The neutral stability curve N with

$$k_N^2 = \varepsilon \quad (4.23)$$

marks the onset of the nonlinear solution (4.14) and the limit of stability of the uniform solution $A \equiv 0$. The Eckhaus boundary E (Eckhaus, 1965) corresponds to a longitudinal instability $\mathbf{Q} = Q \hat{\mathbf{x}}$, and is given by

$$k_E^2 = (1/3) k_N^2 = \varepsilon/3. \quad (4.24)$$

For $k > k_E$ we can calculate the wave number Q of the fastest growing mode and its growth rate by maximizing $\sigma_k(Q)$. This gives (Newell and Whitehead, 1969)

$$Q_{\max} = (3/4) (k^2 - \varepsilon/3) (\varepsilon + k^2) k^{-2} \quad (4.25)$$

and

$$\sigma_k(Q_{\max}) = (9/4) (k^2 - \varepsilon/3)^2 k^{-2}. \quad (4.26)$$

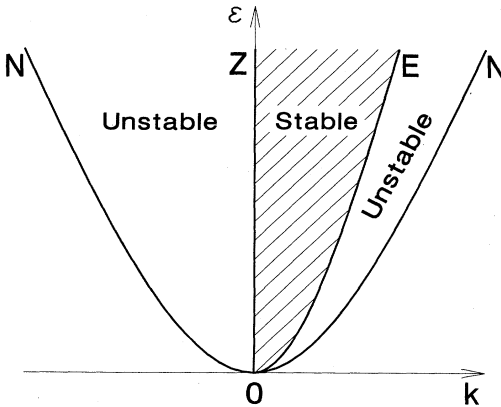


FIG. 9. Stability boundaries from amplitude equation (4.13), showing reduced control parameter vs deviation of wave vector from its critical value, $k = q - q_0$. N neutral; E Eckhaus; Z zig-zag. Hatched region is stable to small perturbations.

Notice that $Q_{\max} \rightarrow 0$ for $k \rightarrow k_E$, i.e. the instability occurs first at long wavelengths. As we shall see, in this limit the instability may also be calculated by considering just the dynamics of the phase of the complex amplitude (see below). The importance of the fastest growing mode in the actual development of an Eckhaus unstable system has been studied theoretically by numerical integration of the amplitude equation (4.13) (Kramer *et al.*, 1988a), and experimentally in nematic convection (Lowe and Gollub, 1985a). Finally, the zigzag boundary Z (Fig. 9) given by (Newell and Whitehead, 1969),

$$k_Z = 0, \quad (4.27)$$

corresponds to a growing transverse modulation with wave vector along the rolls, $\mathbf{Q} = Q \hat{\mathbf{y}}$. In this case the maximum growth rate occurs for

$$Q_{\max}^2 = 2q_0 |k|, \quad k < 0, \quad (4.28)$$

with a value

$$\sigma_k(Q_{\max}) = 3k^2. \quad (4.29)$$

Again $Q_{\max} \rightarrow 0$ at the boundary of the instability and the behavior is captured by a phase dynamics analysis.

When the scales τ_0, ξ_0 , and g_0 are restored, it is found that the instability boundaries take on a scale-independent universal form if they are expressed in terms of k_N in this near-threshold limit. They are therefore typical of all rotationally invariant type I_s systems and do not reflect the details of the underlying microscopic equations.

(iii) Superposition of plane-wave solutions: Squares and hexagons

In Eq. (4.2) the assumption of a single roll solution was made. We can also look for the growth of solutions that are superposition of n sets of rolls at various orientations,

$$U = U_0 \left[\sum_{i=1}^n A_i(x, y, t) e^{i \mathbf{q}_i \cdot \hat{\mathbf{x}}} + \text{c.c.} \right] + O(\varepsilon), \quad (4.30)$$

with $|\mathbf{q}_i| = q_0$. If we leave out spatial variation of the A_i then in general (4.13) is replaced by a set of n equations (Newell and Whitehead, 1969)

$$\partial_t A_i = \varepsilon A_i - \sum_{j=1}^n g_{ij} |A_j|^2 A_i, \quad (4.31)$$

where the constants g_{ij} depend on the angles $\hat{\mathbf{q}}_i \cdot \hat{\mathbf{q}}_j = \cos \theta_{ij}$

$$g_{ij} = \mathcal{G}(\theta_{ij}), \quad (4.32)$$

with $\mathcal{G}(0) = 1$. Actually $\mathcal{G}(\theta)$ is not a smooth function of θ due to mode interference occurring exactly at $\theta_{ij} = 0$. This yields

$$\mathcal{G}(\theta=0) = \frac{1}{2} \mathcal{G}(\theta \rightarrow 0). \quad (4.33)$$

The above equations can be used, for example, to in-

vestigate the competition between rolls and other regular solutions (Schlüter, Lortz, and Busse, 1965) consisting of waves with equal amplitudes at angles $m\pi/n$ around the circle, where n and m are integers. Then $n=2$ gives squares, and $n=3$ gives hexagons. For example squares are described by two equal amplitudes $A_1 = A_2 = A_S$. The solution of Eq. (4.31) is then

$$|A_S|^2 = [1 + \mathcal{G}(\pi/2)]^{-1} \varepsilon, \quad (4.34)$$

compared with the amplitude for rolls $A_1 = A_R$, $A_2 = 0$ with

$$|A_R|^2 = [\mathcal{G}(0)]^{-1} \varepsilon. \quad (4.35)$$

If we look at perturbations about the square solution, i.e., $A_1 = A_S + \delta_1$ and $A_2 = A_S + \delta_2$, and linearize (4.31) we find

$$\partial_t \delta_1 = -2|A_S|^2 \delta_1 - 2\mathcal{G}(\pi/2) |A_S|^2 \delta_2, \quad (4.36a)$$

$$\partial_t \delta_2 = -2\mathcal{G}(\pi/2) |A_S|^2 \delta_1 - 2|A_S|^2 \delta_2, \quad (4.36b)$$

with growth $[\delta_{1,2} \sim e^{\sigma t}]$ at rates

$$\sigma = -2[1 \pm \mathcal{G}(\pi/2)] |A_S|^2. \quad (4.37)$$

Thus squares are stable with respect to rolls [i.e., $\delta_1 = -\delta_2$, leading to the negative sign in (4.37)] for

$$\mathcal{G}(\pi/2) < 1, \quad (4.38)$$

and it is easy to see that rolls are stable with respect to squares in the opposite limit. Notice that in this simple calculation the stable solution is the one with the greater mean-square amplitude $\sum_{i=1}^n |A_i|^2 = n |A_1|^2$, which also gives a lower value of the potential (4.9). An example where squares are in fact the preferred solution is convection between poor conductors (see Sec. VIII.F). The case of rhomboids (two sets of rolls at an angle $\theta \neq \pi/2$) has been considered by Malomed and Tribel'skii (1987). It should be noted that the regular solutions of Eq. (4.30) for $n > 3$ yield patterns that are not a periodic lattice, but rather analogous to a quasicrystal, with quasiperiodic spatial dependence along any direction. Such states have recently been produced experimentally in the parametric surface wave system (Sec. IX.D) by Christiansen *et al.* (1992) and by Edwards and Fauve (1993).

A particularly interesting case is that of three wave vectors mutually at an angle of $2\pi/3$. Then, since

$$\mathbf{q}_1 + \mathbf{q}_2 + \mathbf{q}_3 = 0, \quad (4.39)$$

an additional quadratic nonlinearity occurs and the amplitude equation in the absence of spatial variation becomes (see, e.g., Ciliberto *et al.*, 1990)

$$\begin{aligned} \partial_t A_1 &= \varepsilon A_1 - \gamma A_2^* A_3^* \\ &\quad - [|A_1|^2 + g_1(|A_2|^2 + |A_3|^2)] A_1, \end{aligned} \quad (4.40)$$

with $g_1 = \mathcal{G}(2\pi/3)$, and similar equations for A_2 and A_3 . If the coefficient γ is nonzero the quadratic nonlinearity dominates near threshold. This situation is generic in the absence of the inversion symmetry $A_i \rightarrow -A_i$

(i.e., $U \rightarrow -U$ in the original equations). The hexagon solution $A_1 = A_2 = A_3 = A_H$ then undergoes a transcritical bifurcation (see Sec. III.A). Near threshold both branches of the hexagon solution are unstable; however, all other branches developing at the transition (e.g., rolls) are unstable towards the hexagon solution, so that the latter is preferred (it has the maximum growth rate near threshold.) If the symmetry breaking coefficient γ is $O(1)$ there are no small amplitude stable solutions and nothing can be said rigorously about the ultimate steady nonlinear state from the amplitude equations, although certainly in many cases the backwardly bifurcating hexagon branch will turn around and become the stable solution. If γ is small the behavior is universal and can be calculated from the amplitude equations (Busse, 1967b), as shown in Fig. 10. The quantities ε_A , ε_B , and ε_R , which define the saddle-node bifurcation, the upper limit of stability of the hexagons and the lower limit of stability of the rolls, respectively, are given in terms of the coefficients of the amplitude equation (4.40) by

$$\varepsilon_A = -\gamma^2/4(1+2g_1), \quad (4.41a)$$

$$\varepsilon_B = \gamma^2(g_1+2)/(g_1-1)^2, \quad (4.41b)$$

$$\varepsilon_R = \gamma^2/(g_1-1)^2. \quad (4.41c)$$

Although it took many years for the situation depicted in Fig. 10 to be clarified, it should be emphasized that a hexagonal pattern is generically preferred close to threshold unless the inversion symmetry $U \rightarrow -U$ is present in the system (Pismen, 1980). Note that Eq. (4.40) and the permuted ones form a potential system (Bestehorn and Haken, 1984) a feature which remains true when spatial derivatives are added as in Eq. (4.13). Terms of the form $\gamma A_2^* \partial_x A_3^*$ considered by Brand (1989) are explicitly of higher order for $\gamma \ll 1$, and are among the many such nonpotential terms encountered even in Boussinesq systems.

Having considered the existence of nonlinear solutions consisting of superpositions of different roll states we

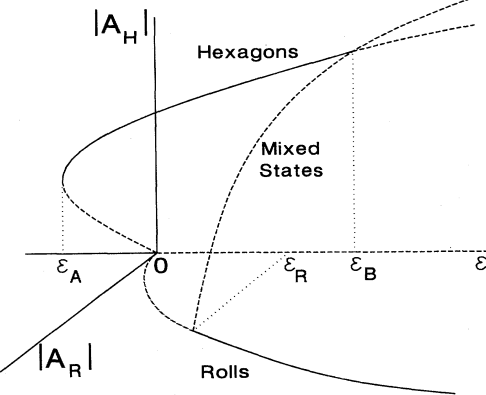


FIG. 10. Amplitude of roll state $|A_R|$ and hexagon state $|A_H|$ as function of control parameter ε , following from Eq. (4.40). Solid lines denote stable states, dashed lines unstable states. The limits of stability ε_A , ε_B , and ε_R are given in Eq. (4.41). (From Ciliberto *et al.*, 1990.)

must also consider the instability of the rolls to such perturbations. The linear growth of a roll solution at wave vector \mathbf{q}_2 making an angle θ with $\mathbf{q}_1 = (q_0 + k)\hat{\mathbf{x}}$, in the presence of the nonlinear saturated solution $A_{1k}(\mathbf{x})$, is again given by linearizing Eq. (4.31). (The maximum growth is for $q_2 = q_0$, so we do not need to include the spatial derivatives in the equation for A_2 .) The equation is

$$\partial_t \delta A_2 = [\epsilon - \mathcal{G}(\theta) |A_k|^2] \delta A_2, \quad q_2 = q_0, \quad (4.42)$$

which gives a positive growth rate when

$$k^2 > k_{CR}^2 = k_N^2 [1 - 1/\mathcal{G}(\theta)]. \quad (4.43)$$

Thus extra instability lines, again varying as $k \propto \epsilon^{1/2}$ and corresponding to “cross-roll” instabilities, may be added to the stability diagram. Depending on the coupling constant $\mathcal{G}(\theta)$ the cross-roll instability may preempt the Eckhaus instability and be important in limiting the band of solutions. Note that when $\mathcal{G}(\theta) > 1$ a superimposed solution is unstable to a single-roll solution, so the ultimate state in this case will be a new single-roll state with the critical wave number but at a rotated angle.

Up to now all the examples in this subsection have concerned two-dimensional systems. Recently De Wit *et al.* (1992) have discussed three-dimensional solutions of the amplitude equation and the relative stability of hexagonal prism, lamellar, and bcc lattice structures.

(iv) Chiral symmetry; Hamiltonian versus dissipative systems

We are usually interested in the case where “chiral symmetry,” $\theta \rightarrow -\theta$, applies. In the presence of external rotation, or for systems in a magnetic field, this symmetry is broken, so that $\mathcal{G}(\theta) \neq \mathcal{G}(-\theta)$. Also in some systems (we are thinking particularly of the parametric wave instabilities) dissipative effects are weak and nondissipative wave interactions dominate the nonlinear terms. In this case there is nearly a “Hamiltonian” symmetry

$$\mathcal{G}(\theta) = -\mathcal{G}(-\theta). \quad (4.44a)$$

Thus a number of symmetry combinations are possible:

(α) Dissipative system, chiral symmetry: The canonical case considered above, as applies for example to Rayleigh-Bénard convection.

(β) Dissipative system, no chiral symmetry: If $\mathcal{G}(\theta) < 1$ for some θ , then the original set of rolls is unstable to the development of a superimposed set of cross rolls at the angle θ , which then grows at the expense of the original set. We expect the first set of rolls to be replaced by rolls at the angle θ , which are in turn unstable to a third set, again rotated through the angle θ , etc. Thus no stable steady state is predicted by the amplitude equation. This phenomenon was predicted to occur in convection in a sufficiently rapidly rotating system by Küppers and Lortz (1969) (Sec. VIII.F.6).

(γ) Near-Hamiltonian system, chiral symmetry: In the Hamiltonian approximation Eq. (4.44a) holds, whereas

chiral symmetry implies $\mathcal{G}(\theta) = \mathcal{G}(-\theta)$, so the nonlinear coefficient is identically zero at this order. Saturation must occur either through the weak nonlinear dissipative effects at this order, or at higher orders in the amplitude expansion (e.g. through nonlinear frequency detuning in parametric wave systems, see Sec. IX.D). The interplay of these two competing small effects may lead to interesting transitions as the control parameter is increased.

(δ) Near-Hamiltonian, no chiral symmetry: In this case we expect large values of $\mathcal{G}(\theta) = -\mathcal{G}(-\theta)$, so that the instability in (β) will always occur. As in (γ) there are no nonlinear saturating effects of a single roll state in the Hamiltonian approximation. Thus one might expect a dynamical state with saturation to occur only at higher orders in the amplitude expansion. This is the starting point for more sophisticated theories of the ferromagnetic parametric spin-wave instabilities discussed in Sec. XII.C below.

(ϵ) Special case: $\mathcal{G}(\theta) = g_0$, independent of θ . In this case the nonlinear saturation occurs through the term

$$\sum_j g_{ij} |A_j|^2 A_i = g_0 \left[\sum_j |A_j|^2 \right] A_i, \quad (4.44b)$$

with j summed over all modes around the critical circle. There is a dynamical degeneracy amongst all states satisfying $\sum_j |A_j|^2 = \epsilon/g_0$; this set contains single roll states with arbitrary orientation, superimposed roll states, as well as states in which the mean square amplitude is distributed continuously around the critical circle, which would not correspond to a definite spatial pattern. In addition, the degeneracy leads to extreme sensitivity to experimental imperfections such as extrinsic noise (see Sec. VIII.F.6 below). In his original analysis of the transversely pumped ferromagnetic resonance system Suhl (1957) arrived at this special case by supposing that the only important nonlinear damping was that of the uniformly precessing mode. Anderson (1981) and Stein (1979) used this example to suggest that systems out of equilibrium do not show robust pattern formation. However we see that this conclusion only applies to the special case represented by Eq. (4.44b), which is not expected to be widespread. In fact a more detailed analysis of the ferromagnetic resonance equations (Sneddon and Cross, 1982) shows that Eq. (4.44b) is not strictly satisfied in this case, although as we have seen in (δ) a dynamic state may still be anticipated due to the weakly dissipative nature of the system.

We remark that the nonlinearity (4.44b) is nonlocal when expressed in real space. Implications of this property for spatial patterns in the ferromagnetic system have been studied by Elmer (1987).

b. Type II_s: Stationary instability with $q_0 = 0$

For the stationary instability in a system with a conservation law, the growth rate $\sigma(q)$ vanishes at $q=0$ and $q_0 \sim \epsilon^{1/2}$ (see Fig. 7). We call this a type II_s instability. In that case a real amplitude is sufficient

$$U = U_0 \psi(x, y, t) . \quad (4.45)$$

If the nonlinear terms of the basic equations are also zero at $q=0$ a consistent long-wavelength expansion of the equations can be made (Gertsberg and Sivashinsky, 1981). The most general amplitude equation then takes the form

$$\partial_t \psi = \varepsilon \nabla^2 \psi - [\nabla^4 \psi + g_1 \nabla \cdot (\nabla \psi)^2 \nabla \psi + g_2 (\nabla \psi)^2 \nabla^2 \psi] , \quad (4.46a)$$

where we have assumed a situation with inversion symmetry so that quadratic nonlinearities are absent. Equation (4.46a) with g_2 identically zero, describes convection between infinitely poorly conducting plates. In this case the equation is potential, whereas in general it is not. A one-dimensional equation without inversion symmetry has quadratic nonlinearities

$$\partial_t \psi = \alpha \partial_y^2 \psi - \partial_y^4 \psi - (\partial_y \psi)^2 , \quad (4.46b)$$

and describes transverse fluctuations of plane interfaces normal to the x direction. When the diffusion constant α becomes negative the system has a linear instability, and is known as the Kuramoto-Sivashinsky equation, introduced in Eq. (3.30) above.

c. Type III_o: Oscillatory uniform

The same expansion about threshold can be carried out for the other classes of linear instability. Again, in these simple cases the results can be written down by inspection. We will describe just some of the more useful ones here, beginning with type III_o.

For this case we need a complex amplitude whose phase describes that of the basic oscillator (see Kuramoto, 1984b)

$$U(\mathbf{x}, t) = [U_0 A(x, y, t) e^{-i\omega_\varepsilon t} + \text{c.c.}] + O(\varepsilon) , \quad (4.47)$$

where

$$\omega_\varepsilon = \omega_0 - c_0 \varepsilon \quad (4.48)$$

is the oscillation frequency of the uniform system ($q = 0$) for $\varepsilon > 0$. The amplitude equation has the form of a complex, time-dependent Ginzburg-Landau equation (in dimensionless units)

$$\partial_t A = \varepsilon A + (1+ic_1) \nabla^2 A - (1-ic_3) |A|^2 A . \quad (4.49)$$

In the limit, $c_1^{-1}, c_3^{-1} \rightarrow 0$, i.e. when the imaginary terms in Eq. (4.49) dominate, the amplitude equation reduces at short times to the nonlinear Schrödinger equation. This differential equation corresponds to a conservative (Hamiltonian) dynamical system which is integrable in one dimension and has been studied in some detail (see Sec. V.B below).

(i) Simple solutions

Let us write down simple solutions of the amplitude equation (4.49) for this case, and discuss their stability. In addition to the spatially uniform nonlinear oscillating solution

$$A(x, t) = a_0 e^{-i\Omega_0 t} , \quad (4.50)$$

$$a_0^2 = \varepsilon , \quad \Omega_0 = -c_3 \varepsilon , \quad (4.51)$$

Eq. (4.49) admits traveling wave solutions

$$A_k(\mathbf{x}, t) = a_k e^{i(\mathbf{k} \cdot \mathbf{x} - \Omega_k t)} , \quad (4.52)$$

$$a_k^2 = (\varepsilon - k^2) , \quad (4.53a)$$

$$\Omega_k = -c_3 \varepsilon + (c_1 + c_3) k^2 . \quad (4.53b)$$

These solutions are known as rotating waves in the chemical literature. Although standing waves are also possible nonlinear solutions, they are always unstable towards traveling waves if the real part of the cubic term in Eq. (4.49) has the correct (negative) sign to yield saturation above onset.

(ii) Stability of plane-wave solutions

The important instability in nonlinear wave systems is the Benjamin-Feir instability (Benjamin and Feir, 1967; Newell, 1974; Stuart and DiPrima, 1978), which corresponds to a wave at (\mathbf{q}, ω) becoming unstable by resonant excitation of sidebands with wave vectors $\mathbf{q}_1, \mathbf{q}_2$ and frequencies ω_1, ω_2 satisfying

$$\frac{1}{2} (\mathbf{q}_1 + \mathbf{q}_2) = \mathbf{q} , \quad \frac{1}{2} (\omega_1 + \omega_2) = \omega . \quad (4.54)$$

For $\mathbf{q}_1, \mathbf{q}_2$ close to \mathbf{q} it becomes a long-wavelength modulational instability, and is then more easily analyzed using the phase equation (see subsection IV.A.2 below).

The analysis of the one-dimensional situation was discussed by Newell (1974) and in more detail by Stuart and DiPrima (1978) starting from the amplitude equation (4.49). The approach is straightforward in principle but algebraically complicated. Restricting ourselves to one dimension, we assume a base state of a traveling wave

$$A_k(x) = a_k e^{i(kx - \Omega t)} , \quad (4.55)$$

and seek an instability in the form

$$\delta A_k(x, t) = e^{i(kx - \Omega t)} [\delta a_+(t) e^{iQx} + \delta a_-(t) e^{-iQx}] , \quad (4.56)$$

with Q the wave number of the perturbations, and linearize in $\delta a_{\pm}(t)$. In many ways this “Benjamin-Feir” instability is the analogue of the Eckhaus instability in the stationary case, although because of the larger parameter space a full analysis becomes quite complicated. In addi-

tion, the instability is more potent, rendering *all* plane wave solutions near onset unstable for

$$1 - c_1 c_3 < 0 \quad (4.57a)$$

(Newell, 1974). The above condition involves a balance between diffusive and dispersive terms. We will refer to it as the Newell criterion though it is often called the Benjamin-Feir criterion. Before this full instability limit is reached, a band of stable solutions is found with

$$k^2 < k_{BF}^2 = \Lambda_{BF} k_N^2 , \quad (4.57b)$$

where $k_N^2 = \varepsilon$ is the neutral stability limit. Here Λ_{BF} is a complicated function of parameters (Stuart and DiPrima, 1978; Malomed, 1984; van Saarloos and Hohenberg, 1992; Brand and Deissler, 1992). For many, but not all values, the instability first occurs for long-wavelength disturbances $Q \rightarrow 0$, in which case it may be calculated from the phase equation quoted in (4.85) and (4.86) below. It is the limit $k^2 = k_{BF}^2$ which we call the Benjamin-Feir instability, though this one is often referred to as the Eckhaus instability, a term we reserve for the stationary case (4.24). For transverse perturbations varying as e^{iQy} the criterion is always (4.57a), and so these are never more unstable than the longitudinal perturbations.

d. Type I_o: Oscillatory periodic

Near a type I_o instability [$\omega_0 \neq 0$, $q_0 \neq 0$] the analogue of (4.47) is

$$\begin{aligned} U(\mathbf{x}, t) = U_0 [& A_R(x, y, t) e^{i(q_0 x - \omega_0 t)} \\ & + A_L(x, y, t) e^{-i(q_0 x + \omega_0 t)}] + \text{c.c.} + O(\varepsilon), \end{aligned} \quad (4.58)$$

where A_R and A_L are right- and left-traveling wave amplitudes, respectively. The one-dimensional case is a simple generalization of the complex Ginzburg-Landau equation (4.49),

$$\begin{aligned} \partial_t A_R + s_0 \partial_x A_R &= \varepsilon A_R + (1 + i c_1) \partial_x^2 A_R - (1 - i c_3) |A_R|^2 A_R \\ &- g_1 (1 - i c_2) |A_L|^2 A_R , \end{aligned} \quad (4.59a)$$

$$\begin{aligned} \partial_t A_L - s_0 \partial_x A_L &= \varepsilon A_L + (1 + i c_1) \partial_x^2 A_L - (1 - i c_3) |A_L|^2 A_L \\ &- g_1 (1 - i c_2) |A_R|^2 A_L . \end{aligned} \quad (4.59b)$$

Compared to Eq. (4.49) there is an extra advective term with s_0 the linear group speed $\partial\omega/\partial q|_{q=q_0}$, and a complex coupling of the right and left moving waves. Again the coefficients of the linear terms are directly given by the linear instability spectrum; the nonlinear terms give amplitude saturation and nonlinear frequency pulling. If only a single wave (e.g., A_R) is present and no boundaries

are involved we can reduce Eq. (4.59a) to the complex Ginzburg-Landau equation (4.49) by introducing a moving frame $\bar{x} = x - s_0 t$, and the analysis of subsection IV.A.1.c then applies.

The full two-dimensional equations are obtained from Eq. (4.59) by the replacements (Brand *et al.* 1986a,b)

$$\begin{aligned} s_0 \partial_x &\rightarrow s_0 [\partial_x - (i/2q_0) \partial_y^2 + (1/2q_0^2) \partial_x \partial_y^2 \\ &- (i/8q_0^3) \partial_y^4] , \end{aligned} \quad (4.60)$$

on the left-hand side and

$$\partial_x^2 \rightarrow (\partial_x - (i/2q_0) \partial_y^2)^2 , \quad (4.61)$$

on the right-hand side. Again these rather complicated looking expressions are given simply by expanding the dispersion relation for $\mathbf{q} = q_0 \hat{\mathbf{x}} + \mathbf{k}$ in small \mathbf{k} and then making the replacement $\omega \rightarrow i\partial_t$, $k_x \rightarrow -i\partial_x$, $k_y \rightarrow -i\partial_y$. Note however that there is no simple rescaling of time, length, and amplitude to remove the small parameter ε from these equations as is possible in Eq. (4.49). It is therefore not clear how to balance the various terms, and the solutions of the equations may not in fact always vary on the slow scales necessary for the amplitude equation approach to be valid.

(i) Superposition of solutions: Traveling versus standing waves

A major question for wave instabilities is the nature of the spatially homogeneous solutions: traveling or standing. At the linear instability these are equally good solutions, and they may be related by linear superposition, but beyond threshold the nonlinear terms give a competition (Coullet *et al.*, 1985). Let us first look at solutions at the critical wave vector q_0 and with frequency $\omega = \omega_0 + \Omega$. Equations (4.59) then yield (i) traveling waves:

$$A_R = a \exp(-i\Omega t + \phi), \quad A_L = 0 , \quad (4.62)$$

with $a^2 = \varepsilon$ and $\Omega = -c_3 \varepsilon$, corresponding to waves traveling to the right, or the alternate solution with A_R and A_L interchanged, corresponding to left-moving waves; and standing waves:

$$A_R = A_L = a \exp(-i\Omega t + \phi) , \quad (4.63)$$

with $a^2 = \varepsilon(1 + g_1)^{-1}$ and $\Omega = -\varepsilon(c_3 + c_2 g_1)/(1 + g_1)$. Traveling waves are stable and standing waves unstable for $g_1 > 1$; the reverse is true for $-1 < g_1 < 1$, and there is no saturation for $g_1 < -1$.

We may also look for solutions with wave vectors away from critical. Traveling waves are given by

$$A_{Rk} = a_k \exp[i(kx - \Omega_k t)] ; \quad A_L = 0 , \quad (4.64)$$

with

$$a_k^2 = \varepsilon - k^2 , \quad (4.65)$$

and

$$\Omega_k = s_0 k - c_3 \varepsilon + k^2(c_1 + c_3). \quad (4.66)$$

In addition, standing waves given by A_{Rk} , $A_{Lk} \neq 0$, and mixed waves A_{Rk} , $A_{Lk'}$, $k \neq k'$, can be constructed (Coullet *et al.*, 1985). Finally, we note that superimposed traveling wave states, e.g. traveling rectangles, have been studied theoretically by Malomed and Gedalin (1989).

(ii) Stability of plane-wave solutions

Once again the important instability is the Benjamin-Feir instability. For a single wave present ($A_R \neq 0$, $A_L = 0$) and in one dimension we may transform to the frame moving with speed s_0 and reduce the equation to (4.49) studied in subsection IV.A.1.c. above. The criterion for the longitudinal Benjamin-Feir instability (Stuart and DiPrima, 1978) goes through unchanged. A theoretical and experimental study of traveling wave stability was recently carried out by Janiaud *et al.* (1992). For transverse perturbations varying as e^{iQy} the diffusive restoring forces are absent, and the condition for the critical wave number to be unstable is simply $c_3 s_0 > 0$ (Brand *et al.*, 1986a,b; Ohta and Kawasaki, 1987). This instability corresponds to a long-wavelength bowing of the wave fronts.

2. Phase equations

a. Stationary systems (type I_s)

(i) Near threshold

The amplitude equation (4.13) for a type I_s instability describes the dynamics of both the magnitude $|A|$ and phase ϕ of the complex amplitude. Consider a small perturbation of the solution $A_k(x) = a_k \exp(ikx)$ describing a periodic state of wave vector $q = q_0 + k$ in one dimension,

$$A(x) = (a_k + \delta a) e^{i(kx + \delta\phi)}, \quad (4.67)$$

with $a_k^2 = \varepsilon - k^2$. From (4.13) we see that the perturbation δa in the magnitude relaxes in a time of order ε^{-1} , which is a slow rate near threshold, but one that remains finite for a fixed control parameter. On the other hand a spatially uniform phase perturbation $\delta\phi$ does not relax at all — it is simply a uniform shift of all the rolls in the x direction. A very slow perturbation, e.g., $\delta\phi = \delta\phi_0 \cos(Qx)$ with $Q \rightarrow 0$, will relax arbitrarily slowly, on a time scale typically of order Q^{-2} . For long-wavelength perturbations (with $Q \ll \varepsilon^{1/2}$) we can assume that after an initial transient the magnitude adiabatically follows any phase variation (actually any phase gradient or wave-number variation). We implement this assumption by substituting (4.67) into (4.13) and multi-

plying through by $e^{-i(kx + \delta\phi)}$. The real part gives the adiabatic amplitude change

$$\partial_k \delta a = -k \partial_x \delta\phi, \quad (4.68)$$

where we may neglect time and space derivatives of δa and also higher-order derivatives. The imaginary part gives the phase variation

$$\partial_t \phi = [\partial_x^2 \phi + (k/q_0) \partial_y^2 \phi + 2k \partial_x \delta a / a_k]. \quad (4.69)$$

Eliminating δa we can derive a single equation for the phase dynamics of slow, long-wavelength perturbations

$$\partial_t \phi = D_{\parallel}(k) \partial_x^2 \phi + D_{\perp}(k) \partial_y^2 \phi, \quad (4.70)$$

with

$$D_{\parallel} = \frac{\xi_0^2}{\tau_0} \left[\frac{\varepsilon - 3\xi_0^2 k^2}{\varepsilon - \xi_0^2 k^2} \right], \quad (4.71)$$

$$D_{\perp} = \frac{\xi_0^2}{\tau_0} \left[\frac{k}{q_0} \right], \quad (4.72)$$

where we have restored the constants ξ_0 and τ_0 of the original amplitude equation (4.3). This “phase diffusion” equation was first derived in the context of convection by Pomeau and Manneville (1979).

(ii) Far from threshold

From the above discussion it should be clear that the validity of the phase equation is not restricted to the vicinity of the threshold, but is in fact *a fortiori* true away from threshold. Here magnitude perturbations (i.e. perturbations of the local structure) relax on a rapid time scale, and long-wavelength phase perturbations again relax arbitrarily slowly. The phase variable can now be defined more generally (Cross and Newell, 1984). Let us consider a perfectly periodic stationary solution with wave vector q

$$U_q(\mathbf{x}, t) = U_{\infty}(\mathbf{q} \cdot \mathbf{x}), \quad (4.73)$$

with $U_{\infty}(\phi) = U_{\infty}(\phi + 2\pi)$, and let η be an independent small parameter. Then we introduce the phase function $\phi(\mathbf{x}, t)$ such that the solution with slow changes (on a scale η^{-1}) in the magnitude or direction of the local wave vector $q(\mathbf{x}, t)$ is

$$U(\mathbf{x}, t) = U_{\infty}[\phi(\mathbf{x}, t)] + O(\eta), \quad (4.74)$$

where

$$\nabla \phi(\mathbf{x}, t) = \mathbf{q}(\mathbf{x}, t), \quad (4.75)$$

and gradients of q are $O(\eta)$. With this general definition we are no longer restricted to small perturbations $\delta\phi$: the solution can describe the variation of the direction of the rolls through large angles, provided this takes place slowly, i.e., over many of the basic periods $2\pi/q_0$. The formulation of the problem in terms of a phase variable defined by Eq. (4.75) is reminiscent of the WKB ap-

proach in nonlinear waves first introduced by Whitham (1974) and subsequently used by Howard and Koppell (1977). The derivation for slow distortions of a stationary periodic state was discussed by Cross and Newell (1984) for various model equations, and is reproduced in Appendix B. As was true for the amplitude equation, the phase equation often takes a universal form when expanded to lowest order in η , reflecting the symmetries of the problem and certain smoothness assumptions. For disturbances of a stationary, locally periodic, rotationally degenerate pattern the result is

$$\tau(q) \partial_t \phi = -\nabla \cdot [qB(q)], \quad (4.76a)$$

$$q = \nabla \phi, \quad (4.76b)$$

where $\tau(q)$ and $B(q)$ are functions of the wave number that depend on the specific system under study. For small perturbations from uniform rolls Eqs. (4.76) reduce to (4.70), yielding expressions for the diffusion constants,

$$D_{\parallel}(q) = -\tau^{-1}(q) (d/dq) [q B(q)], \quad (4.77a)$$

$$D_{\perp}(q) = -\tau^{-1}(q) B(q). \quad (4.77b)$$

The instabilities of straight roll patterns described in subsection IV.A.1 above that correspond to long-wavelength perturbations are contained in the phase equation. In fact, the stability requirement for the solution with wave vector q is simply $D_{\parallel}(q) > 0$, $D_{\perp}(q) > 0$. The passage of D_{\parallel} through zero signals the Eckhaus instability (4.24), and D_{\perp} passing through zero gives the zigzag stability boundary (4.27). Thus Eqs. (4.77) reproduce the earlier results near threshold, and they continue them into the strongly nonlinear regime once $\tau(q)$ and $B(q)$ are known. In this way the Eckhaus and zigzag instabilities are seen to have some universality even away from threshold. Other instabilities which occur at short wavelengths depend more sensitively on the details of the system.

(iii) More complicated situations

The general form of the phase equations (4.70) or (4.76) will be changed if other slow modes exist, i.e., if there are other quantities that may vary independently on the slow time scale of interest in the phase dynamics. The slow phase equation must then be coupled to the dynamical equation for the additional mode, leading to equations that are higher-order in the time derivatives, and often yielding propagating rather than diffusive solutions (Brand and Cross, 1983; Coullet and Fauve, 1985; Fauve, 1987). This may occur, for example, if we have an additional conserved physical quantity, such as the horizontal momentum for convection between free-slip boundaries (Siggia and Zippelius, 1981b). Alternatively, it may be due to an additional broken symmetry as occurs for modulated waves in Taylor-Couette flow (Brand and Cross, 1983). Another example is the long-wavelength dynamics of a spatially periodic solution of the phase

equation (4.76), written as $\phi_0(qx + \zeta_0)$, with the new phase ζ_0 giving translations of the pattern. There are now two spatially uniform perturbations that do not relax (i.e., are at zero frequency),

$$\phi = \phi_0(x) + \delta\phi, \quad (4.78a)$$

$$\zeta = \zeta_0 + \delta\zeta, \quad (4.78b)$$

and coupled dynamics for slowly varying $\delta\phi$ and $\delta\zeta$ must be considered. An alternative scheme for this problem is to introduce a derived “velocity” field $u = \partial_x \phi$. Then we have

$$\partial_t u = \partial_x (\partial_t \phi) = \partial_x f(u, \partial_x u, \dots), \quad (4.79)$$

where f does not depend on ϕ itself, only on its derivatives $u, \partial_x u, \dots$. The quantity u is therefore “conserved” (i.e. a constant u does not relax), and coupled equations for u and ζ are considered as in our previous example. Note that the need for coupled equations is simply implied by the conservation of u . If the field u were also a physical velocity this would imply Galilean invariance,

$$u \rightarrow u + v, \quad \partial_t \rightarrow \partial_t + v \partial_x. \quad (4.80)$$

Although this extra Galilean invariance leads to propagating dynamics (Coullet and Fauve, 1985; Shraiman, 1987) it is not necessary: only the conservation equation (4.79) is needed. Galilean invariance does however give additional restrictions on the parameters of the coupled equations, e.g., in the equation

$$\partial_t \phi = -\alpha u^2 + \dots, \quad (4.81)$$

the coefficient α is unity if Galilean invariance holds. The introduction of the field $u = \partial_x \phi$ bears a strong analogy to the definition of the superfluid velocity $v_s \propto \nabla \phi$ in the theory of superfluidity, where ϕ is the phase of the Bose condensed wave function (see, e.g., Lifshitz and Pitaevsky, 1981). Again v_s need not be a true (i.e., Galilean covariant) velocity; it is not, for example, in the case of superfluidity in a porous medium. However, since it is defined as the gradient of a phase it plays the role of a conserved quantity in the dynamical equations (Bergman *et al.*, 1974).

It turns out that for our canonical fluid system, Rayleigh-Bénard convection, and other similar systems the smoothness assumption used in deriving the general form (4.76) breaks down (Cross, 1983). In fact for a perturbation $\delta\phi \sim \delta\phi_0 \cos(Q \cdot x)$ the expansion in the small wave vector Q of the distortion depends on quantities such as Q_x/Q that are not analytic as $Q \rightarrow 0$. A simple way of incorporating this effect is to include a coupling to a “mean drift” horizontal flow v_D which depends on the vertical coordinate (but gives an integrated flow). This field is averaged over a unit cell of the basic periodic pattern and so varies only slowly (with the pattern) in the horizontal direction. It leads to an additional advection term in Eq. (4.76)

$$\partial_t \phi + \mathbf{V} \cdot \nabla \phi = -\tau^{-1}(q) \nabla \cdot [\mathbf{q} B(q)], \quad (4.82)$$

with \mathbf{V} a horizontal velocity given by a z average of \mathbf{v}_D weighted by a function that depends on the local structure of the rolls and ∇ the (two-dimensional) horizontal gradient. The nonanalyticity arises because \mathbf{v}_D is driven both by distortions of the pattern and by an additive pressure $P_S(x, y)$, also varying only slowly in the horizontal direction, which in turn must be eliminated by the incompressibility condition

$$\nabla \cdot \int_0^d dz \mathbf{v}_D(\mathbf{x}, z) = 0. \quad (4.83)$$

In general Eq. (4.83) is a complicated nonlinear Poisson-like equation for P_S . Since the z -integrated mean flow is divergence free, it can be expressed in terms of a stream function ψ or derived from a vertical vorticity Ω_z , and the singular structure of the perturbation theory can alternatively be controlled by working with these variables, rather than with P_S itself. Formally the breakdown of the smoothness assumption can be traced back to long-range effective forces arising from incompressibility. (If compressible fluid equations were used the effect would presumably arise from eliminating the “slow” sound mode for the time scales of interest in the phase diffusion.) Recently the full structure of the phase equations including mean drift have been worked out from the fluid equations for convection, and this will be described in Sec. VIII.A below. Similar behavior should be found in many fluid systems (see, e.g., Hall, 1984), and it is important to be on the lookout for analogous effects in other cases as well. The breakdown of analyticity has many important consequences. For example with its inclusion a new long-wavelength phase instability which is neither purely transverse ($\mathbf{Q} = Q\hat{\mathbf{y}}$) nor longitudinal ($\mathbf{Q} = Q\hat{\mathbf{x}}$) is found (Cross, 1983). In convection this is known as the skew-varicose instability (Busse, 1978).

b. Oscillatory systems (types I_o and III_o)

We can introduce phase equations for oscillatory systems near threshold in the same way as in the previous subsection, starting from the amplitude equations (4.49) and (4.59). For a single traveling-wave solution in the oscillatory periodic case (type I_o) we use the analogue of Eq. (4.67)

$$A(x, t) = (a_k + \delta a) \exp[i(kx - \Omega_k t + \delta\phi)], \quad (4.84)$$

with Ω_k the frequency of the plane-wave solution (4.53). Magnitude perturbations can be eliminated, with more algebra, as in the stationary case, and we arrive at an equation for small phase variations on long length scales $\gg \epsilon^{-1/2}$ of the form

$$\partial_t \delta\phi + \bar{s}_0 \partial_x \delta\phi = D_{\parallel} \partial_x^2 \delta\phi + D_{\perp} \partial_y^2 \delta\phi, \quad (4.85)$$

with

$$\bar{s}_0 = s_0 + 2k(c_1 + c_3), \quad (4.86a)$$

$$D_{\parallel} = (1 - c_1 c_3) [\epsilon - k^2(3 - c_1 c_3 + 2c_3^2)(1 - c_1 c_3)^{-1}] \times (\epsilon - k^2)^{-1}, \quad (4.86b)$$

$$D_{\perp} = -c_3 s_0 / 2q_0 + (k/q_0)(1 - c_1 c_3 + s_0 c_3 / 2q_0). \quad (4.86c)$$

The zeroes of D_{\parallel} and D_{\perp} again delineate the stability boundaries, here the Benjamin-Feir instability (see above). We see that the whole band becomes longitudinally unstable for $c_1 c_3 > 1$, the classic balance of dispersive and diffusional effects. The transverse instability at $k=0$ simply requires $c_3 s_0 > 0$, and may preempt the more familiar longitudinal instability (Ohta and Kawasaki, 1987; Brand *et al.*, 1986a,b).

Away from threshold the analogue of (4.73) for an ideal plane-wave solution is (Kuramoto, 1984b)

$$U(\mathbf{x}, t) = U_{\infty}(\mathbf{q} \cdot \mathbf{x} - \omega t), \quad (4.87)$$

with a dispersion relation $\omega(q)$ which is characteristic of the fully nonlinear plane-wave state. An Ansatz of the form (4.74) now leads to the phase equation (Biktashev, 1989)

$$\partial_t \phi + \omega(q) = -\tau^{-1}(q) \nabla \cdot [\mathbf{q} B(q)], \quad (4.88)$$

where $\tau(q)$ and $B(q)$ are functions of the plane-wave state. Again one should be concerned about singular terms coming from mean drift effects. These are potentially even more important than in the I_s case, since the steady uniform wave may itself induce mean drifts. Then the vertical vorticity might include terms

$$\Omega_z = \hat{\mathbf{z}} \cdot \mathbf{q} \times \nabla[f(q)], \quad (4.89)$$

which are one order lower in the slow gradients than in the type- I_s case.

In the oscillatory uniform case (type III_o), the equation for slow variations of the uniform state near threshold is the phase equation (Kuramoto, 1984b)

$$\partial_t \phi + \omega_0 = \alpha \nabla^2 \phi - \beta (\nabla \phi)^2, \quad (4.90)$$

with

$$\omega_0 = -\epsilon c_3, \quad (4.91a)$$

$$\alpha = (1 - c_1 c_3), \quad (4.91b)$$

$$\beta = (c_1 + c_3), \quad (4.91c)$$

where we have kept all terms up to second order in the slow variation including nonlinear terms. Away from threshold the phase equation takes the same form, with ω_0, α, β dependent on the fully nonlinear solution. Note that β is just given by the dispersion. In one spatial dimension, this equation becomes more familiar in the form

$$\partial_t u - \alpha \partial_x^2 u + u \partial_x u = 0, \quad (4.92)$$

(with $u = 2\beta \partial_x \phi$) which is the Burgers equation (Burgers, 1948).

c. Higher-order phase equations

If a coefficient of the lowest order diffusive terms in the phase equation passes through zero into the unstable regime it becomes necessary to add higher-order terms to control the dynamics. (The dynamics may not however always remain within the range of validity of the phase equations, in which case a more complete description would be needed). The higher order equations depend more specifically on the problem addressed than the lower order ones. Often it is not convenient to maintain the rotationally invariant description, since a different scaling of the spatial derivatives is needed to give a suitable balance. Kuramoto (1984a) has presented a classification of higher-order equations for small deviations from plane-wave states, either steady or oscillatory (see also Fauve, 1987). The symmetries implied by the different cases may be used to restrict the possible terms. In addition, relationships exist between some terms that are nonlinear in the phase gradients and the linear dispersion relation. The higher-order equations involve a balance between nonlinear terms and higher-order gradient terms when the coefficient of the diffusion term becomes small. The choice of balancing terms, given by suitably scaling space and nonlinearities amongst possible "higher-order" ones is not always unique — often numerical work is needed to test whether the evolution remains within the domain of validity of the chosen scaling, or is robust to the addition of ignored terms (e.g., adding dissipative terms to otherwise conservative equations could change the long-time behavior). Analysis along these lines remains in its early stages. In certain simple cases the equations reduce to well studied models.

A simple example arises from the phase equation near the threshold for the stationary periodic I_s instability. If our reference state is at the critical wave number [$k=0$ in (4.16)], the state is zigzag unstable and the coefficient of the ∂_y^2 term disappears. It is straightforward to repeat the derivation of Eq. (4.70) keeping higher-order terms. If we continue to restrict ourselves to a linear equation we find

$$\partial_t \phi = \left[\partial_x^2 \phi + (k/q_0) \partial_y^2 \phi - \frac{1}{4} q_0^{-2} \partial_y^4 \phi \right], \quad (4.93)$$

where we are assuming $\partial_x \sim \eta$, $\partial_y \sim \eta^{1/2}$, $k \sim \eta$. The nonlinear terms in this equation have been given by Cross and Newell (1984).

Other examples come from studying the variation in one spatial dimension along the basic wave vector $\mathbf{q}=q\hat{\mathbf{x}}$, for our three major classes of instability. [Kuramoto (1978) has also considered transverse y -variations.] To specify the symmetries we will assume that the fundamental equations are symmetric under $x \rightarrow -x$. Since we are usually dealing with dissipative systems, no time reversal symmetry is assumed.

The stationary-periodic system (type I_s) is invariant under $(\phi \rightarrow -\phi, x \rightarrow -x)$. This allows the equation

$$\partial_t \phi = \alpha \partial_x^2 \phi - \gamma \partial_x^4 \phi + \beta (\partial_x \phi) \partial_x^2 \phi + \dots, \quad (4.94)$$

with $\alpha \rightarrow 0$ signaling the diffusive (Eckhaus) instability. For $\alpha < 0$, a simple rescaling leads to the equation

$$\partial_t \phi = -\partial_x^2 \phi - \partial_x^4 \phi + (\partial_x \phi) \partial_x^2 \phi. \quad (4.95)$$

Interestingly, this equation derives from a potential (Fauve, 1987)

$$\mathcal{J} = \frac{1}{2} \int dx [-(\partial_x \phi)^2 + \frac{1}{3} (\partial_x \phi)^3 + (\partial_x^2 \phi)^2], \quad (4.96)$$

which however is not bounded above or below, so that higher-order terms may be needed to control the dynamics. Empirically the dynamics subsequent to the Eckhaus instability is "catastrophic," i.e., it evolves outside the slow variation assumed, eventually "unwinding" the phase to give a new wave number. On the other hand the addition of a term proportional to $(\partial_x \phi)^2 \partial_x^2 \phi$ to Eq. (4.95) leads to a stabilizing $(\partial_x \phi)^4$ term in the potential \mathcal{J} , which can then be used to describe spatially inhomogeneous nonlinear states (Brand and Deissler, 1989; Riecke, 1990).

The oscillatory-uniform (type III_o) system is invariant under $x \rightarrow -x$ by itself. Thus we expect an equation of the form

$$\partial_t \phi = \alpha \partial_x^2 \phi - \gamma \partial_x^4 \phi - \beta (\partial_x \phi)^2 + \dots. \quad (4.97)$$

Note that the nonlinear coefficient is given by the linear dispersion relation $\omega = \omega_0 + \beta q^2$. Beyond the diffusional instability, i.e. for $\alpha < 0$, the above system yields the Kuramoto-Sivashinsky equation (3.30). The same result is expected for transverse y variations in the stationary periodic case, as discussed in Eq. (4.93) above.

The oscillatory-periodic phase equation (type I_o) has no symmetry restrictions and is

$$\partial_t \phi = \alpha \partial_x^2 \phi + \gamma \partial_x^3 \phi - \beta (\partial_x \phi)^2, \quad (4.98)$$

after using a Galilean transformation to eliminate the term in $\partial_x \phi$. For $\alpha > 0$ and small this equation may be transformed to

$$\partial_t u - \partial_x^3 u - u \partial_x u = O(\alpha^{1/2}). \quad (4.99)$$

Equating the left-hand side to zero gives the Kortweg de Vries equation, which balances the dispersive and nonlinear terms. The $O(\alpha^{1/2})$ diffusive correction terms will destroy the integrability of the lowest-order equation (see Kivshar and Malomed, 1989).

All of the above results rely on the apparently innocuous assumptions of symmetries and smooth expansions in slow spatial gradients (compared with the characteristic length scales of the unperturbed pattern). However, as we have already seen in the lowest-order phase equation, these assumptions may break down as a result of the dynamics. Moreover, to make progress it is assumed that the higher-order terms have the "right sign" to saturate the dynamics within the weakly nonlinear, slowly varying

realm for which the equation is valid. In specific situations one must be aware of these restrictions and of the possibility of their breakdown.

d. Control-parameter ramps

An application of the idea of phase equations is to a system with a slow spatial variation ("ramp") of a parameter p in the microscopic equations that contributes to the control parameter ϵ . A particularly interesting case is where p is a function of one space dimension x , and $p(x)$ interpolates slowly between a value yielding a control parameter $\epsilon(x)$ below threshold for $x < 0$, to a constant value p_+ giving $\epsilon_+ > 0$ above threshold for large positive x . Using the same methods as in deriving the phase equation, Kramer *et al.* (1982) showed how to obtain an equation for the spatial dependence of the wave vector q of the stationary solution for slow ramps,

$$f_1(q,p)\partial_x q + f_2(q,p)\partial_x p = 0, \quad (4.100)$$

where f_1 and f_2 are functions that can be calculated for each particular system and for any quantity p . Integrating Eq. (4.100) from the linear state for $x < 0$ where a unique solution $U=0$ exists, we find a precise wave number $q_p(\epsilon_+)$ in the constant region. For spatial variation of a given quantity p contributing to $\epsilon(x)$ the wave number $q(\epsilon_+)$ is unique, independent of the functional form of $p(x)$ for slow enough spatial variation. However different quantities p yield *different* selected wave numbers for the same final ϵ_+ , as demonstrated explicitly by Hohenberg *et al.* (1985). Thus ramping the control parameter slowly to subthreshold values provides a precise and selectable wave number, as opposed to the wide band consistent with stability in a periodic system (see Sec. VI.A below). Precise wave-vector selection was first found by Eagles (1980) in his study of convection with ramped plate separation varying on an $O(\epsilon^{-1/2})$ length scale.

An interesting correction to the perfect selection by slow ramps arises if the variation of the control parameter is not everywhere smooth. It has been shown by Cross (1984) and by Riecke (1986) that abrupt variations in control parameter act as "pinning centers" which lead to nonadiabatic corrections to the phase equation (4.100) (see subsection IV.A.4 below), and to a finite band of states δq . Analytic calculations of this effect have been carried out on models by Riecke (1988), and they agree well with numerical work and qualitatively with experiments on Taylor-Couette flow.

3. Secondary instabilities

We have classified systems by the nature of the bifurcation from the uniform state (types I, II, and III, either o or s). The classification leads directly to different amplitude and phase equations. We may further consider the various secondary instabilities of the ideal nonlinear

states, i.e., the boundaries of the stability balloon. Again it is possible to classify the instabilities by their spatial symmetries and temporal behavior, and to develop amplitude equations describing the evolution of the unstable modes, now expanding in the small increase in the control parameter above the secondary instability threshold. We have already discussed the higher-order phase equations that are valid when the instability is at long wavelengths. Since secondary instabilities occur in already complicated states, the range of possible classes is larger than at the primary instability threshold. We will illustrate the idea for type I_s systems, concentrating on a particular example known as the "drift instability."

A secondary instability in a type I_s system occurs in a spatially periodic system. Thus the unstable mode has the form of a Bloch wave (analogous to the Floquet analysis in a temporally periodic state, see Iooss and Joseph, 1980)

$$u = U_0(qx + \phi) + AU_Q(qx + \phi)e^{iQ\cdot x}e^{i\Omega t}, \quad (4.101)$$

where $U_0(qx + \phi)$ is the nonlinear state with wave vector $q\hat{x}$ with the phase ϕ shifting the pattern as a whole. The second term is the perturbation (with U_Q also a period function of wave vector $q\hat{x}$), Q is the Bloch wave vector which may be taken in the range (the first Brillouin zone)

$$-\frac{1}{2}q < Q_x \leq \frac{1}{2}q,$$

and Ω is the frequency, nonzero for a Hopf bifurcation. Different types of behavior occur for $Q_x=0$ (no breaking of the translational periodicity), $Q_x=\frac{1}{2}q$ (wavelength doubling), or Q_x incommensurate with q , as well as for Ω zero or nonzero (stationary or Hopf), and Q_y finite or zero. In addition, discrete symmetries may be broken; for example, when $Q_x=0$ or $Q_x=\frac{1}{2}q$ there is the question of whether the parity symmetry (which we assume to be present in U_0) is broken. This wide range of possibilities is already manifest in the analysis by Busse and co-workers (see Busse, 1978) of the secondary instabilities in Rayleigh-Bénard convection discussed further in Sec. VIII.A below.

A point not evident from the early work on convection is the importance of the coupling to the *phase* variable ϕ of the *basic* pattern, describing the free translation of the structure: the instability may cause the whole pattern to drift. Coullet and Iooss (1990) have classified all the possible types of behavior for one-dimensional type I_s and I_o systems, and have written down coupled equations for the amplitude A of the new unstable mode (real or complex depending on Q and Ω) and the phase ϕ of the basic periodic pattern, defined in Eq. (4.101).

Consider for example the case of a parity breaking, $Q=0$, stationary bifurcation (Coullet *et al.*, 1989d). This is characterized by a real amplitude A coupled to the phase ϕ . Symmetry restrictions lead to the equations (in

scaled variables)

$$\partial_t A = \partial_x^2 A + g_1(\partial_x \phi) A + \epsilon A - g_0 A^3 + \dots, \quad (4.102)$$

$$\partial_t \phi = D \partial_x^2 \phi + g_2 A, \quad (4.103)$$

with g_0, g_1, g_2, D real constants. The second equation reflects the fact that in a nonequilibrium system, breaking the parity will typically lead to the drift of the whole pattern. (Time reversal symmetry would forbid such a motion at an analogous equilibrium transition.)

An interesting wave-number selection phenomenon occurs in the case of a subcritical bifurcation, $g_0 < 0$ (we insert a high-order term A^5 to stabilize the system). A bubble (or pulse) of the broken parity phase above threshold will propagate in one direction or another depending on the sign of A , and grow for $\epsilon > \epsilon_1 = -(3/16)g_0^2$. Analysis of Eq. (4.103) shows that the propagating, growing bubble leaves behind a uniform state with a shifted wave vector. Passage of successive bubbles changes the wave vector to $\partial_x \phi = -k^*$ given by setting the effective control parameter governing the growth rate equal to ϵ_1

$$\epsilon + g_1 k^* = \epsilon_1, \quad (4.104)$$

at which point the bubble no longer expands. These results seem to correlate well with experimental observations in directional solidification (Coullet *et al.*, 1989d) and in convection in a narrow annulus.

As is clear from the stability balloon in convection discussed in Sec. VIII.A below, the secondary instabilities often reflect subtle details of the microscopic equations, and little can be said in general about which finite- Q instabilities will be present. (We have seen that the long-wavelength instabilities have a wider universality.) Progress can however be made near a degenerate primary bifurcation (e.g., a codimension-2 point, see subsection IV.B below). Then the secondary instability may be understood in terms of the competition between the different states at the degenerate bifurcation, and may often be captured, either approximately or systematically, by the particular amplitude equations valid in this region. Examples occur near the degeneracy point of primary bifurcations at q and $2q$ (Malomed and Tribelsky, 1984; Fauve *et al.*, 1990; Paap and Riecke, 1990; Levine *et al.*, 1991; Rappel and Riecke, 1992; Riecke and Paap, 1992), in the weakly damped parametric wave system (Paap and Riecke, 1990; Milner, 1991), and for Taylor-Couette modulated waves (Chossat and Iooss, 1985).

4. Nonadiabatic effects

Amplitude and phase equations describe the slow evolution of variations of a periodic pattern. They may be derived as smooth equations in a slow scaled spatial coordinate (e.g., $X = \epsilon^{1/2}x$ in the amplitude equation), and the derivation involves a perturbation expansion. The fast underlying spatial variation does not appear in the final answer e.g. Eq. (4.3). An important physical

phenomenon that is not captured by these expansions, even if taken to higher order, is the locking of coherent structures, or regions of spatial variation, to the underlying periodic structure in type I systems. Thus for example the propagation of fronts, or the glide of dislocations (see Sec. V.B.3 below) may cease altogether for small enough driving. This coupling to the fast spatial degrees of freedom is generally put under the heading of “nonadiabatic effects” (Pomeau, 1984), and will be discussed further in subsection V.B.2.b.vi.β below, in the context of a stationary front in the Swift-Hohenberg equation.

5. Rotationally invariant order parameter equations

The phase equation is valid over a wide range of control parameter values and for arbitrarily large reorientations of the rolls, provided the rate of spatial variations is small compared with the local wave number. The whole approach is based on the slow variations of a pattern which locally has a periodic spatial structure. This method does not give a complete description of the pattern in typical situations, since defects — where no locally periodic structure can be identified — are common. The amplitude equation on the other hand allows for more general modulations of the pattern, including amplitude variations. For example, as discussed in detail in Sec. V.B below, the properties of *dislocation* defects may be completely studied near threshold using the amplitude equation (Siggia and Zippelius, 1981a), and boundary effects are easily included. However, large changes in the direction of the wave vector are not permitted. The question arises: can we find a treatment that includes both options?

Near threshold the “order parameter” equation introduced by Swift and Hohenberg (1977) seems a possible candidate. Although we have already discussed this equation as an example of a microscopic model in Sec. III.C, we now wish to consider it as an approximation to a more fundamental microscopic description such as the full fluid equations of convection. The form of the equation can be motivated by returning to the characteristic spectrum of the linear instability I_s of Fig. 7. Starting from a microscopic system (3.4) we define ψ_q to be simply the full amplitude of the plane wave eigenvector at q . To get the correct spectrum Eq. (4.4) must be satisfied in the linear regime. The nonlinear terms may be developed perturbatively by assuming that the modes away from the critical wave number q_0 adiabatically follow the slow time dependence (Haken, 1977). The equation becomes

$$\tau_0 \partial_t \psi_q = [\epsilon - \xi_0^2(q - q_0)^2] \psi_q + \sum_{\substack{q_1 q_2 q_3 \\ q_1 + q_2 + q_3 = q}} g(q_1, q_2, q_3) \psi_{q_1} \psi_{q_2} \psi_{q_3}, \quad (4.105)$$

where g is a complicated function which can be calculated in specific cases (Cross, 1980). We now define a real order parameter in space as

$$\psi(\mathbf{x}) = \sum_{\mathbf{q}} \psi_{\mathbf{q}} e^{i\mathbf{q} \cdot \mathbf{x}}, \quad (4.106)$$

and Fourier transform Eq. (4.105) to give an equation in real space. This procedure encounters three difficulties: the first is that the $(q - q_0)^2$ term does not give a convenient expression, and we transform it to

$$(q - q_0)^2 \psi_{\mathbf{q}} \approx (4q_0^2)^{-1} (q^2 - q_0^2)^2 \psi_{\mathbf{q}} \\ \rightarrow (4q_0^2)^{-1} (\nabla^2 + q_0^2)^2 \psi(\mathbf{x}). \quad (4.107)$$

Secondly, the nonlinear terms give a short-range, but nonlocal interaction. In specific cases physical arguments may suggest various local approximations (e.g., see Manneville, 1983a; Bestehorn and Haken, 1990a,b). However, as emphasized below, these are *not* in general systematic approximations, and the importance or unimportance of the effects left out has not been tested in general. A case where a systematic approximation leads to a local interaction is the type II_s instability (subsection IV.A.1.b above). The full structure is quantitatively important when considering superpositions of singly-periodic states as in subsection IV.A.1.a above [it affects $\mathcal{G}(\theta)$], but we shall for simplicity replace the nonlinear term proportional to g by a local interaction $g_0 \psi^3(x)$ with a constant g_0 . Thirdly, the full effect of boundaries is not included in the projection onto the unstable eigenvector, since “fast” spatial modes are forced by the boundary conditions. With these caveats in mind we are thus led to a simple description given by the Swift-Hohenberg equation

$$\tau_0 \partial_t \psi = \epsilon \psi - (\xi_0^2 / 4q_0^2) (\nabla^2 + q_0^2)^2 \psi - g_0 \psi^3, \quad (4.108)$$

together with the boundary conditions

$$\psi = \hat{\mathbf{n}} \cdot \nabla \psi = 0, \quad (4.109)$$

where $\hat{\mathbf{n}}$ is the normal to the boundary. This equation does indeed reduce to the amplitude equation (4.3) for nearly parallel rolls and reproduces the correct boundary conditions on the amplitude A to lowest order in ϵ (Cross *et al.*, 1983a). Moreover it describes more general patterns containing defects and other large distortions of the roll structure, as discussed in Sec. V below. Often the variables are rescaled to eliminate unnecessary constants, leading to the simple form (3.27).

Near type I_o instabilities complex order parameter equations have been obtained by Ohta and Kawasaki (1987) and more recently by Bestehorn and Haken (1990a,b). The simplest equation is of the form

$$\tau_0 \partial_t \psi = \epsilon \psi + s_0 (\nabla^2 + q_0^2) \psi \\ - (\xi_0^2 / 4q_0^2) (1 + i c_1) (\nabla^2 + q_0^2)^2 \psi \\ - g_0 (1 + i c_3) |\psi|^2 \psi, \quad (4.110)$$

where now ψ is a complex field (its real part is the physical field). More complicated nonlinear terms involving derivatives are of course also possible, as in the real case.

Although rotationally invariant equations such as

(4.108) are instructive models for understanding pattern formation, it should be emphasized that they do not result from any systematic expansion of more fundamental equations. In particular, the order-parameter equations derived by Haken and co-workers for a large number of systems (see Bestehorn and Haken, 1990a,b, and references therein) involve uncontrolled approximations, since some but not all of the corrections to the amplitude equations resulting from the fast spatial modes are retained.

B. Qualitative methods

In the previous section we have mainly been concerned with quantitative perturbation methods. Throughout our discussion we have seen that the role of symmetry is crucial in pattern forming systems, for example in the definition of ideal patterns and in the derivation of amplitude and phase equations. In this section we briefly treat symmetry from a more formal point of view. We then introduce an expansion scheme known as “normal forms,” which systematizes and in some ways extends the amplitude equation approach. This scheme yields qualitative rather than quantitative information, and it shows its real power in complicated situations with symmetric or degenerate bifurcations. (Note however that normal forms are usually restricted to ideal, spatially periodic solutions.) These aspects of bifurcation theory have recently received considerable attention from mathematicians, and we cannot hope to do the subject justice. Our main aim here is to provide a crude translation between these formal developments and our more heuristic approach. The reader is referred to recent books and reviews (Guckenheimer and Holmes, 1983; Golubitsky and Schaeffer, 1985; Crawford, 1991; Crawford and Knobloch, 1991) for a fuller account. Finally we discuss the qualitative implications of the symmetry analysis for the existence of defects in ideal patterns.

1. Formal methods of bifurcation theory

a. Normal forms and nondegenerate bifurcations

As mentioned above the method of normal forms is similar in approach to the use of amplitude equations, but with rather different aims. The idea is again to derive a reduced dynamical description near the bifurcation point by projecting the dynamics onto a lower-dimensional space (the center manifold). For small amplitude solutions this is the space spanned by the marginal eigenvectors, i.e., those with eigenvalue passing through the imaginary axis at the critical value of the bifurcation parameter. The center manifold is however continued into the larger amplitude regions. The emphasis of the approach is on reproducing qualitative features of the dynamics; the expansion is continued to whatever order is needed for the full qualitative behavior

to be displayed, rather than to a definite order in some systematic expansion parameter. Furthermore, although the original expansion might be developed in powers of the mode amplitudes, a systematic procedure of both linear and *nonlinear* transformations is used to reduce the equations to a simple canonical form, with variables that usually bear a complicated relationship to the original variables. This canonical form is then analyzed to make qualitative statements about all (or at least typical) systems with a given type of bifurcation. For example it is often possible to connect the nature of the bifurcation (supercritical or subcritical) with the stability of the ensuing solutions.

A somewhat related technique, known as the Lyapunov-Schmidt reduction, examines periodic or steady state solutions beyond the bifurcation point by solving a reduced, time-independent equation. Although less general than the method of normal forms, the Lyapunov-Schmidt technique provides a rigorous approach to a smaller class of solutions (i.e., the periodic ones) near a Hopf bifurcation.

We will introduce the method of normal forms in the case of nondegenerate bifurcations from a time-independent state, repeating in somewhat more formal language the discussion in subsection III.A.2 above. In the absence of special symmetry or degeneracy the bifurcation can occur in two ways: a real eigenvalue of the linear stability analysis passes through zero (type s); or a complex pair $\sigma_1 = \sigma_2^* = \sigma$ pass through the imaginary axis $\text{Re}\sigma = 0$ (type o; a Hopf bifurcation). Near a type s instability the center manifold is one-dimensional and the simplest normal form in the single variable u is as in Eq. (3.9b)

$$\partial_t u = Ru - u^2, \quad (4.111)$$

corresponding to an exchange of stability at a transcritical bifurcation. If equations have inversion symmetry (corresponding to $u \rightarrow -u$) the quadratic nonlinearity must be absent and the simplest representative is as in Eq. (3.9c)

$$\partial_t u = Ru \pm u^3, \quad (4.112)$$

corresponding to a pitchfork bifurcation. This simple example demonstrates certain results that are characteristic of more complicated situations:

(i) An alternative choice of coordinates $u' = u + u_0$ with u_0 a constant would lead to a more complicated, nonstandard form.

(ii) The amplitude of the new solution scales in a characteristic way with the bifurcation parameter, $u \sim |R|$ for Eq. (4.111) and $u \sim |R|^{1/2}$ for Eq. (4.112).

(iii) Depending on the sign of the cubic term in Eq. (4.112) the transition may be either supercritical or subcritical. There is a prescribed and simply calculated relationship between the stability of the small amplitude solutions and the nature of the transition [subcritical \leftrightarrow unstable; supercritical \leftrightarrow stable, at least in this subspace].

(iv) It may well happen that the original equations only

have quadratic nonlinearities. A simple projection onto the marginally stable eigenspace would then not produce the cubic term in Eq. (4.112). To obtain this term one uses an iterative procedure: calculate the amplitude of the stable eigenvectors driven by the nonlinearity, and then feed these back into the marginal space. This adiabatic elimination, or calculation of the "slaved modes" in the standard amplitude formalism, can be thought of as calculating the curvature corrections to the center manifold when it is extended into the nonlinear regime.

The full power of these methods becomes apparent when considering bifurcations with symmetry or degenerate bifurcations, which we now discuss.

b. Bifurcations with symmetry

In a system with symmetry, many symmetry-related modes may become unstable together and the standard nondegeneracy restrictions of simple bifurcation theory are not satisfied. The theory must be reinvestigated using symmetry analysis. The natural mathematical tool is group theory, and there is a large body of work systematically generalizing the simple bifurcations considered above to situations with particular symmetry groups.

The first step is to construct the group Γ_0 containing all symmetry elements of the system. The fundamental symmetry in pattern forming systems is translational. Since, in the ideal situation, we are looking for spatially periodic solutions, it is often mathematically convenient to restrict the translations to a compact group by taking *periodic boundary conditions* over periods L_i , $i = 1, \dots, d$ in a d -dimensional space (so that translations T_i and $T_i + L_i$ are identified). Note however that the assumption of periodic boundary conditions is not consistent with continuous rotational symmetry in space. The Taylor-Couette system is an example of a physical situation with such boundary conditions (in the azimuthal direction). Each translational symmetry is then isomorphic to that of a circle, and is often described in the mathematical literature as S_1 or $\text{SO}(2)$ symmetry. Spatial parity symmetry ($x \rightarrow -x$) would enlarge the group to $O(2)$. Thus the important case of wave instabilities (type I_o) with parity symmetry can be described as a Hopf bifurcation with $O(2)$ symmetry.

To perform a symmetry analysis for Hopf bifurcations it is useful to incorporate the time dependence in the symmetry description. The original autonomous system (3.4) is invariant under all time translations. If we are seeking periodic solutions of period τ (to be determined) it is again convenient to consider time translations T_τ modulo τ . This corresponds to another S_1 symmetry. The Hopf bifurcation leads to a solution breaking this symmetry, the operation of T_τ on a solution translating the phase of the oscillator. Thus the Hopf bifurcation with one-dimensional translation and parity symmetry can be described by the full group $\Gamma_0 = O(2) \times S_1$.

In a pattern forming bifurcation there is a transition to a state of lower symmetry, which is the phenomenon of

spontaneously broken symmetry. The symmetry of the new state will be represented by an “isotropy group” Γ_1 that is a subgroup of Γ_0 (i.e., contains fewer symmetry elements). The question of which subgroups of Γ_0 can typically characterize the new state seems hard to answer in general (Golubitsky and Schaeffer, 1985). Subsequent bifurcations can lead to further reductions in symmetry, so that a chain of possible groups is formed, called the “isotropy lattice” [Fig. 11(a)], with successively smaller numbers of elements, each one a subgroup of the higher level group (at least to within a “conjugacy,” see Golubitsky *et al.*, 1988). The symmetry analysis is often sufficient to produce a nondegenerate bifurcation scheme for which the usual theorems hold. The reduced symmetry state can be analyzed using the method of normal forms, which must now respect the remaining symmetry. The polynomial expansions are continued to high enough order so that solutions showing this minimal symmetry may be found — often low-order truncations lead to solutions with artificially high symmetry. Nondegeneracy conditions, i.e., the assumption that coefficients in the normal form will not be zero typically, may rule out certain candidates in the isotropy lattice. For compact groups the expansion to any order is given by combinations of a finite number of low-order polynomials. Again, general results may be found linking, for example, the nature of the bifurcation to the stability of the new solutions.

An example of the formalism is the Hopf bifurcation with $O(2)$ symmetry considered by Golubitsky and Stewart (1986). The symmetry elements of the full group $\Gamma_0 = O(2) \times S_1$ are displacements in space through T_x and spatial parity P [the $O(2)$ symmetry], plus translations in time through T_t (the S_1 symmetry). The isotropy lattice is shown in Fig. 11(b). States above the transition may be represented by two complex numbers z_1 and z_2 . (These are just the wave amplitudes A_R and A_L in the notation of subsection IV.A.1.d). The state with symmetry $SO(2)$ is either $z_1=0$ or $z_2=0$: this is just the traveling or rotating wave case, and the symmetry is a combined translation in space and time. The state with symmetry $Z_2 \times Z_2^c$ is $z_1=v$, $z_2=v$, and is the standing wave with inversion symmetry, plus the symmetry Z_2^c which is a change of sign of the amplitudes z_1 , $z_2 \rightarrow -z_1$, $-z_2$, together with a time translation through half a period. These are the only two oscillatory modes that typically appear. The state with residual symmetry Z_2^c is the general mixed-wave state (z_1, z_2) and only occurs in degenerate cases (Golubitsky *et al.*, 1988, p. 341). The normal form equations are the amplitude equations of subsection IV.A.1.d., with spatial dependence neglected. These can be rewritten in the form

$$\partial_t \begin{bmatrix} z_1 \\ z_2 \end{bmatrix} = (p + iq) \begin{bmatrix} z_1 \\ z_2 \end{bmatrix} + (r + is) \delta \begin{bmatrix} z_1 \\ -z_2 \end{bmatrix}, \quad (4.113)$$

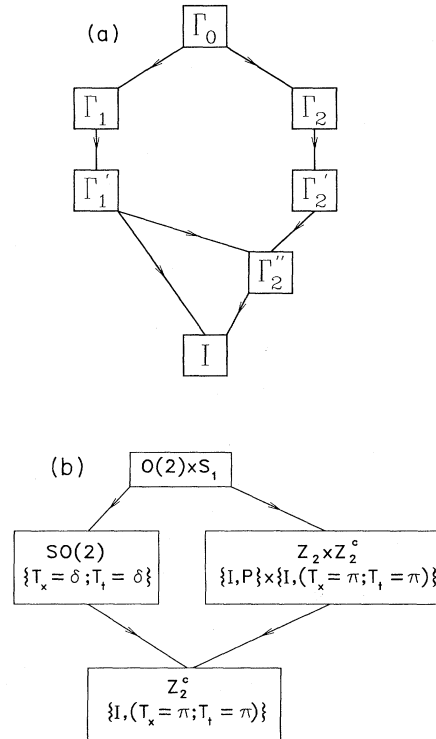


FIG. 11. Isotropy lattice for bifurcations with symmetry. (a) Schematic representation of the isotropy lattice showing successive symmetry breaking bifurcations, starting from the original symmetry group Γ_0 and passing through a number of possible chains, through lower symmetry states represented by groups Γ_1 , Γ'_1 , etc. The end point is the identity I . (b) Isotropy lattice for the Hopf bifurcation with $O(2)$ symmetry of spatial translations and parity, showing its decomposition into the subgroups $SO(2)$, the two-member group Z_2 (or Z_2^c), and products $Z_2 \times Z_2^c$. The symmetry elements shown in the figure are parity P , the identity I , translation through space by an amount δ ($T_x=\delta$), and translation in time by an amount δ ($T_t=\delta$), with $\delta=2\pi$ corresponding to a complete period.

with $\delta = |z_2|^2 - |z_1|^2$, and p, q, r, s functions of the two invariants $N = |z_1|^2 + |z_2|^2$ and $\Delta = \delta^2$. Depending on signs and ratios of the coefficients $r(0)$ and $p_N(0)$ the different bifurcations in Fig. 11(b) are possible [$r(0)=r(N=0, \Delta=0)$ and $p_N(0)=(\partial p / \partial N)_{N=\Delta=0}$]. It is easy to see that for either rotating waves or standing waves to be stable both must branch supercritically, and then one is stable and the other is unstable.

c. Degenerate bifurcations

It is possible to tune system parameters so that a number of eigenvalues, not related by symmetry, become unstable together. These are known as co-dimension- n degenerate bifurcations if n system parameters must be tuned. Now the center manifold is higher-dimensional and the normal form equations must be developed as polynomials in the amplitude of all the marginal modes.

Symmetry classification again plays an important simplifying role. The behavior as the system parameters are varied slightly away from the codimension- n point can be investigated using the normal forms (the universal unfolding). The full behavior is often complicated, depending on various signs and ratios of coefficients in the normal forms, which may vary from system to system.

2. Phase variables and topological defects

The symmetry classification of a bifurcation provides a useful way of generalizing the idea of phase variables (see, e.g., Coullet *et al.*, 1987, 1989b, 1991). Consider a state with *broken symmetries* beyond a particular bifurcation. Some symmetry elements of the system are no longer symmetry elements of the solution. The action of one of these elements on a solution will give a different state, but one that is entirely equivalent. The class of different equivalent states generated by all the *continuous* symmetry elements must be distinguished by parameters ϕ_i such that action by the group elements changes these variables. We will call the ϕ_i *phase variables*, since they are a natural generalization of the phase generated by translations, discussed in subsection IV.A.2. A spatially uniform change of any of the ϕ_i corresponds to producing a new equivalent solution, so such a change does not lead to any dynamics. A slowly varying change $\phi_i(\eta \mathbf{x})$, $\eta \ll 1$, would therefore be expected to relax slowly at a rate $\sigma \sim \eta^p$, with $p > 0$ and typically equal to 2. Thus the generalized phase variables will describe the dynamics of slow spatial variations of the basic state.

The introduction of phase variables has implications beyond dynamical equations. The global constraints resulting from the requirement that the phase field should lead to a single-valued microscopic U field can be used to give a topological classification of possible patterns. Let us consider the case of a two-dimensional roll system with phase variable ϕ corresponding to $\mathbf{q} \cdot \mathbf{x}$ in the undistorted pattern as in subsection IV.A.2. Now consider a pattern in which over some large closed loop C the phase varies slowly, but accumulates a total “phase winding” of 2π over the loop, leading to a winding number

$$W = (1/2\pi) \int_C \nabla \phi \cdot d\ell = 1. \quad (4.114)$$

We can ask whether such a variation is consistent with a slow variation of ϕ everywhere. The answer is clearly no, since if the contrary were true we could smoothly shrink our integration contour always through regions of slow variation, and the integer winding number W could not change. Eventually a 2π phase winding would occur over an arbitrarily small loop, contradicting the assumption of slow variation. Thus an integer winding number generated by the behavior in regions where the phase variation is slow, necessarily implies the existence of at least one *point defect*, where the assumption of slow variation, and hence the phase description, break down. (An

amplitude equation or a fully microscopic description would still be valid, however.) This construction is familiar from the definition of the Burgers vector of a dislocation in a crystal, or of a vortex in a superfluid. The existence of these “topological defects” depends both on the space of phase variables (order parameter space), and on the spatial dimension of the pattern. Defects exist if there is a nontrivial mapping of the contour in physical space (the loop C above) onto the order parameter space (the circle 0 to 2π for the phase variable ϕ above). Defects are mathematically characterized by the homotopy theory of such maps. [A review in a condensed matter context is given by Mermin, 1979.] In addition to point defects, defined by a surrounding sphere in three dimensions, a circle in two dimensions and a pair of points ($x = \pm \infty$) in one dimension, we may look for higher-dimensional defects, e.g., a line in three dimensions. We will discuss simple examples in Sec. V without using the mathematical formulation explicitly. The importance of topological methods increases with the complexity of the patterns, and they have played a useful role, for example in the study of wave instabilities in excitable media discussed in Sec. X.

Although the topological classification of defects is a useful exercise, the importance of regions of slow phase variation allowing such a classification in real patterns is not clear in many situations. The main difference with condensed-matter systems, as discussed by Mermin for example, is the absence of a Lyapunov function for dynamical equations. A condensed system near equilibrium seeks to minimize the free energy of various field configurations, and thus favors slowly varying phases over most of the system. The core of a defect usually represents a higher energy state, but its elimination involves overcoming a macroscopic energy barrier. Thus topological stability often implies dynamical stability. For dynamical systems on the other hand, topological stability is neither necessary nor sufficient for dynamical stability, though topological defects often appear as persistent features of solutions. An example of a topologically stable defect which disappears will be encountered in our discussion of traveling waves in Sec. V.B. It is a kink pair formed of right- and left-traveling waves for a convectively unstable system. Conversely, an example of a stable defect with no topological stability is a stationary pulse in an oscillatory state, which may exist over a broad region of parameter space (see Sec. V.B). Finally, topological defects may be created spontaneously in spatial regions where the phase description breaks down, either near boundaries or in the bulk as a consequence of instabilities, and unlike near-equilibrium cases, there is no way to assign an “energy cost” associated with this creation process.

V. ELEMENTS OF REAL PATTERNS

Having described the ideal patterns that exist above threshold for the different classes of instabilities, we now

wish to study the main modifications brought about by "real" conditions. One important deviation from the ideal state arises from the presence of boundaries. Another obvious feature of real patterns is the existence of local structures or defects, either inside domains of roughly ideal states or at the boundaries between such domains. We review these subjects here, and then attempt to combine them in Sec. VI.

A. Effects of boundaries

1. Type I_s: Stationary periodic

Let us consider a type I_s instability in a rotationally invariant system whose ideal state consists of parallel rolls. We shall introduce the various types of boundary conditions through their effects on the linear threshold, and then discuss in considerable detail the constraints on nonlinear solutions arising from what we will call "rigid" boundary conditions.

a. Threshold effects

(i) Periodic boundary conditions

The simplest boundary conditions to discuss are ones that are consistent with a subset of the ideal solutions of the laterally infinite system. For example, periodic boundary conditions over a rectangular box of dimensions $L \times M$

$$U(x+L)=U(x), \quad (5.1a)$$

$$U(y+M)=U(y), \quad (5.1b)$$

are consistent with spatially periodic solutions, the only difference being that the wave vectors are restricted to the discrete set $\mathbf{q}=(2\pi\ell/L, 2\pi m/M)$ for ℓ, m integers. If L and M are small enough there may be very few, or even a unique ℓ and m , giving a wave vector \mathbf{q} within the band of stable states: in this case strict wave-number selection may occur by a rather trivial mechanism. The same set of solutions may also be consistent with other boundary conditions, e.g., no flux (or Dirichlet) conditions, which simply require zero normal gradients of the solution at the boundary. In this particular case the solutions extend to the nonlinear regime: the boundary conditions merely select a discrete set of the nonlinear ideal solutions. Although these boundary conditions may be natural from the microscopic physics, they are not generic in systems yielding instabilities at finite wave numbers.

(ii) Inhomogeneous boundary conditions

If the boundary conditions are not consistent with the spatially uniform solution $U=0$, we call them *inhomogeneous*. These boundary conditions render the bifurcation imperfect (Sec. III.A). Since the evolution of the small amplitude state near the ideal system bifurcation is very sensitive to such small imperfections the transient evolution is strongly affected. If the control parameter is increased slowly through threshold often a unique solution will develop, corresponding to the smoothly developing branch in Fig. 6(f).

For large systems a small imperfection may be treated using the amplitude equation (4.13) (in one dimension for simplicity)

$$\partial_t A = \epsilon A + \partial_x^2 A - |A|^2 A, \quad (5.2)$$

with an inhomogeneous boundary condition (see Cross *et al.*, 1983a, and references therein)

$$A(x) = a_{\pm}, \quad x=0, L, \quad (5.3)$$

and a_{\pm} complex numbers. For small systems a useful approach (Shaeffer, 1980) is to "switch on" the imperfection with a parameter $0 < \eta < 1$. For small η the passage from an ideal bifurcation to an imperfect one may be analyzed in detail. The qualitative behavior may then be the same even for larger imperfections, $\eta \rightarrow 1$. This approach is particularly useful in determining the choice between degenerate or almost degenerate solutions (e.g., between the 3 and 4 roll states in a system of size 3.5, see Sec. IX.B below).

(iii) Rigid boundary conditions

Typically, the lateral boundary conditions will not be consistent with the structure of the ideal solution: it will not be possible to satisfy *all* boundary conditions by a choice of the *one* free variable — the phase of the ideal solution at the boundary. Homogeneous boundary conditions (those consistent with the uniform state $U=0$) will therefore usually *shift* the onset of the instability. We can identify two different classes of boundary conditions depending on whether the instability is enhanced or suppressed.

Perhaps most commonly we might expect the boundaries to suppress the instability. This is the case for Rayleigh-Bénard cells where the sidewalls impede the fluid flow through viscous effects. Let us consider a system described by the general *pde* (3.4) in a box of size $L \times L$ with "rigid" boundary conditions consistent with $U \equiv 0$

$$U(\mathbf{x})=0, \quad \nabla U(\mathbf{x})=0, \dots \quad (5.4)$$

(depending on the order of the *pde* one may need conditions on higher derivatives). The instability threshold $R_c(L)$ will be shifted from its value R_c^∞ in the infinite system as a result of the rigid boundary conditions (5.4), by an amount

$$\epsilon_c = [R_c(L) - R_c^\infty] / R_c^\infty. \quad (5.5)$$

We say that the system is small if $Lq_0 = O(1)$, and

large if $Lq_0 \gg 1$. For large systems we expect that $\epsilon_c \ll 1$, and rigid boundary conditions can be treated within the amplitude equation (5.2). For example in a one-dimensional situation the incompatibility of (5.4) with the ideal solutions U_∞ induces a boundary condition of the form (Ahlers *et al.*, 1981; Cross *et al.*, 1983a)

$$A(x)=0, \quad x=0, L, \quad (5.6)$$

on the amplitude A . The onset solution is then [Fig. 12(a)]

$$A = a \sin(\pi x/L), \quad (5.7)$$

leading to a threshold suppression proportional to L^{-2} ,

$$\epsilon_c = \pi^2/L^2, \quad (5.8)$$

with L the system size measured in units of ξ_0 . More generally, for arbitrary L Eq. (5.2) no longer applies. One finds an overall increase in the suppression as L decreases, but with modulations periodic in L with period π/q_0 , corresponding to the fitting of discrete numbers of periods into the finite geometry as discussed for example by Charlson and Sani (1971) and shown in Fig. 13. For small systems [$Lq_0 = O(1)$] we expect $\epsilon_c = O(1)$ also.

The second possibility is that the boundary conditions *enhance* the instability. In a small system this will simply lead to a lower critical value of the control parameter R_c . For large systems a surface instability develops, leading to a solution localized near the boundaries and decaying in the bulk, for control parameter R_c less than the value R_c^∞ of the ideal bulk instability. Typically $|\epsilon_c|$ will be $O(1)$, i.e., the surface solution develops far below the bulk instability. As R is increased to approach R_c^∞ the surface solution may drive the bulk solution, in a manner similar to the inhomogeneous boundary conditions described above: the bifurcation which occurs at R_c^∞ in the ideal case has now become imperfect [Fig. 6(f)]. Howev-

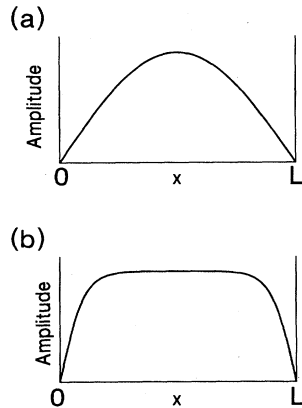


FIG. 12. Amplitude $A(x)$ in one-dimensional system for the amplitude equation (5.2) with boundary conditions $A(x=0)=A(x=L)=0$. (a) Very close to the shifted threshold $\epsilon - \epsilon_c \ll \epsilon_c$. (b) Further away from shifted threshold $\epsilon - \epsilon_c \gtrsim \epsilon_c$.

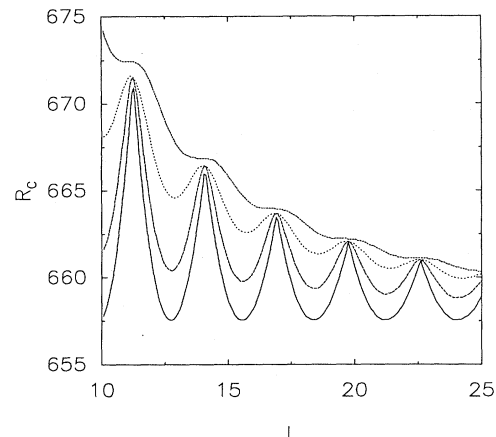


FIG. 13. Threshold Rayleigh number R_c for onset of convection in a one-dimensional system of size L for the model of free-slip convection. The boundary conditions at the ends interpolate from free-slip thermal insulators (bottom line) to rigid good thermal conductors (top line). (From Y.-Y. Chen, 1992.)

er, any of the symmetry related solutions may occur, depending on the symmetry breaking at R_c . For $R > R_c^\infty$ the solution will be like the ideal solution in the bulk, with amplitude scaling as $\epsilon^{1/2}$ for not too small ϵ , but it will already have grown to $O(1)$ at the boundaries. Kramer and Hohenberg (1984) have called these type II solutions, in contrast with type I solutions which suppress the instability.

Although the second class of solutions is less common in physical systems, examples are easily found in model equations. Kramer and Hohenberg investigated the Swift-Hohenberg model (3.27) with general homogeneous boundary conditions, and found that depending on the values of parameters in the boundary conditions, either type I or type II solutions were stable, but never both. Hohenberg *et al.* (1985) subsequently extended the study to a reaction-diffusion system (3.32) and found similar results. From this study we may see that no-flux boundary conditions for reaction-diffusion systems are the special point just intermediate between the two cases of suppressing and enhancing boundaries, and in this sense they are nongeneric. They will produce the periodic shift in onset with L , but *not* the overall trend growing as L^{-2} when L decreases. The lower envelope of the $R_c(L)$ curve which touches the minima will remain at $\epsilon_c = 0$ in this case, as shown for example in the lowest curve in Fig. 13. Rotating convection is an experimental system showing an enhanced instability to a boundary mode (Kuo and Cross, 1993).

b. Constraints on nonlinear solutions: Rigid boundaries

Rigid boundary conditions have a strong effect on patterns, both in *perturbing* solutions of the infinite system and in *selecting* particular solutions. In large systems these effects can be studied near threshold using the am-

plitude equation with the appropriate boundary conditions. Many conceptual questions are most easily understood in this framework. Very close to threshold the restricted nonlinear solutions are conveniently calculated using a mode expansion. Beyond this very restricted region the full differential amplitude equation must be solved. Here we are particularly interested in the selection of the wave number in one-dimensional systems, and orienting effects in two dimensions.

(i) Mode expansion

For simplicity we will consider a one-dimensional system (5.2) of length L , with boundary condition (5.6), which changes both the character and the number of solutions compared to the infinite system. The solutions may be expanded in the form

$$A = \sum_n A_n \sin(n\pi x/L), \quad (5.9)$$

in terms of the linear solutions satisfying the appropriate boundary conditions. The constraints on the nonlinear solutions are thereby automatically included. Two regimes may be distinguished (Ahlers *et al.*, 1981):

- Very near threshold $\varepsilon - \varepsilon_c \lesssim \varepsilon_c$ (remember $\varepsilon_c \ll 1$ by assumption). In this regime the expansion is dominated by the lowest mode of amplitude $A_1 \sim (\varepsilon - \varepsilon_c)^{1/2}$,

$$A(x) = \sqrt{2} A_1(t) \sin(\pi x/L) + O(\varepsilon - \varepsilon_c). \quad (5.10)$$

A Landau equation for the transient evolution of A_1 can be derived by substituting (5.10) into the amplitude equation and projecting onto the $\sin(\pi x/L)$ mode:

$$\partial_t A_1 = (\varepsilon - \varepsilon_c) A_1 - \bar{g} |A_1|^2 A_1, \quad (5.11)$$

with $\bar{g} = (4/L) \int_0^L \sin^4(\pi x/L) dx = 3/2$. Note that there is a unique steady state solution $A_1 = [(\varepsilon - \varepsilon_c)/\bar{g}]^{1/2}$ except for an overall phase factor. [In fact the continuous phase symmetry is removed by higher-order terms in the amplitude equation, see subsection (ii) below]. Small inhomogeneous boundary effects or other forces rendering the bifurcation imperfect may be included through a term $f_1(t)$ on the right-hand side of Eq. (5.11). This force may be static, time dependent but determined by the details of the experiment, or stochastic (Ahlers *et al.*, 1981). In each case $f_1(t)$ is arrived at by again projecting the local forcing $f(x, t)$, which is added to Eq. (5.2), onto the first unstable mode.

- Further away from threshold, $\varepsilon \gtrsim \varepsilon_c$, but still with $\varepsilon \ll 1$. As ε increases a larger number of linear modes come into play, and the saturated solution changes from a sine function to a “top hat” shape with $|A(x)|$ constant over most of the range, as in the infinite system [Fig. 12(b)]. The number of linear modes needed grows rapidly, and the expansion in Eq. (5.9) loses its simplicity. Instead the full partial differential amplitude equation must be solved.

(ii) Wave number selection in one dimension

It turns out that the reduced amplitude near the boundaries imposed by rigid boundary conditions leads to a vastly reduced set of nonlinear solutions (as compared to the infinite system) in the bulk of the cell, far from the boundaries. In this region the solutions can be characterized by the local wave number, and only a narrow band of wave numbers exist as steady state solutions, much narrower than the ideal stability band.^{5.1}

The simplest case in which to demonstrate this effect is a semi-infinite system in one dimension, i.e., the region $x \leq 0$ with a single boundary at $x=0$, say. Then as shown by Cross *et al.* (1980, 1983a) the continuous band of solutions with $|q - q_0| \leq \varepsilon^{1/2}$ which exists in the infinite system collapses to a much smaller band

$$|q - q_0| \leq c \varepsilon, \quad (5.12)$$

where c depends on the details of the system. This large reduction in the band of wave numbers affects the behavior *arbitrarily far from the boundaries*. Continuity with the laterally infinite system is maintained not in the existence of steady state solutions, but in the time scale for these solutions to be established. Thus if the boundary conditions are changed suddenly from no-flux say, to rigid, then the restricted range of solutions is established in a region a distance L from the boundary only after the time necessary for the influence of the change to propagate over this distance. For type I_s systems this time is L^2/D with D an appropriate diffusion constant. We emphasize again that the stationary solutions are severely constrained compared with the infinite system.

Since this somewhat surprising result answers the old question of how a long system approaches the ideal infinite system, and also provides a wave-number selection mechanism to be discussed in Sec. VI.A below, we will analyze the problem in some detail here. We again start from some arbitrary microscopic U equation (3.4) with a stationary (type I_s) instability. We initially restrict ourselves to a semi-infinite system. Near threshold an amplitude equation exists in general, so we first illustrate the effect using the static form of Eq. (5.2) (i.e. $\partial_t A = 0$) and the *phenomenological* inhomogeneous boundary condition

$$A(x=0) = \lambda \varepsilon^{1/2}, \quad (5.13)$$

^{5.1}The effect of rigid boundaries in restricting the wave-number band was first noticed numerically for the Swift-Hohenberg and Kuramoto-Sivashinsky equations by Pomeau and Manneville (1980), but these authors mistakenly concluded that the selection was perfect, as did Pomeau and Zaleski (1980). The restriction to a linear band quoted in Eq. (5.12) was first obtained by Cross *et al.* (1980, 1983a) for the free-slip model of convection as well as for the order-parameter models treated by Pomeau and Manneville (1980). The model results were then derived in a simpler fashion by Pomeau and Zaleski (1981).

with λ a small parameter.^{5.2} Equations (5.2) and (5.3) may be solved perturbatively in λ (Cross *et al.*, 1983a) though in fact exact analytic solutions exist (Kramer and Hohenberg, 1984). The magnitude $|A|$ approaches saturation for $|x| \gtrsim \varepsilon^{-1/2}$. The allowed wave numbers $k = q - q_0$ of A fall in the restricted band

$$-\lambda \varepsilon^{1/2} / \sqrt{2} < k < \lambda \varepsilon^{1/2} / \sqrt{2}. \quad (5.14)$$

This restriction can be easily understood by constructing two “adiabatic invariants” for the x integration (Cross *et al.*, 1980; Pomeau and Zaleski, 1981)

$$Q = a^2 \partial_x \phi, \quad (5.15)$$

$$E = \frac{1}{2} (\partial_x a)^2 + Q^2 / 2a^2 + \frac{1}{2} \varepsilon a^2 - \frac{1}{4} a^4, \quad (5.16)$$

where

$$A(x) = a(x) e^{i\phi(x)}. \quad (5.17)$$

We can bound E using the point in the cell where a reaches its minimum value a_m :

$$E \geq Q^2 / 2a_m^2 + \frac{1}{2} \varepsilon a_m^2 - \frac{1}{4} a_m^4. \quad (5.18)$$

Analogously, if a_M is the maximum value of a , Eqs. (5.15) and (5.16) yield

$$Q^2 \leq a_M^2 a_m^2 \left[\varepsilon - \frac{1}{2} (a_m^2 + a_M^2) \right] \leq \frac{1}{2} a_m^2 \left[\varepsilon - \frac{1}{2} a_m^2 \right]^2, \quad (5.19)$$

where the last inequality is obtained by maximizing with respect to a_M . Finally, we evaluate $k = \partial_x \phi$ in the bulk where $a = a_k = \varepsilon^{1/2}(1 - k^2)$ so that

$$\begin{aligned} k &\leq [a_m / \sqrt{2} a_k] \left[\varepsilon - \frac{1}{2} a_m^2 \right] \\ &\simeq a_m / \sqrt{2} \text{ for } a_m \ll a_k, \end{aligned} \quad (5.20)$$

showing that the wave number is bounded by the smallest amplitude occurring anywhere in the cell. Physically this is reasonable, since the minimum amplitude represents a weak spot in the cell and allows the phase to unwind if the “stress” from $k \neq 0$ somewhere in the cell is too great. The behavior for k outside the band can be followed by integrating the evolution equation (5.2) in time. It is found (Cross *et al.*, 1982) that the periods are indeed eliminated in the small a region near the boundary. This local relaxation (analogous to the mechanism of the Eckhaus instability) eventually affects the wave number everywhere.

^{5.2}With homogeneous boundary conditions on the U equation the amplitude $A(0)$ at $x=0$ in fact turns out to be $O(\varepsilon)$. Thus small λ may be used to understand the behavior, although for $\lambda = O(\varepsilon^{1/2})$ terms neglected in arriving at Eq. (5.2) become important.

As discussed above, rigid boundary conditions of the form (5.4) on the U equation lead to the condition $A(0)=0$, Eq. (5.6), on the $O(\varepsilon^{1/2})$ amplitude. This corresponds to $\lambda=0$ in Eq. (5.13), so the wave-number band obtained from this calculation is

$$q = q_0 \pm 0 \times \varepsilon^{1/2} + O(\varepsilon). \quad (5.21)$$

This means that the $O(\varepsilon^{1/2})$ Eckhaus stable band is completely eliminated by the boundary condition! On the other hand taking $\lambda=O(\varepsilon^{1/2})$ suggests a band of width $O(\varepsilon)$. To calculate this band the amplitude expansion has to be taken to higher order and stationary solutions sought. The general^{5.3} form at next order is (Cross *et al.*, 1983a)

$$\begin{aligned} 0 = &\partial_x^2 A + \varepsilon A - |A|^2 A - i b_1 \varepsilon \partial_x A - i b_2 \partial_x^3 A \\ &+ i(b_3 + b_4) |A|^2 \partial_x A \\ &+ i(b_3 + b_5) A^2 \partial_x A^* + O(\varepsilon^{5/2}), \end{aligned} \quad (5.22)$$

with b_i ($i=1, \dots, 5$) numerical constants which depend on the details of the system. The boundary condition becomes

$$0 = A - \alpha \partial_x A - \beta \partial_x A^*, \quad x=0, \quad (5.23)$$

where the complex numbers α and β depend on the boundary conditions for the U equation. The solutions of (5.22)–(5.23) turn out to have bulk wave numbers restricted to the band (Cross *et al.*, 1983a)

$$k_- < k < k_+, \quad (5.24)$$

with

$$k_{\pm} = -\frac{1}{2} |\beta| (\eta \pm 1) \varepsilon, \quad (5.25a)$$

$$\eta = (\text{Im } \alpha - \gamma) / |\beta|, \quad (5.25b)$$

$$\gamma = \frac{1}{2} (2b_1 + b_2 - 2b_3 - b_4 - b_5). \quad (5.25c)$$

In a finite system the boundary conditions (5.13) or (5.23) must be applied at both ends of the sample. For convenience we let the sample length be $2L$, with boundary conditions at $x=\pm L$. Specifically, the boundary condition (5.23) becomes

$$0 = A - \alpha_{\pm} \partial_x A - \beta_{\pm} \partial_x A^*, \quad x=\pm L, \quad (5.26)$$

^{5.3}The perturbative procedure of Cross *et al.* (1983a) can be more formally (and elegantly) justified in terms of a normal form expansion (Iooss *et al.*, 1990). The variable x may be considered as a “time” coordinate and the degenerate bifurcation unfolded at $\varepsilon=0$. In fact a suitable nonlinear transformation yields a much simpler, but completely general, equation. However in actual calculations on physical systems it is probably easier to maintain a simple relationship of $A(x)$ to the microscopic variables U , so that the b_i , α , and β in Eqs. (5.22)–(5.23) can be calculated explicitly.

with $\alpha_+ = -\alpha^* = \alpha$, $\beta_+ = -\beta^* = \beta$. It should be noted that β contains a phase factor $\exp(2iq_0L)$, so that the equations "know" about the quantizing of solutions at this (but not lower) order. Then for a large system [$L \gtrsim \epsilon^{-1}$] the wave number is still restricted by the conditions (5.24) and (5.25), but the additional condition at $x = -L$ has the effect of quantizing the solutions to a finite set of values inside the band, separated by amounts of order π/L . Because of the dependence of β on q_0L the dependence of the discrete wave vectors on control parameter ϵ obtained in a finite system is rather complicated (see Cross *et al.*, 1983a). The important point, though, is that this complex behavior occurs entirely inside the $O(\epsilon)$ band given by (5.24) (see Fig. 14).

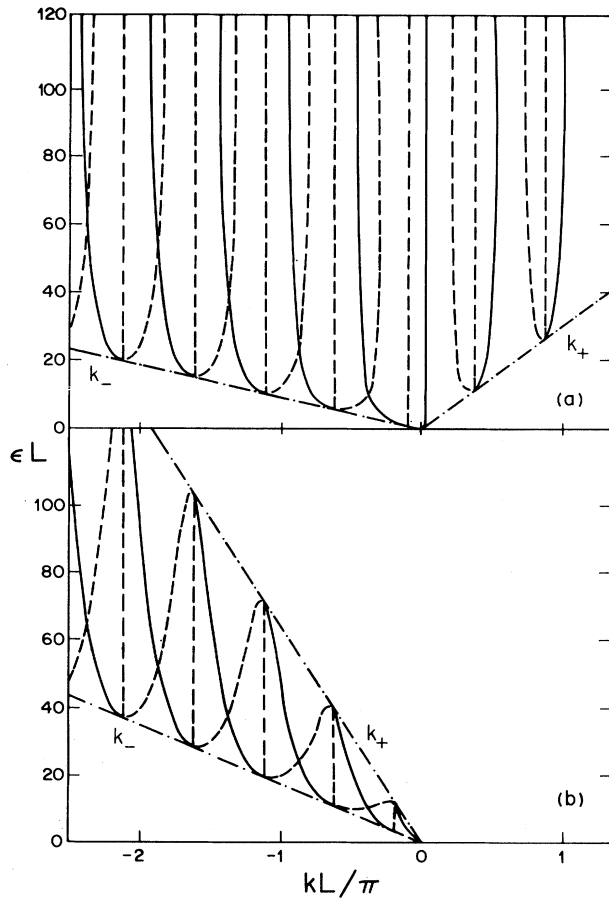


FIG. 14. Allowed wave vectors in the bulk of a one-dimensional system of size $2L$ near threshold given by solving Eqs. (5.22) and (5.26). The reduced Rayleigh number ϵ is plotted vs the deviation k of the wave vector from its critical value q_0 . Solid and dashed lines correspond to different solution branches. The dashed branches are unstable, the solid branches stable (Daniels, 1984). Dash-dotted lines are k_{\pm} from Eq. (5.25). Note that the allowed wave vectors in the finite system fall between these bounds derived for the semi-infinite system. The parameters used correspond to free-slip convection with Prandtl number $\sigma = 0.78$ and perfectly insulating rigid sidewalls in (a), and perfectly conducting rigid sidewalls in (b). (From Cross *et al.*, 1983a.)

The effect of finite geometry on the Eckhaus boundary (4.24) has been studied by Tuckerman and Barkley (1990). These authors showed that in a finite system the neutral and Eckhaus curves are no longer tangent, but are parabolas that intersect at two points with the Eckhaus line below the neutral one. Experimental manifestations of these effects are noted in Sec. IX.B.2.c below.

(iii) Orientational effects in two dimensions

In large two-dimensional geometries we must also consider the direction of the local wave vector, and in particular how it is affected by the boundaries. Empirically in Rayleigh-Bénard convection a rather strong tendency is observed for the rolls to come in normal to the walls (i.e., \mathbf{q} parallel to the wall). This result may be partly understood from the linear analysis of the onset in a rectangular box, since with rigid boundaries the first unstable mode has rolls perpendicular to the long side of the box (Davis, 1967). The argument may be extended to the weakly nonlinear regime by considering how the amplitude approaches zero at a plane boundary. Cross (1982b) showed that any angle of approach of the rolls is possible. However the healing length near the wall over which the rolls are suppressed is $\epsilon^{-1/2} \cos\theta$ (for θ not too near $\pi/2$) with θ the angle between \mathbf{q} and the normal $\hat{\mathbf{s}}$. If we define a surface contribution to the Lyapunov potential (4.9) for the amplitude equation, this quantity is minimized when the healing length is shortest, i.e., by $\theta \rightarrow \pi/2$. [In this limit the healing length depends only on the fourth order y derivatives in Eq. (4.13) and becomes $O(\epsilon^{-1/4})$.] However since variation of θ affects the state arbitrarily far away from the surface it is not obvious that this motion will occur until we consider the pattern as a whole. Pomeau and Zaleski (1981) showed that for rolls parallel to a *plane* boundary there is a linear instability towards nucleation of a normal set of rolls in the boundary layer, but again in a finite system this may be suppressed by other sidewalls or by the curvature of the surface. This brings us to the global question of pattern selection in two dimensions, which we defer to Sec. VI.

Both of the above arguments (the linear analysis and the Lyapunov function) rely on general features that follow from the symmetry of the system, rather than on any detailed properties of the equations. In each case the crucial element is that near threshold rapid spatial variation is preferred along the rolls rather than perpendicular to them. In addition, in these limits a global meaning can be given to the statement "the rolls want to approach the wall normally," using either the lowest linear mode or the Lyapunov function. Further away from threshold it is not clear that either of these concepts still apply, and the preference for normal rolls relies in the end on evidence from experiment and numerical simulations.

An extra complication that has not been fully incorporated into our arguments was found by Zaleski *et al.* (1984) who noted that solving the amplitude equation in the $O(\epsilon^{1/4})$ healing layer near normal incidence yields a

curvature to the rolls in this region, so that the optimum approach angle for the rolls in the bulk differs from $\pi/2$ by an amount of order $\epsilon^{1/4}$. There is perhaps some evidence for this in numerical simulations of the Swift-Hohenberg equation by Greenside and Coughran (1984) and in experiments by LeGal (1986) shown in Fig. 41 below, but the general applicability of this result is not understood.

2. Type III₀: Oscillatory uniform

Little theoretical work has been done on boundary effects for the oscillatory uniform case. In part this is due to the paucity of controlled studies of boundaries in the corresponding experimental systems (chemical waves, excitable biological media). Boundaries can act as sources, sinks or reflection sites for waves and defects (see Sec. V.B below). The only study we are aware of which is based on amplitude or phase equations is the work of Riecke and Kramer (1985) who considered Eq. (4.90) for $x < 0$ with the surface boundary condition

$$\partial_x \phi = -G/\alpha, \quad x=0. \quad (5.27)$$

Then depending on the sign of $G\beta$ [where β is the coefficient appearing in Eq. (4.90)] they found either a disturbance propagating into the bulk (for $G\beta > 0$), or a weak disturbance localized near the surface (for $G\beta < 0$).

3. Type I₀: Oscillatory periodic

The effects of boundaries turn out to be very important in type I₀ systems because the instability, at least at a supercritical bifurcation, is always *convective* in the infinite system due to the propagation of disturbances at the group velocity s_0 (see Sec. III.A.2). It is therefore only the *reflecting* properties of the boundaries that cause a perturbation in the finite system to grow locally in this regime. Let us characterize the boundaries by a reflection coefficient r for linear waves, defined as the ratio of amplitudes of a reflected wave to that of an incoming wave of constant magnitude and critical wave number at threshold (Cross, 1986b). Then we can estimate the threshold of the instability ϵ_c in a finite system by balancing the growth of the disturbance with the growth rate ϵ_c over one traverse of the length $2L$ of the cell, with the loss in amplitude due to reflection (we assume $|r| < 1$)

$$|r| e^{2\epsilon_c L/s_0} = 1, \quad (5.28)$$

with s_0 the group velocity of the waves and L/s_0 the traversal time. Equation (5.28) gives

$$\epsilon_c = s_0 (2L)^{-1} \ln(1/|r|), \quad (5.29)$$

i.e., a shift for large L which is $O(L^{-1})$ rather than $O(L^{-2})$ as in the stationary case, Eq. (5.8). Also, this result gives ϵ_c diverging as $|r| \rightarrow 0$. Actually we would then expect $\epsilon_c = O(1)$, where the instability becomes ab-

solute, as discussed by Zaleski *et al.* (1985). [These authors used the linearized amplitude equation but with boundary conditions $A_R = A_L = 0$ to determine ϵ_c .] Equation (5.29) gives the leading term in L^{-1} , but there will also be quadratic corrections for smaller L .

The onset mode in a large system can be easily found by using the amplitude equations (4.59). Since the diffusive terms play a secondary role in the structure of the solution we may write (Cross and Kuo, 1992)

$$A_R(x, t) = a_R e^{\epsilon x/s_0} e^{i(kx - \Omega_k t)}, \quad (5.30a)$$

$$A_L(x, t) = a_L e^{-\epsilon x/s_0} e^{i(-kx - \Omega_k t)}, \quad (5.30b)$$

with A_R and A_L related at the ends $\pm L$ by

$$A_L(L) = r e^{2iq_0 L} A_R(L), \quad (5.31a)$$

$$A_R(-L) = r e^{-2iq_0 L} A_L(-L). \quad (5.31b)$$

This leads to Eq. (5.29) together with $a_R = \pm a_L$ and an expression for $k = O(L^{-1})$ given by a phase matching condition

$$2(q_0 + k)L + \phi_r = n\pi, \quad (5.32)$$

$$a_R = a_L, \quad n \text{ even}, \quad (5.33a)$$

$$a_R = -a_L, \quad n \text{ odd}, \quad (5.33b)$$

where ϕ_r is the phase of r . The shift in wave number k will lead to a change in the onset frequency and $O(L^{-2})$ corrections to ϵ_c , whose calculation however requires the reinstatement of the diffusive terms in the amplitude equation. The discrete set of k defined by Eq. (5.32) will usually lead to a single mode with the smallest ϵ_c , which is seen from Eqs. (5.30) to be in the form of counterpropagating traveling waves, with the amplitude of right-moving waves large in the right-hand end of the system and left-moving waves dominant in the left half. For particular values of L two modes will be degenerate at threshold, and their superposition will lead to a beating phenomenon (Kolodner *et al.*, 1989).

It should be noted that this calculation has sidestepped the difficulties in the type I₀ amplitude equation discussed below Eq. (4.61), since the short healing length region near the ends is not described in Eqs. (5.30) but rather is parametrized by the reflection coefficient r .

To obtain an estimate of the reflection coefficient from the amplitude equation we generalize the type of boundary conditions used in the stationary case, assuming again that the sidewalls suppress the instability. In a one-dimensional situation the general homogeneous linear boundary conditions consistent with the symmetries $x \rightarrow -x$, $A_R \leftrightarrow A_L$ are

$$A_R - \alpha_{\pm} \partial_x A_R - \beta_{\pm} \partial_x A_L = 0 \quad (5.34a)$$

$$A_L + \alpha_{\pm} \partial_x A_L + \beta_{\pm} \partial_x A_R = 0 \quad (5.34b)$$

with $\alpha_{\pm}, \beta_{\pm}$ dependent on the underlying microscopic boundary conditions. It is easy to solve the linear problem of an incoming right-moving wave of unit magnitude and an outgoing left-moving wave at $x = +L$ near threshold. Setting

$$A_R = 1 + a_1 e^{-(L-x)/\xi_s}, \quad (5.35a)$$

$$A_L = r, \quad (5.35b)$$

$$\xi_s = (1 + i c_1) / s_0, \quad (5.35c)$$

where the second term in (5.35a) represents a correction with amplitude a_1 , localized at the endwall, we find the reflection coefficient

$$r \approx s_0 \beta_- (1 + i c_1)^{-1}, \quad (5.36)$$

for small $\alpha_{\pm}, \beta_{\pm}$. However we emphasize that unless s_0 is small, so that ξ_s is much larger than the basic length scale of the problem, treating the boundary region within the amplitude equation formalism is not consistent. If s_0 is not small we have a complicated problem at the boundary (with both nonlinearity and rapid spatial variation) which has not yet been solved, although the linear problem has been studied for the free-slip case by Cross and Kuo (1992).

As in the type I_s system a mode truncation scheme may be used very near threshold. At lowest order this simply yields the nonlinear saturation of the counterpropagating waves represented by Eqs. (5.30). This calculation yields (Cross and Kuo, 1992) $|a_R| = |a_L| = a$ with

$$a^2 = \frac{4L}{s_0(|r|^{-1} - |r|)} \frac{(\epsilon - \epsilon_c)}{(1 + g_1)}. \quad (5.37)$$

Notice that if instead we had assumed an inverted bifurcation in the infinite system, the coefficient $(1 + g_1)^{-1}$ in (5.37) would become $(g_1 - 1)^{-1}$. Thus if $g_1 > 1$ the instability will be supercritical in the finite geometry, even though it is subcritical in the infinite geometry. This is clearly related to the strong standing wave component of the onset solution in the finite geometry.

The mode truncation may be extended to dynamic states in particular simple limits. Dangelmayr *et al.* (1991) have studied the limit of small group speed $s_0 = O(L^{-1})$, perturbing in the small reflection amplitude. Dangelmayr and Knobloch (1991) perform a normal forms analysis of the resulting coupled *ode*'s. Knobloch and de Luca (1992), on the other hand, look at the limit $r \rightarrow 1$. An interesting feature of these calculations is the extreme sensitivity of the periodic or chaotic states to the system size via the parameter Lq_0 , reminiscent of the beating states in the linear analysis.

B. Defects and coherent structures

1. Introduction

An important element in the structure and formation of real patterns is the existence of well-defined local

structures or “defects” in or at the edges of regions that otherwise approximate quite well an ideal pattern. These local structures may have a topological origin, as outlined in Sec. IV.B, in which case topological arguments are useful to *motivate* the search for solutions with particular geometries and to suggest their *stability*. On the other hand, as mentioned earlier, many important local structures do not have topological significance. Since the theory and phenomenology of both types of local structures follow similar lines we will consider them together. The defects we will study are often referred to as “coherent structures,” a term which emphasizes the local perturbation rather than the background in which it is embedded.

We will divide the discussion into two parts. First (subsection V.B.2) we discuss the structure of stationary defects, or of uniformly moving defects for which we can make the replacement $\partial_t \rightarrow \mathbf{v} \cdot \nabla$. In these cases the problem reduces to the solution of an ordinary differential equation (*ode*) in one dimension, or to a purely spatial partial differential equation (*pde*) in higher dimensions. We then (subsection V.B.3) discuss the motion of defects caused by various perturbations. (The above division is not a clean one, since sometimes it is convenient to calculate uniformly moving defects perturbatively starting from the stationary solutions.)

An important feature of the search for local defect solutions (stationary or uniformly moving) is that their existence places *constraints* on the background pattern arbitrarily far away from the defect, where the latter produces negligible distortions from an ideal state. Thus, for example, demanding a stationary dislocation in a type I_s pattern such as a Rayleigh-Bénard roll structure fixes the background wave number of the ideal pattern far away. Defects may therefore provide an important pattern *selection* mechanism, as discussed in Sec. VI below.

2. Structure of defects

We first briefly review the principles of calculation of the structure of defects, leaving the details to the discussion of specific examples.

a. Calculation methods

(i) Far-field calculations

As discussed earlier, topological defects may be characterized by a winding number in a generalized phase variable:

$$\int_C \nabla \phi \cdot d\ell = 2n\pi, \quad (5.38)$$

where C is any contour surrounding the defect. If C is taken at large distances where the deviations from the ideal pattern are on a slow spatial scale, this equation together with the phase equation may be used to fully cal-

culate the far field of a stationary or uniformly moving defect. The dislocation defect discussed in subsection V.B.2.c below provides a good illustration of this method. The phase description breaks down at small distances, however, where Eq. (5.38) implies rapid variations, and a more complete description is in principle required. Often this core region can be parametrized simply in terms of a core size r_c .

It should be clear that this approach is only useful for defects in a continuous symmetry variable: defects resulting from a discrete broken symmetry (such as parity) are not characterized by a phase variable.

(ii) Phase-space methods

In systems that are effectively one dimensional, the calculation of defect solutions can be formally reduced to a problem in dynamics, where the “time” is the continuous dimension of spatial variation. Examples are point defects in one spatial dimension, line defects in two dimensions, or point defects in two dimensions in cases where one direction can be eliminated by symmetry (e.g., for an axisymmetric defect only the radial coordinate need be considered). In such cases the defect solution appears as an orbit in a phase space defined by a finite set of *ordinary* differential equations, whose number is determined by the order of the starting partial differential equation in the spatial variable (see Howard and Kopell, 1977; Kopell and Howard, 1981). Besides the obvious simplification of reducing a *pde* to a finite set of *ode*'s, this reformulation allows use of powerful qualitative methods from dynamical systems theory to obtain various results without numerical calculation. As illustrated below, phase space methods are particularly useful when the ideal states appear as fixed points, and defects are heteroclinic or homoclinic orbits joining these fixed points. The real and complex Ginzburg-Landau equations (4.13) and (4.49), as well as their generalizations (Sec. III.C.2.d) are notable examples where this is the case, and a rather general enumeration of the types and multiplicities of simple defect solutions can be given for these systems (see subsection V.B.2.b below). Besides such simple defects one can look for limit cycles of the *ode* which may represent periodic patterns or nonlinear wave trains, characterized by a dispersion relation $\omega(q)$, or chaotic orbits which represent spatially disordered states.

A severe drawback of these methods, on the other hand, is that the stability of the solutions under the (physical) time evolution of the original *pde* is not tested, so that a great deal of effort may be expended calculating appealing but unstable, and therefore physically irrelevant, solutions. The questions of stability and accessibility under the physical dynamics (i.e., the basin of attraction) must always be considered in discussions of possible solutions obtained from phase-space methods. Some information on stability can be obtained using perturbative methods.

(iii) Special solutions

Calculating the structure of defects may be easier in special limits or at special points in parameter space where there are extra *symmetries* or additional *conservation laws* which make a reduced analysis possible. An example of a special limit is the calculation of dislocations in the lowest-order amplitude equation. Special points are also a useful tool for understanding fronts and pulses in the generalized complex Ginzburg-Landau equation discussed in subsection V.B.2.b.(v) below.

(iv) Perturbation methods

When a particular solution to an equation is known it is often possible to calculate nearby ones using perturbation methods. For example, perturbing away from the dislocation solution of the lowest-order amplitude equation by adding the next order terms in $\epsilon^{1/2}$ yields the structure and wave number selected by the stationary dislocation at order ϵ , which turns out to be nontrivial. For example the case of (Darcy-Rayleigh) convection in a porous medium for which $q_0 = \pi$ was calculated by Pomeau *et al.* (1983) who found^{5,4}

$$q_d = q_0 + \alpha\epsilon, \quad \alpha = 1.04. \quad (5.39)$$

The methods used for this type of calculation will be discussed in the section on dynamics (subsection V.B.3.a).

Another example occurs in the Ginzburg-Landau model, which leads to an integrable dynamical system in certain limiting cases. Then the defects or coherent structures can be found analytically and they form a continuous family indexed by their velocity and/or their frequency. Perturbing away from these limits we find a discrete set of solutions, which can often be divided into a stable and an unstable subset. A well-known example of this phenomenon is the perturbation of the nonlinear Schrödinger equation by small dissipative terms (see, e.g., Kivshar and Malomed, 1989).

b. One-dimensional defects

(i) Classification of defect solutions: Coherent structures

We have seen in Sec. IV that pattern forming systems possess finite amplitude “ideal” solutions which are characterized by a wave vector and/or a frequency. In one dimension defects can be created by the spatial juxtaposition of different types of ideal solutions and of the zero amplitude solution. We shall define three classes of such coherent structures which can be considered ele-

^{5,4}These authors had a different definition of ϵ . We have rewritten their expression with $\epsilon = (R - R_c)/R_c$, $R_c = 4\pi^2$.

mentary defects, treating first systems where the uniform $U=0$ state plays a special role (see van Saarloos and Hohenberg, 1992 and references therein).

• **Fronts**, which consist of a finite amplitude ideal state at one end ($x \rightarrow -\infty$, say) and the zero amplitude state at the other ($x \rightarrow +\infty$).

• **Pulses**, which have the zero amplitude state at both ends and nonzero amplitude in a localized region.

• **Domain boundaries**, formed by the juxtaposition of two finite-amplitude states.

For moving fronts one distinguishes between “positive” and “negative” cases depending on whether the nonzero-amplitude state invades the zero-amplitude state or vice versa. For domain boundaries whose ideal states have group velocities of opposite sign one distinguishes between “sources” with outgoing velocity vectors, and “sinks” with incoming ones.^{5.5} In two dimensions, when the solutions on either side are stationary periodic states of different orientations, the domain boundaries are called grain boundaries. In this case there is also y variation (periodic or quasiperiodic), but it is usually easily described.

In the absence of symmetry the zero amplitude state is not singled out, and the above distinctions between different types of structures are less sharp. We will call a front a structure joining two states of unequal amplitude, at least one of which is uniform. A pulse, on the other hand, has uniform states of roughly equal amplitude on either side, while sources and sinks involve periodic wave states.

For the one-dimensional case with symmetry it is convenient to begin with the generalized Ginzburg-Landau model introduced in Sec. III.C.2 above.

(ii) The generalized Ginzburg-Landau model

Consider the equation

$$\begin{aligned} \partial_t A = & (b_1 + i c_1) \partial_x^2 A + f_1(|A|^2) A \\ & + \partial_x [f_2(|A|^2) A] + [\partial_x f_3(|A|^2)] A, \end{aligned} \quad (5.40)$$

where

$$f_\ell(y) = f_{\ell r}(y) + i f_{\ell i}(y), \quad \ell = 1, 2, 3, \quad (5.41)$$

are complex functions of their argument, which are arbitrary for the moment (we typically will consider low-order polynomials). This includes the type I_s amplitude equation (5.2) as a special case. For the sake of uniformity we will refer to the ideal states as “waves.”

(a) The dynamical system

Let us restrict ourselves to a particular class of solutions of Eq. (5.40), the so-called “uniformly translating” solutions, given by the ansatz

$$A(x, t) = e^{-i\omega t} \hat{A}(\xi), \quad (5.42a)$$

$$\xi = x - vt, \quad (5.42b)$$

$$\hat{A}(\xi) = a(\xi) e^{i\phi(\xi)}, \quad (5.42c)$$

where v and ω are arbitrary real constants. Insertion of (5.42) into (5.40) leads to a system of *ode*'s for the variables

$$a(\xi), \quad (5.43a)$$

$$q(\xi) = \partial_\xi \phi, \quad (5.43b)$$

$$\kappa(\xi) = \partial_\xi a / a, \quad (5.43c)$$

which takes the form^{5.6} (see van Saarloos and Hohenberg, 1992, and references therein)

$$\partial_\xi a = \kappa a, \quad (5.44a)$$

$$\partial_\xi q = Q(a, q, \kappa), \quad (5.44b)$$

$$\partial_\xi \kappa = \mathcal{K}(a, q, \kappa), \quad (5.44c)$$

with

$$Q = -\tilde{b}_1 \omega + \tilde{c}_1 v \kappa - \tilde{b}_1 v q - 2 \kappa q$$

$$\begin{aligned} & + \tilde{c}_1 [f_{1r} + 2(f'_{2r} + f'_{3r}) \kappa a^2 + f_{2r} \kappa - f_{2i} q] \\ & - \tilde{b}_1 [f_{1i} + 2(f'_{2i} + f'_{3i}) \kappa a^2 + f_{2i} \kappa + f_{2r} q], \end{aligned} \quad (5.45a)$$

$$\begin{aligned} \mathcal{K} = & -\tilde{c}_1 \omega - \tilde{b}_1 v \kappa - \tilde{c}_1 v q - \kappa^2 + q^2 \\ & - \tilde{b}_1 [f_{1r} + 2(f'_{2r} + f'_{3r}) \kappa a^2 + f_{2r} \kappa - f_{2i} q] \\ & - \tilde{c}_1 [f_{1i} + 2(f'_{2i} + f'_{3i}) \kappa a^2 + f_{2i} \kappa + f_{2r} q], \end{aligned} \quad (5.45b)$$

$$\tilde{b}_1 = b_1(b_1^2 + c_1^2)^{-1}, \quad \tilde{c}_1 = c_1(b_1^2 + c_1^2)^{-1}. \quad (5.45c)$$

The coupled set (5.44) can be considered formally as a *dynamical system* in the pseudo-time variable ξ . Fixed points and trajectories in the phase space of this dynamical system will correspond to different uniformly translating solutions of the original *pde* (5.40). Most of our discussion will refer to the complex Ginzburg-Landau equation obtained by setting

$$f_1 = \epsilon - (b_3 - i c_3) a^2 - (b_5 - i c_5) a^4, \quad f_2 = f_3 = 0, \quad (5.46)$$

in (5.45), for which

^{5.5}The nomenclature for one-dimensional defects is quite inconsistent in the literature: fronts are sometimes called kinks or shocks, pulses are referred to as solitons or *s*-waves, and domain boundaries are known as fronts, pulses, shocks, sources, targets, sinks, holes, or kinks.

^{5.6}The parametrization in terms of the three variables a, κ, q becomes singular for solutions in which $a(\xi)$ has zeros. In that case a four-variable system, involving $\text{Re } A$, $\text{Im } A$, $\text{Re } \partial_x A$, $\text{Im } \partial_x A$, say, should be used (see Landman, 1987).

$$\begin{aligned} Q &= -\tilde{b}_1(\omega + vq + c_3a^2 + c_5a^4) \\ &\quad + \tilde{c}_1(v\kappa + \varepsilon - b_3a^2 - b_5a^4) - 2\kappa q , \end{aligned} \quad (5.47a)$$

$$\begin{aligned} \mathcal{K} &= -\tilde{b}_1(v\kappa + \varepsilon - b_3a^2 - b_5a^4) \\ &\quad - \tilde{c}_1(\omega + vq + c_3a^2 + c_5a^4) + q^2 - \kappa^2 . \end{aligned} \quad (5.47b)$$

We first consider fixed points, which are determined by the conditions

$$\partial_\xi a = \partial_\xi q = \partial_\xi \kappa = 0 . \quad (5.48)$$

These are of two types. First, finite amplitude solutions, which we refer to as "nonlinear," and are characterized by

$$a_N = \text{const}, \quad q_N = \text{const}, \quad \kappa_N = 0 , \quad (5.49)$$

where a_N and q_N are easily calculated as functions of the parameters. This N fixed point corresponds to a plane wave in the original equation (5.40), namely

$$A(x, t) = a_N e^{i[q_N x - (\omega + q_N v)t]} . \quad (5.50)$$

Second, zero-amplitude or "linear" solutions of the form

$$q_L = \text{const}, \quad \kappa_L = \text{const}, \quad a_L = 0 , \quad (5.51)$$

which correspond to evanescent waves in the original equation.

(β) Coherent structures

One-dimensional defects can now be constructed by finding (heteroclinic) trajectories in the phase space of (5.44), i.e., trajectories that join the various fixed points. The three types of simple defects defined above can now be identified (see Fig. 15).

- *Fronts* joining N and L fixed points.
- *Pulses* joining different L fixed points.
- *Domain boundaries* joining different N fixed points.

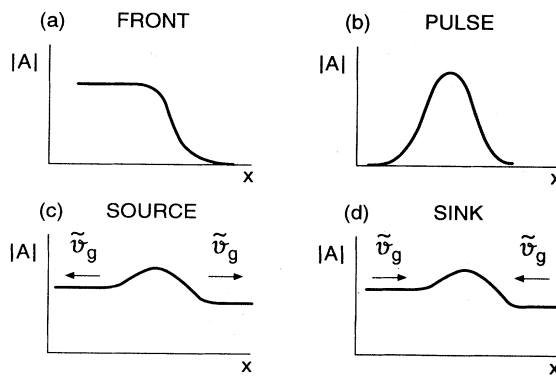


FIG. 15. Schematic sketch of various one-dimensional coherent structures: (a) front; (b) pulse; (c) and (d) domain boundaries of source and sink type, respectively. The quantity \tilde{v}_g is the group velocity of the nonlinear state in the frame moving with the structure [see Eq. (5.62a)].

The condition for the existence of a heteroclinic trajectory is that the stable and unstable manifolds of the fixed points in question should join up. Applying this condition we find predictions for the *multiplicity* of defect solutions as ω and v are varied for fixed parameter values, i.e., predictions of n -parameter continuous families or discrete sets of solutions. It should be emphasized, of course, that such arguments do not prove the existence or nonexistence of solutions, only the possibility of finding nearby solutions if one is known to exist. We shall illustrate the power of counting arguments in paragraph (iii) below.

Besides fixed points and heteroclinic orbits there are also more complicated trajectories such as limit cycles or chaotic orbits (Holmes, 1986; Landman, 1987). Certain limit cycles correspond to nonlinear waves in the original equation (5.40) whose wavelength λ is determined by the period of the limit cycle. If the limit cycle passes near a pair of fixed points the nonlinear wave can be thought of as the spatial juxtaposition of an infinite set of pulses or domain boundaries.

(iii) Multiplicity of solutions

We now wish to analyze the dynamical system (5.44) in various special cases in order to show how the stability of the N and L fixed points determines the multiplicity of defect solutions.

(a) Fronts

Let us begin with the *real* amplitude equation, namely (5.40) and (5.46), with $c_1 = c_3 = c_5 = b_5 = 0$ and $b_3 > 0$. This means we may choose $b_1 = b_3 = 1$. Restricting ourselves first to *real* solutions, which requires picking $\omega = 0$, we obtain

$$\partial_\xi^2 a + v \partial_\xi a + \varepsilon a - a^3 = 0 , \quad (5.52)$$

for uniformly translating solutions. The phase-space equations are

$$\partial_\xi a = \kappa a , \quad (5.53a)$$

$$\partial_\xi \kappa = -v\kappa - \varepsilon + a^2 - \kappa^2 , \quad (5.53b)$$

i.e., the wave vector q does not appear. The nonlinear fixed point N exists for $\varepsilon > 0$ and is given by

$$a_N^2 = \varepsilon , \quad (5.54a)$$

$$\kappa_N = 0 , \quad (5.54b)$$

and the linear fixed points $L_{1,2}$ for $v > v^* = 2\varepsilon^{1/2}$ by

$$L_1 : a_L = 0 , \quad \kappa_{L1} = \frac{1}{2}(-v - \sqrt{v^2 - 4\varepsilon}) , \quad (5.55a)$$

$$L_2 : a_L = 0 , \quad \kappa_{L2} = \frac{1}{2}(-v + \sqrt{v^2 - 4\varepsilon}) , \quad (5.55b)$$

corresponding to the two possible exponential decay rates

in the tails. The phase plane structure is illustrated in Fig. 16(a) for fixed $\varepsilon > 0$, and v .

We now need to ask whether it is possible to find a trajectory that leaves N and arrives at L_1 or L_2 , i.e., how many parameters (v, ε, \dots) must be tuned for this to happen. Clearly, from Fig. 16(a) the trajectory must leave N along the unique direction of the unstable manifold. Since L_2 has no unstable directions, we would expect this trajectory to approach L_2 without tuning parameters. Thus for $v > v^*$ we find a continuum of front solutions corresponding to a heteroclinic trajectory leaving N along the single unstable direction and arriving at the attractive fixed point L_2 . In addition the phase space method allows for a *particular* or *discrete set* of velocities v , with v adjusted so that the unique trajectory leaving N approaches L_1 along its stable manifold. (This requires tuning the amplitude of the unstable eigenvector in the trajectory approaching L_1 to zero, i.e., a one-parameter tuning, here v .) The discrete set turns out not to exist for Eq. (5.52), but it exists and plays an important role in modified equations, e.g., the equivalent one for a subcritical bifurcation treated below. For $v < v^*$ the linear fixed points are complex, i.e., they involve the variable q , but the dynamical system (5.53), as well as its extension to include $q(\xi)$, does not describe the real front solutions of (5.52) that exist in this range [see subsection (iv) below]. In view of the continuum of front solutions with $v > v^*$, which are obtained by our arguments, the question naturally arises as to which front is selected in the common experimental situation where the stable $a^2 = \varepsilon$ state in-

vades the unstable $a=0$ state starting from a localized perturbation. This important selection question has been the subject of an enormous amount of work, and it will be discussed in Sec. VI.B below.

It is interesting to study the existence of front solutions as extra complications are added. We consider first the real equation for a subcritical bifurcation (i.e., we change the sign in front of a^3 and add an a^5 stabilizing term) and we still restrict our attention to real solutions,

$$\partial_\xi^2 a + v \partial_\xi a + \varepsilon a + a^3 - a^5 = 0. \quad (5.56)$$

The fixed-point structure has the same form as in Fig. 16(a) for $\varepsilon > 0$, but now for $\varepsilon < 0$ it takes the form shown in Fig. 16(b). Since L_1 and L_2 now both have one unstable direction the continuous family of fronts disappears, and there is a unique front (or a discrete set) corresponding to the specific value or values of v for which the unstable manifold of N joins the stable manifold of L_1 (this is the fixed point relevant for a positive front where N invades L and $\kappa < 0$). As ε is raised through zero this discrete set of fronts continues to exist, and in addition the continuous family develops in the same way as for the supercritical case shown in Fig. 16(a).

If we now look for *complex* solutions we must allow for a nonzero frequency ω . For complex solutions of the real cubic amplitude equation [(5.40) and (5.46) with $c_1 = c_3 = b_5 = c_5 = 0$] we can seek fronts producing states with finite wave number $q_N = -\omega/v$. This case was considered by Ben Jacob *et al.* (1985) who found that the continuous family that exists for $\omega=0$ persists when $\omega \neq 0$, so that the real equation with complex solutions in fact has a *two parameter* family of front solutions determined by v and ω (or q_N).

The generalization of the above arguments to the complex Ginzburg-Landau equation has been worked out by van Saarloos and Hohenberg (1992), specifically for the case of a subcritical bifurcation where (5.46) becomes (for $b_1 = b_3 = b_5 = 1$, a choice which is always allowed by appropriate scaling of the equation)

$$\begin{aligned} \partial_t A = & \varepsilon A + (1+ic_1) \partial_x^2 A + (1+ic_3) |A|^2 A \\ & -(1-ic_5) |A|^4 A. \end{aligned} \quad (5.57)$$

It turns out that the counting arguments based on the stability of the N and L fixed points allow a rather large multiplicity of front solutions. The basic idea remains that the fronts associated with L_2 form a continuous family (with 1, 2, or 3 parameters), and the fronts associated with L_1 form a discrete set. Clearly, with such a large allowed multiplicity of front solutions one must ask which ones are realized as orbits of the dynamical system (5.44), and more importantly, which ones are realized as persistent solutions in the dynamics of the pde (5.57). This *selection problem* is once again deferred to Sec VI.B. At this stage we may merely remark that some information about stability already follows from the properties of the N state created behind the front. Indeed, if this state is itself unstable, to Eckhaus or Benjamin-Feir instabilities

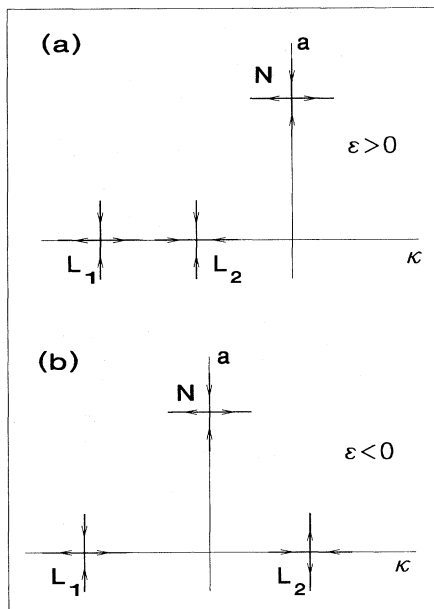


FIG. 16. Phase-plane structure in the a, κ plane for the real amplitude equations (5.52) and (5.56), showing a nonlinear fixed point N , two linear fixed points L_1, L_2 and their stable and unstable directions. (a) $\varepsilon > 0$, Eq. (5.52). (b) Same as in (a) but for the subcritical case (5.56) and for $\varepsilon < 0$.

ties (see Sec. IV.A.1.c), then the front will not be a uniformly translating solution. Nevertheless, a time-dependent front may well be found, with a time-averaged velocity whose value is well approximated by v . Another, more subtle instability of the front due entirely to the properties of the N state occurs if the group velocity of that state (in the moving frame) is *positive*. In that case a small disturbance far behind the front will eventually outrun the leading edge (see van Saarloos and Hohenberg, 1992). The condition for a positive group velocity [see Eq. (5.59) below] is related, but not identical, to the Benjamin-Feir criterion (4.57).

(β) Pulses

Since pulses are represented by $L \rightarrow L$ orbits of the dynamical system the counting argument does not differentiate between Eqs. (5.52) and (5.56) since it only involves the linear part of the equation. The orbit must originate at a fixed point with $\kappa_L > 0$ (for $\xi \rightarrow -\infty$) and end at one with $\kappa_L < 0$ ($\xi \rightarrow +\infty$), so in the real equation it can only exist for $\epsilon < 0$ [see Fig. 16(b)]. Moreover, in order for the orbit to end up at L_1 a parameter must be adjusted, so pulses only exist for discrete velocities. By symmetry it can be shown that if a pulse with velocity v exists then there is also one with velocity $-v$, so in general the stationary ($v=0$) pulse belongs to the discrete set.^{5.7}

For the complex Ginzburg-Landau equation (5.57) van Saarloos and Hohenberg (1992) show that a pair of linear fixed points $L_{1,2}$ with $\kappa_{L1} < 0$, $\kappa_{L2} > 0$ exists for $\epsilon > 0$ also. Thus counting allows a discrete set of pulses for both $\epsilon < 0$ and $\epsilon > 0$, and the stationary pulse ($v=0$) is again in general allowed by symmetry (see footnote 5.7).

(γ) Sources and sinks

We begin by discussing domain boundaries in the generalized Ginzburg-Landau model (5.40) with arbitrary $f_1(|A|^2)$ but $f_2=f_3=0$ (van Saarloos and Hohenberg, 1992; see also Malomed, 1984). The N fixed-point parameters are given by

$$b_1 q_N^2 - f_{1r}(a_N^2) = 0 , \quad (5.58a)$$

$$\omega + v q_N - c_1 q_N^2 - f_{1i}(a_N^2) = 0 . \quad (5.58b)$$

Let us confine ourselves to the stable branch of (5.58a),

^{5.7}More precisely, we can state that if a stationary ($v=0$) pulse exists for one value of the parameter ϵ in Eq. (5.56), it will in general persist as a stationary pulse in a neighborhood of that parameter value. Moving pulses ($v \neq 0$), on the other hand, have a velocity whose value in general depends on ϵ . For Eq. (5.57) which has more parameters, the same remarks apply to the dependence of v on any of the parameters.

i.e., assume that this equation can be inverted to give

$$a_N^2 = f_{1r}^{-1}(b_1 q_N^2) . \quad (5.58c)$$

Then we define the group velocity of the waves in the frame moving with velocity v by

$$\begin{aligned} \bar{v}_g &= (\partial \omega / \partial q_N)_v \\ &= -v + 2c_1 q_N - 2b_1 q_N f'_{1i} / f'_{1r} , \end{aligned} \quad (5.59)$$

where the prime denotes the derivative with respect to the argument a^2 . Consider an orbit $N_1 \rightarrow N_2$ joining two N fixed points. From Eqs. (5.58a) and (5.58b) we find, assuming $q_{N1} \neq q_{N2}$,

$$v = c_1(q_{N1} + q_{N2}) - \left[\frac{f_{1i}(a_{N1}^2) - f_{1i}(a_{N2}^2)}{q_{N1} - q_{N2}} \right] . \quad (5.60)$$

Equations (5.59) and (5.60) thus express v and \bar{v}_g in terms of the wave vectors q_{N1} and q_{N2} of the fixed points alone. For the cubic case

$$f_1 = \epsilon - (b_3 - i c_3) a^2 , \quad (5.61)$$

we find

$$v = (c_1 + b_1 c_3 / b_3)(q_{N1} + q_{N2}) , \quad (5.62a)$$

$$\bar{v}_{g1} = (c_1 + b_1 c_3 / b_3)(q_{N1} - q_{N2}) = -\bar{v}_{g2} . \quad (5.62b)$$

It follows that for this case any domain boundary is either a source ($\bar{v}_{g2} > 0$, \longleftrightarrow), a sink ($\bar{v}_{g2} < 0$, $\rightarrow\leftarrow$), or a homoclinic structure where the nonlinear states on either side are identical [$\rightarrow\rightarrow$, $q_{N1} = q_{N2}$, $\bar{v}_{g1} = \bar{v}_{g2}$, but Eq. (5.62) does not hold]. In this case it can be shown that for small v sources form a discrete set and sinks a continuous family. For the general case represented by (5.59) and (5.60) there are (moving) domain boundaries that are neither sources nor sinks, nor homoclinic structures, i.e., they have unequal group velocities with the same sign. For example, in the quintic equation it can be shown that domain boundaries are again necessarily either sources or sinks for small enough^{5.8} $|v|$, and that sinks form a continuous family indexed by v , and sources form a discrete set. For larger^{5.8} $|v|$ on the other hand, there is a possibility of families of sources also, as well as more general domain boundaries with $|\bar{v}_{g1}| \neq |\bar{v}_{g2}|$.

To conclude this discussion of the use of stability considerations to determine the multiplicity of solutions of the dynamical system, we note that generally speaking these arguments provide an *upper limit* for the number of solutions. This is because the counting only considers the restrictions placed on the orbit by its end points and not by the intermediate parts of phase space. In applying this rule, however, it is important to take proper account of *symmetries* and *conservation laws* which may not be

^{5.8}The limits on $|v|$ can be calculated from the parameters, see van Saarloos and Hohenberg (1992).

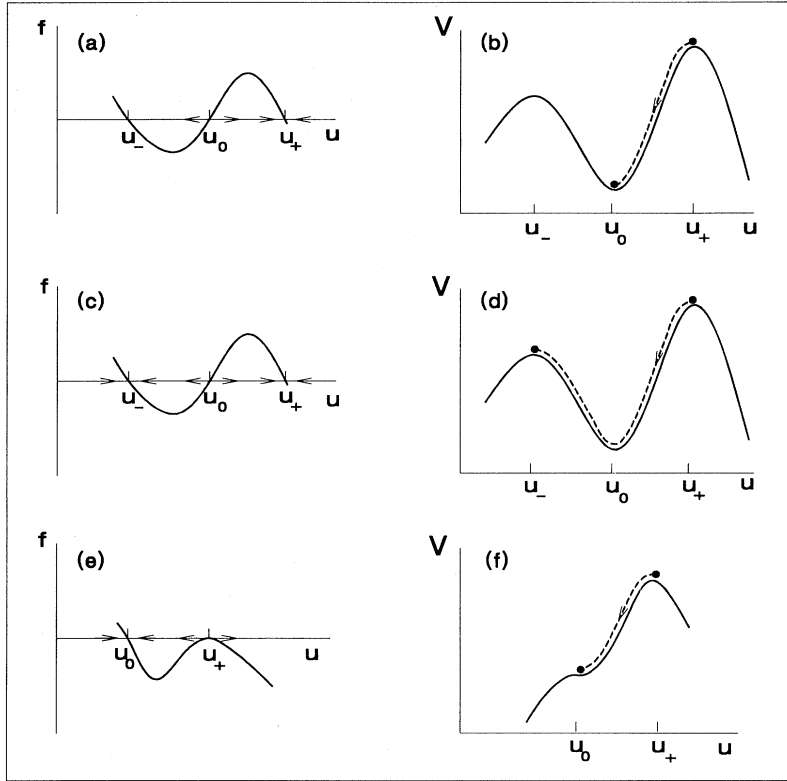


FIG. 17. Illustration of various forms of $f(u)$ and the associated $V(u)$ for the nonlinear diffusion equation (5.64). Arrows in (a), (c), and (e) show stability of fixed points u_+, u_0, u_- corresponding to spatially independent solutions. Trajectories in (b), (d), and (f) (dashed lines) correspond to coherent structures of the pde (5.63).

readily apparent in the stability analysis. An example was provided above in the counting of pulses, where the value $v=0$ (stationary pulse) results from inversion symmetry. As we shall see in subsection (v) below, continuous symmetries and conservation laws lead to families of solutions once a particular solution is known to exist.

We now turn to special cases where information is available on the whole phase space trajectory, and where more detailed results on the existence and multiplicity of coherent structures can be obtained.

(iv) Fronts and pulses in the nonlinear diffusion equation

The real equations discussed above are examples of the nonlinear diffusion equation, for which a more complete analysis of fronts and pulses is possible. This gives some insight into the strengths and weaknesses of the counting arguments. Let us consider the equation

$$\partial_t u = \partial_x^2 u + f(u), \quad (5.63)$$

where for the Ginzburg-Landau case $u = A$, and $f(A_r) = f_{1r}(A_r^2)A_r$, but more generally f need not have any symmetry. We call Eq. (5.63) the nonlinear diffusion equation. The dynamical system (5.44) for uniformly translating solutions $u(x, t) = u(x - vt)$ becomes

$$\partial_\xi^2 u + v \partial_\xi u + f(u) = 0, \quad (5.64)$$

where the function u , in contrast to $a = |u|$, can be both positive and negative. Equation (5.64) describes a classi-

cal particle of unit mass with damping constant v (either positive or negative) moving in the potential (Ben Jacob *et al.*, 1985)

$$V(u) = \int^u f(y) dy. \quad (5.65)$$

Let us consider a function $f(u)$ with three zeros and no symmetry, as in Fig. 17. The points u_\pm that are stable equilibria of (5.64) are maxima of the potential V , and the unstable equilibrium $u = u_0$ is a minimum of V . A front^{5,9} is represented by an orbit that begins at a maximum of V ($u = u_+$, say) and ends up at $u = u_0$ [Figs. 17(a) and 17(b)]. For large v the damping is large and the particle leaving $u = u_+$ will come to rest at $u = u_0$ without overshoot. This corresponds to a monotonic front between u_+ and u_0 . Below some damping $v = v_s$ there will be an overshoot before returning to u_0 . We may also define a critical damping v^* below which the approach to the minimum is underdamped, i.e., occurs through an infinite number of decaying oscillations, and the leading edge of the front is oscillatory. For some value $v = v_{\min} < v_s$ the particle will precisely reach the other maximum at $u = u_-$ [Figs. 17(c) and 17(d)] and this orbit represents a front^{5,9} solution between the two

^{5,9}Since Eq. (5.64) has no symmetry we use the term front to denote a structure joining any two uniform states of different amplitudes [see subsection (i) above].

stable fixed points $u=u_{\pm}$. The sign of the velocity v_{\min} is determined by the relative magnitude of $V(u_+)$ and $V(u_-)$, i.e., by the quantity

$$J_{\pm} = \int_{u_-}^{u_+} f(y) dy , \quad (5.66)$$

such that for $J_{\pm} > 0$, $v_{\min} > 0$, and u_+ invades u_- , while for $J_{\pm} < 0$ the opposite is true. For $v < v_{\min}$ the orbit goes off to $u = -\infty$, so it does not represent a finite solution of Eq. (5.64). (Depending on the form of $f(u)$, v_{\min} may be larger than v^* ; in this case v^* is not relevant to the properties of fronts, although it may appear in the fixed-point analysis.) We thus have a one-parameter family of fronts between u_+ and the unstable state u_0 with velocities $v_{\min} < v < \infty$, and a single front with velocity v_{\min} between u_+ and u_- .

An interesting special case arises at a saddle-node bifurcation where one of the stable states disappears as a parameter is varied, e.g., u_- and u_0 collide as in Fig. 17(e). For this particular case there is a continuous family of fronts from u_+ to u_0 with $v > v_{\min}$ where v_{\min} is the limit of the unique u_+ to u_- front velocity mentioned above. Discrete fronts, e.g., those corresponding to Fig. 17(d) are sometimes known as "trigger" fronts, whereas those belonging to a family, e.g. Fig. 17(f), are known as phase fronts (Fife, 1984a,b; Reusser and Field, 1979).

In the subcritical Ginzburg-Landau model (5.56) we have

$$f(u) = f_{1r}(u^2)u = \varepsilon u + u^3 - u^5 , \quad (5.67)$$

i.e., f is odd. For $\varepsilon > 0$ this leads to a potential as in Fig. 17(b) and 17(d) which is symmetric about $u=0$, and we find $v_{\min}=0$. In this case there is a family of fronts with $0 < v < \infty$, and also a stationary front between u_+ and u_- , i.e., a domain boundary in our classification. A pulse solution is an orbit beginning and ending at $u=u_0=0$, and it is clear that for $\varepsilon > 0$ none exists, since $u=0$ is a minimum of the potential $V(u)$.

Turning now to $\varepsilon < 0$, $V(u)$ has three maxima since $u=0$ is now a stable solution of Eq. (5.64). If we consider only orbits for $u \geq 0$ they may again be represented as in Fig. 17 but now with $u_- = 0$ and u_+ the positive stable solution of Eq. (5.64). A front between a zero and finite amplitude state^{5,9} is represented by an orbit joining these two maxima. There is no longer a family, but rather a unique velocity v^* for such an orbit. Its sign is again determined by a quantity as in Eq. (5.66)

$$J_+ = \int_0^{u_+} f(y) dy , \quad (5.68)$$

such that for $J_+ > 0$, $v^* > 0$ and u_+ invades $u=0$, while for $J_+ < 0$ the opposite is true. Similarly, there is a unique pulse orbit and it has $v=0$, since the trajectory leaving $u=0$ must return to $u=0$. Moreover it exists

only for $\varepsilon_1 < \varepsilon < 0$ where ε_1 is the value such that $V(u=0)=V(u=u_+)$. For $\varepsilon=-3/8$ a saddle-node bifurcation occurs as in Fig. 17(f) and a continuous family of fronts with $v > v^*$ exists.

It is also interesting to consider the asymmetric example

$$f(u) = \varepsilon u + u^2 - u^3 ; \quad (5.69a)$$

$$V(u) = \frac{1}{2} \varepsilon u^2 + \frac{1}{3} u^3 - \frac{1}{4} u^4 , \quad (5.69b)$$

and to compare the actual multiplicity of fronts and pulses found here to the results of the counting arguments of subsection (iii) above. It may be verified (Ben Jacob *et al.*, 1985) that $v_{\min}=1/\sqrt{2}$, and $v^*=2\varepsilon^{1/2}$. For $\varepsilon > 0$, $V(u=0)$ is a minimum and the mechanical model shows that there is one front (between $u=u_+ > 0$ and $u=0$) for each v in the range $v_{\min} < v < \infty$. For $\varepsilon > 1/8$ and $v < v^*$ the approach to $u=0$ is oscillatory with $v^* > v_{\min}$, Figs. 18(a) and 18(b), whereas for $0 < \varepsilon < 1/8$ the asymptotic approach is exponential, although over the whole range $0 < \varepsilon < \varepsilon^+=2$ there is overshoot for $v < v^+(\varepsilon)$ (Fig. 18). On the other hand the counting arguments of subsection V.B.2.b.iii give a continuous family for any $\varepsilon > 0$ and $v > 0$, plus a discrete set.

Thus the counting argument *overestimates* the multiplicity of solutions since it predicts fronts in the range $0 < v < v_{\min}$ where none exist. In addition there is only one front for each $v > v_{\min}$, not a family plus a discrete front. The latter is embedded in the family, at $v=v^+$, and represents a solution connecting smoothly to the family. The anomaly at $v=v^+$ only appears when one plots the *asymptotic* decay rate $\kappa_L(v)$, as in Fig. 18, which experiences a discontinuity at $v=v^+$. This occurs because the solution has the asymptotic form

$$u(\xi) \sim C_1(v) e^{-|\kappa_{L1}|\xi} + C_2(v) e^{-|\kappa_{L2}|\xi} , \quad (5.70)$$

with $|\kappa_{L1}| > |\kappa_{L2}|$, and $C_2(v)$ passes through zero at $v=v^+$. Thus v^+ is the velocity v_s where the solution first experiences an overshoot. It will turn out (see Sec. VI.B below) that the front with $v=v^+$ plays an important role in the selection problem.

For $\varepsilon < 0$, the phase-space argument correctly predicts the existence of a discrete front, as well as discrete pulses, but it does not specify their multiplicity: only stationary, $v=0$, pulses exist, and only for $\varepsilon_1 < \varepsilon < 0$.

(v) Exact solutions

In this section we describe a number of special circumstances which allow us to obtain analytic information about the solutions of the generalized Ginzburg-Landau equation (5.40).

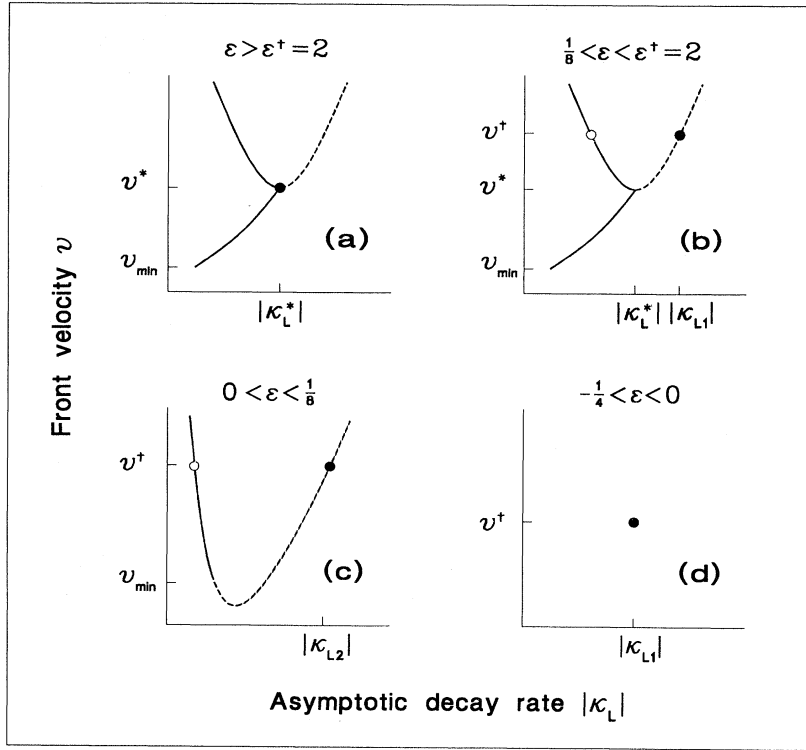


FIG. 18. Velocity v vs asymptotic spatial decay rate $|\kappa_L|$ of fronts in the asymmetric nonlinear diffusion equation (5.69), for various values of control parameter ε . Full lines show the range of velocity for which front solutions exist. Dashed lines show other solutions for the exponential approach given by a linear analysis about $u=0$ that are not, however, the asymptotic approach for nonlinear fronts. Solutions with $v > v^*$ correspond to exponential decay of $u(x)$, while fronts with $v < v^*$ have oscillatory decay (in which case $|\kappa_L|$ is the asymptotic decay rate of the envelope). For $0 < \varepsilon < \varepsilon^+ = 2$ [panels (b) and (c)] the velocity v^+ is the value at which the curve $\kappa_L(v)$ is discontinuous, and it corresponds to a discrete front linking the fixed points N and L_1 in Fig. 16. For $-\frac{1}{4} < \varepsilon < 0$ [panel (d)] only this front exists, and for $\varepsilon < -\frac{1}{4}$ there are no fronts. For $\varepsilon = 0$, $v_{\min} = v^* = v^+$ and there exist “phase fronts” for all $v > v_{\min}$, corresponding to the situation in Figs. 17(e,f). Similarly, for $\varepsilon = -\frac{1}{4}$, Eq. (5.69) has a saddle-node bifurcation and phase fronts exist for $v > v_{\min}$. In each case the solid point indicates the front which turns out to be selected according to the arguments of Sec. VI.B, and the open circle corresponds to a “missing” front.

(a) *Symmetries, conservation laws, and “integrable” systems*

For special points in parameter space a *pde* such as (5.40) may obey additional symmetries or conservation laws. [The well-known connection between the two, expressed by Noether’s theorem (see, e.g., Hill, 1951), presupposes a variational principle which is not in general present in the equations we are considering.] A consequence of continuous symmetries is the existence of *families* of solutions, obtained, e.g., by applying the symmetry transformation to a particular solution. A different method of finding families is to examine the dynamical system (5.44). For special cases this system of *ode*’s may be integrable and may therefore yield exact front or pulse solutions. Unless there are restrictions on v and ω this procedure will in general yield families. Note that the above integrability involves only the particular subclass of uniformly translating solutions (5.42), and it is of course quite different from the integrability of the *pde*, which refers to a general solution.

(b) *Perturbing around exact solutions*

Having obtained families of exact pulse or front solutions in special cases of Eq. (5.40), it is interesting to ask how these are modified when more general terms are added as small perturbations (see Newell, 1978; Doelman, 1989; Kivshar and Malomed, 1989; Fauve and Thual, 1990; Hakim and Pomeau, 1991; Dewel and Borckmans,

1992). For example, van Saarloos and Hohenberg (1992) have shown that the equation

$$\partial_t A = i \partial_x^2 A + i f_{1i}(|A|^2) A + \partial_x [f_{2r}(|A|^2) A] \quad (5.71)$$

(where f_{1i} and f_{2r} are arbitrary real functions) leads to an integrable dynamical system (5.44) with an exact double family of pulses indexed by v and ω , and a single family of fronts indexed by v . When the dissipative perturbation

$$b_1 B = b_1 \partial_x^2 A + f_{1r}(|A|^2) A, \quad (5.72)$$

is added to the r.h.s. of Eq. (5.71) the conservation laws of this equation are broken and a selection of a discrete set of pulses and fronts ensues. For small b_1 this is achieved by showing that the dynamical effect of the perturbation on the family of solutions of (5.71) is to induce a drift of the parameters $v(T)$, $\omega(T)$, according to the slow time variable $T = b_1 t$, towards definite fixed-point values. This type of perturbative calculation therefore does not simply ask how the full manifold of front and pulse solutions is modified, but also which solutions will be *stable* under the perturbation (5.72). Although there certainly are solutions of the perturbed system that are not obtained in this way, those which are will have certain selection properties to which we shall return in Sec. VI.B.

(*vii*) *Particular solutions of the complex Ginzburg-Landau equation*

Even when there are no special symmetries, conservation laws, or integrability conditions it is sometimes possible to find particular exact solutions of the dynamical system (5.44), (5.47). An important one for the selection problem treated in Sec. VI.B below is the so-called “nonlinear front” solution obtained by van Saarloos and Hohenberg (1990, 1992) from the ansatz

$$q(a^2) = q_N + e_0(a^2 - a_N^2), \quad (5.73a)$$

$$\kappa(a^2) = e_1(a^2 - a_N^2), \quad (5.73b)$$

with constants q_N , a_N , e_0 , e_1 to be determined. Insertion of this ansatz into the *ode*'s (5.44), (5.47) leads to two quadratic polynomial equations in the variable $a^2(\xi)$. Requiring that these relations be satisfied identically, one finds six relations (from the coefficients of a^0 , a^2 , and a^4 in the two equations) for the six quantities q_N , a_N , e_0 , e_1 , ω , and v . From these one can in general find explicit expressions for the velocity v^\dagger and the decay rate $\kappa_L^\dagger = -e_1 a_N^2$ in terms of the parameters $\{b_i, c_i, \varepsilon\}$ of (5.47) (there are either 0, 1, or 2 solutions). This particular solution, which was derived independently by Klyachkin (1989), is the discrete $N \rightarrow L_1$ front predicted by the counting arguments of subsection V.B.2.B.iii. It will play an essential role in the *selection* process discussed in Sec. VI.B below.

The existence of “integrable orbits” of the nonintegrable dynamical system, or of particular nontrivial solutions of the *pde* (5.57), has been related to Painlevé conditions by Florjanczyk and Gagnon (1990) and by Powell *et al.* (1991). In particular, Powell *et al.* apply the truncated Painlevé expansion of Weiss *et al.* (1983) to the *pde* directly in order to find the nonlinear front solution (5.73). So far the appeal to this more general framework has not led to new results, but one might hope that further work along these lines will provide additional insights.

Bekki and Nozaki (1985) have presented a *family* of exact solution of the cubic Ginzburg-Landau equation (4.49) which they call “hole” solutions, and which are domain boundaries in our classification. It was noticed by van Saarloos and Hohenberg (1992) that these solutions in fact represent *sources*, which are predicted to have discrete multiplicity according to the counting arguments of subsection V.B.2.B.iii, rather than existing as a family. Since the phase space counting usually overestimates the multiplicity this violation is unexpected, and has tentatively been attributed to a “hidden symmetry” by van Saarloos and Hohenberg (1992).

(*vi*) *Other one-dimensional defects*

(*a*) *Weak sources and sinks in the phase equation*

In oscillatory systems (types I_o and III_o) the domain boundaries we have called “sources” and “sinks” are

often referred to as “targets” (outgoing waves) and “shocks” (incoming waves). Targets are important as point defects in two-dimensional situations and will be considered in subsection V.B.2.c.iii below. If the wave vectors of the two domains are close together a rather complete analysis is possible using the phase equation. We will call these weak sources (sinks).

For the type III_o instability, or in the moving frame for a single type I_o wave, we may use the phase equation (4.90)

$$\partial_t \phi = \alpha \nabla^2 \phi - \beta (\nabla \phi)^2, \quad (5.74)$$

which is valid more generally than the amplitude equation (4.49) [in contrast to (4.90) we here suppress the constant term ω_0]. A complete sink or shock solution of Eq. (5.74) may be found analytically in one dimension (Kuramoto, 1984a,b; Murray, 1989). The transformation

$$u = 2\beta \partial_x \phi \quad (5.75)$$

changes Eq. (5.74) into a Burgers equation

$$\partial_t u = \alpha \partial_x^2 u - u \partial_x u. \quad (5.76)$$

Alternatively, the Cole-Hopf transformation (Whitham, 1974)

$$\tilde{\chi} = \exp(-\beta \phi / \alpha) \quad (5.77a)$$

converts (5.74) to the linear equation

$$\partial_t \tilde{\chi} = \alpha \nabla^2 \tilde{\chi}, \quad (5.77b)$$

which can be solved to yield

$$u(x, t) = u_0 + u_1 \tanh[-(u_1/2\alpha)(x - u_0 t)], \quad (5.78a)$$

or

$$\phi = -\frac{\alpha}{\beta} \left\{ -\frac{1}{2} u_0 (x - u_0 t) + \ln[e^{u_1(x - u_0 t)/2\alpha} + e^{-u_1(x - u_0 t)/2\alpha}] \right\}, \quad (5.78b)$$

where u_0 and u_1 are arbitrary constants. The expression in Eq. (5.78) represents a shock front moving with velocity

$$v = u_0, \quad (5.79)$$

in a medium whose overall phase is given asymptotically, as $x \rightarrow \pm \infty$, by

$$\phi_{\pm} = q_{\pm} x - \omega_{\pm} t, \quad (5.80a)$$

with

$$\omega_{\pm} = \beta q_{\pm}^2, \quad (5.80b)$$

$$q_{\pm} = u_0/2\beta \pm |u_1|/2\beta. \quad (5.80c)$$

The above results can be interpreted simply by noting that (5.80b) is the dispersion relation for nonlinear waves,

and (5.80c) is obtained from the *synchronization* condition

$$\omega_+ - q_+ v = \omega_- - q_- v . \quad (5.81)$$

Note that Eq. (5.80c) is equivalent to Eq. (5.62a) above, with the scaling $b_1 = b_3 = 1$, and $\beta = c_1 + c_3$, as in Eq. (4.91.c).

As a special case of Eq. (5.80) we first consider *stationary sinks*, with $v = 0$. These have $q_+ = -q_-$ and group velocities v_g , so they correspond to a pattern of *incoming* waves

$$v_g^+ = -v_g^- = -|u_1| < 0 . \quad (5.82)$$

Note that the signs of the wave vectors q_{\pm} (or phase velocities) depend on the sign of the dispersion coefficient β , which can in principle be either + or -. For the usual case of $\beta > 0$ the wave vectors are also incoming ($q_+ = -q_- < 0$), but for $\beta < 0$ we have $q_+ = -q_- > 0$. In either case the solution corresponds to a stationary sink at which two equal and opposite waves collide.

For moving sinks we have in general $v \neq 0$, and Eqs. (5.80)–(5.81) imply

$$\omega_+ - \omega_- = v(q_+ - q_-) = -v|u_1|/\beta . \quad (5.83)$$

Thus the direction of motion of the shock depends on the sign of the dispersion: for the usual case of positive dispersions ($\beta > 0$), the higher frequency wave entrains the lower frequency one ($\omega_+ > \omega_- \rightarrow v < 0$), and for $\beta < 0$ the opposite is true.

Note that we obtained a result similar to (5.83) in the complex Ginzburg-Landau model (5.61), but there it was not restricted to weak shocks. Indeed, Eq. (5.62) expressed in terms of $\omega_{N\pm} = \omega \pm vq_{N\pm}$ implies

$$\begin{aligned} \omega_{N+} - \omega_{N-} &= (c_1 + c_3 b_1 / b_3)(q_{N+}^2 - q_{N-}^2) \\ &= v \tilde{v}_g^+ / (c_1 + c_3 b_1 / b_3) . \end{aligned} \quad (5.84)$$

Then for a sink ($\tilde{v}_g^+ < 0$), with normal dispersion ($c_1 + c_3 b_1 / b_3 > 0$), $\omega_{N+} - \omega_{N-} > 0$ implies $v < 0$; i.e., the higher frequency state overtakes the lower frequency one. The situation is reversed for negative dispersion, as well as for sources.

Let us now ask under what conditions (5.78b) represents an appropriate solution of the amplitude equa-

tion (4.49). The condition of validity of the phase equation (5.74) is $\delta a \rightarrow 0$, which corresponds to small differences $q_+ - q_-$, i.e., *weak shocks*. This condition implies $q \ll \epsilon^{1/2}$ near threshold, and when it is violated we have *strong shocks*, for which amplitude variations must be taken into account, as discussed in subsection V.B.2.b.iii above (see also Bernoff, 1988). Another point to note is that there are no one-dimensional source or target solutions of the phase equation (5.74) representing *outgoing* waves, i.e. waves with $v_g^+ \simeq -v_g^- > 0$. It turns out that within the phase equation formalism targets only exist if the medium is *inhomogeneous*, i.e. the targets are “*extrinsic*” (Kuramoto, 1984b). Intrinsic targets that arise in a homogeneous medium require amplitude variations, as discussed in subsection V.B.2.b.iii above, and in subsection V.B.2.c.iii below for the two-dimensional case.

(B) The Swift-Hohenberg model; nonadiabatic effects

For the Swift-Hohenberg model (3.27) in one dimension the phase-space methods discussed above would lead to a rather high-order dynamical system and they are more difficult to implement. Nevertheless, the existence of a two-parameter family of moving fronts has been proved rigorously for this model at small ϵ by Collet and Eckmann (1990), and a number of numerical studies have been carried out (see Sec. VI.B). In the subcritical case localized pulse solutions can be found numerically, not only in one dimension but in higher dimensions as well (see subsection V.B.2.d below).

The Swift-Hohenberg model is also convenient for illustrating nonadiabatic effects discussed briefly in Sec. IV.A.4. Let us consider a stationary front, and make use of the Lyapunov potential to give a simple analysis, although calculations using only the dynamic equations can also be carried out (Bensimon *et al.*, 1988). A front centered at $x = 0$ is described by a real amplitude $A(X)$ with $X = \epsilon^{1/2}x$ in the reduced amplitude equation (4.7), so that

$$u = \epsilon^{1/2} A(\epsilon^{1/2}x) 2\cos(q_0 x + \phi) + \dots , \quad (5.85)$$

where ϕ gives a shift in the position of the rolls, and we do not need to consider higher-order terms. The potential (3.28) is

$$\mathcal{F} = \epsilon^2 \int dx \{ -2A^2(\epsilon^{1/2}x) \cos^2(q_0 x + \phi) + 4A^4(\epsilon^{1/2}x) \cos^4(q_0 x + \phi) + 8q_0^2 [\epsilon^{-1/2} \partial_x A(\epsilon^{1/2}x)]^2 \sin^2(q_0 x + \phi) \} . \quad (5.86)$$

We would usually evaluate this expression by first ignoring the slow variation of A and replacing the oscillating functions by their averages ($\cos^2 \rightarrow \frac{1}{2}$, $\sin^2 \rightarrow \frac{1}{2}$, $\cos^4 \rightarrow \frac{3}{8}$), leaving the integration over the slow variable to obtain

$$\mathcal{F} \simeq \epsilon^{3/2} \int dX \{ -A^2(X) + 4q_0^2 [\partial_X A(X)]^2 + \frac{3}{2} A^4(X) \} . \quad (5.87)$$

Clearly this integral is independent of the position of the

front relative to the rolls. However we have ignored terms such as

$$\Delta \mathcal{F} = \epsilon^2 \int dx [-A^2(\epsilon^{1/2}x) \cos 2(q_0 x + \phi)] . \quad (5.88)$$

Since this is just the Fourier transform at wave number $2q_0$ of a function smoothly varying over a scale $\epsilon^{-1/2}$, this integral is exponentially small. In fact

$$\Delta \mathcal{F} \sim e^{-a/\sqrt{\epsilon}} , \quad (5.89)$$

where α and the prefactors depend on the details of the shape of $A(x)$. However, most importantly, $\Delta\mathcal{J}$ will depend on ϕ , i.e. on the relative position of the front and the rolls.

Formally this correction is “smaller than any power of ϵ ,” however for any nonzero value of ϵ such a locking term may be important. Physically it simply corresponds to a preference of the center of the front to sit on top of or between the rolls. The consequences in the Swift-Hohenberg model will be rather harmless until ϵ becomes sizable and perturbation theory is not applicable. For example, the periodic corrections to the potential will lead to a small modulation of the linear front velocity $v^* = 2\epsilon^{1/2}$, to be discussed in Sec. VI.B below. However in other situations, where the amplitude or phase equations predict a smooth passage of a propagation velocity (relative to the periodic structure) through zero, the modulation will give rise to a *locking* of the velocity to zero over a finite parameter band (Bensimon *et al.*, 1988).

(γ) Grain boundaries

A class of one-dimensional defects arises in a two-dimensional system in the region where two patches of rolls of different orientations come together. In analogy with crystal physics these defects are called “grain boundaries” and they are the *line* topological defects associated with the rotational symmetry of type I_s patterns; they may also be thought of as fronts between two nonlinear states. We can consider symmetric grain boundaries, where the rolls on either side make an angle $\pm\theta$ to the direction of the boundary. More common, however, seem to be perpendicular grain boundaries where one set of rolls is perpendicular, and the other parallel, to the boundary. This structure is presumably favored for the same reasons that rolls tend to terminate normally at a sidewall (see Sec. V.A.1.b.iii). Also, as mentioned earlier, rolls parallel to a long sidewall are unstable to perpendicular rolls.

The structure and dynamics of grain boundaries have been studied in some detail using the amplitude expansion near threshold (Cross, 1982a; Manneville and Pomeau, 1983; Tesauro and Cross, 1987; Malomed *et al.*, 1990). We now need two coupled amplitude equations, for the two sets of rolls, as in Eq. (4.31). This system could be analyzed using phase space methods as in subsection V.B.2.b.iii above, albeit in higher dimensions (variables $a_1, \kappa_1, q_1, a_2, \kappa_2, q_2$), but this has not been pursued in the literature. The interaction parameter $\mathcal{G}(\theta)$, Eq. (4.32), which determines the stability of one set of rolls to superimposed rolls at an angle θ , controls the properties of the structure. Cross (1982a) has considered symmetric grain boundaries and evaluated the extra contribution to the potential (4.9) of the amplitude equation coming from the suppressed amplitudes at the interface.

The perpendicular case, shown schematically in Fig. 21(g) below, has received wider attention since it

provides a mechanism for wave-number selection. We consider the geometry of rolls along the x and y axes with the grain boundary along the y axis. Within the lowest-order amplitude equation, arguments based on the Lyapunov function and direct analysis show that a stationary grain boundary only occurs for $q_x = q_y = q_0$ (Tesauro and Cross, 1987). In an earlier work Manneville and Pomeau (1983) had suggested a one-parameter family, but this was due to their neglect of the phase unwinding of the x rolls that can occur, much as at a rigid lateral boundary. The calculation of the spatial dependence of the amplitudes of the stationary grain boundary is quite delicate because of the different characteristic length scales ($\epsilon^{-1/2}$ and $\epsilon^{-1/4}$) for the variations of the two amplitudes within the boundary, leading in fact to an $O(\epsilon^{-1/5})$ boundary layer for the y rolls (and not $\epsilon^{-1/4}$ as suggested by Tesauro and Cross).

In general the situation has close analogies with front propagation (subsection V.B.2.b.iii.α). For a general value of q_y (consistent with stable y rolls), we expect a *unique* propagation velocity producing a set of x rolls with a determined wave number, since this is analogous to the situation of a front connecting two stable states. If q_y is tuned to reduce the propagation speed, then we expect nonadiabatic effects [see subsection (β) above], whereby the front envelope is locked to the x rolls themselves, over a band of q_y which, however, is exponentially small near onset. The position of the front which is locked to the x rolls can then still relax, but now by stretching the wave number of the x rolls, presumably to a unique selected value for each q_y in the band. Notice that for nonzero front velocity the magnitude and phase of the x rolls are evolving separately, whereas in the stretching motion they are locked together. This picture was tentatively confirmed by Tesauro and Cross (1987) using perturbative calculations on the amplitude equation, and a direct numerical simulation of model equations, although in the latter it was not shown conclusively that transients had been eliminated.

c. Point defects in two dimensions

(i) Dislocations in type I_s systems

A dislocation defect is a point in the cell where a pair of rolls terminates, as shown in Fig. 19. It is the topological defect associated with the discrete translational symmetry of the ideal system, as discussed in Sec. IV.B. The motion that takes an isolated dislocation through symmetry related states occurs in a direction parallel to the rolls and is called *climb*. Since climb has the effect of increasing or decreasing the average wave number of the whole system (for motion up or down in Fig. 19, respectively), we might expect the climb velocity to be related to the background wave number, i.e. the wave number far away from the core where perturbations due to the dislocation are not important. Indeed, there is a particular wave number q_d for which the climb velocity is zero and in subsection V.B.3. below we will investigate the depen-

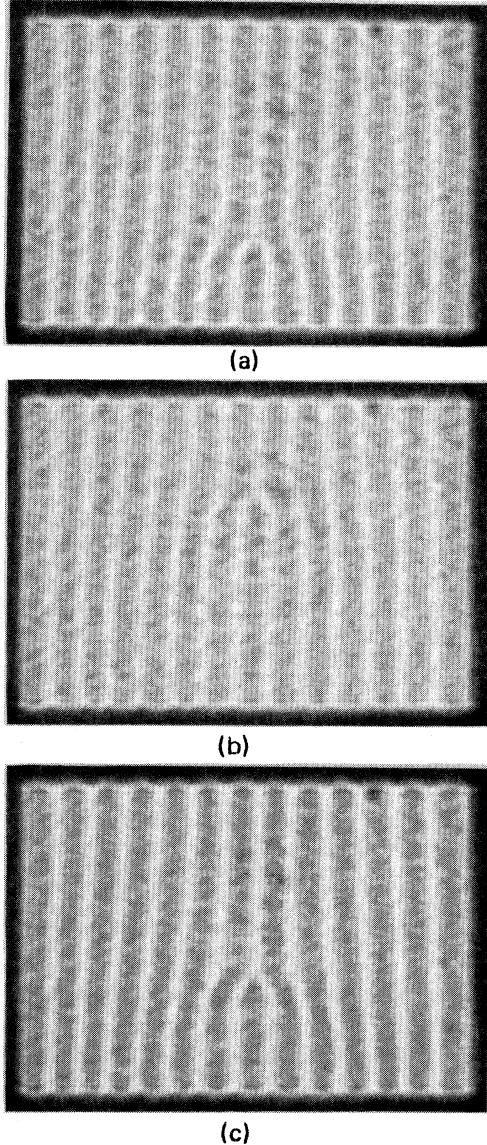


FIG. 19. Dislocation defects in a type I_s system. Photographs are flow visualizations of a Rayleigh-Bénard convection experiment showing a pattern of 14 wavelengths in the lower portion of the cell and 13 in the upper portion. Panels show climb motion of the defect induced by changing the Rayleigh number. (a) $R = 1.2 R_c$: the dislocation is moving towards the bottom of the picture. (b) Lowering the Rayleigh number to $R = 1.15 R_c$ reverses the motion. (c) The Rayleigh number has increased again. (From Croquette, 1989.)

dence of the velocity on wave number, $v(q - q_d)$. Motion along the direction normal to the rolls is called *glide* and, contrary to climb, it does not involve only symmetry-related states because of the underlying periodic structure. In general the dislocation will be pinned to a particular position relative to this structure and a nonzero perturbation will be needed to drive the motion, though this effect does not show up in the amplitude or phase equations, since it is “nonadiabatic.”

In general the far field of a stationary or uniformly climbing dislocation is given by solving the phase equation (4.76) linearized about the background wave number q . Specifically, let us write $\phi = qx + \bar{\phi}$, so that

$$\begin{aligned} v \partial_y \bar{\phi} - D_{\parallel}(q) \partial_x^2 \bar{\phi} - D_{\perp}(q) \partial_y^2 \bar{\phi} \\ = 2\pi D_{\parallel}(q) \partial_x \delta(x - x_d) \Theta(y - y_d), \quad (5.90) \end{aligned}$$

where (x_d, y_d) is the position of the defect in the moving frame and Θ is the Heaviside function. (Actually we could formally choose v in any direction by a simple rescaling of the equation, but as mentioned above only climb is expected to be uniform.) The term on the right-hand side maintains the required phase winding by introducing a 2π jump along $x = x_d$, $y > y_d$. We will assume that the diffusion constants $D_{\parallel}(q)$, $D_{\perp}(q)$ are both nonzero (see below). It should be noted that the velocity v is actually fixed by the background wave number q , though this does not come out of the phase equation analysis. Indeed, Eq. (5.90) may be solved for any (v, q) , so it remains unclear to us how the selection is manifested in an analysis based on the phase equation alone. It appears likely that in general $v(q)$ will depend on the details of the defect core structure where (5.90) breaks down due to the rapid spatial variation (Tesauro and Cross, 1986), so we shall consider $v(q)$ to be given in studying Eq. (5.90).

This equation may be readily solved (Bodenschatz *et al.*, 1988a). Introducing scaled coordinates $X = x/D_{\parallel}^{1/2}$, $Y = y/D_{\perp}^{1/2}$, $V = v/D_{\perp}^{1/2}$, $R = (X^2 + Y^2)^{1/2}$, we have for $v = 0$ simply

$$\bar{\phi} = \tan^{-1}(Y/X). \quad (5.91)$$

For nonzero v this same expression applies close in ($VR \ll 1$), whereas far away ($VR \gg 1$) the result is more complicated and is most easily stated in terms of a gradient related to the tilt angle

$$\partial_Y \bar{\phi} = [(V\pi)^{1/2} X / 2R^{3/2}] \exp[-V(Y+R)/2]. \quad (5.92)$$

A feature of this solution that has important implications for the interaction of defects is the exponential decay of the phase perturbation in front of the uniformly moving defect ($X = 0$, $Y > 0$), rather than the power law decay behind the defect ($X = 0$, $Y < 0$), or for the stationary case ($V = 0$). This is a consequence of the diffusive propagation of the phase, and leads to a short-range interaction between defects moving towards each other with a range set by the velocity, a result first obtained by Siggia and Zippelius (1981a) (see subsection V.B.3.b below).

When the dynamics is derivable from a potential \mathcal{J} (e.g. near threshold), the above equations continue to hold for anisotropic systems. For isotropic systems, on the other hand, the analysis breaks down since the stationary defect solution has $q = q_m$ where q_m minimizes \mathcal{J} , and $D_{\perp}(q_m) = 0$. We must then include higher-order gradient terms in the phase equation, which near threshold becomes (restoring the scales ξ_0 and τ_0)

$$\begin{aligned}
 (\tau_0/\xi_0^2) \partial_t \bar{\phi} &= -(\tau_0 v / \xi_0^2) \partial_y \bar{\phi} + \partial_x^2 \bar{\phi} \\
 &+ (k/q_0) \partial_y^2 \bar{\phi} - (1/4q_0^2) \partial_y^4 \bar{\phi} \\
 &- 2\pi \partial_x \delta(x - x_d) \Theta(y - y_d), \quad (5.93)
 \end{aligned}$$

with $k = q - q_0$. In order to eliminate k and q_0 from this equation we introduce the following scaled variables

$$\tilde{x} = 2kx, \quad (5.94a)$$

$$\tilde{y} = 2(kq_0)^{1/2}y, \quad (5.94b)$$

$$\tilde{t} = 4(k\xi_0)^2 t / \tau_0, \quad (5.94c)$$

$$\begin{aligned}
 \tilde{v} &= (2q_0\xi_0)^{1/2} (k\xi_0)^{-3/2} (\tau_0 v / \xi_0) \\
 &= (\tau_0 / \xi_0^2) (\sqrt{2q_0} / k^{3/2}) v, \quad (5.94d)
 \end{aligned}$$

in terms of which Eq. (5.93) for $\bar{\phi}(\tilde{x}, \tilde{y}, \tilde{t}, \tilde{v})$ becomes

$$\begin{aligned}
 \partial_t \bar{\phi} &= -2^{-3/2} \tilde{v} \partial_y \bar{\phi} + \partial_{\tilde{x}}^2 \bar{\phi} + \partial_{\tilde{y}}^2 \bar{\phi} - \partial_{\tilde{y}}^4 \bar{\phi} \\
 &- 2\pi \partial_{\tilde{x}} \delta(\tilde{x} - \tilde{x}_d) \Theta(\tilde{y} - \tilde{y}_d). \quad (5.95)
 \end{aligned}$$

The linearized equation is easily solved by Fourier transforms for any value of the parameter \tilde{v} (which Siggia and Zippelius, 1981a called β), so the velocity is arbitrary at this level. In the limit $\tilde{v}=0$, the solution is

$$\begin{aligned}
 \bar{\phi} &= (\pi/2) \operatorname{sgn}(\tilde{x}) [\operatorname{erf}(\tilde{y}/2\sqrt{\tilde{x}}) + 1] \\
 &= (\pi/2) \operatorname{sgn}(x) [\operatorname{erf}(q_0^{1/2}y/\sqrt{2x}) + 1], \quad (5.96)
 \end{aligned}$$

close in ($\tilde{y} \lesssim 1, \tilde{x} \lesssim 1$), but it goes over to

$$\bar{\phi} = \tan^{-1}(\tilde{y}/\tilde{x}) = \tan^{-1}[(y/x)(q_0/k)^{1/2}], \quad (5.97)$$

far away ($\tilde{x}, \tilde{y} > 1$), where the ∂_y^4 terms become negligible (for $k \rightarrow 0$ only the small \tilde{x}, \tilde{y} regime remains). Actually the neglect of the nonlinear terms in the phase equation in arriving at Eq. (5.95) is not everywhere correct (Siggia and Zippelius, 1981a), but introduction of these terms does not destroy the scaling given in Eqs. (5.96) and (5.97). In particular, Meiron and Newell (1985) have constructed a similarity solution $\bar{\phi} = \phi_{MN}(\tilde{y}/\sqrt{\tilde{x}})$ of the nonlinear phase equation for the stationary dislocation ($\tilde{v}=0$), with ϕ_{MN} obtained by numerically solving a nonlinear *ode*; they find good agreement with a numerical simulation of a particular model equation.

In the region close to threshold we can obtain information about the core structure using the full amplitude equation (4.3). We will restrict the analysis to $v=0$, which occurs for $q-q_0=k=0$, i.e. for k at the minimum of the potential (4.9). For the isotropic case the situation is complicated by the different ways x and y derivatives appear in Eq. (4.3). Thus we would expect the amplitude to be depressed to zero at the defect position, with the region of depressed amplitude extending over a range scaling as $\epsilon^{-1/2}$ in the x direction and $\epsilon^{-1/4}$ in the y direction. Because of this anisotropy the problem still requires solution of a spatial *pde*. Numerical results are available from Pomeau *et al.* (1983). For the anisotropic

case (4.11) the amplitude equation takes a simpler form, the core structure is axisymmetric in the scaled coordinates $(x/D_{\parallel}^{1/2}, y/D_{\perp}^{1/2})$ and a simple *ode* for the radial dependence can be solved numerically (Bodenschatz *et al.*, 1988a). It should be emphasized that the amplitude $A(x, y)$ is completely smooth: the singularity in the phase variable implied by the winding condition (5.38) is relaxed smoothly (over the core size) by $|A|$ going to zero at a point.

We have calculated the structure of moving or stationary defects, but have not yet described how $v(q)$ is determined. This will largely be discussed in subsection V.B.3 below, on dynamics. However an important point is that there is a unique background wave number $q=q_d$ (or conceivably a discrete set) such that $v=0$ and the dislocation does not climb. The evidence for this assertion comes from experiment (Pocheau and Croquette, 1984), from numerical work on amplitude equations (Siggia and Zippelius, 1981a) and on model equations (Tesauro and Cross, 1986), and from perturbation expansions of the amplitude equation to higher order in ϵ . (Pomeau *et al.*, 1983). However we do not yet have a direct derivation of the existence of the function $v(q)$ starting from the basic properties of a dislocation, namely the phase winding condition and an equation for phase dynamics (with corrections at small distances).

(ii) Disclinations

Disclinations are the point topological singularities associated with the rotational symmetry of the roll wave vector in a rotationally invariant system. They are commonly seen in Rayleigh-Bénard convection, for example, and can be understood as resulting from the tendency of the rolls to approach the boundary normally. Indeed, if this is taken as a constraint, and there are only point defects in the cell, then disclinations are a necessary consequence.

Disclinations may be characterized by their winding number, which is the number of 2π rotations swept out by the wave vector as the defect is circled. Figures 20(a) and 20(b) show a (+1) disclination, and Fig. 20(c) a (-1/2) defect. Notice that the magnitude of the wave vector necessarily varies over a considerable range in Fig. 20(b) even far from the disclination point, and such distortions will only occur if they do not lead to local instabilities. Sometimes the distortion will be relieved by a line of dislocations or by a grain boundary. Only the (+1) and (+1/2) defects can be constructed with a constant wave number. The structure in Fig. 20(a) is often seen in circular domains, and also in other geometries where it is partially obscured by the boundaries such as in Fig. 20(d). This particular disclination is also called a focus singularity.

The focus singularity provides an important wave-number selection mechanism. For a stationary focus singularity there is a unique wave number asymptotically far away from the core, as can be seen quite simply from

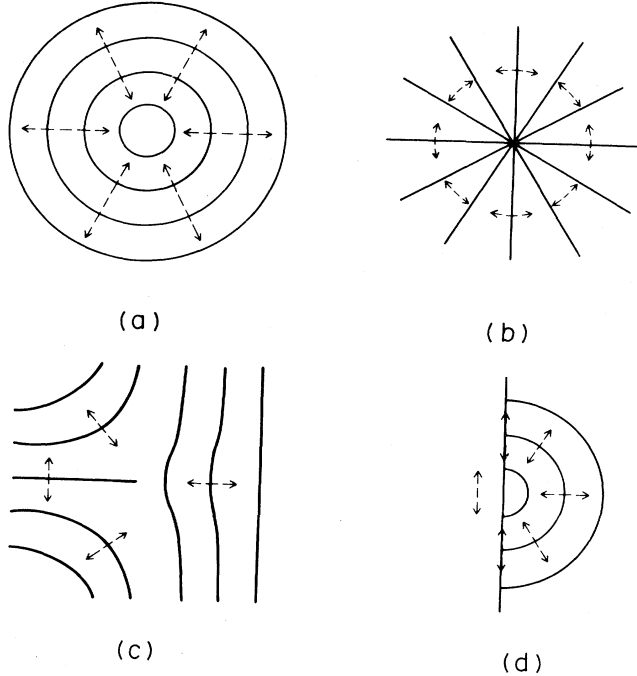


FIG. 20. Schematic diagram of disclination point defects: (a) Focus singularity (strength +1). (b) Alternate +1 defect. (c) Defect of strength $-1/2$. (d) Disclination on lateral sidewall. The full lines denote phase contours (rolls), the dashed arrows are the normals to the rolls.

the phase equation (4.76). If we first consider the axisymmetric case, the solution is

$$q B(q) = c/r , \quad (5.98a)$$

where c is an integration constant. Since c can be shown to be $O(1)$ from the short-distance behavior, we have $q \rightarrow q_f$ at large r , where

$$B(q_f) = 0 . \quad (5.98b)$$

Note that this result is unchanged by the mean-flow effects discussed in Sec. IV.A.2, since no radial mean flows can occur by the constant density assumption. For the non-axisymmetric case, however, the result carries over only for situations where no mean flows exist (Cross and Newell, 1984), and then the asymptotic wave number q_f is at the border of the zigzag instability. These results depend only on the assumption of a smooth phase gradient expansion, and so should have widespread applicability in type I_s systems. How closely q approaches q_f depends on how large r can be made, and also how soft the core structure is (i.e. how small c is).

In the axisymmetric case the full core structure can be investigated near threshold using the amplitude equation in radial coordinates (Brown and Stewartson, 1978; Pomeau *et al.*, 1985). The question is rather delicate, though, since solutions exist with the amplitude diverging at the center. Flows corresponding to these solutions

have been observed in convection experiments (Croquette, 1989).

(iii) Target patterns

The analogue of foci in oscillatory patterns is the axisymmetric target. It is the two-dimensional version of a source or a sink in one dimension. The question of whether intrinsic targets (i.e. ones that do not depend on an externally applied imperfection at the core) exist in various oscillatory systems remains a controversial one. In addition extrinsic targets, such as might be initiated for example by a dust particle in a chemical reaction, have also been investigated. This issue will be discussed further in Sec. X below.

Weak extrinsic targets in type III₀ systems can be understood from the phase equation if we assume an external perturbation at some point in space that raises the frequency of the medium locally. We start from the phase equation in two dimensions (Kuramoto, 1984b)

$$\partial_t \phi = \alpha \nabla^2 \phi - \beta (\nabla \phi)^2 - g(\mathbf{x}) , \quad (5.99)$$

where $g(\mathbf{x}) > 0$ is centered at $\mathbf{x} = 0$ and is assumed to vanish for $r > r_0$ [we denote the circular coordinates for \mathbf{x} by (r, θ)]. We first assume $\beta > 0$. The use of the Cole-Hopf transformation as in (5.77)

$$\tilde{\chi} = \exp(-\beta \phi / \alpha) \quad (5.100)$$

linearizes the phase equation to

$$\partial_t \tilde{\chi} = [\alpha \nabla^2 + (\beta / \alpha) g(r)] \tilde{\chi} . \quad (5.101)$$

Setting

$$\tilde{\chi}(r, t) = e^{-\lambda t} \chi(r) , \quad (5.102)$$

we have a time-independent Schrödinger equation

$$-\alpha \nabla^2 \chi + V(r) \chi = \lambda \chi , \quad (5.103)$$

for a particle of energy λ in a bounded attractive potential $V(r) = -(\beta / \alpha) g(r) < 0$. In two dimensions it is known that there is always at least one bound state $\lambda < 0$, with a positive eigenfunction [a necessary condition in view of (5.100)]. The asymptotic form of the wave function for $r \gg r_0$ is

$$\chi(r) \sim (\bar{q}r)^{-1/2} e^{-\bar{q}r} , \quad (5.104)$$

where $\bar{q} = (-\lambda / \alpha)^{1/2}$. Returning to the phase function ϕ the solution far from the center is

$$\phi(\mathbf{x}, t) = -\omega t + qr , \quad (5.105a)$$

$$\omega = \beta q^2 , \quad (5.105b)$$

$$q^2 = -\lambda \alpha / \beta^2 > 0 . \quad (5.105c)$$

Thus the effect of the perturbation $g(\mathbf{x})$ is to pick out a particular wave vector (5.105c) from the continuous family (5.80c), and to entrain the wave solution to the frequency (5.105b) which is positive [i.e. larger than the fre-

quency $\omega(0)$ of the uniform state, omitted from (5.99)]. If $g(\mathbf{x})$ were negative Eq. (5.103) would have no bound states and no target pattern solution of Eq. (5.99) would exist.

A typical target pattern only extends out a finite distance from the center, at which point there is an abrupt transition to the uniformly oscillating medium. This can be achieved for the solutions of (5.99) with $r \gg r_0$, by terminating the target at a shock front at $r=r_s(t)$, with $\omega=\omega(0)$ and $q=0$ for $r > r_s(t)$ [we have restored the background frequency omitted from (5.99)]. According to Eq. (5.80), this implies that the outer rim of the target pattern will move at the velocity

$$v_s = \beta q = (-\alpha\lambda)^{1/2}. \quad (5.106)$$

Inside the target, in the region $r_0 < r < r_s(t)$, the waves move outwards with the phase velocity $v_{ph} = \omega/q = [\omega(0) + \beta q^2]/q$, which is larger than the velocity v_s of the rim, so that waves periodically annihilate on the rim. Finally, we note that two different target patterns, centered at \mathbf{x}_1 and \mathbf{x}_2 , say, can have their outer rims collide, and the ensuing structure is a shock front or sink as discussed in subsection V.B.2.b.vi above; the pattern having the higher frequency consumes the other one, a feature which corresponds to the experimental behavior discussed in Sec. X below.

It is instructive to recast the shock solution (5.78) into the language of the Schrödinger equation (5.101). According to Eqs. (5.104) and (5.105c) we have $\tilde{q} = \beta q/\alpha$, so a shock (5.80) with $q_+ = -q_- < 0$ corresponds to a one-dimensional wave function $\tilde{\chi} \sim \exp(|\tilde{q}|r)$ with exponential growth. Such a solution is considered unphysical as a wave function $\tilde{\chi}$, but it corresponds to a legitimate phase function ϕ , which describes shocks. As in the one-dimensional case a major difference between targets (sources) and shocks (sinks) is that the former exist for a discrete set of wave vectors and frequencies, whereas the latter are a continuous family (5.80).

The preceding discussion of targets was predicated on the assumption of normal dispersion $\beta > 0$. In fact, the entire derivation also goes through for $\beta < 0$: targets exist only if $g(\mathbf{x}) < 0$, i.e. if the local frequency is reduced at the center and it entrains the pattern ($\omega = \beta q^2 < 0$). Indeed, the potential $V(r) = -(\beta/\alpha) g(r)$ is still negative, and a bound state $\lambda < 0$ exists with decaying wave function (5.104) with $\tilde{q} = (-\lambda/\alpha)^{1/2} > 0$. The corresponding phase function ϕ , Eq. (5.105a), now has a negative wave vector ($q = \alpha\tilde{q}/\beta < 0$) corresponding to incoming phase waves, but the structure is still a target pattern since the group velocity $v_g = \beta q > 0$ is outgoing. [As noted earlier the shock structure (5.78) for $\beta < 0$ has incoming group velocity but outgoing phase velocity and it again corresponds to a wave function $\tilde{\chi}$ with incoming waves.]

In the absence of the external perturbation $g(\mathbf{x})$, the phase equation (5.99) does not support targets. We therefore first consider the complex amplitude equation (4.49) in two dimensions and search for solutions of the form

$$\phi(\mathbf{x}, t) = \omega t + \psi(r), \quad (5.107a)$$

$$a(\mathbf{x}, t) = a(r). \quad (5.107b)$$

The derivation of the amplitude equation (4.90) is now modified to account for the spatial variation of a (Kuramoto, 1984b)

$$\partial_t \phi = \alpha \nabla^2 \phi - \beta (\nabla \phi)^2 + 2\alpha a^{-1} \nabla a \cdot \nabla \phi. \quad (5.108)$$

The last two terms can be thought of as a perturbation of the local frequency $\omega(\mathbf{x})$. The Cole-Hopf transformation (5.100) is now generalized to

$$\tilde{\chi}(r, t) = a \exp(-\beta \phi/\alpha) = e^{-\lambda t} \chi, \quad (5.109)$$

where χ satisfies the Schrödinger equation (5.103) with the potential

$$V(r; a) = (1 + \beta^2/\alpha^2) a^{-1} \nabla^2 a. \quad (5.110)$$

If we assume the asymptotic behavior

$$a(r) = a_0 + a_k r^k, \quad r \rightarrow 0, \quad (5.111a)$$

$$a(r) = a_\infty + a_{-1} r^{-1}, \quad r \rightarrow \infty, \quad (5.111b)$$

we see that

$$V(r; a) \sim \frac{a_k k^2 r^{k-2}}{a_0 + a_k r^k}, \quad r \rightarrow 0, \quad (5.112a)$$

$$V(r; a) \sim (a_{-1}/a_\infty) r^{-3}, \quad r \rightarrow \infty. \quad (5.112b)$$

It is likely that $a_0 = 0$, so that the potential has a universal r^{-2} repulsion near the origin. At large distances, however, we find an *attractive tail*, so long as the amplitude falls below its asymptotic value, i.e. so long as $a_{-1} < 0$. It is thus plausible that the Schrödinger equation (5.103) should admit a bound state with the potential (5.110), from which it follows that (5.108) has a target pattern solution. The analysis of Koppell and Howard (1981) also showed the existence of axisymmetric intrinsic target solutions in the $\lambda-\omega$ system, Eq. (3.34), in two dimensions, though these were shown to be unstable by Ermentrout and Rinzel (1980).

(iv) Spiral patterns

Spirals are the generalization of targets to a case where the pattern is no longer circularly symmetric. In terms of the Schrödinger analysis of the phase equation (5.108) they correspond to bound states with nonzero angular momentum. We define an m -armed spiral as a solution of (5.108) or (4.49) of the form

$$\phi(\mathbf{x}, t) = -\omega t - m\theta + \tilde{\phi}(r), \quad (5.113a)$$

$$a(\mathbf{x}, t) = a(r). \quad (5.113b)$$

We may see immediately that there are no spirals with uniform amplitude $a = \text{const}$, since the transformation (5.109) leads to an additional centrifugal term in the potential of the radial equation (5.103), of the form

$$V_m(r) = -m^2/r^2, \quad (5.114)$$

which is infinitely attractive as $r \rightarrow 0$, and leads to an infinite binding energy (Kuramoto, 1984b). It is therefore necessary to consider a spatially varying amplitude,

$$a(r) \sim_{r \rightarrow 0} a_m r^m, \quad (5.115)$$

leading to a potential (5.110) that cancels the singularity in (5.114). At large distances the amplitude still has the form (5.11b) and it is reasonable to suppose that a bound state will exist in general, since it is expected that $a_- < 0$.

Hagan (1982) has explicitly constructed spiral solutions in the $\lambda-\omega$ system, which (for simple nonlinearity) is equivalent to the complex Ginzburg-Landau model (4.49) with $c_1=0$. Note also that for the construction of periodic solutions the amplitude equation has an additional scaling property: a solution with parameters c_1, c_3 can be related (Bodenschatz *et al.*, 1991c) to the solution of a second amplitude equation with parameters c'_1, c'_3 , provided

$$\frac{c_1 + c_3}{1 - c_1 c_3} = \frac{c'_1 + c'_3}{1 - c'_1 c'_3}. \quad (5.116)$$

Thus the choice $c'_1 = 0, c'_3 = (c_1 + c_3)/(1 - c_1 c_3)$ may be used to transform Hagan's solution valid for $c_1=0$ to the general case (4.49). (Length and time scales are also rescaled.) Hagan constructed solutions both by perturbation in small $c_1 + c_3$ (i.e. about the dislocation solution for the real equation), and numerically (see also Koppell and Howard, 1981). He argued that only the lowest ($m=1$) spiral will in general be stable since higher-order ones can break up into lower-order ones. This argument is based again on perturbing about the potential $c'_3=0$ case. [We remark that stability is not transferable through the scaling (5.116) so there is no direct information on stability for general c_1, c_3 .] Once again spirals exist for a unique value of q and ω , satisfying the far field dispersion relation analogous to (4.53b). Bodenschatz *et al.* (1991c) performed more extensive numerical calculations in the case $c_1=c_3$. For $c_1=c_3>0.63$ they find that the selected wave number is unstable to the finite- q Benjamin-Feir instability (which they call the Eckhaus instability). Spiral solutions have also been obtained numerically by Aranson *et al.* (1989) in a complex generalization of the Swift-Hohenberg model. For further analytic and numerical investigations of spiral waves in model systems we refer the reader to Chap. 12 of Murray (1989), to Aranson and Rabinovich (1989), to Sakaguchi (1989), and to Winfree (1991).

It is amusing to note that a *spiral* solution of the envelope equation, when applied to a type I_o system, yields a dislocation defect in that system [although the solution of the amplitude equation (4.13) corresponding to the rotationally invariant system has not been calculated]. This dislocation is drifting at the group speed s_0 within the amplitude equation, whereas the waves themselves are

moving with the phase speed.

Another approach to spirals is to consider the curling up of a line defect which is the two-dimensional extension of a single one-dimensional pulse traveling in the x direction, say. In its ideal unperturbed state the structure is a straight line parallel to y , moving with the pulse speed v . Under small deformations of the shape of the line, the change in normal velocity v_n is assumed to be given by the eikonal equation (Keener and Tyson, 1986)

$$v_n = v + D_\perp K, \quad (5.117)$$

where K is the local curvature of the line (assumed small), and D_\perp is a constant which has dimensions of a diffusivity. In Eq. (5.117) the sign of K is such that a curvature towards the direction of propagation is positive. The eikonal equation represents an expansion in the curvature of the wave front and, as written, it neglects the influence of nearby waves (e.g. other arms of the spiral) on the velocity v . The curvature expansion can also be applied to a plane-wave train whose velocity depends on its frequency or wavelength, and in lowest order the dispersion relation $v(\omega)$ of the undistorted wave train appears in the eikonal equation. The applicability of Eq. (5.117) to a specific model will be considered in Sec. X below.

Let us suppose that the line defect has a free end and begins to curl up around it. A description of the mechanism for this curling up has been given by Meron and Pelée (1988), but we defer a discussion of this effect to Sec. X. At this stage we focus on the steady-state shape of the spiral, as described by the eikonal equation (5.117), which must be supplemented by boundary conditions at the core and in the far field. It is convenient to define the spiral parametrically in terms of the coordinates of the rigidly rotating pulse, i.e. take $m=1$ in Eq. (5.113a) and describe the coordinates of the point $\phi=0$ as

$$x = r \cos [\theta(r) - \omega t], \quad y = r \sin [\theta(r) - \omega t], \quad (5.118)$$

where r is the radial coordinate and the unknowns $\theta(r)$ and ω determine the shape and frequency of the spiral, respectively. The boundary condition at the core is assumed to be

$$\partial_r \theta = 0, \quad r = r_c, \quad (5.119)$$

i.e. the spiral is assumed to intersect the circle $r=r_c$ radially, with the radius r_c taken as a phenomenological parameter. In the far field we have

$$\partial_r \theta = q_\infty = \omega/v, \quad r \rightarrow \infty, \quad (5.120)$$

representing a pulse train undistorted by curvature. If the pulses are sufficiently far apart (i.e. if the frequency is low enough), the velocity v will be independent of frequency in the far field. In that case it can be shown from

pure geometry (Keener and Tyson, 1986) that (5.118) implies^{5.10}

$$v_n = \frac{\omega r}{(1+\psi)^{1/2}} \quad (5.121a)$$

and

$$K = \frac{\partial_r \psi}{(1+\psi^2)^{3/2}} + \frac{\psi}{r(1+\psi^2)^{1/2}}, \quad (5.121b)$$

where

$$\psi = r \partial_r \theta. \quad (5.122)$$

The eikonal equation (5.117) then becomes

$$-r \partial_r \psi = (1+\psi^2) [(rv/D_\perp)(1+\psi^2)^{1/2} - (\omega/D_\perp)r^2 + \psi], \quad (5.123)$$

which can be viewed as an eigenvalue equation for the frequency ω . Let us rescale the coordinate, setting

$$\tilde{r} = (v/D_\perp)r, \quad \tilde{q}_\infty = (D_\perp/v)q_\infty = \omega D_\perp/v^2, \quad (5.124)$$

whence Eq. (5.123) depends on the single parameter \tilde{q}_∞ ,

$$-\tilde{r} \partial_{\tilde{r}} \psi = (1+\psi^2) [\tilde{r}(1+\psi^2)^{1/2} - \tilde{q}_\infty \tilde{r}^2 + \psi], \quad (5.125)$$

with boundary conditions

$$\psi = 0 \text{ for } \tilde{r} = \tilde{r}_c = r_c v / D_\perp, \quad (5.126a)$$

and

$$\psi \rightarrow \tilde{q}_\infty \tilde{r} \text{ for } \tilde{r} \rightarrow \infty. \quad (5.126b)$$

The solution of Eq. (5.125) with boundary conditions (5.126) leads to an eigenvalue relation of the form

$$\tilde{q}_\infty = Q(\tilde{r}_c), \quad (5.127a)$$

or equivalently

$$\omega = (v^2/D_\perp) Q(r_c v / D_\perp). \quad (5.127b)$$

The numerical solution for Q is well represented by the expression

$$Q(x) \approx 0.331 - 0.097 x^2, \quad (5.128)$$

which provides a relation between the frequency and the velocity, with r_c as a parameter.

Let us ask if the above scheme is self-consistent. The validity of the curvature expansion near the core requires

$$v \gg D_\perp/r_c, \quad (5.129)$$

or $x \gg 1$ in (5.128). Moreover, treating v as a constant in

deriving Eq. (5.123) means that we neglect dispersion, i.e. we fix v to be the pulse velocity v_p , which is appropriate if the pulses in the far field do not overlap significantly. The velocity v_{sp} and frequency ω_{sp} of the spiral solution

$$v_{sp} = v_p, \quad (5.130a)$$

$$\omega_{sp} = (v_p^2/D_\perp) Q(r_c v_p / D_\perp), \quad (5.130b)$$

thus obtained will be self-consistent for any r_c such that Eq. (5.129) is satisfied. Of course, the length r_c must bear some relationship to the microscopic lengths in the system for the solution to be physically meaningful.

The solution of the eikonal equation (5.125) also provides a detailed shape of the equiphase lines $\theta(r)$, obtained by integrating up $\psi(\tilde{r})$ according to (5.122). It is interesting to compare this numerical solution with two limiting cases, the first being an Archimedean spiral obtained by assuming $\theta(r)$ to be linear everywhere. The result is

$$\theta(r) = q_\infty r, \quad (5.131)$$

which implies

$$r_c = 0. \quad (5.132)$$

The second approximation is an involute spiral, obtained by neglecting the curvature correction in the eikonal equation, i.e. by setting $D_\perp = 0$ in (5.117). The constant phase lines in this case are

$$\theta(\tilde{r}) = s(\tilde{r}) - \tan^{-1} s(\tilde{r}), \quad (5.133)$$

with

$$s^2(\tilde{r}) = r^2 q_\infty^2 - 1 = \tilde{r}^2 \tilde{q}_\infty^2 - 1, \quad (5.134)$$

from which it follows that

$$\psi(\tilde{r}) = (\tilde{q}_\infty^2 \tilde{r}^2 - 1)^{1/2}, \quad (5.135)$$

and [cf. Eq. (5.127a)] the core radius is given by

$$\tilde{r}_c \tilde{q}_\infty = r_c q_\infty = 1. \quad (5.136)$$

Note, however, that the curvature K becomes arbitrarily large as $r \rightarrow r_c$ for the involute, so the approximation (5.133) is not self-consistent. Keener and Tyson (1986) have shown in their Figs. 9–11 that the shape function calculated from Eq. (5.125) agrees rather well with the involute spiral for $\tilde{q}_\infty = 0.02$, whereas it is close to the Archimedean spiral for $\tilde{q}_\infty = 0.14$, and disagrees with both for $\tilde{q}_\infty = 0.33$.

d. Three-dimensional defects

(i) The Swift-Hohenberg model

As mentioned above, localized solutions can be found for type I_s systems in two and three dimensions. For example, Aranson *et al.* (1989) have considered the Swift-Hohenberg model with a subcritical bifurcation

^{5.10}There are sign inconsistencies in Tyson and Keener (1988) [compare, e.g., their Eq. (16) and their Fig. 7], so that their equations differ slightly from ours, which agree with Keener and Tyson (1986).

$$\partial_t u = -u + \beta u^2 - u^3 + (\nabla^2 + q_0^2)^2 u , \quad (5.137)$$

as well as a complex generalization

$$\partial_t \psi = -\psi + \beta |\psi|^2 \psi - |\psi|^4 \psi + (\nabla^2 + q_0^2)^2 \psi , \quad (5.138)$$

and have numerically found localized solutions in two and three dimensions over a range of the real parameter β . The existence of stable droplet solutions in models with a Lyapunov function might at first seem surprising, since no such solutions are found in the simpler Ginzburg-Landau model (4.13). It turns out, however, that for the fourth-order system (5.137) the Lyapunov potential has minima associated with variation on the scale q_0^{-1} , so a bubble of the $u \neq 0$ phase can become trapped in the $u = 0$ phase. This is an example of a non-adiabatic effect (see Sec. IV.A.4) which is lost in the amplitude equation (4.13) associated with the "microscopic" model (5.137).

(ii) Scroll waves

Target and spiral solutions can also be constructed in three dimensions. Since the coherent oscillatory state involves a complex order parameter it is analogous to the ordered state of superfluid ${}^4\text{He}$, say, and the three-dimensional defect states will have *line singularities*, rather than point singularities (Mermin, 1979). These structures have been called *scroll waves* by Winfree (1984a). The dynamics of these defects when the ends of the line join to form a loop has recently been treated by Keener (1988) and will be discussed in Sec. X below.

3. Defect dynamics

a. Calculation methods

We may next look at the dynamics of the defects driven by different types of perturbations. These may arise from other distant defects (then we are calculating the interaction between defects) or may be imposed externally, e.g. by compressing the rolls and thereby increasing the wave number or by changing the value of a control parameter. A perfectly periodic structure tends to be a rigid object, whereas the presence of defects allows the whole system to distort. It is then not surprising that the motion of defects is empirically an important feature of the dynamics of spatial patterns, both in transients leading to a final steady state (Siggia and Zippelius, 1981a) and in persistent dynamics. Although the time evolution of ensembles of defects is very complicated, considerable progress has been made in the study of the dynamics of *isolated* or weakly interacting defects, which will primarily concern us here.

Two methods to calculate the dynamics of defects have been used: perturbation theory from an assumed known stationary defect, and nonperturbative methods in those systems (or low-order approximations) whose dynamics is

governed by a potential. We will briefly review these methods in a general context, before discussing specific examples.

(i) Perturbative calculations

If we assume the solution $U = U_d(\mathbf{x} - \mathbf{x}_d)$ for a stationary defect to be known, the dynamics is often given by a solvability condition (see Appendix A). Confining ourselves to stationary (type I_s) systems for the moment, we write an ansatz for the moving defect in the form

$$U(\mathbf{x}, t) = \tilde{U}_d[\mathbf{x} - \mathbf{x}_d(t)] + \eta U_1(\mathbf{x}, t) , \quad (5.139)$$

where η is a small parameter introduced as a measure of the small perturbation causing the motion, \tilde{U}_d is a prescribed distortion of U_d whose form depends on the perturbation (see below), and U_1 is an unknown correction. Substituting the ansatz (5.139) into the general equation of motion (3.4) we find

$$\eta \mathcal{L}_G(U_d) U_1 = -\mathbf{v} \cdot \nabla U_d - \eta \delta G , \quad (5.140)$$

where

$$\mathbf{v} = \partial_t \mathbf{x}_d , \quad (5.141)$$

$$\begin{aligned} \eta \mathcal{L}_G(U_d) U_1 &= \eta \left[\frac{\delta G}{\delta U} \right]_{U=U_d} U_1 \\ &= G[U_d + \eta U_1] - G[U_d] \\ &= G[U_d + \eta U_1] , \end{aligned} \quad (5.142)$$

i.e., \mathcal{L}_G is the linearization of G about U_d , and

$$\eta \delta G \equiv G(\tilde{U}_d) - G(U_d) = G(\tilde{U}_d) . \quad (5.143)$$

[In (5.142) and (5.143) we have used the fact that $G(U_d) = 0$, i.e. that U_d is the stationary defect solution.] Equation (5.140) is formally soluble for the unknown function U_1 as long as the operator \mathcal{L}_G does not have a zero eigenvalue. We are interested in the case where this zero eigenvalue would correspond to the translation of the defect through symmetry related states, and then the corresponding eigenvector is ∇U_d . It follows that \mathbf{v} is given along this symmetry direction \hat{s} by the standard solvability condition (see Appendix A)

$$\mathbf{v} \cdot \hat{s} = -\eta \frac{\int [(\hat{s} \cdot \nabla U_d)^\dagger \delta G] d\mathbf{x}}{\int [(\hat{s} \cdot \nabla U_d)^\dagger (\hat{s} \cdot \nabla U_d)] d\mathbf{x}} . \quad (5.144)$$

There are two difficulties with this expression: one is that the zero-eigenvalue adjoint eigenvector, schematically written as $(\hat{s} \cdot \nabla U_d)^\dagger$ may not be easy to calculate (and is *not* in general the derivative of the adjoint defect solution); the second difficulty is that the integral in the denominator may not be finite, an indication that the perturbation scheme has broken down. In very simple situations it may be straightforward to guess the appropriate cutoff to be imposed. However in most interesting cases, such as systems of many interacting defects, a more so-

phisticated approach is necessary (see subsection V.B.3.b.iii below).

Let us present some examples of the distortion \tilde{U}_d that appears in Eq. (5.143). We first suppose that the driving force is a compression or dilatation of the background wave vector from $\mathbf{q} = q_d \hat{\mathbf{x}}$ which characterizes the far-field of U_d , to $\mathbf{q}' = q_d(1+\eta) \hat{\mathbf{x}}$. Then the distortion \tilde{U}_d is given by

$$\tilde{U}_d = U_d(x(1+\eta) - x_d(t), y - y_d(t)), \quad (5.145)$$

i.e. it is the stretched stationary defect solution. Similarly, if the driving force comes from a change in control parameter $\delta\epsilon$, the above scheme applies with $\mathbf{q}' = q_d(\epsilon + \delta\epsilon)$. Alternatively if the defect is driven by N other defects with fixed positions \mathbf{x}_j ($j = 1, \dots, N$) then we take

$$\tilde{U}_d = U_d(\mathbf{x} - \mathbf{x}_d(t)) + \sum_{j=1}^N [U_d(\mathbf{x} - \mathbf{x}_j) - U_\infty(\mathbf{q}_d \cdot \mathbf{x})], \quad (5.146)$$

where

$$U_\infty = \lim_{|\mathbf{x} - \mathbf{x}_d| \rightarrow \infty} U_d. \quad (5.147)$$

Notice that this simple ansatz only applies when the asymptotic state U_∞ is the same for all the defects in the region of interaction. This is *not* true for example in the case of interacting sources or spirals, where the asymptotic states between the defects correspond to waves traveling in opposite directions. In some cases one might try to allow for a slowly varying phase field between the defects (see subsection V.B.3.b.iii below).

(ii) Potential systems

For potential systems an alternative, more direct method is available (Siggia and Zippelius, 1981a). One equates two expressions for the time evolution of the potential [we use Eq. (4.9) for concreteness]. The first is

$$\partial_t \mathcal{F} = \mathbf{v} \cdot \frac{d\mathcal{F}_d}{d\mathbf{x}_d}, \quad (5.148)$$

where $\mathcal{F}_d = \mathcal{F}(U_d)$, and the effective force $d\mathcal{F}_d/d\mathbf{x}_d$ depends on the perturbation. The second expression is

$$\begin{aligned} \partial_t \mathcal{F} &= -2\tau_0 \int |\partial_t U_v|^2 d\mathbf{x} \\ &= -2\tau_0 \int |\mathbf{v} \cdot \nabla U_v|^2 d\mathbf{x}, \end{aligned} \quad (5.149)$$

where U_v is the moving defect solution. Equating these two expressions we find for motion in a direction $\hat{\mathbf{e}}$ the expression

$$v = -v^{-1} \hat{\mathbf{e}} \cdot d\mathcal{F}_d / d\mathbf{x}_d, \quad (5.150)$$

with

$$v = 2\tau_0 \int |\hat{\mathbf{e}} \cdot \nabla U_v|^2 dx. \quad (5.151)$$

Since the right-hand side of Eq. (5.149) is already $O(v^2)$ it may be possible to use the stationary defect solution U_d for U_v , but this does not always yield a finite integral, and then the full moving solution must be used.

b. Examples

(i) Dislocations

(a) Climb

Much of the formalism for considering the dynamics of defects was developed in the context of dislocations in type I_s systems. We first consider the climb of an isolated dislocation near threshold, where we can make use of the potential. Using Eq. (4.9) and the scheme outlined in Eqs. (5.150)–(5.151) above we find for the climb velocity

$$v = -\frac{d\mathcal{F}_d/dy_d}{2\tau_0 \int |\partial_y A_d|^2}. \quad (5.152)$$

This result can be thought of as a Peach-Köhler force divided by an effective drag v which depends on the direction of motion. To evaluate the force we consider the change in \mathcal{F}_d from a displacement δy_d of the defect in a system of extent L_x in the x direction (which we will put to infinity at the end). The only change in the evaluation of \mathcal{F}_d after a displacement δy_d is that an area of the cell $L_x \delta y_d$ has effectively had the wave number $q_+ = q(y \rightarrow +\infty)$ replaced by $q_- = q(y \rightarrow -\infty)$. Thus

$$\delta\mathcal{F} = -[\partial_q \mathcal{F}_\infty(q)] (q_+ - q_-) L_x \delta y_d, \quad (5.153)$$

where $\mathcal{F}_\infty(q)$ is the dependence of the potential of the ideal state on the wave number q . Now $(q_+ - q_-) L_x$ is simply the phase winding 2π , and using the explicit expression for \mathcal{F}_∞ in the amplitude equation (4.3) we find

$$d\mathcal{F}_d/dy_d = -2\pi \partial_q \mathcal{F}_\infty = 4\pi \xi_0^2 |A_\infty(k)|^2 k, \quad (5.154)$$

with $|A_\infty(k)|$ the magnitude of the ideal solution with wave number $\mathbf{q} = (q_0 + k) \hat{\mathbf{x}}$. It turns out that the drag term is dominated by the far region where

$$|\partial_y A_d|^2 \approx |A_\infty|^2 |\partial_y \bar{\phi}|^2, \quad (5.155)$$

and we must use the moving defect solution $\bar{\phi}$ to obtain finite answers.

For the isotropic case we use Eqs. (5.152), (5.155), and (5.94) to obtain an equation for \bar{v} which reads

$$\bar{v} = 4\sqrt{2} \pi \left[\int \int d\bar{x} d\bar{y} [\partial_y \bar{\phi}(\bar{x}, \bar{y}, \bar{v})]^2 \right]^{-1}. \quad (5.156)$$

Since the nonlinear phase equation has not been solved the above result has not been adequately tested, but an approximation was obtained by Siggia and Zippelius (1981a) who inserted the $\bar{\phi}$ obtained from the linear phase equation (5.95). Their result is $\bar{v} = 1.47$, which compares reasonably well with the value $\bar{v} = 0.84$ they extracted from a direct numerical simulation of the amplitude

equation. Thus, although the numerical value of \bar{v} has not been accurately calculated from (5.156), the result that $\bar{v} \sim \text{const}$, i.e. $v \propto k^{3/2} = (q - q_0)^{3/2}$ (independent of ϵ) is a definite prediction. This unusual scaling can be traced back to the fact that $D_{\perp} \rightarrow 0$ at the wave vector of the stationary defect.

The anisotropic case was treated by Bodenschatz *et al.* (1988a). Here using the stationary solution (5.91) in Eq. (5.152) leads only to weak logarithmic divergences. For the conveniently scaled equation

$$\partial_T \bar{A} = \bar{A} + (\partial_X^2 + \partial_Y^2) \bar{A} - |\bar{A}|^2 \bar{A}, \quad (5.157)$$

they find for $k, V \rightarrow 0$

$$V = 2k / \ln(3.29/V), \quad (5.158)$$

in a very large system where the velocity provides the cutoff at long distances (cf. subsection V.B.2.c.i above). In a system of scaled size L with $L \ll V^{-1}$ the velocity cutoff in the logarithm is replaced by a number proportional to L . It may be remarked that due to the isotropy of the amplitude equation, this same result applies to climb (V in the Y direction driven by a wave number change $k = \partial_X \bar{\phi}$) and to glide (V in the X direction driven by a tilt of the rolls $k = \partial_Y \bar{\phi}$), as well as to intermediate cases. Physically, we again expect that for small enough k or for increasing control parameter, glide will be affected by pinning to the underlying periodic rolls, but these effects are not captured by the amplitude equation.

Using the same method it is easy to include the interaction between defects. It is then important to remember the anisotropic distribution of the phase distortion of a moving defect displayed in Eq. (5.92), so that the interaction falls off exponentially in some directions, unlike the stationary defect which yields a power-law falloff.

Away from threshold in general no potential exists, and the velocity of climb has only been calculated perturbatively. [Also away from threshold we expect glide motion to be quenched, at least for small driving strengths accessible to perturbation theory, by the pinning, see Sec. IV.A.4 above.] The starting point of the calculation is to assume the stationary defect solution to be known, including of course the background wave number q_d selected by the stationarity condition. As far as we can see the value of q_d is fixed by the details of the core structure on $O(1)$ length scales, and in general we have no way of finding it except numerically or through some other perturbation scheme (Pomeau *et al.*, 1983). In general we expect $D_{\perp}(q_d) \neq 0$, so that the far field is given by Eqs. (5.91) and (5.92).

If the stationary defect solution U_d is assumed known, then it is relatively easy to investigate the climb velocity induced by a change in the background wave number, at least formally (Kawasaki, 1984a,b; Tesauro and Cross, 1986). The ansatz (5.145) becomes

$$\tilde{U}_d = U_d((1+\eta)x, y-vt), \quad (5.159)$$

with $\eta = (q - q_d)/q_d$. The general procedure outlined in Eq. (5.144) above then gives

$$v = \eta v^{-1} \int (\partial_y U_d)^\dagger \delta G(U_d), \quad (5.160)$$

with

$$v = \int (\partial_y U_d)^\dagger (\partial_y U_d), \quad (5.161)$$

where $(\partial_y U_d)^\dagger$ is the zero-eigenvalue adjoint eigenvector (adjoint to the translation mode $\partial_y U_d$), and now δG arises from the $O(\eta)$ terms produced by the replacement $\partial_x \rightarrow (1+\eta) \partial_x$ in the evolution operator G . In the denominator we again try replacing U_d by its value in the large-distance region

$$U_d(x, y) \simeq U_0(\mathbf{q}_d \cdot \mathbf{x} + \bar{\phi}), \quad (5.162)$$

where U_0 is the ideal periodic solution with wave number $\mathbf{q}_d = q_d \hat{\mathbf{x}}$, and in this approximation U_d satisfies a self-adjoint equation so that

$$(\partial_y U_d)^\dagger \simeq q_d^{-1} [\partial_x U_0(q_d x)] \partial_y \bar{\phi} \simeq \partial_y U_d. \quad (5.163)$$

The effective damping (5.151) is then

$$v = \langle q_d^{-2} [\partial_x U_d(q_d x)]^2 \rangle \int (\partial_y \bar{\phi})^2, \quad (5.164)$$

where $\langle \dots \rangle$ denotes an average over the periodic solution. If $\bar{\phi}$ is evaluated for the stationary solution, i.e. (5.91), the integral in v diverges logarithmically, so we need a long-distance cutoff either from finite system size or from the velocity itself. In the latter case the result is

$$v \propto (q - q_d) / \ln(v/v_0), \quad (5.165)$$

where v_0 represents a short-distance cutoff. The analogy to Eq. (5.158) should be clear and the result basically stems from the assumption $D_{\perp}(q_d) \neq 0$. In numerical simulations of nonpotential model systems (Tesauro and Cross, 1986) the linear dependence on $(q - q_d)$ has been verified (there the system was quite small, and finite size provided the long-distance cutoff), in contrast to results indicating a $(q - q_d)^{3/2}$ law for a potential model, where $D_{\perp}(q_d) = 0$.

(B) Glide

Near threshold, dislocation glide in the isotropic system can also be studied by calculating the effect on the potential. The relevant term replacing (5.154) is now due to curvature, i.e. $-(1/8q_0^2) |A_{\infty}|^2 (\nabla \cdot \mathbf{k})^2$. It is clear that glide in a constant curvature cannot change the potential, so instead we must look at a background phase of the form

$$\phi = c x y^3, \quad (5.166)$$

with c a constant. We may again evaluate the change in the potential from a displacement δx_d of the dislocation. This is done most easily by transforming the integral to a contribution from the change in the length of the 2π cut

as the dislocation is displaced (Kawasaki, 1984a,b),

$$\delta\mathcal{F}/\delta x_d = (\pi/2q_0^2) |A_\infty|^2 \partial_y(\nabla \cdot \mathbf{k}) . \quad (5.167)$$

Thus the Peach-Köhler force takes the form $\tau \times \nabla(\nabla \cdot \mathbf{k})$ with τ the circulation of the phase around the defect (in the $\pm z$ direction depending on the sign of the winding number). The drag term now takes the form

$$\nu = \int |\partial_x A_d|^2 \simeq |A_\infty|^2 \int (\partial_x \phi)^2 , \quad (5.168)$$

and this integral is finite even when the solution for a stationary defect is used. Shraiman (private communication) has proposed an additional term in the Peach-Köhler force in potential systems proportional to $\nabla(\nabla \cdot \mathbf{k})$, which leads to glide in an axisymmetric situation ($\nabla \cdot \mathbf{k} = q_0/r$). Note that in this case the direction of motion is independent of the sign of the dislocation.

Very little is known about glide motion of dislocations away from the threshold region, where the amplitude equation no longer applies. Pomeau *et al.* (1983) showed that glide *may* be caused by a constant curvature (i.e., $\phi = qx + \gamma y^2$) in a nonpotential system, again by balancing these distortion terms with the higher-order amplitude equation terms in the solvability condition (5.144). However the integrals in the numerator diverge, and the authors suggested a nonanalytic dependence of the glide velocity, varying as $\gamma^{1/2}$. Again we remark that pinning should quench the motion for small driving forces, so that the validity of this perturbative approach is not clear.

(ii) Interaction of pulses

Localized defects such as pulses or fronts (kinks) have been extensively studied in reaction-diffusion systems (see, e.g. Rinzel and Terman, 1982; Gurevich and Mints, 1984; Mornev, 1984; Vasiliev *et al.*, 1987; Gurevich *et al.*, 1989; Murray, 1989; Ohta *et al.*, 1989). The specific problem of the interaction of pulses in a one-dimensional excitable medium provides a fertile example of the methodology we have outlined (Elphick *et al.*, 1988, 1990b, 1991; Elphick and Meron, 1990). The system considered is a general reaction-diffusion system

$$\partial_t U = \mathcal{D} \partial_x^2 U + \mathcal{L} U + \mathcal{N}(U) , \quad (5.169)$$

with \mathcal{D} a diffusion matrix, \mathcal{L} a linear operator, and \mathcal{N} a nonlinear operator. In particular the simple Fitz-Hugh-Nagumo model in one dimension

$$\partial_t u_1 = \partial_x^2 u_1 + 3u_1 - u_1^3 - u_2 , \quad (5.170a)$$

$$\partial_t u_2 = a(u_1 - b) , \quad (5.170b)$$

can be used for illustration. For consistency with our general notation we will define $\bar{u}_1 = u_1 - b$, $\bar{u}_2 = u_2 - (3b - b^3)$ so that the quiescent state is $\bar{u}_1 = \bar{u}_2 = 0$. Since we are dealing with real solutions of a real equation an analysis in terms of the variables \bar{u}_1 , \bar{u}'_1 , \bar{u}_2 is appropriate, and the quiescent state corre-

sponds to the L fixed point $\bar{u}_1 = \bar{u}'_1 = \bar{u}_2 = 0$ (subsection V.B.2 above). A pulse solution corresponds to a homoclinic orbit starting at and returning to L . For some values of the parameters a, b the stability analysis about L yields a complex pair of eigenvalues, as well as one real eigenvalue, so that the approach of the variables \bar{u}_1 , \bar{u}_2 to zero in the trailing edge is oscillatory. In this situation spatial chaos is typical (see Sec. VII.E.6 below).

If $U_d(\xi)$ with $\xi = x - vt$ is the single pulse solution centered around the origin satisfying

$$(\mathcal{D} \partial_x^2 + v \partial_x + \mathcal{L}) U_d + \mathcal{N}(U_d) = 0 , \quad (5.171)$$

we seek a solution for a collection of defects in the comoving frame

$$U(\xi, t) = \sum_i U_d(\xi - \xi_i(t)) + U_1(\xi, t) . \quad (5.172)$$

We assume that the defects are well separated, $\xi_i - \xi_{i-1} \gg 1$, so that the time dependence of the positions ξ_i is slow and the correction term U_1 is small, with an exponential dependence on the separation. (We will not explicitly introduce the small parameter η to display these small quantities.) This is still of the general form (5.146), except that we have made use of the fact that $U_d(\xi \rightarrow \pm \infty) = 0$. Thus we have, following the analysis of subsection V.B.3.a. above,

$$\partial_t \xi_i = \frac{\int [\partial_\xi U_d(\xi - \xi_i)]^\dagger \delta G d\xi}{\int [\partial_\xi U_d(\xi - \xi_i)]^\dagger [\partial_\xi U_d(\xi - \xi_i)] d\xi} , \quad (5.173)$$

with δG determined by the defect interaction through the nonlinear terms

$$\delta G = \mathcal{N} [\sum_j U_d(\xi - \xi_j)] - \sum_j \mathcal{N}[U_d(\xi - \xi_j)] , \quad (5.174)$$

and $(\partial_\xi U_d)^\dagger$ is the zero-eigenvalue adjoint eigenvector, adjoint to the translation mode^{5.11} $\partial_\xi U_d$. It is clear that δG is of order $\exp(-\lambda \xi_d)$ where λ is the exponential decay of the tails of the pulses (we assume front and back have comparable values) and ξ_d is the typical separation of the defects. In general δG contains contributions from the overlap of the tails of the j th defect with the core region of the $(j \pm 1)$ st defects, and also from the overlap of the tails of the j and $(j+1)$ st and the j and $(j-1)$ st defects in the intermediate region $\xi - \xi_j \sim \pm 1/2 \xi_d$. The adjoint eigenvector $\partial_\xi U_d^\dagger(\xi - \xi_i)$ presumably also decays exponentially away from ξ_i with similar decay rates. Thus a number of terms may be identified that are $O[\exp(-\lambda \xi_d)]$: because of the $\partial_\xi U_d^\dagger$ term, in the present case they all arise from the overlap of the tails of the $(i \pm 1)$ st defect with the core of the i th defect rather than the overlap of two tails in the intermediate region. We find terms

^{5.11}Equations (5.173) and (5.174) have a very different form from those of Elphick *et al.*, (1988) who have a $\partial_\xi^2 U$ term in the denominator. This comes from their unorthodox parametrization with $U_d[t - x/v_0 - \tau_j(x)]$ in place of (5.172). Our results do agree with those of Elphick and Meron (1990b).

$$\int (\partial_\xi U_d^\dagger)_i \delta G = \int (\partial_\xi U_d^\dagger)_i \left\{ \left[\left[\frac{\partial \mathcal{N}}{\partial U_d} \right]_{i-1} + \left[\frac{\partial \mathcal{N}}{\partial U_d} \right]_{i+1} \right] (U_d)_i + \left[\frac{\partial \mathcal{N}}{\partial U_d} \right]_i [(U_d)_{i-1} + (U_d)_{i+1}] \right\} d\xi , \quad (5.175)$$

where $(\partial \mathcal{N}/\partial U_d)_i$ is the Jacobian of the nonlinear term with respect to U_d evaluated for the i th defect solution [e.g. if $\mathcal{N}=U^3$, $(\partial \mathcal{N}/\partial U_d)_i=3U_d^2(\xi-\xi_i)$]. The expression in Eq. (5.175) is more general than that of Elphick *et al.* (1988), who do not need the first term in square brackets for the special case they consider. Independently of the details we therefore arrive at the equation of motion

$$\partial_t \xi_i = C_1 \exp[-\kappa_1(\xi_{i+1}-\xi_i)] \cos[q_1(\xi_{i+1}-\xi_i)+\phi_1] + C_2 \exp[-\kappa_2(\xi_i-\xi_{i-1})] \cos[q_2(\xi_i-\xi_{i-1})+\phi_2] , \quad (5.176)$$

where $\kappa_j \pm iq_j$ are the eigenvalues of the L fixed point (see subsection V.B.2.b above), and C_j and ϕ_j depend on performing the detailed integrals. For the specific model (5.170) the trailing edge of the pulses may be oscillatory (i.e., $q_1 \neq 0$), whereas the leading edge is not ($q_2=0$). Then Eq. (5.176) yields an asymmetric interaction in the forward and backward directions, and the equivalent of the Peierls-Nabarro “force” does not satisfy Newton’s third law.

A similar formalism has been developed by Aranson *et al.* (1989) to describe the interaction of localized pulse-like solutions in three dimensions. The equation of motion for the distance R between two pulses is

$$\partial_t R = R^{-1} \partial_R [e^{-\mu R} \cos \nu R] , \quad (5.177)$$

where μ and ν are constants characterizing the asymptotic behavior of the single pulse solution. Recently, Malomed and Nepomnyashchy (1990) have calculated the interaction of pulses in the complex Ginzburg-Landau equation (4.49) by perturbative expansions near the nonlinear Schrödinger ($c_1, c_3 \rightarrow \infty$) and relaxational ($c_1, c_3 \rightarrow 0$) limits. They find evidence for bound states in both cases. Numerical work on this system has been carried out by Brand and Deissler (1989) and Deissler and Brand (1990, 1991).

(iii) Interaction of dislocations and spirals in the complex Ginzburg-Landau model

A long sought goal is the development of a complete “phase field plus defect” dynamical description of a dilute system of defects involving equations of motion of the defect positions \mathbf{x}_k , driven by and in turn modifying the slow phase field ϕ (see, e.g. Cross and Newell, 1984). The effort in this direction has advanced furthest for the Ginzburg-Landau equation. Although the final goal has not yet been reached, the work does illustrate the general problems and potential solutions.

Following the approach of Kawasaki (1984a) and Tesauro and Cross (1986), Rica and Tirapegui (1989) and Elphick and Meron (1991) have used an ansatz for a multidefect solution

$$A(\mathbf{x}, t) = (a^{(0)} + a^{(1)}) e^{i\phi(\mathbf{x}, t)} , \quad (5.178)$$

where $a^{(0)}$ is an ansatz for the magnitude analogous to Eq. (5.145), $a^{(1)}$ is the small correction due to the interac-

tion, and ϕ is the full phase field. (We use a slightly different notation than Rica and Tirapegui.) Based on the solvability conditions with respect to the zero eigenvectors represented by translations of the defects, and on phase symmetry, they propose the coupled equations

$$\partial_t \mathbf{x}_k = 2m_k \hat{\mathbf{z}} \times \nabla \phi^{(k)} \Big|_{\mathbf{x}_k} + 2c_1 \nabla \phi^{(k)} \Big|_{\mathbf{x}_k} , \quad (5.179)$$

together with the usual phase equation (4.90)–(4.91)

$$\partial_t \phi = (1 - c_1 c_3) \nabla^2 \phi - (c_1 + c_3) (\nabla \phi)^2 + c_3 . \quad (5.180)$$

The effect of the defect on the phase is given by the phase winding condition around each defect, e.g., for a contour surrounding just the k th defect at \mathbf{x}_k

$$\int_k \nabla \phi \cdot d\ell = 2\pi m_k . \quad (5.181)$$

In (5.179) $\phi^{(k)}$ is given by subtracting the phase field of the k th defect from the full phase field ϕ . This clearly illustrates the type of result desired. Unfortunately, as far as we can see, this result is only correct in the special case of $|c_1 + c_3| \ll 1$, but not $c_1 = c_3 = 0$ (i.e. the real case). Two difficulties arise.

- The complex case: interacting spirals. As pointed out by Aranson *et al.* (1991) (see also Rica and Tirapegui, 1991a; Pismen and Nepomnyashchy, 1992), in the general complex case the asymptotic wave vectors of the two spirals at a point between them have $O(1)$ magnitude $q_\infty(c_1, c_3)$, but are in opposite directions, so that a shock develops; this happens unless $q_\infty \rightarrow 0$, which occurs when $|c_1 + c_3| \rightarrow 0$. (This special case has been treated in detail by Rica and Tirapegui, 1991b.) Aranson *et al.* treat the shock for small $|c_1 + c_3|$ within the nonlinear phase equation (5.180), applying the Cole-Hopf transformation (5.77a) to obtain a linear system. Then superposition and the exponential falloff in the Cole-Hopf variables immediately lead to an interaction (and a velocity $\partial_t \mathbf{x}_k$) which decrease exponentially with the separation between defects. This effect corrects the r^{-1} dependence in the earlier work (Rica and Tirapegui, 1989; Elphick and Meron, 1991), where a linear superposition of the phase fields of the two defects, not allowing for the nonlinear shock, was erroneously assumed. Although it is expected that the exponential form, including the estimate of the decay rate αq_∞ [with $\alpha = (c_1 + c_3)/(1 - c_1 c_3)$], will persist even for $|c_1 + c_3| = O(1)$, in this

case the shock is strong [see subsection V.B.2.b.(vi) above] and so it cannot be quantitatively captured by the phase equation (5.180). Presumably a complete calculation must also involve the dynamics of the shock line defect (which need not necessarily be midway between the point defects as assumed by Aranson *et al.*, 1991), together with equations such as (5.179) and (5.181). Moreover, the subtraction involved in calculating $\phi^{(k)}$ from the full phase field seems to remain a delicate question in general (see Pismen and Nepomnyashchy, 1992). Despite these subtleties, the physically important basic result, i.e. the exponential decay of the interaction between spirals at large distances, was confirmed by numerical calculations of Aranson *et al.* (1991a,b). These authors also find the possibility of bound states at small separation.

• The real case. For the real case $c_1 = c_3 = 0$, we have seen in Eq. (5.158) above that there are in fact logarithmically divergent coefficients in relating the velocity $\partial_t \mathbf{x}_k$ to the local phase gradient, and these are not apparent in Eq. (5.179). Recently various authors (Neu, 1990; Pismen and Rodriguez, 1990) have shown how to incorporate the logarithmic cutoffs by a careful treatment of the delicate subtraction involved in going from ϕ to $\phi^{(k)}$, in which the stationary solution for the defect cannot be used. We will describe the version by Neu since his approach is analogous to the one discussed earlier, and it seems better suited for generalizations to more complicated cases.

The crucial elements in Neu's analysis involve matching a phase expansion and a core expansion in an overlap region where both are valid, and using an integral expression which is a generalization of the solvability condition, but is evaluated over a finite region so that divergences are eliminated. For a point defect moving with velocity v in a dilute ensemble of other defects the phase equation near the chosen defect is to lowest order in the expansion parameter η (e.g. the inverse of the defect spacing)

$$\nabla^2 \phi = -\mathbf{v} \cdot \nabla \phi , \quad (5.182)$$

since other time derivatives are $O(\eta^2)$. Expansion of the solution of Eq. (5.182) about the defect position in small $r = |\mathbf{x} - \mathbf{x}_d|$ yields

$$\phi(\mathbf{r}) = \phi_0(\mathbf{r}) + \frac{1}{2} (\log r) \mathbf{v} \cdot \mathbf{r} + \mathbf{K} \cdot \mathbf{r} + \dots , \quad (5.183)$$

where ϕ_0 is the unperturbed phase and \mathbf{K} is not given by the expansion but is to be determined by matching to the far field. The core expansion must involve the full amplitude $A = A_0 + A_1$ with A_0 the unperturbed core solution, and A_1 the perturbation satisfying in analogy with Eq. (5.140) above,

$$\mathcal{L} A_1 = -\mathbf{v} \cdot \nabla A_0 , \quad (5.184)$$

where \mathcal{L} is the linearized operator

$$\mathcal{L} A_1 = \nabla^2 A_1 + (1 - 2|A_0|^2) A_1 - A_0^2 A_1^* . \quad (5.185)$$

Matching to the phase equation we obtain

$$A_1 \rightarrow i \left[\frac{1}{2} (\log r) \mathbf{v} \cdot \mathbf{r} + \mathbf{K} \cdot \mathbf{r} \right] A_0 , \quad (5.186)$$

in a matching region where $|A_0| \rightarrow 1$ but the small- r expansion (5.183) of the phase is still valid.

The standard solvability condition is derived from

$$\int [(\nabla A_0)^\dagger \mathcal{L} A_1] d\mathbf{x} = 0 , \quad (5.187)$$

where by $(\nabla A_0)^\dagger$ we mean the zero eigenvalue eigenfunction of \mathcal{L}^\dagger . Since this expression has a logarithmic divergence at large $|\mathbf{x}|$, Neu writes a modified solvability condition on a finite domain D , by making use of the identity

$$\begin{aligned} I &\equiv \int_D \operatorname{Re}(u^* \mathcal{L} w - w^* \mathcal{L} u) d\mathbf{x} \\ &= \int_{\partial D} \operatorname{Re}(u^* \partial_n w - w^* \partial_n u) d\ell , \end{aligned} \quad (5.188)$$

valid for arbitrary functions u and w , with D the disk of radius r_0 centered on the defect, ∂D the boundary of this disk taken to be in the matching regime, and ∂_n a derivative normal to the boundary. Taking $\hat{\mathbf{e}}$ to be an arbitrary direction Neu makes the choices

$$u = \hat{\mathbf{e}} \cdot \nabla A_0 \text{ so that } \mathcal{L} u = 0 , \quad (5.189)$$

and

$$w = A_1 \text{ so that } \mathcal{L} w = -\mathbf{v} \cdot \nabla A_0 . \quad (5.190)$$

The first part of the identity in (5.188) gives

$$I = -\pi(\alpha + \log r_0) \hat{\mathbf{e}} \cdot \mathbf{v} + \dots , \quad (5.191)$$

with

$$\alpha = \lim_{r_0 \rightarrow \infty} \int_0^{r_0} [(d|A_0|/dr)^2 + r^{-2}|A_0|^2] r dr - \log r_0 , \quad (5.192)$$

representing a core integral independent of r_0 and of the perturbations. The second part of the identity gives

$$I = -\pi(\log r_0 + 1) (\hat{\mathbf{e}} \cdot \mathbf{v}) - 2\pi \hat{\mathbf{e}} \cdot \hat{\mathbf{z}} \times \mathbf{K} . \quad (5.193)$$

On equating these two expressions, the logarithmic terms cancel to yield the relation

$$(1 - \alpha) \mathbf{v} = -2\hat{\mathbf{z}} \times \mathbf{K} , \quad (5.194)$$

replacing Eq. (5.179) which is wrong as it stands for the real case. The calculation of the motion of the defect thus reduces to the evaluation of the quantity \mathbf{K} , given by the prescription of solving the phase equation (5.180) with the moving defects as sources, and then performing the subtraction at each defect required by the definition of $\phi^{(k)}$. Since the subtractions involve the unknown velocities and since the phase field and velocities must be mutually consistent, this procedure, although defined in principle, may be quite difficult to carry out in practice for a general situation of many interacting defects. Neu illustrates the method for a single defect in the presence

of a constant background phase gradient \mathbf{q} and finds

$$\mathbf{K} = \mathbf{q} + \frac{1}{2} \log|v| \hat{\mathbf{z}} \times \mathbf{v}, \quad (5.195)$$

which, with (5.194), yields an implicit expression for the velocity and reproduces the results of Bodenschatz *et al.* (1988a) for this simple situation. Here clearly the velocity v provides the long distance cutoff. In other situations some combination of v and variations in the phase gradient field presumably play this role. It would appear straightforward to generalize the above calculation to other simple situations, such as two defects approaching each other from infinity, initially driven by a uniform phase gradient \mathbf{q} . The full solution for an arbitrary dilute defect field remains to be demonstrated. For further discussion of this problem see Pismen and Rodriguez (1990), Pismen and Nepomnyashchy (1991), and Pismen and Rubinstein (1991).

(iv) Scroll waves in three dimensions

In a three-dimensional system that develops spiral line singularities, the lines may connect to form various loop defects which are dynamic due to the mutual interaction of portions of the loop. Keener (1988) has developed a description of this dynamics starting from an assumed known spiral or target solution $U_2(r, \theta)$ for a two-dimensional model, such as a reaction-diffusion equation (5.169). The new idea, beyond our discussion of defects in the plane, is to allow for a slow variation of this solution in the third dimension. The centers of the 2d spirals may now lie on a slowly varying curve $\mathbf{R}(s, t)$ in three-space, called the filament of the scroll wave (s is the arc-length along the filament), and the phase ϕ of the spiral may twist going along this curve. An approximate solution is sought in the form

$$U(\mathbf{r}, t) = U_2(|\mathbf{r} - \mathbf{R}(s, t)|, \theta + \phi(s, t) - \omega t) + U_1, \quad (5.196)$$

where derivatives of the twist ϕ and of \mathbf{R} , as well as the correction U_1 , are assumed to be small. If \mathbf{N} and \mathbf{B} are unit vectors normal and binormal to the curve \mathbf{R} , and \mathbf{T} is the tangent vector, then three-dimensional space can locally be represented along the three orthogonal directions \mathbf{T} , \mathbf{N} , and \mathbf{B} . The basic ansatz is that the curvature $K = \mathbf{N} \cdot \partial_s \mathbf{T}$ and torsion $\tau = -\mathbf{N} \cdot \partial_s \mathbf{B}$ of the curve $\mathbf{X} = \mathbf{R}$ are small, and that the curve moves slowly in space. The lowest-order phase equations are then

$$\omega = \partial_s \phi - \tau, \quad (5.197a)$$

$$\partial_t \phi = \mathbf{B} \cdot \partial_t \mathbf{N} + (\mathbf{T} \cdot \partial_t \mathbf{R}) \omega + \beta_1 \partial_s \omega - \alpha_1 \omega^2 - \gamma_1 K, \quad (5.197b)$$

$$\mathbf{N} \cdot \partial_t \mathbf{R} = \beta_2 K - \gamma_2 \partial_s \omega - \alpha_2 \omega^2, \quad (5.197c)$$

$$\mathbf{B} \cdot \partial_t \mathbf{R} = \gamma_3 K - \gamma_4 \partial_s \omega - \alpha_3 \omega^2, \quad (5.197d)$$

where the coefficients $\alpha_i, \beta_i, \gamma_i$ are expressed in terms of the two-dimensional solution U_2 , as well as the solution of an adjoint problem, as in Eq. (5.144) above.

From these general equations the following results are obtained in special cases.

Untwisted scroll ring: For an untwisted filament in a plane, ϕ is independent of position and the torsion τ can be taken to zero, so the equations become

$$\mathbf{N} \cdot \partial_t \mathbf{R} = \beta_2 K, \quad (5.198a)$$

$$\mathbf{B} \cdot \partial_t \mathbf{R} = \gamma_3 K, \quad (5.198b)$$

$$\partial_t \phi = -\gamma_1 K. \quad (5.198c)$$

If all the diffusion constants in Eq. (5.169) are equal [$\tilde{D} = D_1$], then $\gamma_1 = \gamma_3 = 0$, $\beta_2 = D$, and a planar filament stays in the same plane and moves with normal velocity proportional to DK . A ring collapses at a rate proportional to its curvature $1/r$. For unequal diffusion constants, $\gamma_3 \neq 0$ and there is a drift perpendicular to the plane of the filament. Moreover in this case one can have $\beta_2 < 0$ which implies that a ring expands.

Twisted scroll rings: In (5.197) the equation of motion for the twist ϕ is a diffusion equation with diffusion constant β_1 , so that nonuniform twist will tend to smooth out (assuming $\beta_1 > 0$). A ring with constant twist will collapse or not, depending on the sign of $\alpha_2 \beta_2$, and the perpendicular drift will also be affected by the twist. The reader is referred to Keener (1988) for further discussion.

VI. PATTERN SELECTION

The problem of pattern selection arises because the equations we are considering have many solutions above threshold for given external conditions, whereas observed patterns constitute a much more restricted set. Thus, among the allowed (i.e. linearly stable) solutions some seem to be preferred over others, and we would like to understand the selection process.

The question divides naturally into two parts. First, what is the multiplicity of real solutions, and how does it compare with the multiplicity of ideal solutions? To begin to answer this question we will incorporate the “elements of real patterns” of the previous section into our description of ideal patterns. Second, if real patterns show multiplicity, is there any ordering between them, such that one solution is preferred over the other? In equilibrium thermodynamic systems this is a familiar concept, with the free energy providing the ordering principle. Although we will see that an analogous approach using the Lyapunov potential may be useful in a *restricted* range near threshold, in general we find no evidence for such a global organizing principle to apply in nonequilibrium system. We might then consider that one state is “preferred” over the other if it has a larger basin of attraction for typical initial conditions, or if it evolves from an initial condition where the two states coexist side by side. This then directs our attention to the dynamics

leading to the final steady state rather than to properties of this state itself.

In addition to these general considerations, the final pattern may depend on the specific way in which the control parameters reach their final values, and on the particular dynamics leading to the steady state. For example, if the pattern grows from a uniform state it is very sensitive to small forces as it grows from zero amplitude, and there must be some forcing to make the pattern grow since in the ideal system with no forcing the uniform amplitude state remains a valid solution for all times. Thus quite delicate features may have a substantial effect on the final steady state. This is often useful in biological models where a small source term is added to favor a desired final state (see Sec. XI). Also in Rayleigh-Bénard convection the effects of forcing on the subsequent pattern evolution have been investigated quite carefully both experimentally and theoretically (see Sec. VIII.D).

We therefore divide our discussion of pattern selection^{6.1} in type-I_s systems into two parts: selection via constraints and selection via dynamics. The distinction is not meant to be rigid; it is introduced primarily for pedagogical purposes and seems to disappear for oscillatory systems. We will find it useful to distinguish between “prepared patterns” which are geometrically simple and result from carefully prescribed conditions and growth protocols, and “natural patterns” which are more complicated and typically arise in large systems with less controlled initial conditions.

A. Type I_s: Stationary patterns

1. Selection via constraints

We first focus on the most elementary example of selection, the local wavelength or distribution of wavelengths in regular stationary roll patterns. This means that we wish to know how the ideal stability balloon of Sec. IV.A is modified by adding the real pattern elements likely to be found in practice. This area has been widely studied over the past two decades, and we now have a rather complete understanding of the phenomena. The more general question of disordered patterns in two dimensions, which we turn to next, is much less well understood. The theoretical knowledge we do have is largely

based on numerical studies of simple models such as the Swift-Hohenberg equation.

a. One dimension: Wave-vector selection

The ideal system — in an infinite geometry or with periodic boundary conditions — has considerable rigidity: any solution with wave vector in the stable band is a good solution because the dynamical trajectory in phase space connecting states with two nearby wave vectors involves large excursions. It is clear from the discussion of Sec. V that this is no longer true in real systems, where both boundaries and defects may relax the constraint of a fixed number of wavelengths. We will thus see that there exist situations which lead to simple essentially one-dimensional patterns, perhaps with one or a few defects, but where the wave vector is *selected* to a unique value, or a narrow band, by some constraint. We now list examples of such wave-number selection mechanisms.

(i) Rigid sidewalls

We have seen that rigid sidewalls provide a means whereby the wave number in the bulk of the system (far from the wall) can adjust its value by the creation or the destruction of rolls in the region near the walls where the amplitude of the pattern is suppressed. As discussed in Sec. V.A.1.b, near threshold the bandwidth of allowed states is proportional to ϵ , in contrast to the ideal system where the width goes as $\epsilon^{1/2}$. It should be noted, however, that we are assuming that the rolls are *parallel* to the sidewall, whereas often in the absence of other constraints rolls tend to approach the walls *perpendicularly*. Also, the relaxation mechanism occurring within a coherence length $\epsilon^{-1/2}$ of the wall can become pinned when this length approaches the basic period, so that the reduction in the wave-number band may well be confined to a narrow region near threshold.

(ii) Control parameter ramps

“Soft” boundaries set up by imposing a spatial ramp in the control parameter select a unique wave number in the bulk (Sec. IV.A.2.d). Note that for an arbitrarily slow ramp in a *given* physical quantity (fluid depth or plate temperature in convection for example) the wave number far away is uniquely determined for fixed bulk parameters. However, for ramps in *different* physical quantities leading to the *same* control-parameter variation $\epsilon(x)$, this selected wave number may vary. Ramps therefore provide a useful experimental tool for precise tuning of wave numbers in the bulk (Kramer *et al.*, 1982; Pomeau and Zaleski, 1983; Hohenberg *et al.*, 1985).

(iii) Concentric rolls with focus singularity

The barriers to the creation or destruction of spatial periods become small near the center of a concentric roll

^{6.1}Getling (1991) has advocated a different usage for the term “selection.” He distinguishes between a “preferred pattern” which is reached under “natural” conditions, and a “realized pattern” obtained under specific constraints which he terms “antiselective.” As discussed below, there is some ambiguity in the definition of “natural” conditions, but even if the criterion could be made unambiguous, we see no compelling reason to choose a particular mechanism as leading to the preferred pattern.

pattern, and this provides another mechanism allowing the wave number to relax. We have seen in Sec. V.B.2 that at a large distance r away from the center the wave number approaches the unique value q_f given by the condition $B(q_f)=0$, Eq. (5.98b), with corrections of $O(1/r)$ (Pomeau and Manneville, 1981; Cross and Newell, 1984). This mechanism will still operate even if only portions of the concentric rolls are within the cell, and the center is on or close to a boundary; such a situation often occurs in the corner of rectangular cells [e.g. Fig. 3(e)]. However, once there is no longer axisymmetry mean flow effects may occur in fluid systems, so that the asymptotic wave number is no longer q_f . In the absence of mean flow effects the phase equation is smooth, and the argument for the unique wave number q_f does not rely on axisymmetry (Cross and Newell, 1984). The analysis goes through essentially unchanged with Eq. (4.76) now integrated along the trajectory orthogonal to the roll, and the increasing equiphase distance between nearby orthogonal trajectories playing the role of r on the right-hand side of Eq. (5.98a).

(iv) Dislocations

A single dislocation, as in Fig. 19, provides a competition mechanism between the wave number q_ℓ in the bulk below the core and the wave number q_u above. It is thus reasonable to say that if the dislocation moves up, for instance, the wave number q_ℓ is “preferred” over q_u by this mechanism. Indeed, after the dynamics has ceased the whole region will have wave number q_ℓ , and one spatial period will have been added or lost. If successive dislocations are injected into the system, eventually $q_{\ell,u}$ will be such that the defect is stationary and the preferred wave number q_d must lie between q_ℓ and q_u . For a sufficiently large system these wave numbers become arbitrarily close together, and the optimal wave number q_d can be determined accurately as discussed in Sec. VIII.C below for Rayleigh-Bénard convection. In order for this mechanism to be effective for finding the preferred wave number we must either assume a sufficient preexisting density of dislocations or some creation mechanism for dislocation pairs.

(v) Grain boundaries

We have seen in Sec. V.B that the perpendicular grain boundary configuration of Fig. 21(g) provides a mechanism for the wave number of the central rolls to smoothly adjust, yielding a selected wave number which may depend on the wave number of the cross rolls. It is interesting that this mechanism provides a means additional to (i) above for a rigid boundary to relax the bulk wave number, through the nucleation of cross rolls in the boundary region.

(vi) Competing selection mechanisms

One of the most interesting questions regarding wave number selection is to ask whether the various mechanisms select the same wave number, so that one can truly speak of a “preferred state,” or whether each mechanism for relaxing the rigidity of the ideal solution produces its own wave number. The study of model equations (Cross *et al.*, 1986, see Sec. VIII.C below), calculations on Rayleigh-Bénard convection (Buell and Catton, 1986a,b), and theoretical and experimental results on control parameter ramps in Taylor-Couette flow (Riecke and Paap, 1987, Ning *et al.*, 1990) show that in general different

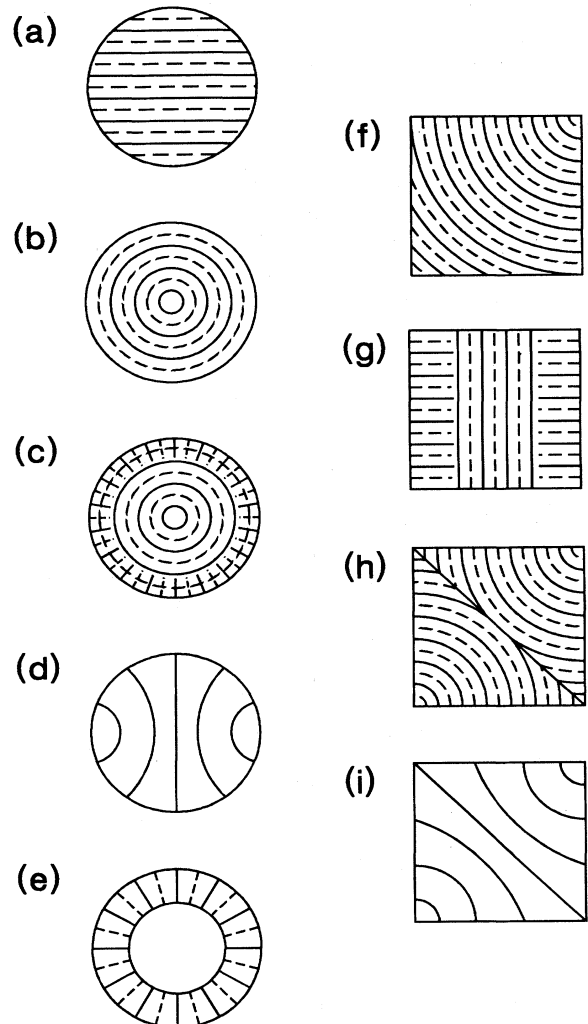


FIG. 21. Schematic of possible patterns in Rayleigh-Bénard convection and other type I_c systems. Solid and dashed lines represent roll boundaries (e.g. upflow and downflow, respectively). In (d) and (i) only a coarse grained representation of the roll boundary directions is shown, and there are many dislocations on a finer scale not shown, which permit the large scale distortions.

selection mechanisms yield different wave numbers. Only in the case of potential systems can one identify a single preferred wave number, which is the one minimizing the potential, but even for that case it appears that front propagation selects a different value (see below). Since we expect typical nonequilibrium systems to be nonpotential this means that in general each mechanism will select a different wave number, though it is clearly necessary to investigate this question in specific systems. In particular, control parameter ramps $\epsilon(x)$ created by variation of different physical parameters provide a useful test case.

If there are indeed different selected wave numbers, it is natural to ask what happens if two mechanisms are operating simultaneously. In general we expect *no* steady solution to exist in these cases, but rather the continual creation of rolls by the mechanism favoring the larger wave number, and the corresponding destruction by the mechanism favoring the smaller one. In the simplest situation the time dependence is periodic, but more complex dynamics is also possible.

This phenomenon can be analyzed quite completely using the phase equation if the two mechanisms operate at well separated locations, for example two different control parameter ramps with a large bulk region in between. We will study the one-dimensional case, but the axisymmetric situation follows quite analogously. For simplicity we neglect the wave-number dependence of $D_{\parallel}(q)$, and seek a temporally periodic solution of the phase equation (4.70) in one dimension, with frequency ω

$$\partial_t \phi = \omega = D_{\parallel} \partial_x q , \quad (6.1)$$

which yields a linearly varying wave number. Also, the frequency is fixed by the requirement that the wave number approaches the selected wave numbers $q_{1,2}$ in the vicinity of each mechanism separated by a distance L ,

$$\omega = (D_{\parallel}/L)(q_1 - q_2) . \quad (6.2)$$

Note that for L large enough ω is small and the individual wave-number selection mechanisms will not be perturbed. The motion consists of the steady drift of rolls between the two regions. Examples of such situations are two incompatible ramps (Cross *et al.*, 1986; Kramer and Riecke, 1985), or the competition between center (focus) and boundary selection in axisymmetric patterns (Cross *et al.*, 1986; Tuckerman and Barkley, 1988; Barkley and Tuckerman, 1989).

b. Two dimensions: general considerations

For large two-dimensional systems the roll direction can vary by large amounts even if the rate of spatial variation is slow, so that the range of possible patterns is much larger than in one dimension. What we would like to do is to put together the various important elements identified in Sec. V, to reach some theoretical understanding of the whole pattern. So far this goal has only been achieved at a semiquantitative level, by analysis of

the Swift-Hohenberg equation near threshold, with confirming evidence from numerical simulations. Further away from threshold our understanding is even more schematic, and is based on the phase equation and on numerical simulations.

(i) Near threshold

As we have seen the Swift-Hohenberg equation (4.108) is a canonical model for type I_s instabilities, and near threshold it can be used as a rotationally invariant generalization of the amplitude equation which holds for any system. Since the equation is governed by a potential which is an integral of local quantities over the whole domain, we can indeed obtain a global description of the system by piecing together elementary contributions. As the potential necessarily decreases in any dynamics, we can never arrive at a final state whose potential value is higher than that of the initial state: in this sense lower potential solutions may be considered "preferred," and we may consider the importance of the various elements discussed in Sec. V according to their relative contribution to the potential (Cross, 1982a).

In the limit

$$\epsilon \ll 1 , \quad \epsilon^{1/2} L \gg 1 , \quad (6.3a)$$

there is a separation of length scales between the roll spacing $q_0^{-1} = O(1)$, the healing length $\xi \approx \xi_0 \epsilon^{-1/2}$, and the system size L such that

$$q_0^{-1} \ll \xi \ll L . \quad (6.3b)$$

In that case one can isolate separate contributions to the potential

$$\mathcal{J} = \int d\mathbf{x} \left[-\frac{1}{2} \epsilon \psi^2 + \frac{\xi_0^2}{8q_0^2} [(\nabla^2 + q_0^2)\psi]^2 + \frac{g_0}{4} \psi^4 \right] , \quad (6.4)$$

coming from the surface and the bulk.

The orientational effect of a rigid boundary was discussed in Sec. V.A: the suppression of the magnitude over a distance of order $\xi_0 \epsilon^{-1/2} (\hat{\mathbf{n}} \cdot \hat{\mathbf{s}})$ [with $\hat{\mathbf{n}}$ the roll normal ($\mathbf{q} = q \hat{\mathbf{n}}$) and $\hat{\mathbf{s}}$ the boundary normal] leads to a boundary contribution to the potential

$$\mathcal{J}_S = (2\sqrt{2}/9 g_0) \xi_0 \epsilon^{3/2} \hat{\mathbf{n}} \cdot \hat{\mathbf{s}} , \quad (6.5)$$

per unit length of boundary. This is minimized for $\hat{\mathbf{n}} \cdot \hat{\mathbf{s}} = 0$, corresponding to rolls approaching the boundary normally. [More precisely, in this limit $\hat{\mathbf{n}} \cdot \hat{\mathbf{s}} = O(\epsilon^{1/4})$, and Eq. (6.5) breaks down due to the neglect of fourth-order derivative terms, the correct answer being $\mathcal{J}_S = O(\epsilon^{7/4})$.]

The bulk term consists of two parts, one arising from slow changes of the roll direction and variations of the wave number, and the other from defects. In the absence of defects the bulk contribution is

$$\mathcal{J}_B = (\xi_0^2/3 g_0) \int d^2x \bar{E} [(1/4q_0^2)(\nabla \cdot \mathbf{q})^2 + (\delta q)^2] , \quad (6.6)$$

with

$$\bar{\varepsilon} = \varepsilon - \xi_0^2 [(\delta q)^2 + (1/4q_0^2)(\nabla \cdot \mathbf{q})^2] \simeq \varepsilon . \quad (6.7)$$

In addition there is a *constraint* (arising from the existence of a phase)

$$(\nabla \times \hat{\mathbf{n}})_z = q_0^{-1} (\hat{\mathbf{n}} \times \nabla \cdot \delta \mathbf{q})_z , \quad (6.8)$$

relating the “bending” of the rolls (in liquid crystal parlance) to spatial variations of the wave number. Now, since $\delta q \lesssim \varepsilon^{1/2}$ from stability considerations, there is only an $O(\varepsilon^{1/2})$ reorientation of $\hat{\mathbf{n}}$ contributing to $(\nabla \times \hat{\mathbf{n}})_z$ over the whole system, so we may put $\delta q = 0$ in predicting possible patterns. We then find

$$\mathcal{J}_B \simeq (\varepsilon / 12g_0) \xi_0^2 \int d^2x (\nabla \cdot \hat{\mathbf{n}})^2 , \quad (\nabla \times \hat{\mathbf{n}})_z = 0 . \quad (6.9)$$

[Note that the contribution of δq to \mathcal{J}_B is *large*, of order $\varepsilon^2 L^2$ even for $\delta q = O(\varepsilon^{1/2})$, so that we must first reduce this term in order to minimize \mathcal{J} . In measuring \mathcal{J} from experiment, on the other hand, it is important to keep the $(\delta q)^2$ term [see Sec. VIII.D.3].]

The constraint on the bend in Eq. (6.8) places severe restrictions on possible patterns. For example, in a circular cell it is not possible to minimize the boundary contribution everywhere and at the same time satisfy the constraint. Instead, the latter can be relaxed by allowing defects in the cell. In fact a distribution of isolated dislocations of density $\rho_D(r)$ leads to a coarse-grained bend as in Figs. 21(d) and (i).

$$\langle (\nabla \times \hat{\mathbf{n}})_z \rangle = 2\pi q_0^{-1} \rho_D(r) , \quad (6.10)$$

with an associated extra defect contribution to the potential

$$\mathcal{J}_D = (q_0 / 2\pi) \langle (\nabla \times \hat{\mathbf{n}})_z \rangle \mathcal{J}_c , \quad (6.11)$$

where \mathcal{J}_c is the contribution from the suppressed magnitude of the order parameter over the core of area $\sim \xi_0^2 \varepsilon^{-3/4}$,

$$\mathcal{J}_c = (\xi_0^2 / g_0) \gamma \varepsilon^{5/4} , \quad (6.12)$$

with γ an $O(1)$ constant which requires numerical evaluation.

Another way the rolls may reorient is via line singularities or grain boundaries, which were discussed in Sec. V.B. They contribute an amount to the potential per unit length

$$\mathcal{J}_{GB} = (1/3g_0) \varepsilon^{3/2} \xi_0 \cos \theta f_{GB}(\theta) , \quad (6.13)$$

in the symmetric case, with θ the angle between the roll normal and the grain boundary normal, and f_{GB} a function of the nonlinear coupling parameter $\mathcal{G}(\theta)$, Eq. (4.32). In the perpendicular case \mathcal{J}_{GB} is also $O(\varepsilon^{3/2})$, and in order to determine the coefficients it is important to replace the point nonlinear kernel of the Swift-Hohenberg model with the full nonlocal but short-range kernel, thus yield-

ing the correct representation of $\mathcal{G}(\theta)$. This should not affect the potential aspects of the equation. Since the scaling with ε and system size is the same as for the boundary terms, there may be changes in the pattern depending on the details of $\mathcal{G}(\theta)$ [e.g. the cases shown in Fig. 21 in a square domain].

Having evaluated the major contributions to the potential we may compare its value for various patterns, to predict which ones are likely to occur. Different contributions scale with different powers of ε and L , and their relative importance varies with these parameters. For example, in a large circular cell it is immediately apparent from Fig. 21 that a pattern of straight rolls (a), essentially ignoring the geometry of the boundary, is preferred over the axisymmetric pattern (b). The comparison is more difficult in the case where radial rolls form at the boundaries (c). Considering the radial rolls as a perpendicular grain boundary, we find a contribution to the potential of the same order as in (a); which one is lower then depends on numerical factors. The solution with distributed dislocations and the rolls approaching the boundary normally (d) always has a higher potential ($\sim \varepsilon^{5/4} L$) for small ε than (a) ($\sim \varepsilon^{3/2} L$), and in general this scaling would suggest that a bending of the pattern due to distributed dislocations over the whole cell will not occur for small ε . This result breaks down in special geometries, e.g. an annulus (e) for $\varepsilon \gtrsim (\delta L / L)^4$ with δL the difference of the radii, where the dislocation solution wins out over a straight roll pattern. In a square cell the defect-free concentric roll solution (f) is preferred over the distributed defect state (i), but if all the dislocations are collapsed onto the diagonal to give a line of defects (h), the comparison with (f) and (g) depends on the details of the interaction function $\mathcal{G}(\theta)$.

Let us mention some of the limitations of the above approach. In any real experiment or simulation the asymptotic state reached need not be the lowest minimum of \mathcal{J} , but merely a *local* minimum which is stable to whatever perturbations are present. Very near threshold the barriers between different minima of \mathcal{J} are expected to be small, but as one raises ε the minima proliferate and the barriers grow. Moreover, the analytic comparison we have attempted of the potential values for various patterns depends on asymptotic scalings in certain combinations of the limits $\varepsilon \rightarrow 0$, $L \rightarrow \infty$, which may be unrealistic in many situations. For example, the restriction $\delta q < \varepsilon^{1/2} \ll 1$ may be violated quite rapidly as ε is raised, so that large-angle bending of $\hat{\mathbf{n}}$ without defects, as well as the creation of disclinations, become possible. The existence of a potential and the expression for it in Eq. (6.4) may or may not remain a good approximation. Its derivation depends on the condition $\varepsilon^{1/2} \ll 1$, and so there is no justification for the use of a potential when δq becomes of order q_0 . Similarly, the estimated difference between various contributions is often very small, for example the factor of $\varepsilon^{1/4}$ between the opposing defect and surface contributions may be swamped in practice by numerical prefactors. Nevertheless some of the broad trends and specific patterns predicted by the above argu-

ments are confirmed experimentally and numerically [e.g. (a) in cylinders, (h) in squares]. An attempt at a quantitative investigation of the potential (6.4) will be discussed in Sec. VIII.D.

The Swift-Hohenberg equation was studied numerically in large systems by Greenside and Coughran (1984). Natural patterns were investigated starting from random initial conditions, in a cell of aspect ratio 29×19 to match the experiments of Gollub *et al.* (1982), and in a square cell of size 16×16 . The results shown in Figs. 3(d), 3(e), and 3(f) are instructive from the point of view of pattern selection. In frame (e), after about 2 horizontal diffusion times, the small-scale structure has largely annealed out, leaving large patches of coherent rolls that approach the sidewall normally, joined sometimes by grain boundaries and sometimes by sharp kinks, as well as a small number of isolated dislocations. This is quite consistent with our qualitative expectations and is somewhat reminiscent of the experimental pattern in Fig. 3(a), which was a steady state. However Fig. 3(e) continues to evolve in time, by the gliding of dislocations away from the high-curvature regions. Eventually, on very long time scales, the pattern simplifies to frame 3(f), which consists of two patches of largely circular arcs joining smoothly, together with small regions of cross rolls near the short boundaries. Remarkably similar results were found using different random initial conditions, and even a different model equation which was nonpotential. However for higher ϵ the simplification at long times was much less dramatic. Simulations for a square shape at small ϵ consistently led to a rather simple symmetric final state [Fig. 3(d)], reminiscent of the prediction in Fig. 21(h). Again, higher ϵ led to a pattern retaining more of the randomness of the initial conditions and less of the geometry.

(ii) Away from threshold

Further away from threshold we have a much less complete picture. We could perhaps still use the Swift-Hohenberg potential as some guide, but this system becomes very rigid, with apparently many small barriers preventing relaxation to simple states, and such behavior does not seem to be generally observed experimentally. Cross and Newell (1984) considered the problem of approach to a steady state based on the phase equation, taking as given a boundary condition that the rolls approach the sidewalls normally. In particular, they studied a situation with focus singularities on the boundaries or in the corners, as suggested by this boundary assumption. They suggested that if the motion on the $O(L^2)$ horizontal diffusion time scale relaxes towards a steady state, this state would generally consist of domains of rolls centered on the foci. The diffusional motion would then relax the wave number in the domains that are close to the focus, to the selected wave number q_f given by $B(q_f)=0$. In fact Cross and Newell showed that the motion on the horizontal time scale is governed by a potential and thus

relaxes to a steady state, but only with the probably unrealistic restriction that $\hat{\mathbf{n}} \cdot \hat{\mathbf{s}} = 0$ everywhere, and the assumption that there are no line defects, no rapidly moving defects, and not too many [$\leq O(L)$] slowly moving defects. Since dislocations with the background wave number q_f typically climb with $O(1)$ velocity [assuming in general $q_f \neq q_d$, see above] the second restriction may be particularly unreasonable. In the absence of a proof of relaxational dynamics, it must again be taken empirically that this dynamics ceases on the $O(L^2)$ time scale. However the system may not have reached a steady state due to the behavior of boundaries between the domains. The subsequent motion of the domain boundaries remains poorly understood. For smooth phase equations the wave vector in the domains, q_f , satisfies $D_1(q_f)=0$. If we naively assume a scaling with the characteristic length scale L (which may now be taken as the domain size) given by the remaining higher (fourth) order derivative terms in the phase equation, we estimate an $O(L^4)$ relaxational time scale. This is consistent with recent numerical simulations in a periodic geometry by Elder *et al.* (1992). Since this argument depends crucially on the relation $D_1(q_f)=0$, it would be interesting to investigate the expected breakdown on adding mean-drift effects, where this relation no longer holds. Note that the argument of Cross and Newell (1984) for an $O(L^3)$ time scale resulting from the dynamics of the domain boundary regions is incorrect: the spatial variation on the $O(L^{1/2})$ scale of a small-angle (phase) domain boundary considered there leads back to the $O(L^2)$ diffusive time scale, and not to $O(L^3)$ as suggested. The motion of dislocation defects may also be important. The expression for the glide velocity is different for potential and nonpotential systems (see Sec. V.B.3.b.i.β), so the time scales would be expected to be different in these two cases if glide is an important mechanism. In addition, a strong dependence on the control parameter might be expected in this case, since glide may become pinned when the nonlinearity grows stronger. Clearly predicting the long-time relaxation depends on a better understanding of defect dynamics, with all the difficulties discussed in Sec. V.B.3.

2. Selection via dynamics

a. External forcing

Suppose the control parameter is raised from a sub-threshold value to above threshold. We must then ask what perturbation initiates the growth of the pattern, and how this affects its detailed evolution. This may depend on specifics of the system (e.g. imposed sources in reaction-diffusion equations, or not quite parallel plates in convection), but some types of forcing may be common to diverse systems.

(i) Boundary forcing

Often the lateral boundaries may force the growth of the pattern (see the discussion in Sec. V.A and in Ahlers *et al.*, 1981). This can then be treated by solving the inhomogeneous amplitude equation, at least near threshold. If the geometry is simple, e.g. a cylinder, the growing pattern will have the symmetry of the boundaries. The subsequent fate — whether the pattern saturates in the simple geometry or breaks up into a more complicated one — depends on the type of considerations discussed in subsection VI.A.1 above.

(ii) Stochastic forcing or stochastic initial conditions

In the absence of the forcing described above, intrinsic thermal fluctuations could initiate the growth. The size of these is *very small* in macroscopic phenomena such as convection (see the estimates in subsection VI.D below) but will be relatively larger as the spatial scale of the basic instability decreases. In addition there must always be other sources of fluctuations coming from noise in the apparatus. A numerical study of pattern evolution in the Swift-Hohenberg model with rather large noise was recently carried out by Elder *et al.* (1992).

For large deterministic systems it is natural to ask how patterns evolve starting from stochastic initial conditions of small amplitude (Newell *et al.*, 1970). In fact Getling (1991) has *defined* the preferred wave vector as the most probable value of the distribution resulting from just such a process (see footnote 6.1). Often it is assumed that the fastest growing mode dominates the evolution under these conditions. However, since the competition between different modes only takes place in the nonlinear regime, this idea is usually too simplistic. For example in a two-dimensional system, stochastically initiated patterns often grow to saturate to a highly disordered nonlinear state. There may then follow slow relaxation to a simpler, more ordered state, whose final configuration depends on the details of the deterministic nonlinear relaxation. Another objection to the fastest growing mode hypothesis is that the initial spectrum of fluctuations may not be independent of wave number (i.e. “white”), and may bias the system towards some other length scale. Indeed, in a careful numerical study of the one-dimensional Swift-Hohenberg equation, Schöber *et al.* (1986) observed that the final wave vector depended on the magnitude and peak position of the initial wave-vector distribution. These results also cast doubt on the notion mentioned above, that stochastic initial conditions provide a way to define an intrinsically preferred pattern (see footnote 6.1). We return to the problem of stochastic and deterministic forcing in Sec. VIII.D below.

b. Threshold protocol

If the control parameter increases *very* slowly through threshold then the details of what initiates the growth

will not be important, since only the first mode which goes unstable will initially grow. Murray (1989) has in particular pointed out the importance of the precise route by which the threshold value is reached. For simplicity we consider a one-dimensional system with periodic (or no-flux) boundary conditions, as described in Sec. V.A. Then we can imagine passing through threshold either by increasing the driving strength ϵ at fixed system size, or by increasing the system size at fixed ϵ . (Other combinations are of course possible, and indeed in some systems a natural definition of the control parameter may lead to an intermediate path.) In the first case (fixed system size) the mode $q = q_0$ develops and will typically persist as ϵ increases since large perturbations are needed to change the number of periods. On the other hand at fixed ϵ the wave number of the mode formed initially will be reduced as the system size increases at fixed number of periods, until a stability boundary (typically the Eckhaus boundary q_E) is reached. Thus in this case the wave number of the final state will tend to be reduced from q_0 towards q_E , although its exact value will depend on the details of the dynamics of the instability.

c. Front propagation

In a large system held above threshold the nonlinear state may grow by the propagation of a *front* away from a localized perturbation. Far enough away from the perturbation the spatial structure will often depend on the intrinsic properties of the front, rather than on details of the initial conditions. As we have seen in Sec. V.B, in the Ginzburg-Landau system (5.57) a continuous family of uniformly translating fronts exist as dynamic solutions interpolating between the stable nonlinear and the unstable uniform states; the family is characterized by the velocity of propagation and by the wave number (or frequency) of the nonlinear state produced. On the other hand if we ask which fronts can develop from localized initial conditions, often a unique one is chosen, propagating with a fixed velocity, and producing a unique wave vector (for each value of control parameter).

This “front selection” question has been much discussed since the 1930s, and even in the simple case of no pattern formation when the velocity of the front is the only variable to be determined (e.g. the nonlinear diffusion equation), the problem continues to attract attention. Since front propagation occurs in both stationary and oscillatory systems we shall discuss this question for types I_s, III_o, and I_o in a unified way.

B. Front and pulse selection

1. The nonlinear diffusion equation

For the case of the simple nonlinear diffusion equation

$$\partial_t u = \partial_x^2 u + f(u), \quad (6.14)$$

in one dimension with $u \geq 0$, the initial value problem has been solved completely starting from the classic work of Kolmogorov *et al.* (1937), and culminating in the rigorous analysis by Aronson and Weinberger (1975, 1978). Let us consider a function $f(u)$ with three zeroes as depicted in Fig. 17. Then as discussed in Sec. V.B.2.b.iv the system has a one-parameter family of uniformly translating fronts with velocities $v_{\min} < v < \infty$, where v_{\min} is the unique velocity of the kink joining the two stable states u_{\pm} . We now ask what will happen if we prepare the system in the (unstable) $u=0$ state and insert a positive localized perturbation with $u \neq 0$ at some point. Then Aronson and Weinberger have proved that a unique front will develop at long times, whose velocity is obtained by considering the set of all fronts with no overshoot (no change in sign of u) and picking the one with the lowest velocity. This selection will hold so long as the initial disturbance has a faster asymptotic spatial decay than the selected front.

The above result is extremely simple to state but its proof requires a sophisticated analysis which depends crucially on the simplicity of the model (a real equation producing a spatially uniform solution). It is therefore useful to rephrase the result and the arguments leading to it in such a way that they might be generalizable to more complicated situations. One reformulation, made by Ben-Jacob *et al.* (1985) is in terms of a concept they call “stability in the moving frame”: If a front $u(x-vt)$ is perturbed slightly in its leading edge, it is stable if it outruns the perturbation and unstable if the perturbation persists at long times. The result of Aronson and Weinberger is then equivalent to the statement that the *stable* front with the lowest velocity is selected.

Another way to state the same result, emphasized particularly by van Saarloos (1989, 1990), is in terms of the $v(\kappa_L)$ curve shown in Fig. 18. The selected front is the one with the *fastest* spatial decay rate, i.e. the maximum $|\kappa_L|$. [Note that with our convention the leading edge decays as $\exp(\kappa_L \xi)$ for $\xi \rightarrow \infty$, so $\kappa_L < 0$.] This means that for $\varepsilon > \varepsilon^{\dagger} = 2$, the selected front has $v^* = 2\varepsilon^{1/2}$ and $|\kappa_L^*| = \varepsilon^{1/2}$, i.e. it belongs to the $N \rightarrow L_2$ family (see Sec. V.B.2.b above), whereas for $0 < \varepsilon < \varepsilon^{\dagger}$ the selected front has $v^* > v^*$, $|\kappa_L^{\dagger}| > |\kappa_L^*|$, and it is the discrete $N \rightarrow L_1$ front. In what follows we attempt to generalize what is known from this soluble example in order to make predictions for arbitrary type I_s, I_o, and III_o systems.

2. General remarks

We consider first a general equation of the form (3.4) and take $\varepsilon > 0$, i.e. assume that the $U=0$ state is unstable. It follows that a given initial condition will appear to propagate faster, the more extended its shape. To be more precise, if a flat initial condition grows with some rate σ , a small disturbance decaying spatially as $e^{-|\kappa|x}$ with $\kappa \rightarrow 0$ will grow essentially as $\exp(\sigma t - |\kappa|x)$ [neglecting the $O(\kappa)$ corrections to σ], and will thus ap-

pear to propagate at a speed $v = \sigma/|\kappa| \rightarrow \infty$. This simply points out the need for considering *restricted* initial conditions, and, in particular, localized or sufficiently rapidly decaying ones in order to create a propagating front. It should be clear that the idea of stability is quite delicate in this situation of rapidly growing disturbances, where we are interested in various asymptotic limits, e.g., $x, t \rightarrow \infty$, $U \rightarrow 0$. It is also useful to distinguish between a *stable* solution, and an *attracting* one, since the type of perturbation of an ideal state that can be considered “reasonable” is different in the two cases. For example, consider the $v > v^* = 2e^{1/2}$ front solutions of the nonlinear diffusion equation (6.14), which have exponential tails decaying more slowly than the selected v^* front. If we perturb the tail region by adding a small *localized* disturbance, then the $v > v^*$ fronts may be considered *stable* as they will outrun the perturbation. On the other hand the example of a small perturbation consisting of a *truncation* of the front far in the tail (e.g. a “localized” initial condition that is “almost” a $v > v^*$ front) shows that the $v > v^*$ fronts are not *attracting* if one starts from a localized initial condition, since eventually the $v = v^*$ front will take over. Notice that in the latter case the perturbation of the $v > v^*$ front is itself delocalized, but it represents a localized initial condition. Conceivably, in some systems these different notions of stability could correspond to differing predictions for front selection depending on the physical situation. For example we can consider propagation from a localized initial condition in a perfectly uniform medium (the usual formulation); then we are concerned with the *attracting* nature of solutions amongst a class, each member of which is defined by an appropriate set of initial conditions. On the other hand we can consider propagation in a medium with small nonuniformities, where dynamic *stability* to a particular class of perturbations is the sensible criterion. Finally it is worth pointing out that generalizations of the Aronson-Weinberger result are, to date, purely heuristic. There is no completely convincing derivation of the selection results to be presented below. The arguments are usually phrased in terms of Gedanken experiments, which do not correspond to realistic dynamics in typical physical situations. Nevertheless, there are now rather complete and precise predictions, and these can be tested by numerical calculations and by experiments.

3. Linear front selection

The simplest approach is the stationary phase argument dating back to Kolmogorov, Petrovsky and Piskunov (1937). A slightly more careful version is the “pinch point” analysis (Lifshitz and Pittaevskii, 1981), both of which are entirely linear. Let us for simplicity restrict ourselves to an equation in one spatial dimension with a single field $U(x, t) = u(x, t)$ and a small *localized* initial condition $u(x, t) = u_0(x)$, but retain the general form (3.4). The solution far in the tail at a later time is given by superposition (linearity assumed!). If we look at

a position $x = vt$ we have

$$\begin{aligned} u(x=vt,t) &= \int dx' u_0(x') \int \frac{dQ}{2\pi} \exp[-iQx'] \\ &\quad \times \exp\{i[Qv - \Omega(Q)]t\}, \end{aligned} \quad (6.15)$$

where initially the wave-number integral is along the real axis, and $\Omega = \Omega_r + i\Omega_i$ is complex. For large t we argue that the Q integral is conveniently evaluated by extending the contour into the complex plane $Q = Q_r + iQ_i$. Note that Q is related to the variables of Sec. V.B via $Q_r = q_L$, $Q_i = -\kappa_L$. After suitably deforming the contour, the integral is dominated by the stationary phase point

$$\frac{d}{dQ} [Qv - \Omega(Q)] \Big|_{Q=Q^*} = 0, \quad (6.16a)$$

i.e.

$$v = \frac{d\Omega(Q)}{dQ} \Big|_{Q=Q^*}, \quad (6.16b)$$

a complex equation for the position of the complex saddle point^{6,2} $Q = Q^*$. The leading order dependence of the integral is then

$$u \sim \exp\{i[Q^*v - \Omega(Q^*)]t\}, \quad (6.17)$$

and the propagation speed of the front is the value $v = v^*$ for which $|u(x = v^*t, t)|$ neither grows nor decays in time, i.e.,

$$\operatorname{Re} i[Q^*v^* - \Omega(Q^*)] = 0, \quad (6.18a)$$

or

$$v^* = \frac{\Omega_i(Q^*)}{Q^*}. \quad (6.18b)$$

All other arguments discussed below based on a linear analysis lead to results equivalent to Eqs. (6.16) and (6.18). Of course, it is not at all obvious why a linear analysis of the whole problem is relevant. Nevertheless the current understanding of the front selection question is that this is the correct answer, except when an intrinsically nonlinear front wins out over the v^* front. Understanding the precise conditions under which this will happen adds content to this otherwise empty statement (see below). Also, it is apparent that the predicted v^* based on a purely linear analysis may not be consistent with a uniformly translating nonlinear front. In that case v^* is expected to be an average of a periodic or even a chaotic velocity.

^{6,2}We warn the reader that we are denoting the stationary phase point as Q^* ; this does *not* signify complex conjugation!

The linear selection conditions (6.16) and (6.18) are thought to apply to both real and complex equations. In the real case the wave vector q_{fp} of the state created by the front is obtained by arguing that each node of $u(x, t)$ formed in the leading edge persists in the fully developed pattern behind the front. It follows that this wave vector is given by

$$q_{fp} = \Omega_r(Q^*)/v^* - Q_r^*. \quad (6.19)$$

Notice that we have assumed that no additional nodes are created in the nonlinear region behind the leading edge, i.e. that there are no phase slips and that nodes do not propagate in the saturated pattern. For the complex Ginzburg-Landau equation (5.57) the velocity v^* and the frequency ω^* can easily be calculated and the wave vector q_N^* is determined by the fixed-point equations (5.58) (see subsection VI.B.6.a below). As shown by van Saarloos and Hohenberg (1992), these equations only possess solutions in certain regions of the parameter space $\{\epsilon, c_i\}$ [they always do for the cubic equation (4.49)], in which case a uniformly translating front will create the corresponding nonlinear state (q_N^*, a_N^*) . For other parameter values no uniformly translating front exists and the state created behind the front cannot be predicted.

As mentioned earlier, the above results coincide with those obtained from the various "marginal stability" argument presented in the literature. For example, Ben-Jacob *et al.* (1985) have obtained (6.16) by requiring that a perturbation of the front should neither grow nor decay in the frame moving with the front speed. It then turns out that all fronts with $v > v^*$ can be considered stable and those with $v < v^*$ unstable, with respect to *localized* perturbations in the moving frame. Implicit in these arguments is a restriction to the one-parameter family of uniformly translating fronts obtained from an equation such as (6.14). More generally, however, the complex dispersion relation $\Omega(Q) = \Omega_r(q_L, \kappa_L) + i\Omega_i(q_L, \kappa_L)$ can be expected to define at least a two-parameter family of complex fronts connecting a nonlinear saturated state U_N to the $U=0$ state. Van Saarloos (1989, 1990) has formulated the "marginal stability" approach to the front selection problem in this case. He shows that Eqs. (6.16) and (6.18) can be interpreted as containing three different statements. (i) The imaginary part^{6,3} of (6.16)

$$\operatorname{Im} \frac{d\Omega}{dQ} = \left[\frac{\partial \Omega_i}{\partial q_L} \right]_{\kappa_L} = 0 \quad (6.20)$$

says that for given κ_L the real part of the wave vector

^{6,3}According to the Cauchy relation for the complex analytic function $\Omega(Q) = \Omega(q_L, \kappa_L)$ we have $\frac{d\Omega}{dQ} = \left[\frac{\partial \Omega_r}{\partial q_L} \right]_{\kappa_L} + i \left[\frac{\partial \Omega_i}{\partial q_L} \right]_{\kappa_L} = - \left[\frac{\partial \Omega_i}{\partial \kappa_L} \right]_{q_L} + i \left[\frac{\partial \Omega_r}{\partial \kappa_L} \right]_{q_L}$.

$q_L(\kappa_L)$ is chosen to maximize growth rate Ω_i , yielding $\Omega_i(\kappa_L) = \Omega_i(q_L(\kappa_L), \kappa_L)$. (ii) Applying Eq. (6.18b) to the wave vector $Q = q_L - i\kappa_L$ one finds

$$v(\kappa_L) = -\Omega_i(\kappa_L)/\kappa_L , \quad (6.21)$$

i.e. a one-parameter family of front velocities characterized by their asymptotic spatial decay rate κ_L . (iii) Finally, the real part of (6.16b) implies that the selected velocity v^* , Eq. (6.18b), is chosen to minimize $v(\kappa_L)$. Indeed, the real part of (6.16b) implies (see footnote 6.3)

$$\begin{aligned} v &= - \left[\frac{\partial \Omega_i}{\partial \kappa_L} \right]_{q_L} = - \frac{d\Omega_i}{d\kappa_L} + \left[\frac{\partial \Omega_i}{\partial q_L} \right]_{\kappa_L} \frac{dq_L}{d\kappa_L} \\ &= - \frac{d\Omega_i}{d\kappa_L} , \end{aligned} \quad (6.22)$$

where (6.20) has been used. Then differentiation of (6.21) leads to

$$\frac{dv}{d\kappa_L} = \frac{1}{\kappa_L} \left[\frac{\Omega_i(\kappa_L)}{\kappa_L} - \frac{d\Omega_i}{d\kappa_L} \right]_{Q=Q^*} = 0 . \quad (6.23)$$

The physical interpretation of the above relations given by van Saarloos (1989) is as follows: Out of the two-parameter family of fronts $\Omega(q_L, \kappa_L)$ only the ones satisfying Eq. (6.20) [i.e. ones whose decay rate is at a maximum with respect to q_L] are "stable" for given κ_L . This condition leads to a one-parameter (κ_L) family of fronts with velocity given by Eq. (6.21). Out of this family he argues that it is the one with the minimum velocity [Eq. (6.23)] that will develop from localized initial conditions, in analogy to the survival of the slowest growing facets in crystal growth (see his Fig. 3). In this way the minimum velocity v^* on the branch (6.21) of Fig. 22 is chosen.

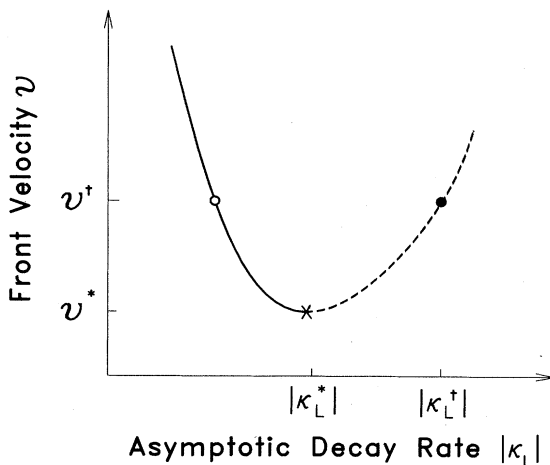


FIG. 22. Front propagation speed as a function of the asymptotic small-amplitude decay rate $|\kappa_L|$ far in advance of the front. Dashed portion corresponds to a value of $|\kappa_L|$ obtained by a linear analysis which however is not the asymptotic decay of a nonlinear front, except at a discrete point marked by a solid circle, at $v^*, |\kappa_L^*|$. (The open circle then corresponds to a discrete missing value on the other branch.) The cross marks the values $v^*, |\kappa_L^*|$ given by the linear selection criterion.

Recently Powell *et al.* (1991) have attempted to understand the selection of v^* by examining the transient dynamics through which the *pde* attains this solution. They suggest that the less localized stable $v > v^*$ fronts are inaccessible from localized initial conditions, so that the system arrives at the selected front by moving through the unstable front states with $v < v^*$, to arrive at the marginally stable $v = v^*$ front at long times. The approach to v^* from below had already been pointed out by van Saarloos (1989), and Powell *et al.* (1991) have attempted to connect this transient evolution to the minimization of a Lyapunov functional. In our view, however, this minimization principle is unconvincing, and the numerical evidence on the behavior of transients is at present somewhat limited. Moreover, for the complex equation (5.57) van Saarloos and Hohenberg have found examples where the approach to v^* is from above.

We know of two ways in which the linear selection criterion (6.16, 18) can fail. The first one is obvious from the previous discussion: if the initial condition is not sufficiently localized, i.e. if its spatial decay rate satisfies $|\kappa_L| < |\kappa_L^*|$, then it is the front with velocity $v(\kappa_L) > v^*$ that is selected (assuming $dv/d|\kappa_L| < 0$ as depicted in Fig. 22). The second violation of linear selection is more interesting, and we turn to it next.

4. Nonlinear front selection

We have seen in Sec. V.B.2.b.iv in studying the nonlinear diffusion equation that in certain cases the $\kappa_L(v)$ curve is not smooth (see Fig. 18). Within the framework of the phase-space counting arguments of Sec. V.B.2.b.iii, the smooth family $v(\kappa_L)$ corresponds to the $N \rightarrow L_2$ orbits, whereas the front $v^\dagger, \kappa_L^\dagger$, where the discontinuity in $v(\kappa_L)$ occurs, is a *discrete* $N \rightarrow L_1$ orbit. Quite generally, for a front advancing into an unstable uniform state ($\epsilon > 0$) van Saarloos and Hohenberg (1990, 1992) have formulated the following (linear and nonlinear) selection conjectures:

The linear front velocity v^* and decay rate κ_L^* can be calculated from Eqs. (6.16) and (6.18). This front will be selected unless there exists a front $v^\dagger, \kappa_L^\dagger$ satisfying the two conditions

$$v^\dagger > v^* , \quad (6.24a)$$

$$|\kappa_L^\dagger| > |\kappa_L^*| , \quad (6.24b)$$

in which case the latter (nonlinear) front will be selected. Moreover, for the complex Ginzburg-Landau equation (5.57), this front is the discrete $N \rightarrow L_1$ orbit obtained from the ansatz (5.73).

In general we expect linear selection at large ϵ , and we can define a value ϵ^\dagger (which may be zero) such that linear selection holds for $\epsilon > \epsilon^\dagger$, while nonlinear selection holds for $0 < \epsilon < \epsilon^\dagger$. The threshold ϵ^\dagger is found to be nonzero at a *subcritical* bifurcation, i.e. nonlinear selection always holds near $\epsilon = 0$ in that case (see Fig. 23). Note also that

the competition between linear and nonlinear selection requires *both* conditions stated in (6.24). In particular if Eqs. (5.73) have a solution with $|\kappa_L^\dagger| > |\kappa_L^*|$, but $v^\dagger < v^*$, it is argued that this front will be unstable in the same way as the other $v < v^*$ fronts. There is limited numerical confirmation for this latter expectation, but it should be said that examples of fronts satisfying the conditions $|\kappa_L^\dagger| > |\kappa_L^*|$ and $v^\dagger < v^*$ have only been found in a small range of the parameter space in Eq. (5.57) (see van Saarloos and Hohenberg, 1992).

The front selection conjectures predict the velocity v and wave vector q_{fp} of the nonlinear state created in the system as a result of the instability of the $u=0$ state. In order to complete the picture we must ask whether the

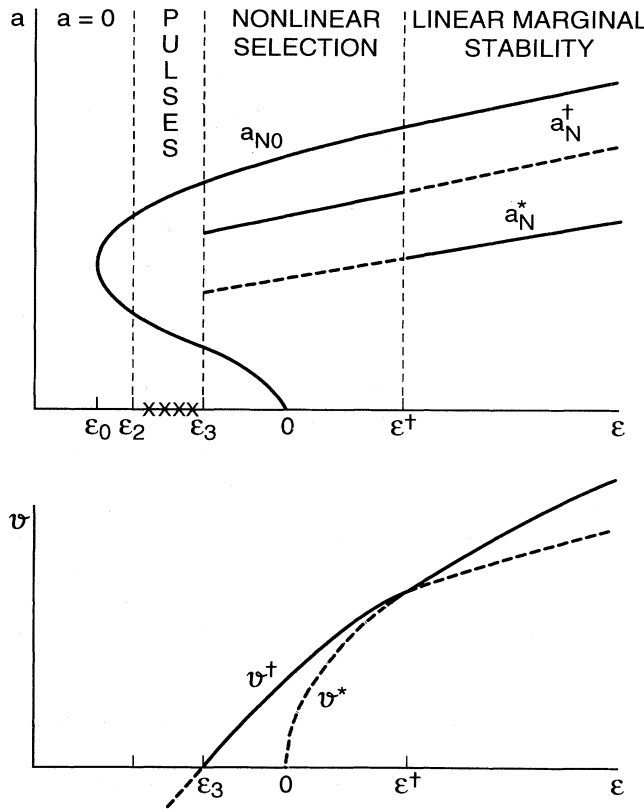


FIG. 23. Front and pulse selection in the complex Ginzburg-Landau equation (5.57) for a subcritical bifurcation. (a) Schematic bifurcation diagram showing the amplitude a vs control parameter ϵ . The solid line marked a_{N0} is the amplitude of the $q_N=0$ plane wave solution bifurcating subcritically at $\epsilon=0$. The line marked a_N^* represents the amplitude of the state created behind the linear marginal stability front which is selected for $\epsilon > \epsilon^\dagger$; the line marked a_N^\dagger is the amplitude of the state created behind the nonlinear front, selected for $\epsilon_3 < \epsilon < \epsilon^\dagger$. In the range $\epsilon_2 < \epsilon < \epsilon_3$ pulses are expected to be stable, and for $\epsilon < \epsilon_2$ a localized perturbation of the $A=0$ state is expected to decay back to $A=0$. (b) Front velocities for the linear (v^*) and nonlinear (v^\dagger) fronts vs control parameter ϵ . In both (a) and (b) the selected front is represented by a solid line and the other one by a dashed line. (From van Saarloos and Hohenberg, 1992.)

nonlinear state is itself stable, a question which can usually be answered from the knowledge of v and q_{fp} . Van Saarloos and Hohenberg (1992) have found, for example, that when q_{fp} is in the Benjamin-Feir unstable band the front is not uniformly translating at long times, though its average velocity agrees well with the value predicted by the selection conjecture.

5. Selection below threshold: Pulses and fronts

The above discussion referred to an *unstable* $U=0$ state being invaded by a stable $U\neq 0$ state, and is thus applicable for $\epsilon > 0$. It answers the selection problem posed by the existence of a family of fronts. For $\epsilon < 0$, we have seen in Sec. V.B above that there may or may not be families of fronts depending on the model, but pulses exist in general at least for complex equations, and one would like to know when a perturbation of the (stable) $U=0$ state will produce a front, when it will produce a pulse, and when it will decay back to $U=0$. Since the linear family $v(\kappa_L)$, Eq. (6.21), no longer exists for $\epsilon < 0$, the question involves *nonlinear* pattern competition. The front selection hypothesis discussed above was extended by van Saarloos and Hohenberg (1992) to this case in the following way:

If a discrete front $(v^\dagger, \kappa_L^\dagger)$ exists with $v^\dagger > 0$ (i.e. the $U\neq 0$ or N state invades the $U=0$ or L state) then this front is selected. If no such front exists or if it has $v^\dagger < 0$, then either a pulse will be formed, or the perturbation will decay to zero (we cannot say which will occur *a priori* nor can we predict whether the pulse will be stable. The state obtained often depends on initial conditions in this case). Typically, fronts are found for $\epsilon_3 < \epsilon < 0$ and pulses for $\epsilon_2 < \epsilon < \epsilon_3$, though both ϵ_3 and ϵ_2 may be zero. In cases where v^\dagger can be calculated ϵ_3 is thus known analytically. The selection conjectures are summarized in Fig. 23.

6. Examples

a. Complex Ginzburg-Landau model

Let us consider Eq. (5.57) which holds for a subcritical bifurcation. Then

$$\Omega(Q) = -i(1+ic_1)Q^2 + i\epsilon = \omega + vQ , \quad (6.25)$$

from which it is easy to see that (6.20) implies ($Q = q - i\kappa$)

$$q_L = -c_1\kappa_L \quad (6.26a)$$

and

$$\kappa_L = -\frac{1}{2}v(1+c_1^2)^{-1} , \quad (6.26b)$$

and then (6.21) yields

$$v(\kappa_L) = -(1+c_1^2)\kappa_L - \epsilon/\kappa_L , \quad (6.26c)$$

which together with (6.23) gives

$$v^* = 2\epsilon^{1/2}(1+c_1^2)^{1/2}, \quad (6.27a)$$

$$\kappa_L^* = -\epsilon^{1/2}(1+c_1^2)^{-1/2}. \quad (6.27b)$$

The frequency ω can then be found from Eq. (6.25) to be

$$\omega^* = -c_1\epsilon, \quad (6.27c)$$

and a uniformly translating front will only be created if Eqs. (5.58) for q_N^* and a_N^* have a solution for the given values of v and ω . Otherwise, the wave vector of the nonlinear state formed by the front cannot be predicted. As mentioned above, the discrete front $(v^\dagger, \kappa_L^\dagger)$ is precisely the one resulting from the nonlinear front ansatz (5.73) discussed in Sec. V.B, which can be obtained analytically as a function of the parameters $(\epsilon, c_1, c_3, c_5)$. Therefore the selection conjectures summarized in subsections 4 and 5 above can be tested in detail, and as shown by van Saarloos and Hohenberg (1992) the results agree with direct simulations of the *pde*. For $\epsilon < 0$, the threshold ϵ_3 for the appearance of pulses (when ϵ is decreased) can be found analytically from the relation $v^\dagger(\epsilon_3) = 0$. The authors also showed that for $\epsilon > \epsilon_3$ the nonlinear front is obtained with the predicted velocity $v^\dagger(\epsilon) > 0$, whereas for $\epsilon_2 < \epsilon < \epsilon_3$ pulses were found. For $\epsilon < \epsilon_2$ a perturbation decayed back to $A = 0$.

Another test of the behavior of fronts and pulses can be made in the perturbative regime near the Hamiltonian limit of the quintic-cubic Schrödinger equation (3.41), corresponding to $|c_1|, |c_3|, |c_5| \rightarrow \infty$ in Eq. (5.57). In particular, for $c_3/c_1 = -c_5/c_1 = 1$, the limits of existence of pulses $\epsilon_2 < \epsilon_3 < 0$ were evaluated perturbatively by van Saarloos and Hohenberg (1992), and more importantly, these authors showed analytically that for $\epsilon_3 < \epsilon < 0$ the discrete front (5.73) with velocity $v^\dagger > 0$ is indeed selected. Thus the behavior of fronts and pulses is well accounted for by the conjectures of subsections VI.B.4 and VI.B.5 above.

b. The Swift-Hohenberg equation

For the Swift-Hohenberg equation (3.27) the phase space methods that form the basis for our conjectures have not been implemented directly, except near the bifurcation point where an amplitude expansion is valid. On the other hand, as mentioned earlier, the existence of a double family of fronts has been proved rigorously by Collet and Eckmann (1990) for this system.

For the supercritical case front propagation was studied in this model by Dee and Langer (1983) and by Ben-Jacob *et al.* (1985). We shall consider the equation with a subcritical bifurcation (van Saarloos, 1989)

$$\partial_t u = -(\partial_x^2 + 1)^2 u + \epsilon u + \mu u^3 - u^5. \quad (6.28)$$

The linear marginal stability prediction for this system was found to be

$$v^* = \frac{4}{3\sqrt{3}}(2 + \sqrt{1+6\epsilon})(-1 + \sqrt{1+6\epsilon})^{1/2}, \quad (6.29a)$$

$$\kappa_L^* = \frac{1}{2\sqrt{3}}(-1 + \sqrt{1+6\epsilon})^{1/2}, \quad (6.29b)$$

and the wave vector selected behind the front is, according to Eq. (6.19),

$$q_{fp} = \frac{3(3 + \sqrt{1+6\epsilon})^{3/2}}{8(2 + \sqrt{1+6\epsilon})}. \quad (6.29c)$$

It should be noted that this wave vector is *different* from the one minimizing the Lyapunov function (3.28), a point which argues against the proposal of Getling (1991, 1992) to use front propagation to define a natural “preferred” wave number (see footnote 6.1).

In general we do not know how to find a discrete front solution for this fourth-order equation, but for $\mu \ll 1$ we can obtain an amplitude equation for (6.28) (see Cross *et al.*, 1983a; van Saarloos, 1989) and reduce the problem to the real Ginzburg-Landau model, for which the nonlinear front ansatz (5.73) can be used. Specifically, for $\epsilon, \mu \ll 1$, Eq. (6.28) leads to the amplitude equation

$$\partial_t A = \partial_x^2 A + \epsilon A - b_3 |A|^2 A - b_5 |A|^4 A, \quad (6.30)$$

with

$$b_3 = -\mu, \quad b_5 = 10/9. \quad (6.31)$$

In this limit we may thus predict ϵ^\dagger , $\kappa_L^\dagger(\epsilon, \mu)$, and $v^\dagger(\epsilon, \mu)$ for sufficiently small values of μ , from the general formulas discussed in Sec. V.B. The results, obtained by van Saarloos (1989), are shown in Fig. 24, from

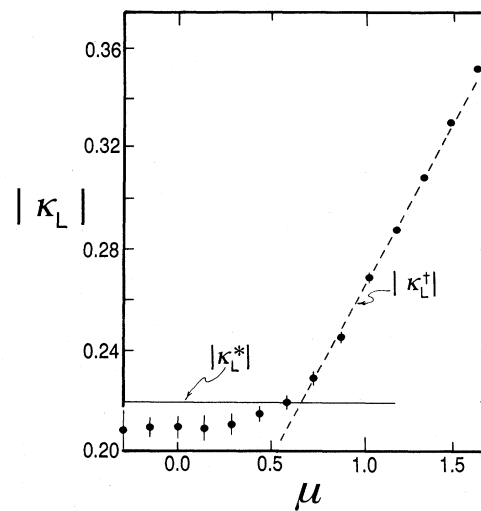


FIG. 24. Decay rate $|\kappa_L|$ for fronts in the Swift-Hohenberg model (6.28) with a subcritical bifurcation, vs the coefficient μ of the cubic term, for $\epsilon = 1/4$. The lines marked $|\kappa_L^*|$ and $|\kappa_L^\dagger|$ are the analytic predictions based on the amplitude equation (6.30), valid for small ϵ . Solid points are results of a numerical simulation of Eq. (6.28). The error bars at low μ arise from the difficulty of estimating the asymptotic decay rate when the solution is the sum of two exponentials with nearly equal decay rates. (From van Saarloos, 1989.)

which it is seen that even for relatively large μ , where the amplitude equation no longer is a good approximation, the departure from linear marginal stability is large and in reasonable agreement with the prediction of the nonlinear selection criterion.

C. Type I_o: Oscillatory periodic

1. Convective versus absolute instability

The type I_o instability point R_c is calculated as the onset point for growth of a plane wave disturbance in a laterally infinite system. If the group speed $s_0 = (\partial\omega/\partial q)|_{q=q_0}$ is nonzero, on the other hand, a small *localized* disturbance will propagate away at this speed, while only growing at a rate that goes to zero as $R \rightarrow R_c$ ($\varepsilon \rightarrow 0$). Thus the instability at R_c is always convective (see Sec. III.A.2), and the system remains absolutely stable at this point. The stationary phase analysis of subsection VI.B.3 above yields a precise estimate for the point of absolute instability, as the value of the control parameter for which the propagation velocity v^* , Eqs. (6.16) and (6.18), away from a localized initial condition goes to zero. For the type I_o amplitude equation (4.59) the criterion for the value of the control parameter ε_a at which this occurs is that the v^* of equation (6.27) modified by the addition of the group speed s_0 , should become zero (Deissler, 1985, 1989). In terms of a convenient scaled group speed $s(\varepsilon)$

$$s = \varepsilon^{-1/2} s_0 \tau_0 / \xi_0 , \quad (6.32a)$$

where for clarity we have restored the scales τ_0 and ξ_0 , the condition for absolute instability becomes

$$s(\varepsilon_a) = \varepsilon_a^{-1/2} s_0 \tau_0 / \xi_0 = 2(1 + c_1^2)^{1/2} . \quad (6.32b)$$

For $0 < \varepsilon < \varepsilon_a$ the system is convectively unstable but absolutely stable; for $\varepsilon > \varepsilon_a$ the instability becomes absolute.

2. Effects of boundaries

Lateral boundaries have a strong effect on the spatial structures observed in the nonlinear propagating wave systems resulting from type I_o instabilities. The study to date has concentrated on the one-dimensional problem of waves traveling down a long rectangular cell, and already in this case rich behavior is found. As mentioned in Sec. V.A the importance of the endwalls is immediately understood, since it is only the presence of reflecting endwalls that allows the instability to grow locally in the range of parameters for which the instability is convective. The wide range of spatial structures observed numerically and experimentally can be thought of as the nonlinear consequences of these properties of the linear state.

Our theoretical analysis will be based on the coupled amplitude equations (4.59a) and (4.59b) together with the

boundary conditions (5.34a) and (5.34b) (Cross, 1986b, 1988b). If we first look for solutions in which the magnitudes $|A_R|$ and $|A_L|$ are time independent, three qualitatively different spatial patterns may be found as the parameters are varied. These are shown in the top 4 panels of Fig. 25, i.e. (a), (b), (g), (h)]. The calculation is based on Eqs. (4.59) with all $c_i = 0$, i.e. the only effect of propagation comes from the group velocity, and only the control parameter ε is being varied.

The first pattern immediately above threshold (a) consists of counter-propagating traveling waves with right-moving waves strong in the right-hand end of the system, and left-moving waves strong in the left-hand end (we assume $s_0 > 0$). This structure is easily understood as a weak nonlinear saturation of the linear onset solution: a small disturbance of, say, right-moving waves grows in time, but simultaneously propagates with the group speed towards the right, producing the characteristic exponential spatial envelope. Reflection at the endwall produces left-moving waves, which in turn grow, simultaneously propagating to the left.

In the more strongly nonlinear regime a remarkable asymmetric pattern is observed [25(b) and 25(g)], which was called the “confined state” by the experimental group who first observed such a structure in binary-fluid convection (Steinberg *et al.*, 1987). For example in the structure of (g) some fraction of the system (which depends on nonlinear parameters but is asymptotically independent of the system size if both endwalls are present) contains essentially the unstable quiescent state, while the remainder of the cell contains nonlinear saturated traveling waves, either right-moving waves at the right-hand end of the cell, or left-moving waves at the left end of the cell. Once again, of course, the structure can be understood in terms of the convective instability. Indeed, a small disturbance of, for example, right-moving waves in the quiescent region of Fig. 25(g) will grow but at the same time it will propagate to the right, leading to large amplitude waves in the right-hand portion of the system. Reflection will produce left-moving waves which are first nonlinearly suppressed by the large amplitude right-moving waves, and then grow once they enter the region of weak right-moving waves. Finally, reflection at the left endwall produces the exponentially growing envelope of right-moving waves, and a self-consistent steady state is established. It should be noted that this steady state depends crucially on the low amplitude waves produced by reflection of the strong waves. In large systems the amplitude of these waves becomes exponentially small near the center of the cell, and the system may become sensitive to external noise (Deissler, 1987b, 1989). This would then be readily observable as a fluctuation in the rise position of the strong waves.

Finally, for stronger nonlinearity a confined to filling transition occurs, and a state appears (h) in which only one set of waves are evident throughout the whole cell (although there may again be low amplitude reflected waves). The difference between (g) and (h) may be identified as a sharp transition by considering the limit of

a semi-infinite system. Then for parameters corresponding to (g) there is no self-consistent nonlinear solution of right-moving waves. As we have seen a disturbance propagates to the right and reflection at an endwall is essential to maintain a steady disturbance. On the other hand for parameters corresponding to (h) reflection at an endwall for large x is not necessary, and a steady nonlinear solution may be maintained. The transition (g) \leftrightarrow (h) results from a reduction in the propagation effects; in fact the parameter values at which the transition occurs seem to correspond exactly to the change from convective (g) to absolute (h) instability in the linear problem [Eq. (6.32)]. This was first suggested for the spe-

cial case of *real* parameters [$c_i = 0$ in Eqs. (4.59)] by Cross (1986b) based on numerical work, and the generalization to the complex case ($c_i \neq 0$) was conjectured by Fineberg *et al.* (1988a,b). The result can be derived analytically using phase plane trajectory methods (Cross and Kuo, 1992).

In fact the states [(a), (b), (g), (h)] with time-independent magnitudes do not exhaust the possible solutions observed numerically for the complex amplitude equations. The appearance of new states depends strongly on both the scaled system size $L/\xi = L\epsilon^{1/2}/\xi_0$ and the scaled group speed s , Eq. (6.32), as well as on the details of the boundary condition parameters $\bar{\alpha}_\pm = \alpha_\pm \epsilon^{1/2}$, and

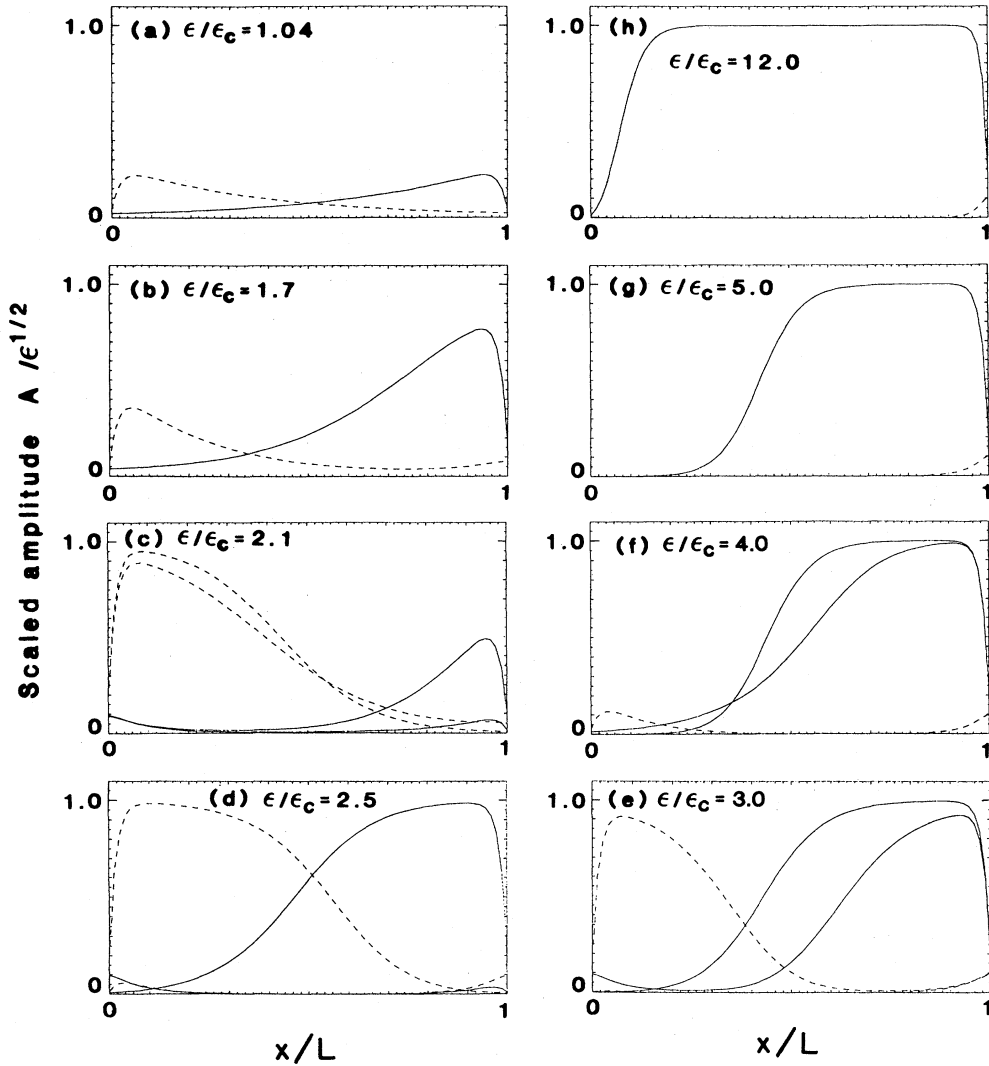


FIG. 25. States predicted near threshold for a traveling wave instability in a one-dimensional finite geometry using the amplitude equations (4.59a,b) with real coefficients ($c_i = 0$) and boundary conditions (5.34a,b). Solid lines show the magnitude $|A_R|$ of right-moving waves, and dashed lines the magnitude $|A_L|$ of left-moving waves. Panels (a)–(h) correspond to fixed values of the group speed s_0 , the system size L and boundary parameters α_\pm, β_\pm for increasing control parameter $\epsilon > 0$ as marked, with ϵ_c the shifted value of onset in the finite geometry. In panels (c)–(f) the state is dynamic, and two traces for each amplitude are shown, corresponding to the extreme values in the cycle, roughly a half period out of phase (see text for details). (From Cross, 1988b.)

$\bar{\beta}_{\pm} = \beta_{\pm}\epsilon^{1/2}$ of Eqs. (5.34). Other states observed are ones in which the envelopes also oscillate in time, typically on the long time scale L/s_0 . This oscillation may be a small amplitude modulation of the rise position of the confined state [“modulated state” Fig. 25(c)] or a complete to and fro motion in which first large amplitude right-moving waves are seen at the right end of the container, to be replaced half a cycle later by the symmetry-related state of large amplitude left-moving waves at the left end of the container [“blinking state” Fig. 25(d)]. The phase diagram as a function of L/ξ and s for a particular choice of the parameters α_{\pm} and β_{\pm} is shown in Fig. 26. It should be noted that an experimental regimen of increasing the control parameter ϵ at fixed L and s_0 corresponds to a hyperbolic trajectory on this diagram. It can be seen that the dynamic states are only evident for large system sizes.

There are more possibilities if the I_o bifurcation in the infinite system is subcritical. This means that the sign in front of the $|A_R|^2 A_R$ term in Eq. (4.59a) is positive, and additional quintic terms must be subtracted to saturate the growth in the infinite system. In addition, for consistency, nonlinear gradient terms such as $|A_R|^2 \partial_x A_R$, a

nonlinear correction to the group velocity, must be included. Clearly there are now even more parameters to be fixed and a systematic search through this parameter space has not been carried out, but two striking results have been discovered. First, it has been found that the hysteresis present in the transition in the infinite system may be strongly reduced or eliminated (Sullivan and Deissler, 1989). Indeed if the sign in front of the first cubic term in Eq. (4.59) is positive and $g_1 > 1$, then there ensues a continuous transition to the same small amplitude counter-propagating traveling wave state [Fig. 25(a)] as found at the forward bifurcation. This occurs because this state has a considerable standing wave component, which stabilizes the system for $g_1 > 0$ (Cross and Kuo, 1992). Sullivan and Deissler (1989) studied a range of parameters with all $c_i \neq 0$ and found quite complicated phase diagrams.

The second new type of behavior is the existence of self-sustaining pulse solutions in the bulk, for the case with $c_i \neq 0$, as discussed in Sec. V.B.2 above. The interaction of these pulses with boundaries remains to be studied in detail, although states with localized pulses stationary at one end (the end towards which the waves in the pulse are moving) have been found, even when only moving pulses exist in the infinite system (Cross, unpublished). We will discuss applications in Sec. IX.A below.

3. External forcing

In type I_o systems the stable ideal states often consist of either right or left traveling waves in one dimension, so the parity symmetry is broken. It has been shown by Riecke *et al.* (1988) that a uniform temporal modulation can stabilize standing waves, i.e. restore the left-right symmetry, provided the modulation frequency is resonant with the original waves, a prediction which has been verified experimentally by Rehberg *et al.* (1988b). A similar effect was obtained by Walgraef (1988b) who considered steady spatial modulation. In two dimensions a richer set of possibilities exists, and both temporal (Walgraef, 1991) and spatial (Pismen, 1987; Coullet and Walgraef, 1989) modulation have been considered.

In a system with endwalls a stable structure can be maintained in a convectively unstable (but absolutely stable) region by reflection at the walls (see subsection VI.C.2 above). It is also of interest to consider the case where, due to variation of the control parameter over the system, an absolutely unstable region sends disturbances into a convectively unstable or even a stable region, leading again to a stable nonlinear state. This type of situation is particularly relevant in open flow systems with a spatially developing flow, such as wakes, jets, and boundary layers, as discussed in Sec. IX.E below.

We start from the amplitude equation (4.59) where now the control parameter $\epsilon = \epsilon(x)$ is a function of position

$$\begin{aligned} \partial_t A + s_0 \partial_x A &= \epsilon(x) A + (1 + ic_1) \partial_x^2 A \\ &\quad - (1 - ic_3) |A|^2 A . \end{aligned} \quad (6.33)$$

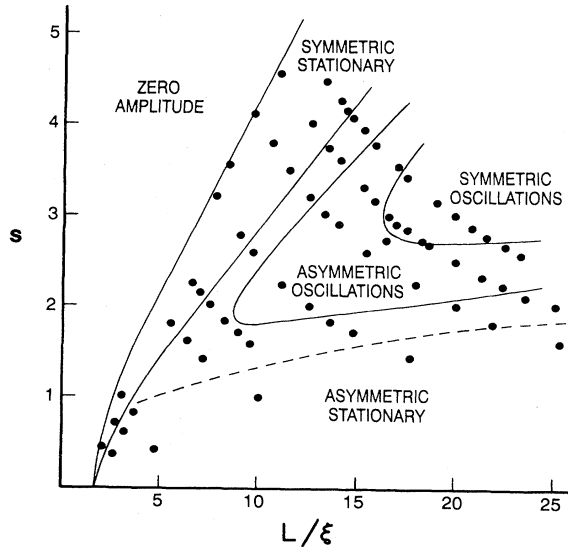


FIG. 26. Phase diagram of states above the threshold of a traveling wave instability showing the reduced group speed $s = s_0 \epsilon^{-1/2} \tau_0 / \xi_0$ as a function of the scaled system size L/ξ , for the amplitude equations (4.59a,b) with $c_i = 0$ and boundary conditions (5.34a,b). The coefficients $\alpha_{\pm}, \beta_{\pm}$ are chosen to yield a reflection coefficient $r = 0.08$ at the endwalls. Numerical calculations were performed at points represented by solid circles. The different regimes are: symmetric oscillations corresponding to panel (d) of Fig. 25; asymmetric oscillations [panels (c), (e), and (f)]; asymmetric stationary states [panels (b), (g), and (h)]; and symmetric stationary states [panel (a)]. Full lines show transitions where the symmetry changes; dashed line indicates the crossover between confined [e.g. panel (g)] and filling [panel (h)] states, which is not a sharp transition in a finite system. (From Cross and Kuo, 1992.)

(We only consider one set of waves, here the right-moving ones.) Two situations have been studied in detail: the case

$$\varepsilon(x) = \varepsilon_0 + \varepsilon_1 x , \quad (6.34)$$

where analytic solution is possible (Chomaz *et al.*, 1988), and the case $\partial_x \varepsilon / \varepsilon \ll 1$, where a WKB approach may be used (Chomaz *et al.*, 1991).

The major qualitative results are illustrated by the linear control parameter case. Chomaz *et al.* use Eq. (6.34) in the domain $x > 0$ with $\varepsilon_1 < 0$ and take the boundary condition $A = 0$ at $x = 0$. The search for a linear instability to self-sustaining solutions at frequency ω is equivalent to the search for bound states in a potential for the Schrödinger equation. Since there is a single additional boundary condition as $x \rightarrow \infty$ (of exponential decay of solutions if this region is stable or of only outgoing waves if it is convectively unstable but absolutely stable), as in the Schrödinger case there are solutions only for a discrete set of frequencies ω_n . Chomaz *et al.* find that for $\varepsilon_0 < \varepsilon_a = 4s_0^2(1+c_1^2)$ there is no region of absolute instability and no self-sustained structure is possible. Such a structure does not develop until there is a finite spatial region of absolute instability, which occurs at a control parameter value

$$\varepsilon_0 = \varepsilon_c = \varepsilon_a + |\delta_1| |\varepsilon_1|^{2/3} (1+c_1^2)^{1/6} \cos[\frac{1}{3} \tan^{-1} c_1] , \quad (6.35)$$

with δ_1 the first zero of the Airy function. Here there is a supercritical Hopf bifurcation to an oscillatory state, sending waves into the convectively unstable region which are eventually damped out in the stable region $x \rightarrow \infty$. (The authors call this a "global bifurcation.") For $\varepsilon_0 > \varepsilon_c$ the linear theory predicts a discrete set of exponentially growing modes, but the nonlinear competition between these modes has not been investigated. An important feature of this result is that a finite portion of the absolutely unstable spatial region, of extent

$$x_T = -\delta_1(-\varepsilon_1)^{-1/3} (1+c_1^2) \cos[\frac{1}{3} \tan^{-1} c_1] = O(|\varepsilon_1|^{-1/3}) , \quad (6.36)$$

is necessary before self-sustained oscillations will occur. For $0 < \varepsilon_0 < \varepsilon_c$, although there are no self-sustained oscillations, the system will be highly sensitive to externally imposed disturbances, either intentionally added periodic disturbances or noise. In particular, large amplitude saturated states may be maintained in a convectively unstable region down stream of a small noise source (Deissler, 1985, 1987b, 1989; Chomaz *et al.*, 1991).

An interesting result for a general shape of spatial dependence of the control parameter $\varepsilon(x)$, but in the limit of slow variation where a WKB analysis applies, is that the (complex) frequency of the fastest growing global mode is given by the saddle-point condition

$$\frac{\partial \Omega}{\partial k} (k_s, \varepsilon(x_s)) = \frac{\partial \Omega}{\partial x} (k_s, \varepsilon(x_s)) = 0 , \quad (6.37)$$

where $\Omega(k, \varepsilon(x))$ is the dispersion relation with k and x extended into the complex plane. Then x_s is the closest saddle point to the real axis in the complex x plane.

D. Effects of external noise

One of the more difficult aspects of the problem of pattern selection is a proper assessment of the role of extrinsic noise. The problem divides naturally into two parts: (i) How does one represent the stochastic forces acting on a system, i.e. can one derive a canonical model? (ii) Can one solve the model, even approximately?

1. Thermal versus nonthermal noise

Any physical system is subjected to random forces coming from the molecular structure of its constituent parts. Clearly, the importance of these effects depends on the scale of the phenomena under consideration. Typically, for microscopic phenomena such as phase transitions or molecular transport processes, thermal noise plays an essential role. A useful model for discussing dynamic properties near critical points, for example, is the stochastic equation (Hohenberg and Halperin, 1977)

$$\partial_t \psi = \Gamma_0 \frac{\delta \mathcal{J}}{\delta \psi^*} + \xi , \quad (6.38)$$

where

$$\mathcal{J} = \int d^d x [r_0 |\psi|^2 + u_0 |\psi|^4 + \xi_0^2 |\nabla \psi|^2] , \quad (6.39)$$

and ξ is a Gaussian white noise with zero mean $\langle \xi \rangle = 0$ and correlation

$$\langle \xi(x, t) \xi(x', t') \rangle = 2 \Gamma_0' k_B T \delta(x - x') \delta(t - t') , \quad (6.40)$$

with T the temperature. Within the framework of the above model the condition that the system relax to the equilibrium (Gibbs) distribution,

$$\mathcal{P} [\psi] \sim e^{-\mathcal{J}[\psi]/k_B T} , \quad (6.41)$$

is the (detailed balance) relation

$$\Gamma_0 = \Gamma_0' . \quad (6.42)$$

[Note that the white-noise form of the spectrum (6.40) is an approximation, which is typically valid only for calculating the long-wavelength correlations of the ψ field.] This model and its variants are useful for describing continuous phase transitions, which may be thought of formally as qualitative changes in the behavior of the correlation function

$$C_\psi(x) = \langle \psi^*(x, t) \psi(0, t) \rangle \quad (6.43)$$

[this function is independent of t at equilibrium]. For example, as a function of r_0 the function C_ψ can go from exponential decay at large distances

$$C_\psi(x) \underset{x \rightarrow \infty}{\sim} e^{-x/\xi} , \quad r_0 > r_{0c} , \quad (6.44a)$$

to a nondecaying form

$$C_\psi(x) \underset{r \rightarrow \infty}{\sim} m^2, \quad r_0 < r_{0c}, \quad (6.44b)$$

characteristic of long-range order. Such phase transitions often occur as a result of a competition between the deterministic term $\delta\mathcal{F}/\delta\psi^*$ and the stochastic term ξ in Eq. (6.38), or more physically, from the competition between energy and entropy. It follows that the noise term must typically be “of order unity” on the scale of \mathcal{F} since it allows for many rearrangements of the system between the different valleys of \mathcal{F} in phase space. We shall express this idea crudely by the relation

$$k_B T \sim f_0 \xi_0^d, \quad (6.45)$$

taking $f_0 \approx r_0 |\psi|^2$ to be a typical energy density in the system.

Our discussion so far has been based on a particular model of critical dynamics, but the ideas are quite generally applicable in the microscopic domain near equilibrium (Hohenberg and Halperin, 1977). Turning now to the types of macroscopic pattern-forming systems we have been considering, we can still for the present discussion represent them in the form (6.38) with thermal noise (6.40) [or perhaps the more general form (3.15) since the assumption of a potential \mathcal{F} is too restrictive]. The point here is that for *macroscopic* systems the typical length and energy scales are such that Eq. (6.45) is rarely satisfied, i.e. the thermal noise is usually negligible compared to the deterministic forces.

To make these notions more precise, let us suppose that we start from the microscopic equations

$$\partial_t U = f(U; R) + \xi(t), \quad (6.46)$$

where the noise satisfies (6.40). Then if the deterministic part [Eq. (6.46) with $\xi=0$] has a bifurcation at $R=R_c$, it leads to an amplitude equation (4.3) in a type I_s system. It is then interesting to ask what the effect of the noise term ξ will be on the amplitude equation. The simplest answer is to take ξ into account at the linear level, i.e. to project ξ onto the critical mode (4.2) and to add this projection to Eq. (4.3). Such a program has been carried out for the case of Rayleigh-Bénard convection, as explained in Sec. VIII.D below. It is found (Graham, 1974; Swift and Hohenberg, 1977; Hohenberg and Swift, 1992) that Eq. (4.3) becomes

$$\tau_0 \partial_t A = \varepsilon A + \xi_0^2 [\partial_x - (i/2q_0) \partial_y]^2 A - g_0 |A|^2 A + \xi_A, \quad (6.47a)$$

$$\langle \xi_A(\mathbf{x}, t) \xi_A(\mathbf{x}', t') \rangle = 2F_A \xi_0^d \tau_0 \delta(\mathbf{x} - \mathbf{x}') \delta(t - t'), \quad (6.47b)$$

with F_A given by the ratio of the thermal energy $k_B T$ to a typical dissipative energy in a volume ξ_0^d ,

$$F_A \sim k_B T / f_0 \xi_0^d. \quad (6.47c)$$

As explained in Sec. VIII.D below this ratio is usually extremely small, $F_A \sim 10^{-9}$, for a typical convection system with $\xi_0 \sim (1-10)$ mm since it represents the ratio of a microscopic to a macroscopic energy (see Ahlers, 1994). Similar estimates can be made for the other systems we are considering, though it is not always clear what the characteristic energy in Eq. (6.47c) should be [see e.g. Eq. (10.37) below].

In view of the smallness of thermal noise for most macroscopic phenomena of interest we must ask whether there are not other sources of noise acting on the system. These would represent degrees of freedom that are not under control or observation, be they associated with the apparatus or with unknown components of the system under study. Clearly, there is little one can say in general about the correct way to represent stochastic effects, either at the level of “microscopic” equations such as (6.46) or at the level of simplified models or amplitude and phase equations. There is no reason that the form (6.46) should be preferred over other hypotheses; in particular it is expected that besides *additive* noise there will be *multiplicative* noise, e.g. an extra term $\xi_A' A$ on the right-hand side of (6.46) representing a fluctuating control parameter (see Hortschek and Lefever, 1984). Moreover, the noise correlations need not have a white spectrum, either in time or in space. It is thus clear that the relatively simple phenomenology of microscopic stochastic phenomena near equilibrium need not be relevant to macroscopic nonequilibrium systems. Nevertheless, in view of the difficulty of finding plausible alternative models, stochastic equations such as (6.46) or (6.47) are often used to model pattern formation, with F_A taken as a phenomenological parameter (see Moss and McClintock, 1989). It should be remembered however that there is no general physical justification for such a model and the results must be viewed with some skepticism.

2. Effects of noise on bifurcations

For simplicity we will confine our discussion to additive white noise, and briefly consider its effect on bifurcations. There is in fact an enormous literature on this problem (see e.g. Gunton and Droz, 1983; Brand *et al.*, 1989), since the kinetics of ordering and coarsening near phase transitions are often represented by models such as (6.38). We shall discuss the stochastically forced Swift-Hohenberg model and then a single-mode amplitude equation.

a. The Swift-Hohenberg model

Consider the stochastic type I_s system in two dimensions

$$\partial_t \psi = \varepsilon \psi - (\nabla^2 + q_0^2)^2 \psi - \psi^3 + \xi, \quad (6.48a)$$

$$\langle \xi(\mathbf{x}, t) \xi(\mathbf{x}', t') \rangle = 2F \delta(\mathbf{x} - \mathbf{x}') \delta(t - t'). \quad (6.48b)$$

The static ordering properties of this system were dis-

cussed in the original paper by Swift and Hohenberg (1977; see also Hohenberg and Swift, 1992). The critical behavior, applicable to an infinite system in $d = 2$ dimensions, turns out to be quite subtle due to the large degeneracy of the broken-symmetry state, and a proper renormalization-group description of the transition has never been worked out. For finite systems, on the other hand, the bifurcation is rounded on a scale

$$\varepsilon_\zeta \sim F^{2/3}, \quad (6.49)$$

i.e. it is *imperfect* with additive noise.

Pattern formation in the stochastic model is a complicated phenomenon which depends critically on the size of the noise ζ . Very little is known in detail, though the concepts of coarsening and domain growth developed for phase transitions (see e.g. Gunton and Droz, 1983) are certainly applicable here. From a quantitative point of view only the linear problem ($g_0 = 0$) can be calculated exactly. For an arbitrary time-dependent control parameter $\varepsilon(t)$, e.g. a sweep from below to above threshold, the average order parameter is given in linear approximation by (Hohenberg and Swift, 1992)

$$\langle \psi_L^2(t) \rangle = L^{-2} \int d\mathbf{x} \langle \psi^2(\mathbf{x}, t) \rangle = \langle \psi_L^2(0) \rangle + 2F \int \frac{d^2 q}{(2\pi)^2} e^{2Q_q(t)} \int_0^t ds e^{-2Q_q(s)}, \quad (6.50a)$$

$$Q_q(t) = \int_0^t ds [\varepsilon(s) - (q^2 - q_0^2)^2]. \quad (6.50b)$$

We shall discuss an approximate formula for $\langle \psi^2(t) \rangle$ that takes into account nonlinearity in the next section.

b. Single-mode amplitude equation

A nonlinear stochastic model for which some quantitative information is available is the single-mode equation for the real variable $\bar{A}(t)$

$$\tau_0 \partial_t \bar{A} = \varepsilon(t) \bar{A} - \bar{g}_0 \bar{A}^3 + \xi, \quad (6.51a)$$

$$\langle \bar{\xi}(t) \bar{\xi}(t') \rangle = 2 \bar{F} \tau_0 \delta(t - t'). \quad (6.51b)$$

This equation might be applicable to a small system in which only one mode is excited [as in Eq. (5.11) above], or it might be thought of as a crude approximation to the time dependence of the spatial average in Eq. (6.48a), $\langle \psi^2(t) \rangle = \langle \bar{A}^2(t) \rangle$. In that case the relation between \bar{F} and F can be shown to be approximately (Ahlers *et al.*, 1981; van Beijeren and Cohen, 1988; Hohenberg and Swift, 1992)

$$\bar{F} \sim F t^{-1/2}. \quad (6.52)$$

The response of a system such as (6.51a) when its control parameter is swept through the bifurcation has been studied systematically for deterministic equations with, for example, a constant ξ (see Grossman and Mikhailov, 1990; Erneux *et al.*, 1991). In the stochastic case an approximate formula for $\langle \bar{A}^2(t) \rangle$ for arbitrary $\varepsilon(t)$ has

been worked out by Ahlers *et al.* (1981) and by Swift *et al.* (1991), based on ideas developed by Suzuki (1987a,b). The approximation, valid for small noise ($\bar{F} \ll 1$), involves an interpolation between exact solutions of the linear stochastic equation for $\varepsilon(t) < 0$ and $0 < \varepsilon(t) \ll 1$, and the nonlinear deterministic equation for $\varepsilon(t) = O(1)$. The formula is cumbersome to write down,

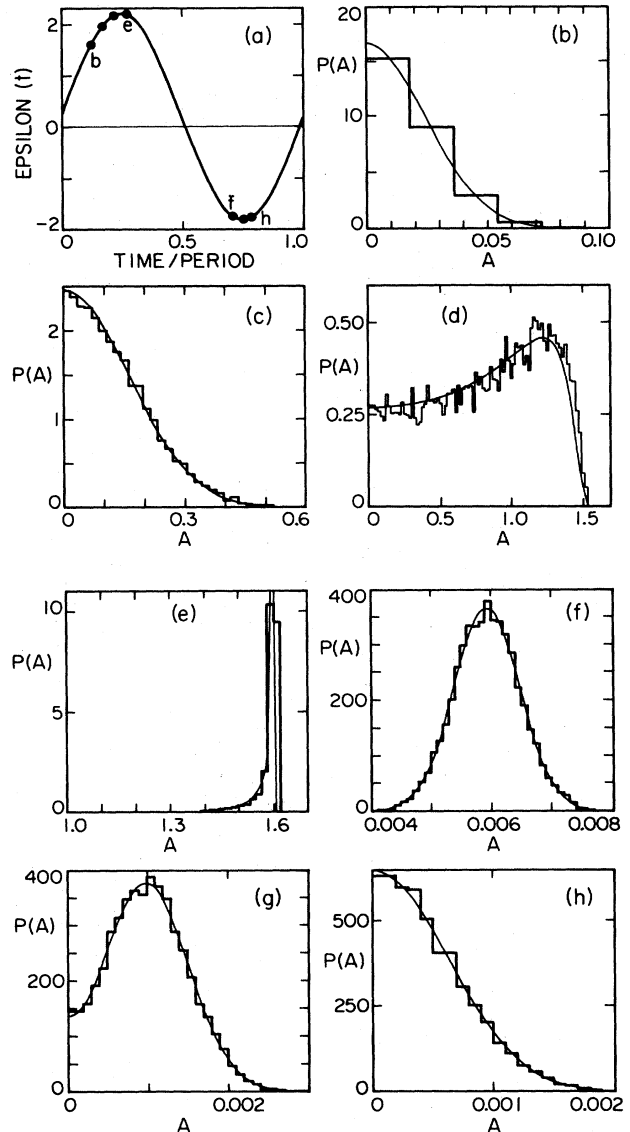


FIG. 27. Probability distribution $P(A)$ vs A at various times for the stochastic amplitude equation (6.51) with $\tau_0 = 0.055$, $\bar{g}_0 = 0.85$, $\bar{F} = 5 \times 10^{-7}$, and $\varepsilon(t)$ given by a sinusoidal modulation, Eq. (8.101) below, with $\varepsilon_0 = 0.2$, $\omega = 5$, $\delta = 2$, as shown in (a). The times in parts (b)–(h) (in units of the period) are $\omega t / 2\pi = 0.1250, 0.1719, 0.2188, 0.2734, 0.7075, 0.7520$, and 0.7822, respectively, as shown by solid dots in part (a). The thin solid lines in (b)–(h) are the analytic approximation of Swift *et al.* (1991), and the jagged line comes from a numerical simulation of the stochastic equation. Since the theory has no adjustable parameters the agreement with the simulation can be considered quite satisfactory. (From Swift *et al.*, 1991.)

so we refer the reader to the paper of Swift *et al.* (1991) for a precise statement, but we note that it provides an analytic approximation to the stochastic equation, whose validity has been verified by comparing it to numerical simulations, as illustrated in Fig. 27. A more systematic treatment has recently been given by Caceres *et al.* (1991).

The above scheme has also been used by Hohenberg and Swift (1992) to provide an approximate solution of the stochastic Swift-Hohenberg model (6.48), and applied to an analysis of experiments in Rayleigh-Bénard convection where the system is ramped through the threshold (see Sec. VIII.D).

We shall have occasion to refer to various models of stochastic behavior in the subsequent discussion of specific systems. Moreover, similar models have been used to represent the effect of chaotic small-scale degrees of freedom on the large scales in *deterministic* systems, as explained in Sec. VII.E. On the whole it must be said that we have little firm knowledge concerning the effects of stochastic forces on nonequilibrium pattern selection, though the problems are important and are being actively studied (see, e.g., Moss and McClintock, 1989; Vasiliev *et al.*, 1987).

VII. CHAOS

A. General features

Chaos is the name given to intrinsic randomness, i.e. random behavior arising in a deterministic system. The existence of chaos was known to Poincaré and others (see, e.g., Miles, 1984c; Jackson, 1989; Gaponov-Grekhov and Rabinovich, 1992), but it was Lorenz (1963) who first clearly identified the phenomenon in dissipative systems, and he and Ruelle and Takens (1971) who first appreciated its significance for understanding fluid flow. This simplest form of chaos occurs in systems of three or more coupled nonlinear ordinary differential equations, and also in discrete mappings. The temporal behavior of such systems is in many cases random, i.e. describable by continuous Fourier spectra, positive Lyapunov exponents, and strange attractors with fractal structure (see below). The physical significance of this behavior of simple mathematical models arises from the experimental observation that certain real systems, for example confined hydrodynamic flows, show similar temporal behavior. The first convincing experimental demonstrations of this phenomenon are due to Ahlers (1974) and Gollub and Swinney (1975).

The basic question we wish to ask is “what is the relationship of the above-mentioned chaotic phenomena to *spatial patterns?*” This question can be divided into three parts: (i) How does one understand the fact that physical systems which consist of an infinity of (molecular) degrees of freedom, or a continuum of hydrodynamic modes, have temporal behavior well described by models with a few degrees of freedom? (ii) How can one understand the temporal behavior of physical systems that are sufficiently extended in space so that the low-dimensional description does not hold (e.g. infinite systems)? (iii)

What can one say about order and disorder in spatial patterns themselves, independent of the dynamics which leads to these patterns? We are thinking here of analyzing instantaneous spatial configurations, or the patterns obtained as stationary (but not necessarily stable) solutions of dynamical equations.

In what follows we will attempt to provide a brief overview of our understanding of these questions which, it must be admitted, is quite sketchy. The most interesting question is the second one mentioned above, but the subject of spatiotemporal chaos is only beginning to be studied at present. We shall begin by presenting a phenomenological and heuristic picture based on defining characteristic lengths which form the basic framework of our picture of spatiotemporal dynamics. Then we shall attempt to identify the important questions which need to be answered to understand chaotic phenomena, and list some examples of numerical and experimental studies of model systems. The need to distinguish between small system “temporal” chaos and “spatiotemporal” chaos in larger systems first became apparent through the pioneering experiments of Ahlers and Behringr (1978a,b) and Berge and co-workers (Berge, 1979; see also Monin, 1978). For other discussions of spatiotemporal chaos see, for example, Aceves *et al.* (1986), Akhromeyeva *et al.* (1989), Grassberger (1989), and Rabinovich and Sushchik (1990).

1. The characteristic lengths

Following Hohenberg and Shraiman (1989) we distinguish three lengths to characterize the dynamics of a spatially extended nonequilibrium system; these are associated with dissipation, excitation, and correlation, respectively. The *dissipation length* ℓ_D is the characteristic length at which energy is dissipated. The modes on shorter scales are passive or “slaved”, and can be treated by elementary methods. The *excitation length* ℓ_E is the length at which energy is injected into the system. For a system near a linear instability there is an excitation range around the most unstable wavelength $\ell_E \approx q_0^{-1}$. External stirring will also typically occur on some length scale which we define as ℓ_E . The *correlation length* ξ is more difficult to define, since its specification requires a rather complete knowledge of the solutions of the dynamical equations. The simplest definition is in terms of a correlation function

$$C_{ij}(r_1 - r_2) = \langle (u_i(r_1, t) - \langle u_i \rangle)(u_j(r_2, t) - \langle u_j \rangle) \rangle, \quad (7.1)$$

where the angular brackets denote an average over time t or an average over the attractor, as discussed below. If the large distance behavior has the form

$$C_{ij}(r) \sim_{r \rightarrow \infty} \exp(-r/\xi), \quad (7.2)$$

then we define ξ as the correlation length for u_i and u_j . Of course, the behavior may be considerably more complicated than in (7.2), but for the moment we will assume that one or more correlation lengths can be defined in the system. Finally, we need to consider the (linear) system

size L , or system volume L^d , where d is the (Euclidean) dimensionality^{7.1} of the system.

2. Small versus large systems

Having introduced the notions of dissipation length ℓ_D , excitation length ℓ_E , correlation length(s) ξ , and linear system size L , we will now give a schematic description of temporal and spatiotemporal chaos, and of “small” and “large” systems. In a uniform stable state all modes of excitation are damped out. At the threshold for pattern formation a small band of modes is excited near the characteristic scale $\ell_E \sim q_0^{-1}$, which is also typically of the same order as the dissipation scale ℓ_D . In our discussion of regular patterns in the previous sections we distinguished between small and large systems according to the value of the quantity Lq_0 . Let us now imagine increasing the control parameter R until the system becomes chaotic. We then wish to distinguish two limiting cases for describing chaotic states.

- Small systems: $L \sim \ell_D$. When the system size L is of order ℓ_D the number of excited modes is severely constrained by geometry. Since these modes can interact strongly a chaotic state can ensue, and this state will be described by an attractor in a low-dimensional phase space. The correlation length ξ also remains comparable to L , so the spatial dependence is dynamically irrelevant and we refer to the system as “small”, i.e. it has a small number of (active) degrees of freedom.

- Large systems: $L \gg \ell_D$. When L is much larger than ℓ_D the system has many degrees of freedom and any description of the chaotic state must take this multiplicity into account. In general we expect the attractor dimension to be correspondingly large in this case.

From this point of view the simplest way to reach the large-system limit is to increase the system-size L at fixed control parameter R . One can then consider the system to be made up of coherent regions (whose size remains to be determined), that are more or less strongly coupled among themselves. We call this limit (fixed R , large L) the regime of “spatiotemporal chaos,” and expect that for sufficiently large L a coarse-grained statistical description will be appropriate.

A second way to achieve a large-system limit for a chaotic state is to fix L and increase R . Although, as we shall see, this scenario is less general than the previous one, we expect that for many systems the number of excited modes will increase with R , thus leading to an attractor in a high-dimensional space. For example in systems described by hydrodynamics the control parameter is given by a ratio of excitation to dissipation. Since the

^{7.1}The term “dimension” is used in the study of dynamical systems to denote the dimension of the phase space, i.e. the number of effective degrees of freedom in the system. In statistical mechanics on the other hand, the term denotes the number of (Euclidean) directions in which the system is *infinite*. Usually the context makes the distinction clear, but in case of ambiguity we shall use “dimension” for the first meaning and “dimensionality” for the second.

latter increases with the square of the wave vector q , while the excitation generally increases more slowly, large R is associated with a decreasing dissipation scale ℓ_D . A prominent example of the above is strong turbulence in fluids where high Reynolds number creates a scale separation between excitation and dissipation ($\ell_E \gg \ell_D$), all at fixed L (see subsection VII.E.5 below).

For either scenario a number of questions arise which we would like to elucidate. Can one define one or more correlation lengths ξ and how do they behave as one goes from a small to a large system by either route? What is the nature of the attractor, in particular what is its fractal dimension d_f (see below) in the asymptotic limits $R \rightarrow \infty$ or $L \rightarrow \infty$? Our conjecture is that in both cases we have

$$\lim_{R \rightarrow \infty} d_f(R) \sim R^a, \quad (7.3)$$

or

$$\lim_{L \rightarrow \infty} d_f(L) \sim L^b, \quad (7.4)$$

but in the second case we expect $b = d$, d being the Euclidian spatial dimensionality of the system. Equation (7.4) leads to a different definition of correlation length than (7.2), i.e. a length ξ_f such that for $L \gg \xi_f$ the system is made up of cells of volume ξ_f^d , and their number $(L/\xi_f)^d$ gives the fractal dimension $d_f(L)$ of the attractor. We refer to the limit (7.4) with $b = d$ as *extensive chaos*.

In line with our focus on pattern forming instabilities we shall primarily consider systems at moderate R as a function of L (“spatiotemporal chaos”). We shall have little to say about the other limit, of $R \rightarrow \infty$ (“strong turbulence”). Indeed, many of the models and systems we consider do not have a physically interesting large- R limit, either because they possess artificial short-length cutoffs (in the models), or because the systems themselves change their character at large excitation.

B. Small systems

Although our main interest is in systems displaying spatial dependence it is useful for us to summarize briefly the considerable knowledge which has been gained in recent years on chaos in small systems. This is first of all because most of what is known firmly about chaos comes from such studies, and secondly because even in large systems it is possible to make local measurements and to evaluate the same quantities as in small systems (time series, Lyapunov exponents, phase space reconstruction). This then provides a starting point for the study of spatiotemporal chaos.

1. Characterization of chaos

Let us consider a dissipative dynamical system consisting of a finite number of coupled degrees of freedom,

$$\partial_t u_i = f_i(U), \quad i = 1, \dots, N, \quad U = \{u_i\}. \quad (7.5)$$

As discussed in Sec. III.A, for autonomous systems at long times motion takes place on an *attractor* which may be a fixed point, a limit cycle, or an m torus, all of which involve regular behavior in the sense that the motion at

one time is *correlated* with the motion at any subsequent time. Alternatively, the motion may be irregular or chaotic, in which case we say the motion takes place on a *chaotic* or *strange attractor*. [Our discussion of chaos is necessarily rather sketchy and imprecise. The interested reader can find further elaboration for example in Hao (1984, 1987, 1988), Schuster (1984), Eckmann and Ruelle (1985), Mayer-Kress (1986), Berge *et al.* (1987), Manneville (1990)].

Since our main concern will be with the long-time properties of systems under constant external conditions it is useful to define a probability measure for the attractor, which remains invariant with time. Given a measure $\mu(U)$ we can take averages of any function $\phi(U)$ over the attractor, by integrating in phase space

$$\langle \phi \rangle = \int dU \mu(U) \phi(U). \quad (7.6)$$

The measure $\mu(U)$ is *ergodic* if the average in (7.6) can also be obtained by integrating over an arbitrary trajectory

$$\int dU \mu(U) \phi(U) = \lim_{T \rightarrow \infty} \frac{1}{T} \int_0^T dt \phi(U(t)), \quad (7.7)$$

where Eq. (7.7) is supposed to hold for any initial condition $U(t=0)$, except for a set of μ -measure zero (Eckmann and Ruelle, 1985). It turns out that many different invariant measures can be constructed for most dynamical systems, but a particular one has physically appealing robustness properties with respect to small perturbations. This measure is obtained by adding to Eq. (7.5) a stochastic function W representing external noise

$$\partial_t U = f(U) + \eta W(t). \quad (7.8)$$

The stochastic process (7.8) has a unique stationary measure μ_η , in terms of which the physical measure, which presumably corresponds to experimental time averages, is defined by the relation

$$\mu_{\text{phys}} = \lim_{\eta \rightarrow 0} \mu_\eta. \quad (7.9)$$

The above definitions are applicable to regular as well as chaotic attractors, and they can presumably be generalized to the case of spatially continuous systems (see Bromberg and Rechester, 1988).

The distinction between regular and chaotic motion can be expressed in terms of the *power spectrum* of the dynamical variables. Let us consider the temporal Fourier transform $\hat{u}_i(\omega)$ of a dynamical variable $u_i(t)$, and form the quantity $|\hat{u}_i(\omega)|^2$ whose average

$$S_i(\omega) = \langle |\hat{u}_i(\omega)|^2 \rangle, \quad (7.10)$$

defines the power spectrum of u_i . Then for regular motion it will consist of a set of sharp delta functions as in the top panel of Fig. 28, whereas for chaotic motion the spectrum has a smooth component as shown in the lower panels. In terms of the time dependence of $u_i(t)$, we can say that the chaotic signal corresponds to a correlation function

$$C_i(t) = \langle (u_i(t) - \langle u_i \rangle)(u_i(0) - \langle u_i \rangle) \rangle, \quad (7.11)$$

which decays at long times, typically as

$$C_i(t) \sim \begin{cases} e^{-t/\tau_{\text{corr}}} & t \rightarrow \infty \\ \dots & \end{cases}. \quad (7.12)$$

(Correlation functions between u_i and u_j can also be defined.) The existence of chaos is thus usually associated with a decorrelation of the motion in a finite time τ_{corr} . The average indicated by the brackets in Eq. (7.11) is with respect to the measure μ defined above.

Another quantity characterizing the dynamics is the *Lyapunov exponent*, which describes the separation of orbits in phase space that start out infinitely close to each other. Let us consider two initial values $\{u_i(0)\}$ and $\{u_i(0) + \delta u_i(0)\}$ at $t=0$. Then for a chaotic orbit we expect the difference δu_i to grow exponentially in time at early times. More precisely we define the Lyapunov exponent as the long-time limit along the orbit of the rate of separation of points in the tangent motion, i.e.

$$\lambda_\ell = \lim_{t \rightarrow \infty} t^{-1} \ln |(DF^t)|_\ell, \quad (7.13)$$

where

$$(DF^t)_{ij} = \partial u_i(t) / \partial u_j(0) \quad (7.14)$$

is the Jacobian matrix evaluated on the orbit $U(t)$. The notation $|A|_\ell$ denotes the ℓ th eigenvalue of the matrix A , ordered in such a way that $|A|_{\ell-1} \geq |A|_\ell \geq |A|_{\ell+1}$. As defined in Eq. (7.13) the exponents λ_ℓ appear to depend on the initial point $u_i(0)$ of the orbit in phase space, but for most chaotic systems it can be shown (Eckmann and Ruelle, 1985) that the same set $\{\lambda_\ell\}$ is obtained for almost all points $\{u_i(0)\}$ in the basin of the attractor, since the limit in Eq. (7.13) averages over long orbits. The set of Lyapunov exponents λ_ℓ , with

$$\lambda_1 \geq \lambda_2 \geq \dots \geq \lambda_n, \quad (7.15)$$

characterize the stability of the motion in phase space. If $\lambda_1 < 0$, all λ_α are negative, i.e. an infinitesimal perturbation decays and the attractor is a fixed point. If $\lambda_1 = 0$ the attractor is a limit cycle, whereas a positive exponent corresponds to diverging orbits, or *chaos*.^{7.2} Such motion, which is said to take place on a strange attractor, is permanently unstable in the directions along the attractor ($\lambda_\alpha > 0$), but stable in directions transverse to the attractor ($\lambda_\alpha < 0$). A positive Lyapunov exponent is at the origin of the *sensitive dependence on initial conditions* that is a characteristic feature of chaos.

A useful characterization of strange attractors is in terms of *generalized dimensions* which roughly speaking count the number of independent degrees of freedom on the attractor (see, e.g., Farmer *et al.*, 1983). Among the many different types of generalized dimension, one of the simplest is the capacity dimension d_{cap} , defined by

$$d_{\text{cap}} = \lim_{\eta \rightarrow 0} \frac{\ln N_c(\eta)}{\ln(1/\eta)}, \quad (7.16)$$

where $N_c(\eta)$ is the minimum number of hypercubes of size η needed to cover the attractor. For a Euclidean set the above definition reproduces the Euclidean dimension

^{7.2}For continuous time dynamics there is always a vanishing exponent (Haken, 1983b), unless the attractor is a fixed point.

d , and for more complicated sets the dimension d_{cap} can take nonintegral values, in which case one speaks of *fractal* sets, and fractal dimension.^{7.3} Another generalized dimension which is used frequently because it is easier to evaluate numerically is the correlation dimension d_{corr} , given by (Grassberger and Procaccia, 1983)

$$d_{\text{corr}} = \lim_{\eta \rightarrow 0} \frac{\ln \langle \mu(\eta; U) \rangle_U}{\ln \eta}, \quad (7.17)$$

where $\mu(\eta; U)$ is the density of points on the attractor in a ball of radius η centered at the point U in phase space. Here the angular bracket denotes an average over points U on the attractor.

There exists yet another important definition of dimension, the so-called *Lyapunov dimension* which is directly related to the Lyapunov exponents defined above. This is

$$d_L = k - \left[\sum_{\ell=1}^k \lambda_\ell \right] (\lambda_{k+1})^{-1}, \quad (7.18)$$

where k is the largest integer such that $\sum_{\ell=1}^k \lambda_\ell \geq 0$. The Lyapunov dimension d_L increases when the number n_p of positive exponents increases, since we always have $d_L > n_p$. In fact, d_L can be thought of as the (fractional) dimension of the parallelipiped which on average neither grows nor decays along the orbit (Manneville, 1985). Another quantity of interest is the Kolmogorov-Sinai entropy,

$$H = \sum_{\ell=1}^{n_p} \lambda_\ell, \quad (7.19)$$

which only sums the positive Lyapunov exponents. It turns out that with the definitions given above exact inequalities can be derived between the various dimensions (see for example Farmer *et al.*, 1983). In many cases the actual values obtained for the different quantities agree to within numerical or experimental uncertainties.

An important point to note is that all of the above definitions of dimension, plus the multitude of other similar quantities (Farmer *et al.*, 1983), refer to a global property, which is far from providing a complete characterization of the fractal sets encountered in nonlinear dynamics. It is only for *scale invariant* structures that one could hope to find a full characterization via a single exponent or even a finite set of exponents. It turns out that the chaotic attractors encountered even in simple mappings necessitate an *infinite number* of dimensions, which can sometimes be represented by a smooth function. Such sets have been given the name “multifractals,” and their properties have begun to be elucidated both theoretically and experimentally in recent years (Mandelbrot, 1974, Frisch and Parisi, 1985; Jensen *et al.*, 1985; Halsey *et al.*, 1986; McCauley, 1990). The simplest way to understand the necessity for many exponents is to generalize the correlation dimension (7.17) to higher moments, thereby defining the q th order “Renyi” dimension (Hentschel and Procaccia, 1983)

^{7.3}We will use the term “fractal dimension” to denote any noninteger dimension characterizing a set and denote it as d_f , as in Eqs. (7.3) and (7.4) above.

$$d_q = \frac{1}{q-1} \lim_{\eta \rightarrow 0} \frac{\ln \langle \mu(\eta; U)^{q-1} \rangle_U}{\ln \eta}. \quad (7.20)$$

(We follow Hentschel and Procaccia in denoting the exponent by q , though it should not be confused with a wave vector.) It is clear that the correlation dimension d_{corr} defined in Eq. (7.17) is d_2 , but one can also show that $d_0 = d_{\text{cap}}$ [Eq. (7.16)], and that $d_q < d_{q'}$ for $q > q'$. In a scale invariant system one might expect the pair-correlation function to determine the higher correlations, so that d_q would have a simple functional dependence on q . For chaotic (multifractal) attractors this is generally not the case, and the whole function d_q is an intrinsic characterization of the dynamics. For different values of q (which can have arbitrary sign) portions with higher or lower density in phase space are weighted differently in Eq. (7.20). A transformation analogous to the Legendre transform of thermodynamics leads to the function $f(\alpha)$:

$$f(\alpha) = q \alpha(q) - (q-1)d_q, \quad (7.21a)$$

$$\alpha(q) = (d/dq)[(q-1)d_q], \quad (7.21b)$$

(Feigenbaum *et al.*, 1986; Halsey *et al.*, 1986; Mori *et al.*, 1989). It can be shown that the function $f(\alpha)$ represents the density of singularities on the attractor that are associated with the scaling exponent α (Halsey *et al.*, 1986). This function can be determined directly by analysis of numerical or experimental data, and it constitutes a kind of signature of the statistical properties of the strange attractor (see Glazier and Libchaber, 1988; Barkley and Cumming, 1990, and references therein). Although it is clear that the functions d_q and $f(\alpha)$ provide a fuller characterization of chaos than is obtained from the fractal dimension d_f , it is not known whether this characterization is in any sense complete. In particular, the question of the universality of chaotic dynamics beyond the onset of chaos is still not completely clarified, even for the simplest examples, and sophisticated methods have been developed for analyzing this problem (see, e.g., Argoul *et al.*, 1988; Auerbach and Procaccia, 1990).

In summary, motion on a strange attractor is characterized by positive Lyapunov exponents (sensitive dependence on initial conditions), a continuous frequency spectrum for observables, and an attractor with (multi)fractal structure. Although these properties are not mathematically equivalent, they usually occur together, and make up what we refer to as temporal chaos in small systems.

2. Reconstructing the attractor from time series

The definitions of Lyapunov exponents and dimensions discussed above were all formulated in terms of the equations of motion of the system (7.5), which determine the trajectories in phase space. Since for most experiments a suitable set of equations (involving a finite number of modes!) is not known, it is not clear *a priori* how useful these concepts might be for analyzing experiments. It turns out, however, that observation of a single variable $u_i(t)$ allows one to estimate the complete orbit in phase space and therefore to obtain approximate expressions

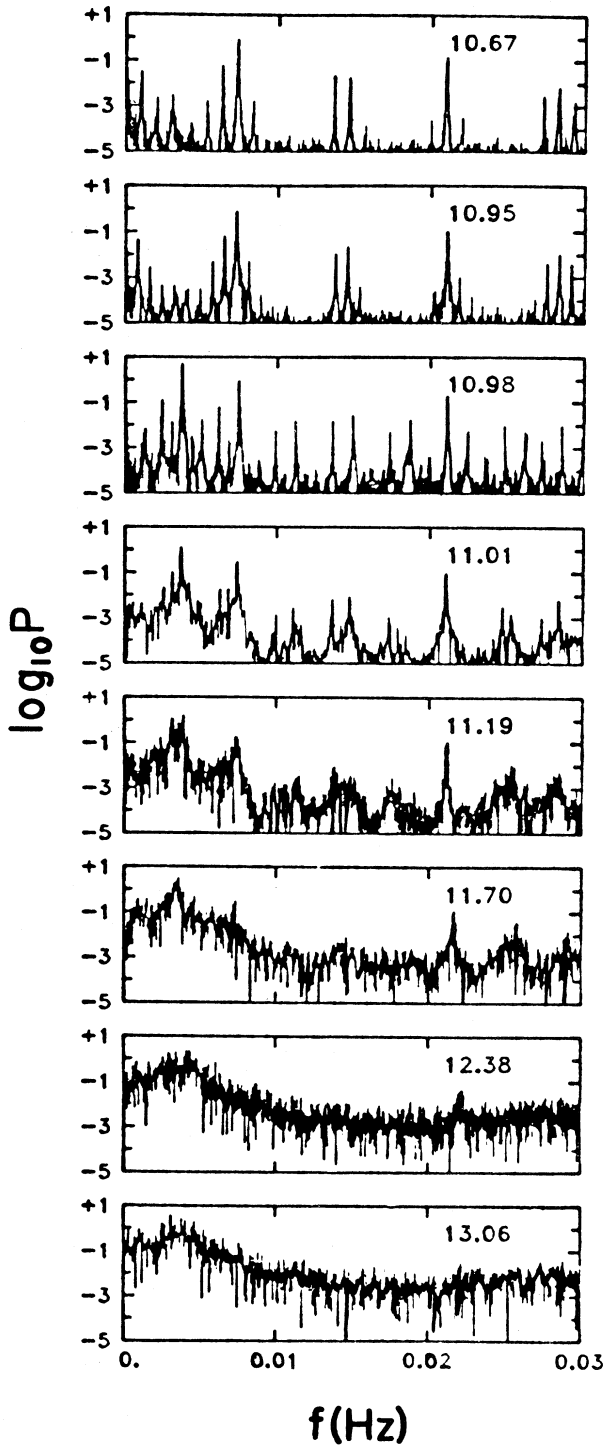


FIG. 28. Power spectrum of temperature fluctuations in a small aspect ratio ($L=2.08$) convection cell. Ordinate is the logarithm of the power spectral density of $\Delta T / \Delta T_c$ in Hz^{-1} as a function of frequency f . Here ΔT is the temperature difference across the cell, ΔT_c its value at the onset of convection, and the heat flow through the cell is maintained constant. The number in each panel is the mean value of $\Delta T / \Delta T_c$. (From Ahlers and Behringer, 1978b.)

for the exponents and dimensions. The method used involves a remarkable *reconstruction technique* (Takens, 1981, 1985; Packard *et al.*, 1980) which consists in the following: the motion on a d_f -dimensional attractor in an N -dimensional phase space is parametrized by taking m displaced values of one of the variables, say u_1 ,

$$\begin{aligned} v_1(t) &= u_1(t), & v_2(t) &= u_1(t+\tau), \dots, \\ v_k(t) &= u_1(t+(k-1)\tau), \end{aligned} \quad (7.22)$$

The reconstruction technique depends on the statement that for almost all values of the time interval τ , the orbit in the space $\{v_k(t)\}$ ($k=1, \dots, m$) is a faithful projection of that in the original space $\{u_i(t)\}$ ($i=1, \dots, N$), so long as $m > 2d_f + 1$, where d_f is the dimension of the attractor. It is important to realize that although the above statement rests on some mathematical theorems (quoted on p. 627 of Eckmann and Ruelle, 1985), the quantitative aspects of the reconstruction method are not entirely clear. For example, it is not known in general how accurately $u_1(t)$ needs to be measured to obtain the attractor of the original $\{u_i(t)\}$ to a given accuracy. Similarly, the total number of data points needed for the reconstruction grows with the dimension of the attractor, but it is not precisely known how fast. Furthermore, the validity of the method depends on a proper choice of the time delay τ , which must be long enough so that each $v_k(t)$ represents new information, but short enough so as not to lose information [see Fraser and Swinney, 1986 and Fraser, 1989 for discussions of these points]. In general, our understanding of the reconstruction method comes both from numerical tests on models whose equations of motion are known, and on applications to experiments where physically plausible answers are obtained. An early careful study of the reconstruction technique was carried out by Eckmann *et al.* (1986), who evaluated the largest Lyapunov exponents for the Lorenz model and for a chaotic Rayleigh-Bénard cell, over a range of values of the control parameter. In the former case they were able to check their results against a direct calculation of the exponents from the equations of motion. There is by now a gigantic literature on the evaluation of fractal dimensions, either from the starting equations or via reconstruction techniques (see e.g. Mayer-Kress, 1986; Gershenfeld, 1988, 1992; Abarbanel *et al.*, 1993), but it is often difficult to assess the reliability of the results obtained (see Guckenheimer, 1984; Ruelle, 1990). Nevertheless, it turns out that in a large number of cases the exponents and dimensions obtained by these techniques yield a reasonably consistent picture of chaotic behavior and the method is clearly of practical value. It should be noted, however, than an important physical limitation of any reconstruction method based on measurements at a single point in a real system is that the motion must in some sense be fully correlated in space. In spatially extended systems such as the ones we consider below, the required input information will necessarily involve data at *different* points in space. We shall discuss this point further, but for the moment we merely note

that some *a priori* criterion should exist to decide whether single-point information suffices, i.e. whether we are truly dealing with a “small” system.

3. Onset of chaos

A remarkable discovery made a few years ago (Feigenbaum, 1978, 1979) is that the transition from regular to chaotic behavior can show *universal* properties, which are formally similar to those found near a thermodynamic critical point. In particular, renormalization group techniques have been applied to such systems and universal *scaling exponents* derived. The two most studied examples of universal routes to chaos are the infinite period-doubling cascade and the transition from quasi-periodicity to chaos; in both cases nontrivial exponents have been calculated and measured. An interesting aspect of the transition is that *external noise* plays the same role as an ordering field at a thermodynamic critical point, i.e. it smears the transition over a range determined by a new critical exponent (Crutchfield *et al.*, 1981; Shraiman *et al.*, 1981). Besides the period-doubling and quasiperiodic transitions, there are routes to chaos involving “intermittency” or “crises,” but they

C. Infinite systems: Extensive chaos

1. Characterizing spatiotemporal chaos

We shall primarily consider the extreme limit of an infinite system, and attempt to make the notions of spatiotemporal chaos and correlation length more precise in this fixed- R large- L limit, since we believe it is conceptually simplest. For infinite systems we cannot hope to produce not seem to possess the same scaling properties or metric universality as the other cases (see Eckmann, 1981). For example the famous transition to chaos discovered originally by Lorenz (1963) is not associated with any simple critical exponent or scaling structure.

4. Continuum models and real systems

Let us now suppose that we are dealing with a continuum model, e.g. the partial differential equations (3.4), which have an infinite number of degrees of freedom. As discussed earlier, since the system is *dissipative* it is reasonable to expect on physical grounds that there is a length scale ℓ_D below which all modes are damped, so that a d -dimensional (see footnote 7.1) system of length L would have an attractor with at most $O[(L/\ell_D)^d]$ degrees of freedom. With increasing forcing, more modes are expected to be excited, which means that ℓ_D decreases as R increases (we use the terms “modes” and “degrees of freedom” interchangeably).

The above picture has been partly validated mathematically both by general theory (Temam, 1988) and by numerical studies (Moon *et al.*, 1983; Doering *et al.*, 1987; Rodriguez and Sirovich, 1990; Sirovich *et al.*, 1990). For a given partial differential equation the attractor is typically a complicated multidimensional set with fractal structure. For mathematical purposes it has been found convenient to embed the attractor in a finite-dimensional *smooth* set called the *inertial manifold*, which is invariant

under the dynamics and is in some sense the minimal smooth set containing the attractor (see Temam, 1990 and references therein). The existence of such an inertial manifold has been proven for models such as the complex Ginzburg-Landau (4.49) and the Kuramoto-Sivashinsky (3.31) equations, but not yet for the Navier-Stokes equation, though approximate inertial manifolds have been found for this case (Temam, 1989). For various systems rigorous bounds have been given for the dimension of the invariant measure, as well as that of the inertial manifold and of the attractor, as a function of either system size or control parameter, (Eckmann and Ruelle, 1985; Temam, 1989).

To the extent that the above program can be carried out, this provides a mathematical explanation of the existence of “small” systems, i.e. of the observed fact that certain continuum systems have dynamics well described by low-dimensional models (Abraham *et al.*, 1984).

vide a detailed theoretical picture of the dynamics, so we adopt a statistical point of view (Hohenberg and Shraiman, 1989; Kraichnan and Chen, 1989). To the extent that we wish to describe chaos this is no restriction, since even in small systems chaotic motion can only be analyzed statistically. Moreover, the traditional description of strong turbulence in fluids is also expressed in terms of statistical correlations (see Monin and Yaglom, 1975).

We will take as our basic definition of spatiotemporal chaos the property of large attractor dimension mentioned in Eq. (7.4) above. Quite generally, a system exhibits spatiotemporal chaos if the attractor dimension diverges with system size. It follows from Eq. (7.18) that the number of positive Lyapunov exponents also diverges. We shall have more to say on the specific dependences of these quantities on L below, but first we discuss various definitions of the correlation length. Clearly, there are an infinite number of possible choices, but most of them will either be physically equivalent or altogether uninteresting. Nevertheless, it is not clear *a priori* how many distinct physically relevant correlation lengths there might be in a given system, so it seems to us worthwhile to explore various possible definitions.

a. Correlation length

We consider a translationally invariant system which is infinite in d directions and is in a statistically stationary state. This means that we can define averages that depend only on *differences* of space-time coordinates. We wish to elucidate the nature of spatial correlations and to define one or more correlation lengths to characterize the dynamics. Rather than seek to guess the unique definition that will fit all cases, we shall list a number of possible candidates. To the extent that the different lengths are qualitatively different this might tell us something significant about the dynamics.

(i) Decay of correlation function

For notational simplicity in this section we consider an equation for a single field $u(x, t)$

$$\partial_t u = G[u, \nabla u, \nabla^2 u, \dots], \quad (7.23)$$

and introduce the correlation function

$$C(x-x';t-t') = \langle (u(x,t) - \langle u \rangle)(u(x',t') - \langle u \rangle) \rangle, \quad (7.24)$$

the average being over the measure μ of Eq. (7.6) or equivalently over the time t with fixed $t-t'$. The corresponding Fourier transforms are given by

$$C(q,\omega) = \int dx dt e^{-i(q \cdot x - \omega t)} C(x,t). \quad (7.25)$$

An important property of correlation functions is their long-range decay, as in the form given in Eq. (7.2) above, which defines a decay length ξ . The actual behavior may be more complicated than simple exponential decay, or a different correlation function than (7.24) may be appropriate, for example if the spatial average of u has periodic time dependence. Alternatively, the correlation function may not decay exponentially, but only algebraically, in which case we say that the corresponding correlation length is infinite. This situation will be discussed further in subsection VII.E.2 below. For the present discussion we assume for simplicity that we are dealing with systems having finite correlation lengths.

(ii) Statistics of fluctuations

The existence of a finite correlation length implies that quantities measured inside a correlation volume will have nontrivial statistics. In contrast, quantities that depend on data spread out over many correlation volumes will have a Gaussian distribution. For example the Fourier transform

$$u(q) = \int dx u(x) e^{-iq \cdot x}, \quad (7.26)$$

has a Gaussian distribution if the volume $\Omega \approx L^d$ contains many correlation volumes ($L \gg \xi$), even if $q^{-1} \ll \xi$. In practical cases one is often interested in more local quantities, such as $u(x)$, or a wave packet inside some volume $\delta\Omega$ which may be smaller or larger than ξ^d .

We can use the statistics of fluctuations to define a correlation length by examining the transition between Gaussian and non-Gaussian statistics. Specifically, let us consider the quantity (Kaski *et al.*, 1983)

$$K(\ell) = \frac{\langle (\Delta u)^4 \rangle_\ell}{3 \langle (\Delta u)^2 \rangle_\ell^2} - 1, \quad (7.27)$$

where

$$\langle A \rangle_\ell = \int_{\Omega(\ell)} dx A(x) \quad (7.28)$$

is an average over a volume $\Omega(\ell) \sim \ell^d$, and

$$\Delta u(x) = u(x) - \langle u \rangle_\ell. \quad (7.29)$$

(For simplicity we assume here that all moments exist.) For $\ell \gg \xi$ we expect the statistics of u to be Gaussian so $K(\ell) \rightarrow 0$, but for $\ell \ll \xi$, $K(\ell)$ has some nonzero value. We can thus define ξ as the value of ℓ at which $K(\ell)$ becomes small when ℓ grows large. Generalizations of the quantity defined in Eq. (7.27) to higher powers of Δu can

be considered, and it is interesting to ask how the corresponding ξ 's will depend on the precise moment under consideration. There may of course be systems with a number of intrinsically different correlation lengths and the above simple scheme will not apply.

As a result of the Gaussian nature of correlations in a large system we expect each Fourier transform variable $u(q,\omega)$ to be governed by a probability functional

$$P\{u(q,\omega)\} \sim \exp[-D(q,\omega)|u(q,\omega)|^2], \quad (7.30)$$

whose Gaussian measure is directly related to the dynamic structure factor

$$C(q,\omega) = \langle |u(q,\omega)|^2 \rangle = \frac{1}{2} D^{-1}(q,\omega). \quad (7.31)$$

The Gaussian nature of (7.30) does not contradict our earlier statement that local variables have non-Gaussian statistics, since in inverting the Fourier transform higher-order correlations between different Fourier modes come into play.

(iii) Other definitions

Besides the decay of correlation functions and the statistics of moments, other lengths can be considered as measures of spatial correlations. Kaneko (1989, 1990a) has defined Fourier transforms over finite spatial domains and obtained a correlation length from the dependence of the spatiotemporal correlations on the domain size. A more physical definition arises when the system itself possesses a domain structure, for example when there exist alternating laminar and turbulent regions (see subsection VII.E.2.a below). Then one can define a distribution function $\tilde{P}(\ell)$ as the fraction of laminar domains with characteristic dimension ℓ and obtain a correlation length from the decay of $\tilde{P}(\ell)$ at large ℓ (see Chaté and Manneville, 1987). A set of correlation lengths can also be defined from purely dimensional considerations by taking ratios of averages of spatial derivatives (or moments in Fourier space), for example (Stassinopoulos *et al.*, 1990)

$$\xi_1^2 = \frac{\langle (u - \langle u \rangle)^2 \rangle}{\langle (\partial_x u)^2 \rangle}, \quad (7.32a)$$

$$\xi_2^2 = \frac{\langle (\partial_x u)^2 \rangle}{\langle (\partial_x^2 u)^2 \rangle}, \quad (7.32b)$$

and so forth. Of course, it is not clear that the lengths so defined will reflect the *long-range* correlations in the system, though some evidence that they do has been presented by Stassinopoulos *et al.* for a simple coupled-map model.

Another possible set of correlation lengths will arise when we discuss Lyapunov exponents and dimensions for extended systems. We will see in the next section that the spatial extent of a Lyapunov vector defines a characteristic length that is presumably some measure of spatial correlation in the system. Also, the length scale over which pointwise measures of the dimension of the attractor are correlated can be used to define a correlation length (see below).

b. Exponents and dimensions

The definitions of exponents and dimensions discussed in subsection VII.B for small systems can be carried over to the infinite case as well. The Lyapunov exponents are defined by a generalization of Eq. (7.13) to a continuum case

$$\lambda_\alpha = \lim_{t \rightarrow \infty} \frac{1}{t} \ln |DF^t|_\alpha, \quad (7.33a)$$

where

$$DF^t = \delta u(x, t) / \delta u(x', 0) \quad (7.33b)$$

is the Jacobian matrix corresponding to the dynamics (7.23). (The notation $|A|_\alpha$ still denotes the α th eigenvalue of the matrix A , which is now infinite dimensional.) Corresponding to each eigenvalue λ_α there is an eigenvector $\tilde{u}_\alpha(x, t)$. For the largest exponent λ_m , Eq. (7.23) has the more transparent form

$$\lambda_m = \frac{1}{2} \lim_{t \rightarrow \infty} \frac{1}{t} \ln \left[\frac{\phi(t)}{\phi(0)} \right], \quad (7.34a)$$

$$\phi(t) = \int dx |\delta u(x, t)|^2, \quad (7.34b)$$

where δu satisfies the equation

$$\partial_t \delta u(x, t) = \left[\frac{\delta G}{\delta u} \right]_{u(x, t)} \delta u(x, t). \quad (7.34c)$$

which is a linearization of Eq. (7.23) about the orbit $u(x, t)$. In writing Eq. (7.34) we have for simplicity taken a single component equation as in Eq. (7.23) and also as-

sumed that the results are independent of the initial values $u(x, 0)$ and $\delta u(x, 0)$. In this way $\delta u(x, t)$ will become proportional to the corresponding eigenvector $\tilde{u}_m(x, t)$ at large t and the maximum eigenvalue λ_m will emerge. In principle one would have to vary the initial conditions but we will assume that this is not necessary.

In a numerical study of the Kuramoto-Sivashinsky equation (3.31), Manneville (1985) has confirmed that the Lyapunov exponents remain bounded as the system size grows. It is their density $\mathcal{D}(\lambda)$ which grows with size (Ruelle, 1982), as shown in Fig. 29, where

$$i(\lambda) = \int_{-\lambda_m}^{\lambda_m} \mathcal{D}(\lambda') d\lambda', \quad (7.35)$$

is plotted for various system sizes. The curves for different sizes are not very different, only the density fills in for larger systems. From these data it is possible to evaluate the Lyapunov dimension, defined in Eq. (7.18), and the result is quoted in Eq. (7.53) below.

As mentioned above, the Lyapunov vector $\tilde{u}_\alpha(x, t)$ associated with a particular exponent λ_α can be used to define a correlation length ξ_α by the relation

$$\frac{[\int d^d x \tilde{u}_\alpha^2(x, t)]^2}{\int d^d x \tilde{u}_\alpha^4(x, t)} = \xi_\alpha^d. \quad (7.36)$$

Although this length is formally still a function of time t it is expected that for an extended eigenvector in an infinite system the spatial integral will have the effect of averaging over time. For a localized eigenvector or a finite system the quantity $\xi_\alpha^d(t)$ could be averaged over

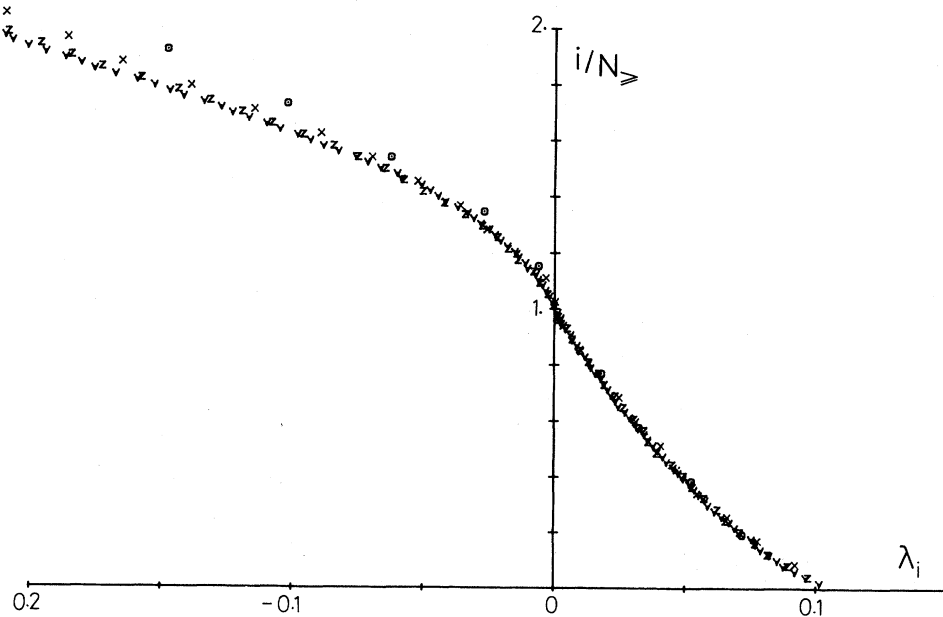


FIG. 29. Number i of Lyapunov exponents larger than the value λ_i , scaled by the number N_{\geq} of non-negative Lyapunov exponents, plotted vs λ_i for the Kuramoto-Sivashinsky model (3.31). Results are shown for sizes $L = 100, 200$, and 400 , showing the intensive nature of the Lyapunov density. (From Manneville, 1985.)

time. The length defined in this way is analogous to the "participation ratio" defined in the theory of electron localization (see Wegner, 1980; Kaneko, 1986a): if ξ_α turns out to be finite for an infinite system this means the eigenvector \tilde{u}_α is *localized*, otherwise it is *extended*. Another correlation length can be obtained from the large distance behavior of the correlation function for the positive density \tilde{u}_α^2 ,

$$C_\alpha(r) = \frac{\int d^d x \tilde{u}_\alpha^2(x+r) \tilde{u}_\alpha^2(x)}{\int d^d x \tilde{u}_\alpha^4(x)}. \quad (7.37)$$

We expect that $C_\alpha(r)$ will decay exponentially at large r for localized states, though with a length $\xi'_\alpha \neq \xi_\alpha$ in general. For extended states $C_\alpha(r)$ remains finite for $r \rightarrow \infty$, and at the "mobility edge" we might have a power-law falloff of C_α .

As mentioned in subsection VII.A above, whenever an attractor dimension is obtained we can ask how it scales with system size L , and thereby define a correlation length. In typical cases for large L , d_f is *extensive* (i.e. proportional to volume) and we can define a correlation length ξ_f by the relation

$$\lim_{L \rightarrow \infty} d_f(L) = (L/\xi_f)^d. \quad (7.38)$$

All of the dimensions defined in subsection VII.B.1 for low-dimensional systems can in principle be calculated for spatially extended systems as well, albeit with large requirements of computer capacity. An interesting question raised by Grassberger (1989) concerns the possibility of defining the fractal dimension of a *subsystem* of volume Ω' embedded in a large system (volume $\Omega \gg \Omega'$). In particular he showed for a system of coupled logistic maps (see below) that the correlation dimension d_{corr} , Eq. (7.17), of the subsystem was also intensive

$$d_{\text{corr}} \propto \Omega', \quad (7.39)$$

though the coefficient of proportionality is not in general the same as for a closed system.

In the above discussion we have assumed that the equations of motion are known, and that the dimensions and exponents were obtained from these equations. As discussed earlier, however, in many experiments an appropriate theoretical model is not available and it is useful to obtain information from experimental data directly. The natural question to ask is, does the reconstruction method described in subsection VII.B.2 above apply to attractors in large systems? The answer to this question is in large measure unknown even for the simplest models. We may conjecture, however, that a natural generalization of the reconstruction method of subsection VII.B.2 is to divide the system into cells of size ξ^d and to measure a vector $u(t) = \{u^{(\alpha)}(t)\}$, with $u^{(\alpha)}(t) = u(x_\alpha, t)$ and x_α placed in cell α . Then the reconstructed vector would be $v_\beta^\alpha(t) = u^{(\alpha)}(t + \beta\tau)$.

If data at two points a distance ℓ apart are used to estimate the dimension, then a simple conjecture might be

(Pomeau, 1985)

$$d(\ell) = \rho_f \xi^d, \quad \ell \ll \xi, \quad (7.40a)$$

$$d(\ell) = 2 \rho_f \xi^d, \quad \ell \gg \xi, \quad (7.40b)$$

since the measurements in Eq. (7.40b) represent two independent samples. The dimension density ρ_f can then be estimated for a linear system (dimensionality $d=1$) as

$$\rho_f = \frac{d(\ell) - d(0)}{\ell}, \quad (7.41)$$

in the interpolation region. Similar formulas can be found for systems of higher dimensionality ($d=2$ or 3). In proposing the above scheme, Pomeau has suggested that the correlation length ξ in Eq. (7.40) will depend on the measurement precision η and should be replaced by $\xi \ln \eta^{-1}$. A preliminary attempt at numerical implementation in a coupled-map model was undertaken by Mayer-Kress and Kurz (1987), but so far the results have been rather inconclusive. Grassberger (1989) has questioned the validity of the above proposal, suggesting that the crossover assumed in Eq. (7.40) will not be observed.

Attractor reconstructions and dimension estimates have been undertaken in a number of spatially extended systems, both numerical and experimental (see Grappin *et al.*, 1986; Mayer-Kress, 1986; Brandstatter and Swinney, 1987; Ciliberto, 1987; Aranson *et al.*, 1988; Gromov *et al.*, 1987). Clearly, the quantity of data required for a precise description grows rapidly with the size of the system, and it is not at present clear how much information can be extracted from this type of analysis.

2. Response and transport

It may be useful to borrow some ideas from linear response theory (Forster, 1975; Hohenberg and Shraiman, 1989). For that purpose let us introduce an external perturbation $h(x, t)$ into the dynamical equation for the field $u(x, t)$, Eq. (7.23), and define the response function R as

$$R(x, x'; \tau) \equiv \left\langle \frac{\delta u(x, t+\tau)}{\delta h(x', t)} \right\rangle, \quad (7.42)$$

where the average is once again over t . The response function quantifies the rate of relaxation to the "equilibrium" measure given by $P\{\hat{u}\}$, Eq. (7.30). Then the relaxation rate for a given spatial mode with wave vector q is determined by the nearest pole of the Laplace transform of R with respect to τ .

Another interesting object first used by Sompolinsky, Crisanti, and Sommers (1988) is the quadratic response

$$\begin{aligned} \Lambda(z) &= (1/\Omega) \int_0^\infty d\tau e^{-z\tau} \\ &\times \int dx \int dx' \left\langle \left(\frac{\delta u(x, t+\tau)}{\delta h(x', t)} \right)^2 \right\rangle, \end{aligned} \quad (7.43)$$

where $\Omega \sim L^d$ is the volume of the system. This function can be used to define the spectral density $n(\lambda)$ of the growth (or susceptibility) exponents

$$\Lambda(z) = \int d\lambda \frac{n(\lambda)}{z - 2\lambda}. \quad (7.44)$$

These exponents are similar, but except for the largest one not exactly equivalent, to the Lyapunov exponents.

One interesting issue is to understand the relation between the correlation and response functions defined above. For example, for the case of dynamics near thermal equilibrium there exists a fluctuation-dissipation theorem which in the classical regime has the form (see, e.g., Hohenberg and Halperin, 1977)

$$C(q, \omega) = (2T/\omega) \text{Im } R(q, \omega), \quad (7.45)$$

where T is the temperature. Note that in equilibrium Eq. (7.45) holds for all q and ω . In the present case we can introduce a function

$$T(q, \omega) \equiv \frac{\omega C(q, \omega)}{2 \text{Im} R(q, \omega)}, \quad (7.46)$$

whose low-frequency long-wavelength limit (if it exists) defines an effective temperature

$$T_0 = \lim_{\substack{q \rightarrow 0 \\ \omega \rightarrow 0}} T(q, \omega). \quad (7.47)$$

Another effective temperature can be obtained from the equal-time correlation function and the static response $R_s(q)$

$$T_e = \lim_{q \rightarrow 0} \frac{C(q, t=0)}{R_s(q)}. \quad (7.48)$$

In equilibrium $T(q, \omega)$ is independent of q and ω and the equality of T_0 and T_e follows from the dispersion relation

$$R_s(q) = P \int_{-\infty}^{\infty} \frac{d\omega}{\pi} \frac{\text{Im} R(q, \omega)}{\omega}, \quad (7.49)$$

where P denotes the principal value. Hohenberg and Shraiman (1989) proposed using Eqs. (7.47) and (7.48) to characterize the spatially extended chaos, and to use the difference between T_0 and T_e , or the ω, q dependence of $T(q, \omega)$ as a measure of the departure from equilibrium. However an important ingredient of the derivation of Eq. (7.49) in equilibrium systems is that the field used to define the response function is introduced into the Hamiltonian, and not into the dynamical evolution equation as we are forced to do in the dissipative chaotic systems. Even for an equilibrium system the function $T(q, \omega)$ defined by Eq. (7.46), with R the response function to a field added to the dynamical equations, is not simply related to the thermodynamic temperature, and it may have a complicated dependence on q and ω . The simplicity of the usual equilibrium result derives from adding the field through a term in the Hamiltonian H , which then has a direct effect on the probability measure, e.g., $\exp[-\beta H]$. This measure determines both the new mean value (the response) and the fluctuations (the corre-

lation functions). On the other hand the independence of $T(q, \omega)$ on ω for small q may result from the long-wavelength Langevin description of extended chaotic systems (see subsection VII.E.1 below), so that equality between T_e and T_0 might not in itself signify that the system is close to equilibrium.

One can also attempt to define effective transport coefficients from the Fourier transform $R(q, \omega)$ of the response function R , using the analogue of Kubo relations familiar from statistical mechanics near equilibrium (Forster, 1975). Such an approach is close to the phenomenological point of view adopted in the study of strong turbulence [see, e.g., Monin and Yaglom, 1975; Dwoyer *et al.*, 1985], where the eddy viscosity is a fundamental ingredient in many approximate treatments. It would be interesting to study the response to deterministic and stochastic forces in chaotic states, and perhaps a connection can be found between exponents and dimensions on the one hand, and transport and response on the other. An attempt at a thermodynamic characterization of extensive chaos has been presented by Ciliberto and Caponeri (1990).

3. Chaos and turbulence

The terms chaos and turbulence are used to denote a number of different phenomena, and considerable debate and confusion have arisen concerning the “proper” use of these words. In discussing this issue here our aim is not to legislate one more set of definitions, but rather to clarify the different types of behavior involved, as well as the terms used by different authors to refer to them (see, for example, Newell, 1986; Bohr, 1989; Busse, 1989). What is generally meant by *chaos* is any type of random behavior resulting from deterministic equations with regular initial conditions. Since we defined temporal chaos by the existence of a finite correlation time, Eq. (7.12), we could similarly consider *spatiotemporal chaos* to be defined by both a finite correlation time and a finite correlation length. The term “turbulence,” when used in fluid dynamics, traditionally signifies disordered flow, particularly flow involving the generation and transport of vorticity (Monin, 1978). In this usage the question of deterministic or stochastic origin of the phenomenon is not central to the terminology, since it refers to observed phenomena rather than to their explanation. Recently the word turbulence has come to be used more widely, sometimes as a synonym for chaos, but more particularly for what we have called spatiotemporal chaos.

The chaos that occurs near threshold in models such as the complex Ginzburg-Landau (4.49) or Kuramoto-Sivashinsky (3.31) equations for large L is referred to as “weak” or “phase” turbulence (Kuramoto, 1984). This is in contrast to “amplitude” or “defect mediated” turbulence, which occurs further away from threshold and involves the motion of phase singularities (see, e.g., Shraiman *et al.*, 1992). It is unclear whether there is a precise distinction between these regimes, or indeed between this

type of turbulence and “strong turbulence,” which occurs in real fluids for large R . The term “spatiotemporal intermittency” refers to a particular scenario for the onset of weak turbulence, where laminar and chaotic attractors coexist at the onset point (see Kaneko, 1985; Pomeau, 1986; Chaté and Manneville, 1987, 1988b; and subsection VII.E.2.a below). Zakharov defines weak turbulence to be the state of a nonequilibrium system consisting of propagating and dispersive waves with weak interactions. In this case the statistical properties of the system can be calculated approximately by means of a kinetic equation. Zakharov calls all other types of turbulence in spatially extended systems “strong turbulence” (see Zakharov, 1984; Goldman, 1984; Dyachenko *et al.*, 1990).

Oono and Yeung (1987) have proposed a mathematical distinction between chaos and turbulence in terms of a quantity they call P entropy. Although their treatment is rather abstract, it appears that their definition of turbulence requires the *propagation* of disturbances and the transmittal of information from one spatial point to the other. It would be interesting to attempt to formulate these notions in terms of response and correlation functions, and to apply them to experimental systems. A numerical study of information transport in a system with a local source of chaos was carried out by Vastano and Swinney (1988).

4. Open systems: Convective instability

The discussion given above does not apply directly to open systems (see Sec. IX.E), in which the assumption of translational invariance and of a statistical steady state are not valid. Some of the same ideas can be applied, however, and in simple cases correspondences can be set up between open and closed systems (Deissler, 1987b, 1989; Bohr and Rand, 1991). Since in a convectively unstable system the unstable eigenvector corresponds to a propagating disturbance, Eq. (7.34) must be calculated in a moving frame if it is evaluated on a finite domain. This yields the velocity-dependent Lyapunov exponents of Deissler and Kaneko (1987). Note, however, that Eq. (7.34) would also give the correct answer in the rest frame if it were evaluated in an infinite domain, as it must be since the leading eigenvector is not localized in the rest frame. The velocity-dependent exponent is merely a calculational device to transform to a reference frame in which the Lyapunov vector is localized, and the calculation in Eqs. (7.34) can be performed in a finite domain (Deissler, 1989).

D. Examples of spatiotemporal chaos

Although there are innumerable studies of extended chaotic systems we will discuss primarily those which focus on the statistical concepts introduced above.

1. The complex Ginzburg-Landau equation

A basic source of chaos in the complex Ginzburg-Landau equation (4.49) is the Benjamin-Feir instability (4.57), i.e. the interplay between spatial and temporal dispersion. In one dimension interest originally focused on intermediate-sized systems, i.e. on the chaotic dynamics of coherent structures such as confined states, fronts, and pulses (Cross, 1986b; Deissler, 1987a, 1989; van Saarloos and Hohenberg, 1992). More recently Shraiman *et al.* (1992) carried out a numerical study of a large system ($L \sim 10^3$) and identified two different chaotic states, one with “space-time defects” (places where the field A vanishes at a single time) and one with only phase fluctuations and no defects. The authors found that correlation functions behaved rather differently in the two cases, but were unable to show conclusively that there is a sharp transition, rather than a smooth crossover, between the two regimes. A related model, consisting of a discrete chain of coupled oscillators in the form

$$\begin{aligned} \partial_t A_j = & A_j - (1 - ic_3) |A_j|^2 A_j + s_0(1 + ic_0)(A_j - A_{j-1}) \\ & + D(1 + ic_1)(A_{j+1} + A_{j-1} - 2A_j), \\ & j = 1, \dots, N, \end{aligned} \quad (7.50)$$

has been studied by Aranson *et al.* (1985, 1986). These authors gave analytic and numerical estimates for the dependence of the dimension of the attractor on N , s_0 , and D , as well as on the nature of the boundary condition at $j=1$ which is important for cases where the system is convectively unstable. For the subcritical case Schöpf and Kramer (1991), following earlier work of Bretherton and Spiegel (1983), have carried out a numerical study of Eq. (5.57) *without* the stabilizing fifth order terms, and have found chaotic as well as stationary and time-periodic solutions.

In two-dimensions the model is particularly rich since the point defects described in Sec. V.B (targets and spirals) participate in the chaotic dynamics. This problem has been studied numerically by Brand *et al.* (1986a,b) and Coullet *et al.* (1987), and also in a discrete form by Bohr *et al.* (1990a,b). At long times a steady state is reached with some average density of defects which was found to depend on the parameters c_1 and c_3 relevant to the Newell criterion (4.57a). The precise nature of the onset of the defected state has not yet been elucidated, however. Dimension estimates for a small two-dimensional system have been given by Bartuccelli *et al.* (1989) for arbitrary c_1 and c_3 . These authors note that the attractor dimension is uniformly bounded by a linear function of ϵ , whereas the dimension of the inertial manifold is bounded by an exponentially growing function of ϵ in the limit of large c_1 and c_3 (near the nonlinear Schrödinger equation). This difference arises due to the influence of wave collapse in two dimensions (see also Landman *et al.*, 1988; Bartuccelli *et al.*, 1990; Zakharov, 1991; Dyachenko *et al.*, 1992). Much work remains to be done in elucidating the role of the different types of

perturbations to the nonlinear Schrödinger limit (3.40) (see Bretherton and Spiegel, 1983; Bartuccelli *et al.*, 1989; Kivshar and Malomed, 1989). A two-dimensional Ginzburg-Landau model of plasma turbulence, which has added forcing and dissipation acting on different scales, has been discussed by Newell *et al.* (1988) with primary focus on the role of coherent structures in turbulent transport and dissipation.

2. The Kuramoto-Sivashinsky equation and its extensions

Let us consider the damped version of this model, (3.31) (Chaté and Manneville, 1987)

$$\partial_t u(x,t) = -\eta u - \partial_x^2 u - \partial_x^4 u - u \partial_x u, \quad (7.51)$$

where η is the control parameter and $x \in [0, L]$, with periodic boundary conditions. We will be interested in the $L \rightarrow \infty$ limit. The stability of the quiescent state $u=0$ is analyzed by linearizing Eq. (7.51). The rate of growth σ of the Fourier mode q is

$$\sigma(q) = -\eta + q^2 - q^4. \quad (7.52)$$

For $\eta < 1/4$ the quiescent state is unstable with the fastest growing mode at $q = q_0 = 1/\sqrt{2}$. The bifurcation is stationary (type I_s) and leads to a spatially periodic structure $u = u_\lambda(x)$ with wavelength $\lambda \approx 2\pi/q_0$. In fact, away from the threshold $\eta = 1/4$, one expects a band of linearly stable cellular solutions. For a system of finite size the band will be reduced to a discrete set. The stability and uniqueness of the cellular solutions is a complicated matter (Hyman *et al.*, 1986) and depends on both η and L . It is known, however, from the work of Frisch, She, and Thual (1986) that for $\eta=0$ cellular solutions with $\lambda \in [\lambda_m, \lambda_M]$ are linearly stable, which implies that for L large enough (so that $L = n\lambda$ can be satisfied for some integer n , and λ in the stable range) there exists at least one linearly stable cellular structure. We expect this to be true also for $0 < \eta < 1/4$. However, a typical numerical simulation of Eq. (7.51) near $\eta=0$ exhibits only chaotic behavior, characterized by stationary statistics and revealing no convergence towards the time-independent cellular state. Nevertheless, we will argue below that the system is quite close to the cellular state *locally* much of the time.

Let us summarize some properties of the chaotic state which was studied by a number of authors, starting with the early work of Manneville (1981). As mentioned above, Manneville (1985) has shown that for $\eta=0$ this state possesses a spectral density of positive Lyapunov exponents, a Lyapunov dimension d_L and an entropy H proportional to L (i.e., they are extensive). His results may be expressed in the form

$$d_L = 2.04(Lq_0/2\pi) - 2.70, \quad (7.53a)$$

$$H = 0.05(Lq_0/2\pi) - 0.09. \quad (7.53b)$$

The spectrum of static fluctuations $\langle |u(q)|^2 \rangle$ studied for $\eta=0$ by Pomeau, Pumir and Pelcé (1984), has a pro-

nounced peak near q_0 and a shoulder at low q . This spectrum has been calculated approximately by Toh (1987), using a statistical model of interacting pulses. The temporal power spectrum for local fluctuations $\langle |u(\omega)|^2 \rangle$ exhibits a power-law rise at low frequencies, although the precise value of the exponent is not known. Finally, Pumir (1985) has shown that the distribution function for static fluctuations of $u(q)$ approaches a Gaussian as L increases. For large L the chaotic state is expected to display short-range order corresponding to the peak in the structure function at $q = q_0$, and long-range disorder represented by the flat behavior at small q . The onset of chaos in the large system has been studied numerically by Chaté and Manneville (1987) who considered the damped equation (7.51), and varied the parameter η from the onset of the spatially periodic state at $\eta = 1/4$ down to the value $\eta = 0$ where the chaos is most pronounced. The authors suggest that for $L \rightarrow \infty$ the onset of chaos as η is varied occurs via a continuous transition which they termed "spatiotemporal intermittency," as illustrated in Fig. 30. This figure represents a space-time plot of

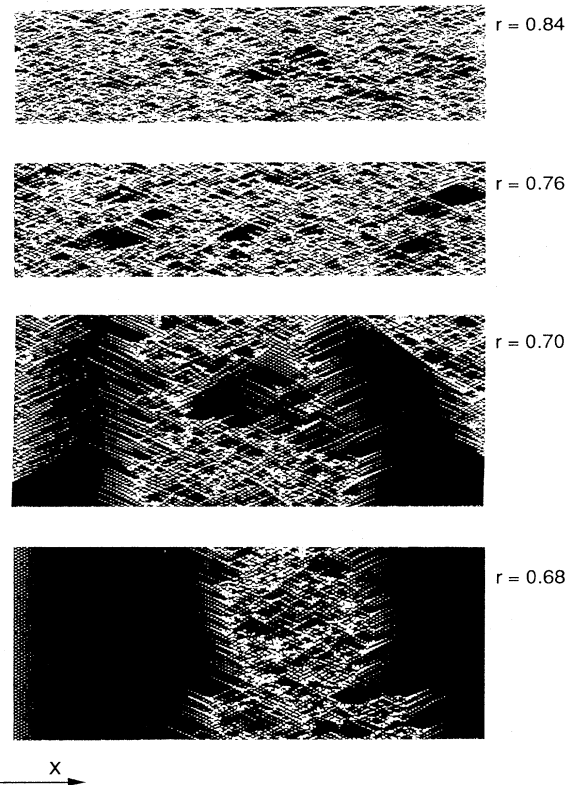


FIG. 30. Transition to extended spatiotemporal chaos via the intermittency route. Pictures show a space-time plot of chaotic regions (white) identified as regions where $u > u_1$ for the damped Kuramoto-Sivashinsky equation (7.51), where u_1 is some chosen threshold value, and laminar regions (black) where $u < u_1$, for different values of the control parameter r , related to η in Eq. (7.51) by $r = 1 - 4\eta$. As r approaches $r_c = 0.688$ from below ($\eta \rightarrow \eta_c = 0.078$ from above) laminar regions acquire macroscopic size (i.e. approach the system size). For $r < r_c$ only isolated chaotic regions remain. (From Manneville, 1990.)

$u(x,t)$ in which the continuous field u has been discretized into two values, “laminar” (in black) and “turbulent” (in white). The criterion distinguishing the two regimes is somewhat arbitrary but the scaling results discussed below do not depend on the precise cutoff u_1 , within the accuracy of the calculation. Chaté and Manneville found that when the control parameter η is varied, there is a change in the behavior of *interfaces* between laminar and chaotic regions. For $\eta > \eta_c \approx 0.078$ the laminar regions invade the transient chaotic regions which could arise from disordered initial conditions. For $\eta < \eta_c$ the chaotic regions win out, but they are themselves made up of chaotic and laminar subdomains. As mentioned in subsection VII.C.1.a above, the distribution $\tilde{P}(\ell)$ of sizes of laminar subdomains defines an exponential correlation length ξ which is finite for $\eta < \eta_c$ and diverges at $\eta = \eta_c$. [For $\eta > \eta_c$, $\tilde{P}(\ell)$ appears to have a power-law dependence, which corresponds to $\xi = \infty$.] The transition occurring at $\eta = \eta_c$ is of a type that was conjectured by Grassberger (1982) and by Pomeau (1986) to be in the universality class of *directed percolation*, but the analogy appears to be qualitative rather than precise in this case (see subsection VII.E.2.a below).

An extension of the Kuramoto-Sivashinsky model, known as the Kolmogorov-Spiegel-Sivashinsky equation, involves the addition of a cubic nonlinear term to Eq. (7.51); it is usually written in the integrated form (Chaté and Nicolaenko, 1990)

$$\partial_t \phi = -\eta \phi - \partial_x^2 \phi - \partial_x^4 \phi - (\partial_x \phi)^2 + \delta \partial_x (\partial_x \phi)^3. \quad (7.54)$$

The additional unfolding parameter δ leads to a shift of the threshold for the appearance of chaos $\eta_c(\delta)$, as well as an apparent modification of the character of the transition. In particular long-lived defect states appear in the transition region, and the bifurcation to chaos becomes strongly subcritical (discontinuous). The qualitative behavior of Eq. (7.54) in the parameter space (η, δ) has also been obtained using coupled maps (Chaté and Manneville, 1989b), so there is some hope that it may provide a generic example.

Many of the theoretical ideas that have been proposed to understand spatiotemporal chaos were either developed for the Kuramoto-Sivashinsky equation or applied to it early on. These include stochastic methods, defect-mediated chaos, and analogies to percolation and other critical phenomena. We shall describe these theoretical approaches briefly in subsection VII.E below.

3. Coupled map lattices

Since any partial differential equation can be discretized into a system of coupled maps there is no sharp difference between the two classes of models. Nevertheless, in the two continuum equations discussed above the chaos had its origin in instabilities such as the Benjamin-Feir instability (4.57), where the coupling between nearby points in the system leads to a negative diffusion constant. For coupled maps what has generally been con-

sidered are systems that are already chaotic in the absence of coupling. The ensuing spatiotemporal dynamics of the coupled systems displays enormous variety, and these models have been widely studied due to the relative ease of generating large amounts of data. Alternatively, coupled map lattices can be considered as coarse-grained versions of continuum systems, but the correspondence between the instability mechanisms in the two types of models is often obscure. For early work on coupled maps see Kaneko (1985), Oppo and Kapral (1986), and references therein, and Kuznetsov and Pikovsky (1986).

Systems of coupled logistic maps have been particularly popular, since the chaotic behavior of the individual elements is so well understood. Kaneko (1987, 1990a), in particular, has identified many different phases in the system, ranging from ordered patterns, to disordered frozen ones, defect dominated phases, and what he calls “fully turbulent” phases. The types of diagnostics he has used include space-time spectra and Lyapunov exponents as well as different types of entropy functions and “pattern distribution functions” (see also Crutchfield and Kaneko, 1987, and Keeler and Farmer, 1986). A careful study of the Lyapunov exponents and their density (7.35) has been carried out for this system by Everson (1989). In particular, he studied the dependence of these quantities on the relative magnitude of the diffusive and convective couplings [analogous to the parameters s_0 and D in Eq. (7.50)], which determines whether the instabilities are absolute or convective [see Sec. III.A]. The propagation of disturbances has also been studied by Brindley and Everson (1989).

As mentioned above, Chaté and Manneville (1988a,b) have introduced a coupled map system to model the transition to chaos via spatiotemporal intermittency originally found in the damped Kuramoto-Sivashinsky equation (7.51). The local map consists of two states, a chaotic one generated by a tent map, and a laminar state represented by a fixed point, with chaotic transients. A simple example of such local dynamics is the map

$$\begin{aligned} f(u) &= r u, & 0 \leq u \leq 1/2, \\ f(u) &= r(1-u), & 1/2 \leq u \leq 1, \\ f(u) &= u, & u > 1, \end{aligned} \quad (7.55)$$

and the coupled model links these maps diffusively, as in Eq. (3.47). Chaté and Manneville have shown that this system displays a transition to chaos via spatiotemporal intermittency as a function of the coupling constant g for fixed $r > 2$. In view of the simplicity of the dynamics it was possible to characterize the transition more precisely than for the Kuramoto-Sivashinsky case, and to measure critical exponents with reasonable accuracy for this supercritical bifurcation.

Let us also mention a particular coupled map lattice constructed by Bunimovich and Sinai (1988), for which they were able to prove that the steady state is chaotic with exponential decay of space and time correlations, in the weak-coupling limit. Further numerical work at

larger coupling has been carried out by Bunimovich *et al.* (1990) and by Livi *et al.* (1990). More recently Rand and co-workers have considered various concrete examples in the *weak coupling limit* in some detail. They were thus able to discuss in a precise way many of the ideas we have introduced heuristically in our earlier discussion. These include thermodynamic limit, natural measure, limiting distribution of characteristic exponents, spatial entropy, exponential decay of correlations, phase transitions, geometric structure of attractors (Gundlach and Rand, 1992a,b,c; Campbell and Rand, 1993). Finally, we note that models consisting of coupled oscillators have attracted growing attention due to their relevance to chemical and biological phenomena (see, e.g., Kuramoto, 1984a; Strogatz and Mirollo, 1988; Sompolinsky *et al.*, 1991).

E. Theoretical approaches

In this section we summarize some of the theoretical approaches that have been proposed to obtain statistical information on systems displaying spatiotemporal chaos. These approaches all involve some attempt to go beyond a pure simulation of the dynamics in order to calculate the correlation and response functions discussed in subsection VII.C above. Sometimes the proposal involves replacing one model by a simpler one, where the latter may still require numerical solution. A question to be answered is: in what way is the system under study different from an infinite collection of independent degrees of freedom? An important element at the present rather primitive stage of development of the field is the search for circumstances where the system has scaling properties in space and time (see subsection VII.E.2).

1. Stochastic models

a. Stochastic dynamics

As mentioned earlier, stochastic models are often used to represent systems interacting with external noise, be it of thermal or other origin (see, e.g., van Kampen, 1981; Gardiner, 1983). The same types of equations can also arise as coarse-grained models representing the long-wavelength, low-frequency dynamics of *deterministic* systems displaying spatiotemporal chaos. The basic idea usually involves an assumption of separation of scales, whereby the unstable short-range degrees of freedom are replaced by a stochastic force with correlations of range ℓ_E , assumed small. This force acts on the macroscopic degrees of freedom which satisfy a stochastic equation whose deterministic part is obtained by coarse graining the starting equations. The resulting model is thought to reflect the essential features controlling the macroscopic correlations, and must take proper account of the symmetries and conservation laws of the original model (see, e.g., Le Berre *et al.*, 1990). The above program has been

partially implemented for the Kuramoto-Sivashinsky equation which becomes a stochastic Burgers equation (in one dimension)

$$\partial_t \phi = \nu \partial_x^2 \phi + \phi \partial_x \phi + \zeta(x, t), \quad (7.56)$$

with short-range noise correlations [Yakhot, 1981; Yakhot and She, 1988; Zaleski, 1989]. The diffusive form of Eq. (7.56) is already suggested by the starting equation (7.51) for $\eta = 0$; the main difference between the two models is that the negative diffusion constant of (7.51), which leads to chaos, is renormalized at long wavelength into an effect diffusion constant ν assumed positive, plus a short-ranged noise ζ (see also Goldenfeld *et al.*, 1990). The stochastic model has an upper wave-vector cutoff $q_c \lesssim q_0$ and the noise correlations are supposed to be on the scale q_c^{-1} . The validity of Eq. (7.56) as a representation of the slow dynamics of Eq. (7.51) has been partially checked by Zaleski (1989) in one dimension but it cannot yet be considered to be firmly established.

More generally, let us write a stochastic equation in the form

$$\partial_t U = G[U] + \zeta(x, t), \quad (7.57)$$

where $G[U]$ is some nonlinear function of U and its gradients (U is in general an n -component vector), and the noise correlations are given by

$$\begin{aligned} & \langle \zeta(q, \omega) \zeta(q', \omega') \rangle \\ &= (2\pi)^d \delta(\omega + \omega') \delta(q + q') \mathcal{D}_0(q, \omega), \end{aligned} \quad (7.58)$$

where the function $\mathcal{D}_0(q, \omega)$ is regular as $q, \omega \rightarrow 0$ for short-ranged noise correlations. Models of the above form have been used by many authors to study nonequilibrium systems. For example, Forster, Nelson, and Stephen (1977) studied long-time tails in fluids and the breakdown of hydrodynamics in two dimensions, using techniques borrowed from the theory of dynamic critical phenomena (Hohenberg and Halperin, 1977; see also Bonilla, 1988; Medina *et al.*, 1989; Cardy, 1992).

It is natural to ask whether renormalization group methods can also be used to study the *short-scale* behavior of fluids, say. For an equation such as the Navier-Stokes equation at high Reynolds number this is the interesting regime of strong turbulence. Forster *et al.* (1977) investigated this question and not surprisingly found that the models flowed to *strong coupling* at small distances, thus invalidating a strict perturbative approach. We shall briefly return to the question of describing strong turbulence within a renormalization group framework in subsection VII.E.5 below.

When studying stochastic dynamics various authors have discussed the question of the stability of phases, in analogy to the corresponding question in thermodynamics (e.g. Bennett *et al.*, 1990). For example, a solution $u_0(x, t)$ of the deterministic equations (7.23) will be tested for stability by adding a Gaussian white noise source $\zeta(x, t)$ as in Eq. (7.57), but of infinitesimal strength ($D_0 \rightarrow 0$). Then the “phase” represented by $u_0(x, t)$ is

said to be stable if the disturbances introduced by ζ are negligible in the large-system limit ($L \rightarrow \infty$), i.e. if perturbations do not propagate out to infinity. This notion of stability, which we might call “phase stability,” is different from simple *linear stability* of the solution $u_0(x, t)$ of the deterministic equations. On the one hand phase stability is more difficult to achieve since although the noise strength D_0 is infinitesimal on average, the Gaussian nature of ζ implies that there are rare perturbations of arbitrary strength. On the other hand phase stability is less stringent than linear stability, since the disturbance must survive the thermodynamic limit $L \rightarrow \infty$ in order to destabilize $u_0(x, t)$. An infinitesimal disturbance that remains localized will not destroy phase stability even if it grows large, though such a disturbance would render $u_0(x, t)$ linearly unstable. It remains to be seen whether this notion of phase stability is a useful characterization of large nonequilibrium systems.

b. Quenched randomness

An interesting limit occurs when the time scale of the external random force becomes very long, i.e. when the randomness is *quenched*. An experimental example might be convection in a cell with rough boundaries. Models with quenched randomness are frequently introduced to study the critical behavior of disordered magnets or other solids. One example consists of a set of coupled oscillators with random internal frequencies (see, e.g., Kuramoto, 1984a),

$$\partial_t \phi_i = \omega_i + \sum_j J_{ij} \sin(\phi_i - \phi_j), \quad i = 1, \dots, N, \quad (7.59)$$

where the ω_i are independent random variables with a fixed probability distribution. Another model, representing collective transport in sliding charge density waves or phase separation of binary fluids in porous media, has the form

$$\partial_t \phi_i = -h_i \sin(\phi_i - \beta_i) + \sum_j J_{ij} (\phi_i - \phi_j) + F, \quad i = 1, \dots, N, \quad (7.60)$$

where now the randomness is introduced in the phases β_i . In each case the average frequency

$$\Omega_i = \lim_{T \rightarrow \infty} \frac{1}{T} \int_0^T dt \partial_t \phi_i(t), \quad (7.61)$$

can be defined for each oscillator, and the distribution of these frequencies $P(\Omega_i)$ over the whole ensemble can be examined. A particular phenomenon of interest is *collective locking*, i.e. when all or a finite fraction of the modes have the same frequency Ω (Kuramoto and Nishikawa, 1987; Bonilla, 1988; Strogatz *et al.*, 1989; Lumer and Huberman, 1991).

2. Critical points

Among all the chaotic states in a large system perhaps the most interesting ones are those associated with long-range spatial or temporal correlations. We have seen that in certain model systems the *transition* to chaos appeared to be *continuous*, and to have many properties in common with critical points of thermodynamic phase transitions, in particular an infinite correlation length.

a. Spatiotemporal intermittency

As mentioned in subsection VII.D.2 Grassberger (1982) and Pomeau (1986) had suggested that the onset of chaos via spatiotemporal intermittency might be analogous to a process of *directed percolation*. This process is most simply expressed as a probabilistic cellular automaton with 2 states per site. The essential characteristic lies in the asymmetry between the two states, one of them being absorbing and the other one not. The absorbing state remains unchanged if its neighbors are also absorbing, whereas the other (active) state has a nonzero probability of remaining active or changing to absorbing, depending on the state of the neighbors. As this probability changes its value one can have a propagation of active sites over the whole system. The directed percolation transition has been studied in some detail; it is continuous and the universal critical exponents (independent of the detailed rules) have been determined in one and two dimensions (Kinzel, 1983). In the dynamical system the laminar state corresponds to an absorbing site and the chaotic or turbulent state to an active one. At the onset of spatiotemporal intermittency a chaotic fluctuation can propagate to infinity. The order parameter for this transition can be defined as the density of turbulent (or active) sites in steady state. Below threshold chaotic fluctuations have a finite lifetime so the homogeneous absorbing state is the steady state configuration and the order parameter is zero.

As discussed above, numerical simulations of various models based on *pde*'s, coupled maps, and cellular automata have confirmed the above picture qualitatively, but the precise nature of the transition and its critical exponents were in some cases shown to differ from those of directed percolation. The situation has been considerably clarified by Grassberger and Schreiber (1991), who note that the analogy is only precise if the laminar state is unique and nondegenerate (e.g. not a modulated phase). Moreover, there can be subtle long-range correlations in the laminar state which introduce additional length scales and thus destroy universality. The reader is referred to the paper by Grassberger and Schreiber (1991) for a more complete discussion (see also Stassinopoulos and Alström, 1992).

We note that above the intermittency threshold, when there is a finite density of active or chaotic sites one can study the steady state patterns from the point of view of *ordinary percolation* of chaotic domains in space and

time. This has been done by Chaté and Manneville (1988c) for the coupled maps based on Eq. (7.55), and they found agreement with the percolation exponents in two dimensions (one space and one time), though the reasons for this are not understood.

b. Self-organized criticality

Besides transition points associated with special parameter values, there might be systems in which the chaotic state has long-range correlations (e.g. spatiotemporal power laws) over a wide parameter domain. This phenomenon has been denoted "self-organized criticality" by Bak, Tang, and Wiesenfeld (1987) who have studied a number of models displaying self-similarity, and have emphasized its ubiquitous nature in nonequilibrium systems as diverse as earthquakes, galaxy formation, fluid turbulence, or $1/f$ noise in conductors. They suggest that scaling behavior is a *natural* outcome of nonequilibrium dynamics, in particular that long-range correlations develop spontaneously as a result of the time evolution, without any special tuning of parameters (see also Tang *et al.*, 1987). Originally intended as an explanation of $1/f$ temporal noise, the paper of Bak, Tang, and Wiesenfeld has generated enormous interest in spatiotemporal scaling phenomena, but it is fair to say that most of the issues raised remain to be clarified.

For illustrative purposes Bak and co-workers considered a pile of sand on a flat surface, which is being fed from above by slowly dropping grains of sand. The slope gradually builds up to a critical value at which the system is marginally stable. If the slope becomes larger the pile will collapse, creating an avalanche, until it reaches the critical state once again. The concept of a self-tuned critical state was introduced by Beam (1962) to describe collective transport in type-II superconductors, and the analogy to a sandpile was already discussed by de Gennes (1966). To model their system Bak *et al.* introduced a simple cellular automaton which in the one-dimensional case has the following form [we use the generalization of Kadanoff *et al.*, 1989]: In a chain of length L , associate with each site j and time t an integer height variable $h(j, t)$. The evolution rules may be written as

$$\left. \begin{aligned} h(j, t+1) &= h(j, t) - h_0 \\ h(j \pm 1, t+1) &= h(j \pm 1, t) + h_0 \end{aligned} \right\} \quad \text{iff } h(j, t) - h(j \pm 1, t) > \Delta, \quad (7.62)$$

otherwise h remains unchanged. The quantities h_0 and Δ are assumed to satisfy $h_0 > 2$ and $\Delta > 2h_0$ but are otherwise arbitrary. The boundary conditions are $h(0, t) = h(1, t)$ (the $j = 0$ end is closed) and $h(L+1, t) = 0$ (the $j = L$ end is open). The transport is initiated by dropping sand at a slow rate

$$J_{\text{in}} = p L, \quad (7.63)$$

at random points in the system. (Injection at the boundary has also been studied.) Bak *et al.* and many subsequent authors performed simulations of this sandpile model and found a power-law distribution of cluster sizes, as well as $1/f^\alpha$ frequency spectra for avalanche lifetimes. The state reached by the sandpile at long times is the prototype for what Bak *et al.* call self-organized criticality.

In our view, the essential questions concerning this phenomenon are as follows: (i) Can one define it precisely? (ii) Can one understand what theoretical models and mechanisms will produce it? and (iii) Do these phenomena appear in nature, and how ubiquitous are they?

(i) Definition

Let us first define "generic scale invariance" (Grinstein *et al.*, 1990) as the appearance of power-law *spatial* correlations in an extended system, over an open range of parameters (i.e. without special tuning). It may turn out that this is a sufficient definition of self-organized criticality, but the heuristic picture presented by Bak *et al.* implies in addition the existence of large events or "avalanches," and the evolution of the system to a marginal state in which a small localized perturbation can produce a large response extending over the whole system (they refer to this state as one of local minimal stability). For want of a better term we shall call this an "avalanche state," though we must stress that a precise definition is lacking. Self-organized criticality is then the spontaneous evolution of a system to an avalanche state exhibiting generic scale invariance.

(ii) Models and mechanisms

We begin by listing theoretical mechanisms for producing generic scale invariance.

• Conservation laws. It is known from equilibrium statistical mechanics that *conservation laws*, which are at the origin of hydrodynamics, lead to power-law correlations in many cases. The important point for the present discussion, which has been emphasized by Hwa and Kardar (1989), Grinstein *et al.* (1990, 1991), and especially Garrido *et al.* (1990), is that this is *even more true* outside of equilibrium. Consider, for example, the anisotropic sandpile model of Hwa and Kardar in d dimensions, a continuum variant of (7.62),

$$\partial_t u = D_{||} \partial_{||}^2 u + D_{\perp} \nabla_{\perp}^2 u - (\lambda/2) \partial_{||}(u^2) + \xi, \quad (7.64)$$

with white-noise correlations

$$\langle \xi(\mathbf{x}, t) \xi(\mathbf{x}', t') \rangle = 2 [\Gamma_0 + \Gamma_{\perp} \nabla_{\perp}^2 + \Gamma_{||} \partial_{||}^2] \times \delta(\mathbf{x} - \mathbf{x}') \delta(t - t'), \quad (7.65)$$

where ∇_{\perp} refers to the $(d-1)$ components transverse to the "downhill" direction $\mathbf{x}_{||}$. The deterministic system satisfies the conservation law

$$\partial_t u + \nabla \cdot \mathbf{j} = \partial_t u + \nabla_{\perp} \cdot \mathbf{j}_{\perp} + \partial_{||} j_{||} = 0, \quad (7.66a)$$

$$\mathbf{j} = -D_{\perp} \nabla_{\perp} u - [D_{||} \partial_{||} u - (\lambda/2) u^2] \hat{\mathbf{x}}_{||}, \quad (7.66b)$$

and in general the full system (7.64) is expected to have power-law correlations in space and time. In the special cases of *equilibrium*, given by the detailed balance condition [see Eq. (6.42) above],

$$\Gamma_0 = 0, \quad \Gamma_\perp / D_\perp = \Gamma_\parallel / D_\parallel = T, \quad (7.67)$$

or of isotropy where the right-hand sides of Eqs. (7.64) and (7.65) are functions of $\nabla^2 = \nabla_\perp^2 + \partial_\parallel^2$ only, some of the correlation functions (e.g., the spatial ones) may become short-ranged despite the existence of a conservation law, but it is this equilibrium behavior that one might regard as nongeneric. When these conditions are not satisfied, i.e. in most nonequilibrium systems, the conservation law (7.66) leads to power laws, i.e. to generic scale invariance.

Hwa and Kardar (1989, 1992) have applied the dynamic renormalization group method to the stochastic system (7.64) and (7.65), and have found the scaling relation

$$\langle [u(\mathbf{x}, t) - u(0, 0)]^2 \rangle \sim x_\parallel^{2\chi} \tilde{C}(t/x_\parallel^z, x_\perp/x_\parallel^\phi). \quad (7.68)$$

The exponents have their bare values for spatial dimension $d > 4$

$$z = z_0 = 2, \quad \chi = \chi_0 = (2-d)/2, \quad \phi = \phi_0 = 1, \quad (7.69)$$

but for $d < 4$ the nonlinearity λ in Eq. (7.64) is relevant, and the exponents take on the nontrivial values

$$z = 6/(7-d), \quad \chi = (1-d)/(7-d), \quad \phi = 3/(7-d). \quad (7.70)$$

(See also Grinstein and Lee, 1991.)

• Goldstone modes. Another mechanism for power laws is a symmetry which may or may not be broken, but nevertheless leads to a type of Goldstone mode in the long-wavelength dynamics (Obukhov, 1990). For example, the interface model

$$\partial_t u = \nu \nabla^2 u + f[(\nabla u)^2] + \zeta(\mathbf{x}, t), \quad (7.71)$$

of Medina *et al.* (1989) with arbitrary function $f(\alpha)$, does not conserve u in general, yet the equal-time correlation functions have power-law behavior for short-range temporal correlations of the noise ζ . [Of course, there is an underlying conservation law, namely for $\mathbf{v} = \nabla u$, but the field u itself is not conserved]. In the special case of a quadratic function, $f = \frac{1}{2} \lambda (\nabla u)^2$, the model possesses an additional Galilean symmetry

$$u' = u + \mathbf{a} \cdot \mathbf{x}, \quad (7.72a)$$

$$\mathbf{x}' = \mathbf{x} + \lambda \mathbf{a} t, \quad (7.72b)$$

$$t' = t, \quad (7.72c)$$

for arbitrary \mathbf{a} , which leads to exact exponent identities for the correlation functions (Medina *et al.*, 1989).

Next we ask whether there is any precise theoretical basis for distinguishing the avalanche state referred to above from generic scale invariance. Although we do not have a satisfactory answer to this question, we note that Carlson, Chayes, Grannan, and Swindle (1990a,b) have

analyzed a simplified version of the sandpile model, and have proven that the dynamics drives the system to a critical point with *diverging diffusion constant*. They have also verified numerically that the same holds true for the original sandpile model (7.62) of Bak *et al.* (1987), as well as for variants thereof. Carlson *et al.* consider the above effect to be an essential element of self-organized criticality, in that the average slope of the sandpile is brought to its critical value by the dynamics. In the model (7.64) of Hwa and Kardar (1989), on the other hand, u represents the fluctuations of the height about an arbitrary steady state, and there is no apparent mechanism for tuning to criticality. Although this point of view on the distinction between the avalanche state and generic scale invariance is appealing to us, it falls short of a precise definition of the avalanche state, and a number of specific points still need clarification.

First, the field-theoretic model (7.64) also leads to an infinite diffusion constant whenever there is “superdiffusive behavior,” i.e. $z < 2$ in Eq. (7.68) or by virtue of (7.70), $d < 4$. What is the difference between the criticality of Carlson *et al.* (1990a,b), and that encountered in (7.68) when $z < 2$?

A second question concerns the tuning of parameters. In the original sandpile model (7.62), the sand is deposited at a sufficiently slow rate p , Eq. (7.63), so that avalanches of arbitrarily large size can take place before the next grain is dropped. This would correspond to a noise source in Eq. (7.64) which depends on the dynamical state of the system and has extremely low frequency correlations. Carlson *et al.* replace (7.62) and (7.63) by a model in which the sand is dropped at unit rate, but the deterministic rearrangements take place according to an interaction $\gamma(j)$ with power-law dependence on space $\gamma(j) \sim j^{-\sigma}$. Criticality then only ensues for sufficiently long-range interactions, i.e. for $0 < \sigma \leq 3$, and the critical exponents are determined by σ . It may thus be argued that in the model of Carlson *et al.* there is a nontrivial dynamic tuning to a critical state (i.e. the infinite diffusion constant), but it is not “self-organized.” It is rather a dynamic response to the long-range interaction assumed in the starting model ($\sigma < 3$).

Finally, we note that Hwa and Kardar (1992) have suggested a rather different interpretation of the distinction between the avalanche state and the scale invariant state described by the field-theoretic model. They propose that the avalanche state is obtained for the lowest values of the deposition rate p in the sandpile model (7.63), and that it corresponds to an ensemble of independent avalanches. The scale invariant state (7.68) on the other hand, corresponds to overlapping avalanches, and it is found for higher values of p and lower frequencies. Hwa and Kardar have presented numerical evidence based on simulations of (7.62) and (7.63) to substantiate their proposal.

From the above discussion we thus arrive at the following theoretical questions: Assuming that we understand the phenomenon of generic scale invariance as described by models such as (7.64), can one give a precise

definition of an avalanche state which is different? If so, can this state be produced by purely dynamical means, without assuming long-range interactions in the model, or the tuning of a parameter? Finally, can generic scale invariance with or without the avalanche property be obtained without assuming conservation laws or a continuous symmetry? Concerning this last issue it is important to note that numerical simulations of many models without conservation laws yield scaling behavior over a number of decades (Bak *et al.*, 1989, 1990; Feder and Feder, 1991; Christensen and Olami, 1992; Olami *et al.*, 1992). Although as far as we know all of these models tune an external parameter analogous to the dropping rate p , Eq. (7.63), to zero, and some of the simulation results have been shown to change when larger systems are investigated (Bennett and Bourzutschky, 1991; Grassberger and Kantz, 1991), it is still fair to say that the appearance of large power-law scaling ranges in the dynamics of these systems remains an important unexplained effect. Moreover, tuning a dropping rate or a current to zero seems more natural than simply setting a parameter to its (finite) critical value.

(iii) Natural phenomena

The notion of self-organized criticality was motivated by the observation of power-law distributions in many static and dynamic natural phenomena (Mandelbrot, 1983). In laboratory experiments, on the other hand, such as the ones mentioned in subsection VII.F below, spatiotemporal chaos only rarely exhibits scaling behavior, and if it does it is the result of parameter tuning. For example, the inertial range of strong turbulence (subsection VII.E.5) arises because the Reynolds number is chosen large ($R_e^{-1} \rightarrow 0$). A chaotic state of convection in a large box, on the other hand, is expected to have exponentially decaying correlations, except at special parameter values. Also there are laboratory examples of avalanche phenomena (soap froth coarsening, Stavans *et al.*, 1991; magnetic bubble domains, Babcock and Westervelt, 1989) where the steady-state distribution does not involve true power laws. Thus the existence of fractals and large avalanche phenomena in nature seems to be the result of some inherent separation of scales in the systems under consideration, and we do not have good theoretical or experimental models as yet to fully understand the origin of these effects.

c. Correlation-length inequalities

Bohr and collaborators (Bohr *et al.*, 1987; Bohr, 1989) have argued that for deterministic chaotic systems with short-ranged interactions the correlation length should always be finite, by virtue of the conjectured inequality

$$\xi \leq v/\lambda_1 , \quad (7.73)$$

where λ_1 is the largest Lyapunov exponent and the constant v , which has dimensions of a velocity, is bounded for $L \rightarrow \infty$. We note that according to Eq. (7.73) a diverging correlation length is necessarily associated with a vanishing Lyapunov exponent, i.e. the disappearance (or marginality) of chaos. For the case of diffusively coupled logistic maps, Rasmussen and Bohr (1987) originally proposed the relation $\xi \propto \lambda_1^{-1}$, but Kaspar and Schuster (1986) showed that $\xi \propto \lambda_1^{-1/2}$ near the onset of chaos; in either case the result satisfies (7.73).

Similarly, Bak *et al.* (1990) and Chen *et al.* (1990) have evaluated Lyapunov exponents in the self-organized critical state reached in a number of models, and have found that orbits in phase space diverge algebraically rather than exponentially, corresponding to $\lambda_1 = 0$. This observation led the authors to state that "turbulence is not chaotic," by which they mean that there are no positive exponents in the turbulent state since the latter is "critical" (see also Crutchfield and Kaneko, 1988; Bohr *et al.* 1992).

It should be noted that in this regard there may be important differences between deterministic and stochastic models, but even in the deterministic case it is clear that the inequality (7.73) cannot be generally valid though some relation might be found to express dynamic scaling properties near continuous transitions to chaos. The problem lies in the meaning of ξ . If ξ is "the length beyond which the motion is basically uncorrelated" as stated by Bohr (1989), then it is also the correlation length for regular (nonchaotic) motion. In that case a counter-example can be constructed by means of a coupled-map lattice each element of which is chaotic (so that $\lambda_1 > 0$), but which undergoes a phase transition as a function of coupling from a regime with short-range correlations to one with *long-range order*. Such a model was alluded to in the paper of Bohr *et al.* (1987), and universal properties of ordering transitions in nonequilibrium systems were already studied by Grinstein *et al.* (1985). A particularly simple deterministic example, due to Miller and Huse (1993), has the form

$$u(j,t+1) = (1-g)f(u(j,t)) + (g/z) \sum_{\delta} f(u(j+\delta,t)) , \quad (7.74)$$

where δ joins j to its z nearest neighbors, and the map $f(u)$ is given by

$$\begin{aligned} f(u) &= 3u, & 0 < u < 1/3 , \\ f(u) &= 2 - 3u, & 1/3 < u < 1 , \\ f(u) &= -f(-u), & -1 < u < 0 . \end{aligned} \quad (7.75)$$

Since $f(u)$ is odd, the system has "Ising symmetry" and can therefore show Ising-type order for suitable values of the coupling g . On the other hand, $f(u)$ is a chaotic map with largest Lyapunov exponent $\lambda_1 = \ln 3 = 1.1$ for $g = 0$, and the exponent for the coupled system varies smoothly with g . Miller and Huse have simulated the system (7.74)

in two dimensions and find that long-range order ($\xi = \infty$) appears for $g \approx 0.82$, at which point $\lambda_1 \approx 0.53$, in violation of the inequality (7.73). [Note that the maximum velocity v of signals is unity for the system (7.74).] Thus an inequality such as (7.73) can only be correct if ξ refers to spatial correlations of temporally chaotic motions, with the correlations of the average being subtracted out. It is not clear to us precisely how to define such a length. Another counterexample was presented by Aranson, Golomb, and Sompolinsky (1992), who considered a coupled-map lattice with asymmetric coupling, representing an open system, in which they showed that stable long-range coherence can coexist with temporal chaos.

In discussing the scaling of attractor dimension with system size we introduced an exponent b , Eq. (7.4), and a characteristic length ξ_f , Eq. (7.38). It is interesting to ask whether exact inequalities could be obtained for b and ξ_f . Analogous results are known to exist for the invariant measure associated with the Navier-Stokes or Ginzburg-Landau equations (see Eckmann and Ruelle, 1985; Temam, 1989). In the absence of exact information we may conjecture the exponent inequality

$$b \leq d . \quad (7.76)$$

3. Defect-mediated turbulence

An interesting proposal for understanding spatiotemporal chaos is that its onset is due to the spontaneous appearance of defects and that the macroscopic behavior can be modeled by a system of interacting defects, with or without a stochastic force. For example in the Kuramoto-Sivashinsky system, Shraiman (1987) has argued that the dominant excitations are viscoelastic waves which collide to form space-time dislocations. From this picture it follows that for a finite system of length L the chaos is transient but the relaxation time to the laminar (periodic) state grows exponentially with L , a result that Shraiman verified in a numerical calculation, albeit with rather small systems ($L/2\pi \lesssim 13$). Another example is the defect state identified in the one-dimensional complex Ginzburg-Landau model by Shraiman *et al.* (1992) (see subsection VII.D.1).

The chaotic state of the two-dimensional complex Ginzburg-Landau model can also be viewed as an ensemble of defects. It has been proposed (Occelli *et al.*, 1983; Walgraef *et al.*, 1983) that the spiral excitations form a vortex gas and undergo a phase transition of the Kosterlitz-Thouless type, as found in two-dimensional superfluids or magnets (Kosterlitz and Thouless, 1978). Although some aspects of this picture may be valid, it should be remembered that the Kosterlitz-Thouless transition comes from a balance between the energy and entropy of the vortex gas, for which thermal noise (see Sec. VI.D) plays an essential role. For the systems under consideration here there may be chaotic degrees of freedom acting on the defects (e.g. via phase turbulence), but the

chaos does not necessarily have white noise character and we see no reason why the critical behavior should be the same as in the thermodynamic case.

Eckmann and Procaccia (1991) (see also Eckmann *et al.*, 1991) have attempted to relate their results on *spatial* chaos of stationary solutions (see subsection VII.E.6 below) to the appearance of defect-mediated turbulence. They conjecture that spatially chaotic states are important in the dynamics, in that the typical time evolution will approach such states on their stable manifold and remain close for some time. We are not aware of any concrete signature of this phenomenon in numerical simulations or in experiments. For further work on defect mediated chaos see Elphick *et al.* (1988, 1990a,b, 1991).

4. Mean-field dynamics

A simplified limit of systems with large numbers of degrees of freedom is obtained when each mode interacts with all the others. This case, which we refer to as the “mean-field” limit, has no spatial dependence or patterns, but it presents some of the mathematical properties of large systems, such as the possibility of extensive chaos. One might also hope to expand about this limit to treat more realistic systems. The limit of a long-range interaction can be considered for most of the models introduced previously, since these are made up of interacting elements (Houlik *et al.*, 1990; Kaneko, 1990c; Strogatz *et al.*, 1989; Golomb *et al.*, 1992). For example the systems (7.59) and (7.60) with quenched randomness become (Fisher, 1985; Kuramoto and Nishikawa, 1987).

$$\partial_t \phi_i = \omega_i + \frac{J}{N} \sum_{j=1}^N \sin(\phi_i - \phi_j) , \quad (7.77)$$

and

$$\partial_t \phi_i = -h_i \sin(\phi_i - \beta_i) + \frac{J}{N} \sum_{j=1}^N (\phi_i - \phi_j) + F , \quad (7.78)$$

respectively. Thus, each mode in (7.78), for example, interacts with the other modes only via the mean field

$$\bar{\phi}(t) = N^{-1} \sum_{j=1}^N \phi_j(t) , \quad (7.79)$$

and the primary difficulty in solving the dynamical model is to enforce the self-consistency condition (7.79). For the collective transport model (7.78), the noninteracting system with $J=0$ is a simple driven pendulum

$$\partial_t \phi = -h \sin \phi + F , \quad (7.80)$$

whose average frequency Ω , Eq. (7.61), has a bifurcation at a particular value of F , such that

$$\Omega = 0 , \quad F < F_c , \quad (7.81a)$$

$$\Omega = \Omega_0 [(F - F_c)/F_c]^\zeta , \quad F > F_c , \quad (7.81b)$$

with $\zeta = 1/2$. In the interacting case $J \neq 0$, Fisher

(1985) has shown that the mean-field system displays perfect locking and has a bifurcation of the form (7.81) but with

$$\xi = 3/2 . \quad (7.82)$$

This example shows that even an elementary Hopf bifurcation changes its character when it involves an infinite number of degrees of freedom.

An interesting mean-field model has been analyzed by Sompolinsky, Crisanti and Sommers (1988). It consists of N real degrees of freedom $\{u_i(t)\}$, $i=1, \dots, N$, coupled together by a quenched random interaction

$$\partial_t u_i = -u_i + \sum_{j=1}^N J_{ij} g(u_j) , \quad (7.83a)$$

with

$$g(u) = \tanh(\gamma u) , \quad (7.83b)$$

a nonlinear gain function, and a random coupling given by

$$J_{ii} = 0, \quad \langle J_{ij} \rangle = 0, \quad \langle J_{ij} J_{k\ell} \rangle = \delta_{ik} \delta_{j\ell} J^2 / N . \quad (7.83c)$$

In the mean-field limit, $N \rightarrow \infty$, the dynamics can be reduced at long times to a single self-consistent equation

$$\partial_t u = -u + \xi(t) , \quad (7.84a)$$

with

$$\langle \xi(t) \xi(t+\tau) \rangle = J^2 C(\tau) , \quad (7.84b)$$

and $C(\tau)$ can be calculated by solving a second-order *ode*. The interesting result obtained by the authors is that for $\gamma J < 1$ the dynamics leads to a fixed point, but for $\gamma J > 1$ the system becomes chaotic. The largest Lyapunov exponent has also been calculated, using an analogy to the spectrum of the Schrödinger equation for a particle in a potential. The authors have also investigated the case of large but finite N numerically, and they find intermediate periodic phases for $\gamma J = O(1)$.

A model that has some features of mean-field dynamics is the differential-delay equation

$$\partial_t u = G[u(t), u(t-\tau)] , \quad (7.85)$$

where $G(u, v)$ is some simple function. The system is strictly speaking infinite dimensional for any delay τ , in the same sense as for a partial differential equation on a finite interval, since in both cases the models can only be integrated exactly with initial data given by a continuous function, here $u(t)$ for $t_0 \leq t \leq t_0 + \tau$, and any t_0 . The dimension of the attractor, on the other hand, is expected to be of order τ so the system (7.85) is only large in the sense of subsection VII.A.2 for $\tau \rightarrow \infty$. This case has been studied by Farmer (1982), who found a Lyapunov dimension roughly linear in τ , though interestingly the entropy, Eq. (7.19), remains constant as τ increases (see Figs. 12 and 13 of Farmer, 1982).

It has been noticed by Chaté and Manneville (1991) that coupled-map lattices in high but not infinite dimen-

sion (e.g. $d \geq 5$) appear to show many features associated with mean-field dynamics rather than the spatiotemporal complexity discussed above for systems with $d \leq 2$. These authors have obtained evidence that in $d=4$ and 5, for example, the coupled map based on (7.55) executes coherent collective motion over distances much larger than the interaction range (say 10–15 times larger). These observations have been in part confirmed by Gallas *et al.* (1991) who carried out simulations on larger systems, but obtained conflicting evidence on the stability of the periodic and quasiperiodic states. Of course, it is difficult to simulate systems of large linear size in high dimension, but there appears to be a qualitative difference between low and high dimension, which merits further study.

5. Strong turbulence

Let us consider fluid flow above the onset of chaos. The short-scale behavior of correlations ($\ell \ll \ell_E$) depends critically on the control parameter R which here is the Reynolds number $R_e = L v / \nu$, where v is a typical velocity and ν is the kinematic viscosity. For R_e not too large, the dissipation scale ℓ_D introduced in subsection VII.A.1 is of the same order as the excitation scale ℓ_E , so all modes with ℓ well below ℓ_E are dissipated. For systems such as the Navier-Stokes equation the dissipation scale shrinks with growing control parameter and the short-distance behavior is highly nontrivial (see, e.g., Monin and Yaglom 1975; Frisch and Orszag, 1990; Nelkin, 1992). The phenomenological theory of isotropic turbulence (Kolmogorov, 1941) introduces in addition to the excitation scale ℓ_E a rate of energy dissipation $\bar{\epsilon}$. The main assumption of the theory is that the velocity correlation function depends on this single parameter $\bar{\epsilon}$, which governs (i) the rate at which energy is injected at large scales ℓ_E , (ii) the (constant) rate at which energy is transferred down to smaller scales by the nonlinear terms in the Navier-Stokes equation (the “cascade”), and (iii) the rate at which energy is dissipated at the smallest scales ℓ_D . At large Reynolds number the lengths ℓ_E and ℓ_D are well separated, and scaling is assumed to occur in the *inertial sub-range*

$$\ell_E \gg \ell \gg \ell_D . \quad (7.86)$$

The Kolmogorov theory follows from the above physical assumptions and dimensional analysis. The Reynolds number is given by

$$R_e \sim \bar{\epsilon}^{1/3} \ell_E^{4/3} / \nu , \quad (7.87)$$

and the dissipation scale ℓ_D is obtained from the condition that the Reynolds number corresponding to that scale should be unity, which yields

$$\ell_D \sim R_e^{-3/4} \ell_E . \quad (7.88)$$

Thus the condition for a substantial inertial range $\ell_D \ll \ell_E$ is just $R_e \gg 1$. The equal-time velocity corre-

lation function $C(q)$ is conventionally written in terms of the energy spectrum

$$E(q) \approx q^{d-1}C(q), \quad (7.89)$$

which in the Kolmogorov theory has the form

$$E(q) \sim \bar{\epsilon}^{2/3}q^{-5/3}, \quad (7.90)$$

in the inertial range. Since strong turbulence theory focuses primarily on this range of scales, one generally assumes $L = \ell_E$, and there is no correlation length in the problem as long as scaling strictly applies.

Recent modifications of Kolmogorov's picture (see Frisch and Orszag, 1990; Nelkin, 1992) recognize the existence of coherent structures within the inertial range, but since these can exist on all scales there is still no well-defined correlation length. Indeed, the statistical theory retains the notion of scaling in the inertial range, though it is no longer assumed that the rate of energy transfer is constant throughout the cascade. Thus the scaling exponents are unknown quantities which depend on the order of the correlation function. Specifically, we can define the p th moment of the velocity u

$$M_p(x) = \langle [u(x) - u(0)]^p \rangle, \quad (7.91)$$

which in real space has the short-distance scaling exponent

$$M_p(x) \sim x^{\beta_p}. \quad (7.92)$$

In the Kolmogorov theory Eq. (7.90) implies $\beta_2 = 2/3$, and it can be shown that for general p the Kolmogorov theory corresponds to

$$\beta_p = p/3. \quad (7.93)$$

The presumed failure of the Kolmogorov theory has been parametrized by the nontrivial dependence of β_p on the index p . This dependence is quite analogous to the dependence of the Renyi dimension of a strange attractor d_q on its index [Eq. (7.20)], and indeed the multifractal nature of strong turbulence was posited before strange attractors had been investigated (Mandelbrot, 1974). For dynamical systems what is studied is the fractal nature of the probability measure of a point in phase space, whereas turbulence focuses on the fractal distribution of equal-time velocity (or vorticity) fluctuations in real three-dimensional space. Fractal structure depends on the existence of a scaling range, which arises from the presence of arbitrarily low frequencies in the spectrum of chaotic dynamical systems, or from the condition $R_e \gg 1$ required for the existence of an inertial range in space for strong turbulence in fluids. An attempt has been made to extend the analysis of turbulent correlations beyond the inertial range, to the dissipative range $\ell \lesssim \ell_D$. The correlation functions were found to obey "multiscaling," which amounts to scaling with logarithmic variables, rather than power laws (Wu *et al.*, 1990). As shown by Jensen *et al.* (1991) multiscaling is a natural, though approximate, consequence of the assumption of a lower

cutoff for probabilities in a multifractal. The description of strong turbulence in terms of multifractals is an active area of research (see Meneveau and Sreenivasan, 1987; McCauley, 1989; Meneveau *et al.*, 1990; Sreenivasan, 1991). For an opposing point of view, however, see Miller and Dimotakis (1991).

It should be noted that, contrary to the equal-time velocity correlations in space which are expressible entirely in terms of \bar{e} within the Kolmogorov theory, the velocity correlations in time at a point in space have been suggested to be of the form

$$E(\omega) \sim \bar{e}^{2/3} \bar{u}^{2/3} \omega^{-5/3}, \quad \omega < \bar{u}/\ell_D, \quad (7.94)$$

where $\bar{u} = [\langle u^2 \rangle]^{1/2}$ is the mean-square velocity which is dominated by large scales (Nelkin and Tabor, 1990). Thus even within the Kolmogorov theory it is important to distinguish which correlation functions can be expressed universally in terms of the cascade and which ones involve the nonuniversal large scales (Chen *et al.*, 1989).

As mentioned above, there have been many attempts to apply renormalization-group techniques to strong turbulence (see Dwoyer *et al.*, 1985). Following up on early work of De Dominicis and Martin (1979), Yakhot and Orszag (1986) have proposed a renormalization-group ε expansion for the Navier-Stokes equation with additive correlated noise $D_0(q, \omega) \sim q^{4-d-\varepsilon}$ [see Eq. (7.58)]. The theory displays the Kolmogorov energy spectrum (7.90) for $\varepsilon = 4$, and a one-loop calculation of the effective viscosity to linear order in ε yields a universal amplitude (known as the Kolmogorov constant), as well as other similar amplitudes, in good agreement with experiment. The success of this procedure is somewhat puzzling and the program has been criticized by a number of workers (Kraichnan, 1987; Bhattacharjee, 1988b).

6. Spatial chaos

A number of authors have focused on the purely spatial aspects of nonequilibrium systems by analyzing the disorder that exists in the dependence of stationary solutions on the coordinate x . For one-dimensional systems in particular, the stationarity condition for Eq. (7.23)

$$G[u, \partial_x u, \partial_x^2 u, \dots] = 0, \quad (7.95)$$

is an ordinary differential equation which can formally be considered as a dynamical system with pseudo-time x as in Sec. V.B. Diffusive systems are then frequently Hamiltonian in character and they display the chaotic properties of Hamiltonian dynamical systems (KAM surfaces, Arnol'd diffusion, etc.; see, e.g., Guckenheimer and Holmes, 1983). The corrections to this behavior arising either from non-Hamiltonian terms or from the effects of higher dimensions in the spatial coordinate x , have been considered by Coullet and Elphick (1987), Coullet *et al.* (1991), and by Eckmann and Procaccia (1991). Although this type of analysis can often be pushed quite far it must be remembered that a solution of the stationarity condi-

tion (7.95) need not have any dynamical significance in terms of the original system (7.23). Indeed, a stationary state is only physically important if it is *stable* (or at least long-lived) and if it is *reachable*, i.e. if its basin of attraction includes physically relevant states. Such considerations have often been overlooked in treatments of spatial chaos.

An example of the application of ideas from dynamical systems theory to spatial chaos arises in the system of interacting pulses in the Fitz-Hugh-Nagumo model (Sec. V.B.3.b.ii). Elphick *et al.* (1988) have derived the dynamical equation for the position ξ_i of the i th defect

$$\begin{aligned}\partial_t \xi_i = & C_1 \exp[-\kappa_1(\xi_{i+1} - \xi_i)] \cos[q_1(\xi_{i+1} - \xi_i) + \phi] \\ & + C_2 \exp[-\kappa_2(\xi_i - \xi_{i-1})].\end{aligned}\quad (7.96)$$

To look for time independent solutions they set $\partial_t \xi_i = 0$ and find

$$\begin{aligned}\cos[q_1(\xi_{i+1} - \xi_i) + \phi] \\ = -\frac{C_2}{C_1} \frac{\exp[-\kappa_2(\xi_i - \xi_{i-1})]}{\exp[-\kappa_1(\xi_{i+1} - \xi_i)]}.\end{aligned}\quad (7.97)$$

This equation will have many solutions, with $\xi_{i+1} - \xi_i$ of order δ say, but differing by multiples of $2\pi/q_1$; such solutions may be chosen to be spatially chaotic and they exist providing the right-hand side of Eq. (7.97) is smaller than unity. In the large separation limit, $\delta \gg 1$, this condition reduces to a condition on the fixed-point eigenvalues

$$\kappa_2 > \kappa_1. \quad (7.98)$$

As we have seen in Sec. V.B.3.b.ii, a single pulse corresponds to a homoclinic orbit leaving the fixed point along the eigenvector corresponding to the real eigenvalue κ_2 and returning along a combination of the eigenvectors with complex eigenvalues $\kappa_1 \pm iq_1$ (Fig. 31). In dynamical systems theory it has been proven that in this situation there are many nearby chaotic orbits, providing a condition on the eigenvalues is satisfied, which turns out to be precisely (7.98). This is known as the Sil'nikov mechanism for chaos (Guckenheimer and Holmes, 1983), and we see that it has a direct manifestation in the spatially chaotic array of pulses.

F. Experimental studies

In this section we wish to review briefly experimental work aimed at understanding the large-scale properties of chaotic systems, and to suggest some possible directions for research. Hydrodynamic experiments involve either visualization techniques (shadowgraph) or point measurements of velocity or temperature. Roughly speaking the large-scale properties begin to appear when $L \gg \max(\ell_E, \ell_D, \xi)$, say $L/\max(\ell_E, \ell_D, \xi) = 50 \sim 100$. For experiments in hydrodynamic systems, e.g. Taylor-Couette or Rayleigh-Bénard flows or parametric waves, this implies an aspect ratio 50–100, and R not too near

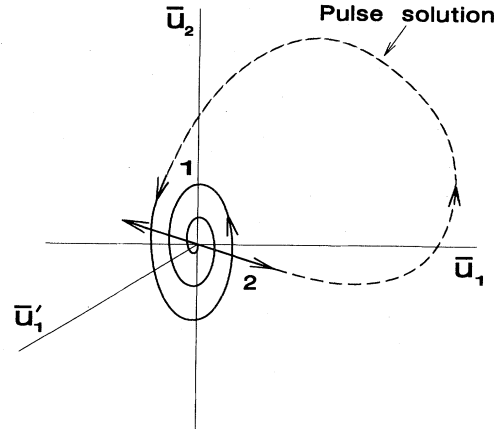


FIG. 31. Trajectory of a pulse solution for Fitz-Hugh-Nagumo model (5.170) in the $\bar{u}_1(\xi)$, $\bar{u}'_1(\xi)$, $\bar{u}_2(\xi)$ phase space. Dashed line corresponds to a single pulse solution leaving the linear fixed point at the origin along the unstable direction corresponding to eigenvalue κ_2 , and returning to the linear fixed point along a direction in the plane spanned by the pair of eigenvectors corresponding to the complex eigenvalues $\kappa_1 \pm iq_1$. Nearby trajectories will be chaotic, and lead to spatial chaos in the pde (5.170).

threshold. (If there are large coherent structures, i.e. $\xi \gg \ell_E, \ell_D$, then the requirements could be more stringent.) In general, such experiments are certainly feasible and a number have been undertaken, starting with the pioneering studies of Ahlers and Behringer (1978) on large aspect-ratio Rayleigh-Bénard convection. More recent work on this system has focused on quasi one-dimensional geometries (Ciliberto and Bigazzi, 1988; Bergé, 1989; Daviaud *et al.*, 1989). Some other experimental systems where large geometries can be obtained are electrohydrodynamic convection in nematics (Nasuno and Sawada, 1989; Rehberg *et al.*, 1989a,b; Braun *et al.*, 1991), parametric waves (Tuffilaro *et al.*, 1989), Taylor-Couette flow (Hegseth *et al.*, 1989), flow between two cylinders (Rabaud *et al.*, 1989) and convection in binary fluid mixtures (Steinberg *et al.*, 1989; Kolodner *et al.*, 1990), or convection under rotation (Bodenschatz *et al.*, 1992).

We shall describe some of these experiments as part of the discussion of specific systems in the following sections, but we can already state that so far only sketchy information is available concerning long-range correlations in space and time. It is our hope that more studies of these questions will be undertaken.

In the case of strong turbulence, experiments have primarily focused on point measurements of velocity or temperature, though some visualizations of the overall flow and correlation function measurements have also been undertaken (Goldburg *et al.*, 1989; Sreenivasan, 1991). For open systems the Taylor hypothesis allows conversion of temporal information at a point to spatial information, from which the scaling properties discussed above have been inferred (see Anselmet *et al.*, 1984).

The validity of this hypothesis has been tested under some circumstances, but its applicability to the study of large-scale correlations is not established. Moreover, for strong turbulence the large range of scales in the inertial subrange (7.86) provides many challenges, but it might also be interesting to study correlations on scales outside of this range, in particular for scales *longer* than ℓ_E (Wu and Libchaber, 1992). Is there a response on long scales $\ell \gg \ell_E$ coming from the cascade? In the spirit of the stochastic approach discussed for the Kuramoto-Sivashinsky model in subsection VII.E.1, one might say that this case represents a system with “infinitely colored” noise since the noise correlations extend over a large range.

An interesting suggestion for an experimental probe of turbulence via ultrasound was recently made by Lund and Rojas (1989). The method has been implemented by Baudet *et al.* (1991).

VIII. RAYLEIGH-BÉNARD CONVECTION

A. General features

Investigations of Rayleigh-Bénard convection have played a vital role in developing ideas of pattern formation in nonequilibrium systems, and this system is often used as the canonical example. It has a number of advantages over other systems: first the basic equations underlying the phenomena are well known, and second there is a close connection between theory and experiment which has permitted detailed tests of many theoretical concepts. There are, of course, approximations involved in arriving at a tractable theory but these are controlled and well understood and can be improved upon if necessary. The experiments are also well controlled: the apparatus construction depends mainly on geometrical considerations (flat plates, etc.) and the maintenance of uniform temperatures. The thermal properties are most precisely controllable in low temperature experiments using helium as the fluid. However flow visualization has not been carried out at these temperatures and so the spatial structure, our main interest here, has not been determined. We refer to Behringer (1985) for a review of this work. For general convection experiments the value of the control parameter is determined by fixing the temperature. The spatial structures are conveniently displayed by noninvasive flow visualization techniques on short time scales compared with typical characteristic times, for the moderate Rayleigh numbers which we are primarily concerned with. In addition, very precise quantitative measurements are possible, involving the integrated heat flux across the cell, as well as point quantities such as local flow velocities (laser Doppler velocimetry) or the local temperature (using dyes or bolometers at the plates).

There are of course some disadvantages. The intrinsic time and length scales are rather long, at least in liquids.

In principle both can be reduced by reducing the separation of the plates, but since the control parameter varies as the third power of this separation and should be accurately uniform across the cell, there are practical limits to this approach. This restriction becomes particularly severe for the slow evolution of the spatial structure in large systems, where characteristic time scales may be on the order of weeks. Another complication of convection is that the easily measured quantities are nonlocal functions of the basic variables, such as averages over the depth of the cell, or nonlinear averages across the cell as in the lensing effect used in shadowgraph visualizations (Croquette, 1989). Careful design of the experiment and appropriate calibration of the probes does however alleviate these problems and allows a determination of absolute intensities, at least in principle.

In this section we will review more quantitatively the basic features of Rayleigh-Bénard convection introduced qualitatively in Sec. II.A. Since our discussion is by no means complete we refer the reader to other reviews for more details; see, for example, Koschmieder (1974, 1993), Palm (1975), Normand *et al.* (1977), Busse (1978, 1981), Ahlers (1989, 1991), Croquette (1989), Manneville (1990), Getling (1991), Newell *et al.* (1993). Our primary emphasis will be on spatial patterns and the comparison between experiment and theory.

1. Basic equations

The microscopic equations describing Rayleigh-Bénard convection are the Navier-Stokes equation for the velocity field (Landau and Lifshitz, 1959)

$$(\partial_t + \mathbf{u} \cdot \nabla) (\rho \mathbf{u}) = -\nabla P + \nabla \cdot \boldsymbol{\sigma} - \rho g \hat{\mathbf{z}}, \quad (8.1a)$$

with

$$\boldsymbol{\sigma}_{ij} = \eta [\partial_i u_j + \partial_j u_i - \frac{2}{3} \delta_{ij} \partial_\ell u_\ell] + \xi \delta_{ij} \partial_\ell u_\ell, \quad (8.1b)$$

mass conservation

$$\partial_t \rho + \nabla \cdot (\rho \mathbf{u}) = 0, \quad (8.1c)$$

and the conservation law for heat

$$(\partial_t + \mathbf{u} \cdot \nabla) (C_p T) = \nabla \cdot (K \nabla T), \quad (8.1d)$$

where we have neglected the heat produced by the viscous dissipation in the last equation. The variables in Eqs. (8.1) are the density $\rho(\mathbf{x}, t)$, the velocity $\mathbf{u}(\mathbf{x}, t) = (u, v, w)$, the pressure $P(\mathbf{x}, t)$ and the temperature $T(\mathbf{x}, t)$, and the parameters are the shear viscosity η , the bulk viscosity ξ , the constant-pressure specific heat C_p , the thermal conductivity K , and the acceleration of gravity g . To close the equations the dependence of the parameters η, ξ, K on temperature and density, and the equation of state $P(\rho, T)$ must be known. The approximations leading to these equations are well understood and essentially rest on the large ratio between the length scales of the spatial variations and the mean free path of the constituent molecules. As mentioned in subsection

VIII.D.1.c below, extra residual effects of the small-scale degrees of freedom appear as stochastic forcing of Eqs. (8.1) with an intensity depending on temperature and given by the fluctuation dissipation theorem (Landau and Lifshitz, 1959; Graham, 1974; Swift and Hohenberg, 1977). Due to simple averaging these terms are small on the scales typical of convection, but they may conceivably be important at bifurcations such as the onset of convection, where the system is very sensitive to small effects.

We are interested in the situation where a temperature difference ΔT is maintained between two horizontal plates. In general the parameters η , C_p , and K will depend on temperature and density and therefore position, and very complicated equations result. The “Boussinesq approximation” (see Normand *et al.*, 1977; Busse, 1978) includes these temperature dependences only in the all important buoyancy term

$$\rho = \bar{\rho} [1 - \alpha(T - \bar{T})] \quad (8.2)$$

(with $\bar{\rho}$, \bar{T} reference values and α the thermal expansion coefficient), and otherwise assumes an incompressible fluid. The Oberbeck-Boussinesq equations are

$$(\partial_t + \mathbf{u} \cdot \nabla) \mathbf{u} = -\nabla(P/\rho) + \nu \nabla^2 \mathbf{u} + g\alpha T \hat{\mathbf{z}}, \quad (8.3a)$$

$$(\partial_t + \mathbf{u} \cdot \nabla) T = \kappa \nabla^2 T, \quad (8.3b)$$

$$\nabla \cdot \mathbf{u} = 0, \quad (8.3c)$$

with $\nu = \eta/\rho$ the viscous diffusivity (kinematic viscosity) and $\kappa = K/C$ the thermal diffusivity. Notice that now the pressure term occurs only in the equation of motion for the velocity \mathbf{u} , and no longer implicitly through the dependence of density on pressure via the equation of state. The incompressibility condition (8.3c) effectively replaces the equation of state, and indeed taking the divergence of (8.3a) and using (8.3c) we obtain a Poisson equation for the pressure, which can then be eliminated in favor of \mathbf{u} and T . (We have dropped the bars signifying reference quantities on these equations and have also absorbed some constants into the pressure term.) The approximations made in going from Eqs. (8.1) to (8.3) are quantitatively justified for most fluids (Busse, 1967, 1978). However Eqs. (8.3) turn out to have an additional inversion symmetry over Eqs. (8.1) in the Rayleigh-Bénard geometry, so that small “non-Boussinesq” symmetry-breaking terms may be qualitatively important in certain regions of parameter space. An example is the roll-hexagon competition discussed in subsection VIII.F.3 below.

The dynamical equations (8.3) must be supplemented by boundary conditions on the flow variables. The ideal system is considered to be infinite in lateral extent, with perfectly conducting top and bottom plates so that the temperature may be assumed fixed

$$T(z = -d/2) = T_u + \Delta T, \quad (8.4a)$$

$$T(z = d/2) = T_u. \quad (8.4b)$$

Experimental realizations approximate this condition very well by making the plate conductivity of order 10^2 to 10^3 times that of the fluid. At a rigid boundary all components of the velocity are zero

$$\mathbf{u} = 0, \quad z = \pm \frac{1}{2} d. \quad (8.4c)$$

We will take these conditions as *defining* the ideal system. In practice of course sidewalls leading to lateral boundary conditions must also be present. This defines the *aspect ratio* or dimensionless lateral size

$$L = \tilde{L}/d, \quad (8.5)$$

where \tilde{L} is a lateral dimension of the container, e.g. the radius for a cylindrical container. For later reference we also define the idealized free-slip boundary conditions, which lead to considerable simplification in the analysis of the instability

$$\partial_z \mathbf{u}_\perp = w = 0, \quad z = \pm \frac{1}{2} d, \quad (8.6)$$

where \mathbf{u}_\perp and w are the 2D horizontal and vertical components of \mathbf{u} , respectively.

In the absence of flow in the ideal system we have the conducting solution

$$T = T_0(z) = T_u + \Delta T(1/2 - z/d), \quad (8.7)$$

and also $P = P_0(z)$ to balance the buoyancy force. To study deviations from the conducting solution it is convenient to subtract off this reference temperature and pressure

$$\theta = T - T_0(z), \quad (8.8a)$$

$$p = P - P_0(z). \quad (8.8b)$$

Finally, dimensionless variables are introduced. We shall use the characteristic *thermal* diffusion time d^2/κ across the depth of the cell as the time unit, d as the length unit and the Rayleigh number

$$R = \frac{\alpha g \Delta T d^3}{\kappa \nu} \quad (8.9)$$

as the dimensionless temperature difference. The dimensionless heat current can be expressed in terms of the Nusselt number \mathcal{N} defined as the ratio of the total heat current to the conducted heat current at the same ΔT . Equations (8.3) and (8.4) then become

$$\sigma^{-1} (\partial_t + \mathbf{u} \cdot \nabla) \mathbf{u} = -\nabla p + \theta \hat{\mathbf{z}} + \nabla^2 \mathbf{u}, \quad (8.10a)$$

$$(\partial_t + \mathbf{u} \cdot \nabla) \theta = R w + \nabla^2 \theta, \quad (8.10b)$$

$$\nabla \cdot \mathbf{u} = 0, \quad (8.10c)$$

$$\mathbf{u} = \theta = 0, \quad z = \pm \frac{1}{2}, \quad (8.10d)$$

where again some pure gradient terms have been absorbed in the pressure. These equations depend on two parameters: the dimensionless driving strength R , the Rayleigh number, and the ratio of thermal and viscous

diffusivities

$$\sigma = v/\kappa , \quad (8.10e)$$

known as the Prandtl number. Notice that σ gives the relative importance of time derivatives and nonlinearities for the temperature vs. the velocity. Equations (8.10) are the starting point for most theoretical work on convection. It should be reemphasized that the approximations leading to these equations are well understood (and improved ones can be made if necessary): they provide a secure basis for theory.

Theoretical work on this problem has been in three phases. The linear stability analysis was the focus of attention from the work of Rayleigh (1916) on the free-slip model, to the calculation of Pellew and Southwell (1940) on the realistic model defined by Eqs. (8.4). This work is described in detail in Chandrasekhar (1961). The ideal nonlinear states and their stability to small perturbations were studied by Busse and co-workers in the 1960s and 1970s (see Busse, 1967a, 1978). [It should be noted that the calculation of the nonlinear states in the appendix of Chandrasekhar (1961) is incorrect.] More recently attention has shifted to the more complex states we have called "real patterns," and the methods of amplitude and phase equations, as well as the study of models.

2. Linear instability and ideal solutions

The linear instability of the conducting solution ($\mathbf{u} = \theta = 0$) is fairly straightforward. It was proven (see Joseph, 1976) that in the ideal system it is stationary i.e. type I_s. This considerably simplifies the calculation. It is also then clear that the Prandtl number drops out of the calculation of the critical Rayleigh number, the critical wave vector (which must therefore be of order d^{-1} with no dependence on the fluid parameters) and the onset solution at threshold. It is straightforward to look for onset solutions varying as e^{iqx} and these can be found in essentially closed form (see the Appendix of Manneville, 1990). The critical Rayleigh number is

$$R_c = 1707.76 , \quad (8.11a)$$

at a critical wave vector

$$q_0 = 3.117 . \quad (8.11b)$$

Note that q_0 is very close to π , so that the roll size (half-wavelength) is very close to the thickness.

Theoretical work on the nonlinear states in a perturbation expansion near threshold was initiated by Gor'kov (1958) and Malkus and Veronis (1958) for convection and by Stuart (1958) for the Taylor-Couette system. It was subsequently developed systematically by Schlüter, Lortz, and Busse (1965) who studied ideal roll solutions and also nonlinear superpositions of rolls in the form of squares, hexagons, and other regular patterns (Sec. IV.A.1). They calculated the interaction parameter equivalent to $\mathcal{G}(\theta)$ of Eq. (4.32) as a function of Prandtl

number and found that rolls are the stable solution near threshold in the ideal system, for all Prandtl numbers. As we have seen, small effects that break the symmetry $(\mathbf{u}, \theta) \rightarrow (-\mathbf{u}, -\theta)$ render the transition subcritical by strongly coupling to the hexagonal solution.

In a long series of papers Busse and co-workers numerically solved for the nonlinear solutions using a truncated (Galerkin) expansion (see Normand *et al.*, 1977; Busse, 1978)

$$U = \sum_{mn} U_{mn} \cos(mqx) \mathbf{u}_n(z) , \quad (8.12)$$

with $\mathbf{u}_n(z)$ some convenient basis functions satisfying the fluid boundary conditions. The parameters $U_{mn}(R, \sigma)$ are determined by requiring the fluid equations to be satisfied when projected onto the mn basis vectors.

3. Stability balloon

The stability analysis of these ideal nonlinear solutions is formulated as a Bloch wave analysis, i.e. the perturbation takes the form

$$\delta \mathbf{u}(x, y, z; \mathbf{Q}) = e^{i(Q_x x + Q_y y)} \delta U_q(x, z; \mathbf{Q}) e^{\sigma_q(\mathbf{Q})t} , \quad (8.13)$$

where δU_q is periodic in x with wave number q and the Bloch wave vector \mathbf{Q} can be restricted to the range

$$-\frac{1}{2} q < Q_x \leq \frac{1}{2} q , \quad (8.14)$$

without loss of generality. (The growth rate σ_q should not be confused with the Prandtl number σ .) The instabilities can be characterized further by the symmetries of δU_q under parity operations. Busse and co-workers calculated the $\sigma_q(\mathbf{Q})$ using the Galerkin expansion (8.12). The stability analysis is converted into an $mn \times mn$ matrix eigenvalue problem for each q and \mathbf{Q} , and then the positive (unstable) $\sigma_{q\alpha}(\mathbf{Q})$ are maximized as a function of \mathbf{Q} to give the most unstable wave vector and the stability boundaries. This process must be repeated for each wave vector q , and each Rayleigh number and Prandtl number desired. There are many possible instabilities with different symmetries. Based on their visual appearance Busse gave colorful names to the various instabilities (e.g. knot, oscillatory, skew-varicose, cross-roll) and calculated the stability boundaries. The region of (q, R, σ) space of stable solutions bounded by these instabilities forms the "Busse balloon" (Fig. 32), which has provided enormous insight into the dynamics of convection, and makes this the best characterized nonlinear pattern forming system. A great deal of the detailed physics of the fluid-heat system is contained in this stability diagram, and it is often possible to arrive at an intuitive understanding of the various instability mechanisms (shear layer instabilities at low Prandtl numbers, thermal boundary layer instabilities at high Prandtl numbers, etc.). However since we are here mainly interested in how well the system is characterized as a canonical example, we will not discuss these details. The reader is referred to the review by

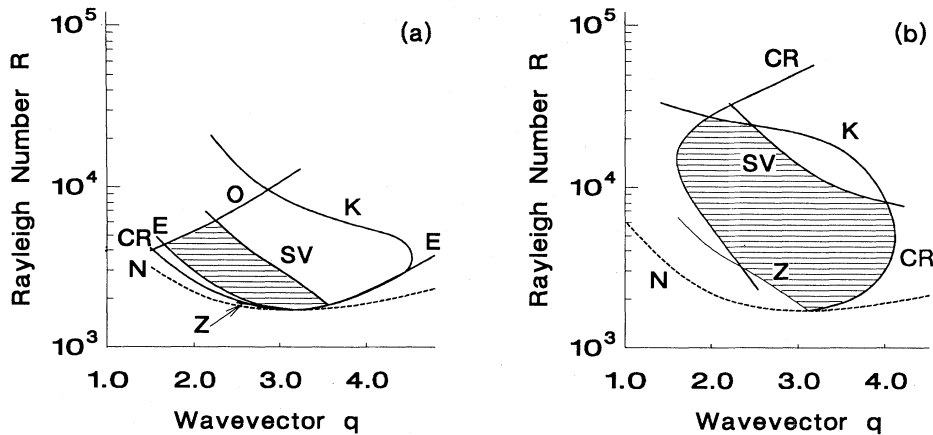


FIG. 32. Stability diagram for ideal roll states in Rayleigh-Bénard convection (a) Prandtl number $\sigma = 0.71$; (b) $\sigma = 7.0$. Diagram shows range of Rayleigh number R and wave vector q for which the ideal roll states are stable (hatched regions), as well as the various instabilities of the roll states: E Eckhaus; Z zig-zag; SV skew-varicose; K knot; O oscillatory; CR cross-roll. The dashed line labeled N is the neutral stability line giving the instability of the conducting state to a convection state at wave vector q . (Adapted from Busse and Whitehead, 1971, and Busse and Clever, 1979.)

Busse (1978), to the recent work of Clever and Busse (1987, 1989), and to a more pedagogical discussion by Manneville (1990) for further reading.

A precise experimental test of the predicted stability diagram is not easy to carry out since the ideal geometry of the theory cannot be realized, but the predictions are borne out at least semiquantitatively, both in the approximate *location* of the stability boundaries and in the nature of each instability (i.e. the form of the eigenvectors). There are two classes of experiments. Busse and Whitehead (1971) used very large aspect ratio systems with a transient ideal state established by thermal imprinting. The instabilities were then investigated in the time window after the nonlinear state was established but before the influences of the lateral boundaries were felt over the interior of the system. These very large systems are probably not spatially homogeneous, and as a result the parameters at which the instabilities occur are modified, as is also the long-time development of the system (e.g. whether the instability leads to a restabilization of the pattern at a new wave vector within the stable band, or leads to persistent time dependence).

A second class of experiments has studied the instabilities in smaller systems by investigating well established steady-state patterns, but both the patterns and the perturbations may be quite strongly influenced by the lateral boundaries. Gollub, McCarriar, and Steinman (1982) worked with Prandtl number 2.5 and aspect ratios 20–30, to study the onset of time dependence in spatially disordered states. Kolodner, Walden, Passner, and Surko (1986) studied the evolution of simple states, but in quite small geometries (aspect ratio 10 × 5) at Prandtl numbers between 2 and 20 (see also Nasuno *et al.*, 1988). Croquette (1989) has reviewed work at low Prandtl numbers in aspect ratios (7–20). In general the conclusion from this work is that the behavior is qualitatively con-

sistent with the theoretical predictions but with considerable shifts in the stability boundaries due to finite geometry, as might be expected. Typically the instabilities are shifted to higher values of the Rayleigh number, with the exception of the cross-roll instability which is often driven downward by the side walls parallel to the dominant roll direction.

4. Amplitude equations

The convection system, albeit with artificial boundary conditions (see below), is the one in which the spatially dependent amplitude equation was first introduced in the study of fluid instabilities (Newell and Whitehead, 1969; Segel, 1969). As we have seen, ironically this “simple” model is actually a situation where the standard amplitude equation breaks down (except in the limit of infinite Prandtl number), due to mean flow effects that are undamped by the free-slip boundaries (see below).

For the experimentally realized rigid boundaries the lowest-order amplitude equation *does* take the general form for a type I_s instability: its form is therefore dictated by general symmetry arguments. For a single set of rolls nearly parallel to the y axis the equation for the complex amplitude $A(\mathbf{x}, t)$ is (Cross, 1980)

$$\tau_0 \partial_t A = \epsilon A + \xi_0^2 [\partial_x - (i/2q_0)\partial_y]^2 A - g_0 |A|^2 A . \quad (8.15)$$

Given this form, individual parameters may be picked out for evaluation by comparison with other calculations (Wesfreid *et al.*, 1978). For example τ_0^{-1} is simply $\partial\sigma(q_0)/\partial\epsilon$, the derivative of the linear growth rate at the critical wave number with respect to the reduced Rayleigh number (Behringer and Ahlers, 1977). Similarly,

the full Prandtl number dependence of g_0 , for a given normalization of the amplitude in terms of the fluid variables, may be evaluated from the work of Schlüter *et al.* (1965), who considered spatially independent amplitudes. A systematic derivation of Eq. (8.15) for the rigid boundary case was given by Cross (1980) using mode projection techniques. In Appendix A we derive the amplitude equation using the original multiple scales perturbation technique of Newell and Whitehead and Segel, going far enough to illustrate the application of the method to this general (nonseparable) example, but without displaying the complicated algebra necessary to evaluate the coefficients.

The parameters appearing in Eq. (8.15) are found to be

$$\tau_0^{-1} = \frac{19.65\sigma}{\sigma + 0.5117}, \quad (8.16a)$$

$$\xi_0^2 = 0.148, \quad (8.16b)$$

and

$$g_0 = 0.6995 - 0.0047\sigma^{-1} + 0.0083\sigma^{-2}, \quad (8.16c)$$

where we have normalized the amplitude A so that the convective heat transport per unit area is

$$(\mathcal{N}-1)(R/R_c) = \langle w\theta \rangle / R_c = |A|^2, \quad (8.17)$$

where \mathcal{N} is the Nusselt number and the bracket denotes a spatial average. For the situation of superimposed rolls the interaction parameter $\mathcal{G}(\theta)$ of Eq. (4.32) was evaluated by Cross (1980) from the calculations of Schlüter *et al.* (1965). It is convenient to write $\mathcal{G}(\theta)$ in terms of another function $g_\sigma(\cos\theta)$ (which also depends on Prandtl number)

$$\mathcal{G}(\theta) = \frac{2g_\sigma(\cos\theta) + 2g_\sigma(-\cos\theta) + 2g_\sigma(-1)}{g_\sigma(1) + 2g_\sigma(-1)}, \quad \theta \neq 0, \quad (8.18a)$$

$$= 1, \quad \theta = 0, \quad (8.18b)$$

where the Prandtl number dependence is given by

$$g_\sigma(\cos\theta) = A(\cos\theta) + B(\cos\theta)\sigma^{-1} + C(\cos\theta)\sigma^{-2}, \quad (8.18c)$$

and A, B, C can be interpolated from Table 1 of Cross (1980). (There A is called g_0 , B is g_{-1} , and C is g_{-2} .)

From these results, of course, the boundaries of the stability balloon may be calculated for small ϵ [i.e. $q - q_0 = O(\epsilon^{1/2})$], reproducing the results of the numerical Galerkin calculations in this limit. Interestingly, for $\sigma \gtrsim 1$ the “cross-roll” instability — the instability of one set of rolls to the growth of another set at some angle θ — preempts the universal Eckhaus line as the bounding instability for $q > q_0$. The universal transverse zigzag instability $q_Z = q_0$ at $O(\epsilon^{1/2})$ forms the boundary on the small wave-number side.

It should be remarked that in spite of what may appear from Eqs. (8.15) and (8.16) it turns out that the amplitude

equation is quite smooth as $\sigma \rightarrow 0$, once the viscous timescale d^2/ν rather than the thermal timescale d^2/κ is used to render the fluid equations dimensionless. Even in this limit complications such as mean flow effects or the onset of the oscillatory instability only appear at higher order in ϵ .

For one-dimensional patterns in a geometry with restricted transverse aspect ratio L_y Daniels and Ong (1990) have evaluated the coefficients τ_0 , ξ_0 , and g_0 of the one-dimensional version of Eq. (8.15) as a function of L_y and σ , for realistic boundary conditions.

5. Phase equations

Pomeau and Manneville (1979) first pointed out the importance of the phase equation (4.70) in the context of Rayleigh-Bénard convection, although since they derived the equation for $\epsilon \rightarrow 0$ from the amplitude equation, their results apply quite generally to type I_s systems; in particular their expressions (4.71) and (4.72) for the diffusion constants D_{\parallel} and D_{\perp} in terms of ξ_0 and τ_0 are generally valid.

The specific features of the convective system arise at the next order in ϵ . In particular Manneville and Piquemal (1982) calculated D_{\perp} to $O(\epsilon)$, which yields the slope of the zigzag boundary $(q_Z - q_0)/\epsilon$, and its strong Prandtl number dependence. In fact, as was mentioned in Sec. IV.A.2 above, the phase equation for convection has nonanalytic behavior due to mean drift effects at any order in ϵ beyond the lowest one (Cross, 1983). This arises because, due to the incompressibility of the fluid, only ∇P enters (and not P via the equation of state), so adding a constant P_S to the pressure makes no difference. However if the added pressure is now made a slowly varying function $P_S(x, y)$ of the horizontal coordinates, the gradients of P_S will drive a horizontal flow which further distorts the convective pattern. The final link in the chain of arguments is that slow distortions of the convective pattern do indeed induce a slowly varying $P_S(x, y)$ which must be determined by the incompressibility condition. Thus $P_S(x, y)$ constitutes an independent slow field determined by a nonlocal (static) constraint.

The importance of the mean flow in reduced descriptions of convection was discovered by Siggia and Zippelius (1981b) in their study of the amplitude equation for free-slip convection (Sec. VIII.B.2 below). There, a horizontal mean flow, constant across the depth of the cell, is undamped and must be included as an independent mode in the slow dynamics. These authors also suggested a phenomenological extension to the rigid-boundary case, where the horizontal flow is damped by viscous coupling to the top and bottom plates. Although now formally of higher order in ϵ in an amplitude equation approach, the mean flow is important to include in the phase equation description since it leads to nonanalyticities at small q , as noted by Cross (1983) and by Cross and Newell (1984), who carried out a perturbative calculation in the weak nonlinearity near threshold.

The technical difficulties of a full calculation starting from the Boussinesq equations for convection away from threshold are formidable, and the complete calculation relying only on the assumption of slow spatial variations has only recently been accomplished (Newell *et al.*, 1990a,b, 1991, 1993). We clearly cannot present this full calculation here, but since the general phenomenon should be quite widespread in fluid systems we will outline what we believe to be the content of the theory, although Newell and co-workers use a different choice of variables.

The starting point is the observation that a horizontal flow, varying slowly with x and y , is driven by distortions of the pattern and by gradients of P_S ; by symmetry it must take the form

$$\mathbf{v}_D(x, y, z) = [f_1 \mathbf{1} + f_2 \hat{\mathbf{q}}\hat{\mathbf{q}}] \cdot \nabla_{\perp} P_S + [f_3 \mathbf{1} + f_4 \hat{\mathbf{q}}\hat{\mathbf{q}}] \cdot \nabla_{\perp} q + f_5 \hat{\mathbf{q}}(\nabla_{\perp} \cdot \mathbf{q}), \quad (8.19)$$

where the functions $f_i = f_i(q, z)$ depend on the full nonlinear structure of the rolls, and ∇_{\perp} is the horizontal gradient. Notice that because the pressure P_S is driving the flow in a medium effectively made anisotropic by the rolls, there are complicated anisotropy factors in Eq. (8.19). In particular the flow is *not* in general along $\nabla_{\perp} P_S$ and it does *not* have the z dependence of Poiseuille flow, although these simplifications do occur in the perturbative calculation near threshold. The incompressibility enforces an important constraint on the mean flow

$$\nabla_{\perp} \cdot \int_0^1 dz \mathbf{v}_D(x, y, z) = 0. \quad (8.20)$$

This determines P_S through an anisotropic Poisson-like equation,

$$\nabla_{\perp} \cdot [(b_1 \mathbf{1} + b_2 \hat{\mathbf{q}}\hat{\mathbf{q}}) \cdot \nabla_{\perp} P_S + (b_3 \mathbf{1} + b_4 \hat{\mathbf{q}}\hat{\mathbf{q}}) \cdot \nabla q + b_5 \hat{\mathbf{q}}(\nabla \cdot \mathbf{q})] = 0, \quad (8.21)$$

with b_i now functions only of q (and control parameters),

$$b_i(q) = \int_0^1 dz f_i(q, z). \quad (8.22)$$

Finally the flow v_D advects the pattern, giving

$$\partial_t \phi \rightarrow \partial_t \phi + \mathbf{V} \cdot \mathbf{q}, \quad (8.23a)$$

with

$$V(x, y) = \int_0^1 dz v_D(x, y, z) g(z), \quad (8.23b)$$

where $g(z)$ is a weighting function again depending on the full nonlinear structure of the rolls. This means that \mathbf{V} is *not* simply the integrated flow. Notice that the last two terms in Eq. (8.19) for \mathbf{v}_D , when inserted into $\mathbf{V} \cdot \mathbf{q}$ give terms in the phase equation which are of the same form as those already present on the right-hand side, and they may be absorbed into these terms. Thus the new effects of the pressure P_S and induced "mean drift" \mathbf{V} may be summarized by the equation

$$\partial_t \phi + \mathbf{V} \cdot \mathbf{q} = -\tau^{-1}(q) \nabla \cdot [\mathbf{q} B(q)], \quad (8.24a)$$

with

$$\mathbf{V} = [b_6(q) \mathbf{1} + b_7(q) \hat{\mathbf{q}}\hat{\mathbf{q}}] \cdot \nabla_{\perp} P_S, \quad (8.24b)$$

and P_S determined by Eq. (8.21). The task of the full calculation is then to determine the parameters $b_i(q)$, $i = 1$ to 7 (in fact only the combination $b_6 + b_7$ is needed for $i = 6, 7$), $\tau^{-1}(q)$ and $B(q)$, as functions of the control parameter R , and the Prandtl number σ .

We note that since the velocity field v_D is *not* simply a uniform flow, the mean drift is not equivalent to transforming to a moving frame of reference. As well as translating the pattern, the drift v_D will also distort the local structure of the rolls. Thus the effect cannot be related to a "gauge invariance" of the original equations, as Pocheau (1988) attempts to do, except at the lowest order of the expansion where the resulting phase equation does show this extra symmetry.

Newell *et al.* (1990a,b, 1991) have chosen to implement this calculation in a slightly different way which brings out more clearly the relationship to the dangerous vertical vorticity mode in the free-slip calculation of Siggia and Zippelius (1981b). Since the integrated mean drift $\int_0^1 dz v_D(x, y, z)$ is divergence free, it can be written in terms of a stream function ζ

$$\int_0^1 dz \mathbf{v}_D(x_{\perp}, z) = \nabla_{\perp} \times \hat{\mathbf{z}} \zeta(\mathbf{x}_{\perp}), \quad (8.25)$$

where $\mathbf{x}_{\perp} = (x, y)$. They then control the singularities by writing the horizontal velocity as

$$\mathbf{u}_{\perp} = f(z) \nabla_{\perp} \times \hat{\mathbf{z}} \zeta(\mathbf{x}) + \mathbf{u}'_{\perp}, \quad (8.26)$$

where \mathbf{u}'_{\perp} has zero mean flux

$$\int_0^1 \mathbf{u}'_{\perp} dz = 0, \quad (8.27)$$

and $f(z)$ is an arbitrary function with mean 1,

$$\int_0^1 f(z) dz = 1. \quad (8.28)$$

Of course different choices of $f(z)$ lead to different "correction" terms \mathbf{u}'_{\perp} ; Newell *et al.* choose a Poiseuille form for convenience. The quantity \mathbf{u}'_{\perp} must be calculated through an iteration procedure, but since it has zero net flux, the calculation does *not* depend on P_S , although it does depend on the (as yet unknown) ζ . Finally ζ is determined by eliminating P_S from the horizontal momentum equations averaged over the fast horizontal variation. This formulation gives an extra advection in the phase equation by the solenoidal velocity field $\tilde{\mathbf{V}} = \nabla_{\perp} \times \hat{\mathbf{z}} \zeta$,

$$\partial_t \phi \rightarrow \partial_t \phi + \gamma(q) \tilde{\mathbf{V}} \cdot \mathbf{q}, \quad (8.29)$$

where $\gamma(q)$ is a weighting function, and a rather compli-

cated differential equation for ζ ensues:

$$\begin{aligned} \nabla_{\perp} \times \hat{\mathbf{q}}\alpha(q)(\hat{\mathbf{q}} \times \nabla_{\perp}\zeta) \cdot \hat{\mathbf{z}} - \nabla_{\perp} \cdot [\hat{\mathbf{q}}\beta(q)\hat{\mathbf{q}} \cdot \nabla_{\perp}\zeta] \\ = \hat{\mathbf{z}} \cdot \nabla_{\perp} \times [\sigma \mathbf{q} \nabla_{\perp} \cdot (\mathbf{q} A^2(q)) - \hat{\mathbf{q}}\tau_{\alpha}^{-1}(q)\nabla_{\perp} \cdot (\mathbf{q} B_{\alpha}(q))] \\ - \nabla_{\perp} \cdot [\mathbf{q}(\nabla_{\perp} \times \mathbf{q} B_{\beta}(q)) \cdot \hat{\mathbf{z}}] , \end{aligned} \quad (8.30)$$

where $\alpha(q)$, $\beta(q)$, $B_{\alpha}(q)$, $B_{\beta}(q)$, $\tau_{\alpha}^{-1}(q)$, and $\gamma(q)$ in Eqs. (8.29) and (8.30) are all functions of q , as well as Prandtl and Rayleigh numbers, which Newell *et al.* explicitly calculate. Note that in the first term on the right-hand side the authors separate out a term involving the real amplitude $A(q)$ of the ideal solution (defined with some convenient normalization), which they also tabulate. This is for convenience of approaching $R \rightarrow R_c$ where the earlier calculation of Cross and Newell (1984) applies; elsewhere this term could be subsumed in a redefinition of B_{α} .

An important application of the phase equation (8.24) is to display the long-wavelength stability boundaries of the Busse balloon. This is accomplished by considering small deviations from a straight roll pattern of wave vector \mathbf{q} which we take in the x direction

$$\phi = qx + \phi_1 \cos(\mathbf{Q} \cdot \mathbf{x}_{\perp}) , \quad (8.31)$$

with $\mathbf{Q} \ll 1$ the wave vector of the perturbation and ϕ_1 small. The mean drift \mathbf{V} may now be found explicitly in terms of ϕ_1 , and an expression for the growth rate of the perturbation is found,

$$\sigma(\mathbf{Q}) = D_{\parallel}(Q_x/Q_y)Q_x^2 + D_{\perp}(Q_x/Q_y)Q_y^2 . \quad (8.32)$$

The effect of the mean drift is thus to make D_{\parallel} and D_{\perp} functions of the ratio Q_x/Q_y (i.e. the direction of the wave vector of the perturbation), so that $\sigma(\mathbf{Q})$ is no longer analytic in Q_x and Q_y when $\mathbf{Q} \rightarrow 0$. Of course D_{\parallel} , D_{\perp} also depend on the wave vector \mathbf{q} of the rolls, as well as on Prandtl and Rayleigh numbers, and they may be calculated in terms of the b_i of Eqs. (8.21) and (8.24), or the equivalent parametrization of Newell and co-workers. The instabilities are given by $\sigma(\mathbf{Q})=0$. Note that for D_{\parallel} , D_{\perp} independent of Q_x/Q_y the instability boundaries are either purely longitudinal $Q_x \neq 0$, $Q_y = 0$ (i.e. Eckhaus) or transverse $Q_x = 0$, $Q_y \neq 0$ (i.e. zigzag). However once the full dependence is taken into account it is found that a new instability preempts the Eckhaus instability on the large wave-vector side, which is neither purely longitudinal nor purely transverse, i.e. it has both $Q_x \neq 0$ and $Q_y \neq 0$. (This is true for all Prandtl numbers, although the difference from Eckhaus is small for large Prandtl numbers.) This instability is the skew-varicose instability found previously in the Galerkin analysis (Busse, 1978). It may now be understood (Cross, 1983) as a modification of the long-wavelength Eckhaus instability, in which the transverse modulation causes a circulating mean drift, forbidden in a purely longitudinal instability, thus enhancing the instability. On the other hand mean drift effects tend to suppress the zigzag instability. From their expressions for the parameters in the phase equa-

tion Newell *et al.* are able to quantitatively reproduce the results of Busse (1978) for the Eckhaus, zigzag and skew-varicose instabilities.

B. Convection models

We have introduced the idea of studying *model equations* in Section III.C, motivated by the impracticality of numerically solving the full microscopic equations in the large systems showing the phenomena of this article. [For recent work that actually solves the full Boussinesq equations, but without attempting to reach quantitative numerical convergence, see Arter, Bernoff, and Newell (1987) and Arter and Newell (1988).] In this section we introduce specific models that have been used to understand convection. These fall into two classes: order-parameter models which are generalizations of the Swift-Hohenberg equation, and free-slip convection where the full Boussinesq equations (8.10) are used, but simplifying unphysical boundary conditions are imposed. A particular truncation of the free-slip equations, known as the Lorenz model (Lorenz, 1963), played a crucial role in the early development of ideas on chaos.

1. Order-parameter models

The Swift-Hohenberg equation was originally introduced to investigate noise-induced fluctuation phenomena very close to threshold $\varepsilon \ll 1$ (Swift and Hohenberg, 1977), and we have discussed its role as a rotationally invariant order parameter equation near threshold in Sec. IV.A.5. Since the equation incorporates the three basic features of type I_s pattern forming systems (onset at a nonzero wave number, growth, and nonlinear saturation), the same equation but with $\varepsilon \approx O(1)$ is useful as a *model system* of pattern formation in general two-dimensional systems, including Rayleigh-Bénard convection (this interpretation is originally due to Pomeau and Manneville, 1980, and Cross, 1982a). Let us write the model in the form

$$\tilde{\tau}_0 \partial_t \psi = \tilde{\varepsilon} \psi - \tilde{\xi}_0^4 (\nabla^2 + \tilde{q}_0^2)^2 \psi - \tilde{g}_0 \psi^3 , \quad (8.33)$$

and determine the parameters by requiring that the amplitude equation derived by the method of Appendix A1, should agree with Eq. (8.15) valid for real convection. A convenient choice is

$$\begin{aligned} \tilde{\tau}_0 &= \tau_0, \quad \tilde{q}_0 = q_0, \quad \tilde{\varepsilon} = (R - R_c)/R_c = \varepsilon , \\ \tilde{\xi}_0^4 &= \xi_0^2/4q_0^2, \quad \tilde{g}_0 = g_0/3 , \end{aligned} \quad (8.34)$$

where τ_0 , q_0 , ξ_0 , and g_0 are as in Eqs. (8.11b) and (8.16). Alternatively, Greenside and Coughran (1984) measured lengths in units of q_0^{-1} and eliminated the other constants by rescaling time and ψ to write Eq. (8.33) as

$$\partial_t \psi = \tilde{\varepsilon} \psi - (\nabla^2 + 1)^2 \psi - \psi^3 , \quad (8.35)$$

with

$$\tilde{\epsilon} = (4/q_0^2 \xi_0^2) \epsilon = 2.78\epsilon . \quad (8.36)$$

There are a number of ways, however, in which the Swift-Hohenberg equation fails to model convection even qualitatively: (i) the model has a Lyapunov function (3.28), so persistent dynamics, periodic or chaotic, is not possible; (ii) the stability diagram shows qualitative differences with the Busse balloon, for example failing to reproduce the general trend of the stable band towards longer wavelengths (smaller q) as the Rayleigh number is increased; (iii) the skew-varicose instability is absent. There may of course be other less obvious flaws. This has led to the search (Manneville, 1983; Greenside and Cross, 1985) for generalizations to remove a number of these imperfections.

The first class of generalizations may be written in the form

$$\partial_t \psi = [\epsilon - (\nabla^2 + 1)^2] \psi - \psi^3 - g_1 \psi (\nabla \psi)^2 + g_2 \psi^2 \nabla^2 \psi , \quad (8.37)$$

where the extra nonlinear terms allow more flexibility. For example in the Swift-Hohenberg equation the cross-roll instability occurs at a particular wave number $q_{CR}(\epsilon)$ which will not match convection even for small ϵ . The extra parameters g_1 or g_2 could be used to tune this boundary. For $g_2 = -g_1$ the equation remains potential: altering this relationship could be used to investigate increasing deviations from this condition. Manneville (1983) and Bestehorn and Haken (1990) have suggested that the choice $g_1 = 1$, $g_2 = 0$ gives a better description of the fluid nonlinearities, although there is no controlled expansion which justifies this choice over Eq. (8.33) which has $g_1 = g_2 = 0$.

A second class of models that generalize Eq. (8.33),

$$\begin{aligned} \partial_t \psi &= [\epsilon - (\nabla^2 + 1)^2] \psi + g_3 \nabla^2 \psi (\nabla \psi)^2 \\ &\quad + (3 - g_3) (\partial_i \psi) (\partial_j \psi) \partial_i \partial_j \psi , \end{aligned} \quad (8.38)$$

is motivated by the work of Gertsberg and Sivashinsky (1981) on Rayleigh-Bénard convection between poorly conducting plates. These authors carried out a systematic expansion in deviations from infinitely poor conductors in the one-dimensional case where the two nonlinear terms in Eq. (8.38) are identical and g_3 drops out. We might thus hope that the characteristic nonlinearities of the fluid equations [all involving spatial derivatives arising from the advection term $\mathbf{u} \cdot \nabla$ in Eqs. (8.10)] are better modeled by Eq. (8.38) than by (8.35). Indeed, the general trend of the stable band to longer wavelengths with increasing driving is reproduced. Note that the case $g_3 = 1$, which was shown to correspond to the case of convection between poorly conducting plates in two dimensions, is potential and leads to square cells for small ϵ . For $g_3 \neq 1$ the system is nonpotential and $g_3 = 3$ is a convenient value to use for nonpotential studies. However for $\epsilon > 1$ the $q = 0$ mode grows without bound, so this limits the range of study.

Both of these classes of models have smooth long-

wavelength expansions so they do not yield the skew-varicose instability. Following Siggia and Zippelius (1981b) and Cross (1983) who analyzed the importance of long-wavelength vertical vorticity or “mean drift” effects, Manneville (1983) and Greenside and Cross (1985) suggested adding an extra advection term caused by the mean drift. Specifically, they took (see the discussion in subsection VIII.A.5 above)

$$\partial_t \psi \rightarrow \partial_t \psi + (\mathbf{V} \cdot \nabla) \psi , \quad (8.39)$$

where \mathbf{V} is a solenoidal mean drift defined in terms of a vertical vorticity potential $\zeta(x, y, t)$

$$\mathbf{V} = (V_x, V_y) = (\partial_y \zeta, -\partial_x \zeta) . \quad (8.40)$$

The potential ζ is in turn driven by distortions of the order parameter field

$$\nabla^2 \zeta = \gamma [\nabla(\nabla^2 \psi) \times \nabla \psi]_z , \quad (8.41)$$

with γ a coupling constant. This rather complicated looking expression correctly reproduces the behavior derived in the amplitude equation to lowest order in ϵ by Cross (1983). Since the importance of mean drift effects grows as the Prandtl number is decreased, the value of γ should be a decreasing function of σ . For large γ the short wavelength components of the vertical vorticity given by Eqs. (8.39)–(8.41) seem to be too large to model low Prandtl number convection (for example the knot instability is enhanced more in the model than in the real system), so Greenside and Cross (1985) also considered models in which these high Fourier components are suppressed.

Clearly as the complexity of the model grows, the justification of the approach becomes more critical. Greenside and Cross suggested that a sensible way to discriminate between different models was to choose the one whose stability diagram most closely approximated the Busse balloon. In particular for pattern formation studies one might try to first reproduce the long-wavelength instabilities (Eckhaus, zigzag, and skew-varicose) and the general trend to smaller wave vector as ϵ increases. In this regard the second class of models, (8.38) with $g_3 = 3$, and the added mean drift term seems to be the optimal choice, namely

$$\partial_t \psi + (\mathbf{V} \cdot \nabla) \psi = [\epsilon - (\nabla^2 + 1)^2] \psi + 3 \nabla^2 \psi (\nabla \psi)^2 , \quad (8.42a)$$

$$\mathbf{V} = \nabla \times (\zeta \hat{\mathbf{z}}) , \quad (8.42b)$$

$$\nabla^2 \zeta = \gamma F [\nabla(\nabla^2 \psi) \times \nabla \psi]_z , \quad (8.42c)$$

where F is an operator that suppresses high Fourier components (for a specific representation see Greenside and Cross, 1985). We show the stability balloon for this model in Fig. 33, and this should be compared with the one for convection with Prandtl number $\sigma = 0.7$ in Fig. 32(a).

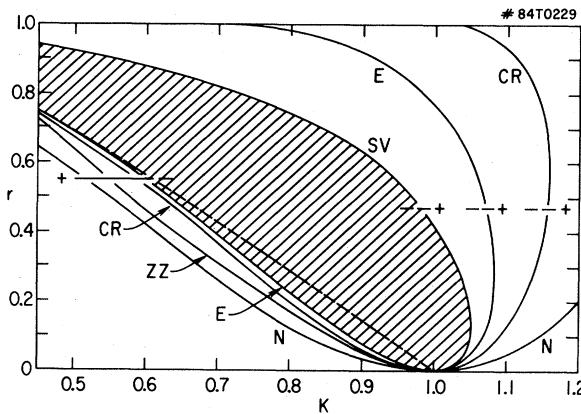


FIG. 33. Stability boundaries for a model of convection given in Eq. (8.42), with $\gamma=10$. (The reduced control parameter ϵ is denoted r in the figure.) The instability lines are labeled as in Fig. 32. The dashed line inside the stable region is the wave number selected in an axisymmetric pattern (see Sec. VIII.C.2.a). The + and - symbols near the lines indicate instability and stability, respectively. The similarity with Fig. 32(a) should be noted. (From Greenside and Cross, 1985.)

2. Free-slip convection

A widely used model system consists of the full fluid equations (8.10), but with the physical no slip boundary conditions ($\mathbf{u}=0$) at the upper and lower boundaries replaced by “no stress” or free slip, as in Eq. (8.6) above. This is at first sight an innocuous physical change, and it allows considerable analytic progress since the linear stability problem is separable and the eigenfunctions are simple sines and cosines, for example

$$\theta(x, z) \propto \cos(\pi z) \sin(\pi x / \sqrt{2}), \quad (8.43)$$

i.e. $q_0 = \pi / \sqrt{2}$, with a critical Rayleigh number $R_c = 27\pi^4/4 = 657.5$. Many calculations have first been performed in the framework of this much simpler problem, including the original derivation of the amplitude equation by Newell and Whitehead (1969) and Segel (1969). The calculation is presented in Appendix A and yields $\xi_0^2 = 8/3\pi^2$, $\tau_0 = (2/3\pi^2)(\sigma+1)/\sigma$, and for the normalization (8.17), $g_0 = \frac{1}{2}$. As first pointed out by Siggia and Zippelius (1981b), however, this change in the boundary conditions is far from harmless, and has enormous consequences for the qualitative behavior. The reason for this is clear from the discussion in Sec. IV.A.2.a.iii above: the free-slip boundary conditions introduce an extra conserved quantity, the mean horizontal momentum, and this drastically changes the long-wavelength slow dynamics. Since the flow is divergence free by the incompressibility assumption we need only consider the transverse part, i.e. we must include an additional slow vorticity mode, leading to a transverse velocity field that advects the convection pattern. This modifies the amplitude equation, even at lowest order, by

introducing the advection $(\mathbf{V} \cdot \nabla)(e^{iq_0x} A) \approx V_x iq_0 A$, so that $\partial_t A \rightarrow (\partial_t + iq_0 V_x) A$. The amplitude equation then becomes

$$\begin{aligned} \tau_0(\partial_t + iq_0 V_x) A &= \epsilon A + \xi_0^2 [\partial_x - (i/2q_0)\partial_y^2]^2 A \\ &\quad - g_0 |A|^2 A, \end{aligned} \quad (8.44a)$$

together with the equation for the vorticity $\Omega = -\nabla^2 \zeta$ from which $V_x = \partial_y \zeta$ can be deduced,

$$\begin{aligned} (\gamma \partial_t - \nabla^2) \Omega &= g_1 \partial_y [A^* (\partial_x - (i/2q_0)\partial_y^2) A + \text{c.c.}] , \\ &\quad (8.44b) \end{aligned}$$

with $\gamma = \sigma^{-1}$ and $g_1 = 3\pi^2/\sigma$. (The extra terms we have included, compared to Siggia and Zippelius may be formally of higher order but they display the physics more clearly; we have also used a different scaling, so the parameters γ and g_1 take on different values than quoted there.) As noted by Siggia and Zippelius (1981b), for the rigid boundary problem the corresponding corrections to the phase equation are given by putting a damping term into Eq. (8.44b), i.e. $\gamma \partial_t - \nabla^2 \rightarrow \eta_{\text{eff}}$.

The stability analysis, performed near threshold by Siggia and Zippelius (1981b) and later corrected by Busse and Bolton (1984), has quite different results in the free-slip case. For example for $\sigma < 0.543$ all states are unstable immediately above threshold, and states at the critical wave number are unstable just above threshold for all σ . Clearly the behavior near threshold of rigid boundary convection is not well described by the free slip model, since for rigid boundaries the $\sigma \rightarrow 0$ limit is completely smooth. On the other hand $\sigma \rightarrow 0$ is a complicated singular limit for the free slip case. Nevertheless Siggia and Zippelius suggest that the free slip model may qualitatively describe low Prandtl number convection between rigid boundaries away from threshold. The idea is based on the observation that in the strongly nonlinear regime boundary layers develop isolating the interior from the rigid boundaries (Jones *et al.*, 1976; Proctor, 1977; Clevenger and Busse, 1981). It is not clear, however, if this idea can be made the basis of a quantitative analysis. As in subsection VIII.B.1 above its validity can perhaps be judged by comparing the stability boundaries of free slip convection away from threshold (Bolton and Busse, 1985; Schnaubelt and Busse, 1989) with those for low Prandtl number rigid convection.

3. The Lorenz model

For completeness we mention here the Lorenz model (Lorenz, 1963) which was motivated by the problem of Rayleigh-Bénard convection. Although the model was extremely important in demonstrating the existence of chaos in coupled ordinary differential equations (cf. Sec. VII.B), we now know that the phenomena displayed by the equations have little quantitative overlap with actual phenomena in convection. The model is arrived at by a lowest nontrivial truncation in a Galerkin expansion of

the Boussinesq equations for free slip convection. Periodic lateral boundary conditions are assumed over a distance $L_x = m 2\pi/q_0$, with $q_0 = \pi/\sqrt{2}$, and with no spatial variation in the y direction. The modes retained are the linearly unstable temperature and vertical velocity modes (the horizontal velocity is then given by the incompressibility condition)

$$w_{11} = 2\sqrt{3}\pi X(t) \cos q_0 x \cos \pi z, \quad (8.45a)$$

$$\theta_{11} = 9\sqrt{3}\pi^3 Y(t) \cos q_0 x \cos \pi z, \quad (8.45b)$$

and the nonlinear temperature mode that couples to these linear modes through the Boussinesq equations,

$$\theta_{02} = (27\pi^3/4)Z(t) \sin 2\pi z. \quad (8.45c)$$

It is a curious feature of the free slip case that there is no coupling to any of the other possible quadratic nonlinear modes, so that a truncation at this order leads to three coupled nonlinear *ode*'s for rescaled variables $X(t)$, $Y(t)$, $Z(t)$

$$\partial_t X = \sigma(Y - X), \quad (8.46a)$$

$$\partial_t Y = rX - Y - XZ, \quad (8.46b)$$

$$\partial_t Z = -b(Z - XY), \quad (8.46c)$$

with $r = R/R_c$, $b = 8/3$. Since the derivation is just a second-order Galerkin truncation, in general such an approach will lead to equations that systematically include no more of the physics than the lowest order amplitude equation. In fact the possibility of slow phase and amplitude modulations is not allowed by Eqs. (8.45) so that the model should be qualitatively best in very small systems ($m = 1$). However because the free slip equations are separable, in this particular case the truncation leads to equations that correctly reproduce the *full* linear behavior of the unstable modes even at high frequencies, whereas the amplitude expansion is predicated on the assumption of slow time behavior even at the linear level. This makes the Lorenz model a useful semi-quantitative tool to investigate modulated convection (subsection VIII.F.5).

The interesting chaotic phenomena (Lorenz, 1963) appear in the Lorenz equations for $r \gtrsim 28$, where the second-order Galerkin expansion is certainly not valid as a representation of convection. Indeed it has been shown (Curry *et al.*, 1984) that if sufficient modes are retained for numerical convergence, but still restricted to no y spatial variation, then the chaos disappears. Low-order truncations including y variations were investigated by McLaughlin and Martin (1975).

C. One-dimensional patterns

We begin by discussing one-dimensional patterns, by which we mean systems for which the transverse dimension is sufficiently small so that the dependence on the transverse coordinate is uniquely prescribed. [Usually

this means $L_y = O(1)$.] Such systems are described by one-dimensional amplitude or phase equations, and by one-dimensional models, though from the point of view of the hydrodynamic equations (8.10) they of course correspond to three-dimensional solutions.

1. Verification of the amplitude and phase equations

Various experiments have been carried out to test or demonstrate the predictions of the perturbative methods described in Sec. IV.A.

a. Amplitude equation

The amplitude equation has the form of a Ginzburg-Landau equation at a thermodynamic phase transition, and predicts characteristic mean-field critical effects for length, time, and velocity scales. Each of these has been studied independently.

(i) The time scale for the amplitude to respond to a perturbation (e.g. a small change in ϵ) is $\tau = \tau_0 |\epsilon|^{-1}$ (Behringer and Ahlers, 1977; Wesfreid *et al.*, 1978).

(ii) The first harmonic of the velocity or temperature field varying as $\cos(q_0 x)$ grows as $\epsilon^{1/2}$ for $\epsilon > 0$ (Wesfreid *et al.*, 1978), and the convective heat current grows as ϵ (Behringer and Ahlers, 1977). The p th higher harmonics should vary as $\epsilon^{p/2}$, and this has been shown to lesser accuracy (Dubois and Bergé, 1978).

(iii) The length scale for magnitude changes varies as $\xi = \xi_0 |\epsilon|^{-1/2}$. This was verified for $\epsilon < 0$ by studying the spatial decay of convection induced by an imperfect sidewall, and for $\epsilon > 0$ by studying the suppression of convection over the length ξ near a perfect rigid sidewall (Wesfreid *et al.*, 1978). Since this is a dramatic confirmation of the predictions of the amplitude equation approach with wide consequences in pattern formation, we show the results in Fig. 34. Notice that the important fact that the envelope $A \rightarrow 0$ at the boundaries [Eq. (5.6)] is also confirmed.

It should be remarked that quantitative agreement is typically obtained both for the power law dependences and also (to the 10% accuracy of the experiments) for the prefactors, which are well known from theory.

b. Phase equation

The dynamics of long-wavelength perturbations of the positions of the rolls should be governed by the phase equation. Wesfreid and Croquette (1980) tested this in a cell of aspect ratio 30×5 and Prandtl number $\sigma = 492$. The straight roll pattern was perturbed by periodically injecting and extracting fluid through slots on the upper and lower plates in the middle of the cell. The spatial dependence of the longitudinal modulation of the phase was fit to the form

$$\phi(x, t) = \phi_0 \exp(-m_1 |x|) \cos(m_2 |x| - \omega t), \quad (8.47)$$

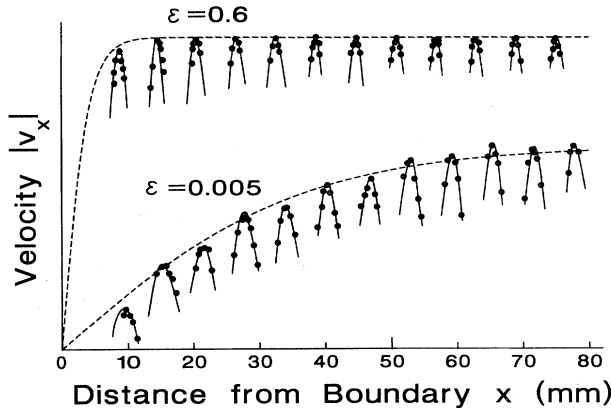


FIG. 34. Suppression of convection near a sidewall: comparison of predictions of amplitude equation with experiment, for two values of the reduced control parameter ϵ . Solid points represent measured values of the magnitude of the horizontal component of the fluid velocity at the mid-plane. The lines drawn through the points are guides to the eye to display the roll structure. The dashed lines are the predictions of the amplitude equation $A = A_0 \tanh(x/\sqrt{2}\xi)$ with $\xi = \epsilon^{-1/2}\xi_0$ and $\xi_0 = 0.385$, with the asymptotic amplitude A_0 fit to the data. (Adapted from Wesfreid *et al.*, 1978.)

where the phase diffusion equation (4.70) yields $m_1 = m_2 = (\omega/2D_{\parallel})$. The experiments were consistent with these forms, and gave a value of D_{\parallel} consistent with theoretical expectations.

Pocheau *et al.* (1987), instead of looking at the frequency response, studied the decay of a spatial modulation with wave vector $\mathbf{Q} = (Q_x, Q_y)$ on a straight roll pattern of wave number q . The initial pattern was set up by thermal masking techniques. An exponential decay of the modulation is expected with a decay rate

$$\tau^{-1} = D_{\parallel} \left[Q_x^2 + \frac{q - q_0}{q_0} Q_y^2 \right], \quad (8.48)$$

where Eq. (4.72) for D_{\perp} near threshold has been used, so mean-drift effects do not enter at this order. Although the precision was rather low ($\sim 30\%$) the quadratic dependence on Q and the linear dependence on the background wave number q were verified, and the measured values of D_{\parallel} were consistent with theoretical expectations.

c. Forced phase drift by mean flows

Since spontaneously generated mean flows are expected to play an important role in the phase dynamics of convective rolls (cf. subsection VIII.A.5), it is interesting to attempt to measure their effect directly. Pocheau *et al.* (1987) accomplished this by imposing an externally driven flow, injecting and removing fluid at a constant flow rate at diametrically opposed points in an annulus. We expect the one-dimensional equation for the phase

around the annulus to be modified to

$$\partial_t \phi + V \partial_x \phi = D_{\parallel}(q) \partial_x^2 \phi, \quad (8.49)$$

where V is determined from Eq. (8.24b), with P_S now the contribution from the externally applied pressure, and small deviations from a uniform background wave number q have been assumed. Since this V involves a complicated overlap integral between the Poiseuille flow and the convection eigenfunctions, it is strictly speaking not the simple mean velocity U used by Pocheau *et al.* in their analysis, although the two quantities are proportional. For stationary patterns Eq. (8.49) predicts a linear variation of the wave number around the annulus, compressed towards the outflow and stretched near the inflow, and this was clearly observed for small U . If U is increased the inhomogeneity grows (Fig. 35), and eventually time dependence occurs when the local wave number at the extreme points becomes Eckhaus unstable. The stability boundary agrees well with the predictions. In addition, measuring U directly from the initial advection of an unmodulated pattern allowed a determination of $D_{\parallel}(q)$, again giving good agreement to the 10% accuracy of the experiment. Croquette *et al.* (1986a,b) have also

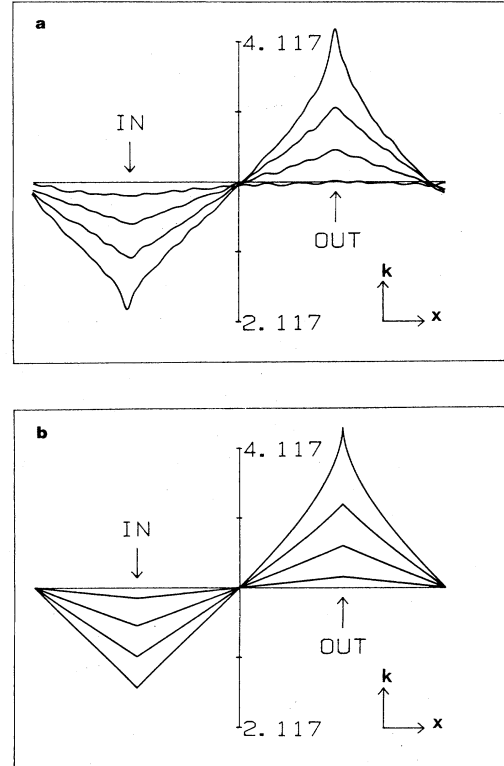


FIG. 35. Roll compression forced by an imposed fluid flow. Local wave vector q (labeled k in the figure) at position x around an annulus for a series of flow rates. The arrows marked in and out indicate filling and outflow holes. (a) Experiment, for $\epsilon = 0.517$ and velocities (increasing from bottom trace to top trace): $U = 0.084 \text{ mm/s}, 0.336, 0.588, 0.840$. (b) Theoretical results obtained from Eq. (8.49), for $\epsilon = 0.5$: $U = 0.075 \text{ mm/s}, 0.275, 0.500, 0.716$. (From Pocheau *et al.*, 1987.)

identified the mean flows in non-axisymmetric convection (see below), by following the motion of a line of tracer dye.

2. Wave-vector selection

The general ideas on wave-vector selection discussed in Sec. VI.A have been tested in considerable detail for fluid convection by experiment, by calculations on model equations and by quantitative calculations of specific results for the full fluid equations. Although certain gaps in our knowledge remain, a rather clear and coherent picture has emerged, with generally good agreement between theoretical expectations and experimental or numerical results. We can now say that the fundamental question of wave-vector selection in simple patterns is well understood.

a. Axisymmetric convection

Perhaps the most ideal “one-dimensional” situation in convection is an axisymmetric pattern in a cylindrical

geometry, where there is dependence only on the radial horizontal coordinate. The conditions for this situation to be stable in large geometries are rather complicated, and will be discussed in subsection VIII.D.1.a below. Theoretically, axisymmetric patterns in large geometries are predicted to possess a unique radial wave number q_f asymptotically far away from the center. If there is a smooth gradient expansion this wave number is the value for which $D_\perp = 0$, which is also the boundary of the zig-zag instability. If mean drift effects are important this is no longer the case. These general conclusions were confirmed by numerical work on the model equations (8.33) and (8.38) by Cross *et al.* (1986).

For the specific case of convection, quantitative predictions were made by Manneville and Piquemal (1982) for the slope near onset $(q_f - q_0)/\varepsilon$ for $\varepsilon \rightarrow 0$, and by Buell and Catton (1986a) for $q_f(\varepsilon)$ at general ε . The results for different values of the Prandtl number are compared with experiment in Fig. 36(a). There is considerable hysteresis in the experimental data, indicating deviations from the

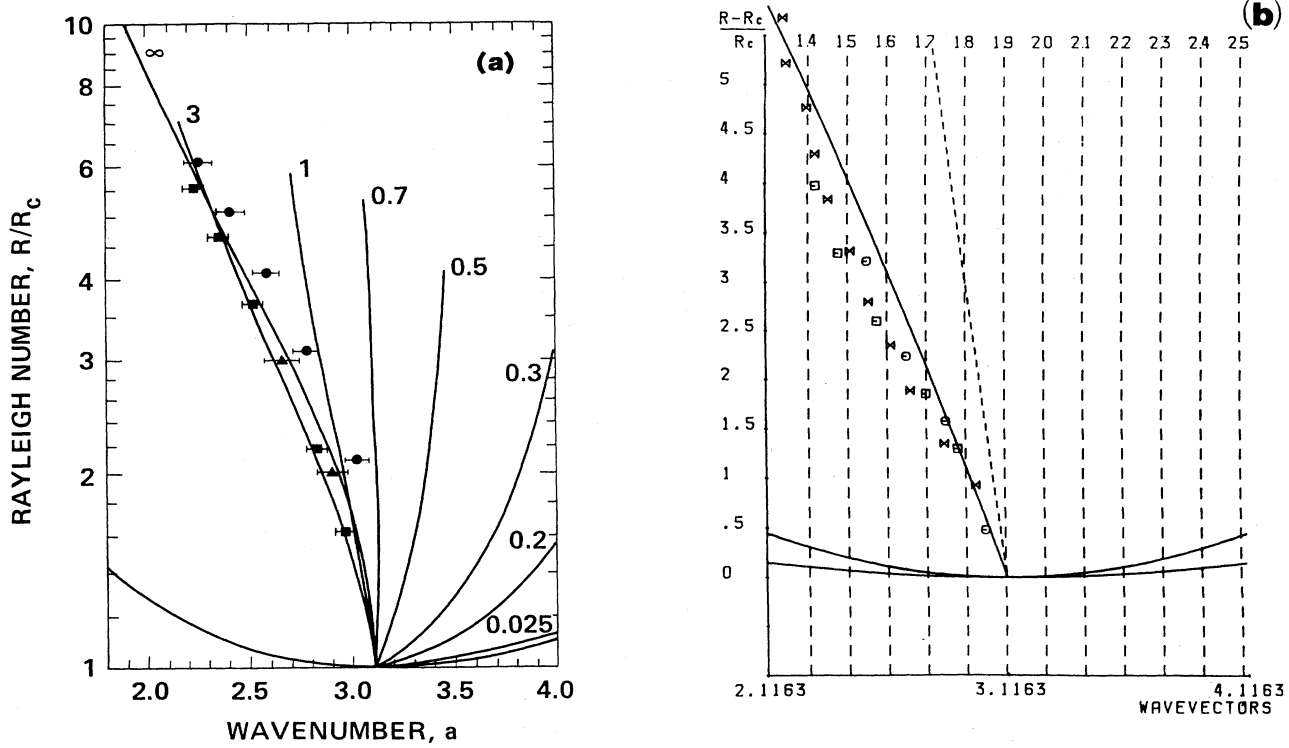


FIG. 36. Wave vector selection in Rayleigh-Bénard convection. (a) Wave vector selected in axisymmetric convection as a function of reduced control parameter. Lines are prediction of Buell and Catton (1986a) for various Prandtl numbers σ indicated next to each line (unlabeled lowest line is neutral stability). Points are experimental data: triangles $\sigma = 6.1$ (Steinberg *et al.*, 1985); circles $\sigma = 511-916$ (Koschmieder and Pallas, 1974); squares $\sigma = 14$ (Croquette and Pocheau, 1984). Notice that all the data are at rather high Prandtl numbers and are consistent, within the scatter, with the $\sigma = \infty$ result. The predicted strong dependence on low Prandtl numbers remains untested. (From Buell and Catton, 1986a.) (b) Wave vector selected by defects in Rayleigh-Bénard convection ($\sigma = 70$). Circles, zero dislocation climb velocity (mean of wave vectors above and below the stationary defect); squares, same as circles but zero velocity point determined from fit to $v(q)$ curves; crosses, wave vector of central set of rolls bounded by two grain boundaries. The solid line shows the initial slope of the zig-zag instability line $q_z(\varepsilon)$, and the tilted dashed line the initial slope of the wave vector selected in axisymmetric convection $q_f(\varepsilon)$. The vertical dashed lines indicate the wave vectors for integer numbers of rolls shown on the top scale. (From Pocheau and Croquette, 1985.)

limit of an asymptotically large system, particularly in the smaller cell of Steinberg *et al.* (1985) (the midpoint of the measured values is plotted). Nevertheless the agreement must be considered very satisfactory, except for the early experiments of Koschmieder and Pallas (1974). Initial inferences by Croquette and Pocheau (1984) that agreement was less good resulted from comparison of $\epsilon \sim 1$ results with the small- ϵ calculation of Manneville and Piquemal (1983). From the more general calculations it turns out that the initial slope is much more sensitive to Prandtl number in the range $3 < \sigma < \infty$, than the curves for large ϵ . The dramatic dependence predicted for small Prandtl number has not been tested experimentally, and to do so will require a scheme to eliminate the instability that breaks axisymmetry (e.g. a hot wire at the center).

b. Selection by sidewalls

In general, if convection rolls approach a sidewall in the parallel orientation, the amplitude of convection is suppressed near the sidewall. This "weak spot" allows the number of convective rolls in the system to relax and provides a wave-number selection mechanism as discussed in Sec. VI.A. Near threshold the predictions of the extended amplitude equation (5.22) is that the wave number will be confined to a reduced band given by Eqs. (5.24) and (5.25), where α and β characterize the effect of the fluid boundary conditions on the amplitude, and the parameters b_i ($i = 1$ to 5) are numerical coefficients in the higher-order amplitude equation. Cross, Daniels, Hohenberg, and Siggia (1980, 1983a) calculated the constants b_i for free slip horizontal boundaries and α and β for the same model, but with rigid sidewalls (zero velocity boundary conditions) of arbitrary thermal conductivity K_w and thickness t . To date these already laborious calculations have not been extended to the realistic no-slip case, and so only predictions of unknown reliability can be made. The free slip calculations lead to the restriction of the band of wave numbers given by Eq. (5.25) with

$$\eta = (32\sqrt{3})^{-1} (5 + 21\sigma^{-1} + 40\sigma^{-2}) \times (1 + 4\bar{\mu} + 6\bar{\mu}^2)^{-1/2}, \quad (8.50a)$$

$$|\beta| = [(1 + 4\bar{\mu} + 6\bar{\mu}^2)/6\pi^2]^{1/2}, \quad (8.50b)$$

where

$$\bar{\mu} = (1 + 2\mu/\pi)^{-1}, \quad (8.50c)$$

$$\mu = (K_w/K_f) \pi \tanh(\pi t_w), \quad (8.50d)$$

K_w and K_f are the wall and fluid thermal conductivities and t_w is the thickness of the wall.

The constants b_i and α, β are more easily evaluated for various model equations (Cross *et al.*, 1983a; Kramer and Hohenberg, 1984; Hohenberg *et al.*, 1985), but no numerical simulations have been done to test the predic-

tions of the perturbation analysis of Cross *et al.* (1983a), or its range of applicability. Numerical work on the full fluid equations with rigid boundaries, but with the flow restricted to be two dimensional (i.e. one "slow" dimension) has been carried out by two groups. Mitais *et al.* (1986) investigated aspect ratio $L = 15$ and Prandtl numbers 0.71 and 0.071, and both thermally insulating and conducting sidewalls, and Arter *et al.* (1987) studied $L = 16$, $\sigma = 2.5$ with insulating sidewalls. The qualitative picture of a restricted band of wave numbers delineated by roll gain or loss near the sidewalls is confirmed. Mitais *et al.* find a much narrower band for conducting than for insulating sidewalls as was also found by Cross *et al.*, but little dependence on the (low) Prandtl number. From the results for those aspect ratios the linear ϵ dependence of the bands predicted by the perturbation theory cannot be discerned. Mitais *et al.* also generalized the calculation to three dimensions in a fairly small box (aspect ratios 6×3) and found the band of solutions further restricted by three-dimensional instabilities.

The only experiment that has been done on Rayleigh-Bénard convection in this connection is by Martinet *et al.* (1982, 1984) in air ($\sigma = 0.7$) with containers of aspect ratios 18×6 and 12×6 having good conducting sidewalls. One problem that arises in comparing with the theory is that the assumption made in the calculation of a one-dimensional spatial variation may never be justified in rectangular geometry. Indeed, in narrow cells the spatial variation of the amplitude in the y direction may not be neglected, although a one-dimensional amplitude equation with different coefficients may be used for the structures in the x direction (Daniels and Ong, 1990), and in wide cells roll curvature especially near the endwalls, or the cross-roll or skew-varicose instabilities, may become important. Indeed Martinet *et al.* found that on increasing ϵ the change in the number of rolls was mediated by three-dimensional disturbances, although on decreasing ϵ the flow remained close to two dimensional. The experiment does, however, show a restricted band of solutions near threshold ($\epsilon < 1$), which is in fact remarkably consistent with the estimates from free slip convection by Cross *et al.*, but apparently not consistent with the 2D numerical work of Mitais *et al.* Probably three-dimensional effects are important and the agreement with Cross *et al.* is fortuitous, but clearly more work on cells of various sizes is needed for a quantitative comparison. Perhaps the best geometry for experimental investigation is the cylindrical one, where the wave number of stationary axisymmetric patterns (if they can be stabilized!) should be consistent with the predicted band at large radii, or a narrow rectangular container where however the theoretical predictions will be harder to calculate.

c. Dislocation climb

The role of dislocation climb in an otherwise one-dimensional pattern of rolls was discussed in Sec. VI.A.1. In some elegant experiments Pocheau and Croquette

(1984) (see also Croquette, 1989) investigated this phenomenon in convection cells (Fig. 19). They established a single dislocation in an otherwise parallel roll system in a rectangular cell using thermal imprinting, by shining an intense beam of light through an optical mask onto the sensitive, slightly subcritical system, and then raising the Rayleigh number to allow the pattern to grow. [This method was pioneered by Chen and Whitehead (1968) in their study of a line of dislocations.] Pocheau and Croquette also had a thermal wire at the longitudinal sidewalls to eliminate the cross-roll boundary instability. For a range of roll numbers n and $n+1$ in the bottom and top half of the cell, the velocity of the dislocation climb up or down the rolls was measured as a function of the Rayleigh number. This yields discrete values of $q_d(\epsilon)$ where q_d is taken as the mean wave number (i.e. for $n+1/2$ rolls) and ϵ is the value at which the dislocation is stationary. In addition the climb velocity could be measured as a function of the deviation from the stationarity condition. Similar experiments were carried out numerically on model equations (8.35) and (8.42) by Tesauro and Cross (1986).

Theoretically, it is expected that near threshold the wave number is given by

$$\frac{q_d(\epsilon) - q_c}{q_c} = 0 \times \epsilon^{1/2} + q'_d \epsilon + \dots . \quad (8.51)$$

A scheme for calculating q'_d was proposed by Pomeau *et al.* (1985), but it has not been implemented for Rayleigh-Bénard convection. The values of $q_d(\epsilon)$ measured by Pocheau and Croquette (1984) for Prandtl number $\sigma=70$ are shown in Fig. 36(b). In subsequent measurements Croquette (1989) has found a shift to smaller q at $\sigma=0.7$. The analogous tendency was seen in the numerical work of Tesauro and Cross, where a shift to smaller q was observed as the coupling to the vorticity flow was increased. Also in that work when the vorticity coupling was zero an analytical calculation of q'_d gave

$$q_d \approx q_0 (1 - \epsilon/4 \dots) , \quad (8.52)$$

which was consistent with the simulation results. The exact dependence of the climb velocity on deviations from the stationarity condition $q_d(\epsilon)$ was hard to extract, either from the numerics or the experiments, but the two were at least qualitatively consistent.

d. Grain boundaries

A wave-number selection mechanism by perpendicular grain boundaries was proposed and implemented experimentally by Croquette *et al.* (1983). The required pattern (see Sec. VI.A.1) was again imposed by a thermal mask. As discussed in Sec. V.B.2 the situation is really quite complicated, depending on whether new y rolls may be produced by the motion or only continuous stretching occurs. In the latter case a unique wave number q_x of the rolls normal to the x direction is expected, which

may however depend on the wave number q_y of the rolls normal to y . This latter effect was not investigated experimentally, and Croquette *et al.* obtained a selected $q_{gb}(\epsilon)$ for Prandtl number 70 that was, within their resolution, identical to the wave numbers selected by dislocation motion [see Fig. 36(b)].

Tesauro and Cross (1987) investigated the phenomena for the models introduced in subsection VIII.B.1 above. For the Swift-Hohenberg model (8.35) and for $\epsilon < 0.5$ a stationary solution was obtained only for $q_x \approx 1.0$, $q_y \approx 1.0$. The value of q_x is consistent (within errors) with the value minimizing the potential. For Eq. (8.38) with $g_3 = 3$ a stationary state was obtained for $q_x \approx 1.00 - 0.53\epsilon$, consistent with the amplitude equation result of $q_x = 1 - \epsilon/2$ for this model, and $q_y \approx 1 - 0.12\epsilon$, although the data were also consistent with a small stationary band in q_y (of width up to 0.02) as expected from the pinning effect of the front discussed in Sec. IV.A.4. Note that the selected value of q_x is quite different from the value selected by dislocations for this model. A complete investigation of the dynamics was precluded by the very long computer runs needed, and it was not clear that the long-time asymptotic limit was ever reached.

e. Ramps

Wave-number selection by slow ramps in the Rayleigh number has been studied both theoretically (Eagles, 1980; Kramer and Riecke, 1985; Buell and Catton, 1986b) and experimentally (Rehberg *et al.*, 1987). Buell and Catton implemented the theoretical scheme of Sec. IV.A.2.d for ramps in the temperature of rigid upper and lower boundaries to calculate the unique selected wave number $q_r(\epsilon, \sigma)$. This is important work since it shows a clearly resolved difference with the same authors' calculation of axisymmetric convection, thus conclusively demonstrating the nonuniqueness of wave-vector selection, although the overall trends are quite similar for both mechanisms. Kramer and Riecke calculated the selected wave numbers for various different combinations of temperature and thickness ramps in the free slip model, and showed that any wave number in the Eckhaus stable band could be selected by a suitable choice of ramps.

f. Front propagation

The velocity of front propagation in Rayleigh-Bénard convection has been investigated experimentally by Fineberg and Steinberg (1987) and numerically by Getling (1983) and by Lücke *et al.* (1987a,b). In the experiments convection was initiated at the ends of a long (aspect ratio 27) cell. (The long sidewalls had fins attached so that convection was not directly forced there.) The measured velocity near threshold ($\epsilon < 0.1$) was $v/\epsilon^{1/2} = 2.01 \pm 0.02$, in excellent agreement with the linear selection predictions from the amplitude equation quoted in Eq. (6.27a) (note, here $c_1 = 0$). Similar agreement was found

in the numerical work. However the measured wave number of the rolls produced behind the front was clearly different from the critical wave number q_0 even for $\epsilon \rightarrow 0$, and then showed a decrease proportional to $\epsilon^{1/2}$. This should be contrasted with the general theoretical expectation of a linear dependence on ϵ on approaching the critical wave number at threshold, as obtained for example from Eq. (6.29c) above.

g. Competing mechanisms

The general conclusion from the body of work described in subsections a-f is that, except in the special case of potential systems, different wave-number relaxation mechanisms lead to different selected wave numbers: there is no “preferred” wave number. This is clearly true in the model calculations of Cross *et al.* (1986) shown in Fig. 37. For the actual Rayleigh-Bénard system the conclusion rests on the numerical work of Buell and Catton (1986a,b) mentioned above, who show that different wave numbers are selected by a control parameter ramp and by an axisymmetric geometry for all Prandtl numbers (including $\sigma \rightarrow \infty$). Experiments have not yet been precise enough to completely resolve the different selected wave numbers, but this is not surprising based on the rather small differences found theoretically for the two mechanisms.

As we have seen in Sec. VI.A.1.a.vi, if two wave-

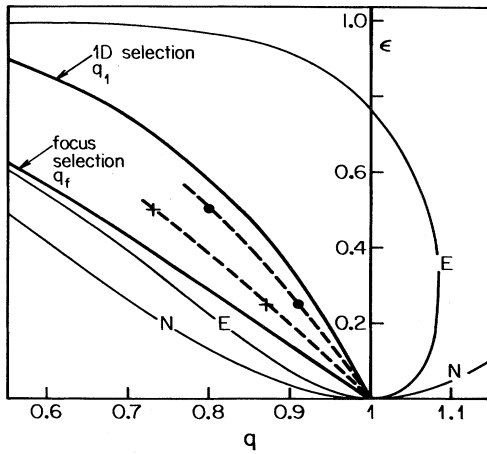


FIG. 37. Wave vector q selected in a model of convection [Eq. (8.42), $\gamma=0$] as a function of control parameter ϵ . Heavy lines show results for focus selection q_f and for the midpoint q_1 of the band selected in a one-dimensional geometry by ends with boundary conditions $\psi=\partial_x\psi=0$. The wave vector q_d selected by zero dislocation climb velocity is denoted by solid circles, and the wave vector q_{gb} selected by zero grain boundary motion is denoted by crosses. The values of q_1 and q_f were calculated analytically. The circles and crosses were obtained by numerical simulations. Dashed lines are drawn through the numerical points and the small ϵ analytically calculated asymptotic slopes. E and N label the Eckhaus and neutral stability boundaries, respectively. (From Cross *et al.*, 1986.)

number relaxation mechanisms leading to incompatible wave numbers are both operating, then a persistent dynamics is expected, corresponding to a drift of rolls from the local region selecting the smaller wave number to the region selecting the larger one. This phenomenon has been seen in convection in two different one-dimensional situations, and has also been proposed as the mechanism behind the persistent dynamics in a more complex pattern in a numerical simulation. Rehberg *et al.* (1987) experimentally demonstrated the persistent phase dynamics forced on a parallel roll state by two different control parameter ramps. The wave numbers selected by the individual ramps were not measured, so no quantitative comparison with theory could be made, but a periodic motion corresponding to the steady (or unsteady if the ramp had a sharp corner) drift of the rolls was seen. Tuckerman and Barkley (1988) and Barkley and Tuckerman (1989) observed a similar state in their numerical simulations of the full fluid equations constrained to axisymmetry in a cylindrical cell of aspect ratio 5. For Prandtl number 10, and with good conducting sidewalls, a periodic state was seen with rolls drifting towards the center and annihilating there. Interestingly, no such state was found for insulating sidewalls. We would interpret the dynamics as arising from the incompatibility of the wave number selected by the focus and the band selected by the outer sidewalls. We note that the latter is indeed narrower for conducting sidewalls in the free slip model calculation although a larger aspect ratio might be necessary for the asymptotic phase dynamics analysis to be valid quantitatively. This motion had previously been predicted for free slip convection by Pomeau *et al.* (1985) and was also found in a numerical simulation of Eq. (8.38) with $g_3 = 0$ by Cross *et al.* (1986). Experimental realization of the above effect will depend on the delicate question of the stability of axisymmetric convection to non-axisymmetric perturbations.

D. Two-dimensional patterns

1. Simple versus natural patterns: The effects of forcing

In a given two-dimensional geometry for a convection experiment, often many different possible steady state and stable patterns are found, some of them simply reflecting the symmetries of the container, and others possessing many defects and a more disordered appearance (i.e. what we have called natural patterns). In addition we would like to know how the convecting solution grows from the uniform state which remains a solution for all times in the ideal system. The physics responsible for initiating the growing nonlinear solution, and the resulting pattern selection, have been studied carefully and systematically in convection, particularly in intermediate aspect ratio cylinders ($L = 5$ to 10). This is a study of how very delicate phenomena can drastically affect the nonlinear state due to the extreme sensitivity of the system to small perturbations in the vicinity of the bifurca-

tion. For example in these cylindrical geometries we may have concentric roll patterns, largely straight roll patterns, or quite disordered states.

a. Imperfect bifurcations and static forcing

The condition for a perfect bifurcation at the (shifted) critical Rayleigh number in a finite geometry is that the zero velocity conducting state remain a solution even when the physical boundary effects at the lateral sidewalls are included. A moment's thought shows that a horizontally uniform vertical temperature gradient does not require that the thermal conductivity of the sidewalls be exactly matched to the fluid (which would be difficult to arrange): instead a sharp bifurcation demands only that the sidewalls should be of uniform thickness, thermally well attached to the top and bottom plates that are perfect conductors, and should lose no heat to the environment outside. (The system should also of course be geometrically perfect, i.e. flat upper and lower plates and vertical sidewalls.)

Modifying any of these constraints will lead to an imperfect bifurcation: typically, thermal imperfections will lead to thermal inhomogeneities near the sidewalls, which are then inconsistent with zero flow. On the other hand in experiments where reproducible cylindrical rolls are desired, thermal imperfections such as a hot wire running around the outer wall may be deliberately added. The growth of the convecting solution near threshold is then described by the amplitude equation with an inhomogeneous boundary condition. For axisymmetric states it turns out that the appropriate representation is (Brown and Stewartson, 1978)

$$U = r^{-1/2} A(r) U_0(z) e^{iq_0 r}, \quad (8.53)$$

with the amplitude equation

$$\tau_0 \partial_t A = \epsilon A + \xi_0^2 \partial_r^2 A - (g_0 L / r) |A|^2 A. \quad (8.54)$$

The effects discussed above may be described by the inhomogeneous boundary conditions (see Sec. V.A.1)

$$A(r = L) = a_1, \quad (8.55)$$

on the amplitude satisfying the radial equation (8.54), with a_1 determined by the strength of the imperfection. Close enough to threshold a one-mode projection can be made, and in view of the inhomogeneous boundary condition the analogue of Eq. (5.10) may be written as

$$A(r) = a_1 r / L + \bar{A}_1(t) \cos(\pi r / 2L). \quad (8.56)$$

It follows that

$$\partial_t \bar{A}_1 = (\epsilon - \epsilon_c) \bar{A}_1 - \bar{g}_0 \bar{A}_1^3 + f(t), \quad (8.57)$$

where

$$\epsilon_c = \pi^2 \xi_0^2 / 4L^2,$$

$$f(t) = f_0 = \epsilon a_1 (2/L) \int_0^L dr r \cos(\pi r / 2L),$$

and \bar{g}_0 is the nonlinear coefficient.^{8.1} In evaluating the driving force f we have only retained the most important term coming from a_1 . Equation (8.57) leads to an imperfect bifurcation, with small amplitude convective heat flow for $\epsilon \lesssim \epsilon_c$. These equations may be solved for the evolution of the axisymmetric solution, forced by a_1 via f_0 , as it grows to large amplitudes when ϵ is raised through ϵ_c [see for example Ahlers *et al.* (1981) for numerical solutions of Eq. (8.57)]. Presumably for large L the pattern would be established in the interior by front propagation from the region of convection near the sidewall existing below ϵ_c .

The thermal imperfection of course remains in the nonlinear state in this case. Although small imperfections will not appreciably change coarse features such as the convective heat flow, they may well influence stability properties. Thus thermal sidewall forcing may be used to maintain a stable axisymmetric pattern where it would otherwise be unstable to cross rolls near the sidewall and lead to more complicated patterns. It is also now believed that (unplanned) thermal imperfections were responsible for the concentric rolls observed by Koschmieder and Pallas (1974) for parameters where more recent experiments find nonaxisymmetric states. Note however that in experiments of Steinberg *et al.* (1985) every effort was made to achieve ideal sidewalls, yet steady state axisymmetric convection was observed for $0.16 < \epsilon < 8$, so that this may in fact be a stable state for some parameter values.

b. Transient forcing

Even when the imperfections discussed in the preceding subsection are absent, so that the bifurcation is perfect for static measurements, forcing of the pattern may occur as a transient in real experimental situations, when the control parameter is raised through threshold at a (necessarily) finite rate. If the lateral sidewalls in the convection apparatus have a different thermal diffusivity than the liquid, then the transient conducting thermal profile when the Rayleigh number is increased will no longer have a uniform spatial dependence on the horizontal coordinate, and will not be consistent with the ideal $\mathbf{u} = 0$ state. Again we may obtain the amplitude equa-

^{8.1}This is actually rather tricky in a cylindrical geometry, since the fields apparently diverge as $r^{-1/2}$ for the solution (8.56) when $r \ll L$, and this leads to $\bar{g}_0 = 2g_0 \int_0^L dr r^{-1} [(\cos \pi r / 2L)]^4 \sim (2g_0 \ln L)$. This means that the heat flux $\sim \bar{A}_1^2$ is suppressed by a term of order $(\ln L)^{-1}$ for this mode, and goes to zero in the large L asymptotic limit. In this case the second mode $A \sim A_2 \sin(\pi r / L)$ would yield the first observable convection. However for the values of L of order 5 to 10 used it is probably the mode with large amplitude at the center that is seen (see Ahlers *et al.*, 1981).

tion in the one-mode simplification, where now for slow variations of the control parameter we have

$$f(t) = f_0 + f_1 \beta(t), \quad (8.58a)$$

where

$$\beta = d\epsilon/dt, \quad (8.58b)$$

f_1 is a parameter which may be estimated by projecting the transient conduction solution onto the unstable mode (Ahlers *et al.*, 1981), and f_0 is the same term as in Eq. (8.57) to account for static imperfections. [Equation (8.58) is an expansion in β . The term retained can be considered to be the first correction to the adiabatic slaving of the fast modes used in deriving the amplitude equation.]

c. Stochastic forcing

As mentioned in Sec. VI.A.2 intrinsic stochastic forcing will arise from the thermal fluctuations left out of the hydrodynamic equations we have been considering. An appropriate theoretical framework for studying this forcing is provided by adding Langevin noise sources to the hydrodynamic equations (8.3) (Landau and Lifshitz, 1959)

$$\partial_t \mathbf{u} + \mathbf{u} \cdot \nabla \mathbf{u} = -\nabla(P/\rho) + \nu \nabla^2 \mathbf{u} - g\alpha T \hat{\mathbf{z}} + \nabla \cdot \mathbf{s}, \quad (8.59a)$$

$$\partial_t T + \mathbf{u} \cdot \nabla T = \kappa \nabla^2 T - \nabla \cdot \mathbf{q}_T, \quad (8.59b)$$

and assuming the noise to be Gaussian with correlations

$$\begin{aligned} \langle s_{ij}(\mathbf{x}, t) s_{\ell m}(\mathbf{x}', t') \rangle &= (k_B T / \rho) 2\nu \delta(\mathbf{x} - \mathbf{x}') \delta(t - t') \\ &\times (\delta_{i\ell} \delta_{mj} + \delta_{im} \delta_{j\ell}), \end{aligned} \quad (8.60a)$$

$$\begin{aligned} \langle q_{Ti}(\mathbf{x}, t) q_{Tj}(\mathbf{x}', t') \rangle &= (k_B T^2 / C_v) 2\kappa \delta(\mathbf{x} - \mathbf{x}') \delta(t - t') \delta_{ij}, \end{aligned} \quad (8.60b)$$

where C_v is the constant volume specific heat per unit volume. These terms provide a noise source in the corresponding Swift-Hohenberg equation (8.33), which becomes (Swift and Hohenberg, 1977; Hohenberg and Swift, 1992)

$$\begin{aligned} \tau_0 \partial_t \psi(\mathbf{x}, t) &= \epsilon \psi - (\xi_0^2 / 4q_0^2)(\nabla^2 + q_0^2)^2 \psi \\ &- (g_0/3)\psi^3 + \xi(\mathbf{x}, t), \end{aligned} \quad (8.61)$$

where the Gaussian noise (given by projecting the noise in Eqs. (8.59) onto the unstable mode) has correlations

$$\begin{aligned} \langle \xi(\mathbf{x}, t) \xi(\mathbf{x}', t') \rangle &= 2F_{\text{th}} \tau_0 (\xi_0 / 2q_0) \delta(\mathbf{x} - \mathbf{x}') \delta(t - t'), \end{aligned} \quad (8.62)$$

with

$$F_{\text{th}} = \left[\frac{k_B T}{\rho d \nu^2} \right] \frac{2\sigma q_0}{\xi_0 \tau_0 R_c}. \quad (8.63)$$

This result is essentially the one found by Graham (1974) and Swift and Hohenberg (1977) for free-slip horizontal boundaries (with correction of minor errors), and remarkably it is also identical to the value found by van Beijeren and Cohen (1988) for the rigid case (see Hohenberg and Swift, 1992 for details). The order of magnitude of the noise strength F_{th} is set by the small parameter $k_B T / \rho \nu^2 d \approx 10^{-9}$, which represents the ratio of the typical energy $k_B T$ of a thermal fluctuation to the *dissipative* energy $\rho \nu^2 d$ in one convective cell (i.e. a kinetic energy density $\rho \nu^2 / d^2$ times the volume d^3). As discussed in Sec. VI.D, it is the smallness of this ratio, due to the macroscopic scale of the convection phenomenon, which makes thermal fluctuation effects particularly difficult to observe (Zaitsev and Shliomis, 1970; Graham, 1974; Swift and Hohenberg, 1977). As mentioned in Sec. VI.D, the stochastic Swift-Hohenberg equation (6.48) can be roughly approximated near threshold by a one-mode model (Ahlers *et al.*, 1981; Hohenberg and Swift, 1992)

$$\tau_0 \partial_t \bar{A} = \epsilon(t) \bar{A} - \bar{A}^3 + \bar{f}(t), \quad (8.64a)$$

$$\langle \bar{f}(t) \bar{f}(t') \rangle = 2\bar{F} \tau_0 \delta(t - t'), \quad (8.64b)$$

with \bar{F} given by Eq. (6.52).

d. Experimental investigations

The relative importance of the various forcing terms in subsections a–c, and their effect on the selected pattern were investigated by Ahlers *et al.* (1981) and later by Meyer *et al.* (1987, 1988, 1991) (see the review by Ahlers, 1994). The earlier experiments were carried out in cryogenic helium in a cylindrical geometry of aspect ratio 4.7, without the benefit of flow visualization. Various protocols were used for raising ϵ through threshold; linear variation in time

$$\epsilon(t) = \epsilon_0 < \epsilon_c, \quad t < 0, \quad (8.65a)$$

$$\epsilon(t) = \epsilon_0 + \beta t, \quad t > 0, \quad (8.65b)$$

with a range of ramp rates β , and jumps

$$\epsilon(t) = \epsilon_0 < \epsilon_c, \quad t < 0, \quad (8.65c)$$

$$\epsilon(t) = \epsilon_1 > \epsilon_c, \quad t > 0. \quad (8.65d)$$

The Nusselt number was measured as a function of time, and fit to numerical solutions of the amplitude equation with either the deterministic forcing (8.58) or the stochastic forcing (8.64), whose overall strength was in each case a fit parameter. The solutions showed two quite well separated parts of the dynamics: a “linear” portion where the Nusselt number grows exponentially to a perceptible value driven by whichever small forcing is present and where the nonlinear terms are unimportant, and a “non-

“linear” portion where the growth saturates [or follows the still ramping $\epsilon(t)$ adiabatically]. The onset time t_{on} for the initial growth is quite well defined, not depending much on the reference value of Nusselt number chosen to label the end of the linear regime. For a ramp $\epsilon = \beta t$ the onset time obtained from the deterministic forcing (8.58) $f(t) = f_1 \beta t$ is

$$t_{\text{on}}^d \sim [(\tau_0/\beta) \ln(2\tau_0/\pi\beta f_1^2)]^{1/2}, \quad (8.66a)$$

and from the stochastic forcing (8.54) it is

$$t_{\text{on}}^s \sim [(\tau_0/\beta) \ln(\tau_0\beta/4\pi\bar{F})]^{1/2}. \quad (8.66b)$$

The experimental data for the Nusselt number were then fitted to t_{on} and in this way the parameters f_1 and \bar{F} were determined [both of the forcings (8.58) and (8.64b) gave comparably good fits when used with Eq. (8.64a)]. We should remark that the time evolution of the Nusselt number shows rather complicated behavior in the nonlinear regime. Ahlers *et al.* (1981) ascribed this behavior to a nonlinear competition between different patterns; possibilities might be between rolls and hexagons (as was assumed by the authors), or between axisymmetric rolls driven by deterministic forcing at the walls [see subsection VIII.D.1.a] and a straight roll pattern which emerges as the nonlinearities begin to dominate the forcing. As we have seen, pattern selection is a difficult question, and in the absence of visualization assigning patterns from the measured Nusselt number is fraught with uncertainty. Indeed the subsequent work by Meyer *et al.* (1987, 1991) in a similar but not identical system (aspect ratio 10), which however allowed pattern visualization, reports similar features for the time dependence of the Nusselt number in the nonlinear regime, but without changes in the form of the pattern. Thus the explanation of the quantitative time dependence of the Nusselt number remains a mystery. This uncertainty does not, however, affect the estimates of t_{on} or of the order of magnitude of the forcing.

In addition to the ramp protocol, Meyer *et al.* (1987) investigated modulated convection i.e.

$$[R(t) - R_c]/R_c = \epsilon(t) = \epsilon_0 + \delta \cos \omega t. \quad (8.67)$$

A fuller discussion of modulated convection is given in subsection VIII.F.5 below. For our purposes here we can usefully consider (8.67) (for small ω) as the repeated cycling of the system through threshold, to investigate the forcing phenomenon and pattern selection. In addition this protocol investigates the destruction by noise of the persistence of a small convection amplitude in the $\epsilon < 0$ portion, which subsequently grows back to large amplitudes on the $\epsilon > 0$ portion of the cycle.

We now summarize the results of these studies.

(i) For sidewalls of thermal diffusivity different from that of the fluid the results for ramps and steps are quite consistent with the deterministic forcing (8.58), at least for $\beta \lesssim 0.2$, with a small static imperfection f_0 and a value of f_1 consistent with a first principles estimate by

Cross, Hohenberg, and Lücke (1983b). The pattern visualization experiments by Meyer *et al.* (1987) showed concentric rolls developing, consistent with the symmetry of the forcing [Fig. 38(a)]. The strength of the forcing is extremely small here, $f_1 = 2.70 \times 10^{-4}$, yet it clearly determines the nonlinear pattern of $O(1)$ amplitude. The small static component f_0 , estimated from the fit to (8.58) for different rates should produce an imperfect bifurcation with a rounding width $\delta\epsilon \sim 0.005$, and a rounding of roughly this size was indeed found in separate static experiments (Ahlers *et al.*, 1981).

(ii) For sidewalls with matching thermal diffusivity^{8.2} the situation was quite different. Here it was determined that stochastic forcing was dominant. This was shown by the random spatial appearance of the growing solutions, Fig. 37(b), and the lack of reproducibility of the details of the pattern from run to run. The strength of the stochastic forcing determined by the fit to Eq. (8.64) given in Fig. 38(b) was $\bar{F} \approx 5 \times 10^{-7}$. [This tiny value is still a factor of 10^4 larger than the thermal noise corresponding to Eq. (8.63), and its precise origin is unknown.] The nonlinear evolution led to a characteristically disordered state shown in Fig. 38(b): thus the delicate competition between the two different, tiny forcing mechanisms has an enormous effect on the emerging patterns.

(iii) For modulated convection with matching sidewalls the strength of the stochastic forcing is measured by its effect on the very faint pattern of exponentially decaying amplitude which persists in the sub-threshold portion of the cycle. (An initial condition of essentially straight rolls was established by thermal imprinting.) Near the threshold for appearance of a convective pattern, it was either coherent from period to period and equal to the initial straight roll pattern, or incoherent with an apparently random spatial configuration, depending on the modulation parameters ϵ_0 and δ of Eq. (8.67). In particular, a characteristic boundary $\epsilon_0 = \epsilon_{01}(\delta)$ could be defined such that the pattern was coherent for $\epsilon_0 > \epsilon_{01}$ and incoherent for $\epsilon_0 < \epsilon_{01}$. [Note that $\epsilon_{01} \gg \epsilon_{0c}$, where ϵ_{0c} is the (small) shift in convective threshold due to modulation; in addition, the hexagon region was unobservable in these experiments since the frequency was low, see subsection VIII.F.5 below.] The boundary ϵ_{01} between coherent and incoherent motion from cycle to cycle was calculated by Swift and Hohenberg (1988) using the stochastic single-mode amplitude equation (8.64). The parameter \bar{F} was

^{8.2}A number of experimental methods have been devised to provide a good thermal match between the convecting fluid and the sidewall. One method involves the use of a light porous wall material which becomes filled with the fluid. Alternatively a horizontal fin placed midway between the plates creates a “wall material” which is precisely the same fluid as in the interior of the cell, but with a plate separation $d/2$ and a critical Rayleigh number larger by a factor of 8. This material is thus nonconvecting.

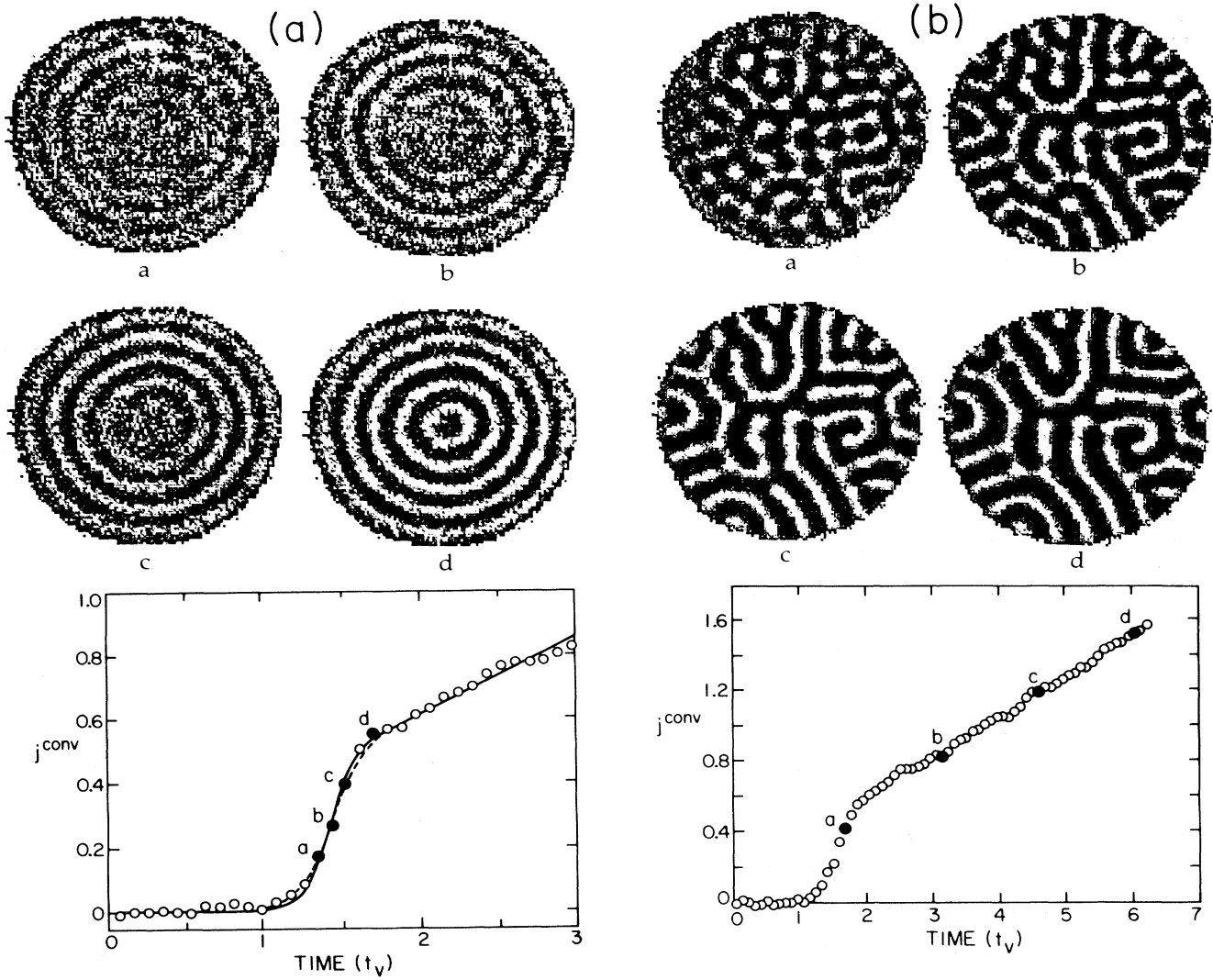


FIG. 38. Shadowgraph images of the emerging pattern and data for the convective heat flux J^{conv} as a function of time for a linear ramp in the applied heat current with ramp rate $\beta=0.27$ [see Eq. (8.58b)]. (a) Cell with polyethylene sidewalls; solid circles correspond to points where images (a)–(d) were taken. (b) Same as (a) but with ‘‘nonforcing’’ sidewalls of matching thermal diffusivity (5% polyacrylamide gel). The emerging pattern has the geometry of the sidewalls in case (a) and is disordered in case (b). (From Meyer *et al.*, 1991.)

fixed from the onset time experiments, so that $\epsilon_{01}(\delta)$ could be predicted with no adjustable parameters; it was found to agree well with the experiment, thus demonstrating the consistency of the stochastic description based on Eqs. (8.61) or (8.64) with adjustable noise strength. As mentioned above, the physical origin of this force is not understood, however, and so far no systematic dependence of \bar{F} on other experimental parameters has been uncovered.

2. Simple two-dimensional patterns

One of the most graphic early examples of pattern formation in nonequilibrium systems was the photograph of

concentric convection rolls in a cylindrical container by Koschmieder and Pallas (1974). [That pattern resembled the one in Fig. 39(c).] The symmetry of this geometry leads to a number of simple patterns, which have been studied in some detail, and which we will now discuss.

At ideal sidewalls, rolls that are normal or nearly normal are often observed. Sometimes radial rolls extending only a small distance into the cell, leaving axisymmetric rolls in the bulk, may be seen as in Fig. 39(d), and another common pattern is the ‘‘Pan Am’’ texture of Fig. 39(b). Very close to onset the solution consists essentially of straight rolls (a), with very little regard to the cylindrical boundaries: clearly the criterion of normal rolls at boundaries is not a strict one (see Kirchartz *et al.*, 1981;

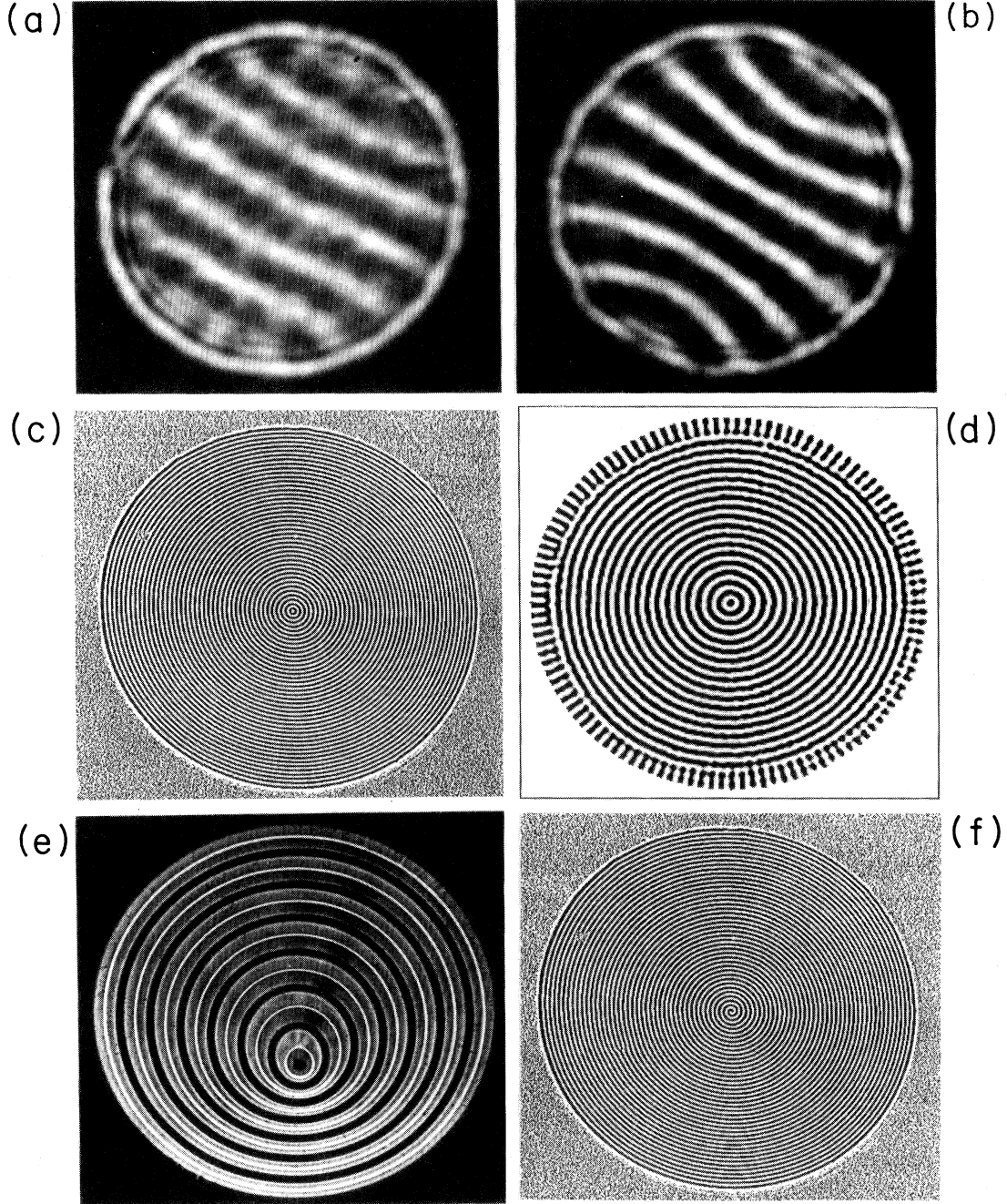


FIG. 39. Simple two-dimensional patterns in a cylindrical geometry obtained for different values of Prandtl number σ , Rayleigh number R , aspect ratio L and different sidewall conditions, showing (a) nearly straight rolls in argon gas with $\sigma=0.7$, $L=7.66$, $R/R_c=1.05$ (with R_c the critical Rayleigh number in the actual geometry); (b) more curved rolls in the same system (Pan-Am texture) at a larger Rayleigh number ($R/R_c=1.12$); (c) concentric rolls in CO₂ gas for $L=86$ with sidewall forcing; (d) convection in CO₂ gas for $L=41$ with very little or no sidewall forcing; (e) off-center pattern (convection in methanol, $\sigma=7$, $R/R_c=7.3$); (f) spiral pattern (convection in CO₂ gas, $R/R_c=1.15$, $L=86$). Both (e) and (f) are stabilized by sidewall forcing. [(a), (b), and (e) from Croquette (1989); (c) and (f) from Bodenschatz *et al.* (1991, and unpublished); (d) from Hu *et al.* (1992).]

Croquette and Pocheau, 1984; Croquette *et al.*, 1986a). Ahlers *et al.* (1981) suggested that the straight roll pattern may be preferred over the axisymmetric one based on evaluating the Lyapunov function for the amplitude equation description of each state. (They used the second axisymmetric mode of Eq. (8.54), but in large systems the logarithmic terms^{8,1} that appear in the analysis of the first mode also favor the straight roll pattern.)

As the control parameter is raised the tendency of the rolls to approach the sidewalls normally grows, and the curvature of the rolls consequently increases [Fig. 39(b)]. This leads to a compression of the rolls in the center of the cell, a feature that has been associated with the transition to chaotic time dependence by defect nucleation (see subsection VIII.E.2.b below). At low Prandtl numbers the mean flow effects driven by roll curvature become important in these simple textures.

An intriguing instability occurs in axisymmetric rolls (with the tangential alignment at the sidewall stabilized by a hot wire): the axisymmetry is broken, with the center of the roll structure moving off the center of the cylinder [Fig. 39(e)]. The displacement may saturate at a finite value, or a dislocation pair may be nucleated and then move to the boundaries leading to a change in the number of rolls. Croquette and Pocheau (1984), Steinberg *et al.* (1985), and Croquette *et al.* (1986a) indeed observe this as a mechanism for wave-number change in this geometry on increasing the control parameter. Pocheau (1989) has suggested that this instability is caused by the mean flows that develop in the off-center pattern [Fig. 40(a)], and Newell and co-workers have developed an analysis of the instability based on the phase equations including mean-drift effects (Newell *et al.*, 1990a,b, 1991). Drift flows are also expected in the Pan Am texture, again serving to enhance the roll curvature [Figure 40(b)] and roll compression at the center, forcing the local wave number out of the stable band.

Pocheau (1989) has constructed a phenomenological model for coupled phase and mean-flow fields and has evaluated the spread in wave vector of the pattern as a function of Rayleigh number. He obtained good agreement with experiment by making the *phenomenological assumption* that the curvature of the rolls increased rapidly with R , immediately above threshold and saturated at a value of curvature of order L^{-1} for $\varepsilon = \varepsilon_t = 0.2$. The difficulty of an *a priori* theory, and of a general prediction of the onset value $\varepsilon_t(L, \sigma)$ thus lies in the sensitivity of the effect to the precise constraints on roll curvature imposed by the sidewalls, which are not understood away from threshold.

An ingenious experiment to support the above theoretical interpretation was devised by Daviaud and Pocheau (1989), who built a cell of aspect ratio $L = 12.5$ with a sidewall boundary which is permeable to large-scale flows. In this case they observed that the crossing point of the maximum wave vector q_m with the skew-varicose instability line, and the consequent onset of defect nucleation, occur at $\varepsilon_t \approx 0.5$ rather than $\varepsilon_t = 0.2$ as in the

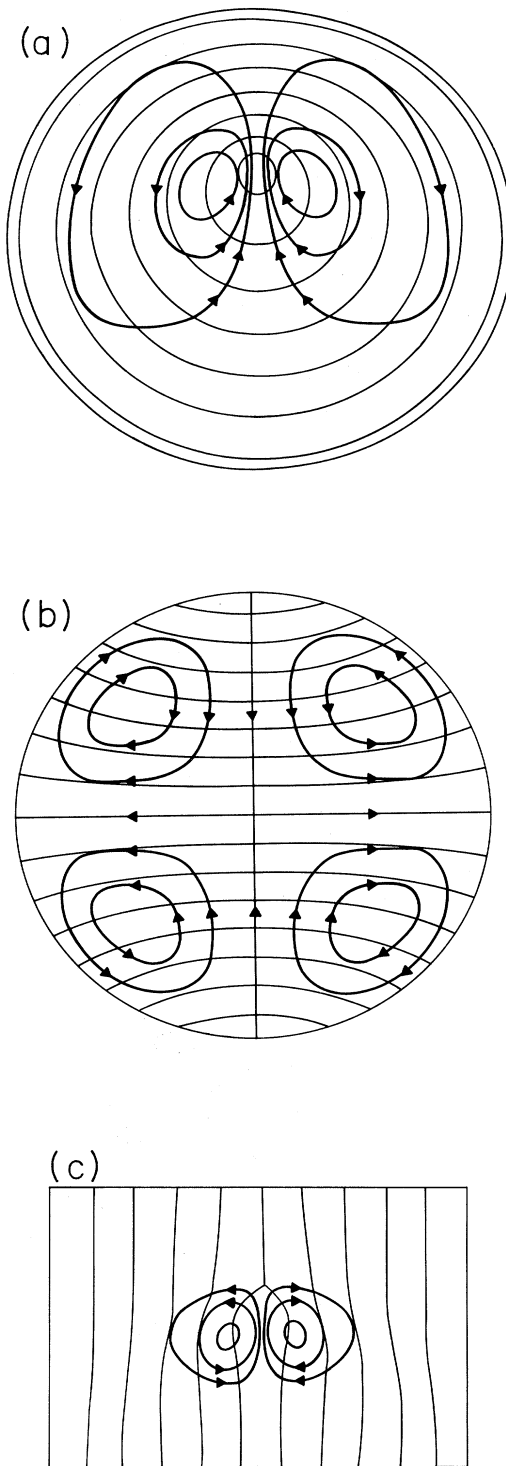


FIG. 40. Sketch of possible large scale mean drift flows in three simple situations. The lines without arrows correspond to the roll boundaries and the lines with arrows to the large-scale flow streamlines. (a) Off-center target pattern [cf. Fig. 39(e)]; (b) "Pan-Am" texture [cf. Fig. 39(b)]; (c) Dislocation [cf. Fig. 19]. (From Croquette, 1989.)

usual impermeable case. An adaptation of the calculation of Pocheau (1989) to this case confirms the larger value of ϵ_t for the onset of time dependence when the large-scale flow is unconfined.

Finally, let us mention an interesting system in which the roll pattern can be controlled externally, namely convection in mercury in the presence of a horizontal magnetic field (Fauve *et al.*, 1984). The effect of the field B is determined by the Chandrasekhar number

$$Q = \bar{\sigma} B^2 d^2 / \rho v, \quad (8.68)$$

where $\bar{\sigma}$ is the electrical conductivity and ρ the density of the fluid. For sufficiently large Q the magnetic field aligns the roll axes and suppresses the instabilities occurring near threshold for this low Prandtl number fluid ($\sigma \sim 0.02 - 0.04$). Studies of chaotic convection in this system will be mentioned in subsection VIII.E.2.

3. Natural two-dimensional patterns

Figures 3(a,b) show two natural patterns at the same system parameters in a rectangular geometry and Fig. 41(a,b) shows an interesting comparison of natural patterns in a large rectangular convection cell and in a numerical simulation of the Swift-Hohenberg model (8.35). There has been considerable experimental work on characterizing steady natural patterns, the transient approach to steady state, as well as the breakdown to persistent time dependence. At present our understanding is mainly descriptive and piecemeal, isolating particular features (Cross, 1982a). A full theory is lacking and we are not even sure of the correct questions to ask. Any

global understanding that we have is based largely on comparing with results or expectations from simple model equations, particularly the Swift-Hohenberg model. We will first attempt to summarize the qualitative features as distilled from a large body of work, and then discuss attempts at more quantitative conclusions.

Let us remark at the outset that we are describing results on "large" systems, with aspect ratios between say 5 and 20. For the experiments we discuss considerable care was taken to approximate an ideal system, i.e. constant external conditions and as perfect a geometry as could be constructed. This is difficult to accomplish in larger cells since transient times become prohibitively long. As will be seen, the steady state patterns ultimately obtained reflect the scale of the system. Indeed, although there may be regions of the pattern where a local roll structure cannot be identified, there are typically also large ordered regions of size comparable with the system size, containing straight rolls or rolls with a radius of curvature also comparable with the size of the system. Thus these system sizes have not reached an asymptotic limit where the size and geometry of the lateral boundaries are no longer important — and perhaps no such limit exists for a truly steady state solution. In the language of Sec. VII.A, the coherence length (as determined empirically from the solution, not the value $\epsilon^{-1/2}\xi_0$ estimated from the amplitude equation) remains of order the system size. It might be expected that under such conditions a complete understanding of the structure would indeed be hard to find. Interestingly, the asymptotic large system limit may arise more easily in simulations of the Swift-Hohenberg model where ϵ can

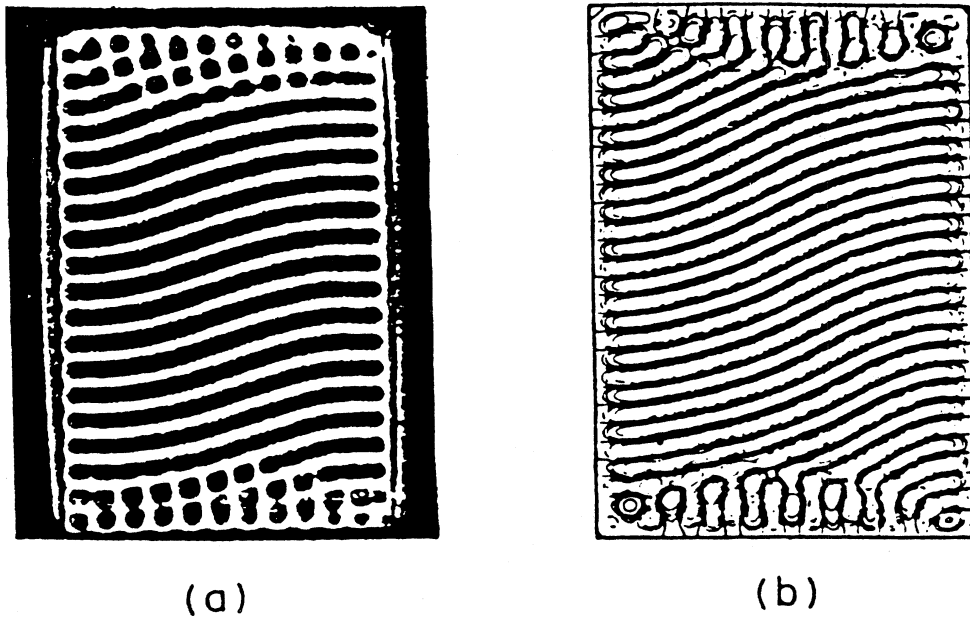


FIG. 41. Comparison of an experimental convection pattern with a numerical simulation of a model equation. Part (a) was obtained by Le Gal (1986) using a shadowgraph method, and part (b) is a calculation by Greenside and Coughran (1984) based on the Swift-Hohenberg model (8.33), for a similar aspect ratio. Note that both patterns are stationary.

be raised, thereby increasing barriers to the evolution of the pattern to simpler configurations, without the danger of persistent time dependence developing. In real convection, by contrast, for values of Rayleigh number at which steady state solutions are obtained, the patterns found at long times still seem to reflect the system size and geometry.

We now summarize the main qualitative results for steady state, natural patterns.

(i) There exists a multiplicity of stable steady state solutions, even when the preparation conditions were nominally the same, for example the patterns in Figs. 3(a) and 3(b).

(ii) Transients leading to the steady state are often very long, sometimes longer than the natural horizontal diffusion timescale $\tau_0 L^2$ (Heutmaker *et al.*, 1985; Ahlers *et al.*, 1985a). Cross and Newell (1984) suggested that a longer timescale could be anticipated from the smooth phase equation (4.76) (see Sec. VI.A.1.b.ii). They proposed local domains in which the wave number evolves to the value q_f selected by focus singularities corresponding to a zero perpendicular diffusion constant, and hence a longer time scale than given by diffusion over the horizontal scale. Note, however, that $D_{\perp}(q_f)$ is not expected to vanish at low Prandtl numbers where mean drift effects are important. (The experiments of Gollub *et al.* were at Prandtl number 2.5.) Other sources of long time scales might be relaxation effects analogous to those occurring in glasses, due to the high initial complexity (Siggia and Zippelius, 1981a), or “barriers” to defect motion which is necessary for the pattern to evolve, although it is not clear how to formulate this notion precisely in a high-dimensional phase space with no potential in the dynamics.

(iii) There is a tendency for the rolls to approach the lateral boundaries at right angles, as for example in Fig. 3. As mentioned earlier, this is not a strict requirement or boundary condition (cf. Sec. V.A.1), but it agrees with the conclusions of amplitude and model equations. The tendency becomes stronger as the Rayleigh number, and hence the curvature of the rolls, increase in these complex patterns, as they do in simple patterns [Figs. 39(a) and 39(b)].

(iv) There are often defects or defected regions in the cell. This is in fact a necessary consequence if the rolls approach the sidewall normally and the roll wave number is fairly constant. Cross (1982a) suggested that the necessary distortions of the rolls could be accomplished by many [$O(L)$] isolated dislocations. Such defects are indeed sometimes seen [see the box in Fig. 3(c)], though more typically one finds disclinations [Figs. 3(b) and (c)], grain boundaries, or complicated defect areas where no simple geometry can be discerned [Fig. 3(a)]. As we have seen, most disclinations can only occur if there is a considerable ($\sim 50\%$) spread of wave numbers, or if there is a line of dislocations. However a theoretical description is then harder than for isolated dislocations.

(v) There is typically a spread of local wave numbers,

with an overall tendency towards smaller values as the Rayleigh number increases. This statement is part of the general folklore of convection (Koschmieder, 1974) and has been investigated by Heutmaker *et al.* (1985), Steinberg *et al.* (1985), and Heutmaker and Gollub (1987). These groups used fluids with Prandtl numbers of 2.5 and 6.1 respectively, so that the conclusions seem to have some generality. The results of Heutmaker and co-workers for the wave-number distribution, are shown in Fig. 42. (The wave number is defined as π times the inverse of the distance between zeroes of the fluctuations of the shadowgraph intensity. This was found to be a more useful characterization than the Fourier transform method of Gollub and McCarriar, 1982.) It is interesting to note, as Newell *et al.* (1990b) point out, that the wave number of the maximum of the distribution follows the wave number selected by an axisymmetric focus (see subsection VIII.C.2.a), although it is not understood why this selection mechanism should operate in disordered patterns, in a system where mean-flow effects are important. Steinberg *et al.* (1985) also state that the mean wave number in natural patterns followed a trend to smaller values similar to the axisymmetric selected wave

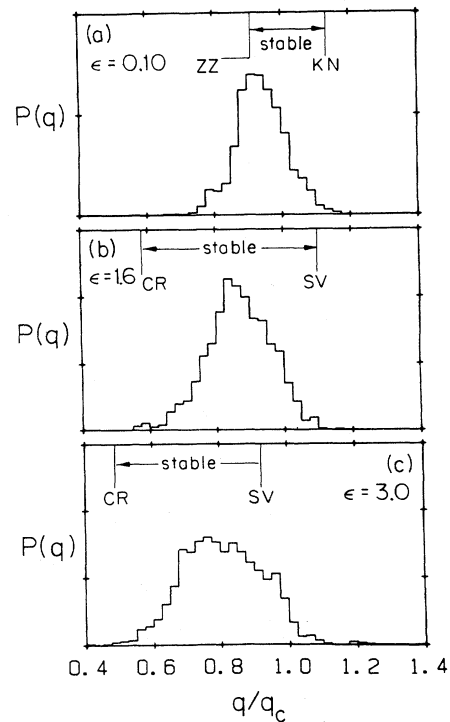


FIG. 42. Wave-vector distribution $P(q)$ in convection patterns in a cylindrical cell of aspect ratio $L=14$ at several values of the control parameter ϵ , for Prandtl number $\sigma=2.5$. The stable wave-vector band as predicted by Busse and Clever (1979) for a laterally infinite system is shown by the horizontal arrows, as well as the instability predicted at the edge of the band (see Fig. 32). $P(q)$ lies within the stable band at moderate ϵ , but partially outside it at low and high ϵ . (From Heutmaker and Gollub, 1987.)

number. It was noted by Heutmaker and Gollub that if the observed wave numbers lie approximately within the stable band of the ideal system the state is usually steady, whereas if the observed wave numbers stray significantly outside the stable band the state usually has persistent time dependence. This result is consistent with the notion that the ideal stability analysis applies approximately (presumably with small shifts of the boundaries) to local regions of rolls without too great curvature. This is particularly likely to be true for the short length scale instabilities (oscillatory, cross-roll); the long wavelength instabilities may depend more on large regions of the flow. On the other hand the phase diffusion equation allows a good theoretical analysis of the stability boundary shifts due to finite size effects in the latter case. An estimate of the effect of finite system size in the longitudinal and transverse directions on the Eckhaus instability has been carried out by Bodenschatz and Kramer (1987), and the same sort of analysis could be done for a local distortion of a large straight roll region. The skew-varicose instability, involving large-scale mean flows is trickier, and finite size effects have not been analyzed in detail for that case.

Experimental results for low Prandtl number ($\sigma = 0.7$) convection with natural patterns are shown in Fig. 43. These are actually dynamic patterns, and the band of wave numbers observed is plotted, together with the type of instability that typically limits the band (Croquette, 1989). Again, small shifts of the boundaries from the ideal predictions are seen. The physics controlling the center and width of the wave-number bands in natural patterns has not been elucidated in this case. Plausible mechanisms are the one-dimensional wave-number selec-

tion mechanisms of subsection VIII.C.2, or truncation of a wide spread of wave numbers induced by the geometry or the initial conditions. Such a truncation would be caused by the instabilities themselves, and could then lead either to a steady state solution with local wave numbers inside the band, or to persistent dynamics. There are however no *predictions* for the onset of time dependence as a function of Prandtl number. Note that for $\sigma \geq 0.7$ the selection mechanisms and the stability balloon both tend to smaller wave number as ϵ is increased, and both of these effects are consistent with the experimental trend. It would be instructive to do experiments for $\sigma < 0.5$ where the known mechanisms select larger wave numbers [see Fig. 36(a), and Buell and Catton, 1986a,b] whereas the center of the stable band continues to tend to smaller wave numbers.

Heutmaker and Gollub (1987) have attempted a quantitative characterization of natural convection using the potential constructed by analogy with the Swift-Hohenberg equation (Cross, 1982). Although this approach involves a crude approximation, the method is important since it is the only global characterization of patterns available. The authors reconstruct the wave-vector field at a large number of points in space, and calculate from their data the bulk [Eq. (6.6)] and surface [Eq. (6.5)] contributions to the potential, as well as a rough estimate of the defect contribution (6.11), using a core size r_c somewhere between one and two times $\epsilon^{-1/2}\xi_0$. They then follow the variation of the potential \mathcal{J} and of the various contributions as the pattern evolves in time. Typically \mathcal{J} is dominated by the bulk and defect terms, with smaller contributions from the surface. Near threshold ($\epsilon \lesssim 2$) the evolution of \mathcal{J} is consistent with a monotonic decrease, as expected for the Swift-Hohenberg model. For $\epsilon > 2$, on the other hand, the evolution of \mathcal{J} is definitely not monotonic: it displays large jumps associated with the spontaneous nucleation of defects, signaling that simple modeling in terms of potential motion is no longer applicable. Although this analysis is pedagogically attractive, it is not actually clear how much is being tested. Since essentially all contributions to \mathcal{J} tend to decrease in time, many other decreasing functionals could be written down (the inverse Nusselt number would probably work for example). The essential dynamics is the steady simplification of the pattern, and although the potential captures and even predicts this trend it does not necessarily *control* the dynamics. It should also be pointed out that the Swift-Hohenberg equation itself, when simulated for analogous values of ϵ to those used in the experiment [see Eq. (8.36)], shows patterns that are held up in complicated metastable minima (Greenside and Coughran, 1984), contrary to what is seen experimentally.

E. Chaotic convection

Convective systems have historically provided some of the most important examples of chaos, due to the ease

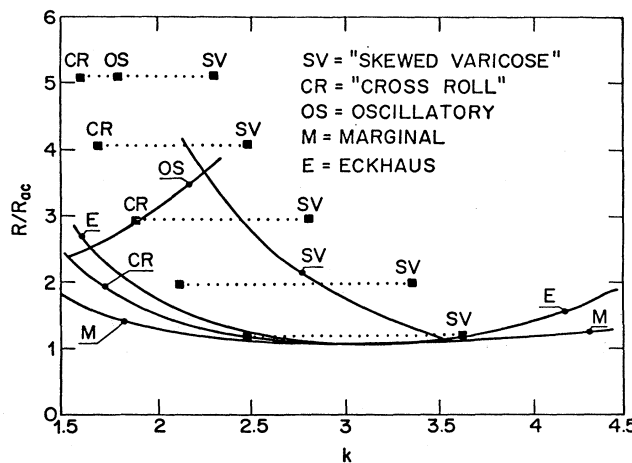


FIG. 43. Wave-vector distribution in time-dependent natural convection patterns in a cylindrical cell of aspect ratio $L=20$ at low Prandtl number ($\sigma=0.7$). Horizontal dotted lines indicate range of wave vectors observed in the pattern at fixed Rayleigh number. The typical instability at each end of the range is labeled as in Fig. 32 (except for the "marginal" stability line M, which is labeled N, "neutral", elsewhere). Full lines are predictions by Busse (1978) for the stability boundaries of the infinite system. (From Croquette, 1989.)

with which different types of spatiotemporal conditions can be set up and controlled. Nevertheless subsequent experimental studies have not succeeded in providing simple examples that might be understood in detail. We shall divide our discussion into the different categories defined in Sec. VII, namely according to the number of modes involved in the dynamics.

1. Small systems

As mentioned earlier, the first clear experimental evidence of chaos was found by Ahlers (1974) in accurate measurements of temperature for a small ($L = r/d = 5.27$) cylindrical container at $R/R_c \approx 2$. Since then many important advances in the elucidation of temporal chaos have resulted from experiments in convection. Examples are the first observations of the period-doubling cascade (Gollub and Benson, 1980, and especially Libchaber and Maurer, 1980, 1982), measurements of the fractal dimension of reconstructed attractors (Malraison *et al.*, 1983), and the observation of the complicated tongue structure of the quasiperiodic route to chaos for convection in mercury (Glazier and Libchaber, 1988). In all of these cases the main advantages of the convective system are the control and stability of external conditions, the sensitivity of measurements of the dynamical behavior, and the ability to visualize the flow in real time. On the other hand, precisely because of the universality of small system chaos the results reveal little about the specifics of convective flow. The interesting behavior of the system is similar to what is seen in many other hydrodynamic systems, as well as in optical or electronic devices (see Mayer-Kress, 1986; Abraham *et al.*, 1984, 1989). We will thus turn to systems with nontrivial spatial dependence to reveal some of the features of chaos that are more specific to convection.

One experimental aspect of chaotic convection in small containers which does not seem to have a simple explanation in terms of low-dimensional dynamical systems is the high-frequency form of the power spectrum illustrated in Fig. 44. As first pointed out by Ahlers and Behringer (1978b) and then observed by many workers, the fall-off at high frequencies obeys a power law $\omega^{-\zeta}$ with $\zeta=2-5$. For a deterministic system with a small number of modes it is expected that the behavior will be exponential when $\omega \gg \omega_{\max}$, where ω_{\max} is the highest characteristic frequency of the modes in the system. As pointed out by Greenside *et al.* (1982) the experimental behavior is most easily interpreted in terms of a stochastic model, though of course it could also be explained by some high characteristic frequency in the low-dimensional model. It might be interesting to explore an alternative deterministic explanation invoking the continuum of modes of a real fluid. It is possible that the concept of a dissipation length (see Sec. VII.A), which we used to argue that a fluid can be represented by a model with a small number of modes, is too simplistic and that a “short-time tail”

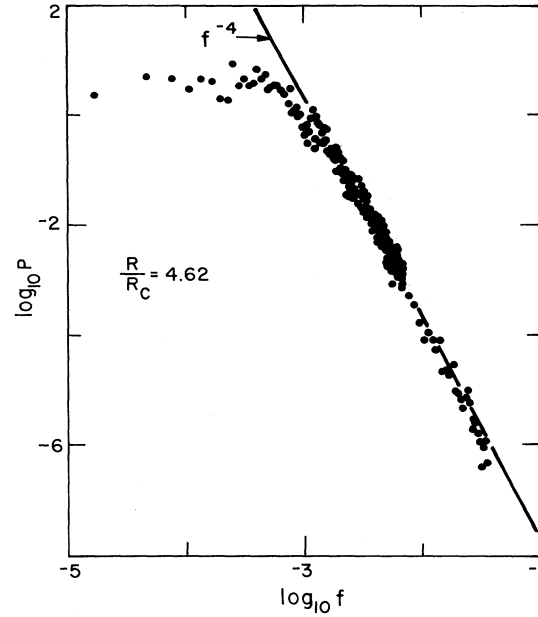


FIG. 44. Power spectral density of temperature fluctuations $\Delta T/\Delta T_c$ in Hz^{-1} across a small aspect ratio cylindrical convection cell ($L = 4.72$) maintained at constant heat flux, as a function of frequency in Hz^{-1} on a log-log plot. The Rayleigh number and Prandtl number are $R/R_c = 4.62$ and $\sigma = 0.7$, respectively. Note the power-law falloff at high frequencies. (From Ahlers and Behringer, 1978.)

persists from interactions with large- q modes. We are not aware of any mathematical studies of this question.

2. Intermediate systems: Defect mediated chaos

Most of the studies of chaotic convection have been in the intermediate-size regime, i.e. aspect ratios in the range $5 < L < 50$, where the system consists of a few defects embedded in domains of regular (ideal) convection. Attention has primarily focused on the *onset* of chaotic time dependence, i.e. on the influence of defects on stability. Very little is known precisely about the chaotic state itself, for example the contribution of each defect to the dimension of the chaotic attractor, or the precise way in which defects influence spatial correlations. As discussed in Sec. VII, these questions are probably very difficult to address in the regime of intermediate sizes where only a few defects are present. We have therefore suggested that it is more promising to consider the large system limit considered in subsection VIII.E.3 below, and to develop a statistical mechanics of defects, though there are certainly technical difficulties in gathering sufficient data to provide meaningful statistical information.

In the present section we summarize what is known about the onset of chaos for systems of intermediate size where the behavior is strongly dependent on Prandtl number.

a. Large Prandtl number: $\sigma \gtrsim 1$

At high Prandtl number convective patterns near threshold are observed to be stationary and to have relatively small variation in local wave vector. Thus we expect an analysis of stability based on the Busse balloon to be appropriate. According to our earlier discussion the roll system will be stable until the wave number crosses the balloon boundaries, and this usually occurs via a cross-roll instability for $\sigma \gtrsim 1$. In this case three-dimensional convection sets in, to form a more or less disordered cellular pattern. The onset of time dependence is then analogous to the melting of this defected solid. We are not aware of any quantitative studies, either experimental or theoretical, of this phenomenon.

b. Low Prandtl number: $\sigma \lesssim 1$

For low Prandtl number the skew-varicose instability is the primary boundary of the Busse balloon, so this mechanism plays a central role in the onset of time dependence (Gollub *et al.*, 1982; Croquette, 1989). An important additional point, though, is the appearance of large-scale flows at low Prandtl number (see subsection VIII.A.5), which deform the roll pattern and lead to a *broadened wave-number distribution* near onset. What usually happens, roughly speaking, is that the local wave number crosses the balloon boundary at some point in space, thus leading to the nucleation of a defect (typically a dislocation). The subsequent time dependence can be either periodic (with regularly spaced nucleation and destruction events) or, more typically, chaotic. The windows of periodic behavior are sensitive to aspect ratio, Prandtl number, and Rayleigh number, and appear to be difficult to predict. Careful measurements as a function of aspect ratio and container shape have been carried out by Behringer and co-workers in liquid ^4He over a limited Prandtl number range ($0.5 < \sigma < 1$), but no visualizations are possible in these cryogenic experiments (see Behringer, 1985; Motsay *et al.*, 1988).

The above defect scenario has been documented by Pochéau, Croquette, and Le Gal (1985) in a careful experimental study in high-pressure argon gas ($\sigma = 0.7$) in a cylindrical container with $L = r/d = 7.66$. The onset of time dependence was found to be at $\epsilon = 0.13$, and was clearly shown to arise from nucleation of a dislocation pair at the center of the Pan Am pattern [Fig. 45(b)]. Greenside, Cross, and Coughran (1988), simulated the experiment using the model in Eq. (8.42) above, which closely reproduces the Busse balloon of argon gas (see Figs. 32 and 33). As in the experiment, a dislocation pair nucleated in the portion of the flow where the rolls were compressed, and the defects subsequently climbed toward the walls of the container, thus producing chaotic motion [Fig. 45(a)]. The authors estimated the onset to be at

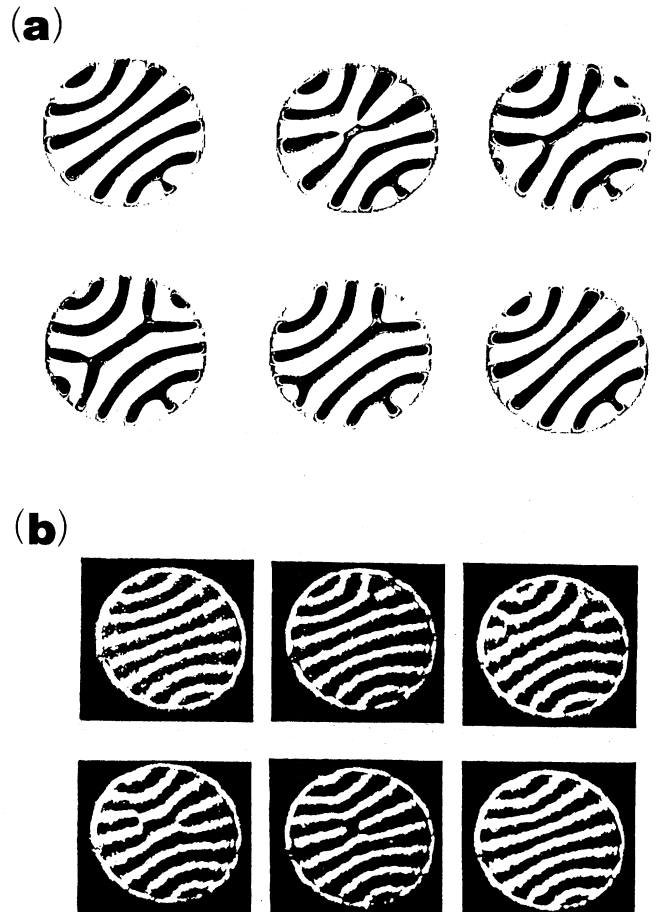


FIG. 45. Comparison of time evolution in an intermediate aspect ratio cell for (a) model equation (8.42) (from Greenside, Cross, and Coughran, unpublished), and (b) an experiment in pressurized argon gas ($\sigma = 0.7$) (from Croquette *et al.*, 1986a).

$\epsilon_t = 0.036$ for $L = 7$ and $\epsilon_t = 0.011$ for $L = 14$, which apart from a large discrepancy in absolute magnitude represents a stronger dependence on L than seen experimentally [$\epsilon_t = 0.13$ for $L = 7.66$ and $\epsilon_t = 0.085$ for $L = 20$, as reported by Croquette, 1989]. The fractal dimension of the chaotic attractor near ϵ_t could also be estimated from the simulation, and was found to be $d_f = 2.9$, suggesting that the dislocations provide effective degrees of freedom for the dynamics. Another interesting aspect of these calculations is that they also showed chaos in a rectangular container (in agreement with the experiments of Motsay *et al.*, 1988), but not in a domain with periodic boundary conditions.

For higher Rayleigh number the pattern becomes increasingly disordered, more defects are created and become mobile. Most of these events can, at least qualitatively, still be associated with instabilities of the Busse balloon (see Sec. 6.5 of Croquette, 1989) but no quantitative theory seems possible in this regime. The behavior is sensitive to geometry and to boundary conditions, as has been demonstrated by a variety of experimental studies

(see Ahlers and Behringer, 1978a,b; Heutmaker *et al.*, 1985; Steinberg *et al.*, 1985; Heutmaker and Gollub, 1987; Motsay *et al.*, 1988; Croquette, 1989). An analysis of the chaotic transition at low Prandtl number has also been carried out by Zaleski (1989).

Finally, we note that in the low Prandtl number fluid mercury experiments mentioned in subsection VIII.D.2 above, Fauve *et al.* (1984) have used a horizontal magnetic field to produce different routes to chaos as the Rayleigh number was raised. For small Chandrasekhar number Q [Eq. (8.68)], the fluid went into a turbulent state immediately above threshold, while for large Q ($Q \gtrsim 700R/R_c$) the pattern was one-dimensional and no chaos was observed in the Rayleigh number range investigated ($R \lesssim 4R_c$). At intermediate Q ($300R/R_c \lesssim Q \lesssim 700R/R_c$) the fluid behaved like a small system with characteristics of temporal chaos (oscillations, period doubling, intermittency).

3. Large systems: Extensive chaos

A small number of experimental studies of convection with large aspect ratio have been carried out, attempting to explore the behavior of the infinite system (see Sec. VII.C). The pioneering investigation of Ahlers and Behringer (1978a,b) found the remarkably small onset value $\epsilon_i \lesssim 0.1$ in cryogenic ^4He ($\sigma \approx 1$), which was quite baffling at the time. We now believe it to be due to the defect nucleation mechanism discussed in subsection VIII.E.2 for argon gas, but we do not know precisely how ϵ_i scales with σ or with L for large systems. It is likely that there are many different types of behavior, dependent on minute details of the system. Most investigations have concentrated on conditions where the onset appears to be clearly away from zero even for large L , such as systems displaying an oscillatory instability. It would nevertheless be interesting to find a system where the onset can be studied in a controlled fashion as a function of L and where it is possible to test how ϵ_i scales for large L .

Experiments on chaotic convection in cells of various geometries have been carried out by Ciliberto and Simonelli (1986), Ciliberto (1987), and Motsay *et al.*, (1988). The most complete studies of large-system convective chaos are experiments on spatiotemporal intermittency in an annular cell, first carried out by Ciliberto and Bigazzi (1988), and later refined and extended by Daviaud and co-workers (Daviaud *et al.*, 1989; 1990). The system used by Ciliberto and Bigazzi was a long thin annulus with aspect ratios $L_y \approx 2$, $L_x \approx 44$, with an oscillatory onset of time dependence at a high value of reduced Rayleigh number ($\epsilon \approx 200$, for Prandtl number $\sigma = 7.5$). The initial time-dependent state consisted of periodic displacements of the roll axes about their mean position. As ϵ was raised the amplitude of the oscillation increased and gave rise to localized turbulent defects caused by the merging of two rolls. Initially these turbulent spots had finite lifetime, but at higher ϵ their spatial extent and their lifetime grew, and eventually they

“percolated” throughout the system. This phenomenon is remarkably similar to the one first observed by Chaté and Manneville (1987) in their simulation of the Kuramoto-Sivashinsky equation discussed in Sec. VII.D.2. As in the simulations, the experimental data were digitized into “turbulent” or “laminar” domains according to various criteria, and the statistics of these domains were analyzed along the lines suggested by Chaté and Manneville. Figure 46 presents the histogram $P(X)$ of the lengths of laminar domains at and above the onset value for spatiotemporal intermittency, showing the crossover from power-law to exponential behavior of the distribution function. In the exponential region above onset the rate of spatial falloff defines a correlation length ξ , which was subsequently shown by Daviaud *et al.* (1989) to have a broad maximum $\xi_{\max} \approx 3.3 \lambda_0$ around the transition point and then to fall off at higher ϵ (λ_0 is the average wavelength of the laminar state). Thus, both the experimentally observed transition and the one found numerically in the Kuramoto-Sivashinsky equation have some features of a critical point, but they do not appear to be sharp in either case, and the rounding seems difficult to account for by finite-size effects alone. More work is necessary to elucidate the nature of the transition to chaos in this system.

4. Large Rayleigh numbers

Thermal convection provides a convenient closed system in which flows with large Reynolds numbers can be

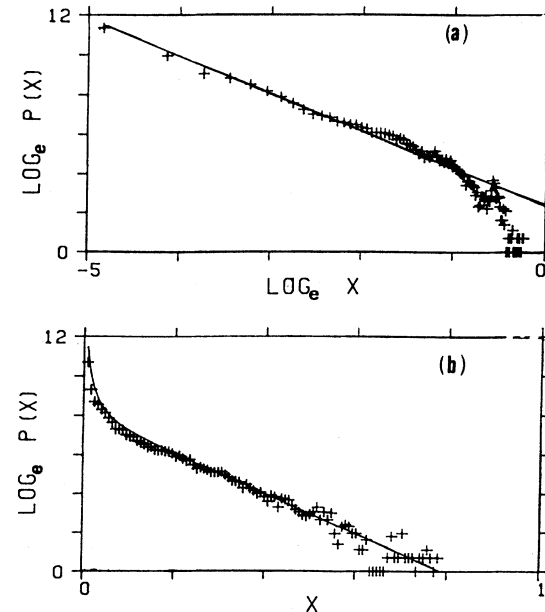


FIG. 46. Distribution $P(x)$ of “laminar” domains of length x for convection in a long thin annulus. (a) At reduced control parameter $\epsilon = 240$ the line shows algebraic decay with exponent 1.9. (b) As in (a) but for $\epsilon = 309$, now showing an exponential decay with decay length $\xi \approx 0.1$. (From Ciliberto and Bigazzi, 1988.)

achieved. (For a recent review see Siggia, 1994.) As first noted by Threlfall (1975), in helium gas at low temperatures Rayleigh numbers can be varied over up to 14 orders of magnitude by changing the pressure. Interestingly, the Prandtl number remains of order unity, varying roughly between 0.5 and 1.5. Early experiments (Threlfall, 1975) found a power-law dependence of Nusselt number \mathcal{N} on Rayleigh number R

$$\mathcal{N} = \mathcal{N}_0 R^\beta, \quad (8.69)$$

with $\beta=0.28$. An exponent $\beta=1/3$ had been obtained in a theory involving the instability of a thermal boundary layer near the bottom plate (see Priestley, 1954; Malkus, 1954; Howard 1966, and other references in Castaing *et al.*, 1989). More recently a careful experimental study of this system was undertaken by the Chicago group (see Castaing *et al.*, 1989), in an effort to characterize both the overall scaling of global quantities such as \mathcal{N} , and the local properties of the flow, e.g. the statistics of temperature fluctuations at different points in the cell, or the nature of boundary layer instabilities and the emission of thermal plumes. The system studied was a cylindrical cell of aspect ratio $L=r/d=0.5$, and the Nusselt number measurements indeed led to a power law as in Eq. (8.69), but the authors distinguished two different regimes. The first, which they termed "soft turbulence" occurs in the range $10^6 < R < 4 \cdot 10^7$ and is consistent with the exponent $\beta=1/3$. For larger R , namely in the range $4 \cdot 10^7 < R < 10^{13}$, which they referred to as "hard turbulence," the exponent changes to $\beta=0.282 \pm 0.006$, with $\mathcal{N}_0=0.23 \pm 0.03$. The distinction between the soft and hard regimes coincides with a change in the distribution of local temperature fluctuations as measured by a probe placed in the center of the cell. For soft turbulence the distribution was found to be Gaussian, whereas it has an exponential tail in the hard turbulence regime. These and a number of other observations have been interpreted by Castaing *et al.* (1989) in terms of a phenomenological theory which modifies the classical picture of Malkus and Howard by introducing an additional "mixing zone" between the thermal boundary layer and the bulk of the fluid. This theory produces the exponent $\beta=2/7=0.286$, in good agreement with the experiment. Further experimental work has been carried out by Sano *et al.* (1989), Wu *et al.* (1990), Chillá *et al.* (1991), Solomon and Gollub (1991), and Wu and Libchaber (1992).

An interpretation of the experiments in terms of standard turbulence phenomenology has recently been offered by Shraiman and Siggia (1990). They identify two nested boundary layers with thicknesses ℓ_T and ℓ_v , representing thermal and viscous processes, respectively, and satisfying the inequality

$$\ell_T < \ell_v. \quad (8.70)$$

The thermal layer is stabilized by the shear flow in the viscous sublayer, which in turn matches the coherent large-scale flow via a turbulent boundary layer. In that case the Nusselt number is related to the shear rate τ by

$$\mathcal{N} \sim \ell_T^{-1} \sim \tau^{-1/3}. \quad (8.71)$$

The shear rate is given in terms of the large-scale Reynolds number R_e and the viscous layer thickness by an empirically verified scaling relation for turbulent boundary layers

$$\tau = \sigma^{1/3} \ell_v^{-2/3}, \quad (8.72a)$$

$$\ell_v = \sigma^2 R_e^3 (2.5 \ln R_e + 6)^{-3}, \quad (8.72b)$$

where σ is the Prandtl number. Combination of Eqs. (8.71) and (8.72) yields the function $\mathcal{N}(R_e)$. In order to relate \mathcal{N} to the Rayleigh number R , the authors use an exact energy balance relation

$$(\mathcal{N}-1) R = \langle (\nabla v)^2 \rangle, \quad (8.73)$$

and estimate the kinetic-energy dissipation by the empirical relation valid for turbulent shear layers

$$\langle (\nabla v)^2 \rangle \sim 100 \ell_v, \quad (8.74)$$

from which, finally, the scaling relation

$$\mathcal{N} \sim 0.27 \sigma^{-1/7} R^{-2/7} \quad (8.75)$$

follows. The domain of validity of this scaling is limited at low Rayleigh numbers by the requirement that the viscous boundary layer be turbulent [so that Eqs. (8.72) should apply], and at high Rayleigh numbers by the nesting condition (8.70). These conditions yield the inequalities

$$5 \cdot 10^7 \sigma^{5/3} \leq R \leq (10^{13} - 5 \cdot 10^{14}) \sigma^4, \quad (8.76)$$

for the validity of Eq. (8.75). The specific Prandtl number dependences in Eqs. (8.75) and (8.76) are new predictions of Shraiman and Siggia which can be tested experimentally. The inequality (8.76) emphasizes the point that the experiments under discussion are not in the asymptotic large R regime of strong turbulence.

The spatial and temporal scaling properties of the temperature and velocity remain controversial. There is some evidence from Sano *et al.* (1989) and Wu *et al.* (1990) for a $k^{-7/5}$ spatial power law for the temperature, which Procaccia and Zeitak (1990) and L'vov (1990) have attempted to explain in terms of the scaling theory of Bolgiano (1959) and Obukhov (1959). However, Shraiman and Siggia (1990) have pointed out that the buoyancy dominated scaling theory of Procaccia and Zeitak and L'vov is inconsistent. Indeed, it also predicts a $k^{-11/5}$ decay for velocity correlations which cannot persist to high k since it is insufficient to dissipate the necessary energy, according to the exact relation (8.73). Finally, we mention that Pumir, Shraiman, and Siggia (1991) have presented a phenomenological model to explain the exponential probability distribution of temperature found by Castaing *et al.* (1989).

Convection in a small cell at large R is a prime example of large-system chaos as discussed in Sec. VII.C, since there is nontrivial space dependence, and the attractor dimension can be expected to grow with R . However,

since the system is highly inhomogeneous in space, and the statistical properties of the flow are very different on small and large scales, the system retains many of the difficulties associated with systems of intermediate size, i.e. it does not display extensive chaos. It is conceivable that high- R convection at large aspect ratio might reveal a simpler phenomenology, so it would be interesting to pursue such experiments (see Wu and Libchaber, 1992).

F. Special topics

1. Convection between poor conductors

Interest in convection between poorly conducting top and bottom plates arises in part because the linear onset problem is analytically soluble in closed form (Sparrow *et al.*, 1964), even for realistic no-slip fluid boundary conditions (the only case we will discuss). From our point of view the system is worth special mention because the onset pattern, taking into account lowest-order nonlinearities, is predicted to be squares rather than the familiar roll pattern (Busse and Riahi, 1980; Chapman and Proctor, 1980). In addition, the weakly nonlinear behavior can be derived via a systematic expansion in slow variations of the flow field, since the onset wave number tends to zero in the limit of very poor conductors (Gertsberg and Sivashinsky, 1981). This is therefore a type II_s system in the nomenclature of Sec. III.B. The resulting order parameter equation provided the basis for the model equation (8.38) studied by Greenside and Cross (1985).

In the limit of infinitely poor conductors the solutions for the velocity \mathbf{u} and temperature perturbation θ near onset become

$$\theta = e^{iq_0^{(0)}x}, \quad (8.77)$$

$$\mathbf{u}^{(0)} = \nabla \times (\nabla \times \hat{\mathbf{z}}\phi^{(0)}), \quad (8.78)$$

with the stream function

$$\phi^{(0)} = \frac{1}{24} (z^2 - 1/4)^2 e^{iq_0^{(0)}x}, \quad (8.79)$$

leading to a critical Rayleigh number

$$R_c^{(0)} = 720, \quad (8.80)$$

and a critical wave number $q_0^{(0)} \rightarrow 0$. Subsequent development is based on perturbing around these solutions using the small parameter

$$K = K_p / K_f, \quad (8.81)$$

where K_p and K_f are the thermal conductivities of the plates and fluid, respectively.

Instead of using the parameter K explicitly, we follow Gertsberg and Sivashinsky (1981) and introduce the finite plate conductivity in terms of the Biot number B , which defines the boundary condition of the thermal field at the

plates via the relation

$$\partial_z \theta = \mp B \theta, \quad z = \pm \frac{1}{2}. \quad (8.82)$$

Then defining the reduced Rayleigh number measured from $R_c^{(0)}$ as

$$\frac{R - R_c^{(0)}}{R_c^{(0)}} = \bar{\epsilon}, \quad (8.83)$$

slow horizontal length scales X, Y and time scale T

$$X = b_0 \bar{\epsilon}^{1/2} x, \quad Y = b_0 \bar{\epsilon}^{1/2} y, \quad T = \frac{1}{2} b_0^2 \bar{\epsilon}^2 t, \quad (8.84)$$

$$Q = b_0^{-1} \bar{\epsilon}^{-1/2} q, \quad b_0^2 = 231/17,$$

and a scaled temperature field Ψ

$$\theta(x, y, z; t) = (0.59/b_0) \bar{\epsilon}^{1/2} \Psi(X, Y, T) + O(\bar{\epsilon}), \quad (8.85)$$

Gertsberg and Sivashinsky show that the convection equations (8.10) can be systematically reduced, using the slow horizontal gradient expansion $\nabla_x, \nabla_y = O(\bar{\epsilon}^{1/2})$. They obtain a single equation for the real function $\Psi(X, Y, T)$

$$\partial_T \Psi = r \Psi - (\nabla^2 + 1)^2 \Psi + \nabla \cdot [(\nabla \Psi)^2 \nabla \Psi], \quad (8.86)$$

where the control parameter r is given by

$$r = 1 - 4B/b_0^2 \bar{\epsilon}^2. \quad (8.87)$$

This equation has a threshold at $r=0$, $Q=1$ leading in the original units to

$$\bar{\epsilon}_c = (R_c - R_c^{(0)})/R_c^{(0)} = (2/b_0) B^{1/2}, \quad (8.88)$$

and a wave number

$$q_0 = (2b_0)^{1/2} B^{1/4}. \quad (8.89)$$

Note that $r=1$ corresponds to $\bar{\epsilon}=\infty$, so the whole range of nonlinearity of Eq. (8.86) is $0 \leq r < 1$. In the convecting state the Nusselt number \mathcal{N} is given by

$$(R/R_c)(\mathcal{N}-1) = b_1 B^{3/2} (1-r)^{-1/2} \langle (\nabla \psi)^2 \rangle, \quad (8.90)$$

with $b_1 = (119/33)^{1/2}/20$. [To derive this result it is necessary to calculate the $O(\bar{\epsilon})$ term in θ .]

The relationship of the phenomenological parameter B to the conductivity ratio K introduces further complications. If the plates have a thickness δ with constant temperature prescribed at the outside surfaces, the boundary condition for a perturbation with horizontal wave number q becomes

$$\partial_z \theta = \pm (K q \coth q\delta) \theta. \quad (8.91)$$

In the thin plate limit, $q\delta \ll 1$ for all q of interest, this gives $B=K/\delta$. Busse and Riahi (1980) also consider the thick plate limit, $q\delta \gg 1$, where the effective Biot number is

$$B = Kq, \quad (8.92)$$

i.e. it depends on the wave number q . The onset wave number in turn scales as $B^{1/4}$ so that for this model $B \sim K^{4/3}$ and $q_0 \sim K^{1/3}$. For the nonlinear problem we must also include the induced modes at $q=0$, for which different boundary conditions must be used in the thick plate case. This makes the problem more complicated: in general for $\delta \gtrsim q^{-1}$ we must add nonlocal terms to Eq. (8.86) to incorporate the extra length scale of the temperature field in the plates. In fact Proctor (1981) shows that the problem may be solved in terms of a two-dimensional order parameter equation similar to Eq. (8.86) with an additional coupling to the three-dimensional diffusion equation for the temperature inside the plates. Since the thin plate limit seems easy to realize experimentally we will restrict our attention to this case.

For Eq. (8.86) it is easy to derive the coupled amplitude equations for superimposed rolls at an angle θ , Eq. (4.31). This leads to an amplitude equation of the form (4.31) with

$$\mathcal{G}(\theta) = \frac{2}{3} (1 + 2\cos^2\theta), \quad \mathcal{G}(0) = 1. \quad (8.93)$$

The general discussion of Sec. IV.A.1 then shows that roll states are unstable and the most rapidly growing perturbation is for a square pattern, so the latter is expected to be stable near threshold for poor conductors. In fact Eq. (8.86) derives from a potential which is minimized for a square. This analysis applies for all Prandtl numbers σ in the limit $K \rightarrow 0$. The full range of (K, σ) for which squares are expected was investigated by Jenkins and Proctor (1984).

Surprisingly, there does not seem to be any experimental work showing square patterns near threshold in pure Rayleigh-Bénard convection between poor conductors. Square patterns were observed in silicone oil between glass conductors (Le Gal *et al.*, 1985), but contrary to expectations the wavelength was not long. Moreover, oscillatory dynamic behavior was observed, in contradiction to the dynamics predicted by Eq. (8.86) which is purely relaxational. This observation was later explained by Moses and Steinberg (1986b) in terms of binary fluid convection effects (the oil was a mixture). Interestingly, there too for some positive values of the separation ratio ψ (see Sec. IX.A below) the onset is predicted to occur at long wavelengths, and would be described by the same equation (8.86). Unfortunately the weakly nonlinear theory is only valid in a tiny range for most binary fluid mixtures because of the slow particle diffusion, and ex-

perimental observations are outside the range of applicability of this simple theory.

2. Oscillatory instability

The oscillatory instability is important in low Prandtl number convection where it limits the maximum Rayleigh number for stationary convection rolls. The instability is periodic in time as implied by the name, has a nonzero wave number along the rolls, and at least initially introduces no extra spatial dependence perpendicular to the rolls. It is therefore an example of a type I_o instability and we will discuss it in this context, concentrating on one-dimensional spatial patterns.

The oscillatory instability was first discussed by Busse (1972). For the physically artificial free-slip case it occurs at long wavelengths and, at low Prandtl numbers, arbitrarily close to threshold. It can therefore be captured analytically by various perturbation techniques. The important degrees of freedom are the translation of the rolls coupled to the mean drift flows discussed in subsection VIII.A.5, which are undamped for free-slip boundaries. The instability has been discussed by conventional perturbation theory (Busse, 1972), amplitude equations (Siggia and Zippelius, 1981b) and phase equation approaches (Fauve *et al.*, 1987).

For rigid boundaries the oscillatory instability occurs at a finite, albeit small, distance above threshold no matter how small the Prandtl number, and at nonzero wave numbers. No systematic expansion scheme has yet been developed to calculate its properties analytically. Fauve *et al.* (1987) phenomenologically modified their phase equation approach by introducing a finite damping on the mean flow, and found quite good agreement with the numerically calculated linear instability curves of Clever and Busse (1974), although systematic deviations are clearly apparent. For quantitatively accurate parameters the numerical Galerkin calculation of Clever and Busse must be used (see also Fauve *et al.*, 1987). A calculation of effects nonlinear in the oscillatory mode amplitude is even more difficult, and we see no reason to expect even qualitatively reliable results from the geometrical arguments of Fauve *et al.*

Experimentally, it turns out that at least for some parameter values (Prandtl number, roll wave number) the oscillatory instability is continuous (supercritical). The behavior near onset is then described by the standard type I_o amplitude equations which we write in the unscaled form as

$$\tau_0(\partial_t + s_0\partial_y)A_R = \epsilon(1+ic_0)A_R + \xi_0^2(1+ic_1)\partial_y^2A_R - [g_0(1-ic_3)|A_R|^2 + g_1(1-ic_2)|A_L|^2]A_R, \quad (8.94)$$

with a similar equation for A_L given by $R \leftrightarrow L$ and $s_0 \rightarrow -s_0$. We have neglected spatial variation along the roll normal (which we continue to label x so that the wave propagation is in the $\pm y$ direction). Unlike many other realizations of type I_o instabilities (such as binary-

fluid convection) which are subcritical, this system provides a direct way to investigate the effect of propagation on weakly nonlinear states, and in particular to test the effects of convective instability and the analysis of Sec. V.B.

Croquette and Williams (1989) and Chiffaudel *et al.* (1989) have carried out such experiments. We shall discuss the former since their setup allowed visualization of the pattern. They used a rectangular cell of aspect ratio 24×32 containing high-pressure argon gas, which yields the low Prandtl number necessary to observe the oscillatory instability, and also permits visualization. The rolls in the convective state were arranged to be parallel to the short side by hot-wire thermal forcing along the walls, and the wave number of the rolls was cleverly manipulated into the right range by the controlled introduction of dislocations which served to reduce the wave number from its threshold value by their climb motion. The oscillatory instability appears without much spatial dependence along the roll normal so that for the central few rolls at least, the one-dimensional treatment given by Eq. (8.94) should be adequate. By measuring the oscillations forced by a small loudspeaker below threshold Croquette and Williams measured the linear parameters of the instability to be,

$$\begin{aligned} g_0 &= 2.3 \pm 1, \quad \omega_0 = 19.8 \pm 1, \\ s_0 &= 5.02 \pm 0.5, \quad \xi_0 = 0.52 \pm 0.15, \\ \tau_0 &= 0.163 \pm 0.05, \quad c_0 = 1.57 \pm 0.3, \\ c_1 &= -0.83 \pm 0.3. \end{aligned} \quad (8.95)$$

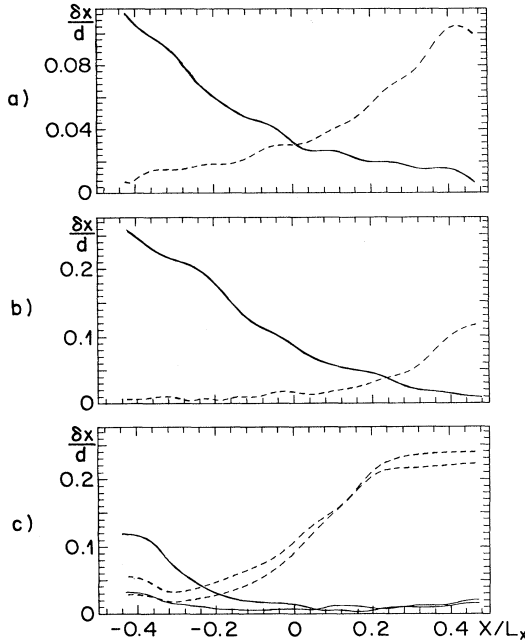


FIG. 47. Amplitude of nonlinear waves near the onset of oscillatory convection, deconvoluted from experimental traces of the roll displacement. Full line is the amplitude of left-moving waves, dashed line that of right-moving waves. (a) $R/R_c = 4.036$, symmetric state; (b) $R/R_c = 4.222$, left-moving waves dominate; (c) $R/R_c = 4.349$, time-dependent “blinking” state, with the two lines corresponding to opposite phases of the modulation. These results should be compared with Fig. 25. (From Croquette and Williams, 1989.)

In addition, the shift in threshold from the infinite system value (estimated by extrapolating the growth rate to zero), $\varepsilon_c = 0.058$, yields an estimate of the reflection coefficient of the waves at the long sidewall via Eq. (5.29), $|r| = 0.183$. Note that at threshold the scaled group speed (6.32) is $s = 6.5 \pm 2$, so that $s(1 + c_1^2)^{-1/2} = 3.0$, and the experiment is well within the “convectively unstable” range (see Sec. VI.C.1).

Unfortunately the nonlinear parameters g_0 , g_1 , c_2 , and c_3 are difficult to measure; Croquette and Williams estimate $g_0 \geq 2$, and also $c_3 = 1$. [This latter value is inconsistent with the one based on the work of Fauve *et al.* (1987), but as we have seen this theory is not expected to be quantitatively reliable.] Also only the combination of boundary parameters α_{\pm} , β_{\pm} of Eq. (5.34) that appears in $|r|$ is determined. Thus several parameters needed for a comparison with theory are not known. Fortunately, the results are not too sensitive to these parameters, and with reasonable choices Cross and Kuo (1992) obtained a remarkably good account of the experiments, as illustrated in Figs. 47 and 48.

3. Non-Boussinesq effects

As discussed in Sec. IV.A, hexagonal patterns are obtained near the threshold of a type I_s instability when the

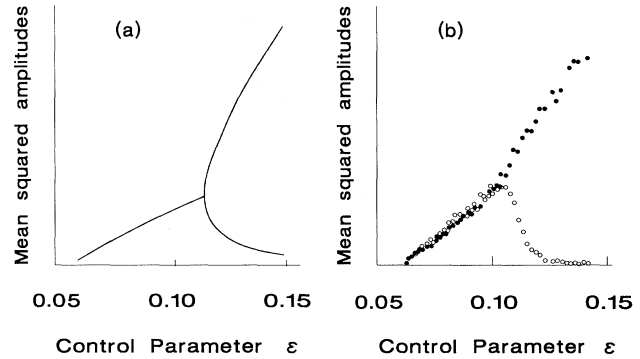


FIG. 48. Comparison of mean squared amplitudes of right and left moving waves as a function of reduced control parameter ε , (a) from solution of amplitude Eq. (8.94); (b) from the experiment shown in Fig. 47. Solid circles denote right-moving waves, open circles left-moving waves. The actual quantity plotted is proportional to $\langle (1 - \cos 2\pi x/L) |A_{R,L}|^2 \rangle$ for $0 \leq x \leq L$, to reduce the sensitivity to the end regions where the experimental measurements were less reliable. For small values of ε the mean square amplitudes of right- and left-moving waves are equal. For $\varepsilon \gtrsim 0.11$ the symmetry is broken and one set begins to dominate. For $\varepsilon \gtrsim 0.15$ (not shown) a dynamic state occurs as in Fig. 47(c). Parameters used in the numerical simulation were $L/\xi_0 = 45.6$, $s_0 \tau_0 / \xi_0 = 1.6$, $c_1 = -0.8$ obtained from independent experimental measurements; boundary condition parameters were $\alpha = -0.22$, $\beta = 0.44$, consistent with the measured reflection coefficient $|r| = 0.18$. In addition the values $g_1 = 2$, $c_3 = -1.15$, which were not determined experimentally, were used. (From Cross and Kuo, 1992.)

inversion symmetry $A \rightarrow -A$ is broken in the system. For Boussinesq convection the $A \rightarrow -A$ symmetry is a consequence of the $z \rightarrow -z$, $w \rightarrow -w$, $\theta \rightarrow -\theta$ symmetry of Eqs. (8.10). For convection, any asymmetry in the boundary conditions at $z = \pm 1/2$ breaks the $z \rightarrow -z$ symmetry, and would be expected to break the $A \rightarrow -A$ inversion symmetry of the amplitude equation. However, Schlüter *et al.* (1965) showed that in the case of rigid boundary conditions on one plate but free on the other, the coefficient γ of Eq. (4.40) is identically zero in the absence of other non-Boussinesq effects, although higher-order asymmetric terms in the amplitude equation (e.g., of order A^4) would not be expected to have zero coefficient. Thus with these particular asymmetries in the boundary conditions there is no subcritical bifurcation to hexagons. The case of an asymmetry in the thermal boundary conditions does not seem to have been investigated, though such a situation often occurs experimentally when optical access is desired through the top plate. Presumably if both top and bottom plates are much better conductors than the fluid the size of the effect (as measured by γ) will be small.

The inversion symmetry is simply broken when the physical properties of the fluid depend on temperature, and therefore on the vertical coordinate (Palm, 1960). This effect is left out of the Boussinesq equations (8.3) since it is generally small, but it can be taken into account perturbatively. Following Busse (1967b) we introduce the parameter

$$Q = \sum_{i=0}^4 \gamma_i P_i , \quad (8.96)$$

where $\gamma_0 = -(\rho_\ell - \rho_u)/\rho_0$, $\gamma_1 = (\alpha_\ell - \alpha_u)/2\alpha_0$, $\gamma_2 = (\nu_\ell - \nu_u)/\nu_0$, $\gamma_3 = (K_\ell - K_u)/K_0$, $\gamma_4 = (C_\ell - C_u)/C_0$, and the quantities ρ, α, ν, K, C are the density, thermal expansion, kinematic viscosity, thermal conductivity, and heat capacity, all of which determine the convective threshold via Eqs. (8.9) and (8.11a). The subscripts ℓ , u , and 0 refer to evaluating the quantities at the temperatures of the lower and upper plates and at the midplane, respectively. The P_i are $O(1)$ coefficients which depend on Prandtl number and have been calculated by Busse for $\sigma \rightarrow \infty$ in the rigid case, and estimated for finite σ . For purposes of describing pattern formation near threshold it suffices to say that a nonzero value of Q leads to the amplitude equation (4.40) with coefficients

$$\gamma(Q) = (3/R_c g_0)^{1/2} Q , \quad (8.97a)$$

$$g_1^{-1} = g_0^{-1} (0.2913 + 0.0815 \sigma^{-1} + 0.0893 \sigma^{-2}) , \quad (8.97b)$$

and g_0 given in Eq. (8.16c). According to the analysis of Sec. IV.A we therefore obtain the characteristic bifurcation diagram in Fig. 10, showing a subcritical bifurcation to hexagons, followed by a region $\varepsilon_R < \varepsilon < \varepsilon_B$ of hexagon-roll bistability, and a roll region for $\varepsilon > \varepsilon_B$ due to an instability of hexagons at ε_B . The basic validity of this theory was verified by Walden and Ahlers (1981) in experiments in liquid ${}^4\text{He}$. More recently Ciliberto, Pam-

olini and Perez-Garcia (1988) performed visualization experiments in water in a cell with aspect ratio $L = r/d = 18$. The authors made a spatial Fourier analysis of the patterns and were able to measure Bragg peaks with considerable accuracy. From the ratio of the peak strengths associated with hexagons and rolls, respectively, they studied the hysteretic transition between the two types of patterns. Moreover they verified quantitatively that the experimental bifurcation diagram agrees with the predictions of Busse (Fig. 10) when an overall correction is made for the threshold shift due to the finite aspect ratio. In particular, the ratio of slopes $(N-1)/\varepsilon$ for hexagons and rolls agrees with theory, and the ratio $(R_B - R_c)/(R_R - R_c)$ agrees to within 15%. Ciliberto *et al.* observed the effect of sidewalls on the patterns, as well as the detailed behavior of defects in the bistable region. These observations have been discussed theoretically by Walgraef (1991). Very recently Bodenschatz, DeBruyn, Ahlers, and Cannell (1991a) carried out experiments in a cylindrical cell of aspect ratio $L = 86$, and were able to obtain a bifurcation diagram unaffected by finite size and to resolve the small quantity ε_A . At larger ε -values they found the remarkably regular hexagonal array shown in Fig. 49(a).

Defects in the hexagon-roll system offer an elegant example of the usefulness of the amplitude equations for describing spatial patterns. Within this approach the hexagonal pattern and its defects are completely determined by the amplitudes of three sets of rolls. In the core one thus expects to see local realizations of roll solutions that are *unstable* in the bulk. One such example, which has been demonstrated experimentally by Ciliberto *et al.* (1990) is a *point dislocation* in the hexagon structure, otherwise known as a “penta-hepta pair.” Let the ideal hexagon structure be made up of the triplet of rolls

$$A_j = a_j(\mathbf{x}) e^{i\phi_j(\mathbf{x})} , \quad j = 1, 2, 3 , \quad (8.98a)$$

with $\nabla_{\mathbf{x}} \phi_j = \mathbf{q}_i$,

$$\mathbf{q}_1 + \mathbf{q}_2 + \mathbf{q}_3 = 0 , \quad (8.98b)$$

and let there be a dislocation at $\mathbf{x} = (x_0, y_0)$. Ciliberto *et al.* measured the pattern shown in Fig. 50(a) by shadowgraph methods, and using Fourier transform decompositions and filtering, were able to determine the local values of the three amplitudes and phases. Then as shown in Figs. 50(e) and (f), they demonstrated that the amplitudes $a_1(\mathbf{x})$ and $a_2(\mathbf{x})$ had a zero at (x_0, y_0) , whereas $a_3(\mathbf{x})$ remains large. The corresponding phases ϕ_1 and ϕ_2 had a singularity, whereas ϕ_3 remains smooth. This demonstrates that the unstable roll solution $a_3 \exp(i\mathbf{q}_3 \cdot \mathbf{x})$ is present in the core of this defect. Another similar example (not shown here) is a grain boundary between three stable roll states with wave vectors also satisfying Eq. (8.98b). In the core of the defect a_1 and a_2 are large whereas a_3 vanishes, and all three phases are smooth. This is an example of the presence of an (unstable) *mixed state*, with two nonzero amplitudes.

These examples illustrate how general symmetry argu-

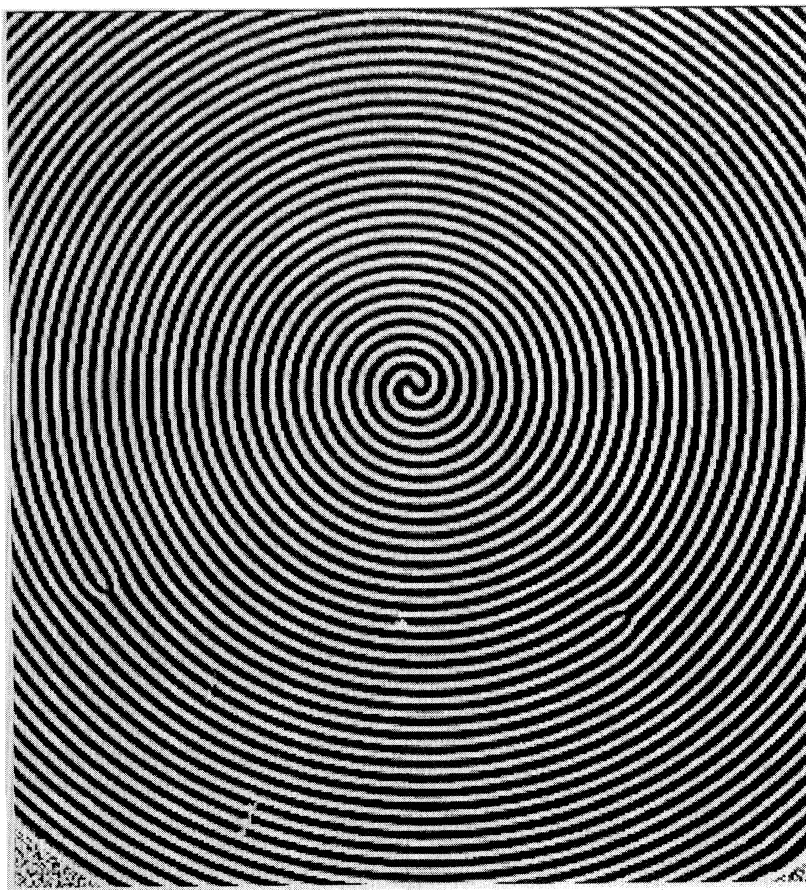
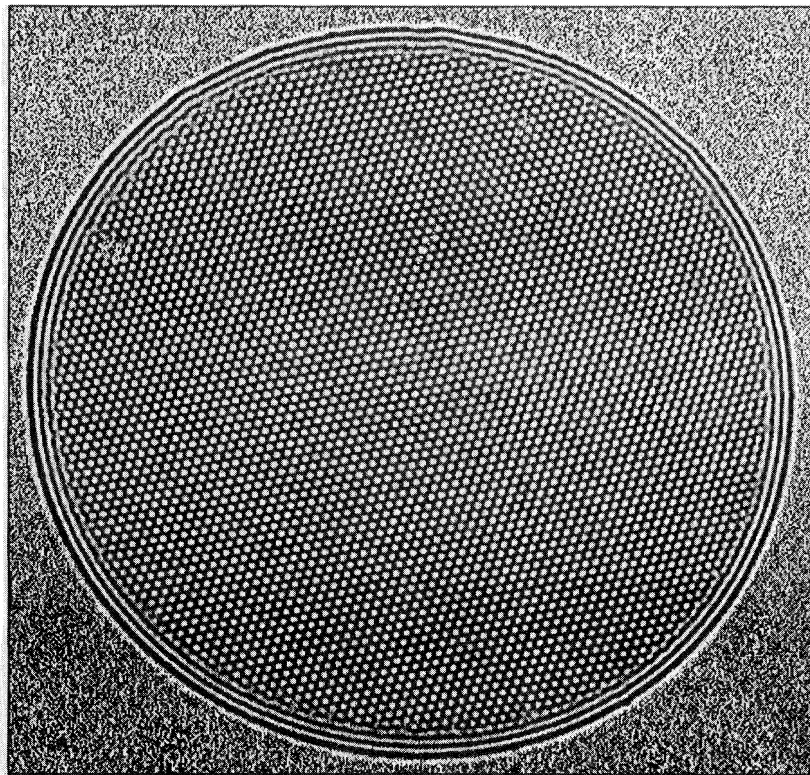


FIG. 49. Patterns in non-Boussinesq convection in an aspect ratio 86 cylindrical cell of gaseous CO_2 . (a) Hexagonal pattern seen near threshold, $\epsilon = 0.06$: notice the remarkably regular hexagonal cells except in a thin layer near the boundary where the cylindrical walls induce circular rolls. (b) Roll state for slightly larger $\epsilon = 0.15$: the rolls here form a two-armed spiral which slowly rotates with a period of 2400 vertical diffusion times. Note that only a portion of the pattern is shown. (From Bodenschatz *et al.*, 1991.)

ments can predict the details of rather complicated spatial patterns. It should be remembered, however, that the analysis relies on the specific amplitude equations used, and a simple description of the core states would not be expected to apply to defects in experiments away from threshold, or in calculations using the Swift-Hohenberg equation, for example. In that case the size of the core is $O(1)$ and the rapid spatial variation may lead to large deviations from a local roll structure.

Lastly, we mention an interesting experiment by Hartung, Busse, and Rehberg (1991) in which a non-

Boussinesq layer of fluid with sinusoidal lateral variation of the temperature showed a time-dependent transition to convective flow.

4. Effect of surface tension: Bénard-Marangoni convection

As mentioned in Sec. II.B convection in a container with a free surface is driven by both surface tension and buoyancy, the competition between the two mechanisms being governed primarily by the thickness d of the layer.

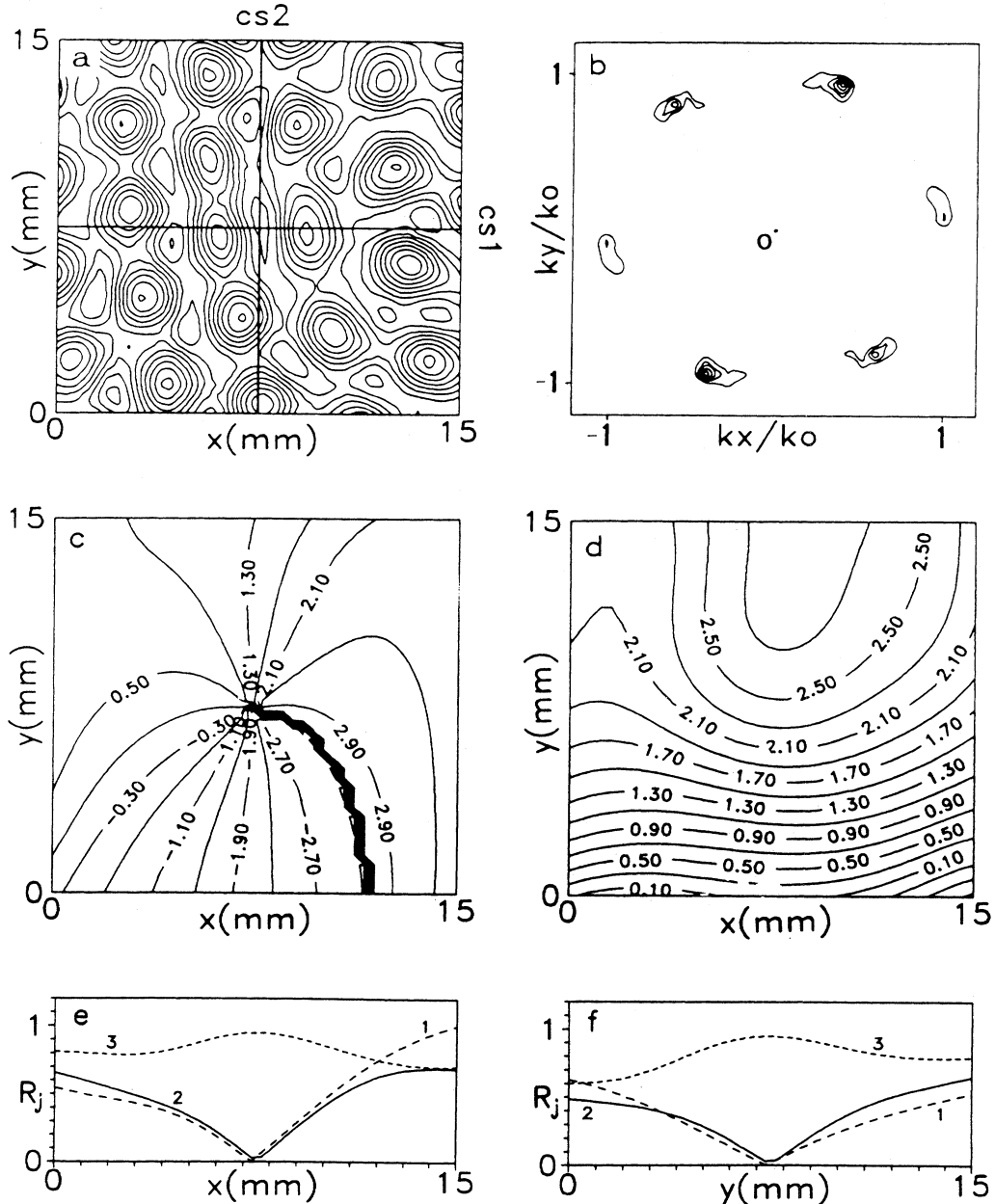


FIG. 50. Defect in a pattern of hexagons: penta-hepta pair. (a) Isotherms of the convective temperature field $T(x,y)$ in a small area of the cell at $\epsilon=0.02$. (b) Spatial Fourier spectrum of the field in (a). (c) Equiphasic lines of ϕ_1 , Eq. (8.98a). (d) Equiphasic lines of ϕ_3 . (e) Cross sections of the amplitudes R_j [denoted a_j in Eq. (8.98a)] with $j=1-3$, along the line labeled CS1 in (a). (f) As in (e) but the cross sections are taken along CS2 in (a). For further explanation see text. (From Ciliberto *et al.*, 1990.)

Again up-down symmetry is broken and a hexagonal pattern is expected. The onset of convection depends on the Marangoni number M , Eq. (2.5), and the Rayleigh number R , Eq. (8.9), and is given to good approximation (Nield, 1964) by

$$\frac{R_c}{R_{co}} + \frac{M_c}{M_{co}} = 1 , \quad (8.99)$$

with $R_{co} = 695$ when the top surface is free, and $M_{co} \approx 90$. [The value of M_{co} depends on the properties of the surface via the Biot number B defined in Eq. (8.82) above, which is generally small (Normand *et al.*, 1977).] The nonlinear properties have been studied by Rosenblatt *et al.* (1982a,b) and by Cloot and Lebon (1984). The corresponding amplitude equation will have the form (4.40), but the coefficients γ , g_0 , and g_1 , are only partially known as functions of Σ and B . The most interesting aspect of this system from our point of view is that large hexagonal patterns have been observed (Cerisier *et al.*, 1987; Perez-Garcia *et al.*, 1988), and their evolution as a function of size L and control parameter can be measured. In particular, defects in the hexagonal lattice appear spontaneously in the system and it would be interesting to study their role in melting the lattice, if large enough systems could be obtained. Moreover, the evolution of the characteristic wave vector, as deduced from the size of the hexagons, has been measured near threshold (Cerisier *et al.*, 1987), and it should be amenable to theoretical analysis.

5. Modulated convection

We have already discussed in subsection VIII.D.1 experiments using a slow periodic modulation of the Rayleigh number through threshold to investigate the small forcing and its dramatic effect on pattern selection. For more rapid modulation there are two new interesting effects. First the threshold is shifted (see Ahlers *et al.*, 1985b, and references therein; Lücke, 1987; Donnelly, 1990), and second an *asymmetric* modulation of the temperatures of the upper and lower plates induces a hexagonal pattern (Roppo *et al.*, 1984; Hohenberg and Swift, 1987; Meyer *et al.*, 1988, 1992).

a. Threshold shift

If we assume that the only effect of modulating the plate temperatures is to provide a time-dependent reduced Rayleigh number $\varepsilon(t)$ and no change in pattern, then near threshold the system is most simply described by the amplitude equation

$$\partial_t \bar{A} = \varepsilon(t) \bar{A} - \bar{A}^3 , \quad (8.100)$$

with

$$\varepsilon(t) = \varepsilon_0 + \delta \cos \omega t \quad (8.101)$$

(we suppress the spatial dependence of A for simplicity).

Now it can be shown quite generally (Ahlers *et al.*, 1985b) that for any periodic $\varepsilon(t)$ the time average of \bar{A}^2 over many periods depends only on the average of ε , i.e.

$$\langle \bar{A}^2 \rangle (t, \delta) = \lim_{\tau \rightarrow \infty} \frac{1}{\tau} \int_0^\tau \bar{A}^2(t, \delta) dt = \langle \bar{A}^2 \rangle (t, 0) . \quad (8.102)$$

Thus according to Eq. (8.102) the bifurcation of $\langle \bar{A}^2 \rangle$ must occur at $\varepsilon_0 = 0$, independent of δ .

On the other hand, the linearized hydrodynamic equations can be analyzed for sinusoidal variation of the lower plate temperature, say

$$T_\ell(t) = T_{\ell o} (1 + \delta \cos \omega t) , \quad (8.103)$$

and the bifurcation studied as a function of the average Rayleigh number R_c , based on $T_{\ell o} - T_u$. It is found in general that the convection threshold shifts as a result of the modulation (see Davis, 1976; Ahlers *et al.*, 1985b). Analytic expressions are available in various limits, particularly for small modulation amplitudes $\delta \ll 1$, where the shift is given by

$$(R_c - R_c^{\text{stat}})/R_c^{\text{stat}} = \varepsilon_{oc} = \delta^2 M(\omega, \sigma) , \quad (8.104)$$

where $M(\omega, \sigma)$ is an $O(1)$ function such that $M(0, \sigma) = M_0 \neq 0$ and $M(\omega, \sigma) \rightarrow 0$ for $\omega \rightarrow \infty$. The existence of a threshold shift in the low-frequency limit is associated with the fact that although we are considering modulation of arbitrarily long period, the response is averaged over many periods [i.e. $\omega \rightarrow 0$, $\tau \rightarrow \infty$, $\omega\tau \gg 1$ in Eq. (8.102)].

In the presence of modulation even the linear problem can only be solved analytically in certain limits, so it is useful to seek approximate treatments of the threshold shift and the near-threshold behavior. A simplified theory based on the Lorenz truncation (8.45), which ignores the spatial variation of the roll amplitudes, was proposed by Ahlers, Hohenberg, and Lücke (1985b). The equations are essentially those of the Lorenz system (8.46), except that the control parameter r is replaced by

$$r(t) = 1 + \varepsilon(t) = 1 + \varepsilon_0 + \delta \cos \omega t , \quad (8.105)$$

and the coefficient b has the value $b = 2$ for rigid horizontal boundaries. The linear problem then reduces to

$$m \partial_t^2 \bar{A} + \partial_t \bar{A} - \varepsilon(t) \bar{A} = 0 , \quad (8.106)$$

i.e. a damped parameterically driven oscillator, or Hill's equation with m a constant depending on σ . It is then easy to show that in general the bifurcation threshold $\varepsilon_{oc}(\omega, \delta)$ is nonzero, and it can be calculated exactly for the special choice of a stepwise constant control parameter $\varepsilon(t) = \varepsilon_0 + \delta s(\omega t / \pi)$, with $s(x) = +1$ for $2n < x < 2n + 1$, $s(x) = -1$ for $2n + 1 < x < 2n + 2$, n an integer. The threshold shift calculated from the Lorenz model has been compared with calculations based on the hydrodynamic equations (8.10) with T given by Eq. (8.103), in limits where these are available, and the agree-

ment is good for both rigid and free boundaries. In addition, the nonlinear behavior can be calculated rather simply in the model (this has only been done very recently for the full equations, see Schmitt and Lücke, 1991) and the comparison with experiment is again satisfactory, provided a time-dependent forcing term such as (8.58) is added to Eq. (8.46a) for $X(t)$. The theoretical predictions of Ahlers *et al.* (1985b) concerning the threshold shifts have been confirmed experimentally by Niemela and Donnelly (1987) and by Meyer *et al.* (1992).

b. Hexagonal patterns

In the simple model discussed above it is assumed that the pattern consists of a single set of parallel rolls and $X(t)$, Eq. (8.45a), [or $\bar{A}(t)$] is their amplitude. When the time dependence of the plate temperatures is *asymmetric* with respect to the top and bottom plates, the fluid response creates an asymmetric temperature profile which favors hexagonal convection near threshold (Roppono *et al.*, 1984) (it is an example of a non-Boussinesq effect discussed in subsection 3 above). This effect can be incorporated into the Lorenz model by including three sets of rolls making angles of $2\pi/3$, plus the higher spatial harmonics that govern their coupling in lowest order (Hohenberg and Swift, 1987). This hexagon-roll system consists of 13 coupled first-order *ode*'s with time-dependent coefficients. In the limit of large Prandtl number and low modulation frequency the threshold shift vanishes, and the model reduces to three coupled amplitude equations of the form (4.40) for the three roll directions, with coefficients that depend on time. The asymmetry parameter $\gamma(t)$ arises from a spatial average of the conduction profile, and it has the form (Swift and Hohenberg, 1989)

$$\gamma(t) = c_2 [\partial_t \phi_u(t) + \partial_t \phi_\ell(t)], \quad (8.107)$$

where c_2 is a known $O(1)$ coefficient and $\phi_{\ell,u}(t)$ are time-dependent upper- and lower-plate temperatures in dimensionless form

$$T_{\ell,u}(t) = \bar{T}_{\ell,u} + R_c \phi_{\ell,u}(t), \quad (8.108)$$

($\bar{T}_{\ell,u}$ are time-averaged temperatures for the lower and upper plates). More general formulas valid at arbitrary frequency and Prandtl number have also been obtained by Swift and Hohenberg (1989), and the asymmetry again involves a parameter like $\gamma(t)$. A bifurcation diagram analogous to the one in Fig. 10 can once again be calculated from the equations of motion, without any adjustable parameters. Note that according to Eq. (8.107) the asymmetry parameter γ , which scales all hexagon effects, vanishes if the upper and lower plate are exactly out of phase [$\phi_\ell = -\phi_u$]. For in-phase modulation on the other hand, it turns out, somewhat surprisingly, that hexagons are still obtained if $\phi(t)$ is not purely sinusoidal. For example, according to Eq. (8.107), a linear variation [$\phi_\ell(t) = \phi_u(t) = \eta t$] produces an asymmetry coefficient

$\gamma(t)$ which is linear in η and a parameter $\varepsilon_A = (R_A - R_c)/R_c$ proportional to η^2 (Krishnamurthy, 1986). An asymmetric modulation $\phi_\ell(t) = \delta \cos \omega t$, $\phi_u(t) = 0$, on the other hand, leads to $\varepsilon_A \sim \delta^4$ for small δ (Hohenberg and Swift, 1987). Some predictions of this theory have been verified quantitatively in experiments of Meyer *et al.* (1988) in a cylindrical cell of aspect ratio $L = 11$, where a clear hexagonal pattern was obtained (see Fig. 51). In particular, the transition points $\varepsilon_R = (R_R - R_c)/R_c$ and $\varepsilon_B = (R_B - R_c)/R_c$ were in good

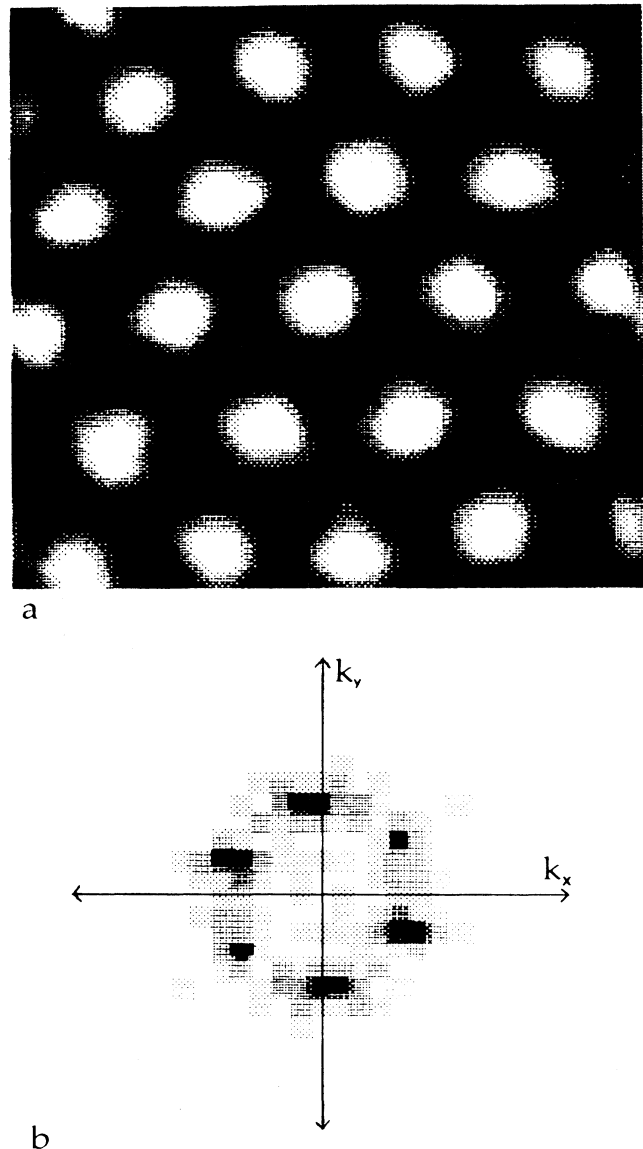


FIG. 51. Hexagon pattern in modulated convection. (a) Shadograph image of a hexagonal convection pattern achieved with modulation parameters $\omega = 1.5$, $\delta = 1.97$, and $\varepsilon_0 = 0.20$ in Eq. (8.101). The bright regions show downflow at the center of the hexagons, while the dark regions show upflow along their outer boundaries. (b) Low-wave-vector portion of the Fourier transform of the image in (a), demonstrating the sixfold symmetry of the pattern. (From Meyer *et al.*, 1988.)

agreement with theory, but no hysteresis was observed in the bistable region. A number of the predictions of Swift and Hohenberg (1989) concerning modulation of upper and lower plates still await experimental tests, and the spatial dependence of the patterns (defects and interfaces) lies completely outside the scope of their simple model.

6. Rotating convection

In a rotating system the Coriolis force may have a significant effect on fluid convection driven by the usual temperature gradient. There are obvious geophysical motivations for studying this phenomenon. The linear instability problem for the onset of convection in a rotating system was studied by Chandrasekhar (1953), and the nonlinear problem with free-slip boundaries by Veronis (1952). From the perspective of this review, our interest in this system goes back to the analysis by Küppers and Lortz (1969) who used the amplitude equation to consider the instability of a nonlinear convective roll state as the rotation rate Ω is increased at fixed temperature gradient. (The analysis was extended to the regime away from threshold by Clever and Busse, 1979.) As discussed in Sec. IV.A.1.a.iv, at a critical rotation rate Ω_c a set of rolls becomes unstable to a second set rotated at some angle θ_c relative to the first set, which in turn become unstable to a set rotated through a further angle θ_c , etc., so that no steady state solution is expected. Furthermore, since the nonlinear coupling constant $\mathcal{G}(\theta)$ in the amplitude equation is no longer symmetric under $\theta \rightarrow -\theta$, the coupled equations are not potential. Thus a dynamic state is expected arbitrarily close to threshold. (Note that we are imagining sitting in the rotating frame, and looking at dynamics relative to the steady state rotation.) An early analysis of the dynamic state by Busse and Heikes (1980) was based on the closeness of θ_c to 60° for a wide range of Prandtl numbers. They used a model consisting of three spatially uniform coupled amplitudes A_1, A_2, A_3 for rolls mutually at 120° . For real amplitudes the equations of motion become

$$\partial_t A_1 = \varepsilon A_1 - [A_1^2 + g_+ A_2^2 + g_- A_3^2] A_1, \quad (8.109a)$$

$$\partial_t A_2 = \varepsilon A_2 - [A_2^2 + g_+ A_3^2 + g_- A_1^2] A_2, \quad (8.109b)$$

$$\partial_t A_3 = \varepsilon A_3 - [A_3^2 + g_+ A_1^2 + g_- A_2^2] A_3, \quad (8.109c)$$

where $g_+ = \mathcal{G}(120)/\mathcal{G}(0)$ and $g_- = \mathcal{G}(-120)/\mathcal{G}(0)$, and the condition for the Küppers-Lortz instability is $g_+ > 1$ and $g_- < 1$, or vice versa. These equations, which were earlier studied by May and Leonard (1975) in a different context, have the interesting property that the orbit continually approaches the heteroclinic orbit connecting the unstable roll fixed points: $(A_0, 0, 0) \rightarrow (0, A_0, 0) \rightarrow (0, 0, A_0) \rightarrow (A_0, 0, 0)$, where (A_1, A_2, A_3) is the vector of amplitudes, and $A_0^2 = \varepsilon/(1+g_++g_-)$. The orbit spends longer and longer in the vicinity of the fixed points, and so the return time diverges at long evolution times. Busse and Heikes suggested that in practice noise

would eventually limit the closeness of approach to the fixed points, yielding some finite mean return time fixed by the noise strength (see also Busse, 1984). The detailed time dependence of the macroscopic variables is unpredictable due to the extreme sensitivity of the orbit to the noise very close to the fixed points. Experiments by Heikes and Busse (1980) seemed to confirm some aspects of the model, although already in this work the importance of spatial domains was apparent. Niemela and Donnelly (1986), using cryogenic helium cells, showed evidence of sensitivity to added noise, although no flow visualization was possible in their experiment. More recently the spatial pattern forming aspects of this system have come under investigation. The importance of defects near the edges of the cell at the onset of time dependence was noted by Zhong *et al.* (1991b) in a cylinder of aspect ratio $L = 10$ containing water. Bodenschatz *et al.* (1992) in a larger cell ($L = 23$), using dense CO_2 as the fluid, see clear evidence for the motion of grain boundaries between patches of rolls oriented at approximately 120° . The motion in both experiments is apparently chaotic, but presumably a length scale set by the system size or the domain size plays the role of the imperfection that keeps the dynamics from converging to the ideal-system infinite period orbit. This system is clearly of great interest for studying the combination of pattern formation and temporal chaos just above onset (Tu and Cross, 1992). The development of the defects or domains into the vortices typical of the high ε state is also of interest (Zhong *et al.*, 1991a).

IX. OTHER FLUID SYSTEMS

A. Convection in fluid mixtures

Convection in binary-fluid mixtures is a well-studied example of a I_o system where space and time scales are roughly as in pure Rayleigh-Bénard convection (see Platten and Legros, 1984 for a general introduction). Since the bifurcation can be oscillatory it immediately leads to a rich phenomenology even in its simplest incarnation, the complex Ginzburg-Landau model. Unfortunately, besides the Hopf bifurcation, there are two other features of the system that complicate the behavior: a subcritical bifurcation to convection and the existence of an additional small parameter, the Lewis number \mathcal{L} representing the ratio of time scales for thermal and solute diffusion, respectively. The last property is not a necessary concomitant of binary fluids since gases have $\mathcal{L} = O(1)$, but for gases the Dufour effect is important and it suppresses the oscillatory instability to unrealistic parameter values in most cases (Hort *et al.*, 1992). Thus all experiments to date have been on liquids with $\mathcal{L} \lesssim 10^{-2}$. The subcritical bifurcation and the small Lewis number imply that theories based on small perturbations of the conducive state will necessarily fail quantitatively in most cases, though it might be hoped that many of the qualitative

features will survive. The situation is somewhat analogous to that encountered in the Belousov-Zhabotinsky reaction in chemistry (Sec. X). For that case a singular perturbation theory exploiting the small parameter has in fact been developed as an alternative to the standard amplitude and phase equations.

Early theoretical work focused on the linear instability, but usually involved unrealistic models such as free-slip permeable boundaries, or the so-called thermohaline model which neglects the Soret effect (see below). Alternatively, attempts were made to describe the realistic rigid impermeable situation, but even at the linear level uncontrolled approximations were made (e.g. Gutkowicz-Krusin *et al.*, 1979). The nonlinear behavior was described for the free-slip or thermohaline models (e.g. Knoblock and Proctor, 1981; Coullet and Spiegel, 1983) by deriving amplitude equations that showed the interesting feature of a codimension-two bifurcation where the stationary and oscillatory bifurcations meet (Brand *et al.*, 1983, 1984). The codimension-two point was studied experimentally by Rehberg and Ahlers (1985) in a cryogenic ^3He - ^4He mixture flowing through a porous medium, and by Ahlers and Rehberg (1986) in a bulk ^3He - ^4He mixture. Although many of the theoretical predictions were verified, a number of discrepancies remained, and the absence of flow visualization complicates the interpretation of the experiments (see also Sullivan and Ahlers, 1988a,b). Interestingly, although the papers of Brand, Hohenberg, and Steinberg (1983, 1984) motivated most of the recent experimental interest in this system, it and all of the early work on the problem (except that of Bretherton and Spiegel, 1983) missed the important distinction between standing and traveling waves, presumably because the implicit assumption was made that lateral walls would stabilize standing waves in a small geometry. Although oscillatory states with no overall oscillation of Nusselt number were first observed by Caldwell (1974), it was only after the pioneering experiment of Walden *et al.* (1985) showed clear evidence of traveling waves above threshold, that the attention of the community was drawn to this system as an example of pattern formation that is intrinsically different from pure Rayleigh-Bénard convection (i.e. type I_o vs I_s).

We shall discuss the basic hydrodynamic equations for binary-fluid convection, as well as the various approximations and numerical methods which have been used to understand this system. Then we shall describe some of the key experiments that test the theory, including ones which are not understood at present.

1. Theory

a. Basic hydrodynamic equations

For miscible binary fluids there is an extra contribution to the buoyancy force coming from concentration perturbations, and the Oberbeck-Boussinesq equations

(8.3) must be supplemented with an equation for the evolution of the concentration field $\tilde{c}(\mathbf{x}, t)$. The buoyancy force arises from the density change [cf. Eq. (8.2)]

$$\rho = \bar{\rho} [1 - \alpha(T - \bar{T}) + \beta(\tilde{c} - \bar{c})] , \quad (9.1)$$

with β the new expansion coefficient. We shall scale the concentration with the ratio of expansion coefficients, defining

$$c = (\beta / \alpha) \tilde{c} , \quad (9.2)$$

so that $\Delta\rho \propto \Delta(T - c)$. The equation of motion for the concentration is then given by (Platten and Legros, 1984; Landau and Lifshitz, 1959)

$$\partial_t c + \nabla \cdot \mathbf{j}_c = 0 , \quad (9.3a)$$

$$\mathbf{j}_c = -D_c (\nabla c + \psi \nabla T) + \mathbf{u} c , \quad (9.3b)$$

with D_c the concentration diffusion coefficient. In Eq. (9.3) the separation ratio

$$\psi = -c(1-c) S_T \beta / \alpha , \quad (9.4)$$

(proportional to the Soret coefficient S_T) provides the important coupling between temperature and concentration variations. (The corresponding extra term in the heat current driven by a concentration gradient, the Dufour effect, is negligible in liquids.) The physical boundary condition on c is that of impenetrable walls

$$\hat{\mathbf{n}} \cdot \nabla (c + \psi T) = 0 . \quad (9.5)$$

Thus the imposed temperature gradient in a Rayleigh-Bénard geometry, Eq. (8.4), also implies a linear concentration profile

$$c = c_0(z) = \bar{c} + \psi \Delta T (z - d/2) . \quad (9.6)$$

This concentration gradient is *destabilizing* for $\psi > 0$ and *stabilizing* for $\psi < 0$. The time scale in Eq. (9.3a), relative to the thermal diffusion time is governed by the Lewis number

$$\mathcal{L} = D_c / \kappa \quad (9.7)$$

mentioned above. As in Sec. VIII.A we now subtract off the reference concentration profile $c_0(z)$, introduce dimensionless units, as well as the auxiliary field

$$\xi = c - c_0(z) + \psi \theta , \quad (9.8)$$

to give the dimensionless equations for the perturbation of the linear conducting profiles,

$$\sigma^{-1} (\partial_t + \mathbf{u} \cdot \nabla) \mathbf{u} = -\nabla p + [\theta(1+\psi) - \xi] + \nabla^2 \mathbf{u} , \quad (9.9a)$$

$$(\partial_t + \mathbf{u} \cdot \nabla) \theta = R w + \nabla^2 \theta , \quad (9.9b)$$

$$(\partial_t + \mathbf{u} \cdot \nabla) \xi = \mathcal{L} \nabla^2 \xi + \psi \nabla^2 \theta , \quad (9.9c)$$

$$\nabla \cdot \mathbf{u} = 0 , \quad (9.9d)$$

with boundary conditions on \mathbf{u} and θ as in Sec. VIII.A.1, and in addition the condition of no solute flux for

impenetrable boundaries

$$\partial_z \zeta = 0, \quad z = \pm \frac{1}{2}. \quad (9.10)$$

b. Linear instability

An approximate analysis of this system was carried out some time ago by a number of authors (see, e.g., the references in Brand *et al.*, 1984), but it is only recently that the linear problem was treated exactly. For $\psi < 0$ the stationary instability is suppressed to larger values of $R = R_{sc}$. However for negative enough ψ (depending on \mathcal{L}) the stationary instability is preempted by an oscillatory instability at R_{oc} . An analysis of this instability with the realistic rigid impermeable boundary conditions must be carried out numerically to give R_{oc} , q_0 , and the frequency ω_0 which all depend on σ , ψ , and \mathcal{L} . Let us define the reduced Rayleigh number as

$$r = R / R_c^{(0)}, \quad (9.11)$$

where $R_c^{(0)}$ is the critical value for a pure fluid. In Fig. 52 we show the dependence of $r_{sc} = R_{sc} / R_c^{(0)}$, $r_{oc} = R_{oc} / R_c^{(0)}$ and the threshold frequency ω_0 on ψ for representative values of ψ and \mathcal{L} . It is seen that the first instability is stationary for $\psi > \psi_2$ and oscillatory for $\psi < \psi_2 < 0$, the point of intersection ψ_2 being a codimension-two bifurcation point^{9,1} where $\omega_0 = 0$. The numerical procedure is made more difficult by the small Lewis number. Actually, an easier $\mathcal{L} = 0$ calculation gives sufficiently accurate results for the values of \mathcal{L} usually found ($\mathcal{L} \approx 10^{-2}$), except for ψ very near zero. A theoretical study of the linear instability has been carried out by Cross and Kim (1988a,b) and by Knobloch and Moore (1988), improving on earlier work of Zielinska and Brand (1987).

Because of the difficulty of displaying the full parameter dependence for the rigid-permeable case, sometimes it is convenient to make use of the results for the unrealistic free-slip, permeable boundary ($c = 0$ at $z = \pm 1/2$) model, which is separable and yields analytic expressions (see Brand *et al.*, 1984)

$$r_{sc}^{fp} = (1 + \psi + \psi \mathcal{L}^{-1})^{-1}, \quad (9.12a)$$

$$r_{oc}^{fp} = (1 + \mathcal{L})(1 + \mathcal{L} + \sigma + \mathcal{L}\sigma^{-1})(1 + \sigma + \sigma\psi)^{-1}, \quad (9.12b)$$

with a frequency

$$(\omega_0^{fp})^2 = -\psi(1 + \mathcal{L})(\sigma + \mathcal{L})(1 + \sigma + \sigma\psi)^{-1} - \mathcal{L}^2. \quad (9.12c)$$

These results differ from the correct ones for rigid impermeable boundaries by factors that are of order unity for realistic ranges of ψ , \mathcal{L} , and σ (Knobloch and Moore 1988). However certain features are qualitatively different, for example the critical wave number remains at $q_{0c} = \pi / \sqrt{2}$ for free-slip permeable boundaries, whereas in the rigid impermeable case q_0 depends on the fluid parameters, and there is a true codimension-two point with no jump in parameters in the free case.

c. Nonlinear states

The linear stability analysis is done about the conductive state where the Soret effect and the very slow particle diffusion produce a linear concentration gradient. Above

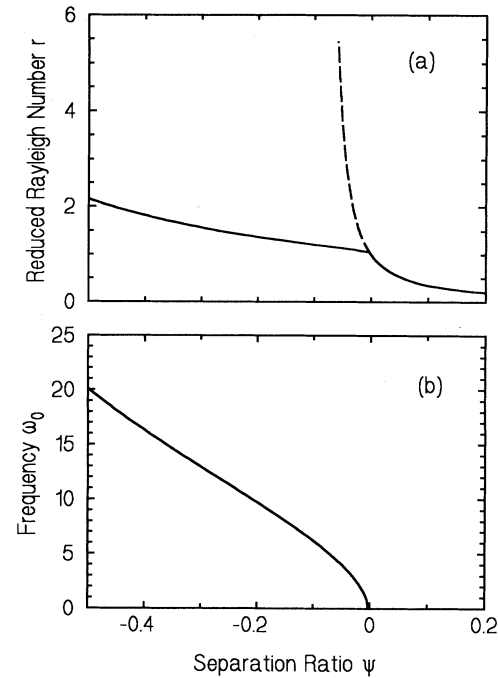


FIG. 52. Critical Rayleigh number and linear instability frequency in a binary fluid mixture with Lewis number $\mathcal{L} = 0.1$ and Prandtl number $\sigma = 10$, as a function of the separation ratio ψ . (a) The parameter r is $R_c / R_c^{(0)}$ with $R_c^{(0)} = 1708$ the critical Rayleigh number for pure fluid convection. The dashed line is the continuation of the stationary bifurcation line above the oscillatory instability. The intersection with the full line marks a codimension-2 degenerate bifurcation point at $\psi = \psi_2 < 0$. Note that ψ_2 is indistinguishable from zero on the scale of the figure since it is $O(\mathcal{L}^2)$. (b) Frequency of the onset state corresponding to (a). Note that for $\psi < \psi_2$ the instability is to a state with a nonzero frequency, whereas for $\psi > \psi_2$ it is to a stationary state. The value $\mathcal{L} = 0.1$ is used for illustrative purposes. For values typical of liquids ($\mathcal{L} \approx 10^{-2}$) the dashed line in part (a) approaches the vertical.

^{9,1}The nature of the codimension-two bifurcation is complicated by the fact that there is a jump in optimal wave number at $\psi = \psi_2$, between the stationary and oscillatory branches (see Cross and Kim, 1988a,b).

threshold the fluid motion would be expected to rapidly mix this concentration gradient, leading to a *uniform* concentration field over most of the depth, with narrow boundary layers of thickness proportional to the small Lewis number \mathcal{L} to which the concentration gradient is confined. Since the concentration gradient away from the boundaries is responsible for the oscillations, we would expect their frequency to decrease rapidly with increasing amplitude of fluid motion, and eventually a transition to stationary convection to take place. Indeed, as discussed below, in experiments in an annular geometry the transition was found to be strongly subcritical for sufficiently negative ψ , leading at R_{oc} to a large amplitude state which is close to the pure fluid convection state (e.g. as measured by the Nusselt number), and consisted of very slow traveling rolls ($\omega \lesssim \omega_0/10$) or, depending on the value of ψ , of stationary rolls sometimes called "stationary overturning convection." Only for very small $|\psi| \sim \mathcal{L}^2$ is the transition expected to become supercritical.

d. Amplitude equations

According to the general discussion of Sec. IV.A we expect an amplitude equation with real coefficients near the stationary instability and one with complex coefficients near the oscillatory instability. The coefficients have been calculated up to cubic order as

functions of ψ , \mathcal{L} , and σ (Cross and Kim, 1988b; Schöpf and Zimmerman, 1989, 1993). Since the sign of the real cubic coefficient is positive rather than negative as in Eq. (4.59) over most of the oscillatory range, the bifurcation to traveling wave convection is in general *subcritical*, and the amplitude expansion is not quantitatively reliable. It is reasonable, however, to try a phenomenological fifth-order equation of the form (5.57) for a semiquantitative description, at least for small $|\psi|$ where the jump at the subcritical bifurcation becomes small. As mentioned above, a separate difficulty involves the smallness of the Lewis number \mathcal{L} , which restricts the amplitude expansion even for the supercritical case. Representative values of the coefficients of the amplitude equation are shown in Table I. Since many unknown higher-order terms are expected to contribute for small \mathcal{L} it is probably preferable to use a fifth-order amplitude equation with fitted coefficients as a phenomenological model.

As discussed in Sec. V.A.3 the endwalls are crucial in allowing the instability to develop in rectangular geometries. Endwalls are naturally incorporated (Cross, 1988b) by adding the boundary conditions (5.34), although the caveats in Sec. V must be remembered, and the approach should be considered phenomenological.

e. Other theoretical methods

In view of the difficulties with the amplitude expansion near threshold, it is natural to search for other methods.

TABLE I. Parameters of the amplitude equation (4.59) for binary-fluid convection for several different values of the Lewis number \mathcal{L} , the Prandtl number σ and the separation ratio ψ . Also shown are the critical Rayleigh number R_{oc} , wave vector q_0 , frequency ω_0 , and parameter c_0 defined in Eqs. (4.58) and (4.48). In addition the value of ψ at the codimension-2 point ψ_2 and at the tricritical point ψ_T (where the real part of the cubic nonlinearity vanishes) are given for each \mathcal{L} and σ . [From Schöpf and Zimmerman, 1990, adapted to our notation.]

	$\mathcal{L} = 0.02 \sigma = 17$		$\mathcal{L} = 0.04 \sigma = 0.75$		$\mathcal{L} = 0.5 \sigma = 1$	
	$\psi_2 = -1.374 \times 10^{-4}$		$\psi_2 = -8.71 \times 10^{-4}$		$\psi_2 = -0.081$	
	$\psi_T = -1.95 \times 10^{-4}$		$\psi_T = -12.59 \times 10^{-4}$		$\psi_T = -0.1363$	
ψ	-1.55×10^{-4}	-0.2	-0.001	-0.2	-0.11	-0.3
R_{oc}	1726.67	2176.74	1769.88	2087.30	2601.12	3216.46
q_0	3.105	3.127	3.069	3.149	2.721	2.759
ω_0	0.072	9.86	0.162	7.51	3.286	8.544
s_0	-0.14	3.08	-0.28	1.95	-0.52	2.28
ξ_0^2	0.149	0.147	0.152	0.147	0.187	0.180
τ_0	0.103	0.102	0.168	0.166	0.143	0.141
c_0	-2.67	0.448	-2.26	0.373	-0.73	0.099
c_1	-2.50	0.114	-1.77	0.056	-0.101	-0.117
c_2	-2.52	-14.9	-2.26	-6.70	-1.09	-1.03
c_3	-260	3.00	-210	5.98	-43.9	4.71
g_1	158	-0.093	135	-0.50	41.6	-2.66

(i) Lorenz models

As already discussed in Sec. VIII.B this method involves the expansion of the hydrodynamic variables in a small number of appropriately chosen modes. The ensuing coefficients satisfy *ode*'s, which are supposed to be valid, at least approximately, beyond threshold.

For the separable free-slip permeable model it is straightforward to generalize the original Lorenz truncation (8.45). We must include extra modes for the concentration variable, and in addition allow for the phase motion of the traveling roll state by taking the amplitudes of the linear modes to be *complex numbers*^{9.2}

$$w = \sqrt{3}\pi [X(t)e^{iqx} + c.c.] \cos\pi z, \quad (9.13a)$$

$$\begin{aligned} \theta = & (9\sqrt{3}\pi^3/2)[Y(t)e^{iqx} + c.c.] \cos\pi z \\ & + (27\pi^3/4)Z(t) \sin 2\pi z, \end{aligned} \quad (9.13b)$$

$$\begin{aligned} \xi = & (9\sqrt{3}\pi^3/2)[U(t)e^{iqx} + c.c.] \sin\pi z \\ & + (27\pi^3/4)V(t) \sin 2\pi z, \end{aligned} \quad (9.13c)$$

with X, Y, U complex and Z, V real. This leads (Cross, 1986a) to the extended Lorenz equations^{9.3}

$$\partial_t X = -\sigma [(X - (1+\psi)Y + U)], \quad (9.14a)$$

$$\partial_t Y = -Y + rX - ZX, \quad (9.14b)$$

$$\partial_t U = -\mathcal{L}U - \psi Y - VX, \quad (9.14c)$$

$$\partial_t Z = -b(Z - XY^* - X^*Y), \quad (9.14d)$$

$$\partial_t V = -b(\mathcal{L}V + \psi Z - XU^* - X^*U), \quad (9.14e)$$

where here we define $r = R/R_{sc}$, $b = 8/3$, and we have taken for the critical wave number $q_0 = \pi/\sqrt{2}$. Solutions of these equations were investigated by Cross (1986a) and by Ahlers and Lücke (1987). They turn out to have a strange degeneracy which is not easily detected by examining the form of the equations: the oscillatory traveling wave solutions exist only at the threshold Rayleigh number r_{oc} , and there they may have a range of amplitudes and frequencies in nonlinear steady states. Above r_{oc} only steady solutions are found. To remove this spurious degeneracy and to reproduce correctly the bifurcation structure of the free-slip permeable model [which, it should be remembered, itself has nongeneric features] Knobloch and Moore (1990) have proposed a “minimal” model with six complex and three real mode amplitudes.

Linz and Lücke (1987), on the other hand, suggest that it is important to include the impermeable boundary condition (9.5), and they have investigated in some detail an intermediate model of free-slip but impermeable boundaries. The linear problem is no longer separable, and the choice of modes even at the linear level is uncontrollable as it was for modulated convection, Sec. VIII.F.5. They used the same choice of modes as in Eq. (9.13), except that they took for the concentration field

$$\xi = \xi_0 \{[U(t)e^{iqx} + c.c.] + V(t)\sqrt{2} \cos(\pi z)\}. \quad (9.15)$$

The resulting equations have the same form as (9.14) but with slightly different coefficients. (Linz and Lücke also calculated these for general q .) The degenerate features of the simple model are removed, for example the critical wave number does indeed show a jump at ψ_2 as in the full equations, and the degeneracy at r_{oc} no longer occurs. However the truncated model contains none of the boundary layer structure expected for small \mathcal{L} , so that quantitative predictions in this limit cannot be expected to be reliable. In addition, some important features are qualitatively inconsistent with results from the full equations with realistic boundary conditions, for example there are apparently no stable nonlinear traveling roll solutions below the tricritical ψ (where the real part of the cubic nonlinearity vanishes), whereas these solutions are certainly conspicuous features of both experimental work and the full theory. Thus this model does not yield a reliable general guide to the experimental phenomena, although judiciously chosen features may be simply investigated.

(ii) Expansion about the pure fluid

For low solute concentration we have $\psi \rightarrow 0$, and it is useful to expand the equations about the (fully nonlinear) equations of pure-fluid Rayleigh-Bénard convection at the same Rayleigh number. In the regime of small $|\psi|$ away from the codimension-two point $\psi_2 \propto -\mathcal{L}^2$, i.e. for

$$\mathcal{L}^2 \ll |\psi| \ll 1, \quad (9.16)$$

(a regime that exists for $\mathcal{L} \ll 1$), Bensimon *et al.* (1989b) have analyzed the convective state using a boundary layer method. In the nonlinear region of saturated traveling waves the characteristic scale for the velocity of convective flow is set by the thermal diffusivity κ , whereas the phase velocity of the waves is determined by the much smaller molecular diffusivity D_c . In the limit (9.16) the mixing due to the flow has a stronger effect on the concentration than on the temperature, so that a sizeable temperature gradient is maintained in the bulk, whereas it is the concentration and not its gradient that is nearly constant. The concentration gradient required by the value of the Soret coefficient occurs in boundary layers of dimensionless thickness \mathcal{L} near the top and bottom plates. From the nonlinear solution with boundary layers the authors predicted the phase velocity v_{tw} of the traveling waves, and in particular the critical Peclet number

^{9.2}The earlier Lorenz-like models missed this crucial point (see e.g. Knobloch and Proctor, 1981).

^{9.3}The definitions of U and V used by Cross (1986a) were in terms of c instead of ξ in Eq. (9.13c), so the corresponding Lorenz equations were somewhat different. It is a simple matter to transform from one set of definitions to the other.

$$P_c = u_c d / D_c , \quad (9.17)$$

at which the velocity v_{tw} vanishes, and the nonlinear convection becomes stationary (u_c is the convective fluid velocity, which depends on R and can be evaluated from the pure-fluid case). The result for P_c is

$$P_c = f(|\psi|/\mathcal{L}^2) , \quad (9.18)$$

where the function $f(x)$ was evaluated numerically, and had the asymptotic form

$$f(x) \sim (16.98 x)^{4/7} , \quad x \rightarrow \infty . \quad (9.19)$$

(iii) Expansion about the codimension-two point

At the codimension-two point ψ_2 four eigenvalues pass through zero. Nearby, the “unfolding” of this degenerate bifurcation leads to a rich range of possible behavior, including traveling and standing waves, stationary rolls and in addition modulated wave states with two temporal frequencies. Knobloch and co-workers (see Knobloch and Moore, 1990, and references therein) have suggested that this structure may be used to understand qualitatively the various states and transitions in spatially homogeneous binary-fluid convection even far away from the codimension-two point, much as we have used the behavior at the nondegenerate bifurcation to understand general nonlinear patterns throughout this work.

Unfortunately the “unfolding of the Takens-Bogdanov bifurcation with $O(2)$ symmetry” (Dangelmayr and Knobloch, 1987) is very complicated, and contains many possibilities depending on parameter values. In addition as we have seen, for small Lewis number there are other bifurcations very nearby, such as the traveling wave tricritical point and the stationary roll saddle node, and these must be included by hand on top of the generic codimension-two behavior to obtain the experimentally relevant behavior. Thus it is hard to make *predictions* based on this approach (beyond local consequences of various types of bifurcations). Near enough to the codimension-two point the degenerate bifurcation theory does provide a rather complete description, and predicts some interesting behavior. If we first ignore spatial inhomogeneities and assume rolls at a fixed wave number q_0 the behavior near the codimension-two point is summarized by a higher-order amplitude equation. We define a complex amplitude $A(t)$ in the usual way

$$U \sim [A(t)e^{iq_0x} + c.c.]U_0(z) , \quad (9.20)$$

so that A satisfies an equation of the form^{9.4}

^{9.4}As mentioned above, earlier work (Knobloch and Proctor, 1981; Coullet and Spiegel, 1983; Brand *et al.*, 1984) had missed the possibility of traveling waves and had derived an equation for a real amplitude describing the standing-wave to stationary-roll codimension-two point. Equation (9.21) has an extra term, with coefficient g_3 , compared to the earlier work which included the $Z_2(q \rightarrow -q)$ symmetry but not the $O(2)$ phase symmetry.

$$\begin{aligned} \partial_t^2 A - (\alpha - g_2 |A|^2) \partial_t A \\ - [\beta + g_1 |A|^2 + g_3 (A \partial_t A^* + A^* \partial_t A)] A = 0 . \end{aligned} \quad (9.21)$$

Here $\alpha = \beta = 0$ defines the codimension-two point, $\alpha \neq 0$, $\beta = 0$ gives the stationary instability, $\alpha = 0$, $\beta \neq 0$ gives the oscillatory instability, and g_1, g_2, g_3 are coefficients of the independent nonlinear terms. The addition of spatial derivative terms, allowing varying wavelengths, is rather complicated. In complete generality we expect the critical wave numbers minimizing the onset Rayleigh numbers for stationary (q_{0s}) and oscillatory (q_{0o}) instabilities to be different at the codimension-two point defined by $R_{co}(q_{0o}) = R_{cs}(q_{0s})$. It is not then possible to extract a single fast spatial dependence $\exp(iq_0x)$ leaving slowly varying amplitudes for both oscillating and stationary rolls. Instead, it is necessary to define two independent amplitudes — one for waves near q_{0o} and one for stationary rolls near q_{0s} , leading to the standard amplitude equations (4.13) and (4.59) except for additional nonlinear coupling terms (Brand and Zielinska, 1986). In binary-fluid convection $q_{0o} - q_{0s} = O(\mathcal{L})$ is typically small, so that one may define a single amplitude $A(x, t)$ giving *both* instabilities through the relation

$$U \sim [A(x, t) e^{iq_{0s}x} + c.c.]U_0(z) . \quad (9.22)$$

We are then led to a single higher-order amplitude equation in one dimension (Cross and Kim 1988b) which is obtained from Eq. (9.21) by the replacement

$$\alpha \rightarrow \alpha + \xi_0^2 [\partial_x - i(q_{0o} - q_{0s})]^2 , \quad (9.23a)$$

$$\beta \rightarrow \beta + \xi_0^2 \partial_x^2 . \quad (9.23b)$$

[Note the first-order spatial derivatives implied by Eq. (9.23a) that were missed in the earlier work of Brand *et al.* (1984).] The parameters appearing in Eqs. (9.21) and (9.23) have all been calculated for binary fluid convection (Cross and Kim, 1988a,b; Zimmerman *et al.*, 1988; we warn the reader that no consistent notation exists for the various coefficients), and properties of the solutions have been investigated by Zimmerman *et al.* (1988). This gives in principle a rather complete description of the codimension-two region, but so far only qualitative comparison with experiment has been possible due to the minuscule range of applicability in experiments with liquids.

(iv) Order-parameter equations

Bestehorn and collaborators (Bestehorn *et al.*, 1989a,b; Bestehorn and Haken, 1990b) have used a phenomenological equation, which is a complex generalization of the Swift-Hohenberg model containing nonlinear gradient terms, to describe binary-fluid convection. The coefficients are chosen so as to fit the function $\mathcal{G}(\theta)$, Eq. (4.32), obtained from an amplitude expansion in the free-slip permeable case. The model then takes the form

$$\begin{aligned} \partial_t \psi = & \epsilon \psi + (\nabla^2 + q_0^2)^2 \psi - g_2(1 - i c_2) |\psi|^2 \psi \\ & - g_3(1 - i c_3) |\nabla \psi|^2 \psi - g_4(1 - i c_4) \psi^* (\nabla \psi)^2. \end{aligned} \quad (9.24)$$

The authors have simulated this model numerically in various two-dimensional geometries and have found a number of features that are qualitatively similar to what is seen experimentally. It must be noted, however, that the values of g_2, g_3, g_4 obtained from the calculation on the free-slip model do not lead to a real nonlinear saturation term for traveling waves in the amplitude equations. It would therefore be interesting to repeat their calculations varying these values to give either a subcritical or supercritical bifurcation to traveling waves. An order-parameter equation such as (9.24) appears to be a minimal model necessary to describe two-dimensional patterns, but even in one dimension it could shed light on the interaction between the fast and slow spatial modes, an effect left out of the complex Ginzburg-Landau equation.

(v) Numerical work

Recently a number of groups have made direct numerical simulations of the hydrodynamic equations. These

fall into two classes: calculations on the free-slip permeable model and calculations for rigid-permeable boundaries. The former are relatively easy (at least for moderate \mathcal{L} where boundary layers are not too thin) and can be carried out in fairly large geometries (e.g., $L = 16$, Knoblock *et al.*, 1986). These investigations of the effect of finite geometries complement the amplitude equation work, but do not have any quantitative applicability to experiment. For the rigid-permeable case the algorithms are less efficient. It is fairly straightforward to study spatially periodic states, since then a small system with only a single period is sufficient. Knoblock and Moore (1990) studied these solutions at small ψ where once again boundary layers are not too tight. However the most complete investigation is that of Barten *et al.* (1989). Their results display the properties of the nonlinear states described above (see Fig. 53), as well as a complex range of behavior depending on the relative magnitudes of the Rayleigh numbers for the traveling-wave saddle node, the oscillatory instability, and the bifurcation point of traveling waves to stationary rolls. The authors investigated mean flow effects and passive particle transport as well. More recently they extended their calculations to large, albeit one-dimensional, systems to study spatial structures, in particular pulse solutions (see subsection IX.A.2.a below).

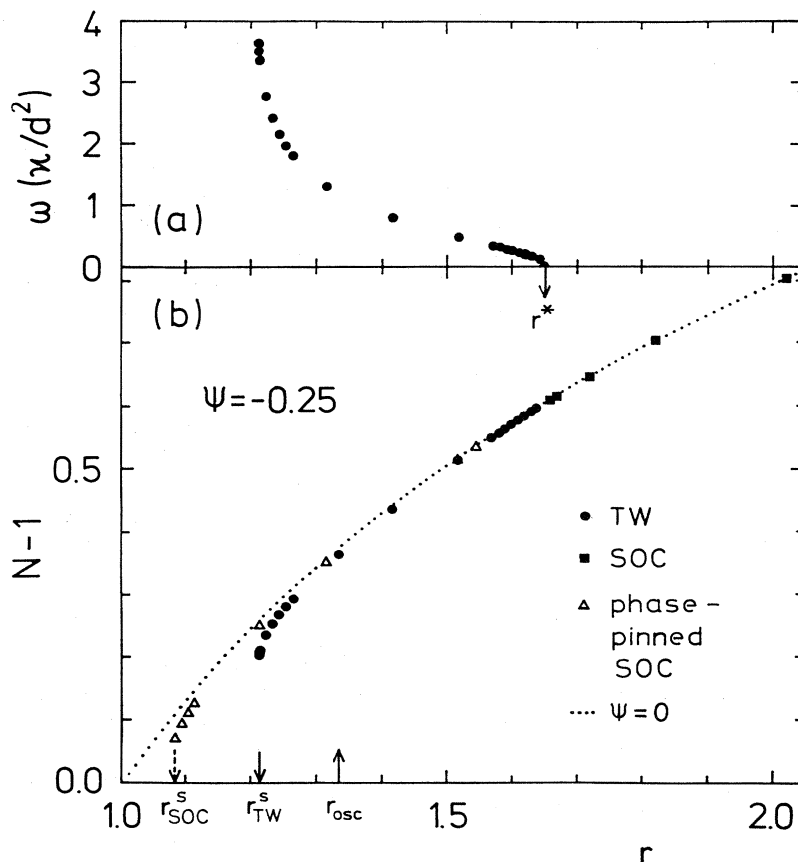


FIG. 53. Properties of the ideal nonlinear states in binary fluid convection between realistic (rigid) plates, obtained numerically for a fluid with Lewis number $\mathcal{L}=0.01$, Prandtl number $\sigma=10$, and separation ratio $\psi=-0.25$. (a) Frequency of nonlinear oscillatory state. (b) Convective heat current measured in terms of the Nusselt number N (denoted N in the figure). Abscissa is the reduced Rayleigh number $r=R/R_c^{(0)}$ with $R_c^{(0)}=1708$, the critical Rayleigh number for pure fluid convection. Solid circles, traveling waves with periodic boundary conditions; squares, stationary rolls (denoted “stationary overturning convection”); triangles, stationary rolls stabilized by adding to the periodic boundary conditions the requirement of zero horizontal velocity, thus effectively quenching the motion of the rolls (“pinning boundary conditions”). The dotted line shows the Nusselt number for pure fluid stationary convection at the same Prandtl number; note how the binary fluid results rapidly approach this curve as r increases. The label r_{osc} denotes the linear instability; r^* is the bifurcation point between traveling and stationary rolls, where the frequency goes continuously to zero; r_{tw}^* is the saddle-node bifurcation point without pinning, and r_{soc}^* the same bifurcation with pinning. (From Barten *et al.*, 1990.)

2. Experiment

a. One-dimensional patterns

(i) Summary of experimental facts

The possibility of constructing long narrow cells with either annular or rectangular geometry offers a unique opportunity to measure the properties of a one-dimensional I_o system near threshold, where the dynamical behavior is expected to be rich, yet one might hope to have a quantitative theory. It turns out, however, that the observed phenomena are quite varied and complicated, so we begin by a brief summary of experimental results (see Surko *et al.*, 1986; Heinrichs *et al.*, 1987; Steinberg *et al.*, 1987, 1989; Bensimon *et al.*, 1989a; Kolodner *et al.*, 1989; Niemela *et al.*, 1990; Anderson and Behringer, 1991; Steinberg and Kaplan, 1991).

- Immediately above threshold the system develops right- and left-propagating waves of *low amplitude*, which can be investigated by dynamically adjusting ϵ to prevent their amplitude from growing or decaying. These states correspond to the unstable branch below the subcritical bifurcation point.

- When ϵ is raised above the linear threshold a number of different *nonlinear* states are seen, depending on ψ , on geometry and on experimental protocol. The nonlinear states can be broadly divided into cell-filling and confined states, and the confined states themselves can be divided into pulses (of fixed small size) and extended states, for which the region of convection has varying, and in principle arbitrary, size. Another distinction which appears primarily for larger $|\psi|$ ($\psi \lesssim -0.1$) is between fast waves whose phase velocity is on the order of the linear velocity ω_0/q_0 , and slow waves with much smaller velocity. The fast waves are seen in confined states and the slow waves primarily (but not always, see below) in cell-filling states. We shall first discuss experiments that can be at least qualitatively understood via the complex amplitude equation and then turn to those that cannot.

(ii) Experiments interpretable by the complex amplitude equation

A fully quantitative experimental test of the amplitude equations has not yet been possible. For large negative ψ the transition is strongly subcritical, and the weakly nonlinear theory is not applicable. The best hope for a quantitative test is to work in the range $-1 \ll \psi \ll -\mathcal{L}^2$ (e.g. $\psi \sim 0.01$) where there is theoretical and experimental evidence that the transition becomes only weakly subcritical. Even here, however, the amplitude equation is not strictly valid because of the small value of \mathcal{L} . Considered as an approximate description it has unknown coefficients, most notably the stabilizing fifth-order terms which must be added if g_0 is destabilizing. In addition the ϵ in Eq. (4.59) is measured from the infinite system

threshold, which may not be well known experimentally. Finally, for experiments performed in rather wide geometries (e.g. $L_y > 4$) two-dimensional distortions may become important, and for those carried out in narrow geometries where this is not important there are no theoretical results for the coefficients of the amplitude equation.

Two novel features which are predicted from the type I_o amplitude equations have been investigated experimentally. The first is the set of extended states with spatial structure and dynamics discussed in Sec VI.C. Here the important features are propagation effects and reflection at the endwalls, with the dispersive terms and the nature of the transition (sub- or supercritical) playing a secondary role. The theory predicts states with spatial structure (e.g. confined states) on the scale of the length of the system, with static or dynamic fronts between different regions and widths determined by the correlation length. The second novel feature predicted by theory is the existence of pulse solutions over a range of parameter values (see Sec. V.B). Here the dispersion and the subcritical nature of the bifurcation are vital, with endwalls being a complication and propagation effects being, as we shall see, a point of discrepancy between theory and experiment. The spatial scale of the pulses is set by intrinsic correlation lengths, and should be essentially independent of the length of the system. In particular experiments, one or the other of the above features may be dominant, and sometimes both may be comparably involved, so that without quantitative predictions the comparison between theory and experiment remains somewhat inconclusive.

The spatial structure of nonlinear states for small ψ has been investigated by Kolodner *et al.* (1989) for ($\psi = -0.021$), by Steinberg *et al.* (1989) (concentrating on $\psi = -0.014$ and -0.058) in rectangular geometries, and by Heinrichs *et al.* (1987) at somewhat larger magnitudes ($\psi = -0.12$ and -0.21) originally in rectangular geometries and later (Niemela *et al.*, 1990) in an annulus where there are no endwall effects. Bensimon *et al.* (1989a) had earlier examined annular geometries for still larger $|\psi|$.

(a) Rectangular cells

The results in rectangular geometries for small $|\psi|$ are quite consistent between different experiments, and seem to largely follow the predictions of Sec. VI.C based on the importance of propagation and reflection, although the role of dispersive effects is evident at larger $|\psi|$. The major results are sketched in Fig. 54. The important features are the following:

- The existence of a weakly nonlinear branch AB of “fast” rolls with frequency of order ω_0 (more closely at A , which is nearer r_{oc} than at the end B). The Nusselt number is also reduced from the corresponding value in pure convection. Inasmuch as the frequency is close to

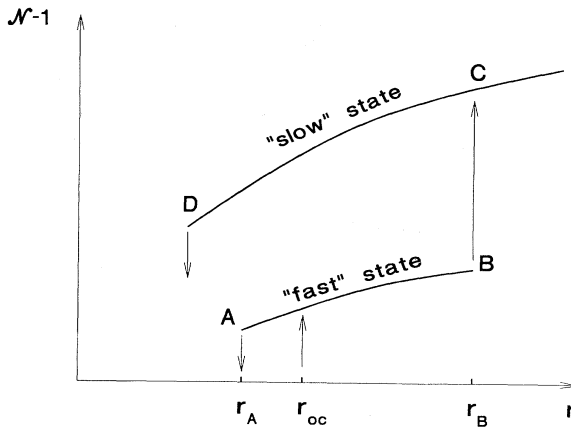


FIG. 54. Schematic diagram summarizing experimental results on binary-fluid convection in a rectangular geometry, plotting Nusselt number vs normalized Rayleigh number. The linear instability occurs at r_{oc} . The state that develops may be a low amplitude “fast” state, with frequency quite close to the linear onset frequency along AB, or a “slow” higher amplitude state along DC, with lower frequencies. Various spatial patterns that do not fill the cell may be traversed reversibly along AB. At r_A a hysteretic decay of convection occurs. At r_B a discontinuous jump to a slow filling state on the branch CD takes place. For larger r a transition to a stationary state (not shown) takes place on this branch. At D a hysteretic jump down to the conduction state occurs. The value of r_{oc} depends on the reflection properties of the endwalls, and in some geometries may be greater than r_B so that the branch AB is not observed.

ω_0 , one might hope that a weakly nonlinear theory might be appropriate for these states.

• The linear onset r_{oc} depends on properties of the endwall, as well as on the fluid properties, consistent with the importance of reflection. At r_{oc} there is a jump to the finite amplitude state which is usually the fast branch AB, although the size of the jump seems to become smaller as $\psi \rightarrow 0$, and the hysteresis $r_{oc} - r_A$ becomes immeasurable in this limit. The dependence on aspect ratio is (Steinberg and Kaplan, 1991),

$$r_{oc}(L) - r_{oc}(\infty) \sim L^{-1}, \quad (9.25)$$

as expected [see Eq. (5.29)] and not the L^{-2} dependence characteristic of pure-fluid (type I_s) convection.

• The values of r_A and r_B , the ends of the fast branch, seem independent of the endwall conditions. Thus for some parameter values and certain endwalls we may have $r_{oc} > r_B$, so that the fast branch AB is not seen. The hysteresis $r_{oc} - r_A$ also depends on the endwall properties.

• The nature and sequence of states along AB is largely consistent with the behavior in Figs. 25 and 26, valid for a supercritical bifurcation if we assume that the effect of the subcritical bifurcation is to eliminate the low amplitude states. We note in particular the following features: a nonlinear “counterpropagating wave” state, reminiscent of Fig. 25(a), at the smallest $|\psi|$; the “blinking” or “sloshing” states of Steinberg *et al.* (1989) and

Kolodner *et al.* (1989), reminiscent of Fig. 25(d); the stationary confined state filling about one half of a large cell ($L = 24$) at small $|\psi|$ (Moses *et al.*, 1987), reminiscent of Fig. 25(g). Figure 55 displays results of Kolodner *et al.* (1989) on an asymmetric blinking state, with the time dependence of the left and right wave envelopes obtained by demodulation techniques from the experimental data: the similarity with results from the Ginzburg-Landau simulations displayed in Fig. 25(d) is striking. At large $|\psi|$, however, the stationary confined states may be more akin to the pulses described below (Steinberg and Kaplan, 1991).

• The value of r_B , the end of the confined states, is consistent with a constant value s_B of the reduced group speed $s = (s_0 \epsilon^{-1/2}) (\tau_0 / \xi_0)$, although this value is around 1.6 whereas theory predicts $s \geq 2$ in the large system limit, depending weakly on ψ in the range studied. Numerical simulations of the amplitude equation by Cross and Kuo (1992) find a reduced value of s_B as the size of the system decreases (see dashed line in Fig. 26), although a precise identification of the confined to filling transition is difficult for the supercritical bifurcation assumed in that work. Fineberg *et al.* (1990) have suggested that the reduction in value of s_B can be ascribed to a nonzero amplitude of the counterpropagating wave at the boundary of the confined state, and with this single parameter they obtain a good fit to the modulation period of the blinking state as the Rayleigh number is reduced. It should be remembered, however, that the character of the state (e.g. its frequency) is significantly different at r_B from the onset solution. Moreover, the transition observed is discontinuous and it is a transition to the “slow” highly nonlinear state, so that the quantitative reliability of the Ginzburg-Landau prediction for s_B is doubtful. In larger aspect-ratio systems Kaplan and Steinberg (1992) show that the transition from confined to filling appears to be triggered by the amplification of fluctuations in the convectively unstable small-amplitude region, much as in the annular geometry (see below), and they study the cross-over between the two mechanisms.

In the model of Cross (1988b) used to explain the above observations it is essential that one consider coupled right- and left-traveling waves, as well as the effects of the sidewalls. In contrast to those confined states, which in general fill a large portion of the cell, another class of states was observed by Steinberg *et al.* (1987) and by Heinrichs *et al.* (1987). These new states were of much smaller extent and apparently less dependent on geometry, though they were localized near the endwall. These observations were explained by Thual and Fauve (1988) in terms of the pulse solutions of a single wave, as discussed in Sec. V.B.2.b.iii.β. We now turn to experiments in annular geometry, where those ideas can be tested more convincingly.

(β) Annular geometry

The explanation of Thual and Fauve (1988) was strikingly confirmed by experiments of Niemela *et al.* (1990)

in an annular cell, which demonstrated that the pulse states were indeed stable without lateral boundaries, and could be quantitatively fit by a simple exact pulse solution of the Ginzburg-Landau equation, albeit with adjustable parameters. This work, and a number of subsequent experiments by various groups (see, Kolodner and Glazier, 1990; Ahlers, 1991; Anderson and Behringer, 1991; Kolodner, 1991a-d; Steinberg and Kaplan, 1991), confirmed that pulse solutions were stable under a variety of experimental conditions, but there remained two qualitative discrepancies between experiment and the simple model. First, the theoretical pulses arising from the sim-

ple Ginzburg-Landau equation (5.57) are at rest in a reference frame moving with the linear group velocity s_0 of the waves, whereas the observed pulses were found to be at rest in the lab frame. Second, the pulses were found to remain stable above the linear threshold, even though the conducting fluid away from the pulses was (convectively) unstable. It turns out that both discrepancies can be plausibly accounted for by corrections to the simple Ginzburg-Landau model. It was first found numerically by Brand and Deissler (1989), and subsequently shown analytically by van Saarloos and Hohenberg (1992), that a nonlinear derivative term $s_2[\partial_x |A|^2]A$ as in Eq. (3.37)

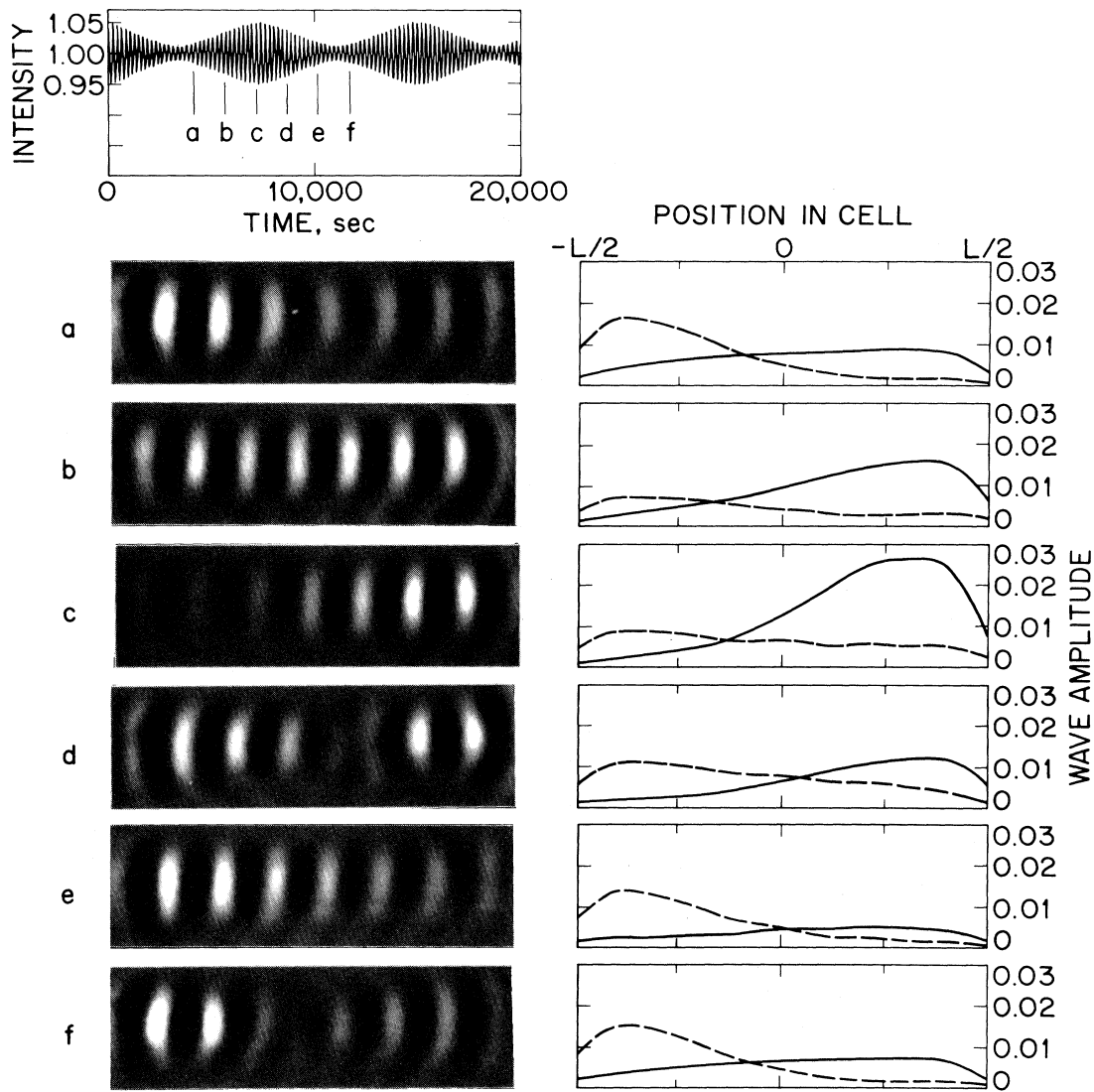


FIG. 55. "Sloshing" or "blinking" state in experimental binary fluid convection. The top trace is the intensity of an optical signal measuring the flow at a single point. The column of pictures on the left is a sequence of shadowgraph images taken at times indicated in the top trace. To the right of each image is the corresponding amplitude computed by demodulation of the optical signal. Full lines, right-moving waves; dashed lines, left-moving waves. Note the similarity with patterns observed in numerical simulations of the amplitude equations shown in Fig. 25(d). (From Kolodner *et al.*, 1989.)

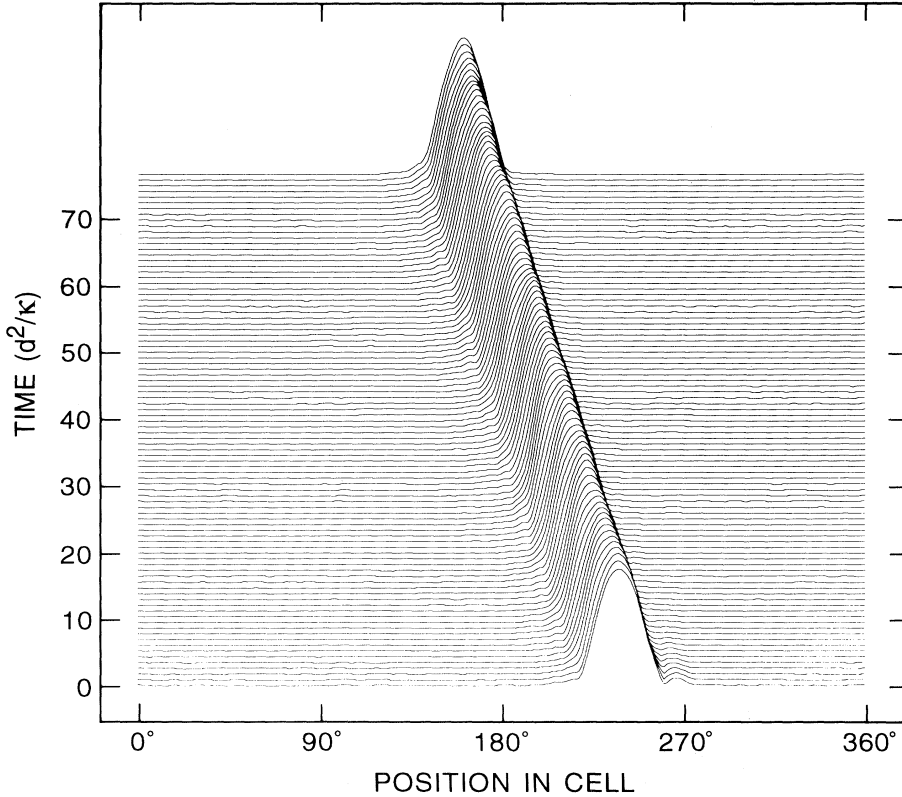


FIG. 56. Drifting pulse in annular convection cell of dimensionless circumference $L = 92$, containing an alcohol-water binary mixture with separation ratio $\psi = -0.12$. Space-time plot of the envelope of the shadowgraph signal representing a localized pulse of convection embedded in a conducting background. The pulse drifts slowly to the left. (From Kolodner, unpublished).

changes the pulse velocity from s_0 to a nontrivial value $v_p(s_2, \epsilon, c_i)$, which depends on all the parameters in the model. Of course this does not explain why the observed velocity was precisely zero, rather than some variable quantity. The numerical simulations of the full hydrodynamic equations by Barten *et al.* (1991), on the other hand, led to a *nonzero* pulse velocity, albeit a very small one $v_p/s_0 \sim 0.01 - 0.03$.

This qualitative discrepancy was removed in a beautiful experiment by Kolodner (1991c), who took particular care to make the control parameter ϵ constant along the cell. As illustrated in Fig. 56, Kolodner found a *moving* pulse with a slow velocity, and in a careful series of measurements was able to show that previous observations could be explained by assuming that the pulse stopped at a point where the local velocity vanished in a slightly nonuniform cell. Although the relationship between an assumed spatial variation $\epsilon(x)$ and the ensuing $v_p(x)$ is no doubt rather subtle, this basic interpretation seems rather convincing to us. Indeed, Kolodner also found that v_p depends on parameters, e.g. the average control parameter $\bar{\epsilon}$, as well as the separation ratio ψ (see Fig. 57 and Kolodner, 1991d).

From the point of view of the Ginzburg-Landau model (3.37), even with a nonlinear derivative term, the small-

ness of v_p/s_0 is nevertheless rather puzzling. An interesting modification of the model which attempts to take into account the slow timescale of solute diffusion, has been presented recently by Riecke (1992). Approximate

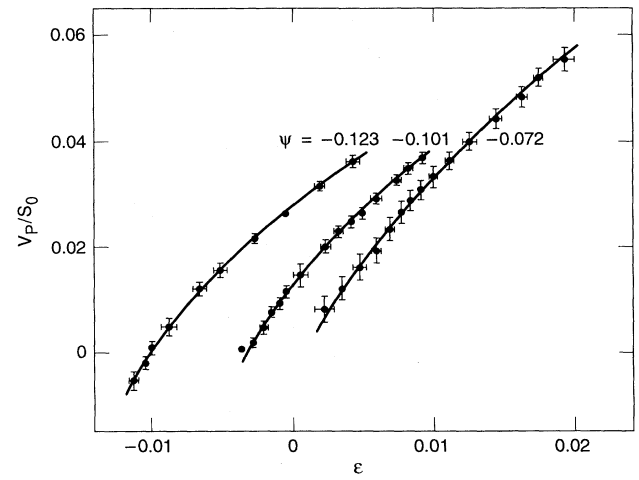


FIG. 57. Pulse velocity v_p normalized by the linear group velocity s_0 vs control parameter ϵ , for pulses such as the one in Fig. 56 and different binary-fluid mixtures. The reduced velocity is seen to be very small in magnitude and to depend on the fluid parameters. (Adapted from Kolodner, 1991d.)

mating the horizontal boundary conditions as free slip and permeable, Riecke arrives at the coupled amplitude equations

$$\begin{aligned}\partial_t A + s_0 \partial_x A &= (1+ic_1) \partial_x^2 A + (\epsilon + d_0 C) A \\ &\quad - (1-ic_3)|A|^2 A - (1-ic_5)|A|^4 A,\end{aligned}\quad (9.26a)$$

$$\partial_t C = d_1 \partial_x^2 C + d_2 C + d_3 \partial_x |A|^2,\quad (9.26b)$$

with the scaling

$$d_2 \sim \mathcal{L}/\epsilon = O(1).\quad (9.27)$$

The above equations possess pulse solutions even in the real case ($c_i = 0$), and Riecke shows numerically that for small d_2 the pulse velocity (equal to s_0 when $d_0 = 0$) remains very small for a range of s_0 . This calculation provides a natural explanation of the observed slowness of the pulse velocity, in terms of the drastic effect of coupling to the slow concentration mode on pulse propagation, even in a model which neglects the thin boundary layers associated with rigid impermeable horizontal boundaries (see subsection IX.A.1.d.ii above).

The second major discrepancy between experiments on pulses and the simple model involves the stability of pulses for $\epsilon > 0$. An explanation was already offered early on by Niemela *et al.* (1990), Barten *et al.* (1991), and Glazier and Kolodner (1991), who noted that in a finite annulus the linear waves created by the convective instability can be reabsorbed by the pulse before they have time to destroy the conducting state. On the other hand the instability mechanism discussed by van Saarloos and Hohenberg (1992) (cf. Sec. VI.B), whereby the pulse expands due to the creation of two outwardly propagating fronts, does not seem to be strongly affected by finite geometry, so the detailed stability properties of pulses remain to be clarified.

A number of experiments have also been carried out on pulse interactions (bound states and scattering) as well as on the effect of low amplitude waves impinging on stationary or moving pulses, and the consequent modifications of pulse stability (see Kolodner and Glazier, 1990; Kolodner, 1991a,b). Most of these effects appear to be qualitatively understood but we are far from a quantitative theory.

(iii) Other one-dimensional experiments

Experiments at more negative ψ emphasize the discrepancies with the complex amplitude equations. In rectangular geometries no weakly nonlinear states with $\omega \approx \omega_0$ are seen, and the system immediately jumps to the slow state (Surko *et al.*, 1986). In annular geometries (Bensimon *et al.*, 1989a) both fast confined states, with ω not too far from ω_0 , and slow filling states, are seen. Ohlsen *et al.* (1990) made careful measurements of the slowing down of the filling states as the Rayleigh number

increases, and found quantitative agreement with the supercritical bifurcation predicted theoretically by Bensimon *et al.* (1989b). Earlier experiments by Walden *et al.* (1985) and Moses and Steinberg (1986a) had seen a subcritical bifurcation, which might be explainable by the rectangular geometry used in that work.

The early experiments in annular geometry at $\psi = -0.25$ by Bensimon and co-workers (Kolodner *et al.*, 1988; Bensimon *et al.*, 1989a) found a whole range of fast confined states, in particular convecting states of arbitrary (large) size bounded by *stationary* fronts. The existence of such fronts over a range of ϵ values remains a mystery, since it is inconsistent with the selection arguments of Sec. VI.B, based on the simple Ginzburg-Landau model (5.57). The observations were confirmed both experimentally (Surko *et al.*, 1991) and numerically (Barten *et al.*, 1991) for a particular value of Rayleigh number but the dependence on ϵ and ψ , and the relation of these large structures to the (small) pulses observed at larger ψ remain to be clarified.

All these different experiments both at large and small negative ψ have a common feature which is *not* understood: states in which the convecting rolls essentially fill the container show a low basic frequency (typically $0.1\omega_0$), whereas states of confined rolls show a higher frequency which approaches the linear frequency ω_0 close to onset, although it may decrease significantly (typically to $0.5\omega_0$ or less) as the nonlinearity increases. Stable slow states usually are cell-filling, though they can be observed as confined states, if the (unstable) trailing edge is pinned by a boundary in rectangular geometry, or by a source defect in annular geometry (Kolodner, 1990). Fast states, on the other hand, have never been observed to fill the cell. The primary mystery, in our opinion, concerns the nature of the stable fast states. The only fast states understood theoretically are the unstable traveling wave states below threshold for a subcritical bifurcation in an infinite system. If a qualitative understanding of the fast states could be achieved we believe that the main features of the one-dimensional system near threshold would be understood.

b. Two-dimensional patterns

(i) Traveling rolls for $\psi < 0$

If the transverse aspect ratio is made greater than about 4 or 5, the behavior becomes more complicated and essentially nothing is understood theoretically. In general the ordered structure across the system breaks down as the lateral aspect ratio is increased, to give more complicated structures often with chaotic dynamics. This tendency to lateral breakup is not surprising if we consider the possibility of the transverse Benjamin-Feir instability. A natural estimate of the instability criterion at a subcritical bifurcation is

$$s_0 \frac{\partial \omega_0}{\partial |A|} \cdot \frac{\partial |A|}{\partial \epsilon} < 0.\quad (9.28)$$

[This is arrived at by allowing more complicated (e.g. fifth order) nonlinear terms but not changing the spatial derivative terms as in Eq. (5.57); the effect of higher-order derivative terms is unknown at present.] The above instability criterion is typically satisfied in nonlinear binary-fluid convection where the frequency decreases as the amplitude grows with increasing ϵ .

The types of behavior observed in two-dimensional systems include (i) a periodic or chaotic “zipper” state in which waves in each half of the cell (lengthwise) propagate from opposite corners, leaving a zipper-like pinching off and rejoining of rolls where the two domains meet down the midline ($\psi = -0.6$, $L = 6 \times 4$) (Walden *et al.*, 1985); (ii) traveling waves confined in both dimensions in domains that evolve chaotically throughout the cell ($\psi = -0.1$, $L = 20 \times 9$) (Steinberg *et al.*, 1987); (iii) traveling waves in various directions largely filling the cell, which again evolve chaotically ($\psi = -0.3$, $L = 20 \times 9$) (Steinberg *et al.*, 1987); (iv) pulse states resembling the one-dimensional ones (Bodenschatz *et al.*, 1992).

The numerical work of Bestehorn *et al.* (1989a,b) on their generalized Swift-Hohenberg model shows structure that is visually strikingly similar to the results (ii) in the preceding paragraph. As mentioned before, however, this model is strongly chaotic even when restricted to one dimension due to the absence of any saturating (real) nonlinearity (Bretherton and Spiegel, 1983). It would be interesting to consider a similar model with and without longitudinal and transverse Benjamin-Feir instabilities to elucidate their relevance to the structures observed (see also Bestehorn and Haken, 1990b).

(ii) Squares and rolls for $\psi > 0$

For positive separation ratio both the temperature and the concentration gradients are destabilizing and the linear theory predicts a dramatic decrease in the stationary convection threshold. If we define a Rayleigh number associated with the concentration as

$$R_S = \frac{\beta g d^3 \Delta \bar{c}}{D_c \nu} , \quad (9.29)$$

[see Eq. (9.2)] then we have $R_S = R \psi / L \gg R$, and we expect the concentration to be destabilized before the temperature. In view of the no-flux boundary condition (9.5), the threshold is analogous to that for thermal convection in the presence of insulating boundaries discussed in Sec. VIII.F. We thus expect to see a *square* pattern with a long wavelength immediately above threshold (Moses and Steinberg, 1986b, 1991; Knobloch, 1989, 1990). Note, however, that since in that case $q_0 \propto B^{1/4}$ [see Eq. (8.89)], the wave vector may rapidly evolve to $q_0 \sim O(1)$ as the effective Biot number increases. Since heat transport is of secondary importance in this state the convected heat is expected to be very small, $(\mathcal{N}-1) \sim 10^{-3}$ to 10^{-4} for small Lewis number, and difficult to detect experimentally. This regime, dominat-

ed by concentration effects, is known as the Soret regime. On the other hand at a Rayleigh number of order the pure fluid critical Rayleigh number $R_c^{(0)}$ a rapid crossover to thermally dominated convection is expected, with a much larger Nusselt number $(\mathcal{N}-1) \sim (R - R_c^{(0)})/R_c^{(0)}$.

The experiments of Moses and Steinberg (1986b, 1991) in an ethanol-water mixture with $\psi \sim 0.02 - 0.2$ agree semi-quantitatively with these ideas. A large-scale flow is first resolved at a small Rayleigh number $r \sim 0.16$ with wave vector $q \sim q_{0p}/8$ (where $q_{0p} = 3.117$), with a clearly defined square structure visible when q has reached $q_{0p}/2$. The wave vector then evolves to $q \sim q_{0p}$ as r increases towards unity. Interestingly, the transition to the roll state for $r > 1$ occurs via a supercritical Hopf bifurcation manifested as an oscillatory competition between the two sets of rolls forming the square pattern. More recently, Bigazzi, Ciliberto, and Croquette (1990), have studied a mixture of methanol with carbon tetrachloride that achieves a separation ratio of order $\psi \sim 0.35$. These authors analyzed the shadowgraph image by a spatial Fourier transform method and used the strength of the Bragg peak as the order parameter for the convective state. In the Soret regime the convection is weak but shows a stationary square pattern, in agreement with theory. The wave vector is of order $q_{0p}/2$ at roughly $2R_{sc}$ (the lowest value of Rayleigh number where the pattern could be detected). Some evidence has been presented by Lhost and Platten (1989) that a large roll appears at onset, but their study does not reveal the square to roll transition seen at higher R . Bigazzi *et al.* thus conclude that a determination of the precise pattern at onset for square-roll convection remains an open (and difficult) experimental problem.

At larger Rayleigh numbers Bigazzi *et al.* also studied the square to roll transition, and did not find the oscillatory behavior found by Moses and Steinberg (1986b) at lower ψ . Instead, the rolls gradually invaded the squares, and also showed time dependence (a traveling-wave instability) as well as an extreme sensitivity to the appearance of defects.

A theoretical analysis of this system was carried out by Müller and Lücke (1988) and by Linz *et al.* (1988; see also Lücke, 1988) using a truncated Galerkin expansion with 10 modes, and a sidewall forcing term as in Sec. VIII.D. In the absence of this forcing the model gives stable rolls immediately above threshold in the “Soret” regime, but a nonzero forcing parameter stabilizes squares. We do not expect the forcing to be an important feature of the experiment, so that the absence of squares without forcing seems to reflect a flaw in the model. At larger R there is a subcritical Hopf bifurcation to a pattern of oscillating rolls and squares, whose frequency decreases with increasing R , until a bifurcation occurs to a state of stationary rolls. This state is itself then predicted to undergo a Hopf bifurcation to a traveling-wave roll state, a feature observed by Bigazzi *et al.*, though the observed bifurcation was supercritical rather than subcritical as predicted.

3. Chaos and noise

Binary-fluid convection is a promising system for studying spatiotemporal chaos since the latter is expected to appear immediately above threshold under certain conditions.

a. Theory

Chaos in the complex Ginzburg-Landau model was discussed in Sec. VII.D. The early work of Bretherton and Spiegel (1983) in one dimension identified a number of parameter regimes with different chaotic patterns. More recently, Schöpf and Kramer (1991) and Shraiman *et al.* (1992) have studied these chaotic states in various regions of the parameter space of the model. In particular, for the subcritical system appropriate to binary-fluid convection, Schöpf and Kramer have shown that the dispersive terms in Eq. (5.57) stabilize a chaotic attractor even in the absence of any quintic terms.

The two-dimensional case has been considered by Brand *et al.* (1986a,b) and by Coullet *et al.*, (1987) and in a discretized form by Bohr *et al.* (1990a,b). A two-dimensional complex order parameter equation was studied by Bestehorn and Haken (1990b), but they did not carry out a detailed investigation of the chaos.

b. Experiments

In the early work of Fineberg *et al.* (1988b) and Kolodner and Surko (1988) in one-dimensional rectangular geometries, a “blinking” state was observed somewhat above threshold. Although some of the properties of this state were captured by the nondispersive model of Cross (1986b), Steinberg and Kaplan (1991) have shown that the temporal behavior is close to that found in the Ginzburg-Landau equation with complex coefficients. Similar observations were made by Kolodner *et al.* (1990) in an annular container. These authors found a state they called “dispersive chaos,” where pulses would grow and collapse in random positions. No detailed analysis of these chaotic states has yet been undertaken, but we consider it to be a candidate for a controlled situation where spatiotemporal chaos might be quantitatively understood.

The two-dimensional system also seems to us to merit further study since very little quantitative experimental work has been done to date. The early experiments of Surko *et al.* (1986) and Steinberg *et al.* (1987) in wide rectangular containers showed “zipper states” and other transverse instabilities associated with two-dimensional chaos. It remains to be seen if these phenomena can be analyzed and clarified.

Finally, we note that Schöpf and Rehberg (1992) have observed fluctuating patterns in the convectively unstable regime of a binary mixture just above the oscillatory threshold. They interpreted these as arising from

amplification of noise, whose magnitude was shown to be consistent with the expected value quoted in Eq. (8.63).

B. Taylor - Couette flow

1. General discussion

The important parameters defining the Taylor-Couette system are geometric — the radius ratio $\eta = a/b$ with a and b the inner and outer cylinder radii, and the aspect ratio $L = \tilde{L}/(b-a)$ with \tilde{L} the length of the fluid column — and driving parameters conveniently chosen as the inner and outer cylinder Reynolds numbers $R_i = a(b-a)\Omega_i/\nu$ and $R_o = b(b-a)\Omega_o/\nu$, with $\Omega_i(\Omega_o)$ the angular velocity of inner (outer) cylinders and ν the kinematic viscosity. In addition the end conditions play a significant role.

Most of our discussion will focus on the case where the outer cylinder is stationary, but we will also briefly describe the variety of states obtained with both cylinders rotating. We will not discuss in detail the dependence of results on η , but the small η limit provides a useful simplification for theoretical analysis. An early review was given by DiPrima and Swinney (1981), which the reader should consult for references to the older literature (see also, Donnelly, 1991). A complete bibliography has been compiled by Tagg (1992).

With the outer cylinder stationary, the first instability when R_i is increased occurs at R_{ic} and leads to the Taylor vortex state of stationary, azimuthal vortices, with complete cylindrical symmetry. As discussed in Sec. II this state is analogous to the roll state of Rayleigh-Bénard convection, but the two directions (axial and azimuthal) are no longer rotationally equivalent. In many situations the cylindrical symmetry remains unbroken and the system provides a good experimental apparatus for investigating one-dimensional pattern formation, analogous to a long thin Rayleigh-Bénard cell. For the Taylor-vortex case the flow is strictly two-dimensional and the theoretical analysis is somewhat simpler. This case will be discussed in subsection IX.B.2.c.

A secondary instability occurs typically at R_i/R_{ic} rather close to unity (≈ 1.1 for $\eta = 0.89$) and it leads to the wavy vortex state, in which a wavy disturbance of the vortices propagates around the cylinder at a speed that is some fraction (depending on η) of the inner cylinder rotation speed. This wave has a coherent phase on the different vortices, and is characterized by an m -fold periodicity in the azimuthal direction

$$\delta\mathbf{U} \sim \exp(i(m\theta - \omega_1 t)) + \text{harmonics}. \quad (9.30)$$

Even in this simple regime there are many possible states characterized by different values of m and different numbers of vortices in the cylinder for each set of system parameters. Coles (1965) dramatically illustrated this diversity of states in a massive experimental study. His challenge to explain in detail the range of solutions and the

transitions between them as system parameters are changed remains largely unanswered. The wavy vortex state is characterized by two slow phase variables, ψ corresponding to translations of the rolls in the axial direction, and ϕ corresponding to translations of the waves in the azimuthal direction. Brand and Cross (1983), assuming a smooth gradient expansion, obtained coupled phase equations which predict propagating rather than diffusive phase dynamics, as well as a long healing length for the perturbation of the wave number by the ends. Hall (1984) has suggested corrections to this theory due to mean flow effects, analogous to those encountered in Rayleigh-Bénard convection.

Typically the next transition as R_i is increased is to the modulated wavy vortex state which shows a quasiperiodic frequency spectrum, i.e. two incommensurate frequencies^{9,5} ω_1 and ω_2 . Remarkably, the two frequencies (the wave frequency and the modulation frequency) do not lock as R_i varies, even when they pass through small rational ratios. Rand (1982) explained this as a result of the time evolution of the waves passing through states related by azimuthal symmetry (cf. Sec. IV.B). Crudely, his argument is that ω_1 is not a “real” frequency of the flow since it is changed by observing from a rotating frame. The modulated wavy state may be characterized as two waves — the original one with m periods and the modulation with n periods — rotating at *independent* rates; this state was analyzed from a symmetry point of view by Gorman *et al.* (1981) and Gorman and Swinney (1982).

Further increase in R_i leads to a chaotic state. The observation by Gollub and Swinney (1975) of the onset of chaos as a definite transition to chaos from a two-frequency state, without intervening many-frequency states, was historically a crucial experimental verification of the applicability of ideas of low-dimensional chaos and strange attractors to real fluid systems. This transition to chaos was later made quantitative by Brandstater *et al.* (1983) who measured the largest Lyapunov exponent, the metric entropy and the attractor dimension in the chaotic regime, using the phase space reconstruction methods discussed in Sec. VII.B above.

If the inner and outer cylinders are allowed to rotate independently, a wide range of flow states are found, as shown in Fig. 58(a) and reviewed by Andereck, Liu, and Swinney (1986). For the counterrotating case with Ω_i sufficiently negative, the first transition from uniform Couette flow is to spiral states

$$\delta\mathbf{U} \sim e^{\pm ikz \pm i(m\theta - \omega t)}. \quad (9.31)$$

For fixed θ we again have waves traveling in the $\pm z$ directions, or a standing wave superposition, correspond-

ing to the situation discussed in Sec. VI.C. Indeed, single dominant spirals, interpenetrating spirals and different spatial regions of upwards and downwards moving spirals with stationary or periodically moving boundaries, have been observed by Andereck *et al.* (1986) and Tagg *et al.* (1989). Their results are quite consistent with predictions based on two coupled complex amplitude equations shown in Fig. 25 above, but no detailed comparison with that theory has been made, although the linear coefficients of the relevant amplitude equation have been calculated (Tagg *et al.*, 1990).

The ideal Taylor-Couette system (idealized by periodic boundary conditions in the axial direction) has many symmetries: translations and parity in the axial direction, translations (but no parity) in the azimuthal direction [$O(2) \times SO(2)$ in the notation of Sec. IV.B]. Mathematical symmetry arguments are therefore important in qualitatively understanding the rich variety of states, dating back to the arguments of Rand (1982) described above. Chossat and Iooss (1985) have investigated the primary and secondary bifurcations at general points in the R_i, R_o diagram. Unfolding the behavior around special degenerate points in the R_i, R_o plane provides further information if symmetry arguments are used. For example Golubitsky and Stewart (1986) and Golubitsky *et al.* (1988) studied the behavior near the codimension-two^{9,6} point R_i^*, R_o^* , where the onsets of spiral and Taylor vortices coincide [point P_2 in Fig. 58(b)]. Here there is a six-fold degenerate bifurcation for fixed axial wave number q and azimuthal quantum number m , with eigenvectors

$$\delta\mathbf{U} \sim e^{\pm(im\theta - i\omega t)} e^{\pm iqz} \quad \text{and} \quad e^{\pm iqz}. \quad (9.32)$$

The authors investigated all the symmetry-allowed states near R_i^*, R_o^* , and obtained results with symmetries corresponding to many of the states observed in experiments. Of course, the range of stable states near the codimension-two point depends on signs and ratios of unknown constants in this approach. Nevertheless, for certain choices of these “nondegeneracy” parameters it is possible to reproduce the sequences of transitions observed on increasing R_i , i.e.

Couette \rightarrow vortices \rightarrow wavy vortices \dots ,

$$R_o > R_o^*, \quad (9.33a)$$

Couette \rightarrow spirals \rightarrow wavy spirals \dots ,

$$R_o < R_o^*. \quad (9.33b)$$

It is intriguing that the wavy vortex state observed for $R_o = 0$ can be qualitatively understood in this unfolding within the six-dimensional space defined by Eq. (9.32). However there does not seem to be any small parameter allowing a quantitative calculation at $R_o = 0$. Indeed, al-

^{9,5}In the experiments of Gollub and Swinney (1975) cited below, a third frequency appears for some range of R_i ; they called this mode ω_2 , and the modulated wave frequency ω_3 .

^{9,6}These authors use a different counting scheme, and label this a codimension-one point.

though states similar to many of the observed ones can be constructed, without further calculation of the unknown constants and even unknown functions, it is not clear how much *predictive* power this method has. Presumably it is fairly straightforward to classify all states that can actually occur at the codimension-two point marked P_2 on Fig. 58(b). In particular, one can calculate the widths associated with the different tongues which appear when one circles this point, i.e. $w_n \sim |\delta R_n|^{P_n}$. In general, how-

ever, the secondary bifurcations typically occur in a regime which is quite nonlinear, so that even qualitative predictions are difficult to obtain reliably.

Langford *et al.* (1988) have embarked on the task of calculating the relevant parameters, initially for the linear instabilities, from the full fluid equations. These authors particularly concentrate on degenerate points where the onset of states with *different* azimuthal symmetries m and m' coincide.

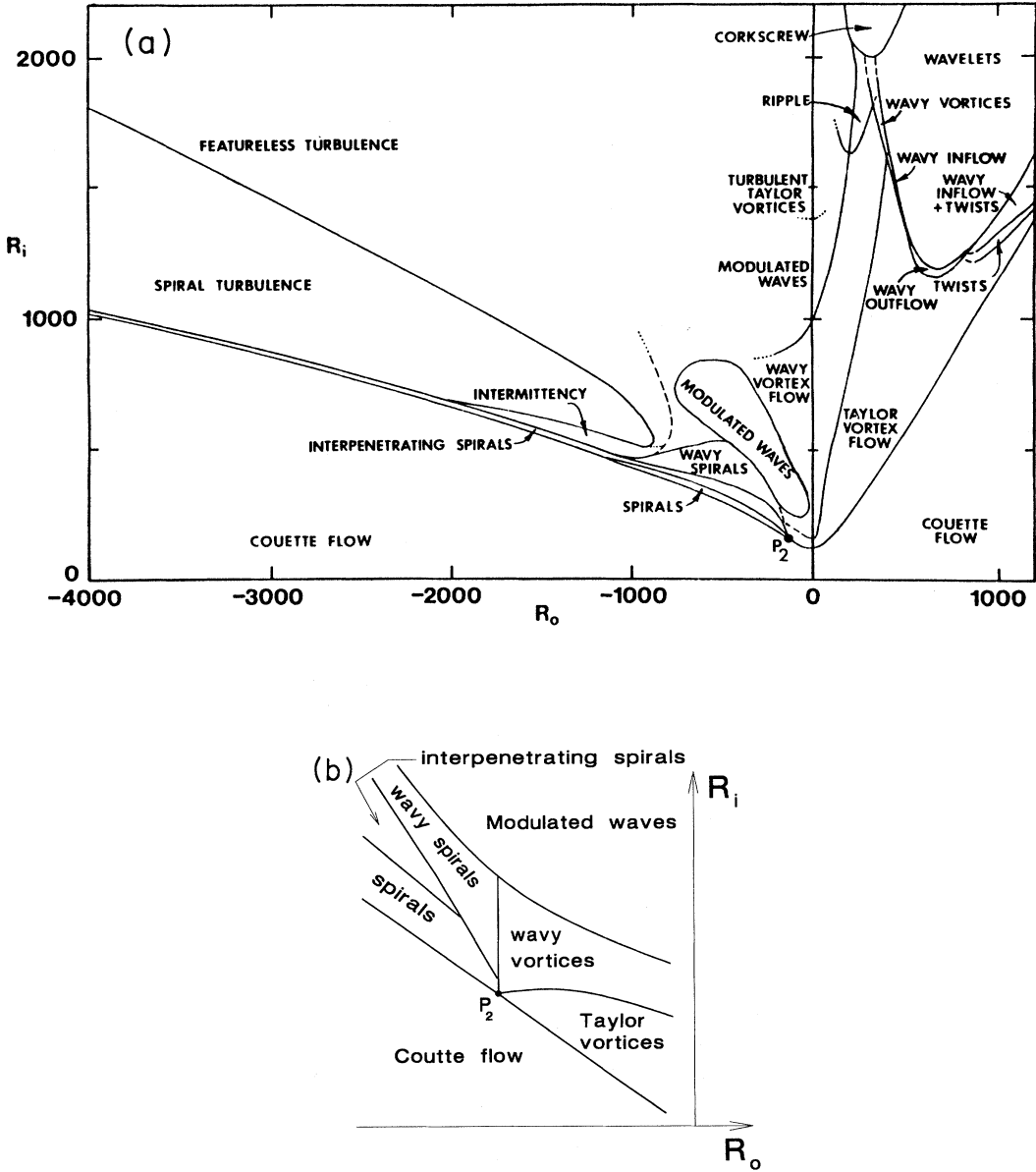


FIG. 58. Diversity of flow regimes observed in the Taylor-Couette system with independently rotating cylinders. (a) R_i and R_o are the Reynolds numbers, proportional to the rotation rates, of the inner and outer cylinders, respectively (from Andereck *et al.*, 1984). (b) Schematic expansion of the region around the codimension-two point P_2 at $R_i = -100$, $R_o = 200$, analyzed by Chossat and Iooss (1985).

2. One-dimensional patterns

a. General considerations

Long Couette cylinders described by amplitude or phase equations backed up by quantitative calculations on the full fluid equations, provide a fertile area for developing and testing ideas on one-dimensional pattern formation. The early work of Pfister and Rehberg (1981) demonstrated the applicability of the spatially dependent amplitude equation for this system. Later, Ahlers and co-workers (Ahlers *et al.*, 1986; Ahlers, 1989) have exploited the azimuthally symmetric Taylor vortex state to demonstrate quite subtle features of pattern selection and competition. This work provides perhaps the most complete quantitative comparison of experiment and theory in the area of nonequilibrium patterns, where often the connection remains at best qualitative.

The first question which naturally arises, that of pattern selection, can in the present case be formulated as the problem of finding the number of vortices in a system of fixed length as the Reynolds number is varied. The characteristic wavelength of these vortices is an important parameter on which further properties of the flow, such as the net torque on the cylinders or the boundaries of secondary instabilities, strongly depend.

It is important to note that the *ends* of a Couette system provide a significant perturbation of the ideal Couette flow which would otherwise occur at low rotation speed. Typically rigid plates, co-rotating with the inner or outer cylinder, are used at least at one end. These do not match the Couette flow which characterizes the ideal infinite cylinder,

$$V_\theta(r) = Ar + B/r, \quad (9.34)$$

with A and B fixed by matching to the rotation rates of the cylinders. Consequently, considerable attention has been devoted to finding a proper description of the approach to the ideal situation as the cylinder length is increased. First, the end perturbation leads to an *imperfect bifurcation* (see Sec. III.A). The boundary condition drives a strong Taylor vortex near the ends even well below the infinite-system threshold, a phenomenon known as "Ekman pumping." Moreover, as the rotation rate is increased the Taylor vortex state spreads from this localized disturbance (Fig. 59) and the boundaries perturb the vortices near the ends significantly. Finally, even in long cylinders the strong Taylor vortex at the end affects the possible wave numbers of the vortices in the bulk, i.e. far from the boundaries. An effect of arbitrarily distant lateral boundaries on wave-vector selection was already encountered in the Rayleigh-Bénard case (Sec. VIII.C), but the details are somewhat different here, since the Ekman vortex pins the phase, rather than allowing it to adjust.

The problem of determining the number of vortices present under given conditions separates naturally into two parts. For short cylinders one studies the bifurca-

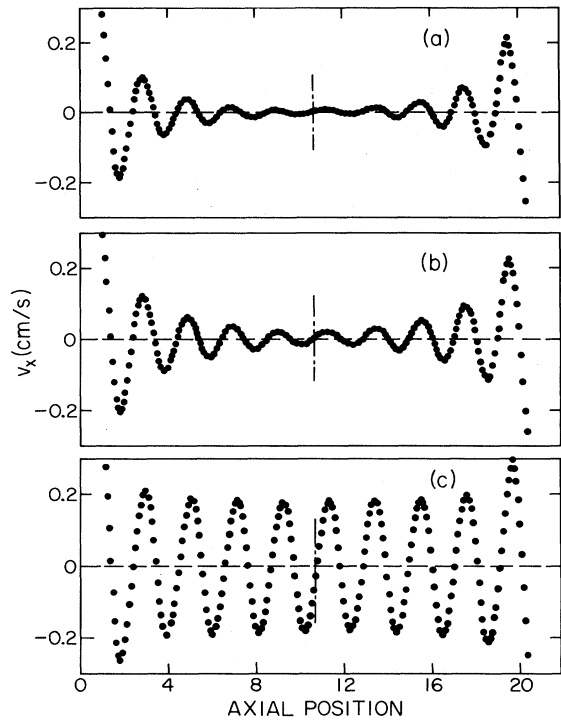


FIG. 59. Ekman pumping by the ends of a Taylor-Couette cylinder. The axial velocity component (denoted v_x in the figure) is shown vs axial position (in units of the gap) in a cylinder of aspect ratio $L=21.27$, for different values of the control parameter $\epsilon=R/R_c-1$, with R_c the onset Rayleigh number of an infinite cylinder, (a) $\epsilon=-0.011$, (b) $\epsilon=-0.003$, (c) $\epsilon=0.023$. Note that strong circulation near the ends occurs even for $\epsilon < 0$, and grows into the bulk as ϵ increases through zero. (From Ahlers *et al.*, 1986.)

tions that occur when the system changes its vortex number upon raising or lowering the angular velocity. For long cylinders the amplitude equation gives an excellent description of the allowed states and their stability as we shall see.

b. Short cylinders

For short cylinders a question of interest is how the Taylor vortex state, which has evolved smoothly from Couette flow via an imperfect bifurcation, changes from a $2n$ vortex state to a $2n+2$ state as the length is increased. (Ekman pumping strongly favors an even vortex state in small cylinders.) This problem was first posed in a precise manner by Benjamin (1978), who studied the 2 to 4 vortex competition. Since the theoretical analysis for $n > 1$ is more straightforward we will describe the later investigation of the 4 to 6 vortex competition by Mullin and Cliffe (1986); the effects are qualitatively the same for both cases.

The experimental results in the region where states with different numbers of vortices first appear are summarized in Fig. 60(a). The crosses correspond to bifurca-

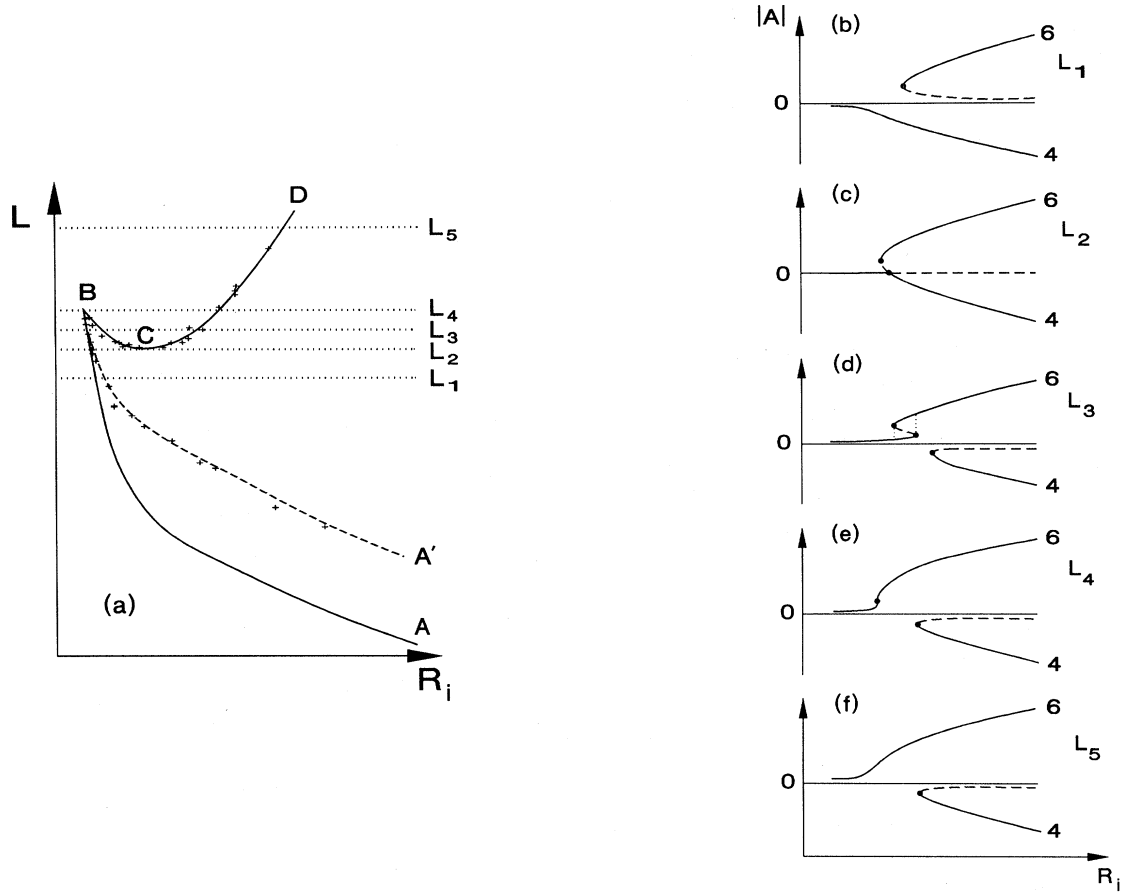


FIG. 60. Bifurcations in a finite Taylor-Couette cell. (a) Results for the competition between four and six rolls on a plot of aspect ratio L vs Reynolds number R_i of the inner cylinder. Full lines indicate a numerically calculated path of bifurcation points [corresponding to the dots in (b)–(f)] with an assumed symmetry. Crosses are experimentally observed bifurcations. For small L the symmetry assumed in the theory is broken in the experiment. The dashed line is a numerical calculation of the locus of this symmetry-breaking bifurcation. (b)–(f) Schematic sketch of the growth of the amplitudes $|A|$ for “four” and “six” roll states as the Reynolds number R_i is increased, for the aspect ratios L_1 to L_5 indicated in (a). Stable branches are denoted by full lines, unstable ones by dashed lines. The dots are the bifurcation points shown by the solid lines in (a). They are saddle-node bifurcation, except at the degeneracy points at L_2 and L_4 [corresponding to points B and C in (a)]. Note that as the aspect ratio changes from L_1 to L_5 the state growing continuously from the zero amplitude state changes from four rolls at L_1 to six rolls at L_5 . At intermediate aspect ratios (e.g., L_3) hysteretic jumps are necessary. (From Mullin and Cliffe, 1986.)

tions between states usually differing by one pair of Taylor vortices, which are observed when the rotation rate is varied at fixed aspect ratio. The solid lines are from a numerical simulation of the fluid equations, restricted to $z \rightarrow -z$ symmetric solutions.^{9,7} The qualitative evolution is shown for various aspect ratios in Figs. 60(b)–60(f), where the solid dots denote the bifurcation points shown in Fig. 60(a). For large R_i , two of the states can be clearly identified as 4 and 6 vortex states, but close to onset the solutions are mixed. Note how the smoothly developing solution changes from the 4 to the 6 vortex state as the

aspect ratio increases from L_1 to L_5 . The lengths L_2 and L_4 yield degenerate bifurcations [at the cusp B and the minimum C of Fig. 60(a)]. Also note that hysteretic jumps occur, for example in the evolution of the 6-vortex state at L_3 .

The full quantitative theoretical prediction in Fig. 60(a) required the massive numerical computation of Mullin and Cliffe (1986), because of the strong Ekman vortices near the ends. Shaeffer (1980) had earlier performed a qualitative analysis which led to the results in Figs. 60(b)–(f). He introduced a parameter $0 < \tau < 1$ characterizing a continuous change of the boundary conditions from ideal ($\tau=0$), where there are perfect bifurcations to the $2n$ and $2n+2$ vortex states, to realistic ($\tau=1$), where the bifurcations are strongly imperfect. In

^{9,7}A symmetry breaking occurs in the experiment for $L < L_1$, and was not allowed for in this simulation (solid line), thus accounting for the discrepancy in this domain.

the ideal case, $\tau=0$, the bifurcations evolve with length, passing through a degenerate point $L=L^*$ and $R_i^*=R_{ic}(L^*)$, where the onset rotation rates coincide. Shaeffer then unfolded the degenerate case perturbatively, treating τ , $L-L^*=h$ and $R_i-R_i^*=\varepsilon$ as small parameters via the equations

$$A_n^3 + g_n A_{n+1}^2 A_n - (\varepsilon + h) A_n - a_n \tau = 0, \quad (9.35a)$$

$$A_{n+1}^3 + g_{n+1} A_n^2 A_{n+1} - (\varepsilon - h) A_{n+1} - a_{n+1} \tau = 0, \quad (9.35b)$$

with g_n , g_{n+1} , a_n , a_{n+1} $O(1)$ coefficients and A_n , A_{n+1} the amplitudes of $2n$ and $2n+2$ vortex states. This “universal unfolding” and the perturbative inclusion of the qualitative effects of the complicated end conditions in the cylinders yield essentially all the results in Fig. 60. Coupled to the experimental data in the figure these provide a striking example of the power of the qualitative methods introduced in Sec. IV.B.

c. Long cylinders

The wave number of Taylor vortices in long cylinders has been studied in a series of experiments by Ahlers, Cannell, Dominguez-Lerma, and Heinrichs (1986). With conventional (nonrotating) ends the Ekman vortex prevents the number of rolls from changing via relaxation at the ends, contrary to the situation in Rayleigh-Bénard convection with rigid sidewalls (Sec. VIII.C). The experiments of Ahlers *et al.* then investigate the rolls far from the ends, where they can be considered as good approximations to states of the infinite system. The wave number of the rolls near the center can be varied over a well-defined band by changing the length of the cylinder at fixed roll number. Eventually, when the wave number reaches extreme limits, time dependence develops, first in the central rolls. This occurs via an instability which initially is well approximated as the Eckhaus instability of the infinite system. The stable band so obtained agrees beautifully with the theoretically calculated Eckhaus boundary as calculated by Riecke and Paap (1986, 1987) and shown in Fig. 61. Notice that the amplitude equation prediction in Eq. (4.24), shown as the dashed line, is good only for very small values of $\varepsilon=(R_i-R_{ic})/R_{ic}$. The sharp upturn on the low- q side is due to a nonlinear resonance of the states at wave numbers q and $2q$, both of which become unstable at this point. This resonance phenomenon was studied earlier by Meyer-Spasche and Keller (1985).

There are of course finite size corrections, which were investigated quantitatively by Ahlers *et al.* (1986) using the amplitude equation. The boundary condition to be applied is not clear *a priori*, since the Ekman vortex leads to a large [$O(1)$ not $O(\varepsilon^{1/2})$] flow amplitude near the ends. Hall (1980) and Graham and Domaradzki (1982) investigated this question, and from their work Ahlers *et al.* used

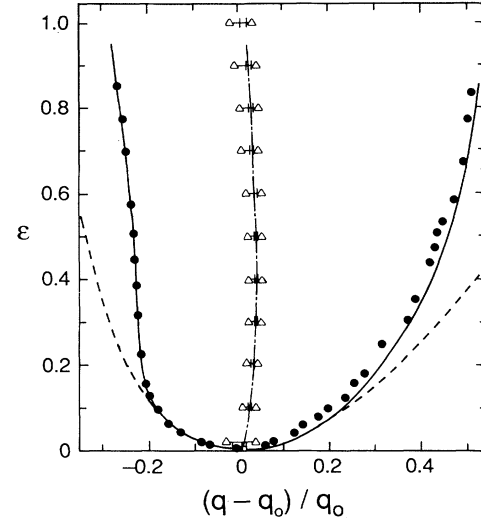


FIG. 61. Comparison between theory and experiment for the wave vector of the Eckhaus instability and the wave vector selected by a control-parameter ramp (created by a slowly varying outer cylinder radius) as a function of reduced control parameter ε . Solid circles, experimental results for Eckhaus instability; solid line, numerical results; dashed line, prediction based on amplitude equations. Triangles and vertical bars give the band of wave numbers selected by a ramp in the outer cylinder with angles $\alpha=0.030$ and 0.015 , respectively; dash-dotted line gives theoretical prediction for wave number selected by ramp with $\alpha\rightarrow 0$. (Adapted from Ahlers *et al.*, 1986; Riecke and Paap, 1986, 1987.)

$$A(0)=A(L)=A_b \gg \varepsilon^{1/2}, \quad (9.36)$$

with A_b a fixed number (chosen to be 1). It is easy to see from Eq. (5.2) that in steady state we have

$$|A|^2 \partial_z \phi = |A|^2 q = \text{const}, \quad (9.37)$$

as in Eq. (5.15). Thus variations in $q(z)=2\pi/\lambda(z)$ are most evident just below threshold where the amplitude is strongly varying in space. Experimental data corresponding to this limit are shown in Fig. 62, from which it is indeed seen that Eq. (9.37) is obeyed, except at the ends due to the strong perturbations caused by the Ekman vortex. This figure shows in particular that the wavelength of the central vortex (where the amplitude is least) becomes most strongly perturbed away from λ_c for $\varepsilon < 0$. Detailed measurements of the dependence of the central wave number on R_i for fixed wave number, and of the onset of time dependence in a finite cylinder, have been compared to numerical predictions from the amplitude equation, and excellent agreement was found. A particularly interesting point involves the onset of the Eckhaus instability in a finite cylinder near threshold. If the only effect of finite size were to quantize the wave vectors then in general the system would have a wave vector different from the critical value q_c and it would enter the Taylor vortex state through the Eckhaus unstable region near

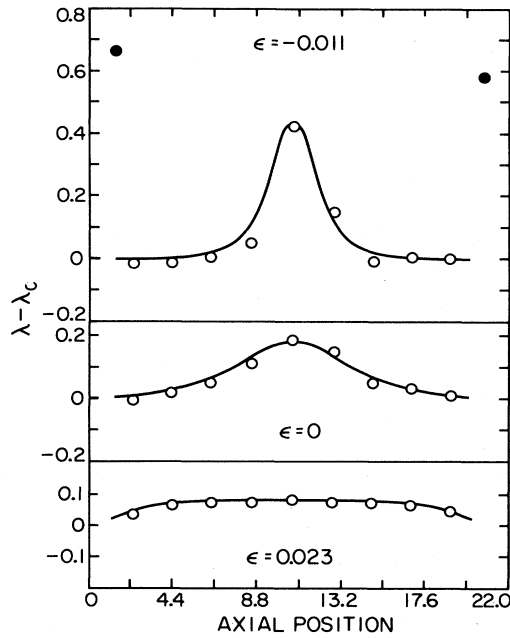


FIG. 62. Local wavelength (vortex-pair width) of Taylor vortices in a system of aspect ratio $L=21.27$ containing 10 vortex pairs, as a function of axial position, for three values of the reduced control parameter ϵ . The solid circles in the top panel represent the Ekman vortex adjacent to each boundary. The solid lines follow from Eq. (9.37). (From Ahlers *et al.*, 1986.)

threshold. Indeed, the modification of the Eckhaus instability by the finite system size calculated by Kramer and Zimmermann (1985; see also Tuckerman and Barkley, 1990) implies that exactly one Eckhaus stable state will exist arbitrarily close to threshold. This result was first noted by Ahlers *et al.* (1986) who also verified it experimentally. These experiments therefore provide a rather complete test of our understanding of the one-dimensional solutions of the fluid equations as well as their stability properties, and lead to quantitative agreement between experiment and theory.

d. Ramped boundaries

The Eckhaus instability still leaves a wide band of possible states in long cylinders above threshold. The actual state obtained must depend on initial conditions and on the experimental protocol. Systems in which this indeterminacy is eliminated, and where a unique wave number is determined by the system parameters, are of particular interest. As we have seen in Sec. IV.A, a slow enough ramp in the control parameter is predicted to yield a unique wave number in a region sufficiently far removed from the ramp. Cannell *et al.* (1983) implemented this idea by axially varying the gap between the cylinders with various small ramp angles α (e.g. $\alpha=0.015$ radians) (for more recent experiments see Ning *et al.*, 1990). They then measured the local wave number of the vortices well away from either end, as a function of the

cylinder length L (see Fig. 63). Figure 61 shows the dramatic reduction compared to the bandwidth in the unramped case as well as the dependence on ramp angle predicted by the theory of Kramer *et al.* (1982). The increasing bandwidth at small ϵ can be understood as arising from pinning of the vortices at the corner of the ramp: this effect was modelled by Cross (1984) through the addition to the amplitude equation of a forcing term localized at the corner,

$$\xi_0^2 \partial_z^2 A + \epsilon A - g_0 |A|^2 A + f(z) = 0, \quad (9.38a)$$

$$f(z) = h \xi_0 \delta(z), \quad (9.38b)$$

with h proportional to the ramp angle. The solution of this equation with the single fit parameter h leads to agreement with the bandwidth at small ϵ shown in Fig. 61, as well as the dependence of the wave number on length, including hysteretic transitions, displayed in Fig. 63. The increasing bandwidth at large ϵ seen in Fig. 61 is attributed to higher-order terms which are beyond the scope of the amplitude equation. This has been demonstrated in model equations by Riecke (1988). The unique wave number found by extrapolation to zero ramp angle agrees with the predictions based on calculations of the Navier-Stokes equations by Riecke and Paap (1987) for the whole range of measured ϵ values. This is one example where a unique wave number is predicted by a general argument, quantitatively calculated, and measured experimentally. As mentioned earlier, a fascinating

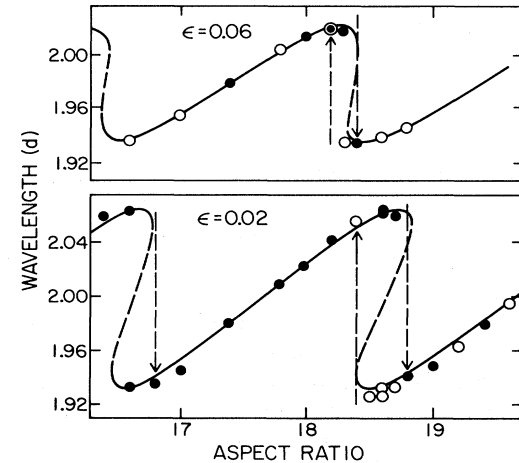


FIG. 63. Wavelength of rolls in the straight supercritical section of a Taylor-Couette system, selected by a control parameter ramp, plotted as a function of aspect ratio L , defined in terms of the length of the straight portion. The control parameter reaches subthreshold values due to an outer cylinder wall sloping at an angle $\alpha=0.03$ at one end of the cylinder. Solid circles were measured with increasing aspect ratio, open circles with decreasing L ; dashed arrows correspond to the observed hysteresis. Solid and dashed lines are theoretical predictions of Cross (1984) based on Eq. (9.38) with the pinning strength h used as a fit parameter. The values of ϵ shown correspond to the control parameter in the straight portion. (From Ahlers *et al.*, 1986.)

prediction is that the wave numbers selected depend on the specific origin of the ramp (inner or outer cylinder ramped, etc). Riecke and Paap (1987) found that if the two cylinders are ramped, at different angles, the unique wave number selected by the ramp should become Eckhaus unstable for some Reynolds numbers, leading to a periodic destruction of vortices, an effect which was again quantitatively confirmed experimentally. Numerical simulations of model equations by Riecke and Paap (1991) suggest that the instability may also lead to chaotic dynamics. Similarly, different ramps at either end may be used to prepare a dynamic state where the vortices are created at one end, drift along the cylinder, and are destroyed at the other end (Paap and Riecke, 1991).

e. Front propagation

Ahlers and Cannell (1983) also investigated the development of the Taylor vortex state by front propagation into the unstable region. In a cylinder of aspect ratio up to 15, they set up an initial state with a localized initial condition corresponding to Ekman vortices at $R_i/R_{ic} = 0.8$. They then jumped up the rotation speed to $R_i/R_{ic} = 1 + \epsilon$ and observed a front between Taylor vortices and Couette flow propagating into the unstable region with an asymptotically constant velocity. For small ϵ the phenomenon should be describable by the amplitude equation, and in particular Eqs. (6.27a) and (6.26a) should apply with $c_1 = 0$, yielding

$$v(\epsilon) = 2(\xi_0/\tau_0)\epsilon^{1/2}, \quad (9.39a)$$

$$q = q_c + O(\epsilon). \quad (9.39b)$$

These scalings were indeed found, but $v\tau_0/\xi_0\epsilon^{1/2}$ was measured to be ≈ 1 instead of 2. (The values of ξ_0 and τ_0 were calculated from the linear stability analysis of Couette flow.) Subsequent numerical calculations based on the full fluid equations (restricted to azimuthal symmetry) by Lücke *et al.* (1984, 1987b) and especially Niklas *et al.* (1989b) were found to be consistent with Eq. (9.39), and therefore disagreed with the experiment. The discrepancy was plausibly explained by Niklas *et al.* as resulting from a surprisingly long transient which was not captured by simulations of the amplitude equation with positive initial conditions carried out by Ahlers and Cannell. Thus the experiment did not measure the asymptotic velocity reached at long times, but rather a (lower) transient value (such an effect was noted independently by van Saarloos, 1989, 1990). The selected wave number was shown by Lücke *et al.* (1987b) to be close to the one obtained from the criterion of fastest growth from the uniform state. However the accuracy of the simulations is at present insufficient to distinguish between this result and the prediction (6.29c) from the Swift-Hohenberg model, say, so the question of wave-vector selection in front propagation remains open.

C. Electrohydrodynamic instabilities in nematic liquid crystals

1. General features

Nematics are liquids, usually formed of long *anisotropic* molecules with properties characterized by a single anisotropy axis, the director \hat{n} . For example the dielectric constant has the form

$$\epsilon_{ij} = \epsilon_0 \delta_{ij} + \epsilon_a \hat{n}_i \hat{n}_j, \quad (9.40)$$

and as a consequence *electrical* forces may be used to couple to the fluid flow. In addition electrical *conduction* is important, together with bulk forces $\rho_e \mathbf{E}$ acting on the volume charge buildup ρ_e . These effects lead to *electrohydrodynamic* instabilities, which are flow instabilities producing roll structures analogous to the Rayleigh-Bénard instability, but driven by electrical forces. Such forces can be made much stronger than gravitational buoyancy forces, so that the characteristic length and time scales of electrohydrodynamic instabilities are typically much shorter (e.g., lengths from 5 to 200 μm). This allows the experimental study of very large aspect ratio systems — up to several hundred — and we will concentrate on this feature of the system. For an introduction to instabilities in nematics see Dubois-Violette *et al.* (1978), Manneville (1990), and Zimmermann (1991).

The geometry we will focus on consists of a thin layer of nematic between two parallel plates separated by 10–100 μm , across which a voltage may be applied. This is usually an a.c. voltage to eliminate ion segregation effects. The plates are treated to favor the alignment of the director in some particular orientation which is in the plane of the plates in the most common configuration (we will pick this as the x axis). (Perpendicular alignment, known as the homeotropic case can also be considered.) The quiescent state consists of the director \hat{n} aligned uniformly in the x direction and no fluid flow. The instability develops when the voltage exceeds a critical value which turns out to be independent of the layer thickness in simple limits. The most familiar instability is to a spatially periodic roll state normal to the x direction known as “Williams domains.” In this state there is fluid circulation coupled to a tilt of the director in the x - z plane.

This electrohydrodynamic system presents a number of advantages in the study of pattern formation. As we have said, the time and length scales are more favorable than in Rayleigh-Bénard convection. The patterns are easily observed optically, since the distortions of the director orientation produce modulations in the index of refraction. The elimination of the rotational symmetry in the plane simplifies the study of large systems which in some cases are well represented by a one-dimensional approximation. There are many physically accessible control parameters, such as the voltage, the frequency, or an applied magnetic field. Moreover there is a rich spectrum of linear instabilities from the quiescent state as parameters are varied (e.g., to stationary normal rolls de-

scribed above, but also to oblique or traveling rolls) as well as interesting instabilities in the nonlinear regime.

The major disadvantage is that the dynamical equations are exceedingly complicated, and the many material properties involved are not always well characterized, so that a full theoretical understanding from the microscopic equations is hard to reach: indeed there remain discrepancies between the *linear* stability analysis and experimental observations despite a great deal of work (Kramer *et al.*, 1989).

An interesting feature of the dissipative electrohydrodynamic instabilities is that they can be tuned continuously into nondissipative regimes, where the instability criterion is given by energy balance arguments and there is no fluid flow in the distorted state (Bodenschatz *et al.*, 1988b). Examples are the Fréedericksz transition, as well as the “splay-twist” transition (Lonberg and Meyer, 1985), which produces a periodic structure with wave vector normal to the alignment direction. This provides the intriguing possibility of following the change in behavior as the nonequilibrium effects become more important while remaining in a fully nonlinear state.

It should be remarked that many other instabilities have been investigated in nematics, where the liquid anisotropy leads to a rich set of phenomena, including thermally driven and shear driven instabilities. We will not touch on this area, but refer the reader to the review by Dubois Violette *et al.* (1978).

2. Linear instability mechanism

As mentioned above, the basic equations of motion are complicated, and we will not write them down completely (see for example Bodenschatz *et al.*, 1988b). Besides the Navier-Stokes equation there are electric current equations of the form

$$\nabla \cdot \mathbf{j} + \partial_t \rho_e = 0, \quad (9.41a)$$

$$\mathbf{j} = \sigma \mathbf{E} + \rho_e \mathbf{v}. \quad (9.41b)$$

The field \mathbf{E} consists of the externally imposed field, the field due to the volume charge ρ_e and in addition a “flexoelectric” contribution from the polarization

$$\mathbf{P} = e_1 \hat{\mathbf{n}} (\nabla \cdot \hat{\mathbf{n}}) + e_3 (\hat{\mathbf{n}} \cdot \nabla) \hat{\mathbf{n}}. \quad (9.42)$$

In addition there is a “torque balance” equation giving the dynamics of $\hat{\mathbf{n}}$ in terms of the dielectric anisotropy energy, the liquid crystal elastic bending energy density

$$F_{\text{el}} = \frac{1}{2} [K_{11}(\nabla \cdot \hat{\mathbf{n}})^2 + K_{22}(\hat{\mathbf{n}} \cdot \nabla \times \hat{\mathbf{n}})^2 + K_{33}(\hat{\mathbf{n}} \times \nabla \times \hat{\mathbf{n}})^2], \quad (9.43)$$

and a viscous torque coupling $\hat{\mathbf{n}}$ to shear and rotation in the fluid. Finally the Navier-Stokes equation is supplemented with extra terms in the stress coming from the volume electrical forces and also from the spatial derivatives of the director $\hat{\mathbf{n}}$.

The stability analysis seeks deviations from the quiescent state — zero fluid velocities, $\hat{\mathbf{n}}$ uniformly aligned in the x direction, forced by an a.c. electric field E_z of frequency ω coming from the voltage V between the confining plates. An example of the types of instabilities encountered is shown by the experimental results in Fig. 64.

The simplest instability is toward convective rolls with normal parallel to the preferred orientation of the director. The onset is divided into two well differentiated regions: at high frequencies (above 470 Hz in Fig. 64) a “dielectric regime” dominated by the oscillating reorientation of the director and consequent dielectric electrical forces; at lower frequencies a “conduction regime” where oscillating charge densities and electric currents dominate. In the absence of flexoelectric effects these instabilities are characterized by different parity symmetries (Bodenschatz *et al.*, 1988b). In addition at very low frequencies, below a critical frequency called the Lifshitz point (120 Hz in the experiments of Rehberg *et al.*, 1989b), the first instability is actually to an oblique roll state with rolls making an angle θ with the alignment direction. Since $+\theta$ and $-\theta$ give equivalent states, domains of each orientation often coexist in the experiment, leading to a zig-zag pattern. The angle θ grows continuously below the Lifshitz point and the analysis of the region near this point is an interesting application of the amplitude equation formalism. The above types of linear instabilities are reasonably well accounted for by theory (Kramer *et al.*, 1988b; Bodenschatz *et al.*, 1990), with quantitative comparison apparently limited mainly by uncertainties in fluid parameters. One discrepancy shown in Fig. 64, involves a small range of frequencies ($350 < \omega < 470$ Hz) in which the transition is to a *traveling* roll state throughout the system, indicated by a nonzero relative frequency. In addition over a wider range of frequencies the transition is found to be weakly hysteretic, and although the small amplitude nonlinear state at onset is stationary, the transients leading to this

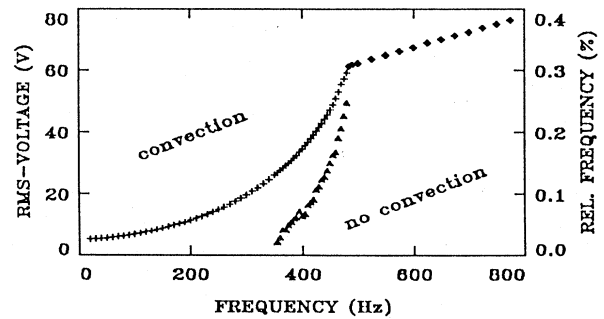


FIG. 64. Example of an experimental linear stability diagram of electrohydrodynamic convection. Pulses show the applied rms voltage of the oscillating drive needed to produce an instability, as a function of the frequency of the driving. Triangles show the relative frequency at onset of the traveling roll pattern (right-hand axis) that develops for a drive frequency between 350 Hz and 470 Hz. (From Rehberg *et al.*, 1989b.)

state are oscillatory, suggesting that the linear instability is in fact oscillatory over this wider range (Rehberg *et al.*, 1991). In other experiments Joets and Ribotta (1988) observed traveling waves near threshold in the form of spatially confined pulses. The mechanism behind these traveling waves is not yet completely understood. Finally, Rehberg *et al.* (1989b) observed a linear growth of the oblique roll angle θ , whereas a square-root dependence is expected at the linear threshold on quite general grounds.

3. Nonlinear states

a. Normal rolls

In the weakly nonlinear regime the normal rolls are described by a complex amplitude $A(x, y, t)$ introduced by writing

$$U = U_0(z) A e^{iq_0x} + \text{c.c.}, \quad (9.44)$$

which satisfies the equation

$$\tau_0 \partial_t A = \epsilon A + \xi_x^2 \partial_x^2 A + \xi_y^2 \partial_y^2 A - g_0 |A|^2 A. \quad (9.45)$$

As mentioned in Sec. IV.A, this equation can be rescaled to read

$$\partial_T A = \pm \bar{A} + (\partial_X^2 + \partial_Y^2) \bar{A} - |\bar{A}|^2 \bar{A}, \quad (9.46)$$

so that the *anisotropic* system (no rotational symmetry in the plane) gives rise to a simple, rotationally invariant (scaled) amplitude equation, whereas rotationally invariant systems such as Rayleigh-Bénard convection lead to a more complicated anisotropic form (4.7). The simplicity of Eq. (9.46) means that a quantitative comparison between theory and experiment in complicated situations is often easier than in Rayleigh-Bénard convection (Kramer *et al.*, 1986). One example is in the dynamics of dislocation defects, which we discuss below. In addition the elimination of the rotational degeneracy allows “one-dimensional” questions to be investigated more easily. An example of this is the experimental study by Lowe and Gollub (1985a) of the development of a straight roll pattern after the onset of the Eckhaus instability, and quantitative comparisons with predictions of Kramer *et al.* (1988a) derived from the amplitude equation.

b. Oblique rolls and the Lifshitz point

The onset of the oblique roll instability is signaled by $\xi_y^2 \rightarrow 0$ in Eq. (9.45). Since the coefficient of a lowest-order derivative term is going to zero, in analogy with a similar phenomenon in equilibrium phase transitions this point ($\epsilon = 0$, $\xi_y^2 \rightarrow 0$) has been called a Lifshitz point (Hornreich *et al.*, 1975). In the electrohydrodynamic case the oblique roll instability occurs as the driving frequency is reduced. The instability is described by two coupled amplitude equations, given by modulating rolls

at angles $\pm \theta$ to the nematic alignment direction

$$U = U_0 e^{iq_0x} [A_+ e^{iq_0y} + A_- e^{-iq_0y}] + \text{c.c.}, \quad (9.47)$$

with $\tan \theta = q_0y/q_0x$ and

$$\begin{aligned} \tau_0 \partial_t A_{\pm} &= \epsilon A_{\pm} + [\xi_x^2 \partial_x^2 + \xi_y^2 \partial_y^2 \pm 2\xi_x \xi_y a \partial_x \partial_y] A_{\pm} \\ &\quad - (g_1 |A_{\pm}|^2 + g_2 |A_{\mp}|^2) A_{\pm}, \end{aligned} \quad (9.48)$$

with $|a| < 1$. For either A_+ or A_- separately the derivative term can be put into the standard form $\partial_X^2 + \partial_Y^2$ by a suitable rotation and scaling of the coordinate axes, again leading to Eq. (9.46), although X is no longer along the nematic alignment direction.

Near the Lifshitz point where the coefficient of ∂_y^2 in Eq. (9.48) goes to zero a new scaling yielding higher-order derivative terms is appropriate. Defining $Y \sim \epsilon^{1/4} y$ and eliminating constant factors, Bodenschatz *et al.* (1990) find

$$\partial_T A = [\partial_X^2 - i\alpha \partial_X \partial_Y^2 + \beta \partial_Y^2 - \partial_Y^4 + 1 - |A|^2] A, \quad (9.49)$$

where β parametrizes the distance from the linear Lifshitz point $\beta = 0$, and α is a numerical constant.

Finally, since the oblique roll instability sets in at long wavelengths, the instability in the nonlinear regime can be analyzed in terms of a higher-order phase diffusion equation

$$\partial_t \phi = \eta \partial_y^2 \phi - \partial_y [\partial_y^3 \phi - (\partial_y \phi)^3], \quad (9.50)$$

where $\eta \rightarrow 0$ signifies the instability, and numerical constants have been eliminated by appropriate scaling. (We have also ignored x derivatives; for the more general case see Sasa, 1990.)

Equations (9.49) and (9.50) have been used to study the onset, development, and instability of the oblique roll state by Bodenschatz *et al.* (1990). In addition, Pesch and Kramer (1986) have analyzed the phenomena in an anisotropic version of the Swift-Hohenberg equation. One interesting question is whether the instability, which may begin as a transverse undulation at nonzero wave number, saturates at a finite amplitude giving a stable undulating or zig-zag solution such as has been observed experimentally (Ribotta *et al.*, 1986), or whether it grows catastrophically to give a uniform reoriented oblique roll structure, with domain boundaries between “zig” and “zag.” An analysis of the amplitude equation (9.49) near the Lifshitz point yields small regions of stable undulating roll solutions. However, to explain the widely observed zig-zag states it is probably necessary to solve the coupled amplitude equations away from the Lifshitz point, and to include the nonadiabatic effects locking the oscillatory decay of the amplitude of the “zig” (say) into the neighboring “zag,” to the underlying periodic structure of the rolls. As discussed in Sec. VII.E.6 spatially chaotic solutions would also be expected in this situation.

4. Convection with spatially periodic forcing

We have emphasized the importance of external forcing on bifurcations, considering mainly small, localized imperfections. External forcing becomes particularly interesting when it is spatially periodic with a period resonant or nearly resonant with the critical wave number of the instability. As well as rendering the bifurcation imperfect (Kelly and Pal, 1978) the driving leads to delicate competition in the nonlinear regime between the externally imposed periodicity and the “natural” wave number of the pattern.

In a series of experiments Lowe and co-workers (Lowe *et al.*, 1985, 1986; Lowe and Gollub, 1985b) investigated this phenomenon for the electrohydrodynamic instability, with external forcing imposed by a grid of electrodes on one of the plates. This particular system was chosen for experimental reasons — the large aspect ratios and easy control of the spatially periodic forcing being important considerations — but the specific mechanism of the instability is not important. The intrinsic anisotropy is however important, since it leads to a simple one-dimensional situation for strong anisotropy. [For weak anisotropy more complicated effects occur; in particular a one-dimensional modulation produces a two-dimensional pattern.]

The results for the one-dimensional situation (electrode grid perpendicular to anisotropy axis) are displayed in Fig. 65 for $\epsilon=0.057$, as a function of the ratio of competing length scales ℓ_0/ℓ_1 ($\ell_0=2\pi/q_0$ being the critical wavelength and ℓ_1 the period of the spatial forcing) and of the strength of the periodic driving α . There is considerable complexity in the results summarized in the figure, and we refer the reader to the original work of Lowe *et al.* (1985, 1986) for a very readable full description. The important competition is between commensurate states (in which an integral number n of rolls are distorted to match m periods of the spatial forcing, with $\ell_0/\ell_1=n/m$ a small rational number), and incommensurate states, in which the mean roll period ℓ does not form a simple ratio with ℓ_1 and, more importantly, varies continuously as parameters are changed. [See Fig. 65(b).] Furthermore, the incommensurate states may be described in terms of local almost undistorted regions of rolls of period ℓ_0 separated by regions of considerable distortion (referred to as solitons by Lowe *et al.*) as shown by the phase plot in Fig. 66(b).

Many of the features of the experiment can be qualitatively reproduced by a one-dimensional amplitude equation description (Coullet, 1986; Coullet and Huerre, 1986). In addition to the usual terms there is one arising from the nearly resonant forcing. Writing $mq_1=n(q_0+k)$ with k small, the appropriately scaled amplitude equation is

$$\partial_t A = \epsilon A - |A|^2 A + \partial_x^2 A + \alpha^m (A^*)^{n-1} e^{inkx}, \quad (9.51)$$

with α proportional to the strength of the driving [note this parameter is unrelated to the α in Eq. (9.49)].

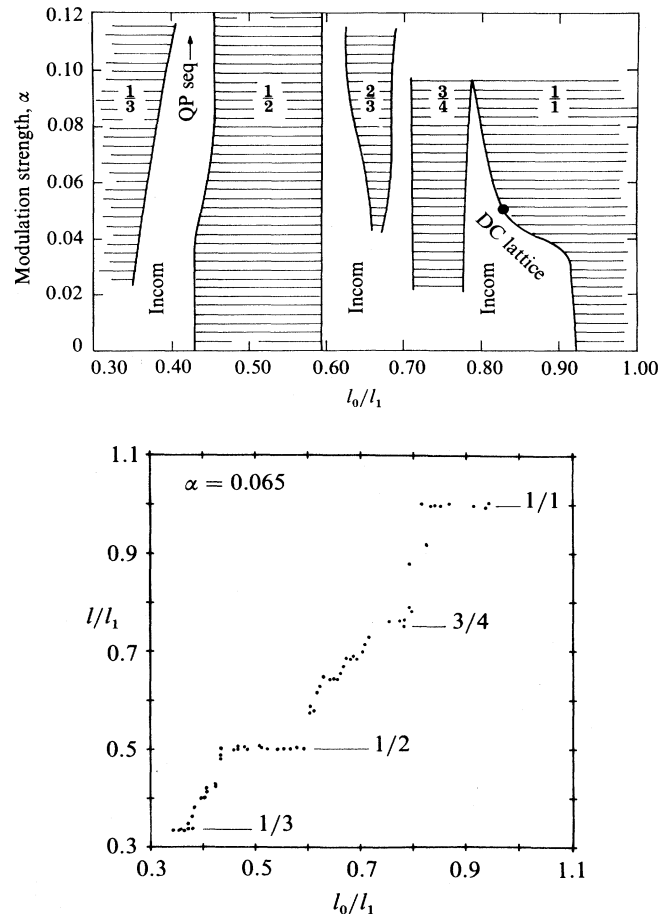


FIG. 65. Electrohydrodynamic convection with spatial forcing. (a) Phase diagram representing the strength of the periodic driving α as a function of the ratio of competing length scales ℓ_0/ℓ_1 , for $\epsilon=0.057$. The commensurate regions are represented by the shaded areas. The incommensurate regions are unshaded. (b) Variation of the inverse of the mean wave number ℓ vs the unperturbed roll wavelength ℓ_0 , both expressed in units of the wavelength ℓ_1 of the periodic forcing, for $\alpha=0.065$ and $\epsilon=0.057$, see Eq. (9.51). Commensurate regions are indicated by plateaus, incommensurate regions by a continuous variation of ℓ with ℓ_0 . (From Lowe *et al.*, 1986.)

Presumably this form is only appropriate for $n \leq 4$, since for $n > 4$ the extra term is formally of higher order in ϵ than other terms in the equation. Note that the resonant case $k=0$, $n=1$ leads to a direct forcing of the critical mode as investigated by Kelly and Pal (1978), and often used experimentally to imprint patterns. Higher-order resonances leave the bifurcation perfect, but may shift the threshold ($n=2$) or make the bifurcation subcritical ($n=3$).

At the present level of approximation, Eq. (9.51) derives from a potential as usual but with the extra term

$$\Delta F = -(\alpha^m/n) \int [(A)^n e^{-inkx} + (A^*)^n e^{inkx}] dx, \quad (9.52)$$

which expresses the tendency of the period of the pattern to lock to the imposed period ($\ell \rightarrow \ell_1$). The theoretical treatment now reduces to minimizing the combined potential, and analogous problems in statistical mechanics are well known to lead to commensurate-incommensurate transitions. The analogy becomes particularly clear when k is so small that a phase treatment is valid

$$A = |A| e^{i\Theta}, \quad \Theta = kx + \Phi, \quad (9.53)$$

at which point the calculation reduces to minimizing the phase potential

$$\begin{aligned} V(\Phi) = & \int [-n^{-1}\alpha^m |A|^{n-2} \cos(n\Phi) \\ & + \frac{1}{2} (\partial_x \Phi)^2 - k(\partial_x \Phi)] dx. \end{aligned} \quad (9.54)$$

This potential is the same as the continuum limit of the Frenkel-Kontorova model (see Aubry, 1983; Pokrovsky and Talapov, 1984), the canonical statistical mechanical model of commensurate-incommensurate transitions, for which results qualitatively analogous to Fig. 65 are well known. The analysis of Eq. (9.54) leads to a continuous transition from the locked commensurate states $\Phi=0$ to incommensurate states with a periodic array of phase slips which are analogous to sine-Gordon solitons, when the mismatch k exceeds a critical value. Since the period of the phase slip array is unrelated to q_1 , this corresponds to an incommensurate solution: the average period ℓ of the rolls is not in general rationally related to the imposed period ℓ_1 and varies continuously with ℓ_0/ℓ_1 . As we have seen, many features of the experiments are captured by this simple analysis, for example the shape of the phase variation for small α depicted in Fig. 66. However some features are not: the locking to higher-order commensurate states including phase slips, and other quasiperiodic or disordered locking phenomena, are not predicted. Presumably these involve locking of the position of the phase slips to the underlying period through nonadiabatic effects (Sec. IV.A.4). Also the change to a discontinuous commensurate-incommensurate transition is not predicted, although other similar systems often show this type of behavior too (see Aubry, 1983).

It is interesting to remark that the theoretical understanding of the experiments of Lowe *et al.* (1985, 1986) is based entirely on potential models: the theory essentially reduces the problem to equilibrium statistical mechanics, where it is safe to talk about the competition between a “preferred” wave number q_0 and an imposed periodicity. It is worth pondering on the implications of the observation of similar phenomena in the more nonlinear regimes, where reduction to a potential description is not guaranteed and often not expected.

5. Motion of dislocations

The simplicity of the amplitude equation (9.46) has allowed a rather complete theoretical treatment of the statistics and dynamics of dislocation defects in the electrohy-

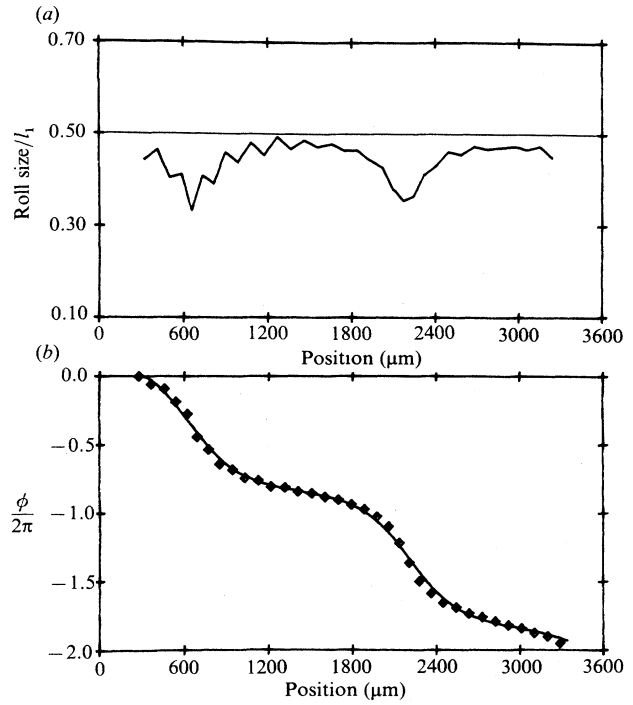


FIG. 66. Spatially forced electrohydrodynamic convection. (a) Roll size (in units of the wavelength ℓ_1 of the forcing) as a function of the position across the cell. Note that over large regions the pattern is nearly commensurate at $\ell=\ell_1/2$, with compressed regions in between. (b) Variation of the phase of the complex amplitude across the sample. The solid line is a fit to Eq. (9.54). (From Lowe *et al.*, 1986.)

drodynamic instability, as well as a direct comparison with experiment (Bodenschatz *et al.*, 1988a, 1990, 1991b; Coron *et al.*, 1991; Weber *et al.*, 1991). The amplitude function defining an isolated stationary defect solution of (9.46) is

$$\bar{A} = \bar{F}(R) e^{i\bar{\phi}}, \quad \bar{\phi} = \tan^{-1}(Y/X), \quad R = (X^2 + Y^2)^{1/2}, \quad (9.55)$$

where $\bar{F}(R) \rightarrow 0$ at the core center $R=0$, and approaches 1 outside the core region in a way that must be calculated numerically [the core size is $O(1)$ in scaled units]. Note that the background wave vector \mathbf{Q} must be zero (i.e., $q = q_d$) for a stationary defect (see Sec. V.B.3).

Perturbations of the background wave number, i.e.,

$$\bar{A} \sim e^{i(Q_X X + Q_Y Y)}, \quad R \rightarrow \infty, \quad (9.56)$$

cause motion of the dislocation. The interpretation of this motion depends on whether one is considering oblique rolls as in Eq. (9.48) or normal rolls. In the latter case, where no coordinate rotation is involved in going from (x, y) to (X, Y) , motion in the $X(x)$ direction is *climb* and is driven by roll compression with wave number Q_X , whereas motion in the $Y(y)$ direction is *glide* and is driven by a small *rotation* of the rolls [$\delta\theta = \varepsilon^{1/2} Q_Y /$

$(q_0 \xi_y)$. As in Rayleigh-Bénard convection, glide will be affected by nonadiabatic effects not included in the amplitude equation.

As we have seen in Sec. V.B.3 the speed V of isolated defects perpendicular to the wave-vector change \mathbf{Q} may be calculated from potential arguments near threshold to give [see Eq. (5.158)]

$$V = 2\mathbf{Q}/\ln(3.29/V), \quad (9.57)$$

where we have assumed that the finite velocity V cuts off the logarithmic divergence in the denominator. If defect pairs get close enough together their interaction will add an extra driving force. It should be remembered that the phase distortion *in front* of a moving dislocation falls off exponentially with a length scale $\sim \xi_0^2/V\tau_0$, and so the interaction between defects moving together will be very small until this separation is reached.

Dislocation motion has been investigated experimentally by Goren *et al.* (1989) and by Rasenat *et al.* (1990); these authors followed a few dislocation pairs remaining from complicated initial conditions, on their way to annihilation. The essential features noted were as follows.

- There exists a regime with a constant relative velocity v_c of the defects. The dependence of v_c on the wave-number distortion was measured.
- There exists a crossover distance r^* below which the motion accelerates.
- This crossover distance varies as $1/v_c$.

These features are all predicted by the above theory. Indeed, the constant velocity is presumed to arise from a compression or rotation of the pattern $v_c \propto Q$ (neglecting small logarithmic corrections). The crossover distance is then the distance at which the phase distortion in front of the defect becomes felt by the second defect. Equation (5.92) predicts $r^* \sim v_c^{-1}$, as measured. We believe there is no merit to the theory developed by Goren *et al.* (1989) to explain the data, which were well accounted for by the prior conventional theory. This is brought out by Kramer *et al.* (1990), who show a comparison of the original theory, using *predicted* values of ξ_x , ξ_y , and τ_0 , with measurements (Fig. 67). It is interesting that glide motion was also observed and showed clear steps, evidence of nonadiabatic pinning effects (Sec. IV.A.4). More detailed measurements of the glide motion have been made by Braun and Steinberg (1991) and await a full theoretical understanding.

6. Fluctuations and chaos

In his early estimates of the effect of thermal fluctuations on the convective instability, Graham (1974, 1975) suggested that electrohydrodynamic convection in nematics would be a favorable system to investigate. Indeed, the characteristic noise strength parameter F_{th} in Eq. (8.63) can be enhanced by a small dissipative coefficient and by use of a thin layer. Recently, Rehberg *et al.* (1991) have reported observing convective fluctua-

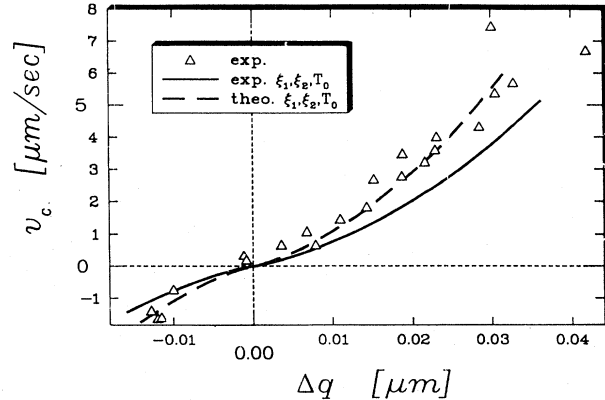


FIG. 67. Climb velocity v_c of a single dislocation in convection rolls in a nematic as a function of the deviation Δq of the wave vector from critical. Triangles are experimentally measured points (Goren *et al.*, 1989). Dashed line is theoretical prediction based on Eq. (9.57), using theoretically calculated values of ξ_0 and τ_0 to return to physical units. There are no adjustable parameters and the agreement is remarkable. (Solid line is obtained using values of ξ_0 and τ_0 estimated from independent measurements.) (From Kramer *et al.*, 1990.)

tions below threshold, and have fitted the measured correlation function to the predictions of Eq. (8.61) above, with a fitted noise strength $F = 2.6 \times 10^{-7}$ close to the *a priori* estimate $F_{th} = 1.8 \times 10^{-7}$.

Finally, we mention that defect mediated chaos has been observed by a number of workers, and this seems to be a promising system for quantitative investigations of extensive chaos (see Nasuno *et al.*, 1989b; Nasuno and Sawada, 1989; Braun *et al.*, 1991).

D. Parametric surface waves

As mentioned in Sec. II.D the parametric excitation of surface waves provides a rich field for pattern formation studies. Although research on this phenomenon has an ancient history, attention has mainly focused on systems with few degrees of freedom, and comparatively little is known about the behavior of the large-system limit. We shall primarily concentrate on this latter case, referring the reader to the literature for studies of small systems (see, e.g., Miles, 1984a; Meron and Procaccia, 1986a,b; Simonelli and Gollub, 1987; Feng and Sethna, 1989; Miles and Henderson, 1990).

1. Theory

a. Basic equations

We begin with the wave equation for oscillation of the free surface of a laterally infinite fluid, whose height is given by $h(\mathbf{x}, t)$ (see Benjamin and Ursell, 1954). Setting

$$h(\mathbf{x}, t) = a_q(t) \cos(\mathbf{q} \cdot \mathbf{x}), \quad (9.58)$$

we have a wave equation

$$\partial_t^2 a_q + \gamma \partial_t a_q + \omega_s^2(q) a_q = 0, \quad (9.59)$$

with γ a phenomenological damping constant, and

$$\omega_s^2(q) = q \tanh(qh_m) [g + \Sigma q^2 / \rho], \quad (9.60)$$

the linear dispersion relation of (unforced) surface waves, g being the acceleration of gravity, Σ the surface tension, ρ the mass density, and h_m the average height of the surface above the bottom of the container. Under parametric forcing the acceleration of gravity is modulated at frequency 2ω according to

$$g \rightarrow \tilde{g}(t) = g(1 + \tilde{\Delta} \cos 2\omega t), \quad (9.61)$$

so that Eq. (9.59) becomes for $q = q_0$,

$$\partial_t^2 a + \gamma \partial_t a + \omega_s^2(q_0) [1 + 2\Delta \cos 2\omega t] a = 0, \quad (9.62a)$$

$$\Delta = \frac{1}{2} \tilde{\Delta} [1 + (\Sigma / \rho g) q_0^2]^{-1}, \quad (9.62b)$$

and q_0 is defined by the resonance condition

$$\omega_s(q_0) = \omega. \quad (9.63)$$

For a small container where a single mode $h_0(x, y)$ with frequency ω_0 is excited we set

$$h(\mathbf{x}, t) = a(t) h_0(x, y), \quad (9.64)$$

and Eq. (9.62a) becomes the Mathieu equation (Landau and Lifshitz, 1976)

$$\partial_t^2 a + \gamma \partial_t a + \omega_0^2 [1 + 2\Delta \cos 2\omega t] a = 0, \quad (9.65)$$

whose solutions of the form

$$a(t) = a_0 e^{\sigma t} + c.c. \quad (9.66)$$

have unstable growth ($\text{Re } \sigma > 0$) inside tongues as shown schematically in Fig. 68. The lowest mode to appear is $n = 1$ and its frequency is centered around $\omega = \omega_0$, with a threshold (see below)

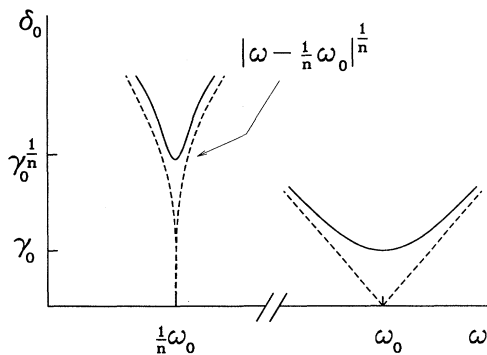


FIG. 68. Neutral stability curves in the driving strength δ_0 vs frequency ω plane for the Mathieu equation (9.65) with parameters defined in (9.68) (only the first and the n th tongues are shown). Instability occurs above the full curves for nonzero damping γ_0 . For $\gamma_0 = 0$ the instabilities occur above the dashed lines.

$$\Delta_c = \gamma / \omega_0, \quad (9.67)$$

or, in terms of the control parameter

$$\delta_0 = \Delta \omega_0 / 2, \quad \gamma_0 = \gamma / 2, \quad (9.68)$$

with dimensions of frequency, $\delta_c = \gamma_0$.

b. Boundary conditions, real fluid effects

In a large but finite system the analysis leading to Eq. (9.65) holds rigorously only for the unphysical lateral boundary condition that the surface should remain horizontal, i.e. perpendicular to the sidewall. A more realistic boundary condition, even for a surface at rest, is that there is a meniscus with some contact angle θ , and a width given by the capillary length

$$\ell_{\text{cap}} = (\Sigma / \rho g)^{1/2}, \quad (9.69)$$

beyond which the stationary surface heals to its bulk position. In the presence of dissipation ($\gamma \neq 0$) and under modulation (9.61), the boundary condition is difficult to describe precisely, but one effect of the boundary is to generate a parasitic surface wave at the *excitation* frequency 2ω , which may propagate inward for a large distance. We are not aware of any quantitative study of this phenomenon. References to the literature on the properties of the meniscus may be found in Miles and Henderson (1990).

It has been suggested by Benjamin and Scott (1954) that if the fluid completely fills the container the surface can become *pinned* to the upper edge, thus leading to the boundary condition

$$h(\mathbf{x}, t) \equiv 0, \quad (9.70)$$

even under modulation (for not too large amplitudes). A difficulty arises, however, because the dissipation coefficient γ , as well as its nonlinear generalizations (see below), are sensitive both to the flow near the boundaries and to large-scale flows caused by the boundary condition (9.70) (see Douady, 1990).

Milner (1991) has summarized the different contributions to the damping constant γ and estimated their magnitude for large systems. There are essentially four important damping mechanisms:

(i) Bulk viscosity, which has contributions from the full surface and leads to a damping constant given by $\gamma_b \sim v q_0^2$.

(ii) Wall damping, whose relative magnitude is reduced by the ratio of perimeter to surface area, and leads to a coefficient $\gamma_w \sim \omega \ell_D / L$, where $\ell_D = (2v/\omega)^{1/2}$ is the dissipation length and L is the system size.

(iii) The moving meniscus [when condition (9.70) does not hold].

(iv) Dissipation due to contaminants at the surface, which can be quite large since it is proportional to the area and since the mechanical properties of the interface can be significantly different from those of the fluid.

Estimates of the last two contributions to the damping in terms of the fluid parameters and the two-dimensional bulk modulus of the contaminant layer are quoted in Milner's paper.

c. Amplitude equations

In the single-mode limit (9.65) we may obtain an amplitude equation for *small* damping ($\gamma/\omega_0 \ll 1$) and *near* resonance ($|\omega - \omega_0| \ll \omega_0$) by expressing $a(t)$ in terms of a slow modulation of the subharmonic mode,

$$a(t) = A(t) e^{-i\omega t} + \text{c.c.} \quad (9.71)$$

The amplitude equation has the form

$$\partial_t A = -(\gamma_0 - ic_0) A - i \delta_0 A^* - (\gamma_3 - ic_3) |A|^2 A, \quad (9.72a)$$

$$c_0 = \omega - \omega_0, \quad (9.72b)$$

together with the equation for A^* , where γ_3 is a nonlinear damping constant and c_3 a nonlinear detuning parameter. These coefficients can in principle be calculated by solving for the flow in the finite container.

The linear spectrum is $A(t) \sim \exp(\sigma t)$ with

$$\sigma_{\pm} = -\gamma_0 \pm (\delta_0^2 - c_0^2)^{1/2}. \quad (9.73)$$

For $c_0 \neq 0$ the dependence of the eigenvalues on δ_0 is shown in Fig. 69. The amplitude equation (9.72) is a faithful representation of the dynamics of Eq. (9.65) provided *both* eigenvalues σ_{\pm} are small (compared to other frequencies in the problem). The actual instability occurs when σ_+ passes through zero at

$$\delta_0 = \delta_c = (\gamma_0^2 + c_0^2)^{1/2}. \quad (9.74)$$

Close enough to this instability we can further reduce the description to a *single* amplitude equation for the real amplitude of the oscillation, appropriately phased to draw energy from the pumping

$$A = B e^{i\alpha}, \quad (9.75a)$$

(the phase α depends on the detuning and is $-\pi/4$ for $c_0=0$). This amplitude equation takes the simple form

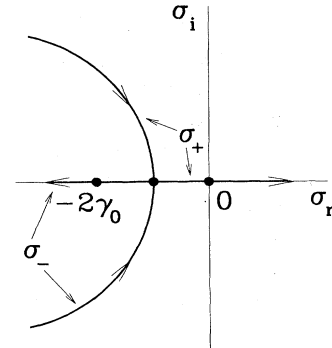


FIG. 69. Path of the complex linear eigenvalues σ_{\pm} [Eq. (9.73)] as the driving strength δ_0 increases. The eigenvalues are a complex pair for $\delta_0 < c_0$, and collide at $\sigma_{\pm} = -\gamma_0$ when $\delta_0 = c_0$. Further increasing δ_0 leads to the instability $\sigma_+ = 0$, where δ_0 takes on the value δ_c given in Eq. (9.74), at which point $\sigma_- = -2\gamma_0$. Note that for small damping γ_0 the σ_- eigenvalue remains small, and the dynamics of the corresponding eigenvector may remain important for $\delta_0 > \delta_c$.

$$\tau_0 \partial_t B = \varepsilon B - g_0 B^3. \quad (9.75b)$$

It should be noted that to arrive at the single amplitude equation (9.75b) we are assuming $|\sigma_+| \ll |\sigma_-|$, so that now the σ_- mode is eliminated as "fast." This delicate interplay between the coupled "near Hamiltonian" amplitude equations (9.72) and the single "unstable mode" amplitude equation (9.75b) is a recurring feature of parametric instabilities in weakly damped wave systems.

For the laterally infinite system, amplitude equations analogous to those of Newell and Whitehead (1969) and Segel (1969) were only studied quite recently. The simplest case is a one-dimensional geometry, considered by Thual *et al.* (1989) and by Douady *et al.* (1989b). They made the ansatz

$$h(x, t) = A_1 e^{i(q_0 x - \omega t)} + A_2 e^{-i(q_0 x + \omega t)} + \text{c.c.}, \quad (9.76)$$

which corresponds to Eq. (9.71), but now includes the degenerate $\pm q_0$ modes defined by the resonance condition

$$\omega_s(q_0) = \omega. \quad (9.77)$$

For small damping we may neglect the wave-vector dependence of the damping and arrive at the amplitude equations for traveling waves:

$$\partial_t A_1 + s_0 \partial_x A_1 = -\gamma_0 A_1 + i c_1 \partial_x^2 A_1 - i \delta_0 A_2^* - [(\gamma_3 - ic_3) |A_1|^2 + (\gamma_4 - ic_4) |A_2|^2] A_1, \quad (9.78a)$$

$$\partial_t A_2 - s_0 \partial_x A_2 = -\gamma_0 A_2 + i c_1 \partial_x^2 A_2 - i \delta_0 A_1^* - [(\gamma_3 - ic_3) |A_2|^2 + (\gamma_4 - ic_4) |A_1|^2] A_2. \quad (9.78b)$$

Again near threshold, $\delta_0 - \gamma_0 \ll \gamma_0$, it is more convenient to rewrite these equations in terms of the standing-wave amplitude $B(x, t)$, which is now complex. Equations (9.78a) and (9.78b) can be reduced using the general procedure outlined in Appendix A. This yields

$$A_1 = B - (s_0/2\gamma_0) \partial_x B + \dots, \quad (9.79a)$$

$$A_2 = iB^* - (is_0/2\gamma_0) \partial_x B^* + \dots, \quad (9.79b)$$

and the amplitude equation with real coefficients of the usual form (see Riecke, 1990)

$$\tau_0 \partial_t B = \varepsilon B + \xi_0^2 \partial_x^2 B - g_0 |B|^2 B, \quad (9.80)$$

with $\tau_0 = \gamma_0^{-1}$, $\xi_0 = s_0/\sqrt{2}\gamma_0$, and $g_0 = (\gamma_3 + \gamma_4)/\gamma_0$, $\varepsilon = (\delta_0 - \gamma_0)/\gamma_0$. The phase of B arises from the spatial translation of the standing-wave pattern. The other combination ($D = A_1 + iA_2^*$ to lowest order) decays to zero for small ε since it is out of phase with the drive, i.e. uniform parametric pumping excites a single standing wave at threshold. For larger ε , Eqs. (9.78) can be shown to have a secondary bifurcation which, depending on the coefficients, is either a drift instability [see Sec. IV.A.3] or a type I_o oscillatory bifurcation (Douady *et al.*, 1989b).

For an infinite two-dimensional system Ezerskii *et al.* (1986) derived an amplitude equation *assuming* a square pattern, treating the detuning as an adjustable parameter

$$\begin{aligned} \partial_t A_j = & -\gamma_0 A_j - i\delta_0 A_{-j}^* - (3\omega/2q_0)(\hat{\mathbf{q}}_j \cdot \nabla) A_j + (3i\omega/4q_0^2)\nabla^2 A_j - (3i\omega/8q_0^2)(\hat{\mathbf{q}}_j \cdot \nabla)^2 A_j \\ & - \sum_{\ell} \{ [\gamma_{j,\ell}^{(3)} - ic_{j,\ell}^{(3)}] |A_{\ell}|^2 A_j + [\gamma_{j,\ell}^{(4)} - ic_{j,\ell}^{(4)}] A_{\ell} A_{-\ell} A_j^* \}, \end{aligned} \quad (9.84)$$

where the linear damping is

$$\gamma_0 = 2\nu q_0^2, \quad (9.85)$$

and the nonlinear damping and dispersion $\gamma_{j,\ell}^{(n)}$, $c_{j,\ell}^{(n)}$ are polynomials in the angle

$$\cos\theta_{j,\ell} = \hat{\mathbf{q}}_j \cdot \hat{\mathbf{q}}_{\ell}, \quad (9.86)$$

given in Eqs. (46), (47), (21), (57), and (58) of Milner's paper. The damping coefficients γ_0 , $\gamma_{j,\ell}^{(n)}$ were obtained under the assumption, valid at high frequencies and for a clean surface, that the dissipation occurs in the bulk of the fluid and is given by

$$\partial_t E = -2\nu\rho \int d^3x (\nabla^2 \phi)^2, \quad (9.87)$$

where E is the energy and ϕ is the potential of the *ideal* (undamped) flow in the bulk.

The complex amplitude equation (9.84) constitutes Milner's basic result. It holds for an arbitrary set of amplitudes A_j , all of whose vectors \mathbf{q}_j have magnitude q_0 given by the resonance condition (9.82). Equation (9.84) represents an expansion of the hydrodynamics near resonance and for weak damping to order A^3 . In order to determine the preferred pattern it is again useful to make the further expansion of this equation, valid in the immediate vicinity of the threshold as in the one-dimensional case (9.80) treated above. Equations (9.79) are generalized by the replacements

$$A_1 \rightarrow A_j, \quad A_2 \rightarrow A_{-j}, \quad \partial_x B \rightarrow (\hat{\mathbf{q}}_j \cdot \nabla) B_j, \quad (9.88)$$

and the group speed s_0 becomes $(3\omega/2q_0)$. This yields the real amplitude equation (Milner, 1991)

$$\begin{aligned} \gamma_0^{-1} \partial_t B_j = & \varepsilon B_j + \frac{1}{2} \left[\frac{3\omega}{2\gamma_0 q_0} \right]^2 (\hat{\mathbf{q}}_j \cdot \nabla)^2 B_j \\ & - \sum_{\ell} \gamma_0^{-1} \Gamma_{j,\ell} |B_{\ell}|^2 B_j, \end{aligned} \quad (9.89)$$

and neglecting nonlinear damping. Quite recently, Milner (1991) attacked the problem from first principles and in a careful analysis obtained a consistent set of amplitude equations near threshold. Starting from the generalization of Eqs. (9.58) and (9.71),

$$h(\mathbf{x}, t) = \sum_{\mathbf{q}_j} A_j(\mathbf{x}, t) \exp i(\mathbf{q}_j \cdot \mathbf{x} - \omega t) + \text{c.c.}, \quad (9.81)$$

with

$$|\mathbf{q}_j|^2 = q_0^2, \quad (9.82)$$

and using the high-frequency limit of (9.60)

$$\omega_s^2(q_0) = (\Sigma/\rho) q_0^3 = \omega^2, \quad (9.83)$$

Milner derived the following amplitude equations:

with

$$\varepsilon = (\delta_0 - \gamma_0)/\gamma_0 \quad (9.90)$$

and

$$\Gamma_{j,\ell} = \gamma_{j,\ell}^{(3)} + \gamma_{j,-\ell}^{(3)} + \gamma_{j,\ell}^{(4)} + \gamma_{j,-\ell}^{(4)}. \quad (9.91)$$

[Presumably there should also be terms in the spatial derivatives transverse to $\hat{\mathbf{q}}_j$ analogous to the ∂_y^2 terms in Eq. (8.15), but Milner did not include these.] From Eq. (9.89) we can identify the coefficient ξ_0 of Eq. (4.3) as $\xi_0 q_0 \sim \omega/\gamma_0 \gg 1$. This system is therefore different from the other type I cases we have encountered, in that the coherence length ξ_0 is necessarily large in the frequency domain where the theoretical analysis applies (small damping). This means that a system may have a large aspect ratio as determined from the parameter $Lq_0 \gg 1$, but nevertheless be small in terms of the quantity $L/\xi_0 \ll 1$.

As usual the amplitude equation derives from a Lyapunov function

$$\begin{aligned} \mathcal{F} = & \int d\mathbf{x} \sum_j \left[-\varepsilon |B_j|^2 + \frac{1}{2} \left| \frac{3\omega}{2\gamma_0 q_0} (\hat{\mathbf{q}}_j \cdot \nabla) B_j \right|^2 \right. \\ & \left. + \sum_{\ell} \frac{1}{2\gamma_0} \Gamma_{j,\ell} |B_j|^2 |B_{\ell}|^2 \right], \end{aligned} \quad (9.92)$$

which may be used to find the preferred pattern near threshold. Indeed, let us assume a solution consisting of an n -sided polygon, so that (9.92) becomes (for a constant $B = B_n$)

$$\mathcal{F} \sim -n\varepsilon B_n^2 + \frac{1}{2} n \gamma_0^{-1} \Gamma_n B_n^4, \quad (9.93)$$

with $\Gamma_n = \sum_{\ell} \Gamma_{j,\ell}$. By evaluating the coefficient Γ_n for various n , Milner shows that squares ($n=2$) are the pre-

ferred pattern, and also that they represent a local minimum of the potential (9.92) with respect to distortions away from $\theta_{j,\ell} = \pi/2$.

It is also possible to test the square pattern for secondary instabilities. Solutions of Eq. (9.89) at nonzero wave vector

$$B_j = B_k e^{ik \cdot x_j}, \quad (9.94)$$

lead to a detuning

$$\beta = \omega_s(q_0) - \omega_s(\mathbf{q}_j + \mathbf{k}) \approx (3\omega/2q_0)[|\mathbf{q}_j + \mathbf{k}| - q_0], \quad (9.95)$$

which parametrizes the band of solutions above threshold. Inserting these into the amplitude equation (9.89) Milner finds the usual longitudinal (Eckhaus) boundary, as well as a transverse instability at $\beta > 0$, just as for the Newell-Whitehead case treated in Sec. IV.A. He notes, however, that squares are also a solution of the traveling-wave equations (9.84), and tests their stability with respect to more general disturbances where A_j and A_{-j}^* are no longer phase locked as in (9.88). The result is a new *transverse amplitude modulation* instability at a nonzero wave vector $\mathbf{p}_m \perp (\mathbf{q}_j + \mathbf{k}_j)$, with

$$p_m^2 = (4q_0^2/3\omega) C' B^2 + \beta, \quad (9.96)$$

where C' is a function of the $c_{j,\ell}^{(n)}$ calculated by Milner, and β is the detuning appropriate to the wave vector $\mathbf{q}_j + \mathbf{k}_j$. The locus of this instability in the (ϵ, β) was also found by Milner, and is shown in Fig. 70.

In principle the amplitude equations (9.84) and (9.89) can be investigated using more general patterns than the regular superpositions of waves that lead to (9.93), but this has not been done. In any case, it is reasonable to assume (just as in convection) that near threshold the preferred pattern in an ideal system is regular, and in that case squares are found.

Milner has attempted to find an “optimal” wave vector by restricting his attention to standing wave patterns with a definite wave vector $\mathbf{q} = \mathbf{q}_j + \mathbf{k}$, $q^2 \neq q_0^2$, and thereby finding higher-order terms in the Lyapunov function (9.92). Minimization of this function then yields an optimal detuning $\beta^*(\epsilon)$ and thus an “optimal” wave vector $k^*(\epsilon)$ which turns out to be destabilized by the transverse amplitude modulation instability at a particular value of ϵ . In our opinion, however, this procedure is unreliable since the actual competition between solutions with different wave vectors involves inhomogeneous (defect) states which are explicitly excluded from the approximate higher-order Lyapunov function. Thus the notion of a preferred wave vector is no better justified away from threshold in this problem than in pure Rayleigh-Bénard convection.

2. Experimental studies

As mentioned above, the most extensive experiments on parametric waves have been carried out on small sys-

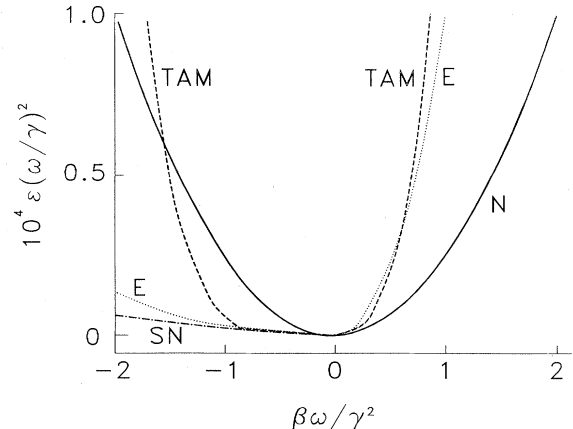


FIG. 70. Stability boundaries for square patterns of standing surface waves as a function of the control parameter ϵ and the detuning parameter β which is a representation of the wave vector q [see Eq. (9.95)]. Solid line (N), neutral stability boundary; dotted line (E), Eckhaus boundary; dashed line (TAM), transverse amplitude modulation; dash-dotted line (SN), saddle-node point for subcritical bifurcation. (From Milner, 1991.)

tems (low frequencies) where a few modes are excited. It is then interesting to study in detail the pattern stability and pattern competition as a function of the modulation parameters, and to make comparisons with theoretical models. In line with our primary interest in nontrivial spatial dependence, however, we shall confine our discussion to experiments on large systems, i.e. those carried out at high frequencies leading to $q_0 L \gg 1$. As mentioned above, however, none of the experiments carried out thus far achieve the true large system limit $L/\xi_0 \gg 1$. To do this one must abandon the weak damping limit and use highly viscous fluids, a situation about which very little is known theoretically (W. S. Edwards, private communication).

a. One-dimensional systems

The only studies of one-dimensional parametric waves we are aware of are the early experiments by Keolian *et al.* (1981) and the more recent work by Douady (1990) in annular containers. The latter experiments observed the standing-wave state at a particular wave vector q_n as well as its limits of stability in the (δ_0, ω) plane. These limits involve Eckhaus-like instabilities ($q_n \rightarrow q_{n+1}$) when ω is varied at fixed δ_0 , and the drift and secondary oscillatory instabilities mentioned above, when δ_0 is raised at fixed ω . These are qualitatively in accord with expectations based on the amplitude equations (9.78), but no detailed comparisons have yet been made. The author states that it is difficult to obtain reproducible results, since the requirements of uniformity and stability of external conditions are particularly severe.

b. Two-dimensional patterns

Douady and Fauve (1988) have performed a series of experiments in square cells with wave vectors in the

range $12 < q_0 L / \pi < 18$. They state that in order to see patterns with different spatial symmetries it was necessary to pin the meniscus at the edge of the cell by filling it to the top [see Eq. (9.70)]. In this way they avoided the strong perturbations of the pattern coming from the waves at frequency 2ω generated at the lateral boundaries by the motion of the meniscus. With the filled cell they found a large multiplicity of regular patterns above threshold, which they analyzed according to the modes

$$h_{mn}(x,y) = \sin(m\pi x/L) \sin(n\pi y/L), \quad (9.97a)$$

with

$$q_0^2 = (m^2 + n^2)(\pi^2/L^2). \quad (9.97b)$$

By symmetry in a square cell there must also exist the mode $h_{nm}(x,y)$, but it need not coexist with h_{mn} . A symmetric pattern with wave vector q_0 is formed by superposition

$$h_s = h_{mn} + h_{nm}, \quad (9.98)$$

whereas a symmetry-breaking pattern is h_{mn} (or h_{nm}) alone. The square pattern has $n=m$, and the symmetric pattern h_s for $m \neq n$ consists of two square patterns tilted at some angle. Douady and Fauve observed essentially all the (m,n) combinations allowed by the resonance condition (9.97b), but found that there was a clean separation between the sets that led to symmetric patterns [which had $0 < \tan^{-1}(m/n) < \pi/8$] and the ones that broke the square symmetry [$\pi/8 < \tan^{-1}(m/n) < \pi/4$].

An interesting hexagonal pattern was also observed at rather large excitation δ_0 and for a high-viscosity fluid where $q_0 \ell_D \gg 1$. The authors noted that this pattern could be interpreted as arising from an accidental degeneracy between asymmetric modes (m_1, n_1) and (m_2, n_2) , such that $m_1^2 + n_1^2 \approx m_2^2 + n_2^2$, with $m_2 \ll n_2$, say. Then if we take $m_1 > n_1$ it can happen that the angle between the vector $\mathbf{q}_1^{(+)} \propto m_1 \hat{\mathbf{x}} + n_1 \hat{\mathbf{y}}$ and $\mathbf{q}_2^{(+)} \propto m_2 \hat{\mathbf{x}} + n_2 \hat{\mathbf{y}}$ is close to $\pi/3$. Since in the particular ansatz (9.97) we also have the vectors $\mathbf{q}_1^{(-)} \propto m_1 \hat{\mathbf{x}} - n_1 \hat{\mathbf{y}}$ and $\mathbf{q}_2^{(-)} \propto m_2 \hat{\mathbf{x}} - n_2 \hat{\mathbf{y}}$, we finally end up with an equilateral triangle formed from $\mathbf{q}_1^{(+)}$, $\mathbf{q}_2^{(+)}$, and $\mathbf{q}_1^{(-)}$, say, which leads to a nearly hexagonal pattern. It would be interesting to understand the sidewall effects that lead to these pattern selection properties, since we note that according to Milner (1991) none of the states with $m \neq n$ (either symmetric or asymmetric) should be stable in the laterally infinite system. However, Milner did not explicitly consider canted pairs of square patterns, so it is conceivable that these would be stable in his theory, thus explaining the experimental observations. A more likely possibility is that the theory only applies to a truly infinite system with $L/\xi_0 \gg 1$, which was not the case in the experiment.

The experiments of Ezerskii *et al.* (1986) and especially those of Tufillaro *et al.* (1989) seem to approximate the large-system limit reasonably well, with an aspect ratio $Lq_0/2\pi \sim 40$ in the latter case (see Gollub and Ramshankar, 1991). The initial pattern did not appear uniformly

in the whole cell, so it was probably forced by spatial inhomogeneities more than by sidewalls, and when it did fill the cell it was not aligned by the sidewalls but rather inclined at an angle which depended on the control parameter as well as weakly on time. Nevertheless, to a good approximation both sets of experiments saw a stationary square pattern near threshold, and a modulation instability at higher forcing, in agreement with the theoretical result of Milner (1991). A quantitative comparison between the work of Tufillaro *et al.* and Milner's prediction of the destabilization of the preferred pattern by the modulation instability gave rather good agreement for p_m , β_m , and h_{\max} without adjustable parameters, and rather worse agreement for ε_m . Milner notes that ε_m depends on the square of the nonlinear damping $\gamma^{(n)}$, and a contribution to $\gamma^{(n)}$ from surface contamination [neglected in Eq. (9.84)], could well account for the discrepancy. In view of the doubts we expressed above on the reliability of the prediction of $\beta^*(\varepsilon)$ we do not take the absolute prediction of β_m seriously, but the relation between p_m , β_m , and ε_m is a nontrivial test. Here again, however, we must reiterate our reservations regarding the value of L/ξ_0 .

c. Large systems: Spatiotemporal chaos

When ε is increased beyond the transverse amplitude modulation instability eventually the system loses spatial coherence and makes a transition to a chaotic state. This was already observed in the experiment of Ezerskii *et al.* (1986), and was investigated quantitatively by Tufillaro *et al.* (1989) and by Gollub and Ramshankar (1991). As shown in Fig. 71, the autocorrelation function obtained from the shadowgraph image has an exponential correlation length which decreases dramatically above a value $\varepsilon \approx 0.1$ (slightly higher than ε_m). The authors also measured correlation spectra in the chaotic state, both spatial and temporal, but so far no theoretical understanding of the data has emerged.

It has recently been suggested by Ciliberto *et al.* (1991) to use as a diagnostic of chaos in large systems the average acceleration of the surface

$$\langle \partial_t^2 h(\mathbf{x}, t) \rangle = \bar{A}(t) \cos 2\omega t, \quad (9.99)$$

where the brackets denote a spatial average over the whole surface. Then the authors claim that at constant input power, the time dependence of $\bar{A}(t)$ is correlated with fluctuations in the position of the surface. This is analogous to the fluctuations of Rayleigh number at constant heat current in convection, and the suggestion is that in both cases one can extract information concerning spatiotemporal chaos from such a diagnostic.

d. Defects

The first observation of a defect in parametric surface waves was by Wu *et al.* (1984) who found a nonpropagat-

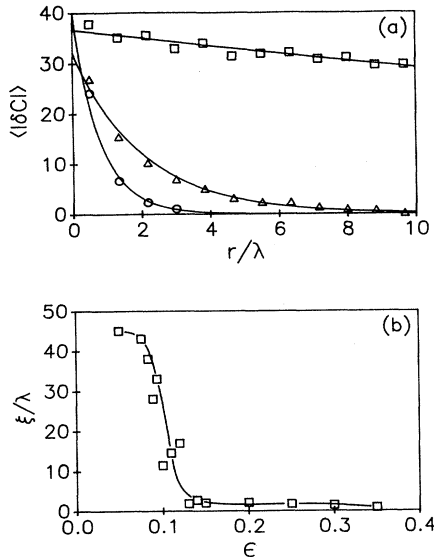


FIG. 71. Spatial correlations in parametrically forced surface wave patterns. (a) Correlation function of square pattern, measured from the optical contrast, for three values of the reduced control parameter ϵ , as a function of distance measured in units of the wavelength λ ($\epsilon=0.07$, squares; $\epsilon=0.15$, triangles; $\epsilon=0.35$, circles). (b) Correlation length ξ derived from data similar to part (a) as a function of control parameter ϵ . (From Tufillaro *et al.*, 1989.)

ing pulse in a narrow one-dimensional channel (they refer to it as a soliton). A theory for this defect was developed by Larraza and Puterman (1984) and by Miles (1984b), based on a perturbed nonlinear Schrödinger equation. More recent treatments, which closely resemble our discussion in Sec. V.B were given by Elphick and Meron (1989), and by Fauve and Thual (1990).

In the one-dimensional situation near threshold the amplitude equation (9.89) admits kink solutions joining the symmetry-related states $\pm B$. Such structures have been observed by Douady (1989) using a stroboscopic method to distinguish between the phases $+B$ and $-B$. However, these solutions are unstable within Eq. (9.89) since the π phase change in the kink can unwind through complex values of B , so the observations remain unexplained. Further from threshold, when the complex amplitude equations (9.78) hold, one expects a large variety of pulse, front and domain boundary defects, but no detailed experimental study has yet been made.

In two dimensions various authors have made visual observations of dislocation and grain boundary defects, but once again a quantitative study is lacking.

E. Open-flow systems

1. General remarks

An important class of problems in fluid dynamics arise when a carefully prepared uniform flow passes through

an observation region containing bodies of various shapes. This of course is the geometry of wind tunnels and many other technologically important systems. Although the main focus of work in this area is usually the development of strongly turbulent flows at high Reynolds numbers, we can also ask whether phenomena exist at lower Reynolds numbers (smaller flow rates), which are analogous to the ones we have been considering. It turns out that these analogies have been the subject of careful experimental investigation in recent years.

Several classic geometries have been studied. We can distinguish geometries that are spatially uniform in the streamwise direction, such as Poiseuille flow in a circular pipe or plane Poiseuille flow between parallel sheets (in both cases the flow is induced by a constant pressure across the system), and geometries in which the base flow develops spatially in the streamwise direction, such as flow past a circular cylinder, the boundary layer that develops for flow incident on the edge of a plate (the Blasius velocity profile), or jets.

The characteristic instability of these situations is the formation of vorticity rolls transverse to the flow direction. The simplest example, which can be motivated by an inviscid theory, is the Kelvin-Helmholtz instability of the infinitesimally thin region of fluid shear between two regions of flow in opposite directions (Fig. 72). The increased flow velocity over a protuberance into the flow induced by a sinusoidal perturbation of the interface leads to a reduced pressure in the region by the Bernoulli effect, which enhances the growth of the perturbation and causes the interface to roll up into vortices. Viscosity acts as a stabilizing effect. Instabilities in systems such as wakes and jets, where the velocity shear has an inflection point, may be understood in terms of the Kelvin-Helmholtz effect. Instabilities in situations where there is no inflection point of the shear, on the other hand, such as Poiseuille and pipe flow, involve the viscosity in an essential way and are more difficult to understand physically (see Tritton, 1988).

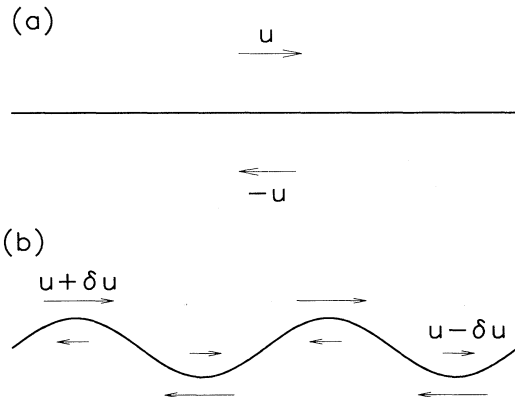


FIG. 72. Schematic of the Kelvin-Helmholtz instability showing (a) unperturbed shear boundary, (b) perturbed shear boundary, with arrow length denoting modulation of the velocity u .

Except in the symmetric situation of Fig. 72 there is typically a net flow which will advect the spatially periodic state of vortices (in a streamwise uniform situation). Thus the instabilities are typically of type I_o, and in this case the difference between convective and absolute instabilities becomes crucial (see Sec. VI.C).

In principle, the type of theoretical analysis we have advocated can be applied to these systems. This involves a linear stability analysis to identify the spatial structure that might develop and the band of possible wave numbers, a nonlinear analysis to produce a saturated state with this spatial structure, and a stability analysis of the nonlinear state to identify the secondary instabilities that might lead to a turbulent flow, via long-wavelength instabilities given by a phase dynamics approach. In practice this procedure typically turns out to be extremely difficult or even impossible to carry out (for a recent review see Drazin and Reid, 1981). Often the instability of the uniform flow is predicted to occur at rather high Reynolds numbers (infinite in the case of pipe flow) and is strongly subcritical, so that the nonlinear states cannot be captured by a weakly nonlinear theory (in some cases they may not have a simple spatial or temporal structure). The secondary instabilities of the nonlinear periodic states that may exist far below the point of the initial linear instability must then be attacked purely numerically. For a recent review of this type of work see Bayly *et al.* (1988). The added complication of a spatially developing base state in the flow over bodies makes these systems even more difficult to understand quantitatively, and often a quasiuniform approximation is made.

Correspondingly, although quite regular patterns of drifting vortices are an obvious feature of experiments on open flows, and indeed yield some of the classic pictures of pattern formation in nonequilibrium systems (Van Dyke, 1982), there exist few experiments where a quantitative comparison with a controlled theory of the nonlinear pattern can be achieved. To conclude this section we will briefly describe experiments on two systems where comparison with small amplitude theories does seem possible.

2. Plane Poiseuille flow

The transition in uniform plane Poiseuille flow is strongly subcritical. The linear instability has been investigated experimentally by Nishioka *et al.* (1975) and results agree well, at the rather low precision of the measurements, with the linear theory. Although saturated nonlinear states of two-dimensional traveling rolls may be constructed theoretically (see Bayly *et al.*, 1988) these are unstable to three-dimensional disturbances (Orszag and Patera, 1980) and no periodic nonlinear state is expected or seen experimentally.

On the other hand Schatz *et al.* (1991) have shown that if a periodic array of cylinders is placed in the flow a *supercritical* (convective) instability occurs, which is well described by an amplitude equation and is also quantita-

tively reproduced by numerical simulations (Fig. 73). In particular for the parameters of Fig. 73 the authors measure a critical Reynolds number $R_e = R_c \approx 128.5$ at which an imposed disturbance begins to grow as it propagates downstream. The behavior of the maximum in the pulse is found to be well described by the amplitude equation

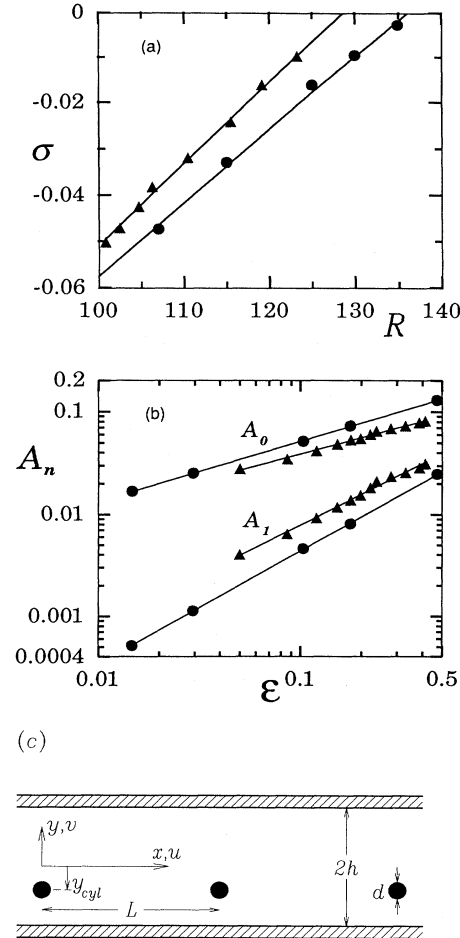


FIG. 73. Channel flow with spatially periodic perturbations. (a) Growth rate σ as a function of Reynolds number, denoted R in the figure, below the transition and (b) saturation amplitudes of the first two Fourier components A_0 and A_1 as a function of reduced Reynolds number ϵ above the transition in periodically perturbed plane Poiseuille flow. Triangles are from experimental measurements of the velocity component u at $x = 3.9$ downstream from cylinder number 18 and $y = 0$. Solid circles are from the velocity component v at $x = 1.6666$ and $y = -0.5$ in numerical simulations. The growth rate measurements σ are consistent with the expected linear dependence on Reynolds number $\sigma \propto (R - R_c)$, yielding estimates for $R_c = 128.5$ (experiment) and $R_c = 136$ (simulation). The dependences of the amplitudes are consistent with $A_0 \propto \epsilon^{1/2}$, $A_1 \propto \epsilon$. (c) Geometry of the experiment: 21 cylinders of separation $L = 6.66$ (defined in units of the channel half depth h) and diameter 0.40, are placed offset from the center by $y = -0.50$. The spanwise dimension z perpendicular to the figure is 40 in the experiment, and is taken to be infinite in the simulations. (From Schatz *et al.*, 1991.)

$$\tau_0 \partial_t A_0 = \varepsilon A_0 - g_0 A_0^3, \quad (9.100)$$

with $\varepsilon = (R_e - R_c)/R_c$, i.e. the amplitude A_0 scales as $A_0 \sim \varepsilon^{1/2}$ and the amplitude of the next harmonic $A_1 \sim \varepsilon$ as expected. Here R_c is the critical Reynolds number for the *convective* instability, since A_0 is measured moving with the pulse, not at a fixed point. (At a fixed point the disturbance eventually decays in time after having passed by.) The spatial derivative terms and complex (frequency shift) coefficients of the full type I_o amplitude equation were not investigated in the above work.

3. von Karman vortices

The periodic appearance of vortex rolls ("vortex street") behind a circular cylinder in a uniform flow is a familiar example of pattern formation. If we consider the instability as occurring in the spatially developing wake behind the cylinder, then the ideas discussed in Sec. VI.C are qualitatively informative: the instability occurs as a global Hopf bifurcation when the region of absolute instability in the vicinity of the cylinder becomes large enough to support a local mode which acts as a source for vortices advected downstream. There are no quantitative calculations of the linear instability based on this idea, however full numerical simulations yield an onset Reynolds number of $R_c \approx 46$ for an infinitely long cylinder, with a dimensionless frequency (known as the Strouhal number) $\omega d / 2\pi v = 0.14$, with d the cylinder diameter and v the fluid velocity (Jackson, 1987, and references therein).

Recent experiments have investigated this transition in detail, showing that it is indeed a supercritical Hopf bifurcation and confirming the applicability of the complex amplitude equations for the oscillating mode.

$$\tau_0 \partial_t A = \varepsilon A - g_0(1 - ic_3)|A|^2 A, \quad (9.101)$$

(Provansal *et al.*, 1987; see also Strykowski and Sreenivasan, 1990). Provansal *et al.* measure both the growth rate of a disturbance above threshold and the decay of imposed disturbances below threshold, and confirm the $|\varepsilon|^{-1}$ dependence of the time scale. This allows an accurate determination of the critical Reynolds number $R_c \approx 47$, agreeing well with the most recent theory. Moreover, the amplitude of the mode above threshold scales as $\varepsilon^{1/2}$. The data show little effect of the nonlinearity on the frequency of the oscillations, so that c_3 must be small. In addition the authors studied forced oscillations for various frequencies close to the critical frequency, both above and below threshold.

4. Type I_s fluid systems with an imposed flow

Rayleigh-Bénard convection in a narrow channel in an imposed flow, or the Taylor-Couette system with imposed axial flow, provide easily controlled experiments to investigate open flow phenomena. Luijkx *et al.* (1981)

studied convection experimentally, while Müller *et al.* (1989, 1992) and Brand *et al.* (1991) investigated this system theoretically, using numerical methods as well as amplitude equations. Tsameret and Steinberg (1991a,b) and Babcock *et al.* (1991, 1992) investigated the Taylor-Couette system.

In an imposed flow the type I_s linear instability is converted to type I_o, with the rolls drifting in the direction of the flow at a velocity proportional to the flow velocity for low speeds (i.e. small Reynolds numbers, denoted R_e). In both the Rayleigh-Bénard and Taylor-Couette systems the threshold is suppressed by the imposed flow, proportional to R_e^2 for small R_e . More importantly the first instability is *convective* (Deissler, 1985), and is described by the amplitude equation

$$\begin{aligned} \tau_0(\partial_t A + s_0 \partial_x A) &= \varepsilon A + \xi_0^2(1 + ic_1)\partial_x^2 A \\ &- g_0(1 - ic_3)|A|^2 A, \end{aligned} \quad (9.102)$$

for type I_o systems. Note here however that there is only one wave, moving in the direction of the flow, so that the reflection phenomena described in Sec. IX.A will not occur. The parameters τ_0 , s_0 , ξ_0^2 , and c_1 have been calculated from a linear stability analysis, and numerical simulations and experiments confirm the basic validity of Eq. (9.102).

In the convectively unstable region $0 < \varepsilon < \varepsilon_a = (s_0 \tau_0 / 2\xi_0)^2(1 + c_1^2)^{-1}$ there is no disturbance in the fluid if the noise in the inflow is small enough, but experimentally a disturbance is usually evident far down the flow, where any small perturbation in the inflow has had sufficient time to grow as it propagates down the cell. This disturbance, even though it may be of large saturated amplitude, shows phase noise, reflecting its origin in the noisy inflow (Deissler, 1985, 1987b, 1989). As ε passes through the point of absolute instability ε_a there is a sharp transition from this noise-sustained structure to a nonlinear solution which shows only very small fluctuations. This solution is analogous to the "filling" states in the binary-fluid case, although the distance from the inflow to where the amplitude becomes large grows as ε_a is approached from above. It is predicted (Cross and Kuo, 1992) to diverge as $(s_{0c} - s_0)^{-1/2}$ in the absence of noise, and this behavior is consistent with experiments at small flow rates.

The sharp disappearance of the noise provides a precise measure of the threshold ε_a (Babcock *et al.*, 1991, 1992; Tsameret and Steinberg, 1991b). To understand the experiment we note that the quantity ε in Eq. (9.102) is given by

$$\varepsilon = [R - R_c(R_e)]/R_c(R_e), \quad (9.103)$$

where R is the Rayleigh number as usual, and $R_c(R_e)$ is the shifted convective instability threshold in the presence of the flow ($R_e \neq 0$). We may also define reduced Rayleigh numbers referred to the threshold in the absence of flow

$$\tilde{\epsilon} = [R - R_c(0)]/R_c(0), \quad (9.104a)$$

$$\tilde{\epsilon}_c = [R_c(R_e) - R_c(0)]/R_c(0), \quad (9.104b)$$

$$\tilde{\epsilon}_a = [R_{\text{abs}}(R_e) - R_c(0)]/R_c(0), \quad (9.104c)$$

so that

$$\epsilon_a = \frac{\tilde{\epsilon}_a - \tilde{\epsilon}_c}{1 + \tilde{\epsilon}_c} = \left[\frac{s_0 \tau_0}{2 \xi_0} \right]^2 (1 + c_1^2)^{-1}. \quad (9.105)$$

The values of $\tilde{\epsilon}_c$ and $\tilde{\epsilon}_a$ measured by Babcock *et al.* are shown in Fig. 74. Since both may be calculated by an analysis of the equations for the linear instability ($\tilde{\epsilon}_a$) is obtained from the stationary phase point using the dispersion relation $\sigma(q)$ in the complex q plane, as in Sec. VI.B) there are reliable theoretical predictions for these quantities. The agreement found by the authors between experiment and theory with no adjustable parameters is remarkable. Similar results were found by Tsameret and Steinberg (1991b). [Earlier measurements by these authors (Tsameret and Steinberg, 1991a) showed less good agreement for $R_e > 1.2$, due to the influence of noise on the onset position in this regime.] Babcock *et al.* also find that Eq. (9.105), which follows from the amplitude equation (9.102), is quite accurately verified. This excellent agreement argues in favor of using models based on the amplitude equation to investigate in detail the stochastic properties of the inflow.

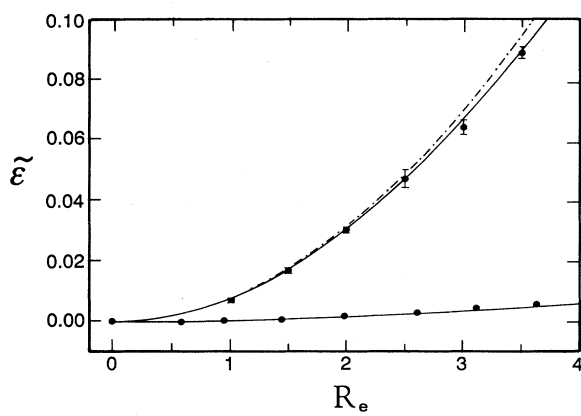


FIG. 74. Stability diagram for axisymmetric rolls in a Taylor-Couette cylinder with axial flow; $\tilde{\epsilon}$ is the reduced azimuthal Reynolds number defined in Eq. (9.104a) and R_e the Reynolds number of the axial flow ($R_e = \langle w \rangle d / \nu$ with $\langle w \rangle$ the mean axial velocity, d the gap and ν the kinematic viscosity). The lower points (experiment) and solid curve (theory) are for the onset of convective instability $\tilde{\epsilon}_c$; the upper points are the absolute instability $\tilde{\epsilon}_a$ identified experimentally by the disappearance of phase noise as $\tilde{\epsilon}$ is raised. The corresponding theoretical predictions for the point of absolute instability are shown by the solid line (hydrodynamic equations) and the dot-dashed line (amplitude equation). (Adapted from Babcock *et al.*, 1991.)

X. PATTERNS IN CHEMICAL REACTIONS

Systems undergoing chemical reactions show many different pattern forming phenomena which combine hydrodynamics with the molecular reactions taking place in chemistry. Many of the traditional spatial patterns occurring in hydrodynamics and in thermodynamic phase transformations are strongly influenced by chemical processes (Mikhailov and Uporov, 1984). As examples we may cite Liesegang patterns (see Dee, 1986), diffusive instabilities in photochemical reactions (Dewel *et al.*, 1983), and various types of catalytic reactions (Bareiko, 1984). The above-named examples involve known pattern forming mechanisms in which chemistry plays a part, but whose basic features can be studied in systems with no chemistry, which are simpler to characterize and to model. We have chosen to concentrate rather on oscillatory chemical reactions since they show distinctive pattern-forming properties and are susceptible to detailed theoretical and experimental study. The theory of wave propagation in chemical media has been reviewed recently in a number of articles and books (see Vasiliev *et al.*, 1987; Tyson and Keener, 1988; Murray, 1989; Winfree, 1991; Kawczynski *et al.*, 1992; Meron, 1992) to which we refer the reader for further details. Our aim here is to present an elementary review of the basic ideas, to relate the work to our general discussion, and to examine the state of comparison of theory and experiment.

A. The Belousov-Zhabotinsky reaction and the Oregonator model

1. Basic experimental facts

Although experimental observations of sustained oscillations in chemically reacting systems date back to the early part of the century, the real growth of interest in the subject occurred in the past 25 years. This growth was sparked by the classic experiments of A. M. Zhabotinsky and co-workers on a metal-ion catalyzed oxidation of organic compounds by bromate ions, an oscillatory reaction which had been discovered by B. P. Belousov in 1951 and now bears the name Belousov-Zhabotinsky (BZ) reaction. (For a history see Field and Burger, 1985, and Winfree, 1984b.) The early work of Zaikin and Zhabotinsky (1970) already revealed the existence of chemical waves in an unstirred reactor, and it is primarily this spatio-temporal aspect of the phenomena that will concern us. The literature on chemical oscillations, and on the BZ reaction in particular, is considerable and it continues to grow [the 1985 book by Field and Burger already has roughly 1000 references!] We shall briefly describe the principal experimental facts and then present a simplified model, the “Oregonator,” which has the reaction-diffusion form (3.32). This model accounts quantitatively for the chemical kinetics in the stirred sys-

tem (no diffusion), and semiquantitatively thus far for the observed wave phenomena in the unstirred case. We shall not inquire into the chemical justification for the model but rather refer the reader to the monograph of Field and Burger (1985). The principal experimental facts about the BZ reaction are as follows:

(i) The *stirred* system under certain conditions shows spontaneous *oscillations* with periods on the order of minutes. These oscillations can be made dramatically visible if ferroin is used as the catalyst, since there is an alternation between the reduced state Fe^{2+} which appears *orange* and the oxidized state Fe^{3+} which appears *blue*.

Under different experimental conditions of average concentrations, temperature etc., the system is *stable* in either the oxidized or the reduced state. Alternatively the system can be *bistable*, so that for fixed average parameter values it can go to either state depending on initial conditions. In both the stable and bistable cases, however, the system is *excitable*, which means that certain initial conditions decay rapidly to the stable state, while others lead to large deviations before the system eventually reaches a stable state.

(ii) If the *unstirred* system is in a steady state it is possible to initiate a local disturbance which propagates out at a constant velocity and with constant shape, in the form of a circular pulse. If the steady state is red, say, the pulse appears as a blue disturbance which decays back to red behind the pulse. Structures such as these, which propagate with constant shape and speed in dissipative media, are referred to in the Soviet literature as "au-towaves" (Krinsky, 1984; Vasiliev *et al.*, 1979, 1987).

(iii) Even more dramatically, there exist *target patterns* in which the above-mentioned pulses are emitted *periodically* from the same "leading center" (also called a "pacemaker"). The different targets are observed to have variable frequencies but produce pulses with rather uniform velocities. If the medium outside the target is oscillatory, the frequency of the targets is higher than the frequency of the medium, so that waves are annihilated at the outer rim of the target. This rim itself is expanding at a speed slower than the velocity of the waves.

When two targets meet they do not penetrate each other. Rather, they annihilate and form angular structures (see Fig. 75). Moreover, the target with the higher frequency consumes the lower-frequency one. There is experimental evidence that most targets are nucleated on extraneous perturbations such as dust particles. Nevertheless it appears that under certain conditions target patterns may exist in a homogeneous medium (see below).

(iv) If a single expanding pulse is broken at a point it begins to curl up around the ends and produces oppositely rotating *spiral patterns*. Besides their geometry, these waves differ from target patterns in that the frequency of rotation, and thus the pitch of the spiral, does not vary from spiral to spiral (Fig. 76). There is thus no tendency for the domain of one spiral to grow at the expense of the other. Spiral patterns are sometimes referred to as "ro-

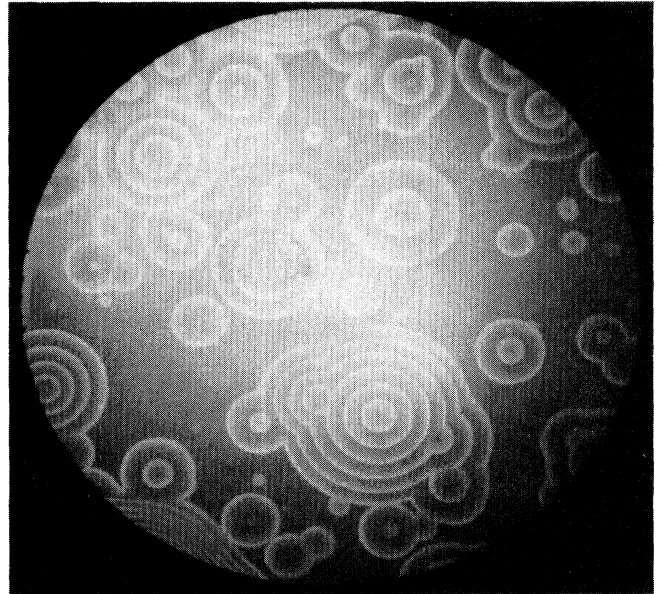


FIG. 75. Target pattern observed in a thin layer of an oscillating Belousov-Zhabotinsky reaction. (From Vidal *et al.*, 1986.)

tors," or "reverberators." They have the form of rotating plane waves over most of their area, except near the core, $r < r_c$, where the chemical compositions and temporal behavior have a different character. (The word "rotor" is sometimes used to denote just the core of the spiral.)

It is possible to perturb the core by replacing it by a hole of perimeter ℓ in the medium. Then the spiral will rotate at a rate $\omega \approx 2\pi v / \ell$, where v is the wave velocity far from the hole. In this way spirals of arbitrary frequency can be created and their interactions studied (Krinsky and Agladze, 1983). It is also possible to create multiarmed spirals by initiating a number of them around a hole in the medium and gradually letting the diameter of the hole shrink to zero (Krinsky and Agladze, 1982). These authors found that multiarmed spirals have lower frequency than single-armed ones, and they are entrained by the latter, but the stability of the multi-armed structures was not demonstrated.

(v) The spatial structures described above have mostly been seen in very shallow Petri dishes, so they can be thought of as two dimensional. There is some experimental evidence, primarily from Winfree and co-workers (Winfree and Strogatz, 1983, 1984; Winfree, 1985), for the existence of three-dimensional "scroll waves" consisting of spirals whose cores form a line, as well as spherical waves emanating from a point.

2. The Oregonator model

Although we have seen in Sec. V.B that targets and spirals are a generic feature in the oscillatory-uniform

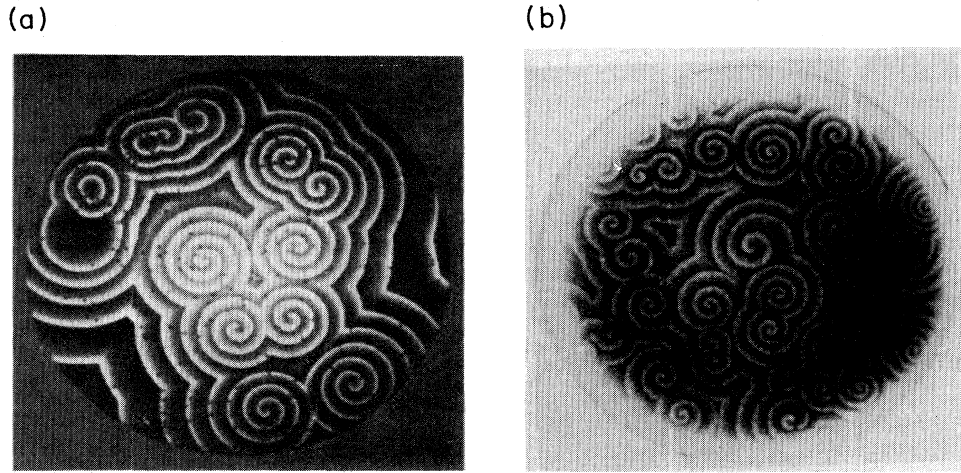


FIG. 76. Spiral patterns in excitable media. (a) Belousov-Zhabotinsky reaction photographed in blue light. Regions of maximum concentration of the blue indicator ferroin appear white. The spirals rotate with a period of about one minute. The dish is 90 mm in diameter with 1 mm depth of reagent. (From Winfree and Strogatz, 1983.) (b) Dark field photograph of a monolayer of slime mold *Dictyostelium discoideum* cells. The contrast is produced by the different refractive properties of the cells responding to a pulse of the diffusing chemical adenosine monophosphate (cAMP). Spirals are evident. They rotate every 5 minutes. The dish is 90 mm in diameter. (From Newell, 1983.)

(type III_o) case, the most successful models that account for the above mentioned observations quantitatively are of the reaction-diffusion type, for example the Oregonator (Field, Körös, and Noyes, 1972; Tyson, 1985). In its simplest version this model retains only the concentration u_1 of the autocatalytic species HBrO_2 and the concentration u_2 of the transition ion catalyst in the oxidized state Ce^{3+} or Fe^{3+} . The large number of other intermediate substances have faster time scales and their concentrations are absorbed in the constants of the model. In dimensionless units a simplified version of the model is given by

$$\partial_t u_1 = \eta^{-1} f(u_1, u_2) + D_1 \nabla^2 u_1, \quad (10.1a)$$

$$\partial_t u_2 = g(u_1, u_2) + D_2 \nabla^2 u_2, \quad (10.1b)$$

where we shall use the functions f and g of Tyson and Fife (1980)

$$f(u_1, u_2) = u_1(1 - u_1) - bu_2(u_1 - a)/(u_1 + a), \quad (10.2a)$$

$$g(u_1, u_2) = u_1 - u_2. \quad (10.2b)$$

For a typical choice of chemical concentrations the parameters take on the values $\eta = 10^{-2}$, $a = 2 \times 10^{-4}$, $b = 3$, $D_1 \equiv 1$, $D_2 = O(1)$; the spatial and temporal units chosen to fix $D_1 \equiv 1$ are 1.7 mm and 20 s, respectively. Equations (10.1) play the role of the microscopic equations for the BZ system, though of course the many approximations that have been made in arriving at this simple form are much less well controlled than in fluid-dynamical systems (see Tyson, 1985). Nevertheless it is hoped that these equations, with the parameters fixed by other ex-

periments, will provide a reasonably accurate description of pattern formation in this system. We will see below that more work is needed to provide a definitive test of the validity of the model.

Throughout this section we will consider a model of the form Eq. (10.1), with f and g of $O(1)$ with nullclines having the qualitative shape shown in Fig. 77. For concrete applications we will often make specific reference to the Oregonator model Eq. (10.2). Notice the small parameter η in Eq. (10.1): this describes the very different reaction rates for the two species u_1 and u_2 . A perturbative description will be built based on this small parameter. Notice also in the Oregonator model Eq. (10.2) the existence of an independent small parameter a , which tends to make the radius of convergence of the expansion small. For early studies of wave patterns in reaction-diffusion systems we refer the reader to Koppell and Howard (1973, 1981), Ortoleva and Ross (1974, 1975); and Shydkrot and Ross (1985). For reviews of the early Soviet literature see Vasiliev *et al.* (1979, 1987). More recent references include Walgraef (1988), Ohta *et al.* (1989), Ohta and Mimura (1990), and Davydov *et al.* (1991).

3. Oscillatory, bistable, and excitable dynamics

It is useful to first set the diffusion coefficients to zero and study the pure reactions.

$$\partial_t u_1 = \eta^{-1} f(u_1, u_2), \quad (10.3a)$$

$$\partial_t u_2 = g(u_1, u_2). \quad (10.3b)$$

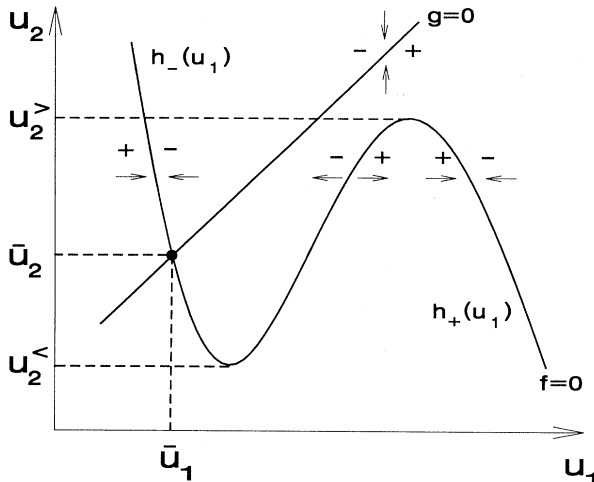


FIG. 77. Schematic plot of the nullclines $f(u_1, u_2) = 0$ and $g(u_1, u_2) = 0$ in the phase space of chemical concentrations u_1 and u_2 for the Oregonator model of the BZ reaction, Eqs. (10.1)–(10.2). (For typical parameters the bends are actually much sharper due to the various small numbers appearing.) The intersection of the nullclines at (\bar{u}_1, \bar{u}_2) yields a stationary solution. The signs of the reaction rates f and g are shown for small deviations of the concentrations from the respective nullclines, leading to the motion towards or away from the nullclines as indicated by the arrows. Since the u_1 nullcline $f = 0$ yields a double-valued function of u_2 , it is convenient to introduce $u_2 = h_+(u_1)$ and $u_2 = h_-(u_1)$ to label the branches indicated. The points $u_2^>$ and $u_2^<$ label the values of u_2 at the maximum and minimum of the u_1 nullcline.

The above equations show the different types of dynamical behavior of the stirred system discussed in (i) above, depending on how the nullclines $f(u_1, u_2) = 0$ and $g(u_1, u_2) = 0$ intersect. For illustration purposes we show a number of cases in Fig. 78, which might occur as we modify certain parameters in the functions f and g [e.g. the constants a and b of Eqs. (10.2)]. The qualitative orbits are easily mapped out by observing the regions of positive and negative $\partial_t u_1$ and $\partial_t u_2$ bounded by the nullclines.

The case shown in Fig. 78(a) corresponds to a Hopf bifurcation, as discussed in Sec. III.A, where the fixed point \bar{u}_1, \bar{u}_2 has an oscillatory instability with a *stable limit cycle* in its immediate vicinity. Note, however, that because of the disparity in time scales introduced by the small parameter η in Eq. (10.1), there is only a small region in parameter space where the limit cycle can be considered to be close to the fixed point and the motion harmonic [this region is typically of order $(a - \bar{a})/\bar{a} < \eta$, $(b - \bar{b})/\bar{b} < \eta$, where \bar{a} and \bar{b} are the parameter values where the Hopf bifurcation occurs]. In the general case shown in Fig. 78(b) the limit cycle will have large amplitude and the motion will be highly anharmonic, corresponding to a *relaxation oscillator*. This behavior can be understood by noting that because of the small parameter η , a trajectory starting at point B , say, will go rapidly to

the vicinity of the attracting branch $h_+(u_2)$ of the nullcline $f = 0$, and then move slowly up this branch until it reaches $u_2^>$. At that point the system jumps to the neighborhood of the other attracting branch $h_-(u_2)$ and moves slowly down that branch until it reaches $u_2^<$, when it jumps back to h_+ . In this way the system reaches a large amplitude limit cycle with alternating fast and slow variations.

Another typical case, shown in Fig. 78(c), represents a *bistable* situation with two different stable fixed points, each one having its own basin of attraction. Finally, in Fig. 78(d) we show a case with a single *stable fixed point*, which can be assumed to be *globally attracting*. Note, however, the different transient motion of a trajectory starting at A which is near the fixed point, and one starting further away, at B , say. The first trajectory decays rapidly to the fixed point, whereas the second one makes a large excursion to the vicinity of $h_+(u_2)$ before eventually ending up at the fixed point. This type of behavior is an example of *excitable dynamics*, and it plays an important role in many other examples drawn from chemistry and biology. In fact similar behavior is expected in the other cases shown in Fig. 78, where the system can make large excursions before settling down to its limit cycle or fixed points. We shall usually reserve the term “excitable” for the specific situation in Fig. 78(d), though it is sometimes used for all the cases shown in Fig. 78. Since the kinetics of u_1 causes excitability in the system and the interaction of u_1 and u_2 causes recovery, u_1 is sometimes referred to as the “trigger” variable and u_2 as the “recovery” variable. According to Tyson and Fife (1980), the Oregonator model (10.3-2) with $\eta \ll 1$ is excitable for $b \lesssim 1/2$ or $b \gtrsim 1-a$, and oscillatory for $1/2 < b < 1-a$.

4. Front and pulse propagation

The interesting question to ask from our point of view is what happens to the system described in the previous section when we add diffusion. The answer turns out to be amazingly rich and varied, and we shall only be able to mention some of the phenomena obtained (see e.g. Fife, 1984a,b; Vasiliev *et al.*, 1987; Tyson and Keener, 1988; Murray, 1989). From what we know in general about the behavior of spatially extended systems close to a Hopf bifurcation (cf. Sec. V.B) we would expect to find propagating plane wave solutions, as well as target and spiral defects in two dimensions. However, as we have seen, a consequence of the small parameters appearing in the model of the actual chemical system is that the systems are strongly nonlinear and thus rarely, if ever, operating close to the instability point. In this regime the simplest and most basic consequence of diffusion is the existence of *propagating pulse solutions* which travel through the system without attenuation. An analysis of these solutions in terms of fronts based on the small parameter η provides a tractable approach to predicting

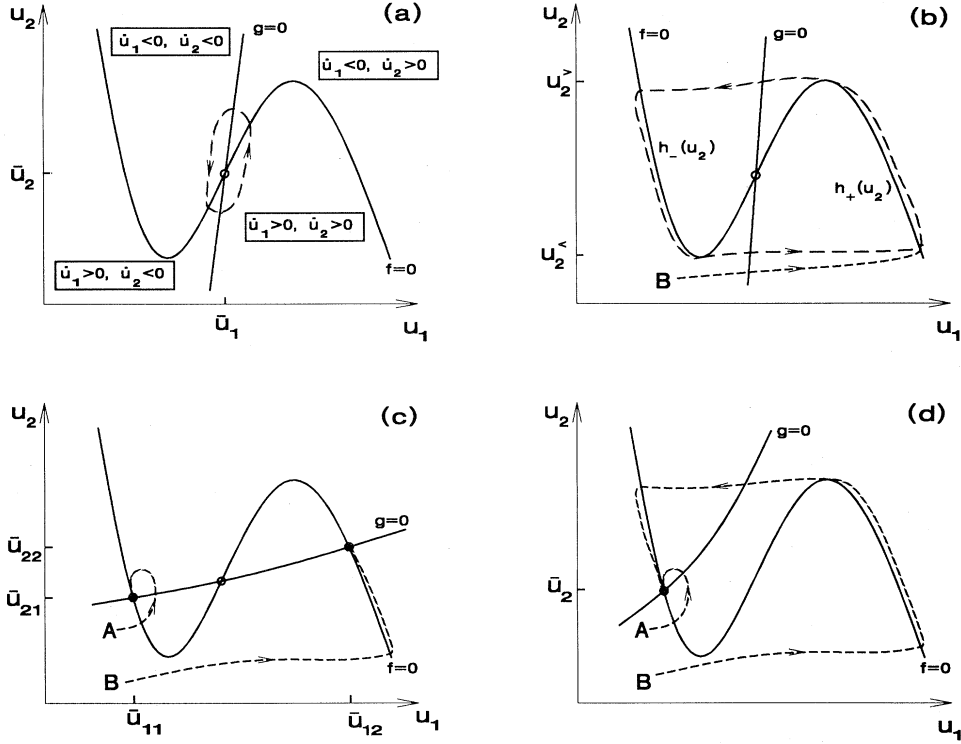


FIG. 78. Schematic of various possibilities for nullclines of Eqs. (10.1) leading to oscillatory or excitable behavior. Although a complete understanding requires quantitative analysis, some features of the trajectories $u_1(t), u_2(t)$ indicated by the dashed lines may be understood from the signs of $\dot{u}_1 = \partial_t u_1$ and $\dot{u}_2 = \partial_t u_2$ indicated in the different regions bounded by the nullclines. Stable stationary solutions (fixed points) are represented by full dots, unstable ones by open dots. (a) Unstable fixed point and small amplitude oscillations (limit cycle). (b) Typical oscillatory case consisting of large amplitude relaxation oscillations, such as would occur for small η , together with an unstable fixed point. The short-dashed line starting from an initial condition B indicates the transient approach to the limit cycle. (c) Bistable case with two stable (and one unstable) fixed points. A large perturbation from the left fixed point (e.g. to B) may lead to dynamics with a final state at the other fixed point, although each fixed point is stable to small perturbations (e.g. to A). (d) Excitable case: small perturbations (e.g. to A) lead to dynamics confined to the neighborhood of the fixed point, whereas slightly larger perturbations (e.g. to B) lead to large excursions before the concentrations ultimately relax back to the fixed point, which is globally stable.

properties of waves, targets and spirals in the strongly nonlinear state, where the presence of a Hopf bifurcation as assumed in Sec. V.B is unnecessary, and the medium may indeed be excitable rather than oscillatory.

The simplest example of such a strongly nonlinear front, namely that occurring in a single variable nonlinear diffusion equation, was discussed already in Sec. V.B.2.b.iv. Let us now turn to the case of Eqs. (10.1) involving the coupled variables u_1 and u_2 and the parameters $\eta \ll 1$ and D_2 . The trigger variable u_1 is also referred to as the “propagator” species. The recovery variable u_2 is sometimes called the “controller” species, since as we shall see its value determines the wave speed and propagation direction (Fife, 1984b). In one dimension, propagating solutions of Eqs. (10.1) can be put into the form $u_1 = u_1(\xi)$, $u_2 = u_2(\xi)$, where

$$\xi = x - vt , \quad (10.4)$$

and

$$\eta \partial_\xi^2 u_1 + \eta v \partial_\xi u_1 + f(u_1, u_2) = 0 , \quad (10.5a)$$

$$D_2 \partial_\xi^2 u_2 + v \partial_\xi u_2 + g(u_1, u_2) = 0 . \quad (10.5b)$$

First setting the small parameter η to zero in Eq. (10.5a) we obtain $f(u_1, u_2) = 0$ which has stable solutions

$$u_1 = h_{\pm}(u_2) , \quad (10.6)$$

for

$$u_2^- < u_2 < u_2^+ , \quad (10.7)$$

[see Fig. 77]. Let us now consider a solution where $u_1 = h_+(u_2)$ for $\xi > \xi_0$ and $u_1 = h_-(u_2)$ for $\xi < \xi_0$. When $\xi = \xi_0$ the derivative terms in Eq. (10.5a) cannot be ignored since the lowest-order solution is discontinuous. In this region there is a boundary layer of width $\sqrt{\eta}$ de-

scribed by the scaling

$$\tilde{\xi} = \xi / \sqrt{\eta}, \quad \tilde{v} = v \sqrt{\eta}, \quad (10.8)$$

in terms of which Eqs. (10.5) becomes

$$\partial_{\tilde{\xi}}^2 u_1 + \tilde{v} \partial_{\tilde{\xi}} u_1 + f(u_1, u_2) = 0, \quad (10.9a)$$

$$D_2 \partial_{\tilde{\xi}}^2 u_2 + \tilde{v} \partial_{\tilde{\xi}} u_2 + \eta g(u_1, u_2) = 0. \quad (10.9b)$$

To leading order in η we have $u_2 = \text{const.}$, and Eq. (10.9a) is precisely of the same form as Eq. (5.64), which has a trigger front solution with a unique velocity $\tilde{v}(u_2) = O(1)$, in the band

$$\tilde{v}^< > \tilde{v}(u_2) > \tilde{v}^>, \quad (10.10)$$

where $\tilde{v}^< = \tilde{v}(u_2^<)$ (see Fig. 79). When $u_2 = u_2^<$ or $u_2 = u_2^>$ there is a family of phase fronts with velocities $\tilde{v} \leq \tilde{v}^>$ and $\tilde{v} \geq \tilde{v}^<$, respectively, as discussed in Sec. V.B.2.b.iv.

From the above discussion we see that in general Eqs. (10.9) have propagating front solutions with velocity $\tilde{v} = O(1)$ or $v = O(\eta^{-1/2})$. In terms of physical variables the wave speed (in dimensional units) is

$$v_{\text{dim}} = \tilde{v}(u_2) \sqrt{k_1 D_1}, \quad (10.11)$$

where \tilde{v} is the $O(1)$ velocity in Eq. (10.10), and k_1 and D_1 are the effective rate constants and diffusion coefficient, respectively, of the propagator species u_1 . Equation (10.11), which is known as Luther's law gives an excellent order of magnitude estimate of wave speeds in an amazing variety of excitable and oscillatory media (see Tyson and Keener, 1988, and Sec. X.A.B.6 below).

It should be noted that the velocity \tilde{v} is $O(1)$ except

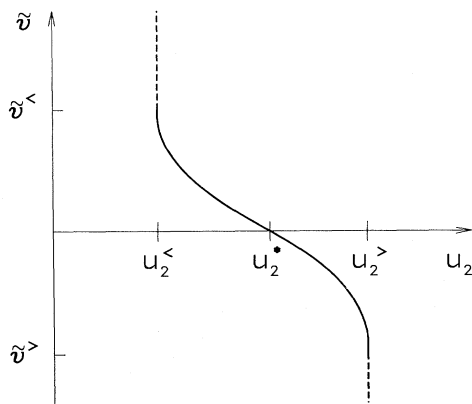


FIG. 79. Schematic of reduced velocity \tilde{v} , defined in Eq. (10.8), as a function of concentration u_2 of the controller species, for a front in the concentration u_1 of a reaction-diffusion system characterized by nullclines such as in Fig. 77. For each value of u_2 in the range $u_2^< < u_2 < u_2^>$ (see Fig. 78) there is a unique propagation velocity corresponding to Figs. 17(c) and (d). Such fronts are often called trigger fronts. For u_2 at the ends of this range there exists a family of fronts with speeds $\tilde{v} > \tilde{v}^<$, for $u_2 = u_2^<$, or $\tilde{v} < \tilde{v}^>$ for $u_2 = u_2^>$, corresponding to Figs. 17(e) and (f). Such fronts are known as phase fronts.

near the special point $u_2 = u_2^*$ where

$$\tilde{v}(u_2^*) = 0, \quad (10.12)$$

which is sometimes called the "stall" solution [see Fig. 79 and Kessler and Levine, 1990a]. The value of u_2^* is obtained implicitly from relation (10.9a), as

$$\int_{h_-(u_2^*)}^{h_+(u_2^*)} f(u_1, u_2^*) du_1 = 0, \quad (10.13)$$

since $\partial_{\tilde{\xi}} u_1$ vanishes at the end points. We shall see below that in the limit $\eta \ll 1$ waves with high frequency and low velocity have $u_2 \approx u_2^*$, in which case the scaling adopted here ceases to be appropriate.

Given the relation $v(u_2)$ for wave fronts, a solitary pulse solution can be constructed in an excitable medium by patching together a wave front (up-jump) with $u_2 = \bar{u}_2$ (the stationary point of the medium, see Fig. 77), and a wave back (down-jump) with $u_2 = u_{2b}$, such that

$$v(\bar{u}_2) = -v(u_{2b}) = v_p, \quad (10.14)$$

where v_p is the pulse velocity. This situation is illustrated schematically in Fig. 80(a), where it is seen that the up-jump and down-jump of u_1 indeed occur at \bar{u}_2 and u_{2b} , respectively. Between the two fronts the variable u_2 satisfies Eq. (10.1b), which we may write as

$$\partial_t u_2 = -v \partial_{\tilde{\xi}} u_2 = g(h_+(u_2), u_2), \quad (10.15a)$$

and behind the second front it reaches its stationary value $u_2 = \bar{u}_2$ according to the equation

$$-v \partial_{\tilde{\xi}} u_2 = g(h_-(u_2), u_2). \quad (10.15b)$$

We have neglected the diffusion of u_2 since according to our previous argument $v(\bar{u}_2) = O(\eta^{-1/2}) \gg 1$. Notice that the down-jump front may be either trigger or phase (Sec. V.B.2.b.iv), depending on whether $v(\bar{u}_2) \gtrless |v^<|$.

5. Periodic wave trains

The solitary pulse considered above can be stimulated by a local disturbance of the medium at a point. Suppose that instead of a one-time stimulation, we excite the system periodically in time in some localized region of space, in order to create a (one-dimensional) wave train. The main difference with the solitary pulse is that the medium in front of the pulse is no longer in a stationary state, thus requiring adjustment of the wavefront value $u_{2f} \neq \bar{u}_2$ and a corresponding change in the wave back u_{2b} , as illustrated in Fig. 80(c). In the present approximation these values are determined by the implicit relations given by integrating Eqs. (10.15) (Tyson and Fife, 1980)

$$P_+ = \int_{u_{2f}}^{u_{2b}} \frac{du_2}{g(h_+(u_2), u_2)}, \quad (10.16a)$$

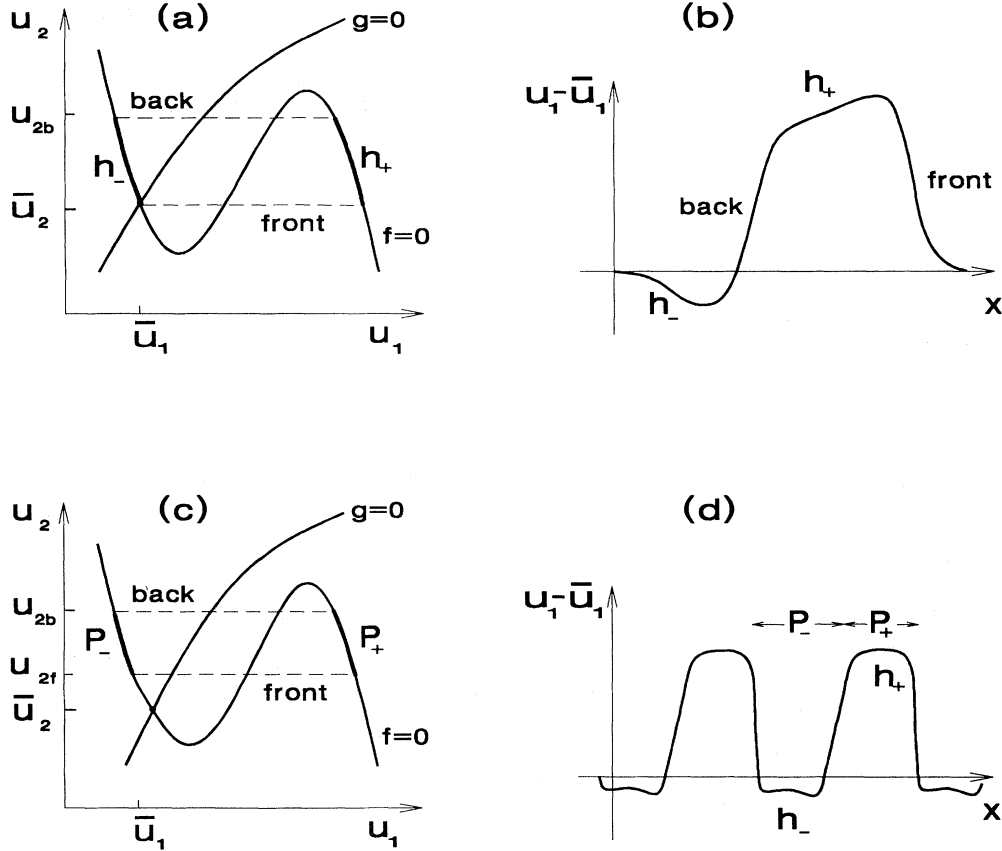


FIG. 80. Propagating pulse (a) and (b) and wave trains (c) and (d) in excitable chemical system. Parts (b) and (d) show the spatial dependence of the propagator species u_1 and parts (a) and (c) map this dependence onto the (u_1, u_2) phase plane, with the fronts and backs of the pulses shown as dashed lines, and the joining regions as heavy lines superimposed on the $f=0$ nullcline. In the regions marked P_+ and P_- in parts (c) and (d) the dynamics of the u_2 variable is governed by Eq. (10.15).

$$P_- = \int_{u_{2b}}^{u_{2f}} \frac{du_2}{g(h_-(u_2), u_2)} , \quad (10.16b)$$

$$P = P_+ + P_- = 2\pi/\omega , \quad (10.16c)$$

$$v(u_{2f}) = -v(u_{2b}) , \quad (10.16d)$$

where $P = 2\pi/\omega$ is the period of the external stimulation, and Eq. (10.16d) determines u_{2b} when u_{2f} is known. In general the above relations have a discrete set of solutions, for given period P , which determine different branches of the dispersion relation

$$\omega = \omega(q) , \quad q = \omega/v , \quad (10.17)$$

obtained by eliminating u_{2b} and u_{2f} from Eqs. (10.16). A plot of the dispersion relation obtained by Keener and Tyson (1986) from the above approximations for the Oregonator model is shown in Fig. 81(a). Notice that for large periods the medium has sufficient time to relax back to the quiescent value \bar{u}_2 , and the propagation velocity approaches a maximum value equal to the velocity of a solitary pulse.

In the derivation of Eqs. (10.16) we used Eqs. (10.15) which neglect the diffusion of the controller species u_2 . This approximation is valid if

$$D_2 \ll v / q , \quad (10.18)$$

and breaks down for low velocities which also implies short wavelengths [see Fig. 81(b)]. [This has been clearly shown by Kessler and Levine (1990a) for a model in which the nonlinear terms in Eqs. (10.1) are replaced by a piecewise linear form.] In the low-velocity limit a new scaling first introduced by Fife (1984b) becomes appropriate. We can estimate the small-velocity scale for which the diffusion of u_2 becomes important, by calculating the slow-front solution in an expansion about the stationary-front (stall) solution of Eqs. (10.9)

$$u_1^*(\xi) = u_1(\xi; u_2^*) , \quad (10.19)$$

where u_2^* is determined from Eq. (10.12). We set

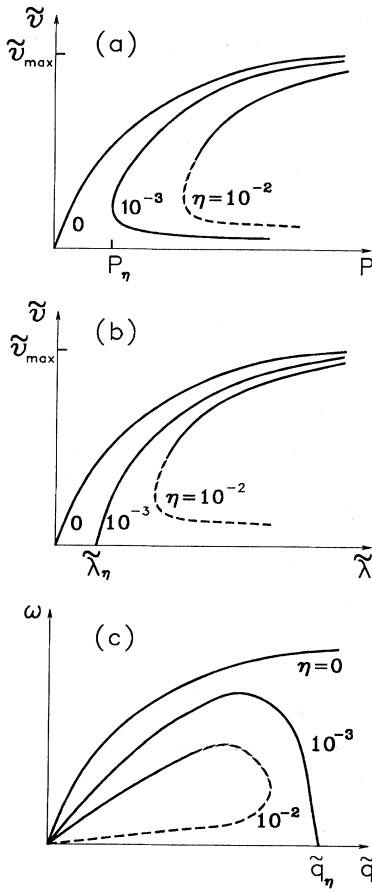


FIG. 81. Various schematic representations of the dispersion relation of chemical wave trains, calculated numerically from Eqs. (10.1)–(10.2), showing the interdependence of the temporal period P , the scaled propagation speed \tilde{v} , wavelength $\tilde{\lambda}$, and wave vector \tilde{q} . Curves for three different values of η are shown. The $\eta=0$ curve is given by the equations of the asymptotic theory (10.16); the $\eta=10^{-3}$ curve is consistent with the new predictions for small \tilde{v} based on the Fife scaling (10.26); the $\eta=10^{-2}$ curve shows significant deviations from these asymptotic predictions, even for this quite small value. Full lines are stable branches, dashed lines unstable. (Adapted from Tyson and Keener, 1988.)

$$u_1 = u_1^*(\xi) + \delta u_1(\xi), \quad (10.20a)$$

$$u_2 = u_2^* + \delta u_2(\xi), \quad (10.20b)$$

and assume that each term in Eq. (10.9b) is of the same order. Then D_2 will be important for

$$\tilde{v} \delta \xi / D_2 = O(1) \quad (10.21)$$

and

$$\tilde{v} \delta u_2 / \delta \xi \sim \eta g(u_1^*, u_2^*) \sim \eta, \quad (10.22)$$

assuming

$$g(u_1^*, u_2^*) = O(1). \quad (10.23)$$

Inserting (10.20a) into (10.9a) to obtain an equation for

the perturbation we find

$$\begin{aligned} \partial_{\xi}^2 \delta u_1 + \frac{\partial f}{\partial u_1^*} \Big|_{u_2=u_2^*} \cdot \delta u_1 \\ = -\tilde{v} \partial_{\xi} u_1^* - \frac{\partial f}{\partial u_2^*} \Big|_{u_1=u_1^*} \cdot \delta u_2, \end{aligned} \quad (10.24)$$

where we can assume that the partial derivatives evaluated at u_1^*, u_2^* as well as the derivative with respect to ξ are $O(1)$. Equation (10.24) leads to a solvability condition with respect to the translation mode of u_1^* , which states that the appropriate average of the rhs vanishes, so to within factors of order unity we have

$$\tilde{v} \sim \delta u_2. \quad (10.25)$$

Putting together Eqs. (10.21)–(10.23) and (10.25) we find

$$\tilde{v} \sim (D_2 \eta)^{1/3}, \quad v \sim D_2^{1/3} \eta^{-1/6}, \quad (10.26a)$$

$$\delta \xi \sim D_2^{2/3} \eta^{-1/3}, \quad \delta \xi \sim D_2^{2/3} \eta^{1/6}, \quad (10.26b)$$

$$\omega \sim \tilde{v} / \eta \delta \xi \sim v / \delta \xi \sim D_2^{-1/3} \eta^{-1/3}. \quad (10.26c)$$

Thus if $D_2 = O(1)$ we see that the dispersion relation (10.17) for plane waves breaks down for $\tilde{v} = O(\eta^{1/3})$, i.e. for slow waves with high frequency and large wave vector. Although this scaling was derived from the condition that diffusion of the controller species should become important for a *planar* front, we can see that it is also the appropriate scaling for the case where the curvature correction $K \sim \delta \xi^{-1} \sim \eta^{-1/6}$ to the propagation of a curved u_1 front becomes comparable to the velocity $v \sim \eta^{-1/6}$ [see Eq. (5.117)]. Thus when the Fife scaling is appropriate, the diffusion of both u_1 transverse to the interface and u_2 are in general important. It turns out that the above argument holds strictly only if η is numerically very small since it requires

$$\eta^{1/3} \ll 1. \quad (10.27)$$

In that case a new scaling of Eqs. (10.5) can be introduced and the dispersion relation can be obtained numerically, for various forms of the functions f and g . An example of the modification of the dispersion relation by controller diffusion D_2 at small velocity (i.e. small wavelength and period) is shown with parameter value $\eta = 10^{-3}$ in Fig. 81 for the Oregonator model (Dockery *et al.*, 1988; see also Kessler and Levine, 1990a). The main effect of the diffusion coefficient D_2 is to introduce a minimum wavelength λ_η and period P_η , i.e. a maximum frequency ω_η for plane-wave trains. There is also, in Fig. 81(b) a bifurcation at wavelength $\lambda = \lambda_\eta$ from stationary pulses ($v = 0$) to traveling waves ($v > 0$).

A numerical evaluation of the dispersion relation using slightly higher (and apparently more realistic) values of η , e.g. the value $\eta = 10^{-2}$ which does not satisfy the condition (10.27) as stringently, was performed by Keener and Tyson (1986), and is also shown in Fig. 81. This case still shows a minimum frequency and wavelength, but no longer has the continuous bifurcation from stationary

pulses to traveling waves. Moreover, the authors have shown that waves with low velocities become linearly unstable, as indicated by the dashed lines in Fig. 81. [They do not comment on the stability of the dispersion relation for $\eta=10^{-3}$.] We shall see below that the detailed properties of low-velocity waves are of some importance physically, since real spiral patterns probe this region in their core, and in general have high frequencies and wave vectors determined by the parameters η and D_2 .

Dispersion relations have also been obtained by Dockery *et al.* (1988) for situations where $D_2 \ll 1$ or $D_2 \gg 1$, in which case there is a subtle interplay between the small parameter η and either D_2 or D_2^{-1} . It should also be noted that although we have generally assumed excitable dynamics in the preceding discussion, the behavior of the uniform system (10.3) does not enter most of the arguments in a sensitive way. Indeed, unlike the case for solitary pulses, in a wave train the system does not have time to reach the steady state between pulses. Thus all of the cases depicted in Fig. 78 are expected to show similar dispersion relations except perhaps near $\omega=0$. The essential ingredients are the bistable nature of the f -function and the separation of time scales coming from the small parameter η .

6. Higher-dimensional patterns

In the previous section we have seen that except for the region of low velocities, one-dimensional wave trains have fronts confined to a spatial region of width $\eta^{1/2}$, which propagate through the medium as a result of the interplay of reaction and diffusion of the propagator species u_1 , at a velocity determined by the level of the controller species u_2 . In two spatial dimensions, the wave front is a line, again of width $\eta^{1/2}$, but the propagation velocity also depends on the shape of this line, in particular on its local curvature K (see Sec. V.B.2.c).

Denoting by v_n the normal velocity of the front we may rewrite Eq. (10.5a) as

$$\eta \partial_\xi^2 u_1 + \eta (v_n - K) \partial_\xi u_1 + f(u_1, u_2) = O(\eta^2), \quad (10.28)$$

where ξ is now the coordinate locally perpendicular to the front. Comparing Eqs. (10.5a) and (10.28) we conclude that for a *fixed* controller concentration u_{2f} at the front, the normal velocity of curved waves is related to the velocity of periodic wave trains by an eikonal equation analogous to Eq. (5.117) (Keener, 1986)

$$v_n = v(u_{2f}) + K, \quad (10.29)$$

where the coefficient D_1 of Eq. (5.117) is just the diffusivity $D_1=1$.

As long as the controller concentration u_{2f} is known, and is far from the stall value u_2^* , Eq. (10.12), the velocity $v(u_{2f})$ is large [$O(\eta^{-1/2})$], so the curvature correction in Eq. (10.29) is small. Equation (10.29) is applicable for example to the case of a curved solitary pulse in two dimensions, for which the effect of controller diffusion D_2 was

also shown to be small. We shall see below, however, that spiral waves have low velocities and short wavelengths, so that both controller diffusion and curvature are important, and u_{2f} cannot be inferred from the properties of plane-wave trains.

a. Target patterns

Since the early observations on targets showed these to have variable periods and to disappear almost completely when the system was purified, most quantitative theories proposed thus far have assumed a *heterogeneous* medium, with a local area of radius r_0 , called a “pacemaker,” assumed to have oscillatory dynamics with a frequency $\omega=2\pi/P$ determined by an unknown external mechanism (Tyson and Fife, 1980; Fife, 1981; Agladze and Krinsky, 1984). This local oscillation then produces expanding concentric waves which form the target pattern. Far from the center, where curvature effects are negligible, the pattern consists of a periodic wave train with frequency ω and speed $v(\omega)$, Eq. (10.17). We thus expect a continuous family of targets whose frequencies and speeds are determined by the external forcing (a similar result was found in Sec. V.B.2.c). From the curves in Fig. 81 it is seen that for long periods P most targets will have roughly the same speed $v_{\max} \approx v(u_2^*)$, and wavelengths proportional to the period. The main effect of curvature is to set a minimum for the size r_0 of the pacemaker region,

$$r_0 > r_0^{\min} = D_1/v_{\max} \approx 5 \times 10^{-3} \text{ cm}, \quad (10.30)$$

for the BZ reaction. [In the strict limit $\eta^{1/3} \ll 1$, condition (10.30) is less restrictive than the condition $q < q_\eta \approx \eta^{-1/3}$, which limits the domain of existence of planewave trains; see Fig. 81(c).]

Tyson and Fife (1980) have explicitly constructed target solutions of the Oregonator model (10.1)–(10.2), assuming the parameter b to vary in space such that $b=b_0$ for $r < r_0$, and $b=b_\infty$ for $r > r_0$, where b_0 and b_∞ correspond to oscillatory [Fig. 78(b)] and excitable [Fig. 78(d)] dynamics, respectively. The passing front then has a form analogous to the one shown schematically in Fig. 80(b), and corresponds to abrupt blue wavefronts (h_+) propagating in a sea of red (h_-), and relaxing slowly back to red. A qualitative prediction of the theory is the possibility of *reducing waves* appearing when the medium is in a quiescent oxidized state. This corresponds to a situation as in Fig. 78(d), but where the stable fixed point is on the $u_1=h_+(u_2)$ branch with a larger value of u_2 .

Target patterns in a *homogeneous* medium were constructed in Sec. V.B.2.c above, based on the amplitude equation and the $\lambda-\omega$ model. More realistic models such as the Oregonator might also be expected to produce intrinsic targets, but they apparently require either three dynamical variables or a nonmonotonic velocity dependence $v(u_2)$ in Fig. 79. In one such model (Fife, 1981) the third variable is a dynamical version of the pa-

parameter b whose variations produced the extrinsic target discussed above. A number of different 3-variable models of intrinsic targets have been presented by Soviet workers. The interested reader is referred to the book by Vasiliev *et al.* (1987).

b. Spiral waves

In Sec. V.B.2.c we discussed spiral solutions to the amplitude equation for type III_o patterns, and observed that in contrast to targets these patterns only exist for discrete wave-vector values. Let us now consider spirals in a system with excitable or bistable dynamics (Winfree, 1991). The simplest way to understand spirals qualitatively is to consider the procedure outlined in Sec. V.B., by which they are actually formed in the BZ system (Fife, 1985). We focus on one of the pulses in a planewave train, which is made up out of a wave front with velocity $v_f = v(u_{2f}) > 0$, and a wave back with $v_b = v(u_{2b}) = -v(u_{2f})$, as depicted schematically in Fig. 82(a). The pulse consists of a region of excited state (h_+) propagating in the rest state (h_-). We then imagine perturbing the pulse by bringing it back to the rest state (h_-) locally. After a short time, we have approximately the situation shown in Fig. 82(b), where the controller variable varies more or less smoothly along the pulse, and passes through the “stall” value $u_2 = u_2^*$, $v(u_2^*) = 0$, somewhere near the tip. As a result the pulse no longer propagates forward uniformly, and it is seen that there is a tendency for each tip to initiate a curling motion which turns clockwise on the left and counterclockwise on the right. Of course, as the spiral curls up the portion near the tip experiences curvature and the simple description in terms of the function $v(u_2)$ will no longer hold. Meron and Pelcé (1988) have investigated a simple model of this phenomenon more quantitatively.

Let us now assume that the above procedure has led to a fully developed steady spiral, shown schematically in Fig. 82(c), with a given rotation frequency ω . We wish to know if a band of frequencies is possible, as in the case of targets. Far from the core the pattern is just a plane-wave train, i.e. curvature effects are negligible and the wave vector is determined, once the frequency is known, from the dispersion relation of the one-dimensional case (10.17). In the core the curvature of the front defines a length scale, and the simplest assumption is that this is not a new length, i.e. that the wave vector q far from the core, the curvature of the front in the core, and the inverse size of the core itself are all of the same order of magnitude. The condition that this be so might then be expected to fix a unique frequency ω and wave vector q (or at least a discrete set). As mentioned above, if this is the case controller diffusion will in general be important in the core region as well as in the plane-wave region far from the core. The width of the propagator front is, however, always negligibly small for small η , so the appropriate framework to establish the full spiral structure is a free boundary calculation with the front acting as a

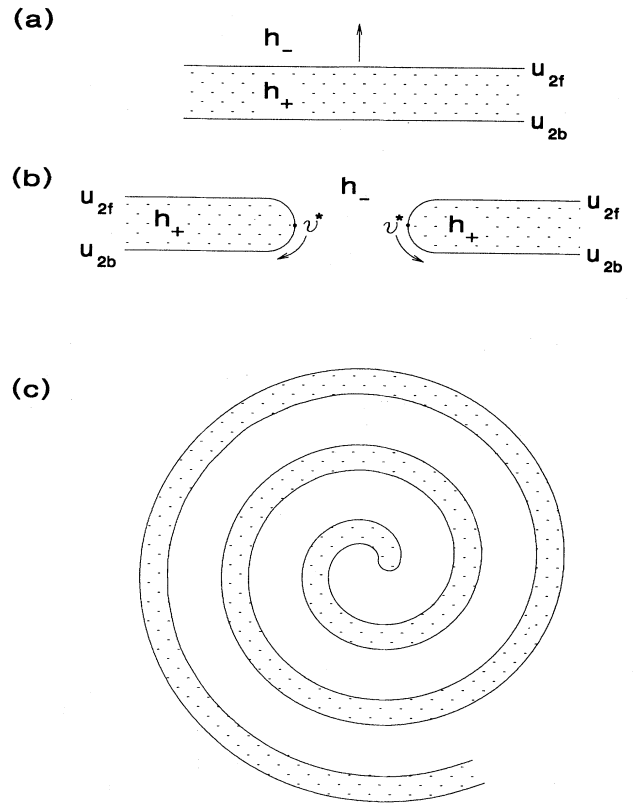


FIG. 82. Schematic illustration of spiral pattern dynamics. (a) and (b) Formation of a spiral by breaking a propagating pulse. Regions of high u_1 concentration are shown hatched. (c) Completed single spiral. See text for details.

source of the diffusing u_2 field, and moving in this field according to the eikonal equation (10.29) (Keener, 1986; Kessler and Levine, 1990b). This difficult calculation has not yet been carried out for $D_2 = O(1)$.

There has been considerable progress for small D_2 , however, leading to the conclusion that only a discrete set of spiral solutions exist, as already found from the amplitude equation. Pelcé and Sun (1991) numerically solved the eikonal equation (10.29) coupled to a dynamic controller field u_2 in the diffusionless limit [$D_2 = 0$ in Eq. (10.5b)]. They assumed a smooth spiral solution as in Sec. V.B.2.c.iv above, but now with the core radius determined self-consistently, rather than taken to be an arbitrary parameter as in the earlier work. Karma (1992) subsequently showed that these solutions are valid small- η solutions of the original pde's (10.5) only in the special “weakly excitable” limit where the value of u_2 in the rest state is close to the stall value u_2^* . In this case he showed that a full spiral solution including a smooth core can be constructed with length and velocity as in the Fife scaling, but with $\omega \rightarrow 0$ corresponding to the degenerate case of $q_\infty \rightarrow 0$ [see Eq. (5.120)]. More recently, the general small D_2 problem, together with the assumption of small η as in the original formulation, has been completely solved in two limits, $\eta^{1/3} \ll D_2 \ll 1$ (Bernoff, 1991) and

$D_2 = 0$ (Karma, 1992; Kessler *et al.*, 1992). We will describe the singly diffusive case $D_2 = 0$ since it is easier to present. Karma (1992) first constructs the solution outside a core region assuming the Fife scaling so that the fronts are near to the stall solution and the length and frequency scales are as in (10.26). (In this region a D_2 in the range assumed by Bernoff is also negligible, so the solution is the same in that case.) The u_2 equation between the fronts reduces to

$$\omega \partial_\theta u_2 = g(h_\pm(u_2^*), u_2^*) + O(\delta u_2), \quad (10.31)$$

with θ the polar coordinate, and where the last term is negligible since $\omega \sim \eta^{-1/3}$. Integration of Eq. (10.31) leads to a consistency requirement *independent of the radial coordinate*

$$\theta^+ - \theta^- = 2\pi \left[\frac{g(h_-)}{g(h_+) + g(h_-)} \right], \quad (10.32)$$

$$(u_2^> - u_2^*) = -(u_2^< - u_2^*) = \pi \omega^{-1} \left[\frac{g(h_+)g(h_-)}{g(h_+) + g(h_-)} \right], \quad (10.33)$$

with $\theta^+(r)$, $\theta^-(r)$ the angles defining the leading and trailing fronts of the spiral [Eq. (5.118)], and $u_2^>$, $u_2^<$ the controller concentrations on these fronts which are constant along each front. Since now, quite nontrivially, the eikonal equation (10.29) is accurate with v the constant velocity defined by the values of $u_2^>$ and $u_2^<$ (which, however, is not the asymptotic large separation velocity), the eigenvalue equation (5.125) derived in Sec. V is an accurate description of the spiral. It is then further assumed that the core size should be chosen as zero on the Fife scale $\eta^{1/6}$, so that the expression reduces to Eq. (5.127b) with $r_c = 0$. For any given set of nullclines all the constant factors may be evaluated to give quantitative predictions for $\omega/\eta^{-1/3}$, $q_\infty \eta^{1/6}$, etc. Karma evaluates these expressions for the FitzHugh-Nagumo model (5.170), and finds very good convergence to numerical results of Winfree for $\eta < 10^{-2}$. Karma notes that on the $\eta^{1/6}$ length scale of the analysis there is a finite angle discontinuity $\theta^+ - \theta^-$ between the fronts at the origin, and that u_2 is also discontinuous. These discontinuities must be resolved on a smaller (e.g. $\eta^{1/2}$) lengthscale for the $D_2 = 0$ model. This region was studied by Kessler *et al.* (1992) who showed that indeed a smooth core on the $O(\eta^{1/2})$ length scale can be constructed, without further restrictions on the far-field solution. A remarkable feature of the core solution is a large $O(1)$ azimuthally constant change in the concentration of the u_2 species which balances the strong diffusion of the u_1 species on the $\eta^{1/2}$ length scale. For the case of small D_2 Bernoff finds a core of size $O(D_2^{1/3})$ and a correction to the $D_2 \rightarrow 0$ frequency by a factor $[1 + O(D_2^{2/3})]$. If $D_2 = O(1)$ it is expected that the singularity will instead be resolved on the $\eta^{1/6}$ length scale.

For a larger value of η , [e.g. $\eta = 10^{-2}$ as in Eqs. (10.1)–(10.2)] there is no obvious scaling which will sim-

plify the equations, and the phenomenological approach of Keener and Tyson (1986) discussed in Sec. V.B is a useful first step. The core radius r_c is taken to be a parameter of the theory, although taking r_c to zero still yields a finite result. The eikonal equation (10.29) has the form of Eq. (5.117) (with $D_1 = D_2 = 1$), so long as we consider the velocity $v(u_{2f})$ to be a given constant. This assumption will be valid if the nonlocal interaction between various arms of the spiral can be neglected, so that $v(u_{2f})$ is equal to the pulse velocity v_p . Then the argument of Sec. V.B determines the spiral frequency ω_{sp} according to the curvature relation (5.127), which now reads

$$\omega_{sp} = v_p^2 Q(r_c/v_p). \quad (10.34)$$

Since v_p and the function $Q(x)$ are known, the above equation determines ω_{sp} as a function of r_c . Keener and Tyson (1986) have attempted to improve upon Eq. (10.34) by replacing v_p by the dispersion relation of planewaves $\omega(v)$ of Fig. 81, i.e. they determine ω_{sp} as the intersection between (10.34) and $\omega(v)$. The results are shown in Fig. 83 for different values of r_c , and they show that the effects of dispersion are by no means negligible for the r_c values considered. Since D_2 was taken into account in the dispersion relation $\omega(v)$ but not in finding $v(u_{2f})$ in the eikonal equation, the procedure of Keener and Tyson is not systematic, but it appears to capture a good part of

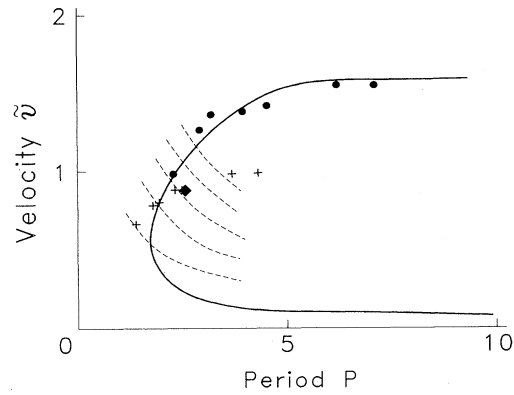


FIG. 83. Dispersion relation for the scaled velocity \bar{v} , Eq. (10.8), vs temporal period P for the Belousov-Zhabotinsky reaction. Full line shows $\bar{v}(P)$ predicted by the Oregonator model (10.1)–(10.2). Dashed lines show a second relationship for waves produced by a spiral in the Keener-Tyson approximation, Eq. (10.34), for values of the core radius r_c ranging from 0.5 (top) to 0.1 (bottom). If r_c were known, the intersection of the appropriate dashed curve and the full curve would give a prediction for the period and corresponding velocity of waves produced by spirals. The diamond is the result for spirals produced by a numerical solution of the original model equations (10.1)–(10.2). The crosses are experimental measurements of the dispersion relation of planar wave trains mapped onto the scaled coordinates using the parameter values of Keener and Tyson (1986). The dots are the same data mapped onto the scaled coordinates using parameters chosen to fit the maximum velocity. (Adapted from Keener and Tyson, 1986 and Tyson and Keener, 1988.)

the physics of this difficult problem. Indeed, the authors have tested their theory against a full numerical simulation of the starting model (10.1)–(10.2), which leads to the solid diamond in Fig. 83. This point is close to the result of the phenomenological theory for the choice of core radius $r_c = 0.3$. Interestingly, the authors report that in the numerical solution the tip of the spiral did not remain stationary in the rotating frame, but carried out a meandering motion which was confined to a circle of radius $r = 0.3$ (see below). The stability of spirals was considered early on by Krinsky and Malomed (1983) and by Keener and Tyson (1986). More recently the transition to meandering motion, which corresponds to a two-frequency oscillation in the laboratory frame, was studied in more detail numerically (Barkley *et al.*, 1990; Karma 1990; Jahnke and Winfree 1991; Barkley 1992), and analytically in the small D_2 limit considered by Bernoff (Kessler *et al.*, 1992).

c. Three-dimensional patterns

We have seen in Sec. V.B that two-dimensional targets and spirals can be generalized to the third dimension by assuming that the core is centered on a line which varies slowly in space (Keener, 1988; Keener and Tyson, 1990, 1991). This theory applies not only to the amplitude equations considered in Sec. V.B, but equally well to reaction-diffusion models such as (10.1)–(10.2), for which the two-dimensional patterns are not described by perturbation theory (see also Brazhnik *et al.*, 1987). The shrinking and drifting of scroll rings discussed in Sec. V.B has been simulated numerically by Jahnke *et al.* (1988), and the structure was seen to vanish abruptly when its radius reached a size comparable to the core radius (see also Panfilov *et al.*, 1989). A topologically more stable scroll ring containing a twist was also simulated by Panfilov and Winfree (1985), but little is known theoretically about its motion. A number of intriguing qualitative experiments and numerical simulations have been carried out over the years by Winfree and collaborators (see Winfree and Strogatz, 1983, 1984; Nandapurkar and Winfree, 1989).

B. Comparisons with experiment

Quantitative experiments on unstirred chemical reactions are difficult to perform, because first of all under usual circumstances the conditions of the experiment have a secular change in time as the reactants become depleted, and secondly it is difficult to measure and control the concentrations of all of the chemicals participating. In the Oregonator model these concentrations enter as parameters and normalization constants, as well as dynamical variables u_1, u_2 . Despite these difficulties considerable effort has been devoted to quantitative measurements of the properties of waves in the BZ reaction, and some nontrivial tests of the theory exist (see Field and

Burger, 1985; Ross *et al.*, 1988b). Moreover, as discussed below, experiments have recently been undertaken in open (unstirred) reactors where the chemicals do not deplete, though few quantitative results have yet been reported.

1. Stirred dynamics

The temporal behavior of the stirred BZ system has been studied in great detail and there is now good agreement between experiments and models containing 7 or more modes (see Richetti *et al.*, 1987). The two-variable Oregonator model (10.1)–(10.2) can be tested by measurements of the reaction rates and the concentrations of the slow reactants. These make up the parameters b and a , and the normalizations of the variables u_1 and u_2 . Given those quantities one can both calculate and measure the time dependence of the variables $u_1(t)$ and $u_2(t)$, for different initial conditions. For example in the oscillatory state the period, the amplitude and the shape of the oscillation can be obtained. Generally speaking (Tyson, 1985) absolute agreement between experiment and theory is no better than a factor of 2, a result which is not too surprising in view of the existence of rather large differences in scales expressed by the smallness of the parameters $\eta \approx 10^{-2}$ and $a \approx 10^{-4}$. A similar situation obtains for the bistable and excitable cases.

2. Pulse propagation

The simplest approximation for the front in a quiescent medium is obtained by neglecting the coupling b in Eq. (10.2a) and yields the dimensionless (Fisher) value (Sec. VI.B)

$$\bar{v} = 2 . \quad (10.35a)$$

This translates into the physical expression (Tyson, 1985)

$$v_{\text{dim}} = 2 [k_3 x_B x_H D_1]^{1/2} , \quad (10.35b)$$

$$= 0.05 (x_B x_H)^{1/2} \text{ cm/s mol} , \quad (10.35c)$$

where $k_3 = 40 \text{ s}^{-1}(\text{mol})^{-2}$ is a measured reaction rate for an intermediate reaction, $D_1 = 1.5 \times 10^{-5} \text{ cm}^2 \text{s}^{-1}$ is the measured diffusion constant of HBrO_2 , and x_B and x_H are the concentrations of BrO_3^- and H^+ respectively (in moles), which were used to obtain the dimensionless u_1 and u_2 in the starting model (10.1)–(10.2).

As discussed above, when the coupling b to u_2 in Eq. (10.2a) is taken into account, the actual pulse velocity in the excitable case depends on the quiescent value \bar{u}_2 of the controller variable, and it turns out (Tyson, 1985) that for the above conditions

$$\bar{v} = \bar{v}(\bar{u}_2) = 1.7 , \quad (10.36a)$$

which translates to

$$v_{\text{dim}} = 0.04 (x_B x_H)^{1/2} \text{ cm/s mol} . \quad (10.36b)$$

Experiments by Showalter *et al.* (1979) and by Wood and Ross (1985) have confirmed the square-root dependence on $x_B x_H$ and have found a prefactor of 0.04–0.05, in good agreement with Eq. (10.36b).

As regards pulse shapes, measurements have been carried out by Wood and Ross (1985), by Agladze and Krinsky (1984) and by Müller *et al.* (1987) but to our knowledge no quantitative comparison with theory has yet been carried out. However the constancy of pulse shape during propagation was dramatically demonstrated by Wood and Ross (1985), who measured the spatial distribution of reactant at one instant of time [Fig. 84(a)], as well as the time dependence at a particular spatial point [Fig. 84(b)], and showed that the two measurements superposed precisely [Fig. 84(c)].

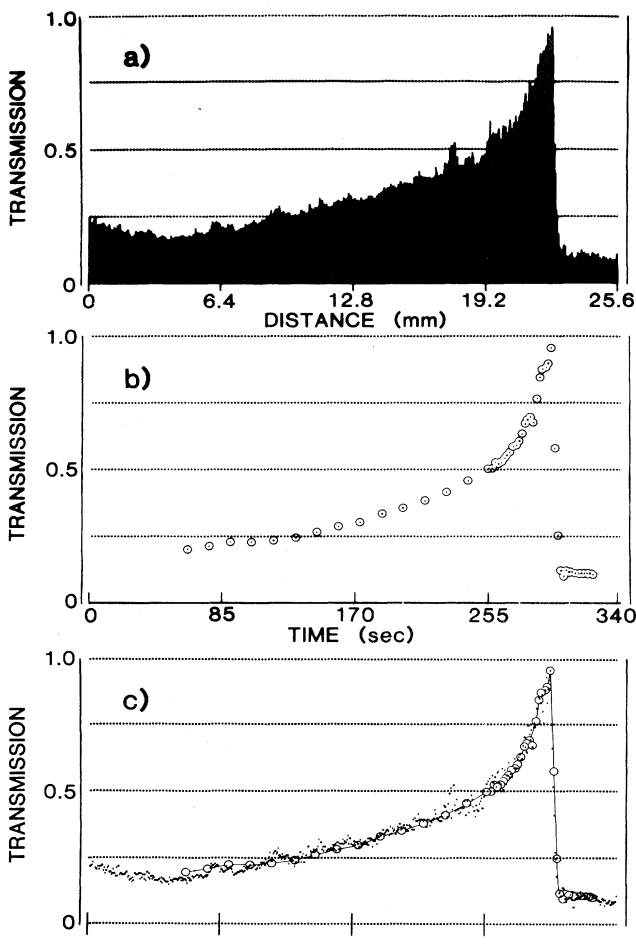


FIG. 84. Profile of a propagating pulse in the Belousov-Zhabotinsky reaction. (A) shows the spatial profile measured at an instant of time by light transmission. (B) shows a similar measurement, but at a fixed point as a function of time. The superposition (C) demonstrates that the pulse is indeed propagating with a constant shape and velocity. (From Wood and Ross, 1985.)

3. Wave trains and target patterns

Successions of pulses are produced periodically in target patterns, the outer regions of which form periodic wave trains which can be compared to the one-dimensional theories discussed in Sec. X.A.5 above. On a qualitative level, the characteristic shape derived by Tyson and Fife (1980) from the Oregonator model, i.e. the succession of sharp wave fronts and diffuse wave backs, agrees well with observations by Wood and Ross (1985), Bodet *et al.* (1987), Müller *et al.* (1987), and Pagola and Vidal (1987). Moreover, the existence of “reducing waves” observed by Smoes (1980) in a system which is in the oxidized state at equilibrium is another qualitative confirmation of the Tyson-Fife theory.

On a more quantitative level, one can set up waves of varying frequencies and attempt to check the calculated dispersion relation. Somewhat surprisingly, a quantitative comparison was carried out only rather recently, in experiments by Pagola, Ross and Vidal (1988), whose results are shown in Fig. 83. The two sets of data actually represent the same measurements, the differences being due to uncertainties in the scaling factors necessary to convert the experimental points to dimensionless units. Specifically, the crosses were obtained using the values of Tyson and Keener (1988), and the circles correspond to an equally plausible set of scale factors adjusted to fit the maximum velocity. The agreement between experiment and theory, which for the crosses involves no adjustable parameters, is in our view encouraging, though the remaining uncertainties associated with the precise relationship between the simple model and the complicated chemistry appear difficult to overcome. This means that many of the subtleties associated with the details of wave propagation in this system are unlikely to be tested quantitatively by experiment. On the other hand, the measured dispersion relation is in good semiquantitative agreement with the theory based on the Oregonator model and certainly different from the perturbative result obtained from the simple phase equation (4.90). This means that we are far from the limit of nearly harmonic waves discussed in Sec. V.B, for which the frequency is almost constant and the velocities vary significantly.

Target patterns have been observed in both excitable and oscillatory reagents. A quantitative experiment in the oscillatory case was performed by Vidal *et al.* (1986), who measured the histogram of wave speeds and periods for a distribution of roughly 100 targets, and found reasonable agreement with the theoretical expectation of constant speed and varying periods (see Tyson, 1987; Vidal, 1987).

Apart from the dispersion relation of the targets, one can ask for the details of the core structure, but this is difficult to observe, since the characteristic core size turns out to be $r_c \sim (D_1/v) \sim 0.2$ mm, as compared to the wavelength $\lambda = 2\pi v/\omega$ which is roughly 2 mm. An interesting suppression of amplitude at the center of a target on a scale of $2 \text{ mm} \approx 10 r_c$, was observed by Pagola

and Vidal (1987). Although the explanation for this effect is not certain, it has been suggested by the authors that it results from the finite thickness of the system, which leads to curvature in the third dimension and could distort the optical measurements of wave intensity.

The most interesting question which has been raised about target patterns concerns their origin as excitations of the system. For excitable reagents it has been found that filtering the medium essentially eliminates spontaneous formation of targets, so it is reasonable to infer that targets are caused by extrinsic dust particles, as discussed above. For certain oscillatory reagents, on the other hand, Vidal *et al.* (1986) reported that filtering did not suppress the appearance of targets, which makes an explanation in terms of spontaneous fluctuations, or noise, more plausible. This noise can itself be either extrinsic to the chemistry, for example thermal noise as suggested by Walgraef *et al.* (1983) and Aguado and Sagues (1990), or intrinsic, i.e. noise caused by chaotic dynamics (Coullet *et al.*, 1987). The strength of thermal noise may be estimated by a formula analogous to Eq. (8.63) for convection

$$F_{\text{th}} = k_B T / \rho \ell D^2 , \quad (10.37)$$

where ℓ is a characteristic core size, D is a diffusion constant and ρ the mass density of the chemicals. Inserting the values $\ell = 0.2$ mm, $D = 10^{-5}$ cm²/s, $\rho = 1$ g/cm³ and $T = 300$ K we find $F_{\text{th}} \approx 0.02$, an intriguingly large value. Chaos, on the other hand, seems ruled out experimentally since the subsequent propagation of the structures is highly regular. Of course, no detailed study exists of the effect of noise on realistic targets based on the Oregonator, but the stochastic mechanism bears further investigation.

An amusing explanation of the appearance of targets has been proposed by Tyson (1987): since it is easier to initiate a target in an oscillatory medium (all that is needed is to increase the frequency locally) there may be dust particles which will be effective in an oscillatory mixture but ineffective in the excitable case. If these particles were too small to be properly filtered in the experiment of Vidal *et al.* (1986) this would explain the persistence of targets in the oscillatory medium. There is a simple and elegant test of this catalytic-particle hypothesis, which was suggested originally by Winfree and Tyson, and was attempted by Agladze and Krinsky (1984). In a system containing filtered oscillatory reagent in which targets have spontaneously appeared, one can erase these structures by creating a high-frequency wave train by external stimulation. When this external source is turned off it leaves behind a phase-gradient which will oscillate at the frequency ω_0 of the medium, with perhaps some spatial structure due to the gradients. If the original targets were created by catalytic particles they should reappear in roughly the same locations and with the same frequencies as before! The experiment of Agladze and Krinsky did find evidence that the targets reappeared in the same place, but the authors did not discuss their frequencies,

nor did they specify whether the solution was filtered. A more careful experiment in filtered oscillatory medium should, however, provide important clues concerning the origin of targets.

4. Spirals and the effects of curvature

Spiral patterns offer perhaps the best test of the theory, since as discussed earlier the core structure determines the frequency and speed of the pattern which can be measured accurately at large distances. Also, spirals are easily created (in pairs) by breaking a wave crest at a point. Müller *et al.* (1987) have obtained a detailed picture of the core of a spiral pattern by measuring the light absorption due to the ferroin component, in a direction perpendicular to the sample. The result is shown in Fig. 85(b) next to a numerical simulation of the Oregonator model presented in part (a). The corresponding point on the dispersion relation agrees well with the solid diamond shown in Fig. 83, within the uncertainties of the transformation from physical to dimensionless units. No quantitative comparison has been made of the experimental and theoretical core structures, but it seems clear from Fig. 85 that the agreement is at best semiquantitative.

Müller and co-workers also measured the overall shape of their spiral and compared the results to the Archimedean spiral, Eq. (5.131), which has $r_c = 0$, as well as to the involute spiral, Eq. (5.133), with $r_c = q_\infty^{-1}$. In both cases the fit turns out to be quite good, but the resolution in the core region is insufficient to determine the phenomenological parameters as was done by Keener and Tyson (1986) in the model calculations.

Another test of the eikonal equation (5.117) was devised in an ingenious experiment by Foerster *et al.* (1988). These authors studied the high curvature region where two circular waves collide and annihilate. The rate of advance of the cusp thus produced can be measured and also calculated using the eikonal approximation. Using time-lapse photography the authors measured the curvature K and rate of advance v_n of the cusp, obtaining the data shown in Fig. 86. A fit to Eq. (5.117) produced a slope $D_1 = 2 \times 10^{-5}$ cm²/s and an intercept $v = 0.95 \times 10^{-2}$ cm/s, in excellent agreement with the bulk values of diffusion constant and velocity for this reagent. However, the linearity of the data out to $K \approx -0.6 (\mu\text{m})^{-1}$ is rather surprising, since one would expect corrections when the spatial scale reaches the core size $r_c \approx 2 \times 10^{-2}$ cm = 200 μm.

5. Further experiments on chemical reactions

A combination of hydrodynamic and chemical influences on patterns has been demonstrated by Agladze *et al.* (1984) in an experiment in which they prepared a pair of spirals in a closed dish, and then opened the system to the ambient air. After a short time, the waves in the spirals become perturbed and disordered and eventu-

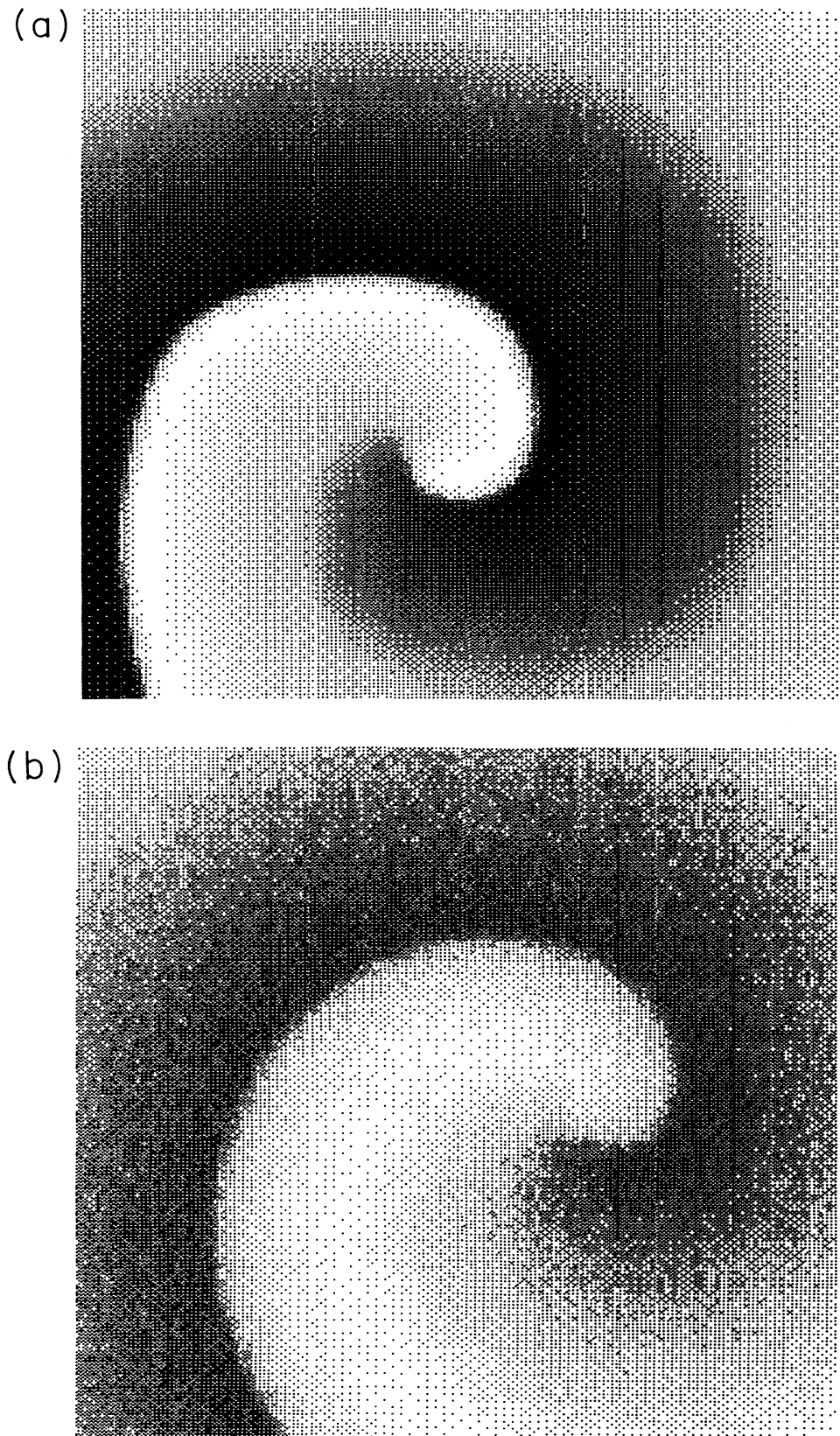


FIG. 85. Spiral core in the Belousov-Zhabotinsky reaction. Comparison of numerical simulations (a) and experimental observation (b). (From Tyson and Keener, 1988.)

ally break up into a chaotic set of small spiral patterns which are continuously created and destroyed. The authors attribute the phenomenon to the interaction of the BZ spirals with *stationary* cellular convective structures, due to surface-tension driven hydrodynamics instabilities in the fluid formed by the chemical reagents.

One of the main limitations of current experimental work on spatial patterns in chemical reactions stems from their operation as closed systems, which therefore run down in finite time (typically less than 100 periods of oscillation). Recently, this problem was overcome by a number of groups (see Castets *et al.*, 1990, and references therein). In particular Noszticzius *et al.* (1987) and Tam *et al.* (1988) constructed a novel type of unstirred *open* reactor in which the chemical reaction occurs in an annular inert gel fed with reagents at the inner and outer rim. In a variant of this original system Skinner and Swinney (1990) were able to make long-time measurements of tip motion in a spiral pattern, and to observe transitions from simple to compound rotation (periodic to quasiperiodic time dependence) as a control parameter is varied.

A goal that for a long time had eluded experimentalists is the seemingly simple one of finding chemical systems with stationary periodic (I_s) structures (Borckmans *et al.*, 1987). As we have seen earlier, the simplest way to obtain such patterns is to choose two substances with sufficiently different diffusion constants [cf. Eq. (2.8)]. Since this appears difficult to accomplish in practice, alternative schemes have been investigated, whereby spatially varying solutions stemming from nonlinear instabilities of a uniform state are obtained in systems with equal diffusion coefficients (Vastano *et al.* 1990). Alternatively, instabilities can be found in systems with macroscopic gradients. Patterns along the gradient are compatible with equal diffusion coefficients of the species (Elezgaray and Arneodo, 1991), but patterns transverse to the gradient (e.g. along an interface separating low- and high-density regions) require a nonscalar diffusion matrix (Boissonade, 1988). General conditions for the appearance of stationary patterns in the presence and absence of gradients have been given by Pearson and Hortschmek (1989), Pearson (1992), and Pearson and Bruno (1993).

On the experimental side considerable progress has recently been achieved, either by creating macroscopic concentration gradients, or by finding methods to enhance the contrast in diffusion constants. Ouyang *et al.* (1989, 1991) reported the observation of a stationary Turing structure in an open chemical reactor in which a macroscopic one-dimensional gradient was imposed externally. The pattern forming stationary instability then occurs along the gradient, and it does not require chemical species with differing diffusion constants. The authors used a "Couette reactor" for which the active chemicals are placed between concentric rotating cylinders, so that the diffusion constant is enhanced by factors of $10^3 - 10^6$ through turbulent mixing, and the characteristic instability length $\ell \sim (D/a)^{1/2}$ [see Eq. (2.8)] is correspondingly

enhanced. The chemical gradients, on the other hand, are along the cylinder axis so they may be controlled independently.

Following suggestions by Borckmans *et al.* (1987) and Boissonade (1988), Castets *et al.* (1990) have recently constructed a different type of unstirred open reactor in which a difference of diffusion constants for the chlorite-iodide-malonic acid reaction is achieved by immersing the chemicals in porous substances (a gel and vycor glass) which affect the diffusion of the constituents differently (see Lengyel and Epstein, 1991). Although their system contained a significant concentration gradient the pattern was transverse to the gradient, and its appearance resulted from the difference of diffusion constants, not from the gradient. Indeed, Ouyang and Swinney (1991a,b) subsequently constructed a reactor without macroscopic gradients and were able to obtain the stationary Turing patterns shown in Fig. 87, with reproducible transitions between uniform, striped, hexagon, and mixed patterns as a function of temperature and concentration. These remarkable recent achievements signal the advent of a new controlled system for the study of spatiotemporal patterns (see Barras and Walgraef, 1992).

6. Nonlinear dissipative waves in other systems

The Oregonator model of Eqs. (10.1)–(10.2) is a prototype for a number of other type-III_o systems with oscillatory or excitable dynamics. Various examples from biology, ecology, and chemistry, taken from Tyson and Keener (1988), are listed in Table III. The basic parameters determining the speed of wave propagation are, according to Luther's law, Eq. (10.11),

$$v_{\text{dim}} \sim (k_1 D_1)^{1/2}, \quad (10.38)$$

where k_1 is a first-order rate constant and D_1 is the diffusion constant of the propagator species. In Table III we list these parameters for various examples of nonlinear dissipative wave phenomena occurring in nature, whose speeds range over a factor of 10^5 ! A more extensive discussion may be found in Vasiliev *et al.* (1979).

Finally, let us cite some references to the extensive literature on purely numerical simulations of chemical and biological patterns based on reaction-diffusion equations and on discretized models, e.g. Pertsov *et al.* (1984), Ermakova *et al.* (1989), Lugosi (1989), Tainaka (1989), Barkley *et al.* (1990), Gerhardt *et al.* (1990), Wu *et al.* (1991).

XI. BIOLOGICAL PATTERNS

The theoretical models used to study biological self-organization are often identical to those discussed in the rest of this article, so it is appropriate to include biological patterns in our review. We are of course dealing with a gigantic topic with a long history of results and conjectures and a host of open questions. Our aim is to elucidate the principal mathematical concepts used by biolo-

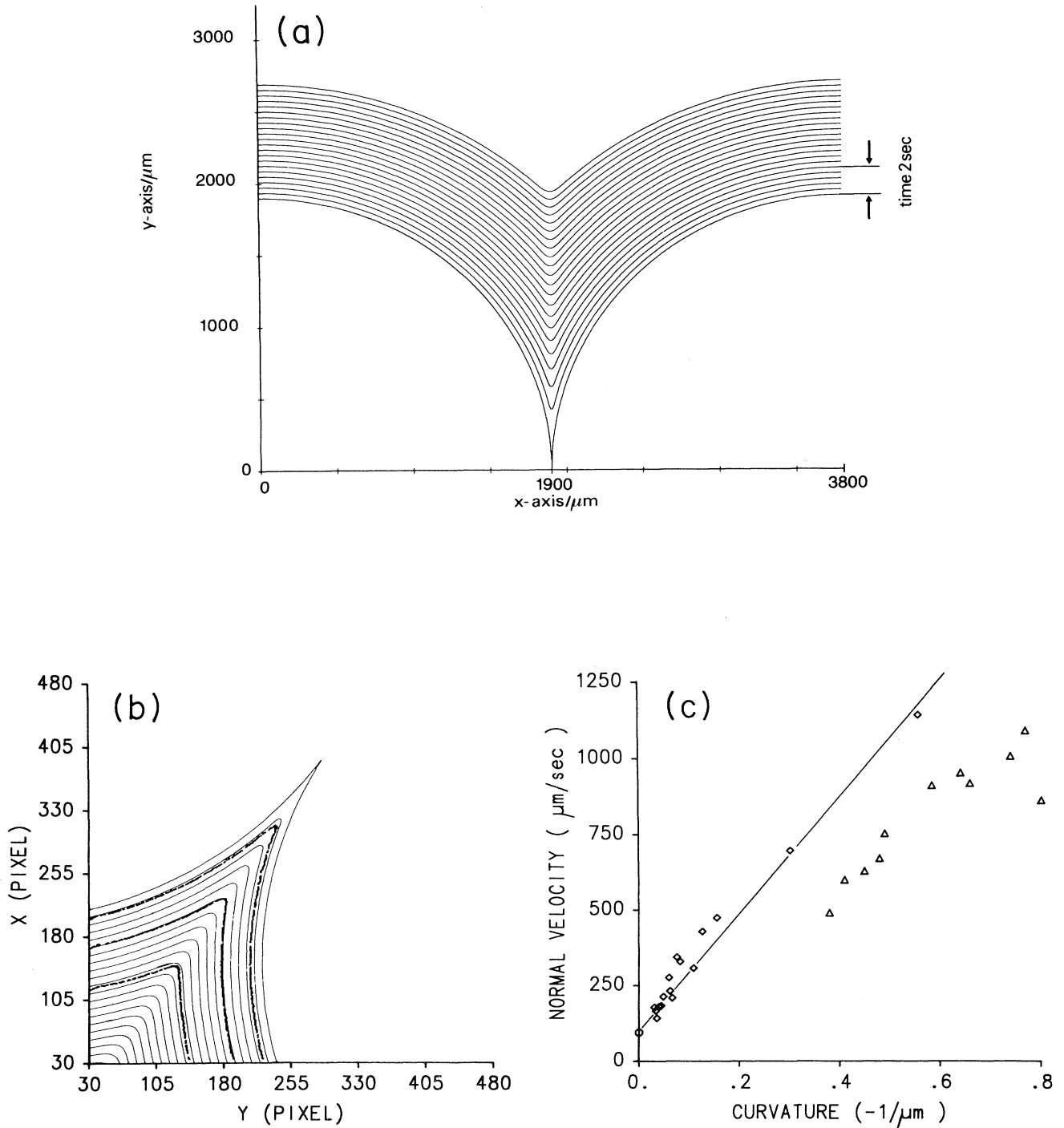


FIG. 86. The effects of curvature on pulse propagation: comparison between experiment and the eikonal equation (10.29). (a) Numerical solution of the eikonal equation for equal time intervals, using parameters v_n and D determined experimentally, for a cusp region such as forms at the boundary between two colliding circular waves. (b) Superimposed experimental (dots) and numerical (lines) measurements of a cusp structure. The time interval between calculated contours starting at $t=0$ is 0.4 s. Experimental results are for $t=0.52$, 1.96 and 4.2 s. Spatial resolution is 4.5 μm per pixel. (c) Relation between curvature and normal velocity determined from cusp structures with spatial resolution 4.5 μm (diamonds) and linear fit showing good agreement with the eikonal equation. (Triangles come from lower resolution measurements.) (From Foerster *et al.*, 1988; Copyright 1988 by the AAAS.)

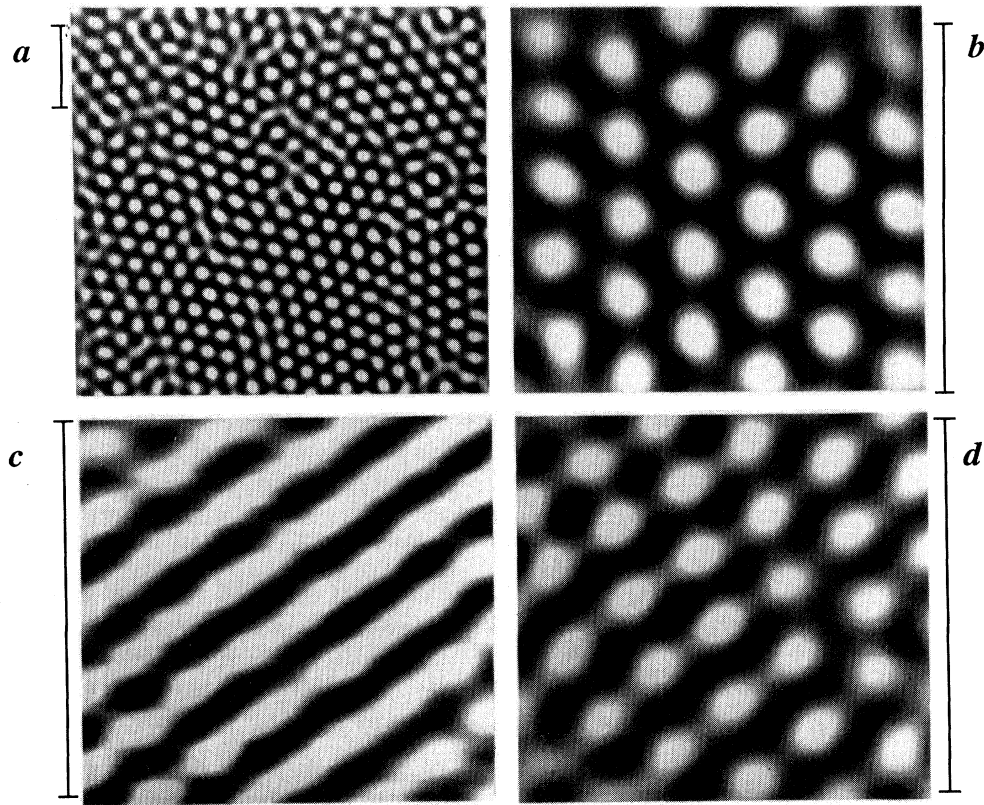


FIG. 87. Stationary Turing patterns in a continuously fed reactor. (a) and (b) hexagons; (c) stripes; (d) mixed state. Light and dark represent the yellow and blue colors of an indicator for the I_3^- concentration in a chlorite-iodide-malonic acid reaction. Patterns (a) and (d) coexist for the same parameter values, whereas (b) and (c) are given by different reactant concentrations. (From Ouyang and Swinney, 1991a; reprinted with permission from Nature, Copyright 1991 Macmillan Magazines Limited.)

gists, and to present a number of examples of applications of these concepts to specific systems.

The study of biological patterns involves two basic ingredients: developing a model which incorporates the main mechanisms and properties under consideration, and analyzing the behavior of the model as a function of its parameters. Due to the complexity and richness of the systems studied, the first phase is by far the most challenging and important one for biology, but it is in large measure beyond the scope of our discussion. We will focus on the second step, since it turns out that at least on an elementary and semiquantitative level the relevant behavior can be inferred by analogy with the preceding discussions of hydrodynamic and chemical models. We will thus for the most part accept the equa-

tions that have been proposed in the literature to describe biological phenomena (see, e.g. Jäger and Murray, 1984; Levin and Segel, 1985; Perelson *et al.*, 1988; Murray, 1989), without inquiring into their justification at the molecular or cellular level. It should be noted, of course, that even if a model accounts reasonably well for the observed phenomena, the molecular picture on which it is founded could be quite incorrect, since the cooperative behavior is often insensitive to the underlying mechanisms. At the somewhat superficial level at which we wish to describe the phenomena this universality is advantageous, but we do not wish to minimize the importance of a detailed molecular understanding of the systems under study.

We will discuss two broad classes of phenomena in-

TABLE II. State variables of some representative excitable media.

System	Propagator (trigger variable)	Controller (recovery variable)
Neuromuscular tissue	membrane potential	ionic conductance
Belousov-Zhabotinsky reaction	bromous acid	ferroin
Dictyostelium discoideum	cyclic AMP	membrane receptor
Epidemics	infectious agent	level of immunity

Table III. Characteristic parameters.

System	Rate constant k_1	Diffusion constant D_1	Wave speed $v = (k_1 D_1)^{1/2}$
BZ reaction	0.2/s	$2 \times 10^5 \text{ cm}^2/\text{s}$	$4 \times 10^{-3} \text{ cm/s}$
Squid giant axon	$3 \times 10^3/\text{s}$	$3.4 \times 10^2 \text{ cm}^2/\text{s}$	10^3 cm/s
Cardiac action potentials	$3 \times 10^2/\text{s}$	$0.6 \text{ cm}^2/\text{s}$	13 cm/s
Cyclic AMP waves in Dictyostelium	$10^{-2}/\text{s}$	$4 \times 10^{-6} \text{ cm}^2/\text{s}$	$2 \times 10^{-4} \text{ cm/s}$
Spread of rabies epidemic by foxes	160/year	200 km^2/year	180 km/year $\approx 1 \text{ cm/s}$

volving spatial patterns: stationary (or slowly varying) patterns that occur in *morphogenesis*, and time-dependent patterns involving *propagating waves*.

A. Morphogenesis

1. General features

Morphogenesis is the development of structure during the growth of an organism. Nowadays, it is widely believed that morphogenesis proceeds sequentially, with finer stages of differentiation laid down on broader features of previous processes. Nevertheless, at the earliest stages of development there arises the question of how spatial differentiation arises in a featureless medium. A mathematical form of this question concerns the breaking of a symmetry: one end of a symmetric egg will become the head and the other the tail. As with any broken symmetry, chance, i.e. fluctuations, can determine which is which, but this choice is only binary — the head will not appear in the middle of the embryo. As the organism grows different parts will develop quite different functions, despite the fact that the material of the embryo is rather homogeneous, at least at the level of the molecular chemistry controlling development. It is true that on its full scale, the embryo is not spatially uniform due to its finite size, and ultimately this limitation will play a vital role. The question remains of how this macroscopic nonuniformity is communicated to the smaller scales.

To explain how this *positional information* is established in the developing organism the existence of chemicals called *morphogens* has been postulated. The local concentration of these morphogens determines cellular development. The basic mechanism was proposed 40 years ago by Turing (1952), who pointed out that if the morphogens obey reaction-diffusion equations they may undergo *symmetry breaking* transitions, producing states with *spatial structure* which might explain the initial stages of development. We shall discuss a number of examples of such patterns below, but we note at the outset that the chemical identification of the morphogens has proved elusive, so that the theories are essentially phenomenological and contain little information on cellular processes.

One argument in favor of the reaction-diffusion mechanism is that with chemically reasonable reaction rates and diffusion constants the length and time scales of the patterns turn out to have the right order of magnitude. This might at first seem surprising, since the lengths obtained are not of molecular size, but rather on the order of microns or larger. According to Crick (1970) the answer lies in the slowness of the diffusion process, which involves large molecules and constrained motion, or hopping over barriers and across membranes. Since we do not, however, wish to further examine the chemical and biological basis for the models used, we will consider the variables and parameters as phenomenological quantities, whose interpretation need not be tied to any particular mechanism. Indeed Turing himself suggested the importance of other mechanisms, and more recently there have been attempts to construct detailed models that reflect known facts about embryonic cells and tissue. The main added ingredient is consideration of *mechanical forces* brought about by shape changes in the growing organism and by transport processes within the medium. The ensuing models are considerably more complex than those involving pure reaction and diffusion, but they presumably incorporate more biological information and they can be tested in more detail (Perelson *et al.*, 1986).

It has been emphasized by Oster (1988), that nearly all models of biological pattern formation involve the interplay between *local activation and lateral inhibition*. From our point of view, this may be interpreted in terms of the condition (2.8) for a type I_s instability in a two-variable reaction-diffusion system, namely

$$2q_0^2 = a_1/D_1 - a_2/D_2 = \ell_1^{-2} - \ell_2^{-2} > 0. \quad (11.1)$$

As mentioned in Sec. II.E this condition states that the diffusion length ℓ_1 for the activator is less than that for the inhibitor, ℓ_2 . Of course within the model (2.7) the condition (11.1) is necessary, but not sufficient: it is also necessary that the system be above threshold, which for (2.7) means that the cross-couplings b_1 and b_2 not be too large. Moreover, (11.1) is by no means a general necessary condition for a type I_s instability. For example, the Swift-Hohenberg model can be interpreted in terms of an off-diagonal diffusion matrix [see Sec. III.C.2] for which Eq. (11.1) does not apply. In our view, therefore, although the notion of local activation and lateral inhibi-

tion is intuitively appealing, it is somewhat restrictive. We prefer the more general concept of type I_s instability.

There are many reviews of theoretical models of morphogenesis, to which we refer the reader (Meinhardt, 1982, 1992; Belintsev, 1983; Segel, 1984; Malacinsky and Bryant, 1984; Perelson *et al.*, 1988; Murray, 1989). Here we wish to place some of these ideas into the framework developed in the previous sections. We will first focus on general principles of methodology, and then study the behavior of specific models which have appeared in the literature. We will attempt to distinguish between results that are robust to small changes in the model, and those that depend more specifically on the detailed assumptions and approximations.

2. Theoretical concepts

a. Positional information

In forming a complex organism different levels of subtlety can be hypothesised for the pattern formation and for subsequent interpretation of a morphogen. A simple gradient of concentration, formed as the diffusion field of a source and sink, could lead to complex segmentation if the subsequent development depended very sensitively on the concentration level of the morphogen. However, such a mechanism seems particularly susceptible to perturbations (Oster, 1988), so the alternative of a Turing mechanism with a true (type I_s) finite-wavelength instability seems more plausible. Of course, if only a single half period of the pattern is present in the organism this again leads to a simple gradient, with subtle interpretation needed to give complex structure. On the other hand, many periods of the pattern and a simpler interpretation rule may apply. An example is the black-white interpretation of complex morphogenic fields in the theory of animal coat markings or shell patterns discussed in Sec. XI.A.5 below.

b. Length scales

The primary feature of the Turing instability is the determination of a length scale fixed by the parameters of the reaction-diffusion system. This has a natural application in explaining a variety of patterns obtained by fitting a fixed length scale phenomenon into varying domain sizes. However, there are immediate problems in accounting for the apparent scale invariance of other morphogenetic processes where the pattern does not change but merely expands for larger domain sizes. In the hydra studied in Sec. XI.A.4 below, changing the overall size does change the resulting development somewhat. This "allometric shift" has been modelled (MacWilliams, 1982) using standard reaction-diffusion equations, but the requirement that similar results be obtained when the length scale is changed by a factor of five places severe,

perhaps untenable constraints on the model. Othmer and Pate (1980) have proposed an ingenious scheme within the reaction-diffusion framework for achieving scale invariance. They propose that the diffusion coefficients of the morphogens are no longer constant but are proportional to the concentration $w(x, t)$ of an additional diffusing species. This species has a uniform source density but does not otherwise react, and has a zero value on the boundaries (i.e., the boundaries are absorbing or leaky). It is then clear that in the steady state w is proportional to L^2 , where L is a typical linear dimension of the domains. Diffusion constants for the morphogens proportional to L^2 then produce scale-invariant patterns. Less precise scale invariance can be achieved, if desired, by modifying the boundary conditions on w . It seems unlikely, however, that this specific mechanism could provide a universal solution to the problem of scale invariance and there seems to be no direct experimental confirmation. Nevertheless, the scheme does demonstrate the possibility of exact or approximate scale invariance within reaction-diffusion systems.

c. Boundary effects

Biological systems are generally quite small ($Lq_0 \approx 1 - 10$), and the patterns are therefore strongly influenced by boundary conditions. As we have seen in Sec. V.A boundary effects are important in a number of ways. Often no-flux boundary conditions are assumed for the diffusing substance, since they are intuitively reasonable from the chemistry, but they are rather special from the point of view of pattern formation. In particular, the resulting behavior is quite analogous to that resulting from idealized periodic boundary conditions in that there is no systematic shift in threshold as the size is reduced (see Sec V.A.1). Also, pattern selection is particularly weak since for each linearly unstable solution with wave number q there is a corresponding nonlinear solution near threshold, and so for $Lq > 1$ there are typically many possible nonlinear steady-state solutions. This leaves unanswered the difficult question of the selection of a unique pattern from the many possibilities, presumably a requirement for robust development.

As we have seen, more general boundary conditions will reduce the choice of solutions, so it is important to distinguish the different roles the boundaries may play. First, boundary constraints may *select* patterns, reducing the number of steady-state solutions. Second, inhomogeneous boundary conditions, inconsistent with a spatially uniform solution, may drive the growth of a particular mode, yielding a preferred solution by changing the *transient evolution* (see below). Arcuri and Murray (1986) have investigated one-dimensional reaction-diffusion equations with both inhomogeneous and rigid boundary conditions, and indeed find a greater selectivity in the former case. Their results can perhaps be usefully analyzed in terms of the above two effects.

d. Initial conditions and transient evolution

If the static analysis of models with the usual no-flux boundary conditions does not yield a unique solution, we must look to the dynamics of the system to understand pattern selection. The evolution will then depend on small effects that initiate the growth from the homogeneous solution $U=0$. One can distinguish the following broad classes of growth conditions:

- An initial condition $U(x,0)=U_0(x)$ is specified on the full spatial domain Ω , with a function $U_0(x)$ which might be regular or disordered. This procedure corresponds to the usual one in dealing with physical systems.

- A pattern is produced in part of the domain Ω and then allowed to expand in successive steps. Examples are aggregation or front propagation models, or row by row growth of an organism (e.g. a mollusk, see Sec. XI.A.5.6 below).

- A natural procedure for biological systems is to consider the spatial domain Ω to be a function of time $\Omega(t)$. Then the dynamics of the differential equations will be supplemented by the stretching of the domain. In the simplest case one might assume that the time scale for variation of $\Omega(t)$ is slow, but nevertheless the final pattern obtained might be very different from the one which would be produced by specifying an initial condition on the fully grown domain $\Omega(t_{\text{final}})$. We are not aware of any systematic studies of the influence of preparation protocols on the final pattern.

- A source term may be added to the equations, thus making the bifurcation imperfect (see Sec. III.A). This may either be through inhomogeneous boundary conditions, or via a distribution of sources of the morphogens within the material. Typically these terms are small and they only determine the evolution when the solution amplitudes are themselves small, while not strongly perturbing the shape of the final nonlinear solution they select. Since to favor the growth of particular modes the sources must break the symmetry and spatial homogeneity, one is then left with the problem of explaining what lays down the pattern of sources. Nevertheless, models with sources have been widely studied, an example being the hydra model discussed below.

3. Modeling the phenomena

The usual procedure adopted in the literature when studying pattern forming models is to choose a particular set of equations with specified parameters and to solve these equations numerically, modifying the parameters until the pattern obtained is a reasonable representation of experiment. It is often difficult to know which aspects of the model are essential and which could be dispensed with or modified. In line with our earlier discussion we would advocate a somewhat more systematic study which seeks to clarify the following issues:

- What is the pattern forming behavior of the model under ideal conditions, i.e. in an infinite geometry with

no sources? Specifically we are thinking of the bifurcation structure as different parameters are varied.

- Is the system near enough to a threshold so that linear instabilities are relevant to the observed patterns?
- How do boundaries and sources modify the behavior?
- What is the effect of discretizing space and/or time? Is this a mathematical approximation or does it have biological significance?
- What is the effect of the growth protocol (see above)?

4. Transplantation and regeneration in hydra

Gierer and Meinhardt (1972) have presented a simple one-dimensional reaction-diffusion model to explain experiments on regeneration and transplantation in hydra after amputation. The hydra is a favorite system for experimentation because its structures regenerate rapidly, frequently within hours. Examples of findings on hydra are these [see Segel (1984)]: (a) If the head is removed, and a small region from just below the head is grafted onto the body, then a head region regenerates. (b) If the grafted piece extends somewhat farther toward the basal disk (i.e., if the graft is less “headlike”), then two heads regenerate. (c) If the graft of (b) incorporates yet more head material, then again only one head regenerates. (d) If a head is amputated and transferred to the anterior portion of the gastric region, then a new head regenerates. (e) If a head is adjoined to the posterior gastric region and the original head is later removed, then no new anterior head regenerates.

The Gierer-Meinhardt model consists of coupled reaction-diffusion equations for an activator $a(x,t)$ and an inhibitor $h(x,t)$,

$$\partial_t a = \rho_a(x)(c_a + c_a a^2/h) - \mu_a a + D_a \partial_x^2 a, \quad (11.2a)$$

$$\partial_t h = \rho_h(x)c_h a^2 - \mu_h h + D_h \partial_x^2 h, \quad (11.2b)$$

with no-flux boundary conditions on the domain $0 \leq x \leq L_H$. The activator is produced by an external source whose density is $c_a \rho_a(x)$, where $\rho_a(x)$ is the density of activator producing cells, and c_a a rate constant which is then enhanced by the activation/inhibition term ca^2/h . Similarly the inhibitor is produced by cells of density $\rho_h(x)$ at an activated rate $c_h a^2$. The densities $\rho_a(x)$ and $\rho_h(x)$, usually taken to be equal, give a preexisting spatial inhomogeneity to the organism, as mentioned earlier.

In Fig. 88(a) we show the source function

$$\rho(x) = \rho_a(x) = \rho_h(x) \quad (11.3)$$

assumed by Gierer and Meinhardt, and the ensuing solutions $a(x)$, $h(x)$ they obtained numerically for the normally configured organism. A high concentration of the activator, which occurs near $x=0$ is assumed to lead to

the growth of a head. Figure 88(b) then shows how a short segment from the center (gastric) region regenerates a head, since it leads to a peak in the activator a . More complicated structures involving grafts are also shown in the figure. For example, it is possible to generate two heads, to inhibit growth of one of them, or to transplant the head from one end of the organism to the other. In each case the only assumption is that the source density $\rho(x)$, which is external to the model, is preserved during the various manipulations. To understand this behavior it is convenient to rescale the variables, defining

$$x' = x / \sqrt{D_a / \mu_a}, \quad (11.4a)$$

$$u_1 = a / [\mu_h c / \mu_a c_h], \quad (11.4b)$$

$$u_2 = h / [c^2 \mu_h / c_h \mu_a^2], \quad (11.4c)$$

$$s(x') = (c_h c_a / c \mu_h) \rho(x), \quad t' = \mu_a t, \quad (11.4d)$$

to give (dropping the primes on x' and t'),

$$\partial_t u_1 = s(x) + \rho(x) u_1^2 / u_2 - u_1 + \partial_x^2 u_1, \quad (11.5a)$$

$$\partial_t u_2 = Q [\rho(x) u_1^2 - u_2 + R \partial_x^2 u_2], \quad (11.5b)$$

$$Q = \mu_h / \mu_a; \quad R = D_h \mu_a / D_a \mu_h, \quad (11.5c)$$

the domain of definition being $0 \leq x \leq L = L_H (\mu_a / D_a)^{1/2}$, with no-flux boundary conditions at the ends. The important control parameter is now R , which represents the square of the ratio of inhibitor to activator decay lengths. The parameter $Q = \mu_h / \mu_a$ affects only the time evolution, not the steady states (rather like the Prandtl number in convection). Note that we have adopted the scalings of Segel (1984), except that we have chosen a different concentration scale so that the source term s may be chosen small. Finally, we normalize $\rho(x)$ such that

$$L^{-1} \int_0^L dx \rho(x) = 1, \quad (11.6)$$

which is always possible with proper choice of the constants c , c_a , and c_h in Eqs. (11.2). The extrinsic spatial inhomogeneity of Eqs. (11.5) is given by the functions $s(x)$ and $\rho(x) - 1$, which are not necessarily small compared to unity (see below). These two source functions are linked in the original model by Eq. (11.4d), but we will consider them as independent in (11.5). Apart from the source functions the parameters of the system (11.5) are R , Q , and L , as well as the number N of "cells," if a discretization is employed where the derivatives are replaced by nearest-neighbor coupling. Often Eqs. (11.5) have been discretized with an artificially small N to simplify the numerics. Then any N dependence is a spurious effect, and can certainly be eliminated with modern day computers, by going to larger N . The time variable is

continuous in either case, and any dependence on discrete time stepping should of course be eliminated.

To place the numerical work in context we will consider the usual linear stability analysis of Eqs. (11.5) for $s(x)=0$, $\rho(x)=1$. The homogeneous solution, stable to long-wavelength perturbations is $u_1=u_2=1$. The linear instability is of type I_s and leads to the instability curve $R(q)$ shown in Fig. 89, with onset parameters $R_c = (3-2\sqrt{2})^{-1} = 5.83$ and $q_0 = (\sqrt{2}-1)^{1/2} = 0.64$. For the hydra solutions of Fig. 88 the parameters are $R_H = 11.7$ ($\approx 2 R_c$) and the initial length [Fig. 88(a)] gives $L = 13.7$, so that the number of full periods which may be contained in the system at onset is $(L q_0 / 2\pi) = 1.4$. The wave number for maximum growth rate q_m gives a similar number. For this value of R the limits of the linear instability are $q_- = 0.325$ and $q_+ = 0.900$. The uniform homogeneous solution [with $\rho(x)=1$ and $s(x)=0$] is unstable to two wave numbers for $L = 13.7$, namely $q_2 = 2\pi/L = 0.46$ and $q_3 = 3\pi/L = 0.69$, leading to four possible final nonlinear solutions, as shown in Fig. 90. Note that according to Fig. 89 the mode with $q_1 = \pi/L = 0.23$, which would grow into the one-humped structure as in Fig. 88(a), decays in the linear stability analysis for $R = 11.7$. It does not develop from a small perturbation of the homogeneous solution in the absence of a spatially dependent source. Such a solution can, however, be formed by applying a large amplitude initial perturbation with wave number q_1 . Therefore in the absence of preexisting inhomogeneities the reaction-diffusion system (11.5) would lead to strange looking hydra!

Let us now consider the system with the sources $s(x)$ and $\rho(x)-1$ employed by Gierer and Meinhardt which, according to Eq. (11.4d) and the parameters listed in the caption to Fig. 88, turn out to be

$$s(x) = 1.5 \quad \rho(x) = 0.27 \exp(-0.16x). \quad (11.7)$$

Solving Eqs. (11.5) with the sources (11.7) numerically, starting from spatially uniform initial conditions, we find the solutions shown in Fig. 91, which have the sought-after one-humped structure. If we now turn off the sources (i.e. set $s=0$, $\rho=1$), the subsequent relaxation of the solutions, also shown in Fig. 91, is rather small and does not spoil the qualitative shape. Thus it is the sources $s(x)$ and $\rho(x)-1$, which are not small in any sense, that allow one to achieve a solution with characteristic wave vector $q_1 \approx \pi/L$ starting from uniform initial conditions. This wave vector is considerably smaller than the most unstable wave vector, which according to Fig. 89 lies between q_2 and q_3 . In this way, however, subsequent runs with more uniform sources and smaller domains, as in Fig. 88(b) or (i) for example, will still lead to a one-humped structure, albeit with a larger characteristic wave vector.

From these remarks we can come to the following conclusions concerning the Gierer-Meinhardt model: The symmetry-breaking character of the type I_s Turing insta-

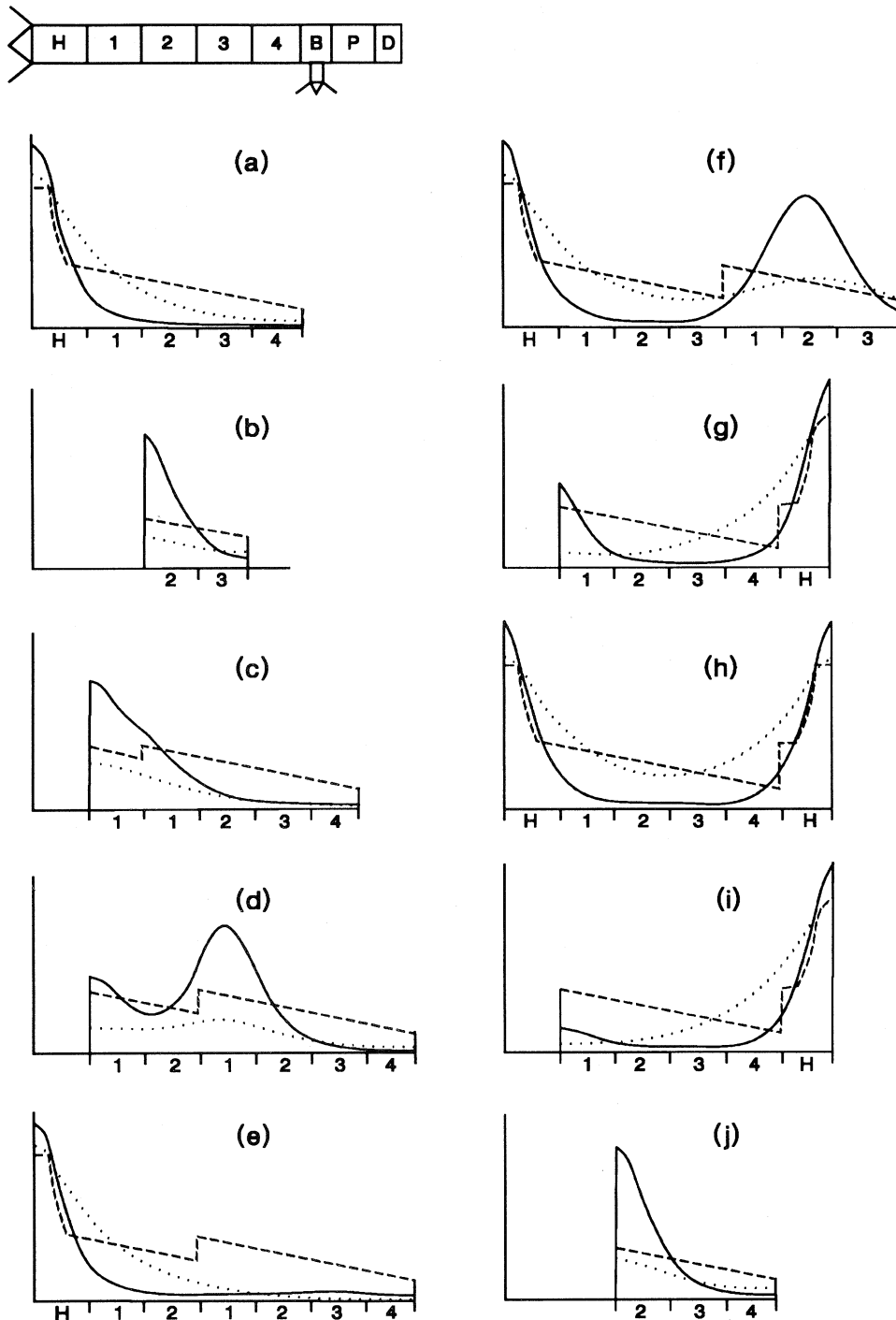


FIG. 88. Gierer-Meinhardt model of hydra. Top figure shows schematic representation of hydra with different sections labeled. Panels (a)–(j) represent predictions for various section and grafting experiments. The assumed source distribution is denoted by the jagged solid line and the resulting concentrations are shown by the solid line (activator, a) and the dash-dotted line (inhibitor, h), respectively. A head is assumed to form in regions of high concentration of activator. (a) Normally configured organism. (b) Short section from center regenerates head. (c) Graft of additional section 1 onto body formed of sections 1234 (we will denote this as 1/1234); head forms only at front end. (d) Graft of additional 12 sections onto 1234 body (12/1234): a secondary head is predicted. (e) Graft H12/1234: H inhibits secondary head formation. (f) Graft H123/123: H does not inhibit secondary head formation. (g) Graft of head onto back end: secondary head develops. (h) Second head is grafted onto back end. (i) Original head in (h) is cut after 10 hours: no second head develops at 1. (j) Section 234 cut from (i) develops head at 2. [Parameters used in Eqs. (11.2) were $c_a = 7.5 \times 10^{-4}$, $c = 0.05$, $\mu_a = 0.0035$, $D_a = 0.03$, $c_h = 0.025$, $\mu_h = 0.0045$, $D_h = 0.45$. Source distributions $\rho_a(x) = \rho_h(x) = \rho(x)$ are shown with full scale corresponding to $\rho = 3.2$.] (From Gierer and Meinhardt, 1972.)

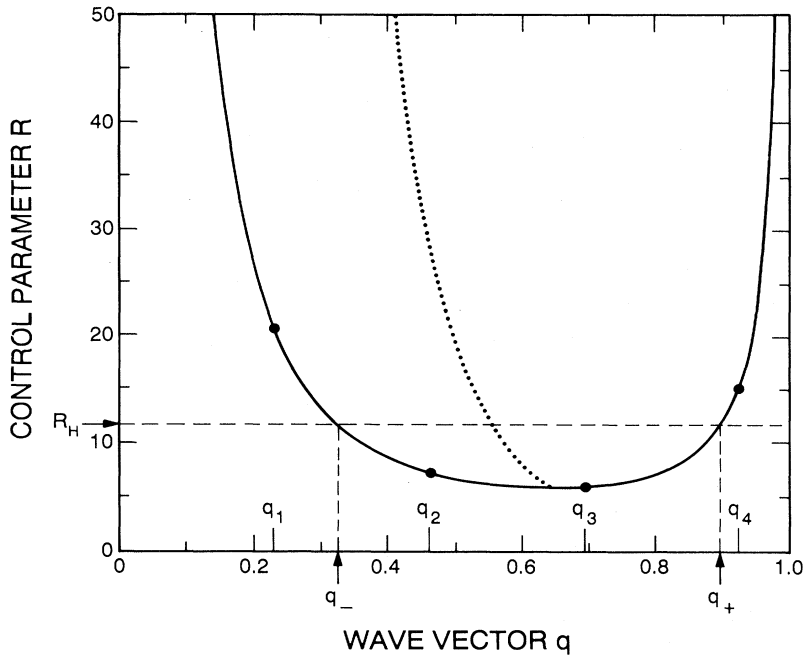


FIG. 89. Linear stability analysis for the Gierer-Meinhardt model (11.5) in an infinite system, with $s(x)=0$ and $\rho(x)=1$, showing neutral stability (full line), in a plot of control parameter R vs wave vector q . Dotted line is the wave vector $q(R)$ of the fastest growing mode. R_H is the control parameter value used in the modeling in Fig. 88, for which the band of unstable wave vectors extends from q_- to q_+ . The wave vectors called q_1 to q_4 are the discrete linear modes for the system size chosen in Fig. 88, and the corresponding values of R for these modes to begin to grow are indicated by solid circles.

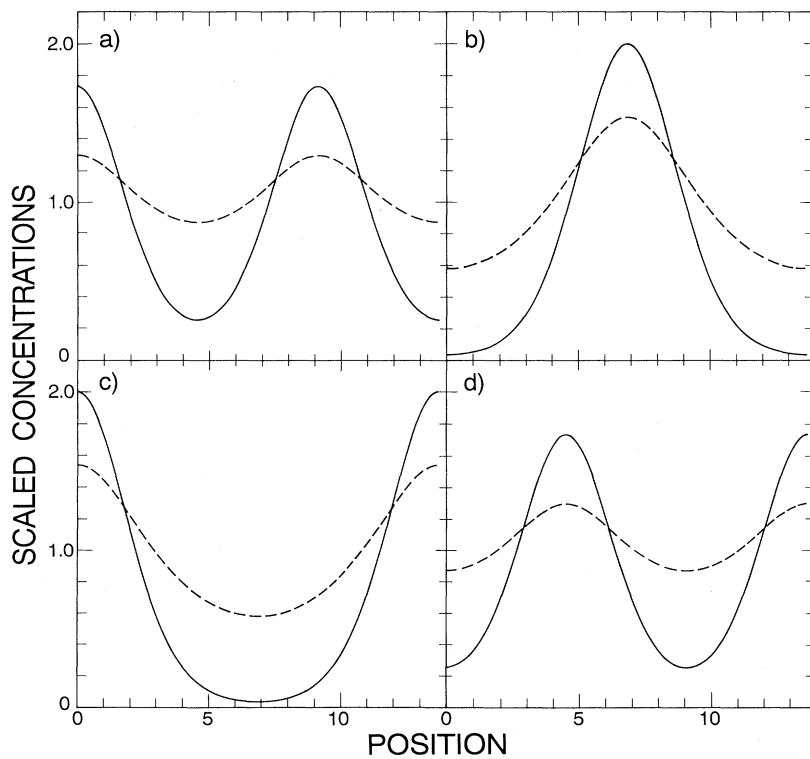


FIG. 90. Linearly growing modes in the absence of inhomogeneous source terms for the Gierer-Meinhardt model of hydra (11.5), showing scaled activator concentration u_1 (full line) and inhibitor concentration u_2 (dashed line) with the parameters used by Gierer and Meinhardt (1972). Panels (b) and (c) correspond to mode q_2 and (a) and (d) to mode q_3 in Fig. 89.

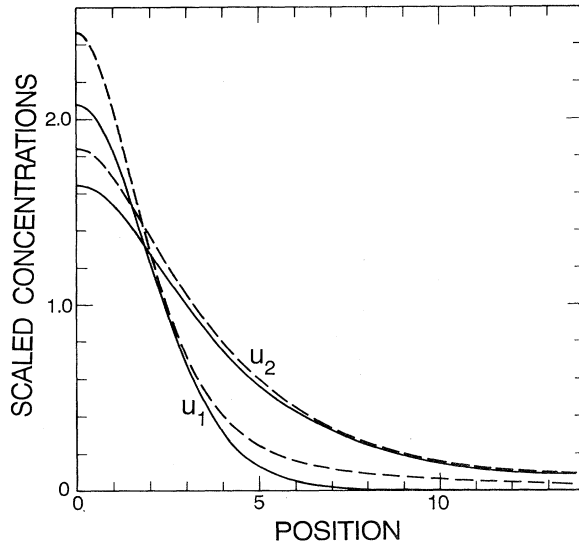


FIG. 91. Solutions for scaled activator concentration u_1 and inhibitor u_2 as a function of position, in the presence of inhomogeneous source terms used by Gierer and Meinhardt (1972), Eq. (11.7) (full lines). The dashed lines show the relaxation if the source terms are subsequently eliminated [i.e., $s(x) \rightarrow 0$, $\rho(x) \rightarrow 1$].

bility is not playing any role in the hydra simulations in Fig. 88; there are strong, externally imposed symmetry breaking effects represented by the inhomogeneous source density $\rho(x)$. The reaction-diffusion system is essentially used to amplify and smooth out this extrinsic inhomogeneity so as to reproduce the regeneration experiments. The critical length in the model is rather larger than the naive estimate. The length L of the normally configured organism is considerably larger than the characteristic length π/q_0 which gives a simple gradient solution in the absence of sources. This choice was presumably forced on the model to allow for the gradient solution in the hydra of reduced size in Fig. 88(b).

MacWilliams (1982) has presented a refinement of the Gierer-Meinhardt model which has somewhat different local chemistry, and only a small inhomogeneous additive source $s(x) \ll 1$, $\rho(x) = 1$. Although the model contains more parameters than Eq. (11.5), these have been estimated rather accurately by fitting to various transplant experiments. The model was then tested on six further experiments and, according to MacWilliams, the results were quite satisfactory. We have also carried out a linear stability analysis of this model and find that the qualitative behavior is similar to that of the Gierer-Meinhardt equations. Specifically, even though the external source is small, the mode selected in the normally configured organism, analogous to the one in Fig. 88(a), corresponds once again to a wave vector at the edge of the unstable band, a factor of 5 smaller than the critical wave vector q_0 . The source term is therefore again very important in favoring the right solution over

the ones that grow faster in the homogeneous system. (Once the solution is obtained its subsequent relaxation after turning off the source is quite small, just as it was with the Gierer-Meinhardt equations.) We conclude that the MacWilliams model is primarily useful to describe the regeneration and transplant experiments, but it does not account for the symmetry breaking and spatial inhomogeneity, which are essential for growing a normally configured organism.

Finally we mention a model by Kemmner (1984) with the important new feature that the inhomogeneous distributions are now *active* chemicals which react with rates controlled by the diffusing activator and inhibitor concentrations (but do not themselves diffuse). No inhomogeneity is imposed externally, and so this model aims to account for the fundamental symmetry breaking of the development, in addition to the regeneration. The model is unfortunately quite complicated, with rates depending on concentrations at various *earlier* times, so we refer the reader to the original paper for a detailed description.

5. Other phenomena

a. Two-dimensional patterns

Meinhardt (1982) has also solved Eqs. (11.5) on two-dimensional domains, for a case which corresponds to parameter values $Q=1.33$, $R=37.5 \approx 6R_c$, $L_x=43$, $L_y=59$ and a discretization with $N=19 \times 26$ cells. From Fig. 89 we see that the fastest growing mode in the infinite medium is $q_m=0.44$ for $R=37.5$. The pattern he obtains is surprising at first sight since it consists of an irregular array of sharp peaks rather than the regular hexagon pattern expected above a type I_s instability. Indeed, Haken and Olbrich (1978) have derived an order-parameter equation starting from the Gierer-Meinhardt model, and find quadratic and cubic nonlinear terms. Their simulations of this equation then lead to hexagonal patterns. It seems likely to us that the main source of the disorder in the pattern found by Meinhardt is the rather coarse discretization of the numerical calculation. We have solved this model in one dimension, first with a fine mesh ($N=100$), and then with a coarser one ($N=20$), starting in each case from small-amplitude random initial conditions. The results, displayed in Fig. 92, show that the system with coarser discretization is considerably more disordered, due to pinning of the nonlinear peaks by the finite mesh. Of course, if the biological system has discrete structure on the scale of the pattern, then the pinning effects are real and dominate the pattern formation, which is then not usefully modelled as a Turing instability.

Another point studied by Meinhardt (1982) is the difference between random initial conditions and a growth algorithm in which the pattern advances into the unstable homogeneous state. The author found that the

more ordered structure is obtained by the latter method, which is another example of pattern formation via front propagation as discussed in Sec. VI.B (see also Oster, 1988). Meinhardt has also used reaction-diffusion models to obtain curved or disordered roll states, as well as branching structures which are designed to model veins, nerves, or leaves. We have not tried to reproduce these patterns, or to test their sensitivity to the parameters and growth protocol, but it seems to us that the branching patterns are not generic structures for type I_s systems.

b. Compartment formation in *Drosophila*

The development of fly eggs provides an example where domain size will determine the pattern at a type I_s instability. As the egg of the fly grows it becomes subdivided into a number of regions which will become different parts of the adult fly. These regions have the geometry of variously shaped discs, and are known as *imaginal discs*. There is evidence to suggest that each disc in turn undergoes successively finer divisions into regions which will play specific roles. (For a discussion of the nature of this evidence see Kaufman *et al.*, 1978; Belintsev, 1983; Murray, 1989). The imaginal disc of the wing has been studied in particular detail. Kauffman *et al.* have suggested that this sequential formation of compartments might be understood as successively unstable modes of a finite-wave number instability fitting into the growing disc. They model the system in terms of the standard pair of reaction-diffusion equations, with no-flux boundary conditions on the diffusing species. In this particular case the equations are separable so the linear eigenmodes of the instability about the uniform state are simply eigenvectors of the Laplacian, $\nabla^2\phi_m = -q_m^2 \phi_m$, with $\mathbf{n} \cdot \nabla \phi = 0$ at the boundaries. The growth rate is $\sigma_m = \sigma(q_m)$, where $\sigma(q)$ is the instability spectrum of the laterally infinite system for a plane wave of wave number q . Thus the *shape* of the imaginal domain only enters through the discrete values of q_m , and the *size* enters through the trivial scaling $q_m = \alpha_m / L$ with α_m a constant depending only on the shape and the mode number. As the domain size changes, successive modes m will pass into the unstable wave number band shown in Figs. 93(a) and 93(b). It is assumed that each such pattern leads to a permanent partition according to the eigenvector ϕ_m . As a simple model Kauffman *et al.* consider an elliptical disc, leading to the modes shown in Fig. 93(c), which will become unstable in succession as the domain grows. Ignoring duplication, this leads to the cumulative sequence of compartments shown in Fig. 93(d). Kauffman *et al.* then suggest a binary characterization of the areas corresponding to a simple \pm interpretation based on the sign of the eigenmode in that case. The point P of Fig. 93(d), for example, belongs to an area with signature $1^+ 2^- 3^- 5^- 6^-$, and the point Q belongs to $1^+ 2^+ 3^+ 5^+ 6^+$ [it is not necessary to include the fourth mode of Fig. 93(c) since this mode does not add an extra partition].

The experimentally determined subareas of the drosophila wing disc, shown in Fig. 93(e), are topologically close to the ideal pattern in Fig. 93(d), and can be interpreted as a distortion of the latter, thus providing some confirmation of the successive partition scheme. Evidence in favor of the specifics of the coding was also presented by the authors in terms of experiments involving mutants.

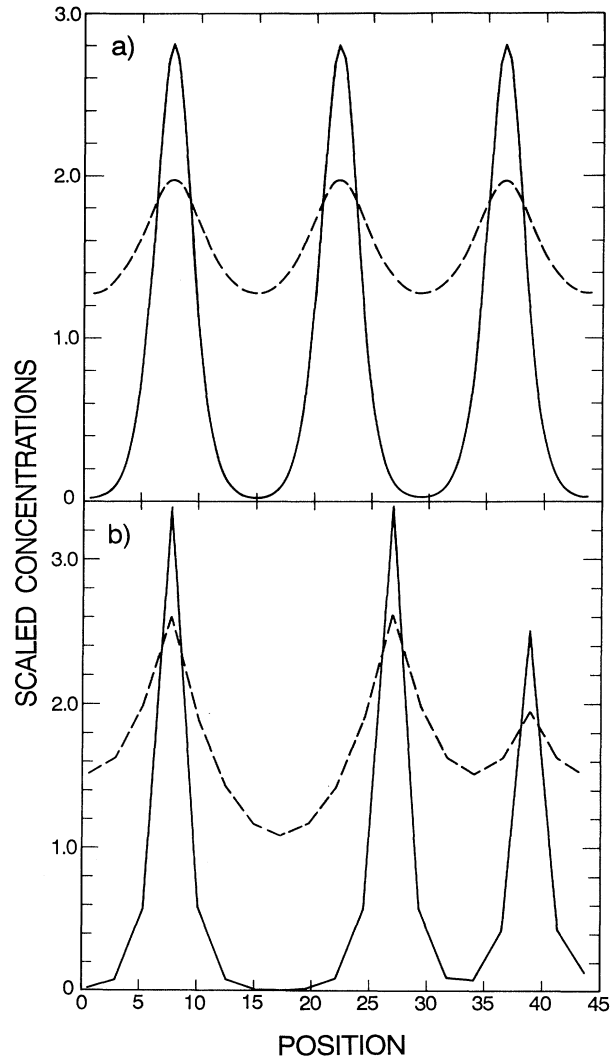


FIG. 92. One-dimensional solution of the Gierer-Meinhardt model, Eq. (11.5), with $Q=1.33$, $R=37.5$, $L=45$, corresponding to the parameters used in their two-dimensional calculation. (a) Fine mesh ($N=100$ points) yielding a good approximation to the solution of the continuum pde. (b) Coarse mesh ($N=20$ points) such as used by Meinhardt (1982), showing an irregular pattern due to locking to the mesh. The result in (b) may be considered a numerical artifact due to insufficient numerical resolution of the continuum model, or as an approximate treatment of a discrete version of the equations corresponding to a 20 cell domain.

The details of the proposed instability are not known at present. For example, is the control parameter very close to critical, so that only one mode is unstable for any given domain size L (as assumed here), or is the driving stronger so that many modes are simultaneously unstable and nonlinear competition must be taken into account? Direct evidence for a reaction-diffusion mechanism as usual does not exist, except for the correct order of magnitude of the length and time scales. We note that here

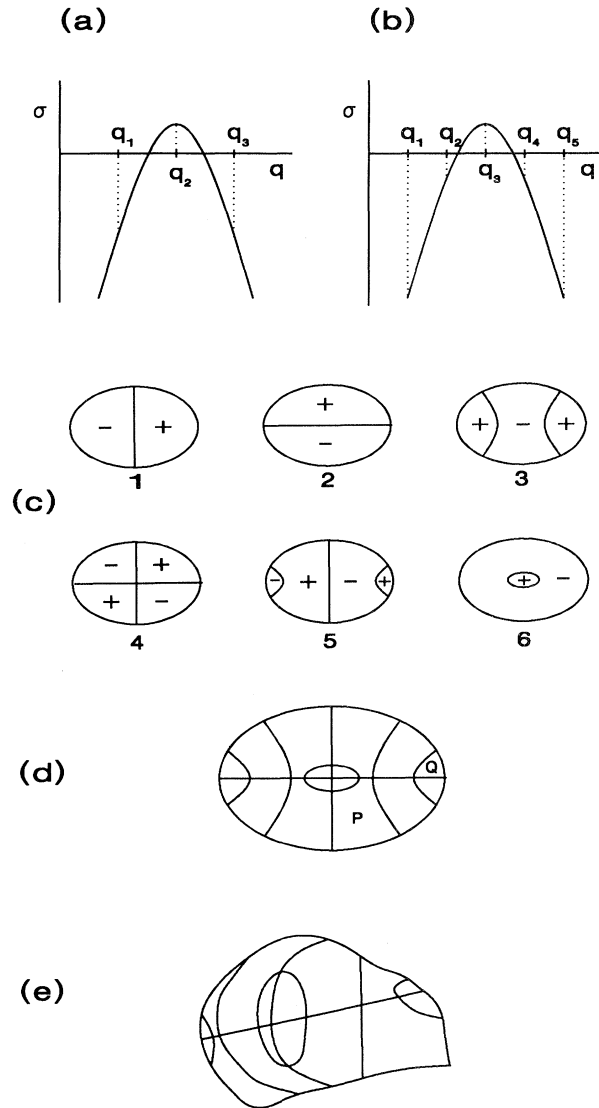


FIG. 93. Sequential compartment formation in *Drosophila*. (a) and (b) Schematic of growth rate $\sigma(q)$ as a function of wave vector in an infinite system, and discrete modes labeled by q_m for two different system sizes. (c) Zero-contours of successive modes that go unstable as the system size increases. (d) Cumulative sequence of compartments resulting from sequence in (c). (e) Experimentally determined subareas of *Drosophila* wing disc. The topological similarity between (d) and (e) should be noted. (Adapted from Kauffman *et al.*, 1978.)

again the atypical no-flux boundary conditions are crucial for the simplicity of the model. As discussed in Sec. V.A, rigid boundary conditions lead to large threshold shifts for $Lq_0 = O(1)$, so the above scheme would either require tuning the control parameter to follow the threshold shift with L , or it would lead to a highly nonlinear situation at the larger sizes if the control parameter is fixed at the threshold value for the smallest size. Also, for rigid boundaries the eigenmodes are no longer the eigenvectors of the Laplacian, but instead depend on the full equations. Perhaps this is one example where the naturalness of the no-flux boundary conditions favors an explanation in terms of a reaction-diffusion mechanism.

c. Mammalian coat markings: The variety of patterns

Pattern forming instabilities have been invoked to explain the external coloration of various organisms, e.g. mammalian coat markings (Murray, 1981a,b, 1989) or the rich variety of shell patterns (see Sec. XI.A.5.d). Comparing the results of model equations with the patterns observed in nature makes it hard to resist the idea that simple finite-wavelength instabilities may indeed account for the phenomena. On the other hand, one must be aware that the results are not unique to the model, or even to the class of models (e.g. reaction-diffusion), although particular details may be highly dependent on arbitrary features of the equations in ways that are not well understood. In this section, rather than assessing the applicability of particular models, we will use the results to display some of the variety of patterns that have been produced.

Murray (1981a,b) in particular has emphasized the importance of the *size of the system* relative to the basic length scale of the instability in producing different patterns from a single model. The production of mammalian coat markings is modelled via a finite-wave-number (type I_s) instability occurring at some stage in the embryo development. The equations used by Murray are

$$\partial_t u_1 = \gamma [u_{10} - u_1 - g(u_1, u_2)] + \nabla^2 u_1, \quad (11.8a)$$

$$\partial_t u_2 = \gamma [\alpha(u_{20} - u_2) - g(u_1, u_2)] + \beta \nabla^2 u_2, \quad (11.8b)$$

with $g(u_1, u_2) = \rho u_1 u_2 (1 + u_1 + \kappa u_1^2)^{-1}$, and $\alpha, \beta, \gamma, \rho, \kappa, u_{10}$, and u_{20} real constants. The details need not concern us, except to note that changing γ changes the length and time scales of the problem, in particular $q_0 \propto \gamma^{1/2}$. As stated in Sec. IV.A the generic pattern in a laterally infinite system is a regular cellular array with hexagonal symmetry. Geometry effects for system sizes comparable to the basic period [$Lq_0 = O(1)$] can strongly perturb the pattern. For example a small rectangular geometry might favor other cellular patterns as in Fig. 94(h); a thin geometry favors stripes perpendicular to the long direction [94(a)]; a small enough geometry restricts the solu-

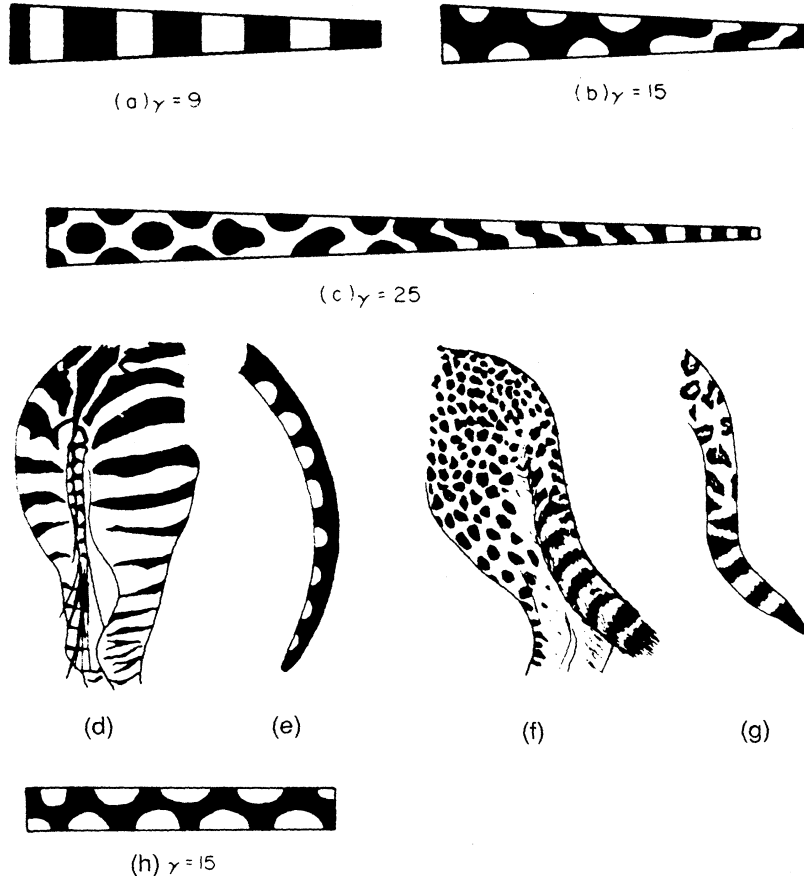


FIG. 94. Model results and natural examples of mammalian coat patterns formed in restricted geometries. Parts (a)–(c) and (h) show nonlinear results from numerical solution of Eqs. (11.8) with random initial conditions, and $\alpha=1.5$, $\kappa=0.1$, $\rho=18.5$, $u_{10}=92$, $u_{20}=64$, and $\beta=10$ (giving steady state values $\bar{u}_1=10$, $\bar{u}_2=9$). (a) $\gamma=9$, dark regions $u_1 > \bar{u}_1$. (b) $\gamma=15$, dark regions $u_1 > \bar{u}_1$. (c) $\gamma=25$ dark regions $u_1 < \bar{u}_1$. (h) $\gamma=15$, dark regions $u_1 > \bar{u}_1$. Note that $q_0 \propto \sqrt{\gamma}$. Parts (d)–(g) show drawings of zebra [(d) and (e)] and leopard [(f) and (g)] coats. Note the similarity between (e) and (h) and between (a) and (f), (g). (From Murray, 1981b.)

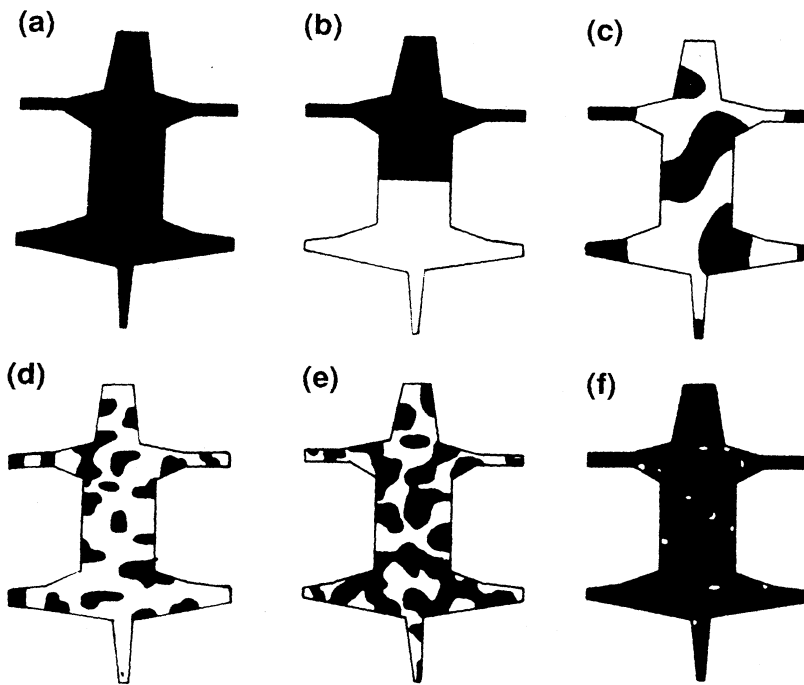


FIG. 95. Mammalian coat patterns formed in complicated geometries as a function of the scale factor γ , obtained from Eq. (11.8). Parameters are $\alpha=1.5$, $\kappa=0.125$, $\rho=13$, $u_{10}=103$, $u_{20}=77$, steady state values $\bar{u}_1=23$, $\bar{u}_2=24$, and $\beta=7$, for (a) $\gamma=0.1$, (b) $\gamma=0.5$, (c) $\gamma=250$, (d) $\gamma=1250$, (e) $\gamma=3000$, and (f) $\gamma=5000$. (From Murray, 1981b.)

tion to be spatially uniform, and more complicated shapes may produce a mixture of patterns. Figures 94(b) and 94(c) show the effect of tapering the domain on the transition between a cellular (spotted) and striped pattern. Figures 95(a) and 95(b) show the transition between a uniform and a simple "gradient" pattern, and Fig. 95(c) shows the coexistence of cellular patterns in the large areas with a spatially constant solution in the restricted regions.^{11.1} Here again, the patterns obtained depend on the assumption of no-flux boundary conditions, though it might be hoped that the general trends would persist under more general boundary conditions as well.

It is clear from the figures that the crucial ingredient in the theory is the relationship of the size of the system to the pattern forming length scale, and Murray has investigated the size of the embryo in various mammals at the time of laying down the prepattern. He concludes that the available information on fetal growth leads to a roughly consistent picture of the variability of coat markings among different animals. Of course, the subsequent evolution of the embryo, when the pattern forming represented by Eqs. (11.8) is no longer operative, may further change the pattern ultimately observed, but the assumption is that the broad features of the patterns are laid down at a time when the model is applicable.

d. Pigment patterns on mollusk shells

A vivid example of pattern formation during growth may be seen on the shells of mollusks. The biological significance of these pigment patterns for the animal itself is unclear since in many cases the animal is active at night or lives burrowed in the sand. The presumed absence of selective value for the organism is thought to facilitate the generation of diversity.

The most interesting aspect of mollusk shell patterns, from our point of view, is that they are generated one row at a time, during growth, so that the two-dimensional pattern on the shell surface represents a space-time record of a one-dimensional solution of the model equations. Patterns appear in the form of lines, stripes or patches of pigmentation with different orientations with respect to the growth direction.

Two different classes of models have been proposed to describe these phenomena, one a standard reaction-

diffusion system with two or three reactants (Meinhardt and Klinger, 1987) and the other a discrete model based on secretory cells stimulated by neural impulses (Ermene-trot et al., 1986; Oster, 1988). Both classes of models

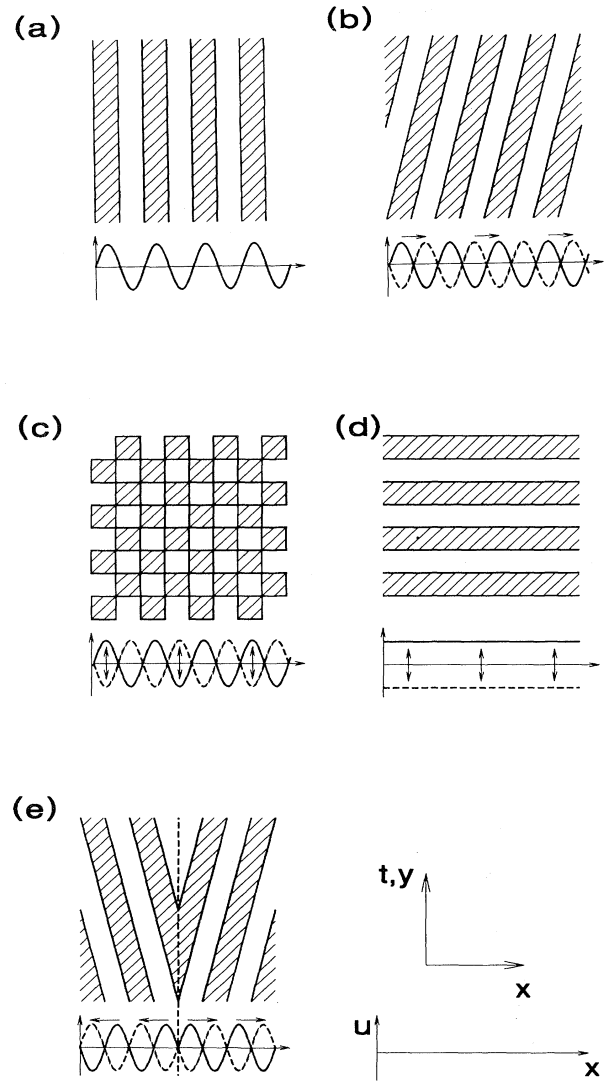


FIG. 96. Types of one-dimensional instabilities and corresponding space-time patterns yielding possible mollusk shell patterns. In each figure the type of linear instability is indicated schematically in the lower portion, and the corresponding pattern laid down by sweeping this one-dimensional pattern through time is shown in the upper portion, with regions of positive signal shaded, and negative ones unshaded (see bottom right-hand panel). (a) Type I_s; (b) type I_o, single traveling wave; (c) type I_o, standing wave; (d) type III_o, uniform oscillation; (e) type I_o, with two oppositely moving traveling waves emanating from a source. In oscillatory cases the solid and dashed curves differ by one half period.

have instabilities which, depending on parameter values, are of either types I_s , III_o , or I_o . In ideal cases their space-time solutions lead to the patterns shown in Fig. 96. Corresponding patterns are often observed in mollusks, as illustrated in Fig. 97, where patterns similar to those in Figs. 96(a) and 96(b) are evident. Abrupt changes in the pattern, such as the one seen in Fig. 97(a), might be caused by changes in parameters during the growth process. Although there is almost no direct biological evidence in favor of either class of models, this application of Turing's ideas seems to us to be particularly striking from a pedagogical point of view, illustrating as it does the different classes of patterns we have identified in our general discussion.

e. Visual hallucination patterns

It has been shown that the early stages of drug-induced visual hallucinations are characterized by the appearance of simple geometric structures which are apparently context-free and independent of previous experiences (see Ermentrout and Cowan, 1979; Murray, 1989). These structures have been classified into "form constants": grating or lattice, cobweb, tunnel, funnel, and spiral. Ermentrout and Cowan have interpreted these structures in terms of a type I_s instability of neuronal activity in the cortex. The remarkable feature of this example is the existence of a mathematical transformation from rectangular cortex coordinates (x, y) to polar retinal coordinates (r, θ) of the visual field. This transformation is a conformal projection which has been shown to take the form

$$x = (4k/\pi\varepsilon)^{1/2} \ln\{\varepsilon^{1/2}r + (w_0^2 + \varepsilon r^2)^{1/2}\}/2 w_0, \quad (11.9a)$$

$$y = (4k/\pi\varepsilon)^{1/2} r\theta/(w_0^2 + \varepsilon r^2)^{1/2}, \quad (11.9b)$$

where k , w_0 , and ε are measurable constants. Let us now inquire what cortical patterns are produced by various retinal patterns under the transformation (11.9). It turns out that the lattice and cobweb retinal patterns (not shown) transform to the simple cellular structures shown in panels (a) and (b) of Fig. 98 and the tunnel, funnel, and spiral retinal patterns on the left in panels (c), (d), (e), go to roll structures that are vertical, horizontal and diagonal, as shown on the right in panels (c), (d), (e), respectively. In all cases it is seen that the cortical patterns which correspond to simple retinal form constants are the regular structures found earlier as ideal solutions of type I_s systems.

Ermentrout and Cowan then introduce a model consisting of a neural network with couplings that are long-ranged in space and retarded in time. Although this model is more complicated than a system of reaction-diffusion equations, it contains the basic elements of local excitation and lateral inhibition, and its linear stability

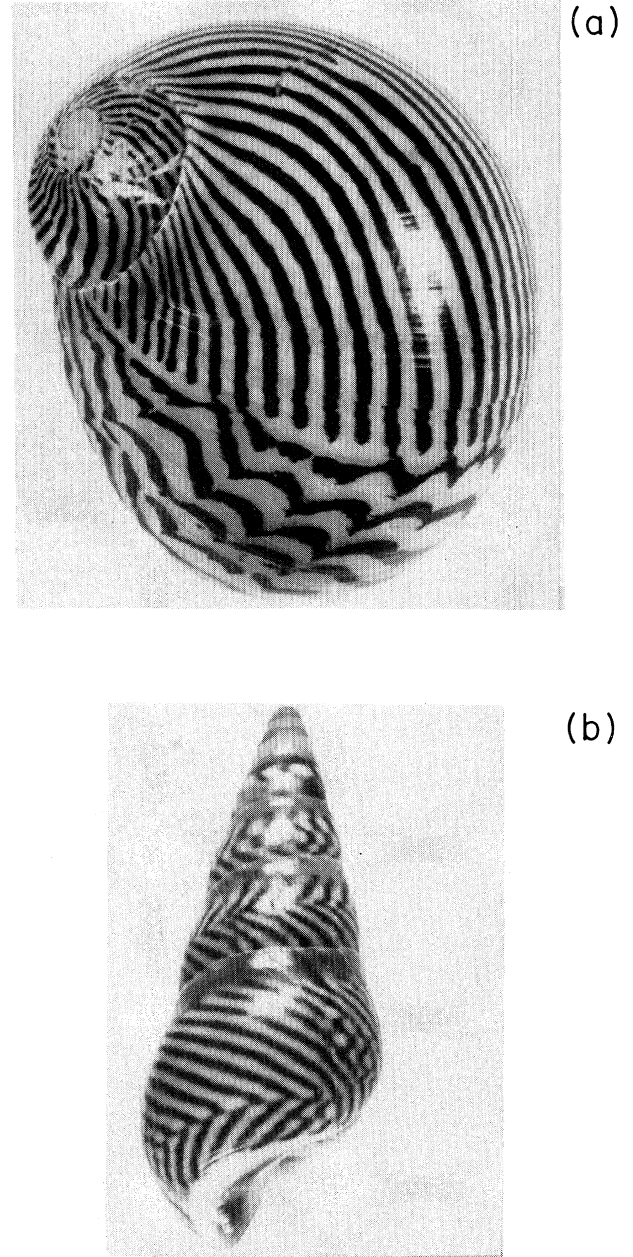


FIG. 97. Patterns on natural mollusks. (a) *Nerita turrita*; (b) *Bankivia fasciata*. (Photos provided by J. Campbell.)

analysis leads to the desired type I_s instability with $q_0 \neq 0$, $\omega_0 = 0$. The authors then find various conditions^{11,2} which will lead to the different cortical patterns, and by the inverse of the transformation (11.9) to the retinal form constants of Fig. 98.

^{11,2}In particular, in order to find roll solutions at all near threshold, it must be assumed that quadratic terms are absent from the equations of motion, though this does not correspond to a symmetry of the starting equations.

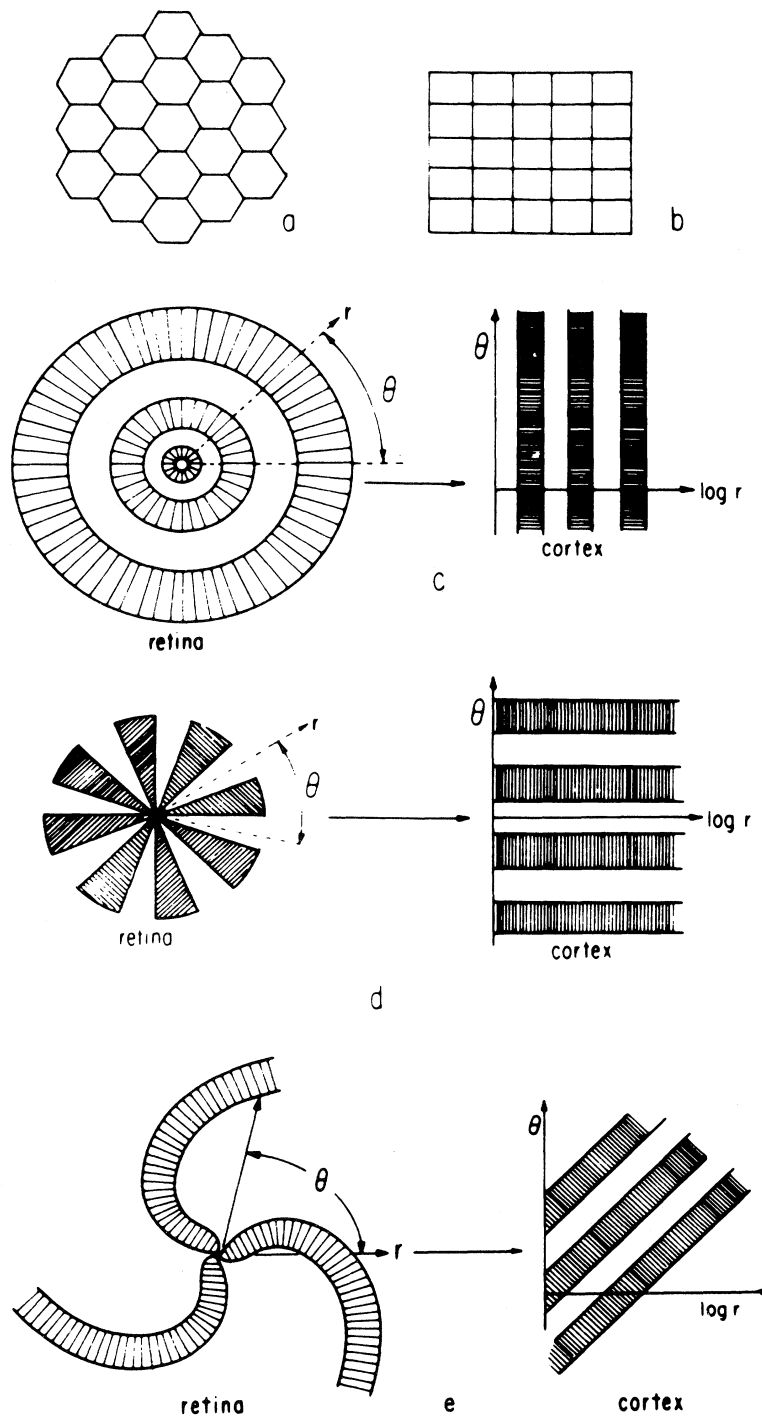


FIG. 98. Visual hallucination patterns on retina and cortex. Panels (c), (d), and (e) show characteristic “form constants” reported in hallucinations interpreted as retinal patterns (left side), and the corresponding cortical patterns given by the transformation (11.9) (right side) for (c) tunnel, (d) funnel, and (e) spiral. Panels (a) and (b) show only the cortical patterns corresponding to grating (or lattice) and cobweb (the corresponding retinal patterns are not shown). Note that for the cortical patterns the axes are labeled with large-distance forms of the coordinates of Eq. (11.9), $x \sim \log r$, $y \sim \theta$. (From Ermentrout and Cowan, 1979.)

f. Mechanical models

As mentioned earlier, a number of authors have introduced mechanical models as an alternative to reaction-diffusion equations for describing pattern and form generation in the development of organisms (see Oster, 1988, and Ch. 17 of Murray, 1989). These models are hydrodynamic-like and incorporate much more of the basic physiology of living cells, concentrating on the balance of mechanical forces and their relation to the biochemistry. The fundamental variables are the cell density $n(\mathbf{x}, t)$, and the density $\rho(\mathbf{x}, t)$ and displacement $\mathbf{u}(\mathbf{x}, t)$ of the extracellular matrix in which the cells are embedded. These variables satisfy a set of three nonlinear equations incorporating cell motion, traction, aggregation and mitosis, as well as the attendant deformation of the extracellular matrix. A simplified version of the model [Eqs. (17.22)–(17.24) of Murray, 1989] still has 9 parameters, and only a linear stability analysis and a few numerical simulations have been carried out so far on this model. The most distinctive feature of the results is the appearance of complicated linear dispersion relations with diverging growth rates at certain q values which depend on the choice of parameters. As noted by Murray, these singularities must be smoothed by the addition of extra terms to the model, which will act as singular perturbations. If it turns out that such dispersion relations are indeed a necessary feature of biological pattern formation, then the point of view we have adopted of classifying systems according to their linear instabilities seems to have little relevance. In particular, the frequent appearance of growth rates that diverge at large wave vectors (see Fig. 17.9 of Murray, 1989) seems to cast doubt on the whole hydrodynamic analysis, and the proliferation of parameters necessary to obtain a sensible theory is a discouraging feature of the approach. It must be said, however, that as far as we are aware no evidence has been presented that the singular dispersion relations correspond to any observable phenomena, so it is too early to tell what the impact of these models will be on our understanding of morphogenesis.

B. Time-dependent patterns: Nonlinear waves

Many biological processes involve periodic activity and transmission of signals via wave motion. Thus the nonlinear wave phenomena described in Secs. V, VI, and X have a number of important applications in biological systems, some of which will be summarized below.

1. Pulse propagation in nerves

Among the earliest examples of the use of reaction-diffusion equations were models for pulse propagation along a nerve fiber. In this case the active medium is the membrane, which uses chemical energy to create a non-

equilibrium distribution of various ions (Na^+ , K^+ , Ca^{++} , etc.), and sustains voltage pulses that serve to transmit information in the nervous system. The empirical model of Hodgkin and Huxley (1952; see also Scott, 1975) has a reaction part with four variables representing currents and potentials for the ionic species, plus the usual derivative terms coming from diffusion. The model was simplified by FitzHugh (1961) and Nagumo *et al.* (1962), who eliminated the two fastest variables and were left with a system, quoted in Eq. (5.170) above, whose nullclines are essentially the same as those of the Oregonator, shown in Fig. 77. Here also, different parameter values take the system from excitable, to periodic, to bistable dynamics, and much of the theoretical work of the past few years on pulse propagation was in fact carried out with reference to the FitzHugh-Nagumo model and with applications to nerve conduction processes in mind (see Ermentrout *et al.*, 1984; Murray, 1989; Elphick *et al.*, 1990a).

2. Excitations of heart muscle

The most natural theoretical approach to the study of cardiac dynamics is to analyze the time-dependent signals obtained from electrocardiograms. It is the detailed shape of these signals that defines the different regimes of normal and abnormal heart function (e.g. arrhythmias such as tachycardia or ventricular fibrillation). These signals have been analyzed from the point of view of nonlinear dynamics, and correlations have been found between heart function and bifurcations or attractor dimensions (see, e.g. Glass and Mackey, 1988; Kaplan *et al.*, 1988; Jalife, 1990). It should be remembered, however, that the cardiogram signal represents a complicated spatial average of the electrical activity of the medium, and as such it is somewhat analogous to the Nusselt number in convection. Just as more detailed information than the average heat transport is useful in characterizing spatiotemporal convection patterns, it is also important to focus on the spatial organization of electrical activity in the heart (see Glass and Mackey, 1988; Glass and Hunter, 1990; Jalife, 1990; Glass *et al.*, 1991).

The cardiac conducting system consists of a large number of cells of different types, where coupling in the intercellular medium is apparently governed by ion currents and special substances called “mediators.” Under normal conditions synchronization of the contractions of the heart cells is due to propagation of electrical waves of excitation in a pattern which resembles the targets discussed for the BZ chemical reaction in Sec. X. Indeed, the excitation originates rather locally, in the cells of the “sinus node” whose characteristic dynamics is of the oscillatory type [see Figs. 78(a), 78(b)] with a period of roughly one second. Outside this region the cells of the myocardium are excitable [Fig. 78(d)], and they transmit the outgoing waves produced periodically in the sinus-node

(the "core").

The earliest attempts to model cooperative excitation effects in the heart were those of Wiener and Rosenblueth (1946), who introduced a discrete automaton model (called the "axiomatic model") of coupled elements as a description of fibrillation. [Early Soviet work is described in Vasiliev *et al.* (1987), pp. 67ff.] In recent years rather detailed kinetic equations have been derived for this system by detailed experimental study of individual cells and groups of cells (Hodgkin and Huxley, 1952; Beeker and Reuter, 1977). The resulting theory is quite complicated, containing up to eight coupled equations (much like the BZ reaction); to our knowledge these have not been analyzed from the point of view of spatial pattern formation. Instead, simpler phenomenological models, such as the FitzHugh-Nagumo equations mentioned earlier in connection with nerve pulse propagation, have been employed. The analysis and results parallel those of the Oregonator model quite closely, so we can draw on the discussion given in Sec. X. Cellular automaton models have also continued to be studied (see Kaplan *et al.*, 1988 and references therein).

As mentioned above, the excitations in a normally functioning heart are represented by a target solution centered at the sinus node. In certain pathological situations other structures may be created which disturb the normal function. For example, if a small region exists with different dynamical characteristics the excitation wave may be perturbed in passing through that region and it may break apart, leaving two free ends (Krinsky,

1984b). As we saw in Sec. X these ends tend to curl up into *spirals* [called "reverberators" in the Soviet literature (Krinsky, 1984a)] which have a *higher* frequency than the targets. This means that the target will be annihilated by collisions with the growing spiral, and eventually the heart tissue will oscillate at the much higher frequency of the spiral. This effect is thought to cause a heart disorder called "paroxysmal tachycardia," where the frequency of the heart beat increases by a factor of ten. In Fig. 99 we show a spiral pattern obtained from multiple probes placed on an isolated rabbit cardiac tissue that has been submitted to external stimulation. The period is shown to be of order 100 ms, as compared with a normal heart beat of 1 s. Numerical modeling of such patterns has been undertaken using a variety of simple equations, and comparisons between *in vitro* experiments, numerical simulations and analytic theory have yielded encouraging results (see Krinsky, 1984a; Tyson and Keener, 1987; Jalife, 1990; Davidenko *et al.*, 1991).

In contrast to tachycardia, in which a single coherent structure takes over the dynamics, fibrillation is thought to involve many different structures vibrating asynchronously. Although no quantitative description of fibrillation has been presented, a natural model to use is that of an inhomogeneous excitable medium in which excitation waves break up to form spirals, which in turn emit high-frequency waves (Krinsky, 1984b). A recent important development is the mapping out of electrical activity in the cardiac medium in real space-time, obtained through multiple implanted probes, and the correlation of the re-

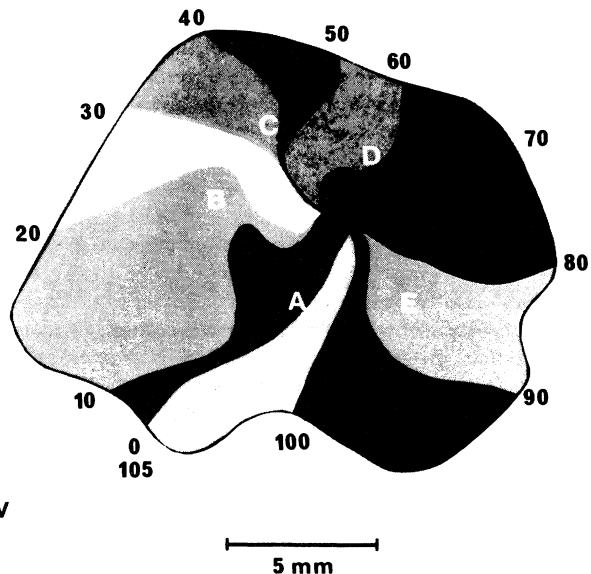
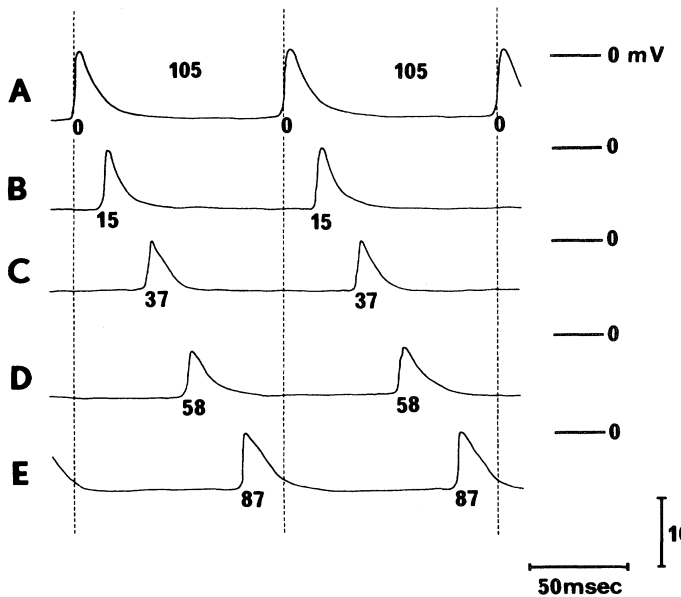


FIG. 99. Rotating spiral waves experimentally induced in a rabbit heart (left atria) muscle: the numbers represent times in milliseconds. Each region was traversed in 10 ms with a complete rotation in 105 ms. On the left panel the transmembrane potentials are shown with the lettering corresponding to the points in the heart muscle on the right. The lines separating different shaded regions in the right-hand panel correspond to the position of the pulse at the times indicated on the periphery. (From Allessie *et al.*, 1977; Copyright 1977 American Heart Association.)

sults with the cardiogram signal (Pogwizd and Corr, 1990). Such experiments provide a fertile field for theoretical interpretation, and many of the issues we have raised in the preceding chapters concerning nonlinear wave propagation arise in attempts to elucidate different aspects of cardiac dynamics (see Glass and Hunter, 1990; Jalife, 1990; Glass *et al.*, 1991). In particular, the following questions may be posed:

- How important is it to have a realistic microscopic picture of the ionic conduction mechanisms, as opposed to "generic models" of excitable media (Chialvo, 1990)?
- Is the spiral defect that is thought to be at the origin of tachycardia caused by extrinsic inhomogeneities in the medium, or can it also arise through suitably timed local stimulation of a homogeneous (healthy) tissue (Allessie *et al.*, 1990; Winfree, 1990)?
- Is ventricular fibrillation chaotic? How does one reconcile different diagnoses of chaos coming from local and global measurements (Pogwizd and Corr, 1990)?
- Can one modify the parameters of the medium so as to make the creation of spirals more difficult, e.g. by increasing the intrinsic core size so that spirals will no longer be produced (Zykov, 1990)?
- How reasonable is the model of a homogeneous medium for representing either the healthy or the abnormal heart tissue? Can one understand the effects of heterogeneity, of anisotropy (due to the structure of muscle fibers), of finite size and of random disorder due to lesions, as perturbations of a basic homogeneous excitable medium (Allessie *et al.*, 1990; Winfree, 1990)?

It should be clear that the potential payoff in the search for an accurate representation of cardiac dynamics is enormous. The specific goals are first predictive: i.e., to understand the patterns of excitation that are likely to lead to arrhythmias such as tachycardia or fibrillation. Secondly, the goals are clinical; namely, the improvement of techniques of *defibrillation*, whereby an external stimulus is supplied to the heart in order to make a transition from a state of fibrillation back to a normal sinus rhythm. Such devices are in use at present, but they are rather crude and based primarily on empirical rules. Theoretical analysis aims to find more reliable schemes for defibrillation using significantly lower power levels, and success in this effort would be of enormous practical value.

3. Slime-mold aggregation

The amoebae of *dictyostelium discoideum* are organisms that begin to aggregate in response to a depletion of their bacterial food supply. This motion is controlled by a signaling substance — cyclic adenosine monophosphate (cAMP) — which the cells secrete more or less rapidly depending on other parameter values. A simple reaction-diffusion model, quite analogous to the Oregonator (10.1)–(10.2), has been proposed for this system, in which u_1 represents the intracellular concentration of cAMP, and u_2 the concentration of an inhibitor sub-

stance. The amount of food reserves is considered to be slowly varying and in the model it merely determines the shape of the functions f and g .

It was remarked by Hagan and Cohen (1981) (see also Belintsev, 1983, 1984) that as the food supply diminishes the system goes gradually from an excitable mode with low cAMP concentration, through an oscillatory state, to an excitable mode with high cAMP concentration. These authors have correlated this evolution with the various stages of development: pulse relaying, spiral and target pattern aggregation, directed locomotion, and tissue buckling, observed in experiments on slime molds. In particular, when the nullclines resemble those for the Oregonator (Fig. 78), we can expect to be able to form target and spiral patterns (Tyson *et al.*, 1989). This is indeed the case, as illustrated in Fig. 76(b) showing an experimental set of spirals that are indistinguishable from those shown in Fig. 76(a) for the BZ reaction. The same model has also been used to describe the aggregation process and the transformation of the spatial shape of the aggregate from a hemispherical mound to an elongated migrating slug (Hagan and Cohen, 1981; Belintsev, 1983). Recently, Levine and Reynolds (1991) have considered the coupling of the reaction-diffusion mechanism to cell motion via chemotaxis. Based on their simple model they conclude that the target and spiral patterns are unstable to a streaming instability which causes them to break up.

Numerous other examples of pattern formation exist in biological systems; these include other nonlinear wave phenomena (Vasiliev *et al.*, 1979; Belousov, 1984; Krinsky, 1984a; Murray 1989), aggregation and precipitation patterns (Oster, 1988; Lauffenburger, 1984), as well as patterns in ecology and epidemiology (for a review see Levin and Segel, 1985).

XII. OTHER SYSTEMS

A. Solidification patterns

Solidification patterns provide an interesting example of the phenomena and methods we have described elsewhere in this article, as well as a link to a much broader class of pattern forming problems where interface growth and diffusion are the dominant processes (for example "diffusion limited aggregation," see Viscek, 1991). In this section we will briefly review this area to establish these links, without any attempt at completeness. Recent reviews of this field include Langer (1987a), Kessler *et al.* (1988), Brener and Mel'nikov (1991), and Flesselles *et al.* (1991).

The basic physical phenomenon is the growth of a stable phase of a material (usually the solid phase at a solid-liquid phase transition but sometimes the ordered phase at a nematic-isotropic liquid crystal phase transition) into the unstable liquid phase, usually prepared by

supercooling. This type of system is of course enormously important in materials preparation. A common experimental protocol is to seed a supercooled liquid with a crystal to nucleate the growth. The process that limits the growth rate is the diffusion away of the latent heat liberated by the solidification or, in the case of the solidification of mixtures, the diffusion away of the component of the mixture that has a lower concentration in the solid, i.e. the "solute."

1. Solidification of a pure supercooled liquid

a. Propagating interface

The quiescent or uniform state upon which pattern formation might be built is the planar solid-liquid interface propagating into the supercooled liquid. We will seek spatial structure in the x coordinate that is parallel to the interface and transverse to the growth direction z .

The dynamical field is the temperature T which may be put into dimensionless form according to

$$u = \frac{T - T_M}{L/C_p}, \quad (12.1)$$

where T_M is the equilibrium melting temperature, L the latent heat, and C_p the specific heat of the liquid phase. The value of $u = u_\infty = \Delta$ in front of the interface is the control parameter and is called the dimensionless undercooling. The equation of motion for u is diffusion in solid and liquid phases. We have in the liquid

$$\partial_t u + D \nabla^2 u = 0, \quad (12.2)$$

where D is the thermal diffusivity of the liquid, and the same equation in the solid but with the solid thermal diffusivity D' replacing D . For simplicity D' is often put to zero, i.e. thermal diffusion in the solid is neglected (the "one-sided model") or sometimes the case $D' = D$ is studied (the "symmetric model"). The interface is coupled to the diffusion field through the latent heat which acts as a source of u with a strength proportional to the interface velocity, so that if the normal velocity of the interface is v_n we have

$$v_n = D [\beta \nabla u|_{\text{solid}} - \nabla u|_{\text{liquid}}] \cdot \hat{n}, \quad (12.3)$$

where \hat{n} is the normal to the interface and

$$\beta = D' C'_p / DC_p, \quad (12.4)$$

with C'_p the specific heat of the solid phase. Finally, the temperature at the interface is given by the Gibbs-Thomson condition^{12.1} (neglecting chemical kinetic effects)

^{12.1}This equation applies in two dimensions i.e. in a thin film. In three dimensions there are two principal components to the curvature tensor. Also in anisotropic systems Σ will depend on the orientation \hat{n} , and some care is needed in its definition. Throughout this section we are considering the growth of a rough interface, i.e. without faceting.

$$u|_{\text{interface}} = -d_0 K, \quad (12.5)$$

where K is the curvature of the interface and d_0 is the capillary length defined in terms of the surface tension Σ via

$$d_0 = \Sigma T_M C_p / L^2. \quad (12.6)$$

The interface propagation problem, between two linearly stable states, is analogous to the discussion in Sec. V.B and we might expect a discrete family of steady state planar solutions parameterized by the propagation velocity v . An extra physical constraint in the present problem, however, is that the heat is *conserved*, so that there is a constraint of unit undercooling $\Delta=1$ on the control parameter for steady state growth. This means that the latent heat released is just sufficient to warm the supercooled liquid to the melting temperature, and steady state growth may proceed. For $\Delta=1$ there is a front for any velocity v , with

$$u = \begin{cases} \exp(-2\xi/\ell) - 1, & \text{for } \xi \geq 0, \text{ liquid} \\ 0, & \text{for } \xi \leq 0, \text{ solid} \end{cases} \quad (12.7)$$

where $\xi = z - vt$ is the coordinate normal to the interface measured from the position of the interface, and the diffusion length

$$\ell = 2D/v \quad (12.8)$$

gives the decay of the temperature field in front of the interface.

b. Linear instability

The characteristic linear instability of diffusion controlled planar interfaces, the Mullins-Sekerka instability (Mullins and Sekerka, 1964; Langer, 1980), is to a transverse undulation of the surface at wave vector q , as illustrated in Fig. 100. The instability may be understood by considering a bulge of the surface which steepens the thermal gradient in front of the interface, thereby enhancing the rate at which the latent heat is diffused

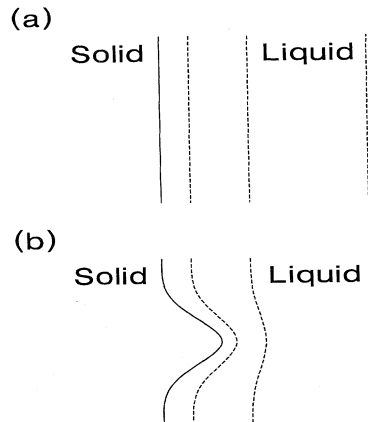


FIG. 100. Mullins-Sekerka instability: full line shows solid-liquid interface and dashed lines temperature contours in the liquid for (a) unperturbed and (b) perturbed system.

away and so increasing the growth rate and the size of the perturbation. The surface tension stabilizes the system via Eq. (12.5), and acts most strongly at large wave vectors. The expression for the growth rate is then determined by the competition between the diffusion and the surface tension and is given approximately^{12.2} by

$$\sigma_q = qv [1 - \frac{1}{2}(1+\beta)d_0\ell q^2]. \quad (12.9)$$

The growth rate is maximized at a wave vector $q_0 \sim (d_0\ell)^{-1/2}$, i.e. a length scale that is the geometric mean of the capillary and diffusion lengths. Note that q_0 depends on the velocity v through ℓ .

The calculation can be generalized to the quasisteady situation of a sphere growing into a supercooled liquid with *arbitrary* undercooling Δ . The same type of expression is obtained with $q \sim m/R$, where m is a mode number, R is the instantaneous sphere radius, and

$$v = \partial_t R = (D/R)(\Delta - 2d_0/R) \quad (12.10)$$

is the corresponding velocity which slowly changes in time. Note that now there is a *unique* solution (in the class considered) for *arbitrary* undercooling, and the role of Δ as the control parameter becomes apparent.

c. Nonlinear state: The dendrite problem

From our point of view the great difference between this solidification problem and the type of systems we have been considering is that the instability is catastrophic, with no saturation at small amplitudes by the nonlinearities. The final growth pattern is far from the planar interface or growing sphere. Experimentally it has been observed (see Fig. 101) that the morphology consists of a growing needle with a parabolic tip but with side branches developing away from the tip. To experimental accuracy, at small undercooling Δ the tip has been shown to move with a constant velocity v (Dougherty and Golub, 1988) uniquely determined by the undercooling Δ and other system parameters. For larger undercooling the side branches approach closer to the tip and an oscillatory component to the velocity is sometimes seen (Raz *et al.*, 1989). This phenomenon as an example of pattern formation has attracted a great deal of attention and considerable progress has been made toward understanding the steady state tip velocity. A full theory of the development and subsequent coarsening of the side branches remains however a major theoretical challenge.

The basic characterization of the growing dendrite is already contained in the formulas discussed above. The only intrinsic length scale in the problem is the capillary

length d_0 determined by the surface tension, and we would expect this to set the basic scale of the structure, namely the tip radius ρ or the side-branch spacing, perhaps modified by the dimensionless control parameter Δ , i.e.

$$\rho = d_0 f_1(\Delta). \quad (12.11)$$

The velocity would then be set by diffusion at this scale as well as the control parameter Δ [cf. Eq. (12.10)], i.e.

$$v = (D/\rho) f_2(\Delta). \quad (12.12)$$

The mathematical treatment of this problem encounters some formidable technical hurdles, which we will not detail here. In the two-dimensional situation attention has focused on steady state needle solutions with no side branching, of the form ($\xi = z - vt$)

$$u = u(x, \xi), \quad v = \text{const.} \quad (12.13)$$

A *discrete* set of possible solutions may be found with ρ and v consistent with the scalings (12.11)–(12.12). Interestingly, however, *no* solutions are found if the surface tension is assumed isotropic. A small crystal anisotropy (e.g. 4-fold), parameterized by a strength α leads to a single stable steady state dendrite with tip radius

$$\rho = c_1 d_0 \Delta^{-2} \alpha^{-7/4}, \quad (12.14)$$

[c_1 is an $O(1)$ constant], as well as a discrete infinity of unstable solutions. (More precisely, the single solution is distinguished as the only one that is *absolutely* stable in the *moving* frame of the tip.) We see from Eq. (12.14) that the tip radius is set by the basic scale d_0 . However, for small undercooling and anisotropy there are two large dimensionless factors on the rhs so that $\rho \gg d_0$. Because of this, one might expect surface tension to have a small effect on the *shape* of the needle.

In fact the experimental shape in the tip region can be very well fit by an “Ivantsov solution” calculated in the absence of surface tension. Indeed the mathematical formulation has proceeded in terms of adding surface tension as a “small” perturbation to the zero surface tension problem. We note that although this is an appropriate and successful *mathematical* procedure there are necessarily considerable technical difficulties, since the only a priori length scale d_0 is not present in the zeroth-order problem and the character of the solutions (discrete set or family) is different in the two cases.

The solution of these problems has required the recent mathematical advance of “asymptotics beyond all orders” (see Kessler *et al.*, 1988; Pelcé, 1988; Segur *et al.*, 1991). The result of the calculation is expressed by two equations. The first is a relation between the “Peclet number”

$$P = \rho v / D, \quad (12.15)$$

and the undercooling Δ , given by

$$\Delta = \sqrt{\pi P} e^{P \operatorname{erfc}(\sqrt{P})}. \quad (12.16a)$$

^{12.2}The “quasi-static approximation” has been used here. See Sec. III.A of Langer (1980) for a discussion and references to a full calculation.

For small undercooling the above equation becomes

$$P \sim \pi^{-1} \Delta^2, \quad \Delta \ll 1, \quad (12.16b)$$

an expression which does not involve d_0 . The second equation is

$$\rho^2 v / d_0 D = c_2 \alpha^{-7/4}, \quad (12.17)$$

which together with (12.16b) implies Eq. (12.14) for small Δ . Recent experimental tests of Eq. (12.17) discussed by Gollub (1991) and by Muschol *et al.* (1992) show agreement within factors of 2, which are, however, outside the quoted errors.

In two dimensions, therefore, the theory is formulated

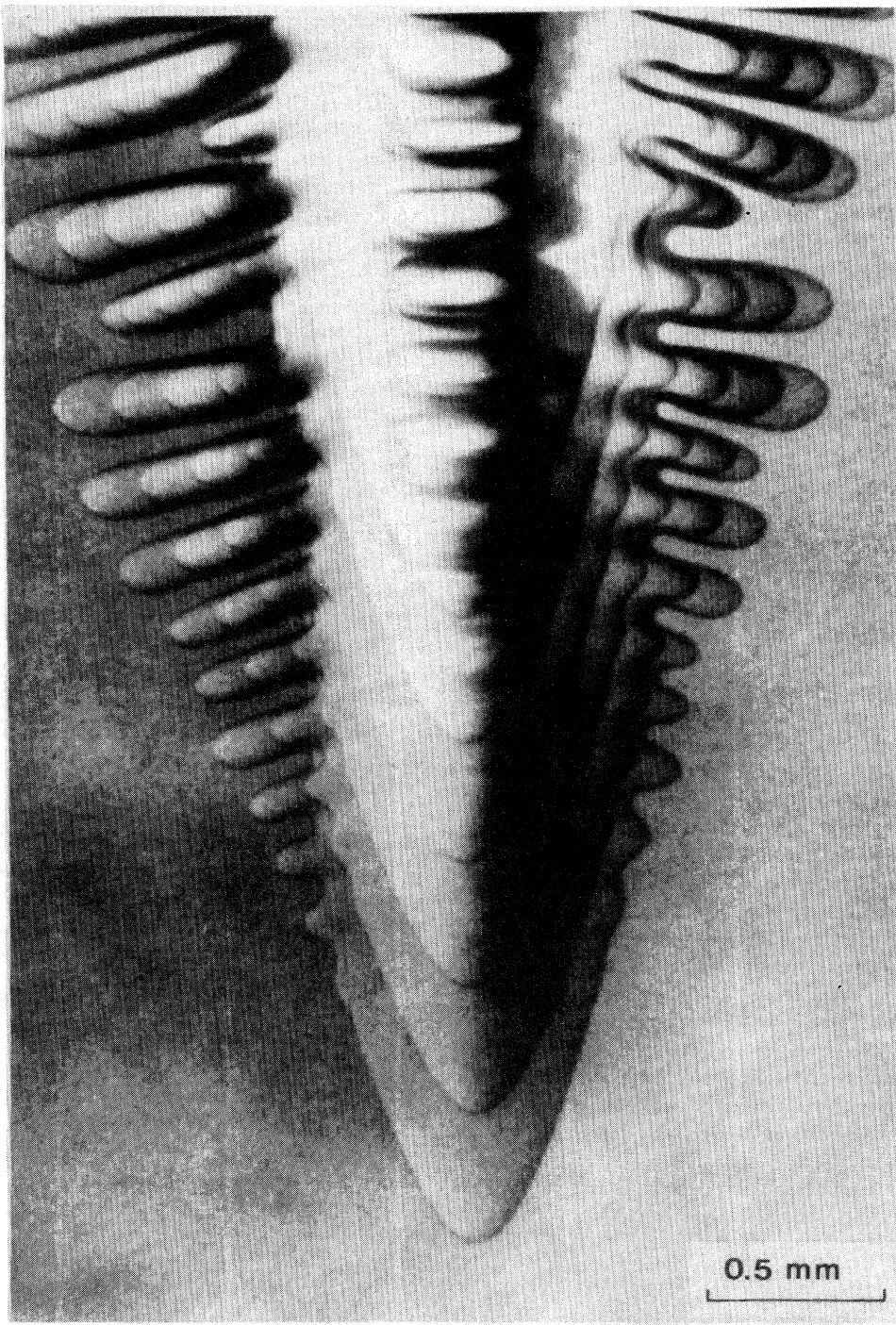


FIG. 101. Multiple-exposure photograph of a succinonitrile dendrite advancing downward. (From Huang and Glicksman, 1981; Copyright 1981 with permission from Pergamon Press Ltd., Headington Hill Hall, Oxford OX3 0BW, United Kingdom.)

in terms of the existence of a steady state propagating needle that is absolutely stable in the moving frame. The side branching, which is so obvious experimentally has *not* been predicted from the original equations. However, since the tip is convectively unstable in the moving frame, one suggestion for the side branches is that they are sustained by thermal noise in the tip region whose effect propagates backwards. Another idea is that the long-range diffusion field may provide a feedback from the region of large side branches to the tip, again supplying an effective (but now deterministic) noise at the tip. There is experimental evidence for the stochastic nature of the side branching from the absence of correlation between the side branches on either side of the tip. The characterization of the large amplitude side branches away from the tip and their coarsening remain completely open.

Despite some obvious successes this picture of the two-dimensional problem remains controversial. The relevance of the steady state solution to the experimental situation, where complicated dynamics (away from the tip) is always seen, is not universally accepted. In fact the mathematical theory depends sensitively on features of the steady state solution far down the needle where it is completely different from the observed behavior, a point that leaves some workers in the field uneasy. The most obvious successes are quantitative predictions for ρ and v which are consistent with experiments carried out thus far, and which may be tested more stringently in the future. On the other hand the three-dimensional problem remains open since no steady state solutions are known in that case.

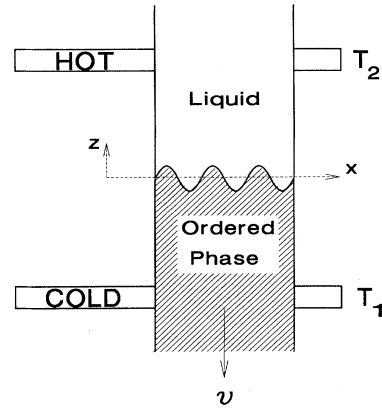


FIG. 102. Directional solidification geometry. Two microscope slides containing a thin film of the material are drawn at a constant velocity v between a hot oven at temperature T_2 and a colder oven at temperature T_1 , bracketing the transition temperature between ordered and disordered phases.

2. Directional solidification

a. Propagating interface

Directional solidification is similar to pure liquid solidification described above except that solute diffusion is the rate limiting process, and an imposed linear temperature gradient serves to limit the instability. This means that patterns close to the planar configuration may be investigated.

The experimental geometry is shown in Fig. 102, and a typical phase diagram which defines the parameters of the problem is shown in Fig. 103. The parameters that

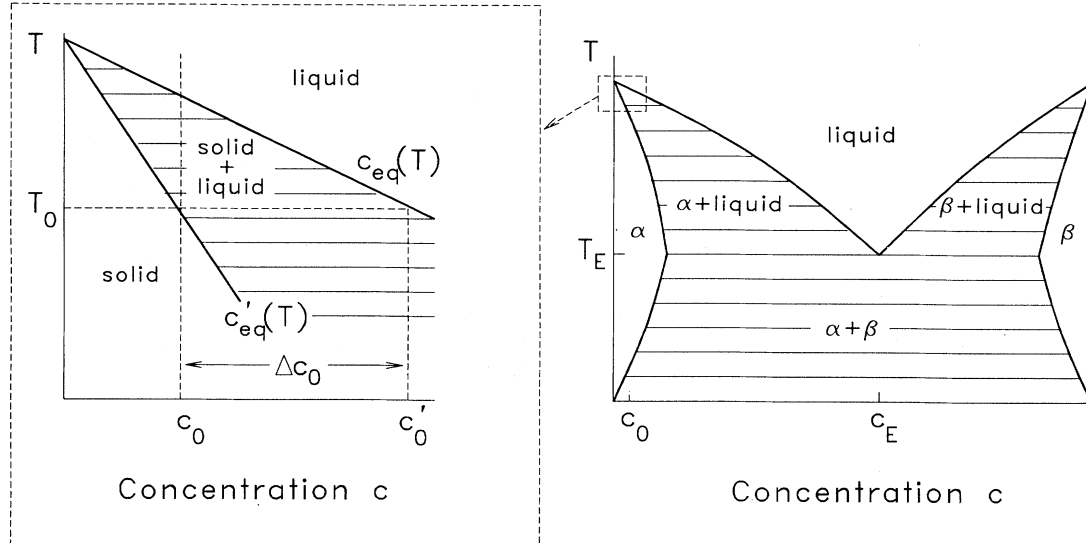


FIG. 103. Phase diagram of eutectic system used in directional solidification experiment, showing phases as a function of the temperature and concentration of the mixture. The two ordered (e.g. solid) phases are denoted α and β . Horizontal lines are two-phase regions consisting of an equilibrium between the phases at the ends of the lines. The eutectic concentration is c_E . In the expanded box c_0 denotes the concentration in the liquid far in front of the interface as well as that of the solid phase, and c'_0 is therefore the concentration in the liquid at the flat interface. The liquidus and solidus curves are denoted $c_{eq}(T)$ and $c'_{eq}(T)$, respectively. They may be approximated as straight lines over this small region.

are readily varied in experiments are c_0 the solute concentration far in front of the interface, the mean temperature gradient \mathcal{G} and the velocity of pulling v , which is also the mean velocity of the interface relative to the fluid. Typically v is used as the control parameter. In steady state the solute concentration in the solid must also be c_0 , and this determines the melting temperature of the planar interface T_0 and thus the position z_0 of the planar interface in the linear temperature gradient.^{12.3} This argument takes the place of the unit undercooling condition for the pure planar interface discussed above. An alternative experimental system replaces the solid-liquid transition by the nematic to isotropic transition in a liquid crystal. As we will see, largely due to the weaker first-order nature of the transition and the smaller diffusion constant it has considerable advantages for comparing theory and experiment.

The coupled equations are essentially as before, but with u now given by the chemical potential μ of the diffusing solute (made dimensionless by dividing by $(\partial\mu/\partial c)\Delta c_0$, with Δc_0 the miscibility gap at T_0). The full details (Langer, 1980) are complicated because of the dependence of parameters on the local temperature, and will not be discussed here. One major difference with the pure case is that the source strength for the diffusing field u for unit interface velocity is no longer a constant (the latent heat), but is instead given by the miscibility gap Δc at the perturbed temperature of the interface^{12.4}

$$\Delta c = \Delta c_0 [1 - (1 - \kappa) \xi / \ell_T], \quad (12.18)$$

with ξ the displacement of the interface, κ the generalized partition coefficient

$$\kappa = \left| \frac{dc'_{eq}}{dT} \right| \left| \frac{dc_{eq}}{dT} \right|^{-1}, \quad (12.19)$$

(see Fig. 103), and ℓ_T a length set by the imposed thermal gradient and defined by

$$\ell_T^{-1} = \frac{\mathcal{G}}{\Delta c_0} \left| \frac{dc_{eq}}{dT} \right|. \quad (12.20)$$

The surface tension length scale is defined by

$$d_0 = \Sigma [(\Delta c_0)^2 (\partial\mu/\partial c)]^{-1}, \quad (12.21)$$

and the diffusion length $\ell \sim D/v$ is now another externally controlled length scale.

^{12.3}For simplicity it is assumed that the thermal conductivities in liquid and solid phases are identical so that the temperature gradient is uniform and simply determined by the temperatures of the ovens.

^{12.4}Langer also introduces a correction to Δc due to the curvature, but this term does not play an important role and is often put to zero.

Various simplifications are often used to make the theory more tractable, and these may be good approximations in specific systems. It is usually assumed that the diffusion of the latent heat away from the interface is sufficiently rapid and that the thermal properties of the two phases are the same, so that the temperature gradient is uniform and independent of the position of the interface. In the one-sided model diffusion of the solute in the growing phase is neglected, a good approximation in the solid-liquid system. On the other hand in the symmetric model the diffusion constants in the two phases are assumed to be equal and κ is also taken to be unity so that Δc , Eq. (12.18), becomes constant. This approximation is better in the liquid crystal system where both phases are liquid and the first-order transition is quite weak so that properties do not change very much at the transition. In the symmetric model the equations of motion can be summarized in a single integrodifferential equation

$$1 - d_0 \kappa(x, t) - \xi(x, t) \ell_T^{-1} = \int_{-\infty}^{\infty} dt' \int_{-\infty}^{\infty} dx' [2 + \partial_t \xi(x', t')] G(x - x', t - t'), \quad (12.22)$$

where G is the Green's function of the diffusion equation, and lengths and times are scaled with $\ell = 2D/v$ and ℓ^2/D , respectively.

b. Linear instability

The analogue of the Mullins-Sekerka stability analysis leads to a growth rate for a transverse perturbation of wave vector q (Langer, 1980) given by

$$\sigma_q \approx q [v - \bar{D} \ell_T^{-1} - \bar{D} d_0 q^2], \quad (12.23)$$

where $\bar{D} = D$ in the one-sided model, $\bar{D} = 2D$ in the symmetric model and we will define the diffusion length as $\bar{\ell} = \bar{D}/v$. Expression (12.23) is derived in the quasistatic approximation valid for small σ_q and not too large velocity, and we have written down the form valid for $q\bar{\ell} \gg 1$.

Equation (12.20) immediately shows that the thermal gradient $\mathcal{G} \propto \ell_T^{-1}$ stabilizes the interface, so that the pulling velocity v must be increased above a critical value v_c , defined simply by $\bar{\ell} = \ell_T$, for the instability to grow. Then Eq. (12.23) may be written

$$\sigma_q = q v_c [\epsilon - (d_0 \ell_T) q^2], \quad (12.24)$$

with $\epsilon = v/v_c - 1$.

Equation (12.23) displays the complexity of the problem since there are three characteristic length scales d_0 , ℓ_T , and $\bar{\ell}$ set by the experimental parameters. Furthermore for typical solid-liquid systems $d_0/\ell_T \sim 10^{-3}$ to 10^{-4} and this small parameter complicates the analysis, for example restricting the range of validity in ϵ of the amplitude equation. For the nematic-isotropic liquid

crystal system on the other hand, this ratio is larger, of order $d_0/\ell_T \sim 10^{-2}$.

Equation (12.24) leads to the impression that we are considering a type III_s instability. However a more careful analysis shows that at small q Eq. (12.23) breaks down, and in fact the interface is weakly stabilized at $q=0$ (the imposed temperature gradient breaks translational invariance so that $\sigma_{q=0}$ is not necessarily zero) leading to a decay of perturbations at a rate (for $q\bar{\ell} \ll 1$) given by

$$\sigma_0 = |\sigma_{q=0}| \sim v\ell_T^{-1} \ll \sigma_m , \quad (12.25)$$

with $\sigma_m \sim v(\ell_T d_0)^{-1/2}$, the maximum growth rate for $\epsilon=O(1)$, setting the scale for typical growth rates away from $q=0$. This more complete analysis predicts a type-I_s instability at a slightly modified value of v_c , and at a critical wave vector q_0 given by (Langer, 1980)

$$q_0 \bar{\ell} \sim (\bar{\ell}/d_0)^{1/3} . \quad (12.26)$$

On the other hand the characteristic wave-vector scale q_m above threshold (as set by the wave vector at maximum growth rate or by the width of the wave-vector band of growing solutions) is seen from Eq. (12.24) to be given by

$$q_m \bar{\ell} \sim (\bar{\ell}/d_0)^{1/2} , \quad \epsilon=O(1) . \quad (12.27)$$

For typical solid-liquid systems we have $\bar{\ell}/d_0 \sim 10^3$, so that $q_m/q_0 \sim 5$, and the wave-vector scale increases rapidly above threshold. Clearly, already at this linear level, the validity of the amplitude equation will be restricted by the small parameter $d_0/\bar{\ell}$ to a small range of ϵ . Again for the liquid crystal system the ratio q_m/q_0 is closer to unity, and we might expect a wider range of applicability of the amplitude expansion.

For large velocities $v \gg v_c$, the planar interface restabilizes. The velocity v'_c at which this occurs is unreasonably large in solid-liquid systems, but quite attainable in the liquid crystal. Interestingly, here the instability for v slightly less than v'_c occurs on a length scale large compared to the diffusion length. Ghazali and Misbah (1992), following Brattkus and Davis (1988), have exploited this to develop a local, long-wavelength expansion of the instability analogous to the Sivashinsky-Gertsberg equation for poor conductors (Sec. VIII.F), although the equation is considerably more complicated.

c. Nonlinear states

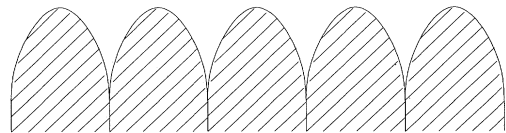
The type I_s amplitude equation for the weakly nonlinear states at small $\epsilon=(v-v_c)/v_c$ can be derived from the full expression for the linear growth rate σ_q (Langer, 1980) and the nonlinear coefficient g_0 has been calculated by Wollkind and Segel (1970) for the one-sided model and by Langer and Turski (1977) for the symmetric model. In the one-sided case and for parameters relevant to solid-liquid systems g_0 is negative and indeed the transi-

tion is experimentally found to be strongly subcritical with a highly nonlinear state of a grooved cellular pattern developing immediately above onset [Fig. 104(a)]: a weakly nonlinear theory does not seem appropriate in this case. On the other hand, for the symmetric model relevant to liquid crystals, g_0 is positive and a supercritical bifurcation is predicted. This was indeed seen by Oswald *et al.* (1987) with a sinusoidal perturbation of the interface growing continuously for $v > v_c$ [Fig. 104(b)], and with v_c and q_0 agreeing well (within the uncertainties of fluid parameters) with the predictions of the linear analysis. Much of the recent experimental and theoretical attention has focused on this system.

Brattkus and Misbah (1990) have calculated the one-dimensional phase equation for the fully nonlinear state appropriate to liquid crystals, from the integrodifferential formulation of the symmetric model. From this they calculate the position of the Eckhaus instability characteristic of the type I_s pattern. Their results, for $d_0/\ell_T = 10^{-3}$ (giving $v_c = 2.50 D/\ell_T^2$ and $q_0 = 1.5 \ell_T^{-1}$) are shown in Fig. 105. Although the results agree with the amplitude equation predictions for small enough ϵ , deviations rapidly become apparent (e.g. of order 35% for $\epsilon=0.04$), consistent with the small range of convergence expected for small d_0/ℓ_T . Also evident in Fig. 105 is the strong effect, on the small- q side of the Eckhaus boundary, of the “ $q \sim 2q$ ” resonance as also found in the Taylor-Couette system (Fig. 61). Although the Eckhaus instability has been observed in this system (Simon *et al.*, 1988) no careful comparison between experiment and the detailed predictions of the theory has yet been presented.

An interesting instability is observed for $\epsilon \sim 2-3$ where domains of an asymmetric state nucleate and then

(a) Solid-liquid



(b) Nematic-isotropic

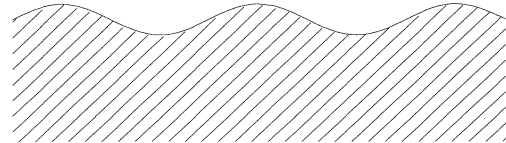


FIG. 104. Cellular states in directional solidification. (a) Solid-liquid interface showing a highly nonlinear state resulting from a subcritical bifurcation. (b) Nematic-isotropic liquid crystal system showing a more weakly nonlinear state. Hatched region is the ordered phase (solid or nematic).

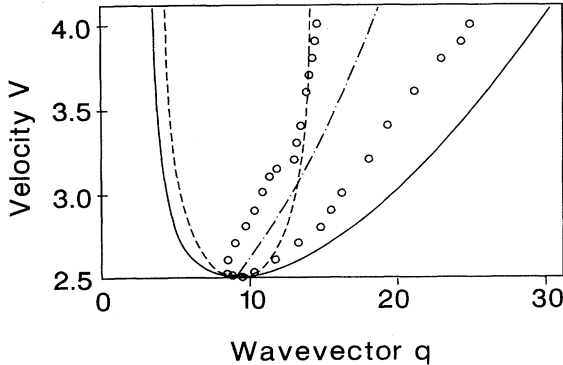


FIG. 105. Stability diagram of velocity vs wave vector for directional solidification in a liquid crystal system. Solid line, neutral stability curve (Mullins-Sekerka); dashed line, Eckhaus instability from amplitude equation; open circles, Eckhaus boundary from numerical simulation of full equations; dash-dotted curve, most unstable mode. (From Brattkus and Misbah, 1990.)

both grow and move through the system. This instability was interpreted by Coullet *et al.* (1989d) in terms of a subcritical secondary bifurcation to a state that breaks the $x \rightarrow -x$ symmetry (see Sec. IV.A.3). The dynamics of these domains is seen to yield a wave-number selection mechanism as described there. The existence of the drifting parity-broken state and its bifurcation from the symmetric state have been calculated from the full equations for the symmetric model by Levine and Rappel (1990) and also in the local model valid for large velocities by Kassner *et al.* (1991). Both calculations predict a *super-critical* bifurcation to the uniform tilted drifting state, rather than the subcritical bifurcation assumed by Coullet *et al.* Recently Caroli *et al.* (1992) (see also Riecke and Paap, 1992) have shown that, due to the feedback of the local wave number on the amplitude of the tilt distortion for spatially localized tilt regions (where the wave number can adjust), elimination of the phase degree of freedom may lead self-consistently to a subcritical bifurcation to tilt domains even when the transition to the uniform state is supercritical. Kassner *et al.* (1991) also predict a zone-boundary Hopf bifurcation (i.e. at $Q = q/2$ with q the wave vector of the unperturbed state), as well as chaotic dynamics.

3. Eutectic solidification

If instead of a small solute concentration c_0 a concentration close to c_E is used, and if also the temperature of the cold contact T_1 is less than T_E , then the solid formed behind the interface will be a mixture of α and β phases (Fig. 103). For small pulling velocities the solids are deposited as alternate lamellae of α and β phases forming a periodic spatial structure with obvious analogies to directional solidification patterns. Many questions similar to the ones we have been addressing, such as wave vector selection and secondary instabilities, arise. In this system, however, there is no spatially uniform state about

which a weakly nonlinear solution can be constructed, and a fully nonlinear theory of the coupled interface and diffusion equations must be developed. We refer the reader to recent literature for a discussion of this work (Karma, 1987; Kassner and Misbah, 1991a,b).

B. Nonlinear optics

Through the discovery of the laser high intensity sources of electromagnetic radiation became available, and many nonlinear phenomena including instabilities were explored. In this section we will focus on systems involving many modes, and briefly indicate some of the analogies that exist with the instabilities and patterns we have studied in the rest of our review. A more detailed treatment can be found in Moloney and Newell (1990, 1992).

1. Basic equations

We start with Maxwell's equation for the electric field $\tilde{\mathbf{E}}$ in a dielectric,

$$\nabla^2 \tilde{\mathbf{E}} - \frac{1}{c^2} \partial_t^2 \tilde{\mathbf{E}} - \frac{1}{c^2 \epsilon_0} \partial_t^2 \tilde{\mathbf{P}} - \frac{2\kappa}{c^2} \partial_t \tilde{\mathbf{E}} = 0, \quad (12.28)$$

where c is the speed of light and ϵ_0 the dielectric constant in vacuum, $\tilde{\mathbf{P}}$ is the polarizability of the medium, and κ (which traditionally has dimensions of frequency!) the attenuation constant of the cavity. The polarizability of the medium is obtained from the Bloch equation for the quantum-mechanical density matrix $\rho_{\ell m}$

$$\begin{aligned} \partial_t \rho_{\ell m} &= -i(\omega_\ell - \omega_m) \rho_{\ell m} \\ &+ (1/\hbar) \tilde{\mathbf{E}} \cdot \sum_j (\mathbf{p}_{\ell j} \rho_{jm} - \mathbf{p}_{jm} \rho_{\ell j}) - \sum_j \gamma_{\ell j} \rho_{jm}, \end{aligned} \quad (12.29)$$

where $\mathbf{p}_{\ell j}$ is the matrix element for the transition from state ℓ to j , whose frequencies are ω_ℓ and ω_j , respectively, and $\gamma_{\ell j}$ is an absorptive coefficient. For a medium consisting of two-level systems with density n_a we define the polarization

$$\tilde{\mathbf{P}} = n_a \mathbf{p} (\rho_{12} + \rho_{12}^*), \quad (12.30)$$

and population inversion

$$\tilde{\mathbf{D}} = n_a (\rho_{22} - \rho_{11}). \quad (12.31)$$

In a dielectric medium we also may relate the polarization to the field via the susceptibility

$$\tilde{\mathbf{P}} = \epsilon_0 \chi \tilde{\mathbf{E}}, \quad (12.32)$$

or the refractive index n ,

$$\tilde{\mathbf{E}} + \epsilon_0^{-1} \tilde{\mathbf{P}} = (1 + \chi) \tilde{\mathbf{E}} = n^2 \tilde{\mathbf{E}}. \quad (12.33)$$

In general, of course, both χ and n are functions of the field $\tilde{\mathbf{E}}$ as well as the frequency ω . It is only in the linear

domain that χ and n are independent of $\tilde{\mathbf{E}}$.

2. Pulse propagation in a dispersive medium

In a purely dispersive medium the refractive index is real and it is usually sufficient to retain two terms in an expansion in $\tilde{\mathbf{E}}$

$$n(\omega, \tilde{\mathbf{E}}) = n_0(\omega) + n_2(\omega) |\tilde{\mathbf{E}}|^2. \quad (12.34)$$

We may then make the familiar Ansatz of a slowly varying envelope

$$\tilde{\mathbf{E}}(\mathbf{x}, z, t) = E(\mathbf{x}, z, t) e^{-i(\omega_0 t - q_0 z)} + \text{c.c.}, \quad (12.35)$$

where z is the propagation direction, \mathbf{x} is the set of transverse directions and q_0 is the wave vector of a linear wave in the medium, satisfying the dispersion relation

$$q_0^2(\omega_0) = n_0^2(\omega_0) \omega_0^2/c^2. \quad (12.36)$$

Neglecting the cavity loss κ , we find upon expanding in E and its gradients

$$\begin{aligned} \partial_z E + q'_0 \partial_t E - (i/q_0) \nabla_{\perp}^2 E \\ + (iq''_0/2) \partial_t^2 E - (iq_0 n_2/n_0) |E|^2 E = 0, \end{aligned} \quad (12.37)$$

with $\nabla_{\perp} = \nabla_{\mathbf{x}}$ and $q'_0 = dq_0/d\omega_0$, etc. In the absence of transverse variation (i.e. neglecting the third term in the above equation) we can change to a moving reference frame ($z \rightarrow z$, $t \rightarrow t - q'_0 z$) to obtain the familiar nonlinear Schrödinger equation

$$\partial_z E = ic_1 \partial_t^2 E + ic_3 |E|^2 E, \quad (12.38)$$

where

$$c_1 \propto q''_0, \quad c_3 \propto n_2. \quad (12.39)$$

Note, however, that the roles of space and time are inverted from the usual ones [e.g. Eq. (4.49)]. It was noticed by Hasegawa and Tappert (1973) that for normal dispersion $q''_0 > 0$ this equation supports solitons if sufficient intensity can be reached, while for $q''_0 < 0$ dark solitons will propagate. There is considerable interest, both scientific and technological, in the details of soliton propagation, particularly in understanding the damping and regeneration of pulses (Hasegawa, 1989; Kumar, 1990).

3. Laser equations

Let us return to Eqs. (12.28)–(12.29) and set

$$\gamma_{12} = \gamma_{\perp}, \quad \gamma_{11} = \gamma_{22} = \gamma_{\parallel}, \quad (12.40)$$

and add a pump parameter D_0 to Eq. (12.29). Then for a two-level system Eqs. (12.28)–(12.29) become in the envelope approximation (12.35)

$$\begin{aligned} \partial_t E + c \partial_z E - (ic/q_0) \nabla_{\perp}^2 E - (i\omega_0/2\varepsilon_0) P + \kappa E = 0, \\ (12.41) \end{aligned}$$

$$\partial_t P + i(\omega_A - \omega_0) P - i(p^2/\hbar) ED + \gamma_{\perp} P = 0, \quad (12.42a)$$

$$\partial_t D - (2i/\hbar)(E^*P - EP^*) + \gamma_{\parallel}(D - D_0) = 0, \quad (12.42b)$$

with $\omega_A = \omega_1 - \omega_2$ the excitation frequency of the two-level system. For a single-mode cavity with frequency ω_c we may make the replacement $c \partial_z E = i(\omega_c - \omega_0) E$, so Eq. (12.41) becomes

$$\begin{aligned} \partial_t E + i(\omega_c - \omega_0) E - (ic/q_0) \nabla_{\perp}^2 E \\ - (i\omega_0/2\varepsilon_0) P + \kappa E = 0. \end{aligned} \quad (12.42c)$$

Let us first consider the usual case where the transverse degrees of freedom are clamped, $\nabla_{\perp} \rightarrow 0$. Then Eqs. (12.42) become three coupled *ode*'s with second-order nonlinearity. For the resonant case

$$\omega_0 = \omega_c = \omega_A, \quad (12.43)$$

this system is identical to the Lorenz model (8.46) with $iE \propto X$, $P \propto Y$, $D \propto Z$, and the control parameter $r \propto D_0$. As is well known (Lorenz, 1963) this model has a stationary bifurcation at $r = 1$, a Hopf bifurcation for

$$r > \sigma(r + b + 3)/(\sigma - b - 1), \quad (12.44)$$

and chaos at larger r . The condition for chaos, $\sigma > b + 1$ requires $\kappa > \gamma_{11} + \gamma_{\perp}$, which implies a “bad” cavity, i.e. large cavity losses. Considerable work has been done to explain the temporal behavior of single-mode lasers and we refer the reader to the literature for further information (Bowden *et al.*, 1984; Chrostowski and Abraham, 1986; Bandy *et al.*, 1988).

Let us ask what happens when the transverse modes are not neglected. As noted by Coullet *et al.* (1989c), the original model (12.42) has a symmetry

$$E \rightarrow e^{i\phi} E, \quad P \rightarrow e^{i\phi} P, \quad D \rightarrow D, \quad (12.45)$$

which may be broken at the Hopf bifurcation. An expansion of the system near the threshold

$$D_0 = D_{0c} = 1 + (\omega_c - \omega_A)/(\kappa + \gamma_{\perp}), \quad (12.46)$$

leads to a complex Ginzburg-Landau equation which we write as

$$\partial_t A = A + (b_1 + ic_1) \nabla_{\perp}^2 A - (1 - ic_3) |A|^2 A, \quad (12.47)$$

with the transverse coordinate defined as

$$\mathbf{y} = \mathbf{x}/L_{\perp}, \quad (12.48)$$

L_{\perp} being the transverse dimension of the cavity; the constants are

$$b_1 = [2\pi FT(1 + \eta)]^{-1} = c[q_0 \kappa L_{\perp}^2 (1 + \eta)]^{-1}, \quad (12.49a)$$

$$c_1 = -2b_1 \theta_0 \eta (1 + \eta)^2 [1 + \eta + \theta_0^2 (1 - \eta)^2]^{-1}, \quad (12.49b)$$

$$c_3 = -\theta_0 (1 - \eta) (1 + \eta)^{-2}, \quad (12.49c)$$

$$\eta = \kappa/\gamma_{\perp}, \quad \theta_0 = (\omega_c - \omega_A)/\gamma_{\perp}, \quad T = \kappa L_{\perp}/c. \quad (12.49d)$$

The important parameter which controls the magnitude

of the transverse variations via b_1 is the Fresnel number

$$F = L_{\parallel}^2 q_0 / 2\pi L_{\parallel}, \quad (12.50)$$

where L_{\parallel} is the longitudinal dimension of the cavity. A large value of F leads to a small b_1 , i.e. the possibility of many transverse modes.

As noted by Coullet *et al.* (1989c), the complex Ginzburg-Landau equation in two dimensions has spiral solutions which are also expected to arise as patterns of the original system (12.42). These authors in fact obtained a spiral in a numerical solution of (12.42) with $b_1 = 4 \times 10^{-4}$, $\eta = 0.04$, $\theta_0 = 0.6$, $\gamma_{\perp}/\gamma_{\parallel} = 1$, $(D_0 - D_{0c})/D_{0c} = 1.2$.

4. Optical bistability

An interesting nonlinear effect, first demonstrated experimentally by Gibbs, McCall, and Venkatesan (1976), is optical bistability of a nonlinear dispersive medium in a Fabry-Perrot interferometer placed inside a ring cavity. Then Gibbs *et al.* showed that according to Eq. (12.37) the effect of nonlinear dispersion is to provide the following relation between the incident and transmitted fields:

$$|E_I/E_0|^2 = f(|E_T/E_0|^2), \quad (12.51)$$

$$f(\alpha) = \alpha[1 + A(1 - \alpha)^2], \quad (12.52)$$

with

$$A = (1 - T)\theta^2/T^2, \quad (12.53)$$

$$E_0 = L_{\parallel} q_0 n_2 / T\theta = \omega_0 n_2 / \kappa\theta, \quad (12.54)$$

where θ is the detuning of the cavity, T the transmission coefficient of the mirrors at the ends of the interferometer whose length is L_{\parallel} , and n_2 the nonlinear dispersion of the medium. It is easy to verify that for $A > 3$ the function f in Eq. (12.52) becomes double-valued, and differential gain and hysteresis ensue. Since A can be tuned by optical means, the necessary condition for observing bistability is that E_0 should be large enough so that E_I/E_0 and E_T/E_0 are of order unity.

The relation (12.51) between the incident and transmitted fields is obtained from Eq. (12.37) neglecting any transverse variation. For media with large Fresnel number (12.50) there is the possibility of obtaining spatial patterns due to the transverse Laplacian in Eq. (12.37). Transverse instabilities of both stationary and oscillatory type are attracting increasing attention (see Abraham and Firth, 1990). Experimental evidence for spatiotemporal chaos in a ring cavity was recently presented by Arechi *et al.* (1990, 1991).

5. Self-induced transparency

Let us consider a medium made up of two-level systems but now tune close to resonance assuming inhomogeneous broadening of the lines. Then neglecting homogeneous broadening ($\gamma_{\perp} = \gamma_{\parallel} = 0$) and diffraction effects,

we may replace P in Eq. (12.42a) by its average $\langle P \rangle$ over a distribution of frequencies resulting from a Maxwellian distribution of atomic velocities. Equations (12.42) now become

$$\partial_t E + c \partial_z E - (i\omega_0/2\varepsilon_0) \langle P \rangle = 0, \quad (12.55a)$$

$$\partial_t \langle P \rangle - (ip^2/\hbar) ED = 0, \quad (12.55b)$$

$$\partial_t D - (2i/\hbar)(E^* \langle P \rangle - E \langle P^* \rangle) = 0. \quad (12.55c)$$

This system turns out to be integrable, as can be seen by making the substitution

$$E = -(\hbar i/2p) \partial_t u, \quad \langle P \rangle = (pD_1/2) \sin u, \quad D = D_1 \cos u, \quad (12.56)$$

so that Eqs. (12.55b)–(12.55c) are automatically satisfied and Eq. (12.55a) becomes

$$(\partial_t + c \partial_z) \partial_t u + \gamma \sin u = 0, \quad (12.57a)$$

$$\gamma = \omega_0 p^2 D_1 / 2\varepsilon_0 \hbar. \quad (12.57b)$$

This equation may easily be transformed into the sine-Gordon equation

$$\partial_r^2 \phi - \partial_z^2 \phi + \sin \phi = 0, \quad (12.58)$$

which has a family of 2π -solitons, as well as a set of breather solutions. The former are nonlinear pulses which travel unattenuated through an absorptive medium. They were first discovered experimentally and described theoretically by McCall and Hahn (1969), who called the phenomenon self-induced transparency. Interestingly, it has recently been suggested by Branis *et al.* (1991) that the existence of a family of such pulses is an artifact of the envelope approximation used to arrive at Eqs. (12.55). When the original Maxwell-Bloch equations (12.28–29) including the fast modes are used instead, these authors find a discrete set of velocities. Moreover, the discrete set does not appear in any order of perturbation theory when fast-mode corrections are added to Eqs. (12.55).

C. Parametric spin-wave instabilities

Parametric wave instabilities analogous to the surface wave instabilities discussed in Sec. IX.D also arise in the case of spin waves in a ferromagnet, and indeed were first studied in this system (Bloembergen and Damon, 1952). Here a spatially uniform oscillating magnetic field drives, above some amplitude threshold, finite wave-vector “spin wave” modes in which the local magnetization precesses with a spatially dependent phase. In the early experiments the oscillating field was applied transverse to the static field and equilibrium magnetization, driving a spatially uniform precession of the magnetization, which in turn drove the parametric instability at nonzero wave vector. Later it was found (Morgenthaler, 1960; Schlömann *et al.*, 1960) that a simpler geometry, with the oscillating field parallel to the static field, also leads

to parametric spin wave instabilities, and this geometry has been favored more recently.

Since it is difficult to diagnose the spatial structure of the nonlinear state beyond threshold, most attention has focused on the complex dynamics that evolves. Also the dissipative effects are weak, as in the fluid surface wave system, so that the quasi-Hamiltonian nature of the system is expected to lead to a highly dynamic state down to driving values very close to threshold. For these reasons spin waves do not provide a good system to demonstrate the phenomena that are the main interest of the present article, and we wish only to make some comparative remarks on the theoretical developments.

Even though the domain of convergence is small, it is convenient to phrase the discussion in terms of the Fourier space amplitude equation analogous to Eq. (4.105)

$$\tau_0 \partial_t \psi_q = [\varepsilon - \xi_0^2 (q - q_0)^2] \psi_q - \sum_{q'} g_{qq'} |\psi_{q'}|^2 \psi_q . \quad (12.59)$$

Here ψ_q is the amplitude of the parametrically excited standing spin wave mode at wave vector q . As usual the phase gives the position of the nodes of the standing wave. The critical circle $q_\perp = |\mathbf{q}_\perp| = q_0$ is in the plane transverse to the static field which we take in the z direction. [Actually, there may be two degenerate critical modes at a given $\mathbf{q}_\perp = (q_x, q_y)$, corresponding to two possible signs of a nonzero q_z (Suhl, 1957). We will not discuss the case with two critical circles, but will only write down expressions for the case $q_z = 0$.] We note in passing that ferromagnetic spin waves are rather complicated even at the linear level, since the frequency of long-wavelength modes depends on the shape of the system (though not its size) due to the dipole form of the interaction, so that actually calculating the parameters of Eq. (12.59) is a formidable task.

In the theoretical analysis of the transverse pumping case, Suhl (1957) proposed that the major dissipative effect leading to saturation of the instability was the suppression of the uniformly precessing mode (at zero wave vector) by the feedback of the parametric modes through the spin-wave interaction terms. Since this feedback is insensitive to the direction of the wave vector q of the wave mode on the critical circle, this immediately leads to the conclusion that in the effective amplitude equation (12.59) we have

$$g_{qq'} = g_0 \quad (12.60)$$

independent of $\hat{\mathbf{q}} \cdot \hat{\mathbf{q}}'$, so that Eq. (12.59) reduces to

$$\tau_0 \psi_q = [\varepsilon - \xi_0^2 (q - q_0)^2 - g_0 \sum_{q'} |\psi_{q'}|^2] \psi_q . \quad (12.61)$$

As a result the nonlinear saturation only depends on the mean square amplitude (intensity) of excited modes $\sum_{q'} |\psi_{q'}|^2$ and *not* on the distribution of this intensity around the critical circle. This led Suhl to propose a *fluctuating* nonlinear state, in which no single mode becomes macroscopically excited. The system therefore

does not possess a well-defined spatial structure, but instead the intensity is distributed amongst all the critical modes, with a distribution that fluctuates in time, responding to some residual noise, perhaps thermal. Anderson (1981; see also Stein, 1980) chose to identify the transversely pumped ferromagnet as the canonical example of pattern forming nonequilibrium systems. He then used the Suhl result to argue that such systems will not form ideal periodic spatial structures. As we have seen, however, the parametric wave systems are atypical cases since they are only weakly dissipative. This means that the dynamics might indeed not be expected to be attracted to a fixed point representing a steady spatial structure. It turns out, moreover, that the Suhl result of a fluctuating nonlinear state depends critically on the assumption (12.60) of a constant mode interaction vertex, which is a result peculiar to the form of dissipation Suhl identifies as dominant. Thus we do not find the Anderson-Stein argument convincing as a general statement on nonequilibrium pattern formation.

The actual nonlinear state of the transversely pumped spin-wave system remains an interesting open question. In a more careful analysis starting from Suhl's dynamical equations, Sneddon and Cross (1982) showed that in fact Eq. (12.60) is not correct. They showed that one can, in general, split $g_{qq'}$ into a part arising from the nondissipative Hamiltonian terms $g^{(h)}$, and a part arising from the nonlinear dissipation $g^{(d)}$ so that

$$g_{qq'} = g_{qq'}^{(h)} + g_{qq'}^{(d)} . \quad (12.62a)$$

Furthermore, symmetry arguments dictate the relation

$$g_{qq'}^{(h)} = -g_{q'q}^{(h)} , \quad (12.62b)$$

and weak dissipation implies

$$g^{(h)} \gg g^{(d)} . \quad (12.63)$$

Note that Eq. (12.62b) implies $g^{(h)} \equiv 0$ in systems in which clockwise and anticlockwise directions around the critical circle are equivalent. This is not the case here, because of the uniform magnetic field.

An immediate consequence of Eqs. (12.62) and (12.63) is that, as in the case of rotating Rayleigh-Bénard convection discussed in Sec. VIII.F.6, a nonlinear state consisting of a single excited standing wave with $\mathbf{q} = q_0 \hat{\mathbf{n}}$, is unstable to a standing wave with $\mathbf{q}' = q_0 \hat{\mathbf{n}}'$ and $\hat{\mathbf{n}}'$ rotated through some angle θ relative to $\hat{\mathbf{n}}$; this state is in turn unstable, and so forth. Thus although the approximations used by Suhl leading to Eq. (12.60) and the dynamic state predicted by him are not correct, the nonlinear state may well be time dependent because of the near Hamiltonian nature of the dynamics.

Since the dissipation is weak in both transverse and longitudinal pumping, Zakharov *et al.* (1975) developed an alternate theory of the nonlinear state, which they called the "S-theory," focusing mainly on the parallel pumping case (see also L'vov and Prozorova, 1988). They propose neglecting the nonlinear damping which leads to the term $g^{(d)}$ in Eq. (12.62a) and to saturation,

since it depends both on the small damping *and* on the small nonlinear terms. Instead the saturation is caused by a “dephasing” of the parametric mode with respect to the pumping. This occurs via terms that are higher-order in $|\psi_q|$ than those retained in Eq. (12.59), but are nondissipative and so do not involve the small dissipation coefficient. The *S*-theory is based on a random phase approximation where $|\psi_q|^2$ is nonzero near the critical circle, but the phase of ψ_q (i.e. the translational position of the mode) is treated as random, either due to thermal or deterministic noise. This theory again leads to a dynamic, fluctuating state but now with

$$|\psi_q|^2 \propto \epsilon^{1/4}, \quad (12.64)$$

rather than the $\epsilon^{1/2}$ dependence resulting from Eq. (12.61). Clearly, close enough to threshold the nonlinear damping must be reintroduced, however over the accessible experimental range Zakharov *et al.* suggest that the *S*-theory should be a good approximation.

D. Further pattern forming systems

In this section we list selected references to pattern forming systems we shall not discuss, but which show many of the phenomena we have described in our review. It should be stressed that neither the list of topics nor the cited references have any pretense of being complete.

- Fluid systems:

- Saffman-Taylor problem (Bensimon *et al.*, 1986).
- Double-layer convection (Rasenat *et al.*, 1989).
- Taylor-Couette flow with partially filled cylinders (Mutabazi *et al.*, 1988, 1990).
- Film flow (Liu and Gollub, 1993).
- Printer’s instability (Rabaud *et al.*, 1991; Cummins *et al.*, 1993; Pan and de Bruyn, 1993).
- Vortex arrays (Willaime *et al.*, 1991).
- Ferrofluids (Bercegol *et al.*, 1987; Silber and Knobloch, 1988).
- Nematics in a rotating magnetic field (Migler and Meyer, 1991).

- Other systems:

- Flame fronts (Sivashinsky, 1983; Clavin, 1985; Schnauer and Haken, 1985; Zel’dovich, 1985).
- Dynamics in ferromagnetic domain walls (Coullet *et al.*, 1990b).
- Beam buckling (Boucif *et al.*, 1991).
- Patterns in catalytic reactions on solid surfaces (Ertl, 1991).
- Flow of granular materials (Baxter and Behringer, 1989; Douady *et al.*, 1989a; Jaeger *et al.*, 1989; Nagel, 1992).

XIII. CONCLUSION

We conclude by briefly reviewing what we believe has and has not been accomplished, and by indicating some useful directions for future research.

A. What has been accomplished

(i) We have analyzed a large array of pattern formation phenomena from a *unified point of view*, which has its origin in the linear instabilities of a homogeneous state. This classification provides a framework for describing seemingly unrelated systems, and suggests useful analogies in theoretical analysis and in the design of experiments. It must be recognized, however, that the classification scheme is most useful in the immediate vicinity of the instability, and it restricts the systems and phenomena under consideration. From a mathematical point of view, the description is expressed in the form of universal *amplitude equations* which are strictly valid only near the bifurcation, but which provide semiquantitative information above threshold as well. Within their range of validity these amplitude equations yield a complete description of the effects that are crucial in pattern formation outside of equilibrium. These are growth of a disturbance with spatial structure, nonlinear saturation, nonlocality through diffusion and, in the case of dynamic instabilities, propagation and dispersion of waves. On the other hand amplitude equations are simple enough so that important but mathematically subtle questions, such as the effects of finite size in restricting ideal patterns, or the dependence of the final state on the protocol of establishing the external conditions, may be analyzed with relative ease.

(ii) In the strongly nonlinear regime above threshold, a complete description of the dynamics must rely on numerical simulation of the starting equations. Some dynamical states of the system, namely those involving slow distortions of an ideal pattern, can be accurately described by the vastly simpler *phase equations* which are consequences of the broken symmetry occurring at the linear instability. A more accurate description in general needs to include *defects*, which are isolated singularities in the phase equation but smooth solutions of the full equations. It is an attractive idea to imagine a description in terms of coupled dynamics of phase and defect degrees of freedom, both in approaching a steady state and in producing persistent dynamics. At the time of writing, the program to establish such a description is almost complete, with most of the technical difficulties overcome, and it will be interesting to see the application to concrete problems in the near future.

(iii) Another way to push the analysis beyond threshold is by inventing *model equations*, designed to incorporate selected pattern forming properties of the starting equations. A necessary (though not sufficient) criterion for the appropriateness of a model is that it should lead to the same amplitude and phase equations as the original system.

This approach is useful to investigate qualitative effects which are beyond the scope of the perturbative amplitude equations. An example is the influence of lateral boundaries in producing large reorientations of the wave vector on long length scales in type I_s systems, which the amplitude equation based on small distortions from a

uniform wave vector is not powerful enough to describe. Another example is persistent dynamics, which is absent from the lowest-order amplitude equation since it is of gradient form in type I_s systems. The approach also gives a way of isolating different features of the full microscopic equations to investigate their influence on the phenomena by judiciously building appropriate model systems. Indeed in the case of chemical reaction-diffusion systems for example, the equations on which much analytic and numerical effort has been expended should properly be thought of as model systems, with a few variables used to describe many complicated reactions, since no systematic justification of the equations has been given. Even in our canonical Rayleigh-Bénard system many new phenomena have historically been predicted from calculations with artificial free-slip boundary conditions. These calculations have the appearance of respectability since they use the full fluid equations for the behavior away from the boundaries, but they are in our view even less controlled than the truncated models we have introduced, since the latter are tuned appropriately by comparing with known results. Indeed the free-slip calculations often produce results which do not qualitatively reflect the behavior of the physical system, as we have remarked at various points throughout the text.

(iv) Armed with the above three classes of approximate equations we have analyzed physically interesting situations (e.g. boundaries, defects) which we call “real pattern” effects. These enter into the problem of *pattern selection*, namely understanding which of the multiplicity of allowed states of a system will actually be found for a given experimental protocol. We do not mean to imply that we have a general solution to the pattern selection problem, only that concrete information is available for a number of physical situations. In discussing real pattern effects it is important to be able to analyze successively more complicated models, in order to elucidate the origin of what are often highly complex phenomena in the realistic equations.

(v) Questions about *universality* and the similarities between different systems are in our view most usefully discussed in terms of the three levels of approximate description mentioned above. The degree of universality of a phenomenon depends on the applicability of one or another of the “universal” approximate equations.

(vi) Among the subjects we have treated, the least well understood is *spatiotemporal chaos*. We have included it in our review partly because it is the main mechanism which disorders nonequilibrium patterns, and partly for its intrinsic interest. We have attempted to confront the questions specific to spatiotemporal chaos which do not arise in studies of systems with a small number of degrees of freedom (temporal chaos). However we do not yet have simple analytic approximations, such as an amplitude expansion, for distortions of a spatiotemporally chaotic state.

(vii) The above theoretical concepts have applicability to a large number of *experimental systems*. Throughout our review we have emphasized the correspondences be-

tween experiment and theory, and the possibility of detailed quantitative comparisons. The range of systems for which the theory has at least some relevance is very large indeed, and in certain cases a significant body of agreement has accumulated. We believe that the tight coupling between theories based on well understood approximations and precise experiments on controlled systems has been vital in developing the growing body of understanding, albeit somewhat piecemeal, of nonequilibrium phenomena. This joint importance reflects to some degree the lack of satisfactory general principles that might make such a pragmatic approach unnecessary (see below).

In summary, we can say that our review attempts an inventory of those pattern formation phenomena that are at least partially understood from our point of view. In this way as new systems are investigated one can distinguish the “easy” problems which have received some attention in analogous systems, from the “hard” ones which demand a fresh and original attack. Before attempting to list some fruitful directions for future research we wish to comment on “what has not been accomplished,” namely on some hoped for general principles which in our opinion fall short of being broadly applicable in the systems considered in this review.

B. What has not been accomplished

(i) A long sought goal of nonequilibrium physics is to find a useful^{13.1} extremum principle such as minimization of the free energy in equilibrium applicable, say, to nonequilibrium steady states reached at long times. Glansdorff and Prigogine (1971, p. 108) state explicitly that “... the search for a universal kinetic potential has proved to be unsuccessful ...,” though they have proposed more specialized variational principles, as well as a “universal evolution criterion” in the form of an inequality involving generalized thermodynamic forces. Landauer (1978, 1988), in particular, has emphasized that the relative occupation of competing states is not determined solely by local properties of these states, but depends on the details of the trajectories joining them. In recent years efforts to find general minimization principles have frequently employed the so-called “maximum entropy formalism” (see Levine, 1987 and references therein, and Landauer, 1981), but we are not aware of new physical results on nonequilibrium pattern formation resulting from this work. Another recent proposal is that of Ross *et al.* (1988a, 1992) focusing on chemical systems, but here again the Lyapunov functional can in general only be found once the equations of motion have been solved.

^{13.1}By “useful” we here mean one that replaces and simplifies the dynamics. As explained in Sec. III.A, the nonequilibrium potential of Graham and coworkers (Graham, 1989) reformulates the dynamics rather than replacing them. We do not mean to imply that it is not useful under certain circumstances, just that it does not correspond to what we have in mind here.

(ii) As mentioned in Sec. VII.E above, the claim^{13.2} that dynamical systems with many spatial degrees of freedom naturally evolve into a self-organized critical state, is also not supported by our detailed studies. Indeed, states with power-law correlation and distribution functions are the exception, not the rule in the experimental systems we have considered. Although scaling phenomena do exist in nature, they apparently result from special circumstances which remain to be fully elucidated.

(iii) Finally, let us mention some more technical issues concerning the proper mathematical description of macroscopic nonequilibrium phenomena. In our view, an appropriate starting point is usually a set of deterministic evolution equations representing the forces acting on the system, on a length and time scale appropriate to the phenomena under study. These equations are sometimes, but by no means always, supplemented by stochastic terms representing thermal or instrumental noise. It is important to remember, however, that such external noise is typically extremely small, or at least very different from the Gaussian white noise often assumed for convenience. Because the starting equations are usually difficult to solve in the large geometries of interest for pattern formation, simplifications are sought, the main ones being perturbation theory near a linear instability (amplitude equations), or expansions about an ideal ordered state (phase equations). Within their domain of validity such equations yield quantitative information on the structure of patterns, which could be obtained (with more difficulty) directly from the starting equations. Outside of this strict domain of applicability, amplitude and phase equations as well as various extensions of these, provide at most semiquantitative information, and results must be interpreted using physical intuition. These remarks apply to the various (phenomenological) order parameter equations we have discussed (see Secs. III.C and IV.A.5), as well as to Ginzburg-Landau models based on symmetry and topology (see, e.g., Coullet and Fauve, 1985). Finally, normal forms (Guckenheimer and Holmes, 1983; Crawford and Knobloch, 1991) are an elegant reformulation of amplitude equations which usually neglect spatial variations, and thus provide a less complete description of patterns.

C. Prospects for the future

It should be clear that even with our somewhat restricted aim of understanding the nonequilibrium states that are related to modes appearing at linear instabilities, much remains to be done. First of all one could hope to improve and extend the work described here. There are as yet only rather few reliable quantitative experiments whose results are fully understood theoretically without resort to *ad hoc* assumptions or adjustable parameters.

We believe that incremental progress in analytic theory, numerical simulations, and laboratory experiments can clarify and deepen our understanding of most of the systems we have discussed. In addition, there no doubt are many new systems and phenomena with similar behavior, some of which will turn out to be amenable to precise experiment and theory. Throughout this review we have attempted to identify open questions and unresolved issues and we hope that a sizeable number of them can be clarified by further work. As was already mentioned earlier, the subject of spatiotemporal chaos seems to us to require the most far-reaching new insights since our understanding is at present rather rudimentary.

Since the remarkable paper by Turing (1952), a long-held dream has been to extend the ideas of pattern formation developed for relatively easily understood chemical or physical systems, to the development of regular structures in biological organisms. We have briefly reviewed work in this direction in Sec. XI, but make no claim to resolving the fundamental issues raised by this research. Answers must rely on careful experimental investigations and on a critical probing of the modeling of the biological phenomena. We might hope, however, that a thorough awareness of the full range of behavior found in chemical and physical experiments and *explained by related simple equations*, may help in assessing the success of the modeling at a more sophisticated level than has been evident in the past.

Apart from improvements in the systems and concepts that we have presented, we can ask whether progress can be made in understanding nonequilibrium systems that are not related in any obvious way to linear instabilities. Examples which come to mind are dendritic patterns, other kinetic phase transitions, fractal growth phenomena, or strong turbulence, to cite only systems where a statistical mechanics approach might still be applicable. Another direction for further work is to analyze the nonlinear models that have been proposed to account for natural phenomena (atmospheric and oceanic flows, geological evolution, physiology, ecology) or to describe technological devices (electronic components) and processes (materials synthesis, corrosion, fracture, etc.). Many of these models bear a strong formal and sometimes physical resemblance to the ones we have studied. We should also concede that there may be some striking new principle or law valid for nonequilibrium phenomena which goes well beyond the concepts we have discussed. Apart from waiting for a bolt from the blue, the most likely method we know of for finding such a general principle is to continue investigating specific systems and phenomena, and testing theoretical ideas by careful experiments.

Finally we will make some remarks on the controversial question of the relevance of our elementary ideas on the nature of nonequilibrium spatial structures to the larger issue of the development of highly complex structures, such as the emergence of life. As a first step towards addressing such questions, Anderson (1981) has focused on the phenomenon of spontaneously broken sym-

^{13.2}See the abstract of Bak *et al.* (1987)

metry, i.e. the existence of states of a system that do not have the full symmetry of the microscopic equations. This concept has unified many diverse phenomena in equilibrium systems, involving the formation of ordered structures such as lattices, superfluids and magnets. Anderson questions the existence or relevance of this phenomenon in dissipative nonequilibrium situations, and argues against the appearance of more complicated emergent properties in this framework. The full importance of the concept of broken symmetry arises in situations where the symmetry involved is a continuous rather than a discrete one. The formation of a regular spatial structure in a previously spatially uniform system is exactly such a situation, and so it is interesting to address Anderson's ideas by bringing to bear the theoretical, and particularly experimental, advances that have occurred in the years since his provocative statements were made.

The existence of states that break translational symmetry seems to us well documented now. Of course this idea must usually represent an idealization in a finite experimental system, though the annular geometry in convection could be thought of as an exception to this statement. Simply from the relative physical scales, the idealization of an infinite system is better for a collection of 10^{23} atoms on a lattice in an equilibrium system, than for $10^4 - 10^6$ convection cells in a "large" nonequilibrium structure. Nevertheless, impressive examples in nonequilibrium systems now exist, as exemplified, in particular, by the structures in Figs. 49(a) and 87. In the former a pattern of hexagonal convection cells in a cylindrical geometry is shown. Certainly the rotational symmetry is broken, but we also see that the hexagonal pattern seems to exist in spite of the boundaries, not because of them. Near the boundary one or two circular rolls are seen, but this disturbance dies out in the bulk, leaving a regular hexagonal lattice. Moreover, when the control parameter is raised slightly, a completely different broken symmetry state appears, in the form of a spiral shown in Fig. 49(b). Figure 87 shows a small portion from a stationary hexagonal pattern in a chemical reaction-diffusion system, confirming Turing's original intuition. This system is particularly noteworthy since the lattice scale is determined entirely by internal parameters (the diffusion and reaction rates, actually both molecular quantities) rather than by geometrical factors such as the height in Rayleigh-Bénard convection (this point was made many years ago by Walgraef *et al.*, 1981, before stationary Turing structures had been realized experimentally). It is perhaps surprising that we invoke hexagonal patterns in our argument, when much of our article has concerned roll states. In fact roll states are much less suited to showing regular structures which are independent of boundary effects and defect free, but this is also true in equilibrium, where the analogous system — a smectic liquid crystal — is notorious for its irregular configurations with many defects (focal conics).

There are of course special situations where regular spatial patterns may not form; for example the type I_o instability when the coefficients are such that the state just

above onset is unstable by the Newell criterion (4.57a). As we have pointed out in Sec. XII.C, the parametric spin-wave instability in ferromagnets quoted by Anderson (1981) and Stein (1979) is another example where this is true. However the idealization of the Suhl analysis followed by these authors, leading to a stochastic distribution of the mean-square amplitude amongst many modes, does not survive a more careful analysis. It is amusing to note that the discussion of Sec. IV.A.1.a.iv shows that regular spatial pattern formation does not occur in that system because it is not dissipative enough! More typically, in dissipative systems the nonlinearities will favor a concentration of the amplitude in a single or a few modes, i.e. a regular pattern in space.

Perhaps more important than simply the existence of broken symmetry states is a unifying set of new properties implied by their presence (Anderson, 1981). We will attempt to point out *experimental* demonstrations of these same properties in nonequilibrium systems.

- New dynamics: the existence of low-frequency modes, often denoted Goldstone modes, reflecting the absence of restoring forces for uniform displacements. In the language of this review this is the phase dynamics, which as we have seen is well verified in experiments, for example in convection (Sec. VIII.C). Often this dynamics is *diffusive*, i.e. a nonoscillatory relaxation with time scale $\tau(Q) \sim Q^{-2}$ for a disturbance of wave vector Q , whereas usually (but by no means always) it is propagating in equilibrium systems. Propagating phase dynamics may also be found in nonequilibrium systems, e.g. the phase dynamics of the wavy vortex state in the Taylor-Couette system recently demonstrated experimentally by Wu and Andereck (1991).

- Generalized rigidity: action at a distance or long-range forces. This feature is well demonstrated by experiments on the Taylor-Couette system with ramped sidewalls over a portion of the length. Here the nature of the ramp may be used to control the steady-state "lattice spacing" (i.e. the roll width) arbitrarily far away (Sec. IX.B.2.d).

- Topological defects which relax the generalized rigidity. We have discussed this point in detail in Secs. V.B and VIII.C. A particularly nice experimental demonstration is the climb of dislocations relaxing the wave vector in the experiments of Pocheau and Croquette (1984) shown in Fig. 19.

These examples demonstrate the same physical consequences of broken symmetry as in equilibrium systems, and there are many other examples throughout this review where ideas motivated by broken symmetry concepts have been tested experimentally in laboratory situations.

The robustness of the spatial structures in nonequilibrium systems is however less clear, and requires some further discussion. Certainly in the absence of principles of time reversal invariance and of global minimization, the range of phenomena leading to a breakdown of spatial order is richer than in equilibrium systems. As a general rule regular structures therefore only survive for

some finite range of control parameter near threshold. Sometimes, particularly in systems with roll type symmetry, the parameters must be chosen quite delicately to yield a stable stationary structure. On the other hand the Taylor-vortex roll structure is found to survive into the strongly chaotic regime, with remarkably clear delineation of the large-scale rolls in a fluid which is strongly chaotic on the small scales. Also we have suggested that, as in equilibrium systems, cellular structures are more robust than striped ones.

Thus, at the laboratory scale we find that the existence of spontaneously broken continuous symmetries, and the relevance of this idea to experimental phenomena (i.e. "Broken Symmetry," not just "broken symmetry" in the language of Anderson, 1981), can be considered to be established.

This conclusion does not address the larger question of whether these structures appearing from nowhere in a dissipative system are an appropriate first step in modeling more exotic (and more interesting!) phenomena such as the emergence of life from the primordial soup. As we have tried to make clear in this review there is no evidence for the existence of any global minimization principles controlling the structure, except as a perturbative statement near threshold. Such a principle would make it easier to generalize from the small scale phenomena of the laboratory (in the sense of number of unit blocks) to the large-scale phenomena of biological complexity. As a modest contribution to the debate we have reviewed tools and ideas which may be relevant to the building blocks of such phenomena. It seems plausible to us (although by no means demonstrated) that reaction-diffusion type mechanisms, perhaps augmented with other phenomena such as forces and flows, *may* provide a mechanism for communicating information encoded at the molecular level up to the cellular level. It is encouraging to note that parameters set by molecular scales can lead naturally to macroscopic length scales, through energy barriers appearing in exponential activation expressions that are large for large molecules. As in many branches of physics, however, it is simply not clear how many conceptual leaps are involved in putting together these building blocks to make the full satisfying edifice.

ACKNOWLEDGEMENTS

The authors have benefited from conversations and collaborations with many colleagues, too numerous to

mention individually, during the many years it took to complete this project. They are particularly indebted to the Aspen Center for Physics for providing a fruitful environment for this collaboration. MCC was supported in part by the NSF under Grants No. DMR-8412543 and DMR-9013984.

APPENDIX A. DERIVATION OF THE AMPLITUDE EQUATION

1. The Swift-Hohenberg equation

We first illustrate the multiple scales approach used to derive amplitude equations on a particularly simple example where the answer can almost be guessed without calculation. We consider the Swift-Hohenberg model (3.27) in two dimensions,

$$\partial_t u = \varepsilon u - (\nabla^2 + q_0^2)^2 u - u^3, \quad (A1)$$

where for clarity we introduce the scale q_0 in the original equation. Near the bifurcation, i.e. for $|\varepsilon| \ll 1$, we wish to separate fast and slow scales for x and t . We therefore define

$$X = \varepsilon^{1/2} x, \quad Y = \varepsilon^{1/4} y, \quad T = \varepsilon t, \quad (A2)$$

anticipating the anisotropic scaling for roll systems in Eq. (4.3). We will consider $u(x, t)$ to be a product of functions of fast and slow variables. From the chain rule for differentiation we therefore must make the replacements

$$\partial_x \rightarrow \partial_x + \varepsilon^{1/2} \partial_X, \quad \partial_y \rightarrow \partial_y + \varepsilon^{1/4} \partial_Y, \quad \partial_t \rightarrow \partial_t + \varepsilon \partial_T, \quad (A3)$$

etc., where on the right-hand side ∂_x , ∂_y , and ∂_t now only act on the rapid dependences. The differential operator in Eq. (A1) becomes

$$(\nabla^2 + q_0^2) \rightarrow \partial_x^2 + 2\varepsilon^{1/2} \partial_x \partial_X + \varepsilon \partial_X^2 + \varepsilon^{1/2} \partial_Y^2 + q_0^2, \quad (A4)$$

where we assume no rapid y dependence, i.e. we are expanding about a roll state with wave vector along x . Let us now set

$$u = \varepsilon^{1/2} u_0 + \varepsilon u_1 + \varepsilon^{3/2} u_2, \quad (A5)$$

and insert (A4) and (A5) into Eq. (A1). Collecting orders of $\varepsilon^{1/2}$ we find

$$\varepsilon^{1/2}: \quad (\partial_x^2 + q_0^2)^2 u_0 = 0, \quad (A6a)$$

$$\varepsilon: \quad (\partial_x^2 + q_0^2)^2 u_1 = -2(2\partial_x \partial_X + \partial_Y^2)(\partial_x^2 + q_0^2) u_0, \quad (A6b)$$

$$\varepsilon^{3/2}: \quad (\partial_x^2 + q_0^2)^2 u_2 = -2(2\partial_x \partial_X + \partial_Y^2)(\partial_x^2 + q_0^2) u_1 - [\partial_T - 1 + u_0^2 + (2\partial_x \partial_X + \partial_Y^2)^2 + 2\partial_X^2(\partial_x^2 + q_0^2)] u_0. \quad (A6c)$$

The first two equations are solved by setting

$$u_0(\mathbf{x}, t) = A_0(X, Y, T) e^{iq_0 x} + \text{c.c.}, \quad (\text{A7a})$$

$$u_1(\mathbf{x}, t) = A_1(X, Y, T) e^{iq_0 x} + \text{c.c.}, \quad (\text{A7b})$$

since Eq. (A7a) implies

$$(\partial_x^2 + q_0^2) u_0 = 0, \quad (\text{A8})$$

so that the rhs of Eq. (A6b) vanishes identically. The last equation (A6c), has a nontrivial rhs so the linear operator on the left must be inverted. Since this operator has vanishing eigenvalues we must impose a *solvability condition*, requiring that the vector on the right should not drive any eigenvector with zero eigenvalue (Stakgold, 1979). The simplest example of such a condition occurs for a matrix equation

$$\tilde{\mathcal{M}}\mathbf{V} = \mathbf{G}. \quad (\text{A9})$$

Let \mathbf{C}_0 be an eigenvector of the adjoint $\tilde{\mathcal{M}}^\dagger$ with zero eigenvalue. Then clearly

$$(\mathbf{C}_0, \tilde{\mathcal{M}}\mathbf{V}) = (\tilde{\mathcal{M}}^\dagger \mathbf{C}_0, \mathbf{V}) = (\mathbf{C}_0, \mathbf{G}) = 0, \quad (\text{A10})$$

i.e. \mathbf{G} is orthogonal to \mathbf{C}_0 . The Fredholm theorem states that Eq. (A10) is also a sufficient condition, i.e. Eq. (A9) has a solution for \mathbf{V} if and only if \mathbf{G} is orthogonal to all zero eigenvectors of $\tilde{\mathcal{M}}^\dagger$. This theorem also holds if $\tilde{\mathcal{M}}$ is replaced by a differential operator.

For Eq. (A6c) the operator

$$\mathcal{L}_0 = (\partial_x^2 + q_0^2)^2 \quad (\text{A11})$$

$$\varepsilon^{1/2}: \quad (\partial_x^2 + q_0^2)^2 u_0 = 0,$$

$$\varepsilon: \quad (\partial_x^2 + q_0^2)^2 u_1 = -4\partial_x \partial_x (\partial_x^2 + q_0^2) u_0 - u_0 \partial_x u_0,$$

$$\varepsilon^{3/2}: \quad (\partial_x^2 + q_0^2)^2 u_2 = -4\partial_x \partial_x (\partial_x^2 + q_0^2) u_1 \\ - [\partial_T - 1 + 4\partial_x^2 \partial_x^2 + 2\partial_x^2 (\partial_x^2 + q_0^2)] u_0 - u_0 \partial_x u_1 - u_1 \partial_x u_0 - u_0 \partial_x u_0.$$

These equations are solved by setting

$$u_0(u, t) = A_0(X, T) e^{iq_0 x} + \text{c.c.}, \quad (\text{A19a})$$

$$u_1(u, t) = A_1(X, T) e^{iq_0 x} + B_1(X, T) e^{2iq_0 x} + \text{c.c.}, \quad (\text{A19b})$$

$$u_2(u, t) = A_2(X, T) e^{iq_0 x} + B_0 + B_2 e^{2iq_0 x} + B_3 e^{3iq_0 x} + \text{c.c.} \\ (\text{A19c})$$

The function $B_1(X, T)$ can be calculated by setting the coefficient of $\exp(2iq_0 x)$ in Eq. (A18b) to zero, yielding

$$B_1 = -i (9q_0^3)^{-1} A_0^2. \quad (\text{A20})$$

With these choices Eqs. (A19a) and (A19b) are satisfied identically, and Eq. (A19c) once again requires a solvability condition, which is obtained by setting the coefficient of $\exp(iq_0 x)$ on the rhs to zero. The result is

is self-adjoint and its zero eigenvectors are $\exp(\pm iq_0 x)$. The Fredholm theorem thus requires that the coefficients of these terms on the rhs of Eq. (A6c) should vanish identically, i.e. A_0 should satisfy the solvability condition

$$[\partial_T - 1 + 3|A_0|^2 + (2iq_0 \partial_X + \partial_Y^2)^2] A_0 = 0. \quad (\text{A12})$$

Returning to unscaled units

$$A(\mathbf{x}, t) = \varepsilon^{1/2} A_0(X, Y, T), \quad (\text{A13})$$

we have the general amplitude equation (4.3)

$$\tau_0 \partial_t A = \varepsilon A + \xi_0^2 [\partial_x - (i/2q_0) \partial_y^2]^2 A - g_0 |A|^2 A, \quad (\text{A14})$$

with

$$\tau_0 = 1, \quad \xi_0^2 = 4q_0^2, \quad g_0 = 3. \quad (\text{A15})$$

[The value of g_0 depends on the arbitrary normalization in Eq. (A7a).]

2. The Kuramoto-Sivashinsky equation

Let us consider the damped KS model (3.31) in one dimension

$$\partial_t u = -\eta u - \partial_x^2 u - \partial_x^4 u - u \partial_x u, \quad (\text{A16})$$

which we rewrite as

$$\partial_t u = \varepsilon u - (\partial_x^2 + q_0^2)^2 u - u \partial_x u, \quad (\text{A17})$$

with $\varepsilon = 1/4 - \eta$, $q_0^2 = 1/2$. The equations corresponding to (A6) are

$$\varepsilon^{1/2}: \quad (\partial_x^2 + q_0^2)^2 u_0 = 0, \quad (\text{A18a})$$

$$\varepsilon: \quad (\partial_x^2 + q_0^2)^2 u_1 = -4\partial_x \partial_x (\partial_x^2 + q_0^2) u_0 - u_0 \partial_x u_0, \quad (\text{A18b})$$

$$\varepsilon^{3/2}: \quad (\partial_x^2 + q_0^2)^2 u_2 = -4\partial_x \partial_x (\partial_x^2 + q_0^2) u_1 \\ - [\partial_T - 1 + 4\partial_x^2 \partial_x^2 + 2\partial_x^2 (\partial_x^2 + q_0^2)] u_0 - u_0 \partial_x u_1 - u_1 \partial_x u_0 - u_0 \partial_x u_0. \quad (\text{A18c})$$

$$[\partial_T - 1 - 4q_0^2 \partial_X^2 + (9q_0^2)^{-1} |A_0|^2] A_0 = 0, \quad (\text{A21})$$

which leads to the general amplitude equation (A14) with $\varepsilon = 1/4 - \eta$, $\tau_0 = 1$, $\xi_0^2 = 4q_0^2 = 2$, $g_0 = (9q_0^2)^{-1} = 2/9$.

$$(\text{A22})$$

3. Rayleigh-Bénard convection

A much more involved calculation is necessary to derive the amplitude equation (A14) from the hydrodynamic equations (8.3) for Rayleigh-Bénard convection. We will once again use the method of multiple-scales perturbation theory. An alternative approach, perhaps more familiar to physicists, is the mode expansion or pro-

jection technique, also known as slaving (Haken, 1983; Cross, 1980). As for the previous models, we will investigate the situation of a single set of slowly varying rolls close to an ideal pattern of straight rolls parallel to the y axis (wave vector along x).

It is convenient first to eliminate the pressure field from Eq. (8.10a) for the velocity field $\mathbf{u}=(\mathbf{u}_\perp, w)=(u, v, w)$, and rewrite Eqs. (8.10) in the form

$$\nabla^2\theta + R w = \partial_t\theta + (\mathbf{u}_\perp \cdot \nabla_\perp)\theta + w\partial_z\theta, \quad (\text{A23a})$$

$$\begin{aligned} \nabla_\perp^2\theta + \nabla^4 w &= \sigma^{-1} \{ \partial_t\nabla^2 w - \partial_z\nabla_\perp \cdot [(\mathbf{u}_\perp \cdot \nabla_\perp)\mathbf{u}_\perp + w\partial_z\mathbf{u}] \\ &\quad + \nabla_\perp^2[(\mathbf{u}_\perp \cdot \nabla_\perp)w + w\partial_z w] \}. \end{aligned} \quad (\text{A23b})$$

We have grouped together terms on the lhs that are involved in the linear threshold calculation. Terms on the rhs are zero in this limit; we will treat these terms by perturbation theory, as well as expanding the operator on the lhs about threshold. In addition to Eqs. (A23) there is an equation for the vertical vorticity $\Omega_z = (\nabla \times \mathbf{u})_z$. Once w and Ω_z are known at each order, \mathbf{u} may be calculated from the continuity equation (8.10c). For rigid top and bottom boundary conditions, to the order of the expansion we will need, $\Omega_z = 0$. In the original derivation of the amplitude equation for the free-slip model (Newell and Whitehead, 1969; Segel, 1969) this same assumption was made. As discussed in Sec. VIII.A, Siggia and Zippelius (1981b) showed that if $\partial_y \neq 0$, and for finite Prandtl numbers, this is in error even for the lowest-order amplitude equation, since the vertical vorticity is not damped in the case of free-slip boundaries.

For pedagogical purposes we will use the infinite Prandtl number limit $\sigma \rightarrow \infty$. For the rigid boundary case this is purely for convenience of exposition, since the many terms on the rhs of (A23b) are eliminated: retaining these terms in an actual calculation simply makes the bookkeeping harder, there is no difficulty of principle. For the free-slip case this assumption eliminates the difficulty of including the vertical vorticity, since $\Omega_z \equiv 0$ when $\sigma \rightarrow \infty$. We will carry the calculation far enough in the rigid case to make the formal procedure clear. Evaluating the expressions is best done numerically, although closed form expressions can be obtained. For the free-slip case we evaluate the expressions explicitly.

We first solve the linear threshold problem, and look for the neutrally stable mode (growth rate zero)

$$\theta(x, z) = \bar{\theta}_q(z) e^{iqx}, \quad (\text{A24a})$$

$$w(x, z) = \bar{w}_q(z) e^{iqx}, \quad (\text{A24b})$$

$$u(x, z) = \bar{u}_q(z) e^{iqx}, \quad (\text{A24c})$$

where the q -dependent onset Rayleigh number $R = R_c(q)$ is given by solving

$$\begin{bmatrix} (\partial_z^2 - q^2) & R_c(q) \\ q^2 & -(\partial_z^2 - q^2)^2 \end{bmatrix} \begin{bmatrix} \bar{\theta}_q(z) \\ \bar{w}_q(z) \end{bmatrix} = 0, \quad (\text{A25})$$

together with the boundary conditions at $z=0, 1$

$$\bar{\theta}_q(z) = \bar{w}_q(z) = \partial_z \bar{w}_q(z) = 0, \quad \text{rigid}, \quad (\text{A26a})$$

$$\bar{\theta}_q(z) = \bar{w}_q(z) = \partial_z^2 \bar{w}_q(z) = 0, \quad \text{free-slip}. \quad (\text{A26b})$$

For the free-slip case we readily find (with an arbitrary overall normalization),

$$\bar{\theta}_q(z) = (4\sqrt{2}/\pi^2)(q^2 + \pi^2)^2 \sin \pi z, \quad (\text{A27a})$$

$$\bar{w}_q(z) = (4\sqrt{2}/\pi^2)q^2 \sin \pi z, \quad (\text{A27b})$$

$$\bar{u}_q(z) = (-4i\sqrt{2}/\pi)q \cos \pi z, \quad (\text{A27c})$$

and for rigid boundaries the solutions may be found in Pellew and Southwell (1940) and Schlüter *et al.* (1965). We choose the value of $q = q_0$ that minimizes $R_c(q)$ and will write $\bar{\theta}_q$, \bar{w}_q , \bar{u}_q as $\bar{\theta}_0$, \bar{w}_0 , \bar{u}_0 at this value. For free-slip, $q_0 = \pi/\sqrt{2}$, $R_c(q_0) = R_{c0} = 27\pi^4/4$ and for rigid boundaries, $q_0 \approx 3.114$, $R_{c0} \approx 1708$.

We now expand Eqs. (A23) consistently in $\varepsilon^{1/2}$, with $\varepsilon = (R - R_{c0})/R_{c0}$,

$$\theta = \varepsilon^{1/2}\bar{\theta}_0 + \varepsilon\theta_1 + \dots, \quad (\text{A28a})$$

$$w = \varepsilon^{1/2}\bar{w}_0 + \varepsilon w_1 + \dots, \quad (\text{A28b})$$

$$u = \varepsilon^{1/2}\bar{u}_0 + \varepsilon u_1 + \dots. \quad (\text{A28c})$$

At $O(\varepsilon^{1/2})$ we have

$$\theta_0 = A_0(X, Y, T) e^{iq_0 x} \bar{\theta}_0(z) + \text{c.c.}, \quad (\text{A29a})$$

$$w_0 = A_0(X, Y, T) e^{iq_0 x} \bar{w}_0(z) + \text{c.c.}, \quad (\text{A29b})$$

$$u_0 = A_0(X, Y, T) e^{iq_0 x} \bar{u}_0(z) + \text{c.c.}, \quad (\text{A29c})$$

where we allow the amplitude of the threshold solution A_0 to vary with the slow space and time scales introduced in Eq. (A2) above. As before, these scalings with ε are formally determined by the ultimate consistency of the expansion, and in particular the balance of terms found in Eq. (A48) below. They are also readily obtained by inspection of the growth rate $\sigma(q, \varepsilon)$, Eq. (4.4).

We rewrite Eqs. (A23) (remember $\sigma \rightarrow \infty$) as

$$\mathcal{L} \begin{bmatrix} \theta \\ w \end{bmatrix} = \begin{bmatrix} \partial_t\theta + (\mathbf{u}_\perp \cdot \nabla_\perp)\theta + w\partial_z\theta \\ 0 \end{bmatrix}, \quad (\text{A30})$$

where \mathcal{L} has the expansion

$$\mathcal{L} = \mathcal{L}_0 + \varepsilon^{1/2} \mathcal{L}_1 + \varepsilon \mathcal{L}_2 + \dots, \quad (\text{A31})$$

with

$$\mathcal{L}_0 = \begin{bmatrix} \partial_z^2 + \partial_x^2 & R_{c0} \\ -\partial_x^2 & -(\partial_z^2 + \partial_x^2)^2 \end{bmatrix}, \quad (\text{A32a})$$

$$\mathcal{L}_1 = \begin{bmatrix} 1 & 0 \\ -1 & -2(\partial_x^2 + \partial_z^2) \end{bmatrix} (2\partial_x\partial_X + \partial_Y^2), \quad (\text{A32b})$$

$$\begin{aligned} \mathcal{L}_2 = & \begin{bmatrix} 1 & 0 \\ -1 & -2(\partial_x^2 + \partial_z^2) \end{bmatrix} \partial_x^2 \\ & + \begin{bmatrix} 0 & R_{c0} \\ 0 & (2\partial_x\partial_X + \partial_Y^2)^2 \end{bmatrix}. \end{aligned} \quad (\text{A32c})$$

On the rhs of (A30) it turns out that the only terms we need are

$$\partial_t \theta + (\mathbf{u}_\perp \cdot \nabla_\perp) \theta + w \partial_z \theta = \varepsilon [u_0 \partial_x \theta_0 + w_0 \partial_z \theta_0] + \varepsilon^{3/2} [\partial_T \theta_0 + (u_1 \partial_x \theta_0 + u_0 \partial_x \theta_1) + (w_1 \partial_z \theta_0 + w_0 \partial_z \theta_1)] + O(\varepsilon^{3/2}) + O(\varepsilon^2), \quad (\text{A33})$$

where the $O(\varepsilon^{3/2})$ terms not displayed [independent of x or proportional to $\exp(\pm 2iq_0x)$] are not needed to the order we will go. At $O(\varepsilon)$ we have

$$\mathcal{L}_0 \begin{bmatrix} \theta_1 \\ w_1 \end{bmatrix} = -\mathcal{L}_1 \begin{bmatrix} \theta_0 \\ w_0 \end{bmatrix} + \begin{bmatrix} u_0 \partial_x \theta_0 + w_0 \partial_z \theta_0 \\ 0 \end{bmatrix}, \quad (\text{A34})$$

and we would like to invert this equation to find (θ_1, w_1) . As above, in order to do this we require that the rhs of Eq. (A34) be orthogonal to all zero eigenvectors of \mathcal{L}_0^\dagger . Since \mathcal{L}_0 is self-adjoint, we know one such eigenvector, namely the onset solution (θ_0, w_0) . The nonlinear terms on the rhs of (A34) depend on the fast variable x as $\exp(\pm 2iq_0x)$, or are independent of x , and they are automatically orthogonal to $(\theta_0, w_0) \propto \exp(iq_0x)$. On the other hand the linear terms in Eq. (A34) do involve the dangerous $\exp(\pm iq_0x)$ factors and we might expect a solvability condition at this order. However, it turns out that since we are expanding about the *minimum* q_0 of $R_c(q)$, this condition is identically satisfied. Indeed, we may write

$$\begin{bmatrix} \theta_1 \\ w_1 \\ u_1 \end{bmatrix} = \begin{bmatrix} \tilde{\theta}_1 \\ \tilde{w}_1 \\ \tilde{u}_1 \end{bmatrix} + (2q_0)^{-1}(2\partial_x \partial_X + \partial_Y^2) A_0 \begin{bmatrix} \bar{\theta}_0(z) \\ \bar{w}_0(z) \\ \bar{u}_0(z) \end{bmatrix} + \text{c.c.}, \quad (\text{A35})$$

where $\bar{\theta}_0(z)$, $\bar{w}_0(z)$, and $\bar{u}_0(z)$ are defined as $\partial_q \theta_q(z)|_{q=q_0}$, etc. Then the functions $\tilde{\theta}_1, \tilde{w}_1$ satisfy the same equation as θ_1, w_1 , except that the linear terms are absent

$$\mathcal{L}_0 \begin{bmatrix} \tilde{\theta}_1 \\ \tilde{w}_1 \end{bmatrix} = \begin{bmatrix} u_0 \partial_x \theta_0 + w_0 \partial_z \theta_0 \\ 0 \end{bmatrix}. \quad (\text{A36})$$

This result depends on the identity, obtained by differentiating Eq. (A25) with respect to q ,

$$\begin{bmatrix} \partial_z^2 - q_0^2 & R_{c0} \\ q_0^2 & -(\partial_z^2 - q_0^2)^2 \end{bmatrix} \begin{bmatrix} \bar{\theta}_0(z) \\ \bar{w}_0(z) \end{bmatrix} - 2q_0 \begin{bmatrix} 1 & 0 \\ -1 & -2(\partial_z^2 - q_0^2) \end{bmatrix} \begin{bmatrix} \bar{\theta}_0(z) \\ \bar{w}_0(z) \end{bmatrix} = 0. \quad (\text{A37})$$

Equation (A36) is now nonsingular and may be inverted to yield

$$\begin{bmatrix} \tilde{\theta}_1 \\ \tilde{w}_1 \end{bmatrix} \sim \left\{ A_0^2 e^{2iq_0x} \begin{bmatrix} f_1(z) \\ f_2(z) \end{bmatrix} + A_1 e^{iq_0x} \begin{bmatrix} \bar{\theta}_0(z) \\ \bar{w}_0(z) \end{bmatrix} + \text{c.c.} \right\} + |A_0|^2 \begin{bmatrix} f_3(z) \\ f_4(z) \end{bmatrix}, \quad (\text{A38})$$

with the $f_i(z)$ determined below. Similarly, the replacement of u_1 by \tilde{u}_1 in Eq. (A35) has the effect of eliminating terms in $\partial_X u_0$ from the $O(\varepsilon)$ continuity equation, which simply becomes

$$\partial_x \tilde{u}_1 + \partial_z \tilde{w}_1 = 0. \quad (\text{A39})$$

(Note that the above procedure was not necessary in the simple examples of Secs. A.1 and A.2, because there \bar{u}'_0 was zero.)

The elimination of a solvability condition at order ε works for any type I_s system. For the free-slip case the term on the rhs of (A36) reduces to $72\pi^3|A_0|^2 \sin 2\pi z$, and the inversion of (A36) yields

$$f_1(z) = f_2(z) = f_4(z) = 0, \quad (\text{A40a})$$

$$f_3(z) = -18\pi \sin 2\pi z. \quad (\text{A40b})$$

The functions $f_i(z)$ can also be obtained, with somewhat larger effort, in closed form for the rigid case. The second term in Eq. (A38) is the complementary function, with A_1 unknown at this stage. Using the expressions for (θ_1, w_1, u_1) from Eqs. (A35) and (A38), we can iterate to the next order, $O(\varepsilon^{3/2})$, obtaining

$$\mathcal{L}_0 \begin{bmatrix} \theta_2 \\ w_2 \end{bmatrix} = G, \quad (\text{A41})$$

where G contains many terms. The requirement that G should not drive the zero-eigenvalue eigenvector of \mathcal{L}_0^\dagger yields at this order a nontrivial *solvability condition*, which finally gives us the amplitude equation. Again we need only collect the terms in $\exp(\pm iq_0x)$, to find

$$\begin{aligned}
\mathcal{L}_0 \begin{bmatrix} \theta_2 \\ w_2 \end{bmatrix} = & - \begin{bmatrix} 1 & 0 \\ -1 & -2(\partial_x^2 + \partial_z^2) \end{bmatrix} \begin{bmatrix} \bar{\theta}_0 \\ \bar{w}_0 \end{bmatrix} \left\{ [2\partial_x \partial_X + \partial_Y^2] A_1 + \partial_X^2 A_0 \right\} e^{iq_0 x} + \text{c.c.} \\
& - \begin{bmatrix} 1 & 0 \\ -1 & -2(\partial_x^2 + \partial_z^2) \end{bmatrix} \begin{bmatrix} \bar{\theta}'_0 \\ \bar{w}'_0 \end{bmatrix} \frac{1}{2q_0} \left\{ (2\partial_x \partial_X + \partial_Y^2)^2 A_0 e^{iq_0 x} + \text{c.c.} \right\} \\
& - \left\{ \begin{bmatrix} -\partial_T A_0 & R_{c0} A_0 \\ 0 & (2\partial_x \partial_X + \partial_Y^2)^2 A_0 \end{bmatrix} \begin{bmatrix} \bar{\theta}_0 \\ \bar{w}_0 \end{bmatrix} e^{iq_0 x} + \text{c.c.} \right\} \\
& + \begin{bmatrix} \tilde{u}_1 \partial_x \theta_0 + u_0 \partial_x \tilde{\theta}_1 + \tilde{w}_1 \partial_z \theta_0 + w_0 \partial_z \tilde{\theta}_1 \\ 0 \end{bmatrix}_{\pm q_0} + B_0 + B_2 e^{2iq_0 x} + B_3 e^{3iq_0 x} + \text{c.c.} . \tag{A42}
\end{aligned}$$

In Eq. (A42) the symbol $(\)_{\pm q_0}$ denotes picking out terms varying with the fast variable x as $\exp(\pm iq_0 x)$. As in Eq. (A34) the first term on the rhs of (A42) contains the factor

$$\begin{bmatrix} 1 & 0 \\ -1 & -2(\partial_x^2 + \partial_z^2) \end{bmatrix} \begin{bmatrix} \bar{\theta}_0 \\ \bar{w}_0 \end{bmatrix} e^{iq_0 x}, \tag{A43}$$

so this term may be subtracted out as in (A35)–(A38).

In the present case, for both free-slip and rigid boundaries, the operator \mathcal{L}_0 is self-adjoint under the scalar product of the vectors $V_a = (\theta_a, w_a)$, $V_b = (\theta_b, w_b)$

$$(V_a, V_b) = \int d\mathbf{x}_\perp dz [(\nabla_\perp \theta_a)^* \cdot (\nabla_\perp \theta_b) + R_{c0} w_a^* w_b], \tag{A44}$$

so that we may simply require orthogonality of G (under this definition of scalar product) to the zero eigenvalue mode (θ_0, w_0) . The free-slip case is particularly simple because the fourth term on the rhs of Eq. (A42) reduces to

$$\begin{bmatrix} & \end{bmatrix}_{\pm q_0} = \begin{bmatrix} w_0 \partial_z \tilde{\theta}_1 \\ 0 \end{bmatrix}_{\pm q_0} = \begin{bmatrix} -72\sqrt{2}\pi^2 |A_0|^2 A_0 e^{iq_0 x} + \text{c.c.} \\ 0 \end{bmatrix}. \tag{A45}$$

Also in view of (A27) we have

$$\frac{1}{2q_0} \begin{bmatrix} \bar{\theta}'_0(z) \\ \bar{w}'_0(z) \end{bmatrix} = \frac{4\sqrt{2}}{\pi^2} \begin{bmatrix} 3\pi^2 \\ 1 \end{bmatrix} \sin \pi z. \tag{A46}$$

Thus the solvability condition reduces to the scalar product

$$\left\{ (\bar{\theta}_0(z), \bar{w}_0(z)), \left[\frac{4\sqrt{2}}{\pi^2} \begin{bmatrix} 3\pi^2 \\ 0 \end{bmatrix} (2iq_0 \partial_X + \partial_Y^2)^2 A_0 + \begin{bmatrix} -\partial_T A_0 & R_{c0} A_0 \\ 0 & (2iq_0 \partial_X + \partial_Y^2)^2 \end{bmatrix} \begin{bmatrix} \bar{\theta}_0 \\ \bar{w}_0 \end{bmatrix} + \begin{bmatrix} 72\sqrt{2}\pi^2 |A_0|^2 A_0 \\ 0 \end{bmatrix} \right] \right\} = 0, \tag{A47}$$

where we define the scalar product in the same way as in Eq. (A44), except that ∇_\perp is replaced by iq_0 , which eliminates the \mathbf{x}_\perp dependence, leaving only the z integral. This finally yields

$$(2/3\pi^2) \partial_T A_0 = A_0 + (8/3\pi^2) [\partial_X + (1/2iq_0) \partial_Y^2]^2 A_0 - (8/3\pi^2) |A_0|^2 A_0, \tag{A48}$$

i.e. Eq. (A14) with

$$\tau_0 = 2/3\pi^2, \quad \xi_0^2 = 8/3\pi^2, \quad g_0 = 8/3\pi^2. \tag{A49}$$

Note that with the choice of normalization defined by (A27)–(A29) the Nusselt number is given by

$$(\mathcal{N}-1)R/R_c = \langle w_0 \theta_0 \rangle / R_c = (16/3\pi^2) |A_0|^2. \tag{A50}$$

We may rescale A_0 to eliminate the factor of $(16/3\pi^2)$ in accordance with Eq. (8.17), which changes the nonlinear

coefficient to

$$g_0 = \frac{1}{2}. \tag{A51}$$

In the rigid case, although the inversion of Eq. (A36) has been carried out analytically for pure-fluid convection by Schlüter *et al.* (1965), a numerical calculation is generally necessary to find the $f_i(z)$ of Eq. (A38). Similarly, the solvability condition resulting from Eq. (A42) involves scalar products of known functions, which may

be evaluated numerically. For cases where \mathcal{L}_0 is not self-adjoint (e.g. the stationary bifurcation in binary-fluid convection) the adjoint of Eq. (A25) must be solved and the appropriate adjoint eigenvector used.

Notice also that in the calculation of \tilde{u}_1 from Eq. (A39) necessary to evaluate the rhs of Eq. (A42) we used the fact that the vertical vorticity $\Omega_z=0$ at this order. As mentioned above, this relation is correct for rigid boundaries, but only in the limit $\sigma=\infty$ for free-slip. If $\sigma < \infty$ in the free-slip case, then Ω_z is a slow mode which must be included as a separate mode in a consistent amplitude equation involving y variation. This was missed in the original derivation of Newell and Whitehead (1969) and Segel (1969), since the difficulty does not become apparent until one calculates terms that are formally of higher order, even though the effect of vertical vorticity enters at the lowest order. As mentioned above, this point was first elucidated by Siggia and Zippelius (1981b).

APPENDIX B. DERIVATION OF THE PHASE EQUATION

As an example of the derivation of the phase equation we will use the model of Eq. (3.29)

$$\partial_t u = \varepsilon u - (\nabla^2 + 1)^2 u + 3(\nabla u)^2 \nabla^2 u , \quad (B1)$$

in two spatial dimensions, $\mathbf{x}=(x,y)$. Since we will study a state in which the direction of the local wave vector varies over large angles, we write the ideal solution in a way that does not single out a preferred coordinate axis by introducing the phase variable ϕ

$$u_{\text{ideal}}(\mathbf{x}) = u^{(0)}(\phi; \mathbf{q}), \quad \phi = \mathbf{q} \cdot \mathbf{x} . \quad (B2)$$

Here $u^{(0)}$ is the fully nonlinear ideal solution which usually can only be obtained numerically. It is important to remember that $u^{(0)}$ has a parametric dependence on \mathbf{q} , in addition to the dependence on ϕ . For illustration purposes we may consider a one-mode Galerkin approximation to $u^{(0)}$

$$\begin{aligned} u^{(0)}(\phi, \mathbf{q}) &\simeq a_q \cos \phi , \\ a_q^2 &= (4/3)q^{-4} [\varepsilon - (q^2 - 1)^2] , \end{aligned} \quad (B3)$$

which is a surprisingly good approximation for Eq. (B1).

We now allow the wave vector to vary slowly in space and time by introducing scaled coordinates $\mathbf{q}=\mathbf{q}(\mathbf{X}, T)$ with

$$\mathbf{X} = \eta \mathbf{x}, \quad T = \eta^2 t , \quad (B4)$$

where the diffusive η^2 scaling of the time is justified *a posteriori* by the nontrivial equation obtained below with this assumption. The small parameter η is a bookkeeping parameter which organizes the perturbation expansion. Its inverse specifies the long length scale over which pattern reorientation occurs, for example η^{-1} might be taken as the system size L .

The phase variable is defined according to

$$\mathbf{q}(\mathbf{X}, T) = \nabla \phi(\mathbf{x}, t); \quad \phi(\mathbf{x}, t) = \int_{\mathbf{x}}^{\mathbf{X}} \mathbf{q}(\mathbf{X}, T) \cdot d\mathbf{x} . \quad (B5)$$

These expressions are somewhat clumsy, involving a mixture of fast and slow coordinates. To eliminate this it is convenient to introduce a *scaled* phase variable Φ

$$\phi = \eta^{-1} \Phi(\mathbf{X}, T) , \quad (B6)$$

where derivatives of Φ with respect to its arguments, the slow coordinates, are assumed to be $O(1)$. Now clearly

$$\nabla \phi = \nabla_{\mathbf{X}} \Phi(\mathbf{X}, T) = \mathbf{q}(\mathbf{X}, T) = O(1) , \quad (B7)$$

with $\nabla_{\mathbf{X}}$ signifying gradients with respect to the slow coordinates $\nabla_{\mathbf{X}} = (\partial_X, \partial_Y)$. Higher derivatives $\nabla_{\mathbf{X}}$ acting on Φ are $O(1)$ corresponding to gradients of \mathbf{q} which are $O(\eta)$ as desired.

We now expand the solution to (B1) in powers of η :

$$u = u^{(0)}(\phi, \mathbf{X}, T) + \eta u^{(1)}(\phi, \mathbf{X}, T) + \dots , \quad (B8)$$

with each $u^{(i)}$ periodic in the variable ϕ with period 2π . Derivatives act according to the rule

$$\nabla f(\phi, \mathbf{X}, T) = \mathbf{q} \partial_{\phi} f + \eta \nabla_{\mathbf{X}} f , \quad (B9)$$

$$\partial_t f(\phi, \mathbf{X}, T) = \eta (\partial_T \Phi) (\partial_{\phi} f) + \eta^2 \partial_T f . \quad (B10)$$

We will also need the following results derived from (B9):

$$(\nabla f)^2 = q^2 (\partial_{\phi} f)^2 + 2\eta (\partial_{\phi} f) (\mathbf{q} \cdot \nabla_{\mathbf{X}}) f + O(\eta^2) , \quad (B11)$$

$$\begin{aligned} \nabla^2 f &= q^2 \partial_{\phi}^2 f + \eta [2(\mathbf{q} \cdot \nabla_{\mathbf{X}}) + (\nabla_{\mathbf{X}} \cdot \mathbf{q})] (\partial_{\phi} f) + O(\eta^2) . \end{aligned} \quad (B12)$$

We now substitute (B8)–(B12) into (B1) and collect terms at each order in η . At $O(\eta^0)$ we obtain

$$[\varepsilon - (q^2 \partial_{\phi}^2 + 1)^2] u^{(0)}(\phi) + 3q^4 (\partial_{\phi} u^{(0)})^2 (\partial_{\phi}^2 u^{(0)}) = 0 , \quad (B13)$$

which defines the ideal solution $u^{(0)}(\phi, \mathbf{q})$. At $O(\eta^1)$ we have

$$\begin{aligned} &[\varepsilon - (q^2 \partial_{\phi}^2 + 1)^2] u^{(1)} + 3q^4 \partial_{\phi} [(\partial_{\phi} u^{(0)})^2 (\partial_{\phi} u^{(1)})] \\ &= (q^2 \partial_{\phi}^2 + 1) [2\mathbf{q} \cdot \nabla_{\mathbf{X}} + (\nabla_{\mathbf{X}} \cdot \mathbf{q})] (\partial_{\phi} u^{(0)}) + [2\mathbf{q} \cdot \nabla_{\mathbf{X}} + (\nabla_{\mathbf{X}} \cdot \mathbf{q})] (q^2 \partial_{\phi}^2 + 1) (\partial_{\phi} u^{(0)}) \\ &- 6q^2 (\partial_{\phi}^2 u^{(0)}) (\partial_{\phi} u^{(0)}) (\mathbf{q} \cdot \nabla_{\mathbf{X}}) u^{(0)} - 3q^2 (\partial_{\phi} u^{(0)})^2 [2\mathbf{q} \cdot \nabla_{\mathbf{X}} + (\nabla_{\mathbf{X}} \cdot \mathbf{q})] (\partial_{\phi} u^{(0)}) + (\partial_{\phi} u^{(0)}) \partial_T \Phi , \end{aligned} \quad (B14)$$

where it must be remembered that \mathbf{q} depends on the slow coordinates, as does $u^{(0)}$ through its dependence on \mathbf{q} .

The details of the right-hand side of Eq. (B14) are not important for pedagogical purposes. Let us write this equation as

$$\mathcal{L}_1 u^{(1)} = \mathcal{N}. \quad (\text{B14a})$$

The important point is that the operator on the lhs, acting on $u^{(1)}$ which is to be determined by Eq. (B14), has a zero eigenvalue eigenvector which is simply the translation mode $\partial_\phi u^{(0)}$. This result follows quite generally from the translational invariance of the system, which is the symmetry leading us to seek a slow phase dynamics. This again leads to a solvability condition requiring that the rhs not drive this translation mode. For the particular example (B1) \mathcal{L}_1 is self-adjoint under the simple scalar product

$$(a, b) = (2\pi)^{-1} \int_0^{2\pi} a(\phi) b(\phi) d\phi \equiv \langle ab \rangle, \quad (\text{B15})$$

so the solvability condition reduces to orthogonality of \mathcal{N} to $\partial_\phi u^{(0)}$. This gives

$$\begin{aligned} \langle (\partial_\phi u^{(0)})^2 \rangle \partial_T \Phi &= 2\mathbf{\nabla}_X \cdot [\mathbf{q} \langle q^2 (\partial_\phi^2 u^{(0)})^2 - (\partial_\phi u^{(0)})^2 \rangle] \\ &\quad + q^2 \mathbf{\nabla}_X \cdot [\mathbf{q} \langle (\partial_\phi u^{(0)})^4 \rangle] \\ &\quad + 2q^2 \langle \mathbf{\nabla}_X \cdot \mathbf{q} \rangle \langle (\partial_\phi u^{(0)})^4 \rangle. \end{aligned} \quad (\text{B16})$$

Equation (B16) may clearly be written in the form

$$\partial_T \Phi = f_1(q) \mathbf{\nabla}_X \cdot \mathbf{q} + f_2(q) (\mathbf{q} \cdot \mathbf{\nabla}_X) q, \quad (\text{B17})$$

consistent with the general form of the phase equation (4.76). The functions f_1, f_2 depend on q , and on averages involving the ideal nonlinear solution $u^{(0)}$ and its derivatives, all of which also depend on q .

From these expressions it is straightforward algebra to derive the diffusion constants $D_{||}$ and D_\perp of Eq. (4.70) which we will quote explicitly,

$$D_\perp(q) = 2\langle q^2 (\partial_\phi^2 u^{(0)})^2 - (\partial_\phi u^{(0)})^2 \rangle + 3q^2 \langle (\partial_\phi u^{(0)})^4 \rangle, \quad (\text{B18})$$

$$D_{||}(q) = \partial_q [2q \langle q^2 (\partial_\phi^2 u^{(0)})^2 - (\partial_\phi u^{(0)})^2 \rangle + q^3 \langle (\partial_\phi u^{(0)})^4 \rangle]. \quad (\text{B19})$$

Then $\tau(q)$, $B(q)$ of Eq. (4.76a) may be evaluated using Eqs. (4.77a,b). We have therefore now derived the nonlinear phase equation with coefficients that depend on the ideal nonlinear solution $u^{(0)}$. In general Eqs. (B18)–(B19) must be evaluated numerically. For the one mode approximation to (B1) we have

$$D_\perp = (q^2 - 1) a_q^2 + \frac{9}{8} q^2 a_q^4, \quad (\text{B20})$$

$$D_{||} = \partial_q [q(q^2 - 1) a_q^2 + \frac{3}{8} q^3 a_q^4], \quad (\text{B21})$$

with a_q defined in (B3).

For the potential analogue of Eq. (B1), i.e. Eq. (8.38)

with $g_3 = 1$, the only change is that the coefficient of the last term in D_\perp , Eq. (B18), becomes 1 in place of 3. In that case

$$D_{||} = \partial_q [q D_\perp]. \quad (\text{B22})$$

REFERENCES

- Abarbanel, H. D. I., R. Brown, and L. S. Tsimring, 1993, "The analysis of observed chaotic data in physical systems", Rev. Mod. Phys. (to be published).
- Abraham, N. B., A. M. Albano, A. Passamante, and P. E. Rapp, 1989, Eds., *Measures of Complexity and Chaos*, NATO ASI Series, Vol. 208 (Plenum, New York).
- Abraham, N. B., and W. J. Firth, 1990, "Transverse effects in nonlinear optics", J. Opt. Soc. Am. B 7, 948.
- Abraham, N. B., J. P. Gollub, and H. L. Swinney, 1984, "Testing nonlinear dynamics", Physica 11D, 252.
- Abraham, R. H., and D. C. Shaw, 1983, *Dynamics: the Geometry of Behavior; Part 1: Periodic Behavior; Part 2: Chaotic Behavior; Part 3: Global Behavior; Part 4: Bifurcation Behavior* (Aerial Press, Santa Cruz).
- Aceves, A., H. Adachihiara, C. Jones, J. C. Lerman, D. W. McLaughlin, J. V. Moloney, and A. C. Newell, 1986, "Chaos and coherent structures in partial differential equations", Physica 18D, 85.
- Agladze, K. I., and V. I. Krinsky, 1984, "On the mechanism of target pattern formation in the distributed Belousov-Zhabotinsky system", in *Self-Organization. Autowaves and Structures Far from Equilibrium*, edited by V. I. Krinsky (Springer-Verlag, Berlin), p. 147.
- Agladze, K. I., V. I. Krinsky, and A. M. Pertsov, 1984, "Chaos in the non-stirred Belousov-Zhabotinsky reaction is induced by interaction of waves and stationary dissipative structures", Nature 308, 834.
- Aguado, M., and F. Sagues, 1990, "Pattern-formation dynamics resulting from a reaction diffusion instability", Phys. Lett. A 143, 283.
- Ahlers, G., 1974, "Low temperature studies of the Rayleigh-Bénard instability and turbulence", Phys. Rev. Lett. 33, 1185.
- Ahlers, G., 1989, "Experiments on bifurcations and one-dimensional patterns in nonlinear systems far from equilibrium", in *Complex Systems*, edited by D. Stein, Vol. 7 (Addison-Wesley, New York), p. 175.
- Ahlers, G., 1991, "Experiments with pattern-forming systems", Physica D 51, 421.
- Ahlers, G., 1994, "Stochastic effects near bifurcations in pattern-forming systems", Rev. Mod. Phys. (to be published).
- Ahlers, G., and R. P. Behringer, 1978a, "Evolution of turbulence from the Rayleigh-Bénard instability", Phys. Rev. Lett. 40, 712.
- Ahlers, G., and R. P. Behringer, 1978b, "The Rayleigh-Bénard instability and the evolution of turbulence", Prog. Theor. Phys. Suppl. 64, 186.
- Ahlers, G. A., and D. S. Cannell, 1983, "Vortex-front propagation in rotating Couette-Taylor flow", Phys. Rev. Lett. 50, 1583.
- Ahlers, G., D. S. Cannell, M. A. Dominguez-Lerma, and R. Heinrichs, 1986, "Wavenumber selection and Eckhaus instability in Couette-Taylor flow", Physica D 23, 202.
- Ahlers, G., D. S. Cannell, and V. Steinberg, 1985a, "Time dependence of flow patterns near the convective threshold in a cylindrical container", Phys. Rev. Lett. 54, 1373.

- Ahlers, G., M. C. Cross, P. C. Hohenberg, and S. Safran, 1981, "The amplitude equation near the convective threshold: application to time-dependent heating experiments", *J. Fluid Mech.* **110**, 297.
- Ahlers, G., P. C. Hohenberg, and M. Lücke, 1985b, "Thermal convection under external modulation of the driving force. I. The Lorenz model. II. Experiments", *Phys. Rev. A* **32**, 3493, 3519.
- Ahlers, G., and M. Lücke, 1987, "Some properties of an 8-mode Lorenz model for convection in binary fluids", *Phys. Rev. A* **35**, 470.
- Ahlers, G., C. W. Meyer, and D. S. Cannell, 1989, "Deterministic and stochastic effects near the convective onset", *J. Stat. Phys.* **54**, 1121.
- Ahlers, G., and I. Rehberg, 1986, "Convection in a binary mixture heated from below", *Phys. Rev. Lett.* **56**, 1373.
- Akhromeyeva, T. S., S. P. Kurdyumov, G. G. Malinetskii, and A. A. Samarskii, 1989, "Nonstationary dissipative structures and diffusion induced chaos in nonlinear media", *Phys. Rep.* **176**, 189.
- Allais, D., and J. E. Wesfreid, "Hexagon-square transition in a ferrofluid instability" (unpublished).
- Allessie, M. A., F. I. M. Bonke, and F. G. J. Schopman, 1977, "Circus movement in rabbit atrial muscle as a mechanism of tachycardia III. The 'Leading Circle' in cardiac tissue without the involvement of an anatomical obstacle", *Circ. Res.* **41**, 9.
- Allessie, M. A., M. J. Schalij, C. J. H. J. Kirchhof, L. Boersma, M. Huyberts, and J. Hollen, 1990, "Electrophysiology of spiral waves in two dimensions: The role of anisotropy", in *Mathematical Approaches to Cardiac Arrhythmias*, edited by J. Jalife, Ann. N.Y. Acad. Sci. **591**, 247.
- Andereck, C. D., and F. Hayot, 1992, Eds., *Ordered and Turbulent Patterns in Taylor-Couette Flow* (Plenum, New York).
- Andereck, C. D., S. S. Liu, and H. L. Swinney, 1986, "Flow regimes in a circular Couette system with independently rotating cylinders", *J. Fluid Mech.* **164**, 155.
- Anderson, P. W., 1981, "Can broken symmetry occur in driven systems?", in *Order and Fluctuations in Equilibrium and Nonequilibrium Statistical Mechanics*, edited by G. Nicolis, G. Dewel, and J. W. Turner (Wiley, New York), p. 289.
- Anderson, K. E., and R. P. Behringer, 1991, "Traveling wave convection patterns in an annular cell", *Physica D* **51**, 444.
- Anselmet, F., Y. Gagne, E. J. Hopfinger, and R. A. Antonia, 1984, "High-order velocity structure functions in turbulent shear flows", *J. Fluid Mech.* **140**, 63.
- Aranson, I. S., A. V. Gaponov-Grekhov, and M. I. Rabinovich, 1985, "The development of chaos in dynamic structure ensembles", *Zh. Eksp. Teor. Fiz.* **89**, 92 [Sov. Phys. JETP **62**, 52].
- Aranson, I. S., A. V. Gaponov-Grekhov, and M. I. Rabinovich, 1988, "The onset and spatial development of turbulence in flow systems", *Physica D* **33**, 1.
- Aranson, I. S., A. V. Gaponov-Grekhov, M. I. Rabinovich, and I. P. Starobinets, 1986, "Strange attractors and the spatial development of turbulence in flow systems", *Zh. Eksp. Teor. Fiz.* **90**, 1707 [Sov. Phys. JETP **63**, 1000].
- Aranson, I., D. Golomb, and H. Sompolinsky, 1992, "Spatial coherence and temporal chaos in macroscopic systems with asymmetric couplings", *Phys. Rev. Lett.* **68**, 3495.
- Aranson, I. S., K. A. Gorshkov, A. S. Lomov, and M. I. Rabinovich, 1989, "Stable particle-like solutions of multidimensional nonlinear fields", *Physica D* **43**, 435.
- Aranson, I. S., L. Kramer, and A. Weber, 1991a, "Interaction of spirals in oscillatory media", *Phys. Rev. Lett.* **67**, 404.
- Aranson, I. S., L. Kramer, and A. Weber, 1991b, "On the interaction of spiral waves in nonequilibrium media", *Physica D* **53**, 376.
- Aranson, I. S., and M. I. Rabinovich, 1989, "Dynamics of spiral waves in nonequilibrium media", *J. Phys. A* **23**, 299.
- Arcuri, P., and J. D. Murray, 1986, "Pattern sensitivity to boundary and initial conditions in reaction diffusion models", *J. Math. Biol.* **24**, 141.
- Arecchi, F. T., 1991, "Space-time complexity in nonlinear optics", *Physica D* **51**, 450.
- Arecchi, F. T., G. Giacomelli, P. L. Ramazza, and S. Residori, 1990, "Experimental evidence of chaotic itinerancy and spatiotemporal chaos in optics", *Phys. Rev. Lett.* **65**, 2531.
- Arecchi, F. T., G. Giacomelli, P. L. Ramazza, and S. Residori, 1991, "Vortices and defect statistics in two-dimensional optical chaos", *Phys. Rev. Lett.* **67**, 3749.
- Argoul, F., and A. Arneodo, 1987, "Symbolic dynamics in the Belousov-Zhabotinskii reaction. An experimental and theoretical approach of Shil'nikov homoclinic chaos", *J. Chem. Phys.* **84**, 1367.
- Argoul, F., A. Arneodo, J. Elezgaray, G. Grasseau, and R. Murenzi, 1989, "Wavelet transform of fractal aggregates", *Phys. Lett. A* **135**, 327.
- Argoul, F., A. Arneodo, and G. Grasseau, 1988, "Fractal dimensions and $f(\alpha)$ spectrum for strange attractors", *Z. Angew. Math. Mech.* **68**, 519.
- Arneodo, A., J. Elezgaray, J. Pearson, and T. Russo, 1991, "Instabilities of front patterns in reaction diffusion systems", *Physica D* **49**, 141.
- Arnold, V. I., 1983, *Geometrical Methods in the Theory of Ordinary Differential Equations* (Springer-Verlag, New York).
- Aronson, D. G., and H. F. Weinberger, 1975, in *Partial Differential Equations and Related Topics*, edited by J. A. Goldstein (Springer-Verlag, Heidelberg), p. 5.
- Aronson, D. G., and H. F. Weinberger, 1978, "Multidimensional nonlinear diffusion arising in population genetics", *Adv. Math.* **30**, 33.
- Arter, W., and A. C. Newell, 1988, "Numerical simulation of Rayleigh-Bénard convection in shallow tanks", *Phys. Fluids* **31**, 2474.
- Arter, W., A. Bernoff, and A. C. Newell, 1987, "Wavenumber selection of convection rolls in a box", *Phys. Fluids* **30**, 3840.
- Aubry, S., 1983, "The twist map, the extended Frenkel-Kontorova model and the devil's staircase", *Physica D* **7**, 240.
- Auerbach, D., P. Cvitanović, J.-P. Eckmann, G. Gunaratne, and I. Procaccia, 1987, "Exploring chaotic motion through periodic orbits", *Phys. Rev. Lett.* **58**, 2387.
- Auerbach, D., and I. Procaccia, 1990, "Grammatical complexity of strange sets", *Phys. Rev. A* **41**, 6602.
- Babcock, K. L., G. Ahlers, and D. S. Cannell, 1991, "Noise-sustained structure in Taylor-Couette flow with through flow", *Phys. Rev. Lett.* **67**, 3388.
- Babcock, K. L., D. S. Cannell, and G. Ahlers, 1992, "Stability and noise in Taylor-Couette flow with through-flow", *Physica D* **61**, 40.
- Babcock, K. L., and R. M. Westervelt, 1989, "Topological 'melting' of cellular domain lattices in magnetic garnet films", *Phys. Rev. Lett.* **63**, 175.
- Bak, P., and K. Chen, 1991, "Self-organized criticality", *Sci. Am.* **264**, Jan. p. 46.
- Bak, P., K. Chen, and M. Creutz, 1989, "Self-organized criticality in the 'game of life'", *Nature* **342**, 780.
- Bak, P., K. Chen, and C. Tang, 1990, "A forest-fire model and some thoughts on turbulence", *Phys. Lett. A* **147**, 297.
- Bak, P., C. Tang, and K. Wiesenfeld, 1987, "Self-organized cri-

- ticality: an explanation of $1/f$ noise”, Phys. Rev. Lett. **59**, 381.
- Bandy, D. K., A. N. Oraevsky, and J. R. Tredice, 1988, “Nonlinear dynamics of lasers”, J. Opt. Soc. Am. B **5**, 876.
- Bareiko, V. V., 1984, “Self-organization phenomena and autowave processes in heterogeneous chemical and physical systems”, in *Self-organization, Autowaves and Structures Far from Equilibrium*, edited by V. I. Krinsky (Springer-Verlag, Berlin), p. 164.
- Barkley, D., 1991, “A model for fast computer simulation of waves in excitable media”, Physica D **49**, 61.
- Barkley, D., 1992, “Linear stability analysis of rotating spiral waves in excitable media”, Phys. Rev. Lett. **68**, 2090.
- Barkley, D., and A. Cumming, 1990, “Thermodynamics of the quasiperiodic parameter set at the borderline of chaos: experimental results”, Phys. Rev. Lett. **64**, 327.
- Barkley, D., M. Knob, and L. S. Tuckerman, 1990, “Spiral-wave dynamics in a simple model of excitable media: The transition from simple to compound rotation”, Phys. Rev. A **42**, 2489.
- Barkley, D., and L. S. Tuckerman, 1989, “Traveling waves in axisymmetric convection—The role of sidewall conductivity”, Physica D **37**, 288.
- Baras, F., and D. Walgraef, 1992, Eds., “Nonequilibrium chemical dynamics: from experiment to microscopic simulations”, Physica A **188**, 1.
- Barten, W., M. Lücke, W. Hort, and M. Kamps, 1989, “Fully developed traveling wave convection in binary-fluid mixtures”, Phys. Rev. Lett. **63**, 376.
- Barten, W., M. Lücke, and M. Kamps, 1990, “Structure and dynamics of nonlinear convective states in binary fluid mixtures”, in *Nonlinear Evolution of Spatio-Temporal Structures in Dissipative Continuous Systems*, edited by F. H. Busse and L. Kramer, NATO ASI Series Vol. 225 (Plenum, New York), p. 131.
- Barten, W., M. Lücke, and M. Kamps, 1991, “Localized traveling-wave convection in binary-fluid mixtures”, Phys. Rev. Lett. **66**, 2621.
- Bartuccelli, M., P. Constantin, C. R. Doering, J. D. Gibbon, and M. Gissel-fält, 1989, “Hard turbulence in a finite dimensional dynamical system”, Phys. Lett. A **142**, 349; Erratum **145**, 476.
- Bartuccelli, M., P. Constantin, C. R. Doering, J. D. Gibbon, and M. Gissel-fält, 1990, “On the possibility of soft and hard turbulence in the complex Ginzburg-Landau equation”, Physica D **44**, 421.
- Baudet, C., S. Ciliberto, and J. F. Pinton, 1991, “Spectral analysis of the von Kármán flow using ultrasound scattering”, Phys. Rev. Lett. **67**, 193.
- Baxter, G. W., R. P. Behringer, T. Fagert, and G. A. Johnson, 1989, “Pattern-formation in flowing sand”, Phys. Rev. Lett. **62**, 2825.
- Bayley, B. J., S. A. Orszag, and T. Herbert, 1988, “Instability mechanisms in shear-flow transition”, Annu. Rev. Fluid Mech. **20**, 359.
- Bean, C. P., 1962, “Magnetization of hard superconductors”, Phys. Rev. Lett. **8**, 250.
- Bechhoefer, J., A. J. Simon, A. Libchaber, and P. Oswald, 1989, “Destabilization of a flat nematic-isotropic interface”, Phys. Rev. A **40**, 2042.
- Beeler, G. W., and H. Reuter, 1977, “Reconstruction of the action potential of ventricular myocardial fibres”, J. Physiol. **268**, 177.
- Behringer, R. P., 1985, “Rayleigh-Bénard convection and turbulence in liquid helium”, Rev. Mod. Phys. **57**, 657.
- Behringer, R. P., and G. Ahlers, 1982, “Heat transport and temporal evolution of fluid flow near the Rayleigh-Bénard instability in cylindrical containers”, J. Fluid Mech. **125**, 219.
- Bekki, N., and K. Nozaki, 1985, “Formations of spatial patterns and holes in the generalized Ginzburg-Landau equation”, Phys. Lett. A **110**, 133.
- Belintsev, B. N., 1983, “Dissipative structures and the problem of biological pattern formation”, Usp. Fiz. Nauk **141**, 55 [Sov. Phys. Usp. **26**, 775].
- Belintsev, B. N., 1984, “Collective phenomena in the multicellular development of *Dictyostelium Discoideum*”, in *Self-organization, Autowaves and Structures Far from Equilibrium*, edited by V. I. Krinsky (Springer-Verlag, Berlin), p. 209.
- Belousov, L. V., 1984, “Synergetics and biological morphogenesis”, in *Self-organization, Autowaves and Structures Far from Equilibrium*, edited by V. I. Krinsky (Springer-Verlag, Berlin), p. 204.
- Ben Amar, M., P. Pelcé, and P. Tabeling, 1991, *Nonlinear Phenomena Related to Growth and Form* (Plenum, New York).
- Bénard, H., 1900, “Les tourbillons cellulaires dans une nappe liquide transportent de la chaleur par convection en régime permanent”, Ann. Chim. Phys. **7** (Ser. 23), 62.
- Ben-Jacob, E., H. R. Brand, G. Dee, L. Kramer, and J. S. Langer, 1985, “Pattern propagation in nonlinear dissipative systems”, Physica **14D**, 348.
- Benjamin, T. B., 1978, “Bifurcation phenomena in steady flows of a viscous fluid”, Proc. R. Soc. London A **359**, 1, 27.
- Benjamin, T. B., and J. E. Feir, 1967, “The disintegration of wave trains on deep water”, J. Fluid Mech. **27**, 417.
- Benjamin, T. B., and C. Scott, 1979, “Gravity-capillary waves with edge constraints”, J. Fluid Mech. **92**, 241.
- Benjamin, T. B., and F. Ursell, 1954, “The stability of the plane free surface of a liquid in vertical periodic motion”, Proc. R. Soc. London A **225**, 505.
- Bennett, C., and M. S. Bourzutschky, 1991, “‘Life’ not critical”, Nature **350**, 468.
- Bennett, C., G. Grinstein, Y. He, C. Jayaprakash, and D. Mukamel, 1990, “Stability of temporally-periodic states of classical many-body systems”, Phys. Rev. A **41**, 1932.
- Bensimon, D., L. P. Kadanoff, S. Liang, B. I. Shraiman, and C. Tang, 1986, “Viscous flows in two dimensions”, Rev. Mod. Phys. **58**, 977.
- Bensimon, D., P. Kolodner, C. M. Surko, H. Williams, and V. Croquette, 1989a, “Competing and coexisting dynamic states of traveling-wave convection in an annulus”, J. Fluid Mech. **217**, 441.
- Bensimon, D., A. Pumir, and B. I. Shraiman, 1989b, “Nonlinear theory of traveling wave convection in binary mixtures”, J. Phys. (Paris) **50**, 3089.
- Bensimon, D., B. I. Shraiman, and V. Croquette, 1988, “Non-adiabatic effects in convection”, Phys. Rev. A **38**, 5461.
- Bergegol, H., E. Charpentier, J. M. Courty, and J. E. Wesfreid, 1987, “Anisotropy effects in ferrofluid instabilities”, Phys. Lett. A **121**, 311.
- Bergé, P., 1979, “Experiments on hydrodynamic instabilities and the transition to turbulence”, in *Dynamical Critical Phenomena and Related Topics*, edited by C. P. Enz, Lecture Notes in Physics 104 (Springer-Verlag, New York), p. 288.
- Bergé, P., 1989, “Chaos and Turbulence in Rayleigh-Bénard Convection”, Phys. Scr. **40**, 381.
- Bergé, P., Y. Pomeau, and C. Vidal, 1987, *Order Within Chaos* (Wiley, New York).
- Bergman, D. J., B. I. Halperin, and P. C. Hohenberg, 1974, “Hydrodynamic theory applied to fourth sound in a moving

- superfluid”, Phys. Rev. B **11**, 4253.
- Bernoff, A.J., 1985a, “Sidewall stabilization of convection” (unpublished).
- Bernoff, A. J., 1985b, “The onset of convection between stress-free boundaries” (unpublished).
- Bernoff, A. J., 1988, “Slowly varying fully nonlinear wavetrains in the Ginzburg-Landau equation”, Physica D **30**, 363.
- Bernoff, A. J., 1991, “Spiral wave solutions for reaction-diffusion equations in a fast reaction/slow diffusion limit”, Physica D **53**, 125.
- Bestehorn, M., R. Friedrich, and H. Haken, 1989a, “Two-dimensional traveling wave patterns in nonequilibrium systems”, Z. Phys. B **75**, 265.
- Bestehorn, M., R. Friedrich, and H. Haken, 1989b, “Modulated traveling waves in nonequilibrium systems: the ‘blinking state’”, Z. Phys. B **77**, 151.
- Bestehorn, M., and H. Haken, 1984, “Transient patterns of the convection instability: A model-calculation”, Z. Phys. B **57**, 329.
- Bestehorn, M., and H. Haken, 1990a, “Synergetics applied to pattern formation in large-aspect-ratio systems”, in *Dissipative Structures in Transport Processes and Combustion*, edited by D. Meinköhn (Springer-Verlag, Berlin), p. 110.
- Bestehorn, M., and H. Haken, 1990b, “Traveling waves and pulses in a two-dimensional large-aspect-ratio system”, Phys. Rev. A **42**, 7195.
- Bestehorn, M., and C. Perez-Garcia, 1987, “Coexistence of patterns with different symmetries in Benard-Marangoni convection”, Europhys. Lett. **4**, 1365.
- Bestehorn, M., and C. Perez-Garcia, 1991, “Modulated rolls and traveling waves in a secondary convective instability”, Europhys. Lett. **16**, 225.
- Bhattacharjee, J. K., 1988a, “Stationary convection in binary liquids, pattern selection by modulation”, Europhys. Lett. **5**, 31.
- Bhattacharjee, J. K., 1988b, “Randomly stirred fluids, mode coupling theories and the turbulent Prandtl number”, J. Phys. A **21**, L551.
- Bhattacharjee, J. K., 1991a, “Homogeneous isotropic turbulence in randomly stirred fluids, self-consistent mode-coupling and perturbation theory”, Phys. Fluids A **3**, 879.
- Bhattacharjee, J. K., 1991b, “Parametric resonance in Rayleigh-Bénard convection with corrugated geometry”, Phys. Rev. A **43**, 819.
- Bhattacharjee, J. K., A. Das, and K. Banerjee, 1991, “Turbulent Rayleigh-Bénard convection in a conducting fluid in a strong magnetic field”, Phys. Rev. A **43**, 1097.
- Bigazzi, P., S. Ciliberto, and V. Croquette, 1990, “Convective patterns in a binary mixture with a positive separation ratio” J. Phys. (Paris) **51**, 611.
- Biktashev, V. N., 1989, “Diffusion of autowaves. Evolution equation for slowly varying autowaves”, Physica D **40**, 83.
- Binder, K., 1973, “Time-dependent Ginzburg-Landau theory of nonequilibrium relaxation”, Phys. Rev. B **8**, 3423.
- Bishop, A. R., G. Grüner, and B. Nicolaenko, 1986, Eds., *Spatio-Temporal Coherence and Chaos in Physical Systems* (Physica **23D**, 1).
- Bloembergen, N., and R. Damon, 1952 “Relaxation effects in ferromagnetic resonance”, Phys. Rev. **85**, 699.
- Boa, James A., and D. S. Cohen, 1976, “Bifurcation of localized disturbances in a model biochemical reaction”, SIAM J. Appl. Math. **30**, 123.
- Bodenschatz, E., D. S. Cannell, R. Ecke, Y-C. Hu, K. Lerman, and G. Ahlers, 1992, “Experiments on three systems with non-variational aspects”, Physica D.
- Bodenschatz, E., J. R. DeBruyn, G. Ahlers, and D. S. Cannell, 1991a, “Transitions between patterns in thermal convection”, Phys. Rev. Lett. **67**, 3078.
- Bodenschatz, E., M. Kaiser, L. Kramer, W. Pesch, A. Weber, and W. Zimmerman, 1990, “Patterns and defects in liquid crystals”, in *New Trends in Nonlinear Dynamics and Pattern Forming Phenomena: The Geometry of Nonequilibrium*, edited by P. Coullet and P. Huerre, NATO ASI Series (Plenum, New York), p. 111.
- Bodenschatz, E., and L. Kramer, 1987, “Influence of lateral boundaries on the Eckhaus instability in anisotropic pattern-forming systems”, Physica D **27**, 249.
- Bodenschatz, E., W. Pesch, and L. Kramer, 1988a, “Structure and dynamics of dislocations in anisotropic pattern-forming systems”, Physica D **32**, 135.
- Bodenschatz, E., A. Weber, and L. Kramer, 1991b, “Interaction and dynamics of defects in convective roll patterns of anisotropic fluids”, J. Stat. Phys. **64**, 1007.
- Bodenschatz, E., A. Weber, and L. Kramer, 1991c, “Structure and dynamics of spiral waves and defects in traveling waves”, in *Nonlinear Wave Processes in Excitable Media*, edited by A. V. Holden, M. Markus, and H. G. Othmer (Plenum, New York), p. 383.
- Bodenschatz, E., W. Zimmerman, and L. Kramer, 1988b, “On electrically driven pattern-forming instabilities in planar nematics”, J. Phys. (Paris) **49**, 1875.
- Boedt, J. M., J. Ross, and C. Vidal, 1987, “Experiments on phase diffusion waves”, J. Chem. Phys. **86**, 4418.
- Bohr, T., 1990, “Chaos and turbulence”, in *Applications of Statistical Mechanics and Field Theory to Condensed Matter*, edited by A. R. Bishop, D. Baeriswyl, and J. Carmelo (Plenum, New York).
- Bohr, T., and O. B. Christensen, 1989, “Size dependence, coherence, and scaling in turbulent coupled-map lattices”, Phys. Rev. Lett. **63**, 2161.
- Bohr, T., G. Grinstein, Y. He, and C. Jayaprakash, 1987, “Coherence, chaos and broken symmetry in classical, many-body dynamical systems”, Phys. Rev. Lett. **58**, 2155.
- Bohr, T., A. W. Pedersen, and M. H. Jensen, 1990a, “Transition to turbulence in a discrete Ginzburg-Landau model”, Phys. Rev. A **42**, 3626.
- Bohr, T., A. W. Pedersen, M. H. Jensen, and D. A. Rand, 1990b, “Vortex dynamics in a coupled map lattice”, in *New Trends in Nonlinear Dynamics and Pattern Forming Phenomena*, edited by P. Coullet and P. Huerre (Plenum, New York)
- Bohr, T., G. Grinstein, C. Jayaprakash, M. H. Jensen, J. Krug, and D. Mukamel, 1992, “Turbulence, power laws and Galilean invariance”, Physica D **59**, 177.
- Bohr, T., and D. A. Rand, 1991, “A mechanism for localized turbulence”, Physica D **52**, 532.
- Boissonade, J., 1988, “Stationary structure induced along a reaction-diffusion front by a Turing symmetry breaking instability”, J. Phys. (Paris) **49**, 541.
- Bolgiano, R., 1959, “Turbulent spectra in a stably stratified atmosphere”, J. Geophys. Res. **64**, 2226.
- Bolton, E. W., and F. H. Busse, 1985, “Stability of convection rolls in a layer with stress-free boundaries”, J. Fluid Mech. **150**, 487.
- Bonifacio, R., and L. A. Lugiato, 1978, “Optical bistability and cooperative effects in resonance fluorescence”, Phys. Rev. A **18**, 1129.
- Bonilla, L. L., 1988, “Nonequilibrium statistical mechanics model showing self-sustained oscillations”, Phys. Rev. Lett.

- 60**, 1398.
- Borckmans, P., G. Dewel, D. Walgraef, and Y. Katayama, 1987, "The search for Turing structures", *J. Stat. Phys.* **48**, 1031.
- Boucif, M., J. E. Wesfreid, and E. Guyon, 1991, "Experimental study of wavelength selection in the elastic buckling instability of thin plates", *Eur. J. Mech. A* **10**, 641.
- Bowden, C. M., H. M. Gibbs, and S. L. McCall, 1984, *Optical Bistability 2* (Plenum, New York).
- Brachet, M. E., P. Coullet, and S. Fauve, 1987, "Propagative phase dynamics in temporally intermittent systems", *Europhys. Lett.* **4**, 1017.
- Brand, H. R., 1988, "Phase dynamics — a review and a perspective", in *Propagation in Systems Far from Equilibrium*, edited by J. E. Wesfreid, H. R. Brand, P. Manneville, G. Albinet, and N. Boccara (Springer-Verlag, Berlin), p. 206.
- Brand, H. R., 1989, "Envelope equations near the onset of a hexagonal pattern", *Prog. Theor. Phys. Suppl.* **99**, 442.
- Brand, H., and M. C. Cross, 1983, "Phase dynamics for the wavy vortex of the Taylor instability", *Phys. Rev. A* **27**, 1237.
- Brand, H. R., and R. J. Deissler, 1989, "Interaction of localized solutions for subcritical bifurcations", *Phys. Rev. Lett.* **63**, 2801.
- Brand, H. R., and R. J. Deissler, 1992, "Eckhaus and Benjamin-Feir instabilities near a weakly inverted bifurcation", *Phys. Rev. A* **45**, 3732.
- Brand, H. R., R. J. Deissler, and G. Ahlers, 1991, "A simple model for the Benard instability with horizontal flow near threshold", *Phys. Rev. A* **43**, 4262.
- Brand, H. R., C. R. Doering, and R. E. Ecke, 1989, "External noise and its interaction with spatial degrees of freedom in nonlinear dissipative systems. Proceedings of a workshop", *J. Stat. Phys.* **54**, 1111.
- Brand, H. R., P. C. Hohenberg, and V. Steinberg, 1983, "Amplitude equation near a polycritical point for the convective instability of a binary-fluid mixture in a porous medium", *Phys. Rev. A* **27**, 591.
- Brand, H. R., P. C. Hohenberg, and V. Steinberg, 1984, "Codimension-two bifurcations for convection in binary fluid mixtures", *Phys. Rev. A* **30**, 2548.
- Brand, H. R., P. S. Lomdahl, and A. C. Newell, 1986a, "Evolution of the order parameter in situations with broken rotational symmetry", *Phys. Lett. A* **118**, 67.
- Brand, H. R., P. S. Lomdahl, and A. C. Newell, 1986b, "Benjamin-Feir turbulence in convective binary fluid mixtures", *Physica* **23D**, 345.
- Brand, H. R., and B. J. A. Zielinska, 1986, "Tricritical codimension-2 point near the onset of convection in viscoelastic liquids", *Phys. Rev. Lett.* **57**, 3167.
- Brandstater, A., J. Swift, H. L. Swinney, A. Wolf, J. D. Farmer, E. Jen, and P. J. Crutchfield, 1983, "Low dimensional chaos in a hydrodynamic system", *Phys. Rev. Lett.* **51**, 1442.
- Brandstater, A., and H. L. Swinney, 1987, "Strange attractors in weakly turbulent Couette-Taylor flow", *Phys. Rev. A* **35**, 2207.
- Branis, S. V., O. Martin, and J. L. Birman, 1991, "Discrete velocities for solitary-wave solutions selected by self-induced transparency", *Phys. Rev. A* **43**, 1549.
- Brattkus, K., and S. H. Davis, 1988, "Cellular growth near absolute stability", *Phys. Rev. B* **38**, 11452.
- Brattkus, K., and C. Misbah, 1990, "Phase dynamics in directional solidification", *Phys. Rev. Lett.* **64**, 1935.
- Braun, E., S. Rasenat, and V. Steinberg, 1991, "The mechanism of transition to weak turbulence in extended anisotropic systems", *Europhys. Lett.* **15**, 597.
- Braun, E., and V. Steinberg, 1991, "Long- and short-range interactions of defects in anisotropic hydrodynamical systems", *Europhys. Lett.* **15**, 167.
- Brazhnik, P. K., V. A. Davydov, V. S. Zykov, and A. S. Mikhailov, 1987, "Vortex rings in excitable media", *Zh. Eksp. Teor. Fiz.* **93**, 1725 [Sov. Phys. JETP **66**, 984].
- Brazovskii, S. A., 1975, "Phase transition of an isotropic system to a nonuniform state", *Zh. Eksp. Teor. Fiz.*, **68**, 175 [Sov. Phys. JETP **41**, 85].
- Brener, E. A., and V. I. Mel'nikov, 1991, "Pattern selection in two-dimensional dendritic growth", *Adv. Phys.* **40**, 53.
- Bretherton, C. S., and E. A. Spiegel, 1983, "Intermittency through modulational instability", *Phys. Lett. A* **96**, 152.
- Brindley, J., and R. M. Everson, 1989, "Disturbance propagation in coupled lattice maps", *Phys. Lett. A* **134**, 229.
- Bromberg, L., and A. B. Rechester, 1988, "Gibbs-type partition in chaotic dynamics", *Phys. Rev. A* **37**, 1708.
- Brown, S. N., and K. Stewartson, 1978, "On finite amplitude Bénard convection in a cylindrical container", *Proc. R. Soc. London A* **360**, 455.
- Bryant, P., C. Jeffries, and K. Nakamura, 1988, "Spin-wave nonlinear dynamics in an yttrium-iron-garnet sphere", *Phys. Rev. Lett.* **60**, 1185.
- Buell, J. C., and I. Catton, 1986a, "Wavenumber selection in large-amplitude axisymmetric convection", *Phys. Fluids* **29**, 23.
- Buell, J. C., and I. Catton, 1986b, "Wavenumber selection in ramped Rayleigh-Bénard convection", *J. Fluid Mech.* **171**, 477.
- Bunimovich, L. A., A. Lambert, and R. Lima, 1990, "The emergence of coherent structures in coupled-map lattices", *J. Stat. Phys.* **61**, 253.
- Bunimovich, L. A., and Y. G. Sinai, 1988, "Spacetime chaos in coupled-map lattices", *Nonlinearity* **1**, 491.
- Burgers, J. M., 1948, "A mathematical model illustrating the theory of turbulence", *Adv. Appl. Mech.* **1**, 171.
- Busse, F. H., 1967a, "On the stability of two-dimensional convection in a layer heated from below", *J. Math.&Phys.* **46**, 140.
- Busse, F. H., 1967b, "The stability of finite amplitude cellular convection and its relation to an extremum principle", *J. Fluid Mech.* **30**, 625.
- Busse, F. H., 1972, "The oscillatory instability of convective rolls in a low Prandtl number fluid", *J. Fluid Mech.* **52**, 97.
- Busse, F. H., 1978, "Non-linear properties of thermal convection", *Rep. Prog. Phys.* **41**, 1929.
- Busse, F. H., 1981, "Transition to turbulence in Rayleigh-Bénard convection", in *Hydrodynamic Instabilities and the Transition to Turbulence*, edited by H. L. Swinney and J. P. Gollub (Springer-Verlag, Berlin), p. 97.
- Busse, F. H., 1984, "Transition to turbulence via the statistical limit cycle route", in *Turbulence and Chaotic Phenomena in Fluids*, edited by T. Tatsumi (Elsevier, Amsterdam), p. 197.
- Busse, F. H., 1989, "Phase turbulence in fluid systems", in *Advances in Turbulence 2*, edited by H. H. Fernholz and H. E. Fiedler (Springer-Verlag, Berlin), p. 152.
- Busse, F. H., and E. W. Bolton, 1984, "Instabilities of convection rolls with stress-free boundaries near threshold", *J. Fluid Mech.* **146**, 115.
- Busse, F. H., and R. M. Clever, 1979, "Instabilities of convection rolls in a fluid of moderate Prandtl number", *J. Fluid Mech.* **91**, 319.
- Busse, F. H., and K. E. Heikes, 1980, "Convection in a rotating layer: a simple case of turbulence", *Science* **208**, 173.

- Busse, F. H., and L. Kramer, 1990, Eds., *Nonlinear Evolution of Spatiotemporal Structures in Dissipative Continuous Systems* (Plenum, New York).
- Busse, F. H., and N. Riahi, 1980, "Nonlinear convection in a layer with nearly insulating boundaries", *J. Fluid Mech.* **96**, 243.
- Busse, F. H., and J. A. Whitehead, 1971, "Instabilities of convection rolls in a high Prandtl number fluid", *J. Fluid Mech.* **47**, 305.
- Busse, F. H., and J. A. Whitehead, 1974, "Oscillatory and collective instabilities in large Prandtl number convection", *J. Fluid Mech.* **66**, 67.
- Caceres, M. O., A. Becker, and L. Kramer, 1991, "Asymptotic probability distribution for a supercritical bifurcation swept periodically in time", *Phys. Rev. A* **43**, 6581.
- Caldwell, D. R., 1974, "Experimental studies on the onset of thermohaline convection", *J. Fluid Mech.* **64**, 347.
- Campbell, D., R. Ecke, and J. M. Hyman, 1990, Eds., *Nonlinear Science: The Next Decade* (North-Holland, Amsterdam), *Physica D* **51**.
- Campbell, K., and D. A. Rand, 1993, "The thermodynamic limit and natural spatiotemporal measures for coupled lattices of chaotic Axiom A attractors" (unpublished).
- Campbell, D., and H. Rose, 1983, Eds., *Order in Chaos*, *Physica D* **7**, Nos. 1–3.
- Cannell, D., M. A. Dominguez-Lerma, and G. Ahlers, 1983, "Experiments on wave number selection in rotating Couette-Taylor flow", *Phys. Rev. Lett.* **50**, 1365.
- Caponeri, M., and S. Ciliberto, 1992, "Thermodynamic aspects of the transition to spatiotemporal chaos", *Physica D* **58**, 365.
- Cardy, J. L., 1992, "Random initial conditions and nonlinear relaxation", *J. Phys. A* **25**, 2765.
- Carlson, J. M., J. T. Chayes, E. R. Grannan, and G. H. Swindle, 1990a, "Self-organized criticality in sandpiles: Nature of the critical phenomenon", *Phys. Rev. A* **42**, 2467.
- Carlson, J. M., J. T. Chayes, E. R. Grannan, and G. H. Swindle, 1990b, "Self-organized criticality and singular diffusion", *Phys. Rev. Lett.* **65**, 2547.
- Caroli, B., Caroli, C., and S. Fauve, 1992, "On the phenomenology of tilted domains in lamellar eutectic growth", *J. Phys. I* **2**, 281.
- Cartwright, M. L., and J. E. Littlewood, 1945, "On nonlinear differential equations of the second order: I. The equation $\ddot{y} + k(1-y^2)\dot{y} + y = b\lambda k \cos(\lambda t + a)$, k large", *J. London Math. Soc.* **20**, 180.
- Castaing, B., G. Gunaratne, F. Heslot, L. Kadanoff, A. Libchaber, S. Thomae, X. Z. Wu, S. Zaleski, and G. Zanetti, 1989, "Scaling of hard thermal turbulence in Rayleigh-Bénard convection", *J. Fluid Mech.* **204**, 1.
- Castets, V., E. Dulos, J. Boissonade, and P. De Kepper, 1990, "Experimental evidence of a sustained standing Turing-type nonequilibrium chemical pattern", *Phys. Rev. Lett.* **64**, 2953.
- Cerisier, P., 1991, "Experimental study of the wavelength selection in a pentagonal vessel in Bénard convection", *Phys. Fluids* **3**, 2061.
- Cerisier, P., J. Pantaloni, and C. Perez-Garcia, 1988, "Thermal technique to induce a preferred initial pattern in Bénard-Marangoni convection", *Physicochem. Hydrol.* **10**, 341.
- Cerisier, P., C. Perez-Garcia, C. Jamond, and J. Pantaloni, 1987, "Wavelength selection in Bénard-Marangoni convection", *Phys. Rev. A* **35**, 1949.
- Chandrasekhar, S., 1953, "The instability of a layer of fluid heated from below and subject to Coriolis forces", *Proc. R. Soc. London A* **217**, 306.
- Chandrasekhar, S., 1961, *Hydrodynamic and Hydromagnetic Stability* (Clarendon Press, Oxford).
- Chapman, C. J., and M. R. E. Proctor, 1980, "Nonlinear Rayleigh-Bénard convection between poorly conducting boundaries", *J. Fluid Mech.* **101**, 759.
- Charlson, G. S., and R. L. Sani, 1971, "On thermoconvective instability in a bounded cylindrical fluid layer", *Int. J. Heat Mass Transfer* **14**, 2157.
- Chaté, H., and P. Manneville, 1987, "Transition to turbulence via spatio-temporal intermittency", *Phys. Rev. Lett.* **58**, 112.
- Chaté, H., and P. Manneville, 1988a, "Continuous and discontinuous transition to spatio-temporal intermittency in two dimensional coupled map lattices", *Europhys. Lett.* **6**, 591.
- Chaté, H., and P. Manneville, 1988b, "Spatio-temporal intermittency in coupled map lattices", *Physica D* **32**, 409.
- Chaté, H., and P. Manneville, 1988c, "Structure of clusters generated by spatiotemporal intermittency and directed percolation in two dimensions", *Phys. Rev. A* **38**, 4351.
- Chaté, H., and P. Manneville, 1989a, "Coupled map lattices as cellular automata", *J. Stat. Phys.* **56**, 357.
- Chaté, H., and P. Manneville, 1989b, "Role of defects in the transition to turbulence via spatiotemporal intermittency", *Physica D* **37**, 33.
- Chaté, H., and P. Manneville, 1991, "Evidence of collective behavior in cellular automata", *Europhys. Lett.* **14**, 409.
- Chaté, H., and B. Nicolaenko, 1990, "Phase turbulence, spatiotemporal intermittency and coherent structures", in *New Trends in Nonlinear Dynamics and Pattern Forming Phenomena*, edited by P. Coullet and P. Huerre (Plenum, New York), p. 215.
- Chen, Y.-Y., 1992, "Finite-size effects on linear stability of pure fluid convection", *Phys. Rev. A* **45**, 3727.
- Chen, K., P. Bak, and M. H. Jensen, 1990, "A deterministic critical forest fire model", *Phys. Lett. A* **149**, 207.
- Chen, K., S. Chen, and R. H. Kraichnan, 1989, "Probability distribution of a stochastically advected scalar field", *Phys. Rev. Lett.* **63**, 2657.
- Chen, M. M., and J. A. Whitehead, 1968, "Evolution of two-dimensional periodic Rayleigh-Bénard convective cells of arbitrary wave numbers", *J. Fluid Mech.* **31**, 1.
- Chialvo, D. R., 1990, "Toward very simple generic models of excitable cells. Order and chaos in cardiac tissues. Facts and conjectures", in *Mathematical Approaches to Cardiac Arrhythmias*, edited by J. Jalife, *Ann. N.Y. Acad. Sci.* **591**, 351.
- Chiffaudel, A., S. Fauve, and B. Perrin, 1987, "Viscous and inertial convection at low Prandtl number: Experimental study", *Europhys. Lett.* **4**, 555.
- Chiffaudel, A., B. Perrin, and S. Fauve, 1989, "Spatiotemporal dynamics of oscillatory convection at low Prandtl number: waves and defects", *Phys. Rev. A* **39**, 2761.
- Chomaz, J. M., P. Huerre, and L. G. Redekopp, 1988, "Bifurcations to local and global modes in spatially developing flows", *Phys. Rev. Lett.* **60**, 25.
- Chomaz, J. M., P. Huerre, and L. G. Redekopp, 1991, "A frequency selection criterion in spatially developing flows", *Stud. Appl. Math.* **84**, 119.
- Chossat, P., Y. Demay, and G. Iooss, 1987, "Interaction de modes azimuthaux dans le problème de Couette-Taylor", *Arch. Rat. Mech. Anal.* **99**, 213.
- Chossat, P., and G. Iooss, 1985, "Primary and secondary bifurcations in the Couette-Taylor problem", *Jpn. J. Appl. Math.* **2**, 37.
- Christensen, K., and Z. Olami, 1992, "Scaling, phase transitions and nonuniversality in a self-organized critical cellular au-

- tomaton model”, Phys. Rev. A **46**, 1829.
- Christiansen, B., P. Alstrom, and M. T. Levinsen, 1992, “Ordered capillary wave states: quasi-crystals, hexagons and radial waves”, Phys. Rev. Lett. **68**, 2157.
- Chrostowski, J., and N. B. Abraham, 1986, Eds. “Optical chaos”, Proc. SPIE **667**, 1.
- Ciliberto, S., 1987, “Fractal dimension and metric entropy in extended systems”, Europhys. Lett. **4**, 685.
- Ciliberto, S., and P. Bigazzi, 1988, “Spatiotemporal intermittency in Rayleigh-Bénard convection”, Phys. Rev. Lett. **60**, 286.
- Ciliberto, S., and M. Caponeri, 1990, “Thermodynamics of spatiotemporal chaos: An experimental approach”, Phys. Rev. Lett. **64**, 2775.
- Ciliberto, S., P. Coullet, J. Lega, E. Pampolini, and C. Perez-Garcia, 1990, “Defects in roll-hexagon competition”, Phys. Rev. Lett. **65**, 2370.
- Ciliberto, S., S. Douady, and S. Fauve, 1991, “Investigating space-time chaos in Faraday instability by means of the fluctuations of the driving acceleration”, Europhys. Lett. **15**, 23.
- Ciliberto, S., E. Pampolini, and C. Perez-Garcia, 1988, “Competition between different symmetries in convective patterns”, Phys. Rev. Lett. **61**, 1198.
- Ciliberto, S., and N. Simonelli, 1986, “Spatial structures of temporal chaos in Rayleigh-Bénard convection”, Europhys. Lett. **2**, 285.
- Clavin, P., 1985, “Dynamic behavior of premixed flame fronts in laminar and turbulent flows”, Energy Combust. Sci. **11**, 1.
- Clever, R. M., and F. H. Busse, 1974, “Transition to time-dependent convection”, J. Fluid Mech. **65**, 625.
- Clever, R. M., and F. H. Busse, 1979, “Nonlinear properties of convection rolls in a horizontal layer rotating about a vertical axis”, J. Fluid Mech. **94**, 609.
- Clever, R. M., and F. H. Busse, 1981, “Low Prandtl-number convection in a layer heated from below”, J. Fluid Mech. **102**, 661.
- Clever, R. M., and F. H. Busse, 1987, “Nonlinear oscillatory convection”, J. Fluid Mech. **176**, 403.
- Clever, R. M., and F. H. Busse, 1989, “Three-dimensional knot convection in a layer heated from below”, J. Fluid Mech. **198**, 345.
- Cloot, A., and G. Lebon, 1984, “A nonlinear stability analysis of the Bénard-Marangoni problem”, J. Fluid Mech. **145**, 447.
- Clune, T., and E. Knobloch, 1991, “Square pattern convection in binary fluids with experimental boundary conditions”, Phys. Rev. A **44**, 8084.
- Coles, D., 1965, “Transition in circular Couette flow”, J. Fluid Mech. **21**, 335.
- Collet, P., and J. P. Eckmann, 1980, *Iterated Maps on the Interval as Dynamical Systems* (Birkhauser, Boston).
- Collet, P., and J. P. Eckmann, 1990, *Instabilities and Fronts in Extended Systems* (Princeton University Press, Princeton).
- Constantin, P., I. Procaccia, and K. R. Sreenivasan, 1991, “Fractal geometry of isoscalar surfaces in turbulence: Theory and experiments”, Phys. Rev. Lett. **67**, 1739.
- Coron, J. M., F. Helein, and J. M. Ghidaglia, 1991, Eds., *Defects, Singularities and Patterns in Nematic Liquid Crystals: Mathematical and Physical Aspects* (Kluwer, Dordrecht).
- Coullet, P., 1986, “Commensurate-incommensurate transition in nonequilibrium systems”, Phys. Rev. Lett. **56**, 724.
- Coullet, P., and C. Elphick, 1987, “Topological defects dynamics and Melnikov’s theory”, Phys. Lett. A **121**, 233.
- Coullet, P., C. Elphick, L. Gil, and J. Lega, 1987, “Topological defects of wave patterns”, Phys. Rev. Lett. **59**, 884.
- Coullet, P., K. P. Emilsson, and F. Plaza, 1991, “Qualitative theory of defects in nonequilibrium systems”, in *Instabilities and Nonequilibrium Structures III*, edited by E. Tirapegui and W. Zeller (Kluwer, Dordrecht), p. 357.
- Coullet, P., and S. Fauve, 1985, “Propagative phase dynamics for systems with Galilean invariance”, Phys. Rev. Lett. **55**, 2857.
- Coullet, P., S. Fauve, and E. Tirapegui, 1985, “Large scale instability of nonlinear standing waves”, J. Phys. Lett. **46**, L787.
- Coullet, P., L. Gil, and J. Lega, 1989a, “A form of turbulence associated with defects”, Physica D **37**, 91.
- Coullet, P., L. Gil, and D. Repaux, 1989b, “The role of topological defects in subcritical bifurcations”, in *Instabilities and Nonequilibrium Structures II*, edited by E. Tirapegui and D. Villarroel (Kluwer, Dordrecht), p. 189.
- Coullet, P., L. Gil, and F. Rocca, 1989c, “Optical vortices”, Optics Commun. **73**, 403.
- Coullet, P., R. E. Goldstein, and G. H. Gunaratne, 1989d, “Parity-breaking transitions of modulated patterns in hydrodynamic systems”, Phys. Rev. Lett. **63**, 1954.
- Coullet, P., R. E. Goldstein, and G. H. Gunaratne, 1990, Comment on “Parity-breaking transitions of modulated patterns in hydrodynamic systems”, Phys. Rev. Lett. **65**, 385.
- Coullet, P., and P. Huerre, 1986, “Resonance and phase solutions in spatially-forced thermal convection”, Physica **23D**, 27.
- Coullet, P., and P. Huerre, 1990, Eds., *New Trends in Nonlinear Dynamics and Pattern Forming Phenomena: the Geometry of Nonequilibrium* (Plenum, New York).
- Coullet, P., and G. Iooss, 1990, “Instabilities of one-dimensional cellular patterns”, Phys. Rev. Lett. **64**, 866.
- Coullet, P., and J. Lega, 1988, “Defect-mediated turbulence in wave patterns”, Europhys. Lett. **7**, 511.
- Coullet, P., J. Lega, B. Houchmanzadeh, and J. Lajzerowicz, 1990b, “Breaking chirality in nonequilibrium systems”, Phys. Rev. Lett. **65**, 1352.
- Coullet, P., and E. A. Spiegel, 1983, “Amplitude equations for systems with competing instabilities”, SIAM J. Appl. Math. **43**, 776.
- Coullet, P., and D. Walgraef, 1989, “Spatial forcing of 2D wave patterns”, Europhys. Lett. **10**, 525.
- Crawford, J. D., 1991, “Introduction to bifurcation theory”, Rev. Mod. Phys. **63**, 991.
- Crawford, J. D., and E. Knobloch, 1991, “Symmetry and symmetry-breaking bifurcations in fluid dynamics”, Annu. Rev. Fluid Mech. **23**, 341.
- Crick, F., 1970, “Diffusion in embryogenesis”, Nature **225**, 420.
- Croquette, V., 1989, “Convective pattern dynamics at low Prandtl number”, Contemp. Phys. **30**, 113, 153.
- Croquette, V., P. Le Gal, and A. Pocheau, 1986a, “Spatial features of the transition to chaos in an extended system”, Phys. Scr. T **13**, 135.
- Croquette, V., P. Le Gal, A. Pocheau, and R. Guglielmetti, 1986b, “Large-scale flow characterization in a Rayleigh-Bénard convective pattern”, Europhys. Lett. **1**, 393.
- Croquette, V., M. Mory, and E. Schosseler, 1983, “Rayleigh-Bénard convective structures in a cylindrical container”, J. Phys. (Paris) **44**, 293.
- Croquette, V., and A. Pocheau, 1984, “Wave-number selection in Rayleigh-Bénard convective structures”, in *Cellular Structures and Instabilities*, edited by J. E. Wesfried and S. Zaleski, Lecture Notes in Physics, 210 (Springer-Verlag, Berlin), p. 106.
- Croquette, V., and H. Williams, 1989, “Nonlinear competition between waves on convective rolls”, Phys. Rev. A **39**, 2765.
- Cross, M. C., 1980, “Derivation of the amplitude equation at the Rayleigh-Bénard instability”, Phys. Fluids **23**, 1727.

- Cross, M. C., 1982a, "Ingredients of a theory of convective textures close to onset", *Phys. Rev. A* **25**, 1065.
- Cross, M. C., 1982b, "Boundary conditions on the envelope function of convective rolls close to onset", *Phys. Fluids* **25**, 936.
- Cross, M. C., 1983, "Phase dynamics of convective rolls", *Phys. Rev. A* **27**, 490.
- Cross, M. C., 1984, "Wave number selection by soft boundaries near threshold", *Phys. Rev. A* **29**, 391.
- Cross, M. C., 1986a, "An 8-mode Lorenz model of traveling waves in binary-fluid convection", *Phys. Lett. A* **119**, 21.
- Cross, M. C., 1986b, "Traveling and standing waves in binary-fluid convection in finite geometries", *Phys. Rev. Lett.* **57**, 2935.
- Cross, M. C., 1988a, "Theoretical methods in pattern formation in physics, chemistry and biology", in *Far from Equilibrium Phase Transitions*, edited by L. Garrido, Lecture Notes in Physics 319 (Springer-Verlag, Berlin), p. 45.
- Cross, M. C., 1988b, "Structure of nonlinear traveling-wave states in finite geometries", *Phys. Rev. A* **38**, 3593.
- Cross, M. C., P. G. Daniels, P. C. Hohenberg, and E. D. Siggia, 1980, "Effect of distant sidewalls on wavenumber selection in Rayleigh-Bénard convection", *Phys. Rev. Lett.* **45**, 898.
- Cross, M. C., P. G. Daniels, P. C. Hohenberg, and E. D. Siggia, 1983a, "Phase-winding solutions in a finite container above the convective threshold", *J. Fluid Mech.* **127**, 155.
- Cross, M. C., P. C. Hohenberg, and M. C. Lücke, 1983b, "Forcing of convection due to time-dependent heating near threshold", *J. Fluid Mech.* **136**, 269.
- Cross, M. C., P. C. Hohenberg, and S. Safran, 1982, "Wavenumber selection in Rayleigh-Bénard convection: a numerical study", *Physica* **5D**, 75.
- Cross, M., and K. Kim, 1988a, "Linear instability and the codimension-2 region in binary-fluid convection between rigid impermeable boundaries", *Phys. Rev. A* **37**, 3909.
- Cross, M. C., and K. Kim, 1988b, "Existence of a codimension-2 point at the threshold of binary-fluid convection between rigid, impermeable boundaries", *Phys. Rev. A* **38**, 529.
- Cross, M. C., and E. Kuo, 1992, "One-dimensional spatial structure near a Hopf bifurcation at finite wavenumber", *Physica* **D 59**, 90.
- Cross, M. C., and A. C. Newell, 1984, "Convection patterns in large aspect ratio systems", *Physica* **10D**, 299.
- Cross, M. C., G. Tesauro, and H. S. Greenside, 1986, "Wavenumber selection and persistent dynamics in models of convection", *Physica* **23 D**, 12.
- Crutchfield, J. P., and K. Kaneko, 1987, "Phenomenology of spatio-temporal chaos" in *Directions in Chaos*, Vol. I, edited by Hao Bai-lin (World Scientific, Singapore), p. 272.
- Crutchfield, J. P., and K. Kaneko, 1988, "Are attractors relevant to turbulence?", *Phys. Rev. Lett.* **60**, 2715.
- Crutchfield, J., M. Nauenberg, and J. Rudnick, 1981, "Scaling for external noise at the onset of chaos", *Phys. Rev. Lett.* **46**, 933.
- Cummins, H. Z., L. Fourtune, and M. Raband, 1993, "Successive bifurcations in directional viscous fingering", *Phys. Rev. E* **47**, 1727.
- Curry, J. H., J. R. Herring, J. Loncaric, and S. A. Orszag, 1984, "Order and disorder in two- and three-dimensional Bénard convection", *J. Fluid Mech.* **147**, 1.
- Cvitanović, P., 1984, Ed., *Universality in Chaos* (Adam Hilger, Bristol).
- Dangelmayr, G., and E. Knobloch, 1987, "The Takens-Bogdanov bifurcation with O(2) symmetry", *Philos. Trans. R. Soc. London Ser. A* **322**, 243.
- Dangelmayr, G., and E. Knobloch, 1991, "Hopf bifurcation with broken circular symmetry", *Nonlinearity* **4**, 399.
- Dangelmayr, G., E. Knobloch, and M. Wegelin, 1991, "Dynamics of traveling waves in finite containers", *Europhys. Lett.* **16**, 723.
- Daniels, P. G., 1977, "The effect of distant sidewalls on the transition to finite amplitude Bénard convection", *Proc. R. Soc. London A* **358**, 173.
- Daniels, P. G., 1984, "Roll-pattern evolution in finite-amplitude Rayleigh-Bénard convection in a two-dimensional fluid layer bounded by distant sidewalls", *J. Fluid Mech.* **143**, 125.
- Daniels, P. G., and C. F. Ong, 1990, "Nonlinear convection in a rigid channel uniformly heated from below", *J. Fluid Mech.* **215**, 503.
- Daubechies, I., 1990, "The wavelet transform, time-frequency localization and signal analysis", *IEEE Info. T* **36**, 961.
- Davey, A., R. C. diPrima, and J. T. Stuart, 1968, "On the instability of Taylor-vortices", *J. Fluid Mech.* **31**, 17.
- Daviaud, F., and A. Pocheau, 1989, "Inhibition of phase turbulence close to onset of convection by permeable lateral boundary condition for the mean flow", *Europhys. Lett.* **9**, 675.
- Daviaud, F., M. Bonetti, and M. Dubois, 1990, "Transition to turbulence via spatiotemporal intermittency in one-dimensional Rayleigh-Bénard convection", *Phys. Rev. A* **42**, 3388.
- Daviaud, F., M. Dubois, and P. Bergé, 1989, "Spatio-temporal intermittency in quasi one-dimensional Rayleigh-Bénard convection", *Europhys. Lett.* **9**, 441.
- Davidenko, J. M., P. Kent, and J. Jalife, 1991, "Spiral waves in normal isolated ventricular muscle", *Physica* **D 49**, 182.
- Davis, S. H., 1967, "Convection in a box: linear theory", *J. Fluid Mech.* **30**, 465.
- Davis, S. H., 1976, "The stability of time-periodic flows", *Annu. Rev. Fluid Mech.* **8**, 57.
- Davydov, V. A., V. S. Zykov, and A. S. Mikhailov, 1991, "Kinematics of autowave patterns in excitable media", *Usp. Fiz. Nauk.* **161**, 45 [Sov. Phys. Usp. **34**, 665].
- DeDominicis, C., and P. C. Martin, 1979, "Energy spectra of certain randomly-stirred fluids", *Phys. Rev. A* **19**, 419.
- de Gennes, P. G., 1966, *Superconductivity of Metals and Alloys* (W. A. Benjamin, New York), p. 83.
- Dee, G. T., 1986, "The patterns produced by precipitation at a moving reaction front", *Physica* **D 23**, 340.
- Dee, G. T., and J. S. Langer, 1983, "Propagating pattern selection", *Phys. Rev. Lett.* **50**, 383.
- Deissler, R. J., 1985, "Noise-sustained structure in the time-dependent generalized Ginzburg-Landau equation", *J. Stat. Phys.* **40**, 371.
- Deissler, R. J., 1987a, "Turbulent bursts, spots and slugs in a generalized Ginzburg-Landau equation", *Phys. Lett. A* **120**, 334.
- Deissler, R. J., 1987b, "Spatially growing waves, intermittency, and convective chaos in an open-flow system", *Physica* **25D**, 233.
- Deissler, R. J., 1989, "External noise and the origin and dynamics of structure in convectively unstable systems", *J. Stat. Phys.* **54**, 1459.
- Deissler, R. J., and H. R. Brand, 1990, "The effect of nonlinear gradient terms on localized states near a weakly inverted bifurcation", *Phys. Lett. A* **146**, 252.
- Deissler, R. J., and H. R. Brand, 1991, "Interaction of two-dimensional localized solutions near a weakly inverted bifurca-

- tion”, Phys. Rev. A **44**, 3411.
- Deissler, R. J., and K. Kaneko, 1987, “Velocity-dependent Lyapunov exponents as a measure of chaos for open-flow systems”, Phys. Lett. A **119**, 397.
- Dewel, G., and P. Borckmans, 1992, “Motionless solitary waves in dissipative systems”, Europhys. Lett. **17**, 523.
- Dewel, G., P. Borckmans, and D. Walgraef, 1983, “Spatial patterns and double diffusion in chemical reactions”, Proc. Natl. Acad. Sci. USA **80**, 6429.
- DeWit, A., G. Dewel, P. Borckmans, and D. Walgraef, 1992, “Three-dimensional dissipative structures in reaction-diffusion systems”, Physica D.
- Dhar, D., 1990, “Self-organized critical state of sandpile automaton models”, Phys. Rev. Lett. **64**, 1613.
- Dockery, J. D., Keener, J. P., and J. J. Tyson, 1988, “Dispersion of traveling waves in the Belousov-Zhabotinskii reaction”, Physica D **30**, 177.
- DiPrima, R. C., and H. L. Swinney, 1981, “Instabilities and transition in flow between concentric rotating cylinders”, in *Hydrodynamic Instabilities and the Transition to Turbulence*, edited by H. L. Swinney and J. P. Gollub (Springer-Verlag, New York), p. 139.
- Doelman, A., 1989, “Slow time-periodic solutions of the Ginzburg-Landau equation”, Physica D **40**, 156.
- Doering, C. R., J. D. Gibbon, D. D. Holm, and B. Nicolaenko, 1987, “Exact Lyapunov dimension of the universal attractor for the complex Ginzburg-Landau equation”, Phys. Rev. Lett. **59**, 2911.
- Donnelly, R. J., 1990, “Externally modulated hydrodynamic systems”, in *Nonlinear Evolution of Spatio-temporal Structures in Dissipative Continuous Systems*, edited by F. H. Busse and L. Kramer (Plenum, New York), p. 31.
- Donnelly, R. J., 1991, “Taylor-Couette flow: The early days”, Phys. Today **44**, Nov., p. 32.
- Doolen, G., R. Ecke, D. Holm, and V. Steinberg, 1989, Eds., *Advances in Fluid Turbulence*, Physica D **37**, 1.
- Douady, S., 1989, “Instabilité paramétrique d’ondes de surface”, Thèse, ENS Lyon (unpublished).
- Douady, S., 1990, “Experimental study of the Faraday instability”, J. Fluid Mech. **221**, 383.
- Douady, S., Y. Couder, and M. E. Brachet, 1991, “Direct observation of the intermittency of intense vorticity filaments in turbulence”, Phys. Rev. Lett. **67**, 983.
- Douady, S., and S. Fauve, 1988, “Pattern selection in Faraday instability”, Europhys. Lett. **6**, 221.
- Douady, S., S. Fauve, and C. Laroche, 1989a, “Subharmonic instabilities and defects in a granular layer under vertical vibrations”, Europhys. Lett. **8**, 621.
- Douady, S., S. Fauve, and O. Thual, 1989b, “Oscillatory phase modulation of parametrically forced surface waves”, Europhys. Lett. **10**, 309.
- Dougherty, A., 1991, “Surface-tension anisotropy and the dendritic growth of pivalic acid”, J. Cryst. Growth **110**, 501.
- Dougherty, A., and J. P. Gollub, 1988, “Steady state dendritic growth of NH4BR from solution”, Phys. Rev. A **38**, 3043.
- Dougherty, A., P. D. Kaplan, and J. P. Gollub, 1987, “Development of side branching in dendritic crystal growth”, Phys. Rev. Lett. **58**, 1652.
- Drazin, P. G., and W. H. Reid, 1981, *Hydrodynamic Stability* (Cambridge University Press, Cambridge).
- Dubois, M., and P. Bergé, 1978, “Experimental study of the velocity field in Rayleigh-Bénard convection”, J. Fluid Mech. **85**, 641.
- Dubois-Violette, E., G. Durand, E. Guyon, P. Manneville, and P. Pieranski, 1978, “Instabilities in nematic liquid crystals”, in *Liquid Crystals*, edited by L. Liebert, Solid State Phys. Suppl. **14**, 147.
- Dubois-Violette, E., E. Guazzelli, and J. Prost, 1983, “Dislocation motion in layered structures”, Philos. Mag. A **48**, 727.
- Dwoyer, D. L., M. Y. Hussaini, and R. G. Voigt, 1985, *Theoretical Approaches to Turbulence*, Appl. Math. Sci. 58 (Springer-Verlag, New York).
- Dyachenko, S., A. C. Newell, A. Pushkarev, and V. E. Zakharov, 1992, “Optical turbulence: weak turbulence, condensates and collapsing filaments in the nonlinear Schrödinger equation”, Physica D **57**, 96.
- Dyachenko, A. I., V. E. Zakharov, A. N. Pushkarev, V. F. Shvets, and V. V. Yan’kov, 1989, “Soliton turbulence in nonintegrable wave systems”, Zh. Eksp. Teor. Fiz. **96**, 2026 [Sov. Phys. JETP **69**, 1144].
- Eagles, P. M., 1980, “A Bénard convection problem with a perturbed lower wall”, Proc. R. Soc. London A **371**, 359.
- Eckhaus, V., 1965, *Studies in Nonlinear Stability Theory*, Springer Tracts in Natural Philosophy, Vol. 6 (Springer-Verlag, Berlin).
- Eckmann, J. P., 1981, “Roads to turbulence in dissipative dynamical systems”, Rev. Mod. Phys. **53**, 643.
- Eckmann, J.-P., G. Goren, and I. Procaccia, 1991, “Nonequilibrium nucleation of topological defects as a deterministic phenomenon”, Phys. Rev. A **44**, R805.
- Eckmann, J. P., S. Oliffson Kamphorst, D. Ruelle, and S. Ciliberto, 1986, “Liapunov exponents from time series”, Phys. Rev. A **34**, 4971.
- Eckmann, J.-P., and I. Procaccia, 1991, “Onset of defect-mediated turbulence”, Phys. Rev. Lett. **66**, 891.
- Eckmann, J. P., and D. Ruelle, 1985, “Ergodic theory of chaos and strange attractors”, Rev. Mod. Phys. **57**, 617; Addendum **57**, 1115.
- Edwards, W. S., and S. Fauve, 1993, “Parametrically excited quasicrystalline surface waves”, Phys. Rev. E **47**, R788.
- Elder, K. R., J. Viñals, and M. Grant, 1992, “Ordering dynamics in the two-dimensional stochastic Swift-Hohenberg equation”, Phys. Rev. Lett. **68**, 3024.
- Elezgaray, J., and A. Arneodo, 1991, “Modeling reaction-diffusion pattern-formation in the Couette-flow reactor”, J. Chem. Phys. **95**, 323.
- Elmer, F. J., 1987, “Strange pattern formation in a model for ferromagnetic resonance instability”, Z. Phys. B **68**, 105.
- Elphick, C., G. R. Ierley, O. Regev, and E. A. Spiegel, 1991, “Interacting localized structures with Galilean invariance”, Phys. Rev. A **44**, 1110.
- Elphick, C., and E. Meron, 1989, “Localized structures in surface waves”, Phys. Rev. A **40**, 3226.
- Elphick, C., and E. Meron, 1990, “Solitary waves generated by subcritical instabilities in dissipative systems”, Phys. Rev. Lett. **65**, 2476.
- Elphick, C., and E. Meron, 1991, “Dynamics of phase singularities in two-dimensional oscillating systems”, Physica D **53**, 385.
- Elphick, C., E. Meron, J. Rinzel, and E. A. Spiegel, 1990a, “Impulse patterning and relaxational propagation in excitable media”, J. Theor. Biol. **146**, 249.
- Elphick, C., E. Meron, and E. A. Spiegel, 1988, “Spatiotemporal complexity in traveling patterns”, Phys. Rev. Lett. **61**, 496.
- Elphick, C., E. Meron, and E. A. Spiegel, 1990b, “Patterns of propagating pulses”, SIAM J. Appl. Math. **50**, 490.
- Engelbrecht, J., 1989, Ed., *Nonlinear Waves in Active Media*

- (Springer-Verlag, Berlin).
- Ermakova, E. A., A. M. Pertsov, and E. E. Shnol, 1989, "On the interaction of vortices in two-dimensional active media", *Physica D* **40**, 185.
- Ermentrout, B., J. Campbell, and G. Oster, 1986, "A model for shell patterns based on neural activity", *The Veliger* **28**, 369.
- Ermentrout, G. M., and J. D. Cowan, 1979, "A mathematical theory of visual hallucination patterns", *Bio. Cybernetics* **34**, 137.
- Ermentrout, G. B., S. P. Hastings, and W. C. Troy, 1984, "Large amplitude stationary waves in an excitable lateral-inhibitory medium", *SIAM J. Appl. Math.* **44**, 1133.
- Ermentrout, G. B., and J. Rinzel, 1980, "One-dimensional λ - ω target patterns: empirical stability tests", *J. Math. Biology* **10**, 97.
- Erneux, T., E. L. Reiss, L. J. Holden, and M. Georgiou, 1991, "Slow passage through bifurcation and limit points. Asymptotic theory and applications", in *Dynamic Bifurcations*, edited by E. Benoit, Lecture Notes in Mathematics 1493 (Springer-Verlag, Berlin), p. 14.
- Ertl, G., 1991, "Oscillatory kinetics and spatio-temporal self-organization in reactions at solid surfaces", *Science* **254**, 1750.
- Evans, D. J., and A. Baranyai, 1991, "Possible variational principle for steady states far from equilibrium", *Phys. Rev. Lett.* **67**, 2597.
- Everson, R. M., 1989, "Lyapunov exponents, dimension and entropy in coupled lattice maps" (unpublished).
- Evesque, P., and J. Rajchenbach, 1989, "Instability in a sand heap", *Phys. Rev. Lett.* **62**, 44.
- Ezerkii, A. B., M. I. Rabinovich, V. P. Reutov, and I. M. Starobinets, 1986, "Spatiotemporal chaos in the parametric excitation of a capillary ripple", *Zh. Eksp. Teor. Fiz.* **91**, 2070 [Sov. Phys. JETP **64**, 1228].
- Faraday, M., 1831, "On the forms and states assumed by fluids in contact with vibrating-elastic surfaces", *Philos. Trans. R. Soc. London* **52**, 319.
- Farmer, J. D., 1982, "Chaotic attractors of an infinite-dimensional dynamical system", *Physica D* **4**, 366.
- Farmer, J. D., E. Ott, and J. A. Yorke, 1983, "The dimension of chaotic attractors", *Physica D* **7**, 153.
- Fauve, S., 1987, "Large scale instabilities of cellular flows", in *Instabilities and Nonequilibrium Structures II*, edited by E. Tirapegui and D. Villarroel (Kluwer, Dordrecht), p. 63.
- Fauve, S., E. W. Bolton, and M. E. Brachet, 1987, "Nonlinear oscillatory convection: a quantitative phase dynamics approach", *Physica* **29D**, 202.
- Fauve, S., S. Douady, and O. Thual, 1990, "Parity-breaking transitions of modulated patterns in hydrodynamic systems", *Phys. Rev. Lett.* **65**, 385.
- Fauve, S., S. Douady, and O. Thual, 1991, "Drift instabilities of cellular patterns", *J. Phys. (Paris)* **1**, 311.
- Fauve, S., C. Larache, A. Libchaber, and B. Perrin, 1984, "Chaotic phases and magnetic order in a convective fluid", *Phys. Rev. Lett.* **52**, 1774.
- Fauve, S., and A. Libchaber, 1981, "Rayleigh-Bénard experiment in a low Prandtl number fluid: mercury", in *Chaos and Order in Nature*, edited by H. Haken (Springer-Verlag, Berlin), p. 25.
- Fauve, S., and O. Thual, 1990, "Solitary waves generated by subcritical instabilities in dissipative systems", *Phys. Rev. Lett.* **64**, 282.
- Feder, H. J. S., and J. Feder, 1991, "Self-organized criticality in a stick-slip process", *Phys. Rev. Lett.* **66**, 2669.
- Feigenbaum, M. J., 1978, "Quantitative universality for a class of nonlinear transformations", *J. Stat. Phys.* **19**, 25.
- Feigenbaum, M. J., 1979, "The universal metric properties of nonlinear transformations", *J. Stat. Phys.* **21**, 669.
- Feigenbaum, M. J., M. H. Jensen, and I. Procaccia, 1986, "Time ordering and the thermodynamics of strange sets: theory and experimental tests", *Phys. Rev. Lett.* **57**, 1503.
- Feng, Z. C., and P. R. Sethna, 1989, "Symmetry breaking bifurcations in resonant surface waves", *J. Fluid Mech.* **199**, 495.
- Fenstermacher, P. R., H. L. Swinney, and J. P. Gollub, 1979, "Dynamical instabilities and the transition to chaotic Taylor vortex flow", *J. Fluid Mech.* **94**, 103.
- Field, R. J., and M. Burger, 1985, Eds., *Oscillations and Traveling Waves in Chemical Systems* (Wiley, New York).
- Field, R. J., E. Körös, and R. M. Noyes, 1972, "Oscillations in chemical systems. II. Thorough analysis of temporal oscillation in the bromate-cerium-malonic acid system", *J. Am. Chem. Soc.* **94**, 8649.
- Fife, P. C., 1979, *Mathematical Aspects of Reacting and Diffusing Systems*, Lecture Notes in Biomathematics 28 (Springer-Verlag, New York).
- Fife, P. C., 1981, "On the question of the existence and nature of homogeneous-center target patterns in the Belousov-Zhabotinskii Reagent", in *Analytical and Numerical Approaches to Asymptomatic Problems in Analysis*, edited by S. Axelsson, L. S. Frank, and A. van der Sluis (North-Holland, Amsterdam).
- Fife, P. C., 1984a, "Current topics in reaction-diffusion systems", in *Nonequilibrium Cooperative Phenomena in Physics and Related Fields*, edited by M.G. Velarde (Plenum, New York), p. 371.
- Fife, P. C., 1984b, "Propagator-controller systems and chemical patterns", in *Nonequilibrium Dynamics in Chemical Systems*, edited by A. Pacault and C. Vidal (Springer-Verlag, Berlin).
- Fife, P. C., 1985, "Understanding the patterns in the BZ reagent", *J. Stat. Phys.* **39**, 687.
- Fineberg, J., E. Moses, and V. Steinberg, 1988a, "Nonlinear pattern and wave-number selection in convecting binary mixtures", *Phys. Rev. A* **38**, 4939.
- Fineberg, J., E. Moses, and V. Steinberg, 1988b, "Spatially and temporally modulated traveling-wave pattern in convecting binary mixtures", *Phys. Rev. Lett.* **61**, 838.
- Fineberg, J., and V. Steinberg, 1987, "Vortex-front propagation in Rayleigh-Bénard convection", *Phys. Rev. Lett.* **58**, 1332.
- Fineberg, J., V. Steinberg, and P. Kolodner, 1990, "Weakly nonlinear states as propagating fronts in the convection of binary mixtures", *Phys. Rev. A* **41**, 5743.
- Fisher, D. S., 1985, "Sliding charge density waves as a dynamic critical phenomenon", *Phys. Rev. B* **31**, 1396.
- Fitz-Hugh, R., 1961, "Impulses and physiological states in theoretical models of nerve membrane", *Biophys. J.* **1**, 445.
- Flesselles, J. M., A. J. Simon, and A. Libchaber, 1991, "Dynamics of one-dimensional interfaces: an experimentalists' view.", *Adv. Phys.* **40**, 1.
- Florjanczyk, M., and L. Gagnon, 1990, "Exact solutions for a higher-order nonlinear Schrödinger equation", *Phys. Rev. A* **41**, 4478.
- Foerster, P., S. C. Muller, and B. Hess, 1988, "Curvature and propagation velocity of chemical waves", *Science* **241**, 685.
- Forster, D., 1975, *Hydrodynamic Fluctuations, Broken Symmetry, and Correlation Functions* (Benjamin, New York).
- Forster, D., D. R. Nelson, and M. J. Stephen, 1977, "Large-distance and long-time properties of a randomly stirred fluid", *Phys. Rev. A* **16**, 732.
- Fraser, A. M., 1989, "Reconstructing attractors from scalar

- time series: a comparison of singular system and redundancy criteria”, *Physica D* **34**, 391.
- Fraser, A. M., and H. L. Swinney, 1986, “Independent coordinates for strange attractors from mutual information”, *Phys. Rev. A* **33**, 1134.
- Frechland, E., 1984, *Synergetics: From Microscopic to Macroscopic Order*, Proceedings of the International Symposium on Synergetics, Berlin, July 4–8, 1983 (Springer-Verlag, Berlin).
- Frisch, U., and S. A. Orszag, 1990, “Turbulence: challenges for theory and experiment”, *Phys. Today* **43**, Jan., p. 24.
- Frisch, U., and G. Parisi, 1985, *Varenna School LXXXVIII*, edited by M. Ghil, R. Benzi, and G. Parisi (North-Holland, Amsterdam), p. 84.
- Frisch, U., Z. S. She, and O. Thual, 1986, “Viscoelastic behaviour of cellular solutions to the Kuramoto-Sivashinsky model”, *J. Fluid Mech.* **168**, 221.
- Gallas, J. A. C., P. Grassberger, H. J. Herrmann, and P. Ueberholz, 1991, “Noisy collective behaviour in deterministic cellular automata”, *Physica A* **180**, 19.
- Gao, H., G. Metcalfe, T. Jung, and R. P. Behringer, 1987, “Heat-flow experiments in liquid ^4He with a variable cylindrical geometry”, *J. Fluid Mech.* **174**, 209.
- Gaponov-Grekhov, A. V., and M. I. Rabinovich, 1990, “Disorder, dynamical chaos and structures”, *Phys. Today* **43**, July, p. 30.
- Gaponov-Grekhov, A. V., and M. I. Rabinovich, 1992, *Nonlinearities in Action* (Springer-Verlag, New York).
- Gaponov-Grekhov, A. V., M. I. Rabinovich, and J. Engelbrecht, 1989, *Nonlinear Waves 1. Dynamics and Evolution* (Springer-Verlag, Berlin).
- Gardiner, C. W., 1983, *Handbook of Stochastic Methods for Physics, Chemistry, and Natural Sciences* (Springer-Verlag, Berlin).
- Garrido, P. L., J. L. Lebowitz, C. Maes, and H. Spohn, 1990, “Long-range correlations for conservative dynamics”, *Phys. Rev. A* **42**, 1954.
- Gerhardt, M., H. Schuster, and J. J. Tyson, 1990, “A cellular automaton model of excitable media. II. Curvature, dispersion rotating waves and meandering waves”, *Physica D* **46**, 392.
- Gershenfeld, N., 1988, “An experimentalist’s introduction to the observation of dynamical systems”, in *Directions in Chaos*, Vol. II, edited by Hao Bai-lin (World Scientific, Singapore).
- Gershenfeld, N. A., 1992, “Dimension measurement on high-dimensional systems”, *Physica D* **55**, 135.
- Gertsberg, V. L., and G. I. Sivashinsky, 1981, “Large cells in nonlinear Rayleigh-Bénard convection”, *Prog. Theor. Phys.* **66**, 1219.
- Getling, A. V., 1983, “Evolution of two-dimensional disturbances in the Rayleigh-Bénard problem and their preferred wavenumber”, *J. Fluid Mech.* **130**, 165.
- Getling, A. V., 1991, “Formation of spatial structures in Rayleigh-Bénard convection”, *Usp. Fiz. Nauk.* **161**, 1 [Sov. Phys. Usp. **34**, 737].
- Getling, A. V., 1992, “Convection-front propagation and wavenumber selection”, *Physica D* **55**, 121.
- Ghazali, A., and C. Misbah, 1992, “Phase instability and local dynamics in directional solidification”, *Phys. Rev. A* **46**, 5026.
- Gibbs, H. M., 1985, *Optical Bistability: Controlling Light with Light* (Academic, New York).
- Gibbs, H. M., S. L. McCall, and T. N. C. Venkatesan, 1976, “Differential gain and bistability using a sodium-filled Fabry-Perot interferometer”, *Phys. Rev. Lett.* **36**, 1135.
- Gierer, A., and H. Meinhardt, 1972, “A theory of biological pattern formation”, *Kybernetik* **12**, 30.
- Giglio, M., S. Muzatti, and U. Perini, 1981, “Transition to chaotic behavior via a reproducible sequence of period-doubling bifurcations”, *Phys. Rev. Lett.* **47**, 243.
- Ginzburg, V. L., and L. D. Landau, 1950, “On the theory of superconductivity”, *Zh. Eksp. Teor. Fiz.* **20**, 1064.
- Glansdorff, P., and I. Prigogine, 1971, *Thermodynamic Theory of Structure, Stability and Fluctuations* (Wiley, London).
- Glass, L., and P. Hunter, 1990, “There is a theory of heart”, *Physica D* **43**, 1.
- Glass, L., P. Hunter, and A. McCulloch, 1991, *Theory of Heart* (Springer-Verlag, New York).
- Glass, L., and M. C. Mackey, 1988, *From Clocks to Chaos. The Rhythms of Life* (Princeton University Press, Princeton, NJ).
- Glazier, J. A., and P. Kolodner, 1991, “Interactions of nonlinear pulses in convection in binary fluids”, *Phys. Rev. A* **43**, 4269.
- Glazier, J. A., and A. Libchaber, 1988, “Quasi-periodicity and dynamical systems: an experimentalist’s view”, *IEEE Transactions of Circuits and Systems CAS* **35**, 790.
- Godrèche, C., 1992, Ed., *Solids Far from Equilibrium* (Cambridge University Press, Cambridge, U.K.).
- Goldburg, W. I., P. Tong, and H. K. Pak, 1989, “A light-scattering study of turbulence”, *Physica D* **38**, 134.
- Goldenfeld, N., O. Martin, Y. Oono, and F. Liu, 1990, “Anomalous dimensions and the renormalization group in a nonlinear diffusion process”, *Phys. Rev. Lett.* **64**, 1361.
- Goldman, M. V., 1984, “Strong turbulence of plasma waves”, *Rev. Mod. Phys.* **56**, 709.
- Goldstein, R. E., G. H. Gunaratne, L. Gil, and P. Coullet, 1990, “Hydrodynamic and interfacial patterns with broken space-time symmetry”, *Phys. Rev. A* **43**, 6700.
- Gollub, J. P., 1991, “An experimental assessment of continuum models of dendritic growth”, in *Nonlinear Phenomena Related to Growth and Form*, edited by M. Ben Amar, P. Pelcé, and P. Tabeling (Plenum, New York).
- Gollub, J. P., and S. V. Benson, 1980, “Many routes to turbulent convection”, *J. Fluid Mech.* **100**, 449.
- Gollub, J. P., and A. R. McCarriar, 1982, “Convection patterns in Fourier space”, *Phys. Rev. A* **26**, 3470.
- Gollub, J. P., A. R. McCarriar, and J. F. Steinman, 1982, “Convective pattern evolution and secondary instabilities”, *J. Fluid Mech.* **125**, 259.
- Gollub, J. P., and R. Ramshankar, 1991, “Spatiotemporal chaos in interfacial waves”, in *New Perspectives in Turbulence*, edited by L. Sirovich (Springer-Verlag, New York), p. 165.
- Gollub, J. P., and H. L. Swinney, 1975, “Onset of turbulence in a rotating fluid”, *Phys. Rev. Lett.* **35**, 927.
- Golomb, D., D. Hansel, B. I. Shraiman, and H. Sompolinsky, 1992, “Clustering in globally coupled oscillators”, *Phys. Rev. A* **45**, 3516.
- Golubitsky, M., and D. G. Schaeffer, 1985, *Singularities and Groups in Bifurcation Theory*, Vol. I (Springer-Verlag, New York).
- Golubitsky, M., and I. Stewart, 1986, “Symmetry and stability in Taylor-Couette flow”, *SIAM J. Math. Anal.* **17**, 249.
- Golubitsky, M., I. Stewart, and D. G. Schaeffer, 1988, *Singularities and Groups in Bifurcation Theory* (Springer-Verlag, New York, Vol. II).
- Goren, G., I. Procaccia, S. Rasenat, and V. Steinberg, 1989, “Interactions and dynamics of topological defects: theory and experiments near the onset of weak turbulence”, *Phys. Rev. Lett.* **63**, 1237.
- Gor’kov, L. P., 1957, “Stationary convection in a plane liquid

- layer near the critical heat transfer point”, *Zh. Exp. Theor. Fiz.* **33**, 402 [Sov. Phys. JETP **6**, 311 (1958)].
- Gorman, M., and H. L. Swinney, 1982, “Spatial and temporal characteristics of modulated waves in the circular Couette system”, *J. Fluid Mech.* **117**, 123.
- Gorman, M., H. L. Swinney, and D. A. Rand, 1981, “Doubly periodic circular Couette flow: experiments compared with predictions from dynamics and symmetry”, *Phys. Rev. Lett.* **46**, 992.
- Graham, R., 1974, “Hydrodynamic fluctuations near the convection instability”, *Phys. Rev. A* **10**, 1762. [Erratum: *Phys. Rev. A* **45**, 4198 (1992)].
- Graham, R., 1975, in *Fluctuations, Instabilities and Phase Transitions*, edited by T. Riste (Plenum, New York).
- Graham, R., 1989, “Macroscopic potentials, bifurcations and noise in dissipative systems”, in *Noise in Nonlinear Dynamical Systems*, Vol. I, *Theory of Continuous Fokker-Planck Systems*, edited by F. Moss and P. V. E. McClintock (Cambridge University Press, Cambridge, U.K.).
- Graham, R., and J. A. Domaradzki, 1982, “Local amplitude equation of Taylor vortices and its boundary condition”, *Phys. Rev. A* **26**, 1572.
- Graham, R., and T. Tél, 1986, “Nonequilibrium potential for coexisting attractors”, *Phys. Rev. A* **33**, 1322.
- Graham, R., and T. Tél, 1990a, “Steady-state ensemble for the complex Ginzburg-Landau equation with weak noise”, *Phys. Rev. A* **42**, 4661.
- Graham, R., and T. Tél, 1990b, “Potential for the complex Ginzburg-Landau equation”, *Europhys. Lett.* **13**, 715.
- Graham, R., and A. Wunderlin, 1987, Eds., *Lasers and Synergetics* (Springer-Verlag, Berlin).
- Grappin, R., J. Leorat, and A. Pouquet, 1986, “Computation of the dimension of a model of fully developed turbulence”, *J. Phys. (Paris)* **47**, 1127.
- Grassberger, P., 1982, “On phase transitions in Schlögl’s second model”, *Z. Phys. B* **47**, 365.
- Grassberger, P., 1989, “Information content and predictability of lumped and distributed dynamical systems”, *Physica Scripta* **40**, 346.
- Grassberger, P., and H. Kantz, 1991, “On a forest fire model with supposed self-organized criticality”, *J. Stat. Phys.* **63**, 685.
- Grassberger, P., and S. S. Manna, 1990, “Some more sandpiles”, *J. Phys. (Paris)* **51**, 1077.
- Grassberger, P., and I. Procaccia, 1983, “Measuring the strangeness of strange attractors”, *Physica* **9 D**, 189.
- Grassberger, P., and T. Schreiber, 1991, “Phase transitions in coupled map lattices”, *Physica D* **50**, 177.
- Greene, J., and J. S. Kim, 1988, “The steady states of the Kuramoto-Sivashinsky equation”, *Physica D* **33**, 99.
- Greenside, H. S., G. Ahlers, P. C. Hohenberg, and R. W. Walden, 1982, “A simple stochastic model for the onset of turbulence in Rayleigh-Bénard convection”, *Physica* **5D**, 322.
- Greenside, H. S., and W. M. Coughran, Jr., 1984, “Nonlinear pattern formation near the onset of Rayleigh-Bénard convection”, *Phys. Rev. A* **30**, 398.
- Greenside, H. S., and M. C. Cross, 1985, “Stability analysis of two-dimensional models of three-dimensional convection”, *Phys. Rev. A* **31**, 2492.
- Greenside, H. S., M. C. Cross, and W. M. Coughran, Jr., 1988, “Mean flows and the onset of chaos in large-cell convection”, *Phys. Rev. Lett.* **60**, 2269.
- N. P. Greis, and H. S. Greenside, 1991, “Implication of a power-law power-spectrum for self-affinity”, *Phys. Rev. A* **44**, 2324.
- Grinstein, G., 1991, “Generic scale invariance in classical nonequilibrium systems”, *J. Appl. Phys.* **69**, 5441.
- Grinstein, G., Y. He, C. Jayaprakash, and B. Bolker, 1991, “Collective behavior of a coupled map system with a conserved quantity”, *Phys. Rev. A* **44**, 4923.
- Grinstein, G., C. Jayaprakash, and Y. He, 1985, “Statistical mechanics of probabilistic cellular automata”, *Phys. Rev. Lett.* **55**, 2527.
- Grinstein, G., and D.-H. Lee, 1991, “Generic scale invariance and roughening in noisy model sandpiles and other driven interfaces”, *Phys. Rev. Lett.* **66**, 177.
- Grinstein, G., D.-H. Lee, and S. Sachdev, 1990, “Conservation laws, anisotropy, and ‘self-organized criticality’ in noisy nonequilibrium systems”, *Phys. Rev. Lett.* **64**, 1927.
- Gromov, P. R., A. B. Zobnin, M. I. Rabinovich, A. M. Reiman, and M. M. Sushchik, 1987, “Finite-dimensional attractors in shear flows with feedback”, *Dokl. Akad. Nauk. SSSR* **292**, 284 [Sov. Phys. Dokl. **32**, 8].
- Grossman, S., and A. S. Mikhailov, 1990, “Sweeping through the critical region”, *Z. Phys. B* **78**, 1.
- Guckenheimer, J., 1984, “Dimension estimates for attractors”, *Contemp. Math.* **28**, 357.
- Guckenheimer, J., and P. Holmes, 1983, *Nonlinear Oscillations, Dynamical Systems and Bifurcations of Vector Fields* (Springer-Verlag, New York).
- Gundlach, V. M., and D. A. Rand, 1992a, “Spatiotemporal chaos. 1. Hyperbolicity, structural stability, spatiotemporal shadowing and symbolic dynamics”, *Nonlinearity* **6**, 165.
- Gundlach, V. M., and D. A. Rand, 1992b, “Spatiotemporal chaos. 2. Unique Gibbs states for higher-dimensional symbolic systems”, *Nonlinearity* **6**, 201.
- Gundlach, V. M., and D. A. Rand, 1992c, “Spatiotemporal chaos. 3. Natural spatiotemporal measures for coupled circle map lattices”, *Nonlinearity* **6**, 215.
- Gunton, J. D., and M. Droz, 1983, *Introduction to the Theory of Metastable and Unstable States*, Lecture Notes in Physics 183 (Springer-Verlag, Heidelberg).
- Gurevich, A. V., and R. G. Mints, 1984, “Localized waves in inhomogeneous media”, *Usp. Fiz. Nauk.* **142**, 61 [Sov. Phys. Usp. **27**, 19].
- Gurevich, A. V., R. G. Mints and A. A. Pukhov, 1989, “Motion of a kink in a bistable medium with hysteresis”, *Physica D* **35**, 382.
- Gutkowicz-Krusin, D., M. A. Collins, and J. Ross, 1979, “Rayleigh-Bénard instability in nonreactive binary fluids. I. Theory”, *Phys. Fluids* **22**, 1443.
- Güttinger, W., and G. Dangelmayr, 1987, Eds., *The Physics of Structure Formation: Theory and Simulation* (Springer-Verlag, Berlin).
- Hagan, P., 1982, “Spiral waves in reaction-diffusion equations”, *SIAM J. Appl. Math.* **42**, 762.
- Hagan, P. S., and M. S. Cohen, 1981, “Diffusion-induced morphogenesis in the development of *Dictyostelium*”, *J. Theor. Bio.* **92**, 881.
- Haken, H., 1975, “Cooperative phenomena in systems far from thermal equilibrium and in nonphysical systems”, *Rev. Mod. Phys.* **47**, 67.
- Haken, H., 1980, Ed., *Dynamics of Synergetics Systems: Proceedings* (Springer-Verlag, Berlin).
- Haken, H., 1981a, Ed., *Synergetics — A workshop: Proceedings of the International Workshop on Synergetics at Schloss Elmau, Bavaria, 1980* (Springer-Verlag, Berlin).
- Haken, H., 1981b, Ed., *Chaos and Order in Nature: Proceedings of the International Symposium on Synergetics at Schloss El-*

- mau, Bavaria, 1981* (Springer-Verlag, Berlin).
- Haken, H., 1983a, *Synergetics, An Introduction. Nonequilibrium Phase Transitions & Self-Organization in Physics, Chemistry & Biology* (Springer-Verlag, Berlin).
- Haken, H., 1983b, "At least one Lyapunov exponent vanishes if the trajectory of an attractor does not contain a fixed point", *Phys. Lett.* **94A**, 71.
- Haken, H., 1987, *Advanced Synergetics* (Springer-Verlag, Berlin).
- Haken, H., 1989, "Synergetics: an overview", *Rep. Prog. Phys.* **52**, 515.
- Haken, H., and H. Olbrich, 1978, "Analytical treatment of pattern formation in the Gierer-Meinhardt model of morphogenesis", *J. Math. Biol.* **6**, 317.
- Hakim, V., P. Jakobsen, and Y. Pomeau, 1990, "Fronts vs. solitary waves in nonequilibrium systems", *Europhys. Lett.* **11**, 19.
- Hakim, V., and Y. Pomeau, 1991, "On stable localized structures and subcritical instabilities", *Eur. J. Mech. B/Fluids* **10**, 137.
- Hall, P., 1980, "Centrifugal instabilities of circumferential flows in finite cylinders: nonlinear theory", *Proc. R. Soc. Lond. A* **372**, 317.
- Hall, P., 1984, "Evolution equations for Taylor vortices in the small-gap limit", *Phys. Rev. A* **29**, 2921.
- Halsey, T. C., M. H. Jensen, L. P. Kadanoff, I. Procaccia, and B. I. Shraiman, 1986, "Fractal measures and their singularities: the generalization of strange sets", *Phys. Rev. A* **33**, 1141.
- Hao, Bai-lin, 1984, Ed., *Chaos* (World Scientific, Singapore).
- Hao, Bai-lin, 1987, Ed., *Directions in Chaos* (World Scientific, Singapore), Vol. 1.
- Hao, Bai-lin, 1988, Ed., *Directions in Chaos* (World Scientific, Singapore), Vol. 2.
- Hartung, G., F. H. Busse, and I. Rehberg, 1991, "Time-dependent convection induced by broken spatial symmetries", *Phys. Rev. Lett.* **66**, 2742.
- Hasegawa, A., 1989, *Optical Solitons in Fibers* (Springer-Verlag, Berlin).
- Hasegawa, A., and F. Tappert, 1973, "Transmission of stationary nonlinear optical pulses in dispersive dielectric fibers; 1. Anomalous dispersion", *Appl. Phys. Lett.* **23**, 142.
- Hegseth, J. J., C. D. Andereck, F. Hayot, and Y. Pomeau, 1989, "Spiral turbulence and phase dynamics", *Phys. Rev. Lett.* **62**, 257.
- Heikes, K. E., and F. H. Busse, 1980, "Weakly nonlinear turbulence", *Ann. N.Y. Acad. Sci.* **357**, 28.
- Heinrichs, R., G. Ahlers, and D. S. Cannell, 1987, "Traveling waves and spatial variation in the convection of a binary mixture", *Phys. Rev. A* **35**, 2761.
- Hentschel, H. G. E., and I. Procaccia, 1983, "The infinite number of generalized dimensions of fractals and strange attractors", *Physica D* **8**, 435.
- Heutmaker, M. S., P. N. Fraenkel, and J. P. Gollub, 1985, "Convection patterns: time evolution of the wave-vector field", *Phys. Rev. Lett.* **54**, 1369.
- Heutmaker, M. S., and J. P. Gollub, 1987, "Wave-vector field of convective flow patterns", *Phys. Rev. A* **35**, 242.
- Hill, E. L., 1951, "Hamilton's principle and the conservation theorems of mathematical physics", *Rev. Mod. Phys.* **23**, 253.
- Hirsch, M. W., and S. Smale, 1974, *Differential Equations, Dynamical Systems and Linear Algebra* (Academic, New York).
- Hjelmfelt, A., and J. Ross, 1992, "Thermodynamic and stochastic theory of electrical circuits", *Phys. Rev. A* **45**, 2201.
- Hodgkin, A. L., and A. F. Huxley, 1952, "A quantitative description of membrane current and its application to conduction and excitation in nerve", *J. Physiol. (London)* **117**, 500.
- Hohenberg, P. C., and M. C. Cross, 1987, "An introduction to pattern formation in nonequilibrium systems", in *Fluctuations and Stochastic Phenomena in Condensed Matter*, edited by L. Garrido (Springer-Verlag, New York), p. 55.
- Hohenberg, P. C., and B. I. Halperin, 1977, "Theory of dynamic critical phenomena", *Rev. Mod. Phys.* **49**, 435.
- Hohenberg, P. C., L. Kramer, and H. Riecke, 1985, "Effects of boundaries on one-dimensional reaction-diffusion equations near threshold", *Physica* **15D**, 402.
- Hohenberg, P. C., and J. S. Langer, 1982, "Nonequilibrium phenomena: outlines and bibliographies of a workshop", *J. Stat. Phys.* **28**, 193.
- Hohenberg, P. C., and B. I. Shraiman, 1989, "Chaotic behavior of an extended system", *Physica D* **37**, 109.
- Hohenberg, P. C., and J. B. Swift, 1987, "Hexagons and rolls in periodically modulated Rayleigh-Bénard convection", *Phys. Rev. A* **35**, 3855.
- Hohenberg, P. C., and J. B. Swift, 1992, "Effects of external noise at the onset of Rayleigh-Bénard convection", *Phys. Rev. A* **46**, 4773.
- Holden, A. V., M. Markus, and H. G. Othmer, 1990, Eds., *Nonlinear Processes in Excitable Media* (Plenum, New York).
- Holmes, P., 1986, "Spatial structure of time-periodic solutions of the Ginzburg-Landau equation", *Physica D* **23**, 84.
- Hornreich, R. M., M. Luban, and S. Shtrikman, 1975, "Critical behavior at the onset of k -space instability on the λ -line", *Phys. Rev. Lett.* **35**, 1678.
- Hort, W., S. J. Linz, and M. Lücke, 1992, "Onset of convection in binary-gas mixtures: role of the Dufour effect", *Phys. Rev. A* **45**, 3737.
- Hortsmek, W., and R. Lefever, 1984, *Noise Induced Transitions* (Springer-Verlag, Berlin).
- Houlrik, J. M., and M. H. Jensen, 1992, "Critical correlations in coupled map lattices", *Phys. Lett. A* **163**, 275.
- Houlrik, J. M., I. Webman, and M. H. Jensen, 1990, "Mean-field theory and critical behavior of coupled map lattices", *Phys. Rev. A* **41**, 4210.
- Howard, L. N., 1966, "Convection at high Rayleigh number", in *Applied Mechanics, Proceedings of the 11th Congress of Applied Mechanics*, Munich, Germany, edited by H. Görtler (Springer-Verlag, Berlin), p. 1109.
- Howard, L. N., and N. Kopell, 1977, "Slowly varying waves and shock structures in reaction-diffusion equations", *Stud. Appl. Math.* **56**, 95.
- Hu, Y. C., R. Eck, and G. Ahlers, 1992 (unpublished).
- Huang, S.-C., and M. E. Glicksman, 1981, "Fundamentals of dendritic solidification — II: development of side branch structure", *Acta Metall.* **29**, 717.
- Huerre, P., 1987a, "Spatio-temporal instabilities in closed and open flows", in *Instabilities and Nonequilibrium Structures I*, edited by E. Tirapegui and D. Villarroel (Reidel, Dordrecht), p. 141.
- Huerre, P., 1987b, "Evolution of coherent structures in shear flows: a phase dynamics approach", *Nucl. Phys. B (Proc. Suppl.)* **2**, 159.
- Huerre, P., and P. A. Monkewitz, 1985, "Absolute and convective instabilities in free shear layers", *J. Fluid Mech.* **159**, 151.
- Huerre, P., and P. A. Monkewitz, 1990, "Local and global instabilities in spatially developing flows", *Annu. Rev. Fluid Mech.* **22**, 473.
- Hwa, T., and M. Kardar, 1989, "Dissipative transport in open

- systems: an investigation of self-organized criticality”, Phys. Rev. Lett. **62**, 1813.
- Hwa, T., and M. Kardar, 1992, “Avalanches, hydrodynamics, and great events in models of sand piles”, Phys. Rev. A **45**, 7002.
- Hyman, J. M., B. Nicolaenko, and S. Zaleski, 1986, “Order and complexity in the Kuramoto-Sivashinsky model of weakly turbulent surfaces”, Physica D **23**, 265.
- Iooss, G., and D. D. Joseph, 1980, *Elementary Stability and Bifurcation Theory* (Springer-Verlag, Berlin).
- Iooss, G., A. Mielke, and Y. Demay, 1990, “Mathematical justification of steady Ginzburg-Landau equation starting from Navier Stokes”, in *New Trends in Nonlinear Dynamics and Pattern-forming Phenomena*, edited by P. Coullet and P. Huerre (Plenum, New York), p. 275.
- Ivantsov, G. P., 1947, Dokl. Akad. Nauk. SSSR **58**, 567.
- Jackson, C. P., 1987, “A finite-element study of the onset of vortex shedding in flow past variously-shaped bodies”, J. Fluid Mech. **182**, 23.
- Jackson, E. A., 1989, *Perspectives of Nonlinear Dynamics* (Cambridge University Press, Cambridge), Vol. I.
- Jackson, K. A., and J. D. Hunt, 1965, “Transparent compounds that freeze like metals”, Acta Metall. **13**, 1212.
- Jaeger, H. M., C.-H. Liu, and S. R. Nagel, 1989, “Relaxation at the angle of repose”, Phys. Rev. Lett. **62**, 40.
- Jäger, W., and J. D. Murray, 1984, Eds., *Modelling of Patterns in Space and Time*, Lecture Notes in Biomathematics **55** (Springer-Verlag, Berlin).
- Jahnke, W., C. Henze, and A. T. Winfree, 1988, “Chemical vortex dynamics in three-dimensional excitable media”, Nature **336**, 662.
- Jahnke, W., and W. T. Winfree, 1991, Int. J. Bifurc. Chaos **1**, 455.
- Jalife, J., 1990, Ed., *Mathematical Approaches to Cardiac Arrhythmias* (Ann. N.Y. Acad. Sci. **591**).
- Janiaud, B., A. Pumir, D. Bensimon, V. Croquette, H. Richter, and L. Kramer, 1992, “The Eckhaus instability for traveling waves”, Physica D **55**, 269.
- Jenkins, D. R., and M. R. E. Proctor, “The transition from roll to square-cell solutions in Rayleigh-Bénard convection”, J. Fluid Mech. **139**, 461.
- Jensen, M. H., 1991, “Multifractals, multiscaling and the energy cascade of turbulence”, in *Spontaneous Formation of Space-Time Structures and Criticality*, edited by T. Riste and D. Sherrington (Plenum, New York).
- Jensen, M. H., L. P. Kadanoff, A. Libchaber, I. Procaccia, and J. Stavans, 1985, “Global universality at the onset of chaos: results of a forced Rayleigh-Bénard experiment”, Phys. Rev. Lett. **55**, 2798.
- Jensen, M. H., G. Paladin, and A. Vulpiani, 1991, “Multiscaling in multifractals”, Phys. Rev. Lett. **67**, 208.
- Joets, A., and R. Ribotta, 1988, “Propagative structures and localization in the convection of a liquid crystal”, in *Propagation in Systems Far from Equilibrium*, edited by J. E. Wesfried, H. R. Brand, P. Manneville, G. Albinet, and N. Boccara (Springer-Verlag, Berlin), p. 176.
- Jones, C. A., D. R. Moore, and N. O. Weiss, 1976, “Axisymmetric convection in a cylinder”, J. Fluid Mech. **73**, 353.
- Joseph, D. D., 1976, *Stability of Fluid Motions Vol. I and II* (Springer-Verlag, Berlin).
- Kadanoff, L. P., S. R. Nagel, L. Wu, and S-M Zhou, 1989, “Scaling and universality in avalanches”, Phys. Rev. A **39**, 6524.
- Kai, S., 1992, Ed., *Physics of Pattern Formation in Complex Dissipative Systems* (World Scientific, Singapore).
- Kaneko, K., 1985, “Spatiotemporal intermittency in coupled map lattices”, Prog. Theor. Phys. **74**, 1033.
- Kaneko, K., 1986a, “Lyapunov analysis and information flow in coupled map lattices”, Physica **23D**, 436.
- Kaneko, K., 1986b, *Collapse of Tori and Genesis of Chaos in Dissipative Systems* (World Scientific, Singapore).
- Kaneko, K., 1987, “Pattern dynamics in spatiotemporal chaos”, Physica D **34**, 1.
- Kaneko, K., 1989, “Spatiotemporal chaos in one- and two-dimensional coupled map lattices”, Physica **37D**, 60.
- Kaneko, K., 1990a, “Simulating physics with coupled map lattices”, in *Formation, Dynamics and Statistics of Patterns*, edited by K. Kawasaki, M. Suzuki and A. Onuki (World Scientific, Singapore), Vol. 1.
- Kaneko, K., 1990b, “Clustering, coding, switching, hierarchical ordering, and control in a network of chaotic elements”, Physica D **41**, 137.
- Kaneko, K., 1990c, “Globally coupled chaos violates the law of large numbers but not the central-limit theorem”, Phys. Rev. Lett. **65**, 1391.
- Kaplan, D. T., J. M. Smith, B. E. H. Saxberg, and R. J. Cohen, 1988, “Nonlinear dynamics in cardiac conduction”, in *Nonlinearity in Biology and Medicine*, edited by A. S. Perelson, B. Goldstein, M. Dembo, and J. A. Jacquez (Elsevier, New York), p. 19.
- Karma, A., 1987, “Beyond steady-state lamellar eutectic growth”, Phys. Rev. Lett. **59**, 71.
- Karma, A., 1990, “Meandering transition in 2-dimensional excitable media”, Phys. Rev. Lett. **65**, 2824.
- Karma, A., 1991, “Universal limit of spiral wave propagation in excitable media”, Phys. Rev. Lett. **66**, 2274.
- Karma, A., 1992, “Scaling regime of spiral wave propagation in single-diffusive media”, Phys. Rev. Lett. **68**, 397.
- Kaski, K., K. Binder, and J. D. Gunton, 1983, “Study of cell distribution functions of the three-dimensional Ising model”, Phys. Rev. B **29**, 3996.
- Kaspar, F., and H. G. Schuster, 1986, “Scaling at the onset of spatial disorder in coupled piecewise linear maps”, Phys. Lett. A **113**, 451.
- Kassner, K., and C. Misbah, 1991a, “Growth of lamellar eutectic structures — The axisymmetrical state”, Phys. Rev. A **44**, 6513.
- Kassner, K., and C. Misbah, 1991b, “Spontaneous parity-breaking transition in directional growth of lamellar eutectic structures”, Phys. Rev. A **44**, 6533.
- Kassner, K., C. Misbah, and H. Müller-Krumbhaar, 1991, “Transition to chaos in directional solidification”, Phys. Rev. Lett. **67**, 1551.
- Kauffman, S. A., R. M. Shymko, and K. Trabert, 1978, “Control of sequential compartment formation in *Drosophila*; a uniform mechanism may control the locations of successive binary development commitments”, Science **199**, 259.
- Kawasaki, K., 1984a, “Topological defects and non-equilibrium”, Prog. Theor. Phys. Suppl. **79**, 161.
- Kawasaki, K., 1984b, “Defect-phase dynamics for dissipative media with potential”, Prog. Theor. Phys. Suppl. **80**, 123.
- Kawasaki, K., Y. Kuramoto, and H. Okamoto, 1989, Eds., “Complex dynamics in nonlinear systems”, Prog. Theor. Phys. Suppl. **99**, 1.
- Kawasaki, K., and T. Ohta, 1986, “Phase Hamiltonian in periodically modulated systems”, Physica A **139**, 223.
- Kawasaki, K., M. Suzuki, and A. Onuki, 1990, Eds., *Formation, Dynamics and Statistics of Patterns* (World Scientific, Singa-

- pore).
- Kawczyński, A. L., W. S. Comstock, and R. J. Field, 1992, "The evolution of patterns in a homogeneously oscillating medium", *Physica D* **54**, 220.
- Keeler, J. D., and J. D. Farmer, 1986, "Robust space-time intermittency and $1/f$ noise", *Physica D* **23**, 413.
- Keener, J. P., 1986, "A geometrical theory for spiral waves in excitable media", *SIAM J. Appl. Math.* **46**, 1039.
- Keener, J. P., 1988, "The dynamics of three-dimensional scroll waves in excitable media", *Physica D* **31**, 269.
- Keener, J. P., and J. J. Tyson, 1986, "Spiral waves in the Belousov-Zhabotinskii reaction", *Physica D* **21D**, 307.
- Keener, J. P., and J. J. Tyson, 1990, "Helical and circular scroll wave filaments", *Physica D* **44**, 191.
- Keener, J. P., and J. J. Tyson, 1991, "The dynamics of helical scroll waves in excitable media", *Physica D* **53**, 151.
- Kelly, R. E., and D. Pal, 1978, "Thermal convection with spatially periodic boundary conditions: resonant wavelength excitation", *J. Fluid Mech.* **86**, 433.
- Kemmner, W., 1984, "A model of head regeneration in hydra", *Differentiation* **26**, 83.
- Keolian, R., L. A. Turkevich, S. J. Puterman, I. Rudnick, and J. A. Rudnick, 1981, "Subharmonic sequences in the Faraday experiment: departures from period doubling", *Phys. Rev. Lett.* **47**, 1133.
- Kessler, D. A., J. Koplik, and H. Levine, 1988, "Pattern selection in fingered growth phenomena", *Adv. Phys.* **37**, 255.
- Kessler, D. A., and H. Levine, 1990a, "Stability of traveling waves in the Belousov-Zhabotinskii reaction", *Phys. Rev. A* **41**, 5418.
- Kessler, D. A., and H. Levine, 1990b, "A geometrical model for spirals: a possible paradigm for Belousov-Zhabotinskii", *Europhys. Lett.* **12**, 465.
- Kessler, D. A., H. Levine, and W. N. Reynolds, 1992, "Spiral core in singly diffusive excitable media", *Phys. Rev. Lett.* **68**, 401.
- Kinzel, W., 1983, "Directed percolation", in *Percolation Structures and Processes*, edited by G. Deutscher *et al.* (Ann. Israel Phys. Soc. **5**, 425).
- Kirchartz, K. R., U. Müller, H. Oertl, and I. Zierep, 1981, "Axisymmetric and non-axisymmetric convection in a cylindrical container", *Acta Mecanica* **40**, 181.
- Kivshar, Y. S., and B. A. Malomed, 1989, "Dynamics of solitons in nearly integrable systems", *Rev. Mod. Phys.* **61**, 763.
- Klyachkin, A. V., 1989, "Modulational instability and autowaves in the active media described by the nonlinear equations of Ginzburg-Landau type" (unpublished).
- Knobloch, E., 1989, "Pattern selection in binary-fluid convection at positive separation ratios", *Phys. Rev. A* **40**, 1549.
- Knobloch, E., 1990, "Pattern selection in long-wavelength convection", *Physica* **41D**, 450.
- Knobloch, E., and J. DeLuca, 1992, "Amplitude equation for traveling wave convection", *Nonlinearity* **3**, 975.
- Knobloch, E., and J. D. Gibbon, 1991, "Coupled NLS equations for counter propagating waves in systems with reflection symmetry", *Phys. Lett. A* **154**, 353.
- Knobloch, E., and D. R. Moore, 1988, "Linear stability of experimental Soret convection", *Phys. Rev. A* **37**, 860.
- Knobloch, E., and D. R. Moore, 1990, "Minimal model of binary fluid convection", *Phys. Rev. A* **42**, 4693.
- Knobloch, E., D. R. Moore, J. Toomre, and N. O. Weiss, 1986, "Transition to chaos in two-dimensional double-diffusive convection", *J. Fluid Mech.* **166**, 409.
- Knobloch, E., and M. R. Proctor, 1981, "Nonlinear periodic convection in double diffusive systems", *J. Fluid Mech.* **108**, 291.
- Kolmogorov, A. N., 1941, "The local structure of turbulence in an incompressible fluid with very large Reynolds number", *Dokl. Akad. Nauk SSSR* **30**, 301 [Reprinted in *Proc. R. Soc. London Ser. A* **434**, 9 (1991)].
- Kolmogorov, A., I. Petrovsky, and N. Piskunov, 1937, "Investigation of a diffusion equation connected to the growth of materials, and application to a problem in biology", *Bull. Univ. Moscow, Ser. Int. Sec. A* **1**, 1.
- Kolodner, P., 1990, "Neutrally stable fronts of slow convective traveling waves", *Phys. Rev. A* **42**, 2475.
- Kolodner, P., 1991a, "Collisions between pulses of traveling-wave convection", *Phys. Rev. A* **44**, 6466.
- Kolodner, P., 1991b, "Stable and unstable pulses of traveling-wave convection", *Phys. Rev. A* **43**, 2827.
- Kolodner, P., 1991c, "Drifting pulses of traveling-wave convection", *Phys. Rev. Lett.* **66**, 1165.
- Kolodner, P., 1991d, "Drift, shape, and intrinsic destabilization of pulses of traveling-wave convection", *Phys. Rev. A* **44**, 6448.
- Kolodner, P., D. Bensimon, and C. M. Surko, 1988, "Traveling-wave convection in an annulus", *Phys. Rev. Lett.* **60**, 1723.
- Kolodner, P., and J. A. Glazier, 1990, "Interaction of localized pulses of traveling-wave convection with propagating disturbances", *Phys. Rev. A* **42**, 7504.
- Kolodner, P., J. A. Glazier, and H. Williams, 1990, "Dispersive chaos in one-dimensional traveling-wave convection", *Phys. Rev. Lett.* **65**, 1579.
- Kolodner, P., and C. M. Surko, 1988, "Weakly nonlinear traveling-wave convection", *Phys. Rev. Lett.* **61**, 842.
- Kolodner, P., C. M. Surko, and H. Williams, 1989, "Dynamics of traveling waves near the onset of convection in binary fluid mixtures", *Physica D* **37**, 319.
- Kolodner, P., R. W. Walden, A. Passner, and C. M. Surko, 1986, "Rayleigh-Bénard convection in an intermediate-aspect-ratio rectangular container", *J. Fluid Mech.* **163**, 195.
- Kopell, N., and L. N. Howard, 1981, "Target patterns and horseshoes from a perturbed central-force problem: some temporally periodic solutions to reaction-diffusion equations", *Studies Appl. Math.* **64**, 1.
- Koschmieder, E. L., 1974, "Bénard convection", *Adv. Chem. Phys.* **26**, 177.
- Koschmieder, E. L., 1993, *Bénard Cells and Taylor Vortices* (Cambridge University Press, Cambridge, England).
- Koschmieder, E. L., and S. G. Pallas, 1974, "Heat transfer through a shallow horizontal convecting fluid layer", *Int. J. Heat Mass Transfer* **17**, 991.
- Kosterlitz, J. M., and D. J. Thouless, 1978, "Two-dimensional physics", in *Progress in Low Temperature Physics*, edited by D. F. Brewer (North-Holland, Amsterdam), Vol. VIIIB, p. 371.
- Kraichnan, R. H., 1987, "An interpretation of the Yakhott-Orszag turbulence theory", *Phys. Fluids* **30**, 2400.
- Kraichnan, R. H., and S. Chen, 1989, "Is there a statistical mechanics of turbulence", *Physica D* **37**, 160.
- Kramer, L., E. Ben-Jacob, H. Brand, and M. C. Cross, 1982, "Wavelength selection in systems far from equilibrium", *Phys. Rev. Lett.* **49**, 1891.
- Kramer, L., E. Bodenschatz, and W. Pesch, 1990, "Interaction and dynamics of defects in anisotropic pattern-forming systems", *Phys. Rev. Lett.* **64**, 2588.
- Kramer, L., E. Bodenschatz, W. Pesch, W. Thom, and W. Zimberman, 1989, "New results on the electrohydrodynamic in-

- stability in nematics”, *Liquid Crystals* **5**, 699.
- Kramer, L., E. Bodenschatz, W. Pesch, and W. Zimmermann, 1986, “Pattern-selection in anisotropic systems”, in *The Physics of Structure Formation: Theory and Simulation*, edited by W. Güttinger and G. Dangelmayr (Springer-Verlag, Berlin), p. 130.
- Kramer, L., and P. C. Hohenberg, 1984, “Effects of boundary conditions on spatially periodic states”, *Physica* **13D**, 357.
- Kramer, L., and H. Riecke, 1985, “Wavelength selection in Rayleigh-Bénard convection”, *Z. Phys. B* **59**, 245.
- Kramer, L., H. R. Schober, and W. Zimmermann, 1988a, “Pattern competition and the decay of unstable patterns in quasi-one-dimensional systems”, *Physica D* **31**, 212.
- Kramer, L., and W. Zimmermann, 1985, “On the Eckhaus instability for spatially periodic patterns”, *Physica* **16D**, 221.
- Kramer, L., W. Zimmermann, E. Bodenschatz, and W. Pesch, 1988b, “Pattern-selection in convective instabilities with axial anisotropy”, in *Propagation in Systems Far from Equilibrium*, edited by J. E. Wesfreid, H. R. Brand, P. Manneville, G. Albinet, and N. Boccara (Springer-Verlag, Berlin), p. 240.
- Krinsky, V. I., 1984a, Ed., *Self-Organization Autowaves and Structures Far from Equilibrium* (Springer-Verlag, Berlin).
- Krinsky, V. I., 1984b, “Autowaves: results, problems, outlooks”, in *Self-organization Autowaves and Structures Far from Equilibrium*, edited by V. I. Krinsky (Springer-Verlag, Berlin), p. 9.
- Krinsky, V. I., and K. I. Agladze, 1982, “Multi-armed vortices in an active chemical medium”, *Nature* **296**, 424.
- Krinsky, V. I., and K. I. Agladze, 1983, “Interaction of rotating waves in an active chemical medium”, *Physica* **8D**, 50.
- Krinsky, V. I., and B. A. Malomed, 1983, “Quasi-harmonic rotating waves in distributed active systems”, *Physica* **9D**, 81.
- Krishnamurti, R., 1968, “Finite amplitude convection with changing mean temperature. Part 1: Theory”, *J. Fluid Mech.* **33**, 445.
- Krishnamurti, R., 1970, “On the transition to turbulent convection. Part 2: The transition to time-dependent flow”, *J. Fluid Mech.* **42**, 309.
- Krishnamurti, R., 1973, “Some further studies on the transition to turbulent convection”, *J. Fluid Mech.* **60**, 285.
- Kumar, A., 1990, “Soliton dynamics in a monomode optical fibre”, *Phys. Rep.* **187**, 63.
- Kuo, E. Y., and M. C. Cross, 1993, “Traveling-wave wall states in rotating Rayleigh-Bénard convection”, *Phys. Rev. E* **47**, 2245.
- Küppers, G., and D. Lortz, 1969, “Transition from laminar convection to thermal turbulence in a rotating fluid layer”, *J. Fluid Mech.* **35**, 609.
- Kuramoto, Y., 1978, “Diffusion-induced chaos in reaction systems”, *Prog. Theor. Phys. Suppl.* **64**, 346.
- Kuramoto, Y., 1984a, “Phase dynamics of weakly unstable periodic structures”, *Prog. Theor. Phys.* **71**, 1182.
- Kuramoto, Y., 1984b, *Chemical Oscillations, Waves, and Turbulence* (Springer-Verlag, Berlin).
- Kuramoto, Y., 1989, “On the reduction of evolution equations in extended systems. The underlying universal structure”, *Prog. Theor. Phys. Suppl.* **99**, 244.
- Kuramoto, Y., 1991, “Collective synchronization of pulse-coupled oscillators and excitable units”, *Physica D* **50**, 15.
- Kuramoto, Y., and I. Nishikawa, 1987, “Statistical macrodynamics of large dynamical systems: case of a phase transition in oscillator communities”, *J. Stat. Phys.* **49**, 569.
- Kuramoto, Y., and T. Tsuzuki, 1976, “Persistent propagation of concentration waves in dissipative media far from thermal equilibrium”, *Prog. Theor. Phys.* **55**, 356.
- Kuznetsov, S. P., and A. S. Pikovsky, 1986, “Universality and scaling of period-doubling bifurcations in a dissipative distributed medium”, *Physica* **19D**, 384.
- Lam, L., and H. C. Morris, 1990, Eds., *Nonlinear Structure in Physical Systems — Pattern Formation, Chaos and Waves* (Springer-Verlag, Berlin).
- Landau, L. D., 1944, “On the problem of turbulence”, *Akad. Nauk. Dok.* **44**, 339. [English translation in *Collected Papers of L. D. Landau*, edited by D. ter Haar, 1965 (Pergamon, Oxford)].
- Landau, L. D., and E. M. Lifshitz, 1958, *Statistical Physics* (Addison Wesley, Reading, MA), Chap. XIV.
- Landau, L. D., and E. M. Lifshitz, 1959, *Fluid Mechanics* (Pergamon, Oxford).
- Landau, L. D., and E. M. Lifshitz, 1976, *Mechanics*, 3rd edition (Pergamon, Oxford), p. 80.
- Landauer, R., 1978, “Distribution function peaks generated by noise”, *Phys. Lett. A* **68**, 15.
- Landauer, R., 1981, “Nonlinearity, multistability, and fluctuations: reviewing the reviewers”, *Am. J. Physiol.* **241**, R107.
- Landauer, R., 1988, “Motion out of noisy states”, *J. Stat. Phys.* **53**, 233.
- Landman, M. J., 1987, “Solutions of the Ginzburg-Landau equation of interest in shear flow transition”, *Studies Appl. Math.* **76**, 187.
- Landman, M. J., G. C. Papanicolaou, C. Sulem, and P. L. Sulem, 1988, “Rate of blowup for solutions of the nonlinear Schrödinger equation at critical dimension”, *Phys. Rev. A* **38**, 3837.
- Langer, J. S., 1980, “Instabilities and pattern formation in crystal growth”, *Rev. Mod. Phys.* **52**, 1.
- Langer, J. S., 1987a, “Lectures in the theory of pattern formation”, in *Chance and Matter*, edited by J. Souletie, J. Vannimenus, and R. Stora (Elsevier, Amsterdam), p. 629.
- Langer, J. S., 1987b, “Dendritic sidebranching in the 3-dimensional symmetric model in the presence of noise”, *Phys. Rev. A* **36**, 3350.
- Langer, J. S., 1989, “Dendrites, viscous fingers, and the theory of pattern formation”, *Science* **243**, 1150.
- Langer, J. S., and L. A. Turski, 1977, “Studies in the theory of interfacial stability I: Stationary symmetric model”, *Acta Met.* **25**, 1113.
- Langford, W. F., R. Tagg, E. Kostelich, H. Swinney, and M. Golubitsky, 1988, “Primary instabilities and bicriticality in flow between counterrotating cylinders”, *Phys. Fluids* **31**, 776.
- Laroche, C., S. Douady, and S. Fauve, 1990, “Convective flow of granular masses under vertical vibrations”, *J. Phys. (Paris)* **51**, 700.
- Larraza, A., and S. Putterman, 1984, “Theory of nonpropagating surface-wave solitons”, *J. Fluid. Mech.* **148**, 443.
- Lathrop, D. P., J. Fineberg, and H. L. Swinney, 1992, “Turbulent flow between concentric rotating cylinders at large Reynolds number”, *Phys. Rev. Lett.* **68**, 1515.
- Lauffenburger, D. A., 1984, “Chemotaxis and cell aggregation”, in *Modelling of Patterns in Space and Time*, edited by W. Jäger and J. D. Murray (Springer-Verlag, Berlin), p. 198.
- Le Berre, M., E. Ressayre, A. Tallet, and Y. Pomeau, 1990, “Dynamical system driven by a retarded force acting as colored noise”, *Phys. Rev. A* **41**, 6635.
- Le Gal, P., 1986, Thèse, Université de Paris (unpublished).
- Le Gal, P., A. Pocheau, and V. Croquette, 1985, “Square versus roll pattern at convective threshold”, *Phys. Rev. Lett.* **54**, 2501.

- Lengyel, I., and I. R. Epstein, 1991, "Modeling of Turing structures in the chlorite-iodide-malonic acid-starch reaction system", *Science* **251**, 650.
- Levin, S. A., and L. A. Segel, 1985, "Pattern generation in space and aspect", *SIAM Review* **27**, 45.
- Levine, R. D., 1987, "Patterns of maximal entropy", in *The Physics of Structure Formation. Theory and Simulation*, edited by W. Göttinger and G. Dangelmayr (Springer-Verlag, Berlin), p. 78.
- Levine, H., and W. J. Rappel, 1990, "Numerical study for traveling waves in directional solidification", *Phys. Rev. A* **42**, 7475.
- Levine, H., W. J. Rappel, and H. Riecke, 1991, "Resonant interactions and traveling solidification cells", *Phys. Rev. A* **43**, 1122.
- Levine, H., and W. Reynolds, 1991, "Streaming instability of aggregating slime mold amoebae", *Phys. Rev. Lett.* **66**, 2400.
- Levinson, N., 1949, "A second-order differential equation with singular solutions", *Ann. Math.* **50**, 127.
- Lhost, O., and J. K. Platten, 1989, "Experimental study of the transition from nonlinear traveling waves to steady overturning convection in binary mixtures", *Phys. Rev. A* **40**, 4552.
- Libchaber, A., and J. Maurer, 1980, "Une expérience de Rayleigh-Bénard de géométrie réduite: multiplication, accrochage et démultiplication de fréquences", *J. Phys. (Paris) Colloq. C* **3**, 51.
- Libchaber, A., and J. Maurer, 1982, "A Rayleigh-Bénard experiment: Helium in a small box", in *Nonlinear Phenomena at Phase Transitions and Instabilities*, edited by T. Riste (Plenum, New York), p. 259.
- Lifshitz, E. M., and L. P. Pitaevskii, 1981, *Physical Kinetics*, Course of Theoretical Physics (Pergamon, New York), Vol. 10, Chap. VI.
- Linz, S. J., and M. Lücke, 1987, "Erratum: Convection in binary mixtures: A Galerkin model with impermeable boundary conditions", *Phys. Rev. A* **35**, 3997.
- Linz, S. J., M. Lücke, H. W. Müller, and J. Niederländer, 1988, "Convection in binary-fluid mixtures: traveling waves and lateral currents", *Phys. Rev. A* **38**, 5727.
- Liu, J., and J. P. Gollub, 1993, "Onset of spatially chaotic waves on flowing films", *Phys. Rev. Lett.* **70**, 2289.
- Livi, R., G. Martinez-Mekler, and S. Ruffo, 1990, "Periodic orbits and long transients in coupled map lattices", *Physica D* **45**, 452.
- Lonberg, F., and R. B. Meyer, 1985, "New ground state for the splay-Fréedericksz transition in a polymer nematic liquid crystal", *Phys. Rev. Lett.* **55**, 718.
- Lorenz, E. N., 1963, "Deterministic nonperiodic flow", *J. Atmospheric Sci.* **20**, 130.
- Lowe, M., B. S. Albert, and J. P. Gollub, 1986, "Convective flows with multiple spatial periodicities", *J. Fluid Mech.* **173**, 253.
- Lowe, M., and J. P. Gollub, 1985a, "Pattern selection near the onset of convection: the Eckhaus instability", *Phys. Rev. Lett.* **55**, 2575.
- Lowe, M., and J. P. Gollub, 1985b, "Solitons and the commensurate-incommensurate transition in a convecting nematic fluid", *Phys. Rev. A* **31**, 3893.
- Lowe, M., J. P. Gollub, and T. C. Lubensky, 1985, "Commensurate and incommensurate structures in a nonequilibrium system", *Phys. Rev. Lett.* **51**, 786.
- Lücke, M., 1987, "Bifurcation behavior under modulated control parameters", in *Noise in Nonlinear Dynamical Systems*, edited by F. Moss and P. V. E. McClintock (Cambridge University Press, Cambridge, U.K.), Vol. 2, p. 100.
- Lücke, M., 1988, "Convection in binary mixtures: propagating and standing patterns", in *Far from Equilibrium Phase Transitions*, edited by L. Garrido (Springer-Verlag, Berlin), p. 195.
- Lücke, M., M. Mihelcic, and B. Kowalski, 1987a, "Propagating convection fronts", *Phys. Rev. A* **35**, 4001.
- Lücke, M., M. Mihelcic, B. Kowalski, and K. Wingerath, 1987b, "Structure formation by propagating fronts", in *The Physics of Structure Formation: Theory and Simulation*, edited by W. Göttinger and G. Dangelmayr (Springer-Verlag, Berlin), p. 97.
- Lücke, M., M. Mihelcic, and K. Wingerath, 1984, "Propagation of Taylor-vortex fronts into unstable circular Couette flow", *Phys. Rev. Lett.* **52**, 625.
- Lugosi, E., 1989, "Analysis of meandering in Zykov kinetics", *Physica D* **40**, 331.
- Luijckx, J.-M., J. K. Platten, and J. C. Legros, 1981, "On the existence of thermoconvective rolls transverse to a superimposed mean Poiseuille flow", *Int. J. Heat Mass Transfer* **24**, 1287.
- Lumer, E. D., and B. A. Huberman, 1991, "Hierarchical dynamics in large assemblies of interacting oscillators", *Phys. Lett. A* **160**, 227.
- Lund, F., and C. Rojas, 1989, "Ultrasound as a probe of turbulence", *Physica D* **37**, 508.
- L'vov, V. S., 1991, "Spectra of velocity and temperature fluctuations with constant entropy flux of fully developed free convective turbulence", *Phys. Rev. Lett.* **67**, 687.
- L'vov, V. S., and L. A. Prozorova, 1988, "Spin waves above threshold of parametric excitations", in *Spin Waves & Magnetic Excitations*, edited by A. S. Borovik-Romanov, and S. K. Sinha (North-Holland, Amsterdam), p. 233.
- Ma, S. K., 1976, *Modern Theory of Critical Phenomena* (Benjamin, Reading, MA).
- MacWilliams, H. K., 1982, "Numerical simulations of hydra head regeneration using a proportion-regulating version of the Gierer-Meinhardt model", *J. Theor. Biol.* **99**, 681.
- Malacinski, G. M., and S. V. Bryant, 1984, Eds., *Pattern Formation, A Primer in Developmental Biology* (Macmillan, New York).
- Malkus, W. V. R., 1954, "The heat transport and spectrum of thermal turbulence", *Proc. R. Soc. London A* **225**, 196.
- Malkus, W. V. R., and G. Veronis, 1958, "Finite amplitude cellular convection", *J. Fluid Mech.* **4**, 225.
- Malomed, B. A., 1984, "Nonlinear waves in nonequilibrium systems of the oscillatory type", *Z. Phys. B* **55**, 241, 249.
- Malomed, B. A., and K. E. Gedalin, 1989, "Stability of cellular wave structures in oscillatory pattern-forming systems near onset", *Physica D* **40**, 33.
- Malomed, B. A., and A. A. Nepomnyashchy, 1990a, "Kinks and solitons in the generalized Ginzburg-Landau equation", *Phys. Rev. A* **42**, 6009.
- Malomed, B. A., and A. A. Nepomnyashchy, 1990b, "Onset of chaos in the generalized Ginzburg-Landau equation", *Phys. Rev. A* **42**, 6238.
- Malomed, B. A., A. A. Nepomnyashchy, and M. T. Tribelsky, 1989, "Two-dimensional quasiperiodic structures in nonequilibrium systems", *Zh. Eksp. Teor. Fiz.* **96**, 684 [Sov. Phys. JETP **69**, 388].
- Malomed, B. A., A. A. Nepomnyashchy, and M. I. Tribelsky, 1990, "Domain boundaries in convection patterns", *Phys. Rev. A* **42**, 7244.
- Malomed, B. A., and M. I. Tribelsky, 1984, "Bifurcation in distributed kinetic systems with aperiodic instability", *Physica* **14D**, 67.
- Malomed, B. A., and M. I. Tribelsky, 1987, "Stability of stationary periodic structures for weakly supercritical convection and

- in related problems”, Zh. Eksp. Teor. Fiz. **92**, 539 [Sov. Phys. JETP **65**, 305].
- Malraison, B., P. Atten, P. Berge, and M. Dubois, 1983, “Dimension of strange attractors: an experimental determination for the chaotic regime of two convective systems”, J. Phys. Lett. **44**, L897.
- Mandelbrot, B. B., 1974, “Intermittent turbulence in self-similar cascades: divergence of high moments and dimension of the carrier”, J. Fluid Mech. **62**, 331.
- Mandelbrot, B. B., 1983, *The Fractal Geometry of Nature* (Freeman, New York).
- Manneville, P., 1981, “Statistical properties of chaotic solutions of a one-dimensional model for phase turbulence”, Phys. Lett. A **84**, 129.
- Manneville, P., 1983a, “A two-dimensional model for three-dimensional convective patterns in wide containers”, J. Phys. (Paris) **44**, 759.
- Manneville, P., 1983b, “Numerical simulation of convection in ‘cylindrical’ geometry,” J. Phys. (Paris) **44**, 563.
- Manneville, P., 1983c, “Towards an understanding of weak turbulence close to the convection threshold in large aspect ratio systems,” J. Phys. Lett. **44**, L903.
- Manneville, P., 1985, “Liapounov exponents for the Kuramoto-Sivashinsky model”, in *Macroscopic Modeling of Turbulent Flows*, edited by O. Pironneau, Lecture Notes in Physics 230 (Springer-Verlag, Berlin), p. 319.
- Manneville, P., 1988, “The Kuramoto-Sivashinsky equation: a progress report,” in *Propagation in Systems Far from Equilibrium*, edited by J. E. Wesfreid, H. R. Brand, P. Manneville, G. Albinet, and N. Boccara (Springer-Verlag, Berlin), p. 265.
- Manneville, P., 1990, *Dissipative Structures and Weak Turbulence* (Academic, San Diego, CA).
- Manneville, P., and J. M. Piquemal, 1982, “Période spatiale sélectionnée par les effets de courbure en convection de Rayleigh-Bénard axisymétrique”, C. R. Acad. Sci. **294**, 681.
- Manneville, P., and J. M. Piquemal, 1983, “Zigzag instability and axisymmetric rolls in Rayleigh-Bénard convection: The effects of curvature,” Phys. Rev. A **28**, 1774.
- Manneville, P., and Y. Pomeau, 1983, “A grain boundary in cellular structures near the onset of convection,” Phil. Mag. A **48**, 607.
- Markin, V. S., V. F. Pastushenko, and Y. A. Chizmadzhev, 1987, *Theory of Excitable Media* (Wiley, New York).
- Markus, M., S. C. Müller, and G. Nicolis, 1988, Eds., *From Chemical to Biological Organization* (Springer-Verlag, Berlin).
- Martinet, B., P. Haldenwang, G. Labrosse, J. C. Payan, and R. Payan, 1982, “Régimes convectifs instationnaires dans l’air en cavité à grands facteurs d’aspect: résultats expérimentaux”, J. Phys. Lett. **43**, L161.
- Martinet, B., P. Haldenwang, G. Labrosse, J. C. Payan, and R. Payan, 1984, “Rayleigh-Bénard instability: experimental study of the wavenumber selection”, in *Cellular Structures in Instabilities*, edited by J. E. Wesfreid and S. Zaleski (Springer-Verlag, Berlin), p. 33.
- Matthews, P. C., R. E. Mirollo, and S. H. Strogatz, 1991, “Dynamics of a large system of coupled nonlinear oscillators”, Physica D **52**, 293.
- Matthews, P. C., and S. H. Strogatz, 1990, “Phase diagram for the collective behavior of limit-cycle oscillators”, Phys. Rev. Lett. **65**, 1701.
- May, R. M., and W. J. Leonard, 1975, “Nonlinear aspects of competition between three species”, SIAM J. Appl. Math. **29**, 243.
- Mayer-Kress, G., 1986, Ed., *Dimensions and Entropies in Chaotic Systems — Quantification of Complex Behavior*, Springer Series in Synergetics Vol. 32 (Springer-Verlag, Berlin).
- Mayer-Kress, G., and K. Kaneko, 1989, “Spatiotemporal chaos and noise”, J. Stat. Phys. **54**, 1489.
- Mayer-Kress, G., and T. Kurz, 1987, “Dimension densities for turbulent systems with spatially decaying correlation functions”, Complex Systems **1**, 821.
- McCall, S. L., and E. L. Hahn, 1969, “Self-induced transparency”, Phys. Rev. **183**, 457.
- McCauley, J. L., 1990, “Introduction to multifractals in dynamic systems theory and fully developed fluid turbulence”, Phys. Rep. **189**, 225.
- McLaughlin, J. B., and P. C. Martin, 1975, “Transition to turbulence in a statically stressed fluid system”, Phys. Rev. A **12**, 186.
- Medina, E., T. Hwa, M. Kardar, and Y. C. Zhang, 1989, “Burgers equation with correlated noise: renormalization-group analysis and applications to directed polymers and interface growth”, Phys. Rev. A **39**, 3053.
- Meinhardt, H., 1982, *Models of Biological Pattern Formation* (Academic, New York).
- Meinhardt, H., 1992, “Pattern formation in biology: a comparison of models and experiments”, Rep. Prog. Phys. **55**, 797.
- Meinhardt, H., and M. Klinger, 1987, “A model for pattern formation on the shells of molluscs”, J. Theor. Biol. **126**, 63.
- Meinköhn, D., 1990, Ed., *Dissipative Structures in Transport Processes and Combustion* (Springer-Verlag, Berlin).
- Meiron, D., and A. C. Newell, 1985, “The shape of stationary dislocations”, Phys. Lett. A **113**, 289.
- Meneveau, C., and K. R. Sreenivasan, 1987, “The multifractal spectrum of the dissipation field in turbulent flows”, Nucl. Phys. Proc. Suppl. B **2**, 49.
- Meneveau, C., and K. R. Sreenivasan, 1991, “The multifractal nature of turbulent energy-dissipation”, J. Fluid Mech. **224**, 429.
- Meneveau, C. M., K. R. Sreenivasan, P. Kailasath, and M. S. Fan, 1990, “Joint multifractal measures: theory and applications to turbulence”, Phys. Rev. A **41**, 894.
- Mermin, N. D., 1979, “The topological theory of defects in ordered media”, Rev. Mod. Phys. **51**, 591.
- Meron, E., 1992, “Pattern formation in excitable media”, Phys. Rep. **218**, 1.
- Meron, E., and P. Pelcé, 1988, “Model for spiral wave formation in excitable media”, Phys. Rev. Lett. **60**, 1880.
- Meron, E., and I. Procaccia, 1986a, “Low-dimensional chaos in surface waves: Theoretical analysis of an experiment”, Phys. Rev. A **34**, 3221.
- Meron, E., and I. Procaccia, 1986b, “Theory of chaos in surface waves: The reduction from hydrodynamics to few-dimensional dynamics”, Phys. Rev. Lett. **56**, 1323.
- Metcalfe, G. P., and R. P. Behringer, 1990, “Critical Rayleigh numbers for cryogenic experiments”, J. Low Temp. Phys. **78**, 231.
- Meyer, C. W., G. Ahlers, and D. S. Cannell, 1987, “Initial stages of pattern formation in Rayleigh-Bénard convection”, Phys. Rev. Lett. **59**, 1577.
- Meyer, C. W., G. Ahlers, and D. S. Cannell, 1991, “Stochastic influences on pattern formation in Rayleigh-Bénard convection: Ramping experiments”, Phys. Rev. A **44**, 2514.
- Meyer, C. W., D. S. Cannell, and G. Ahlers, 1992, “Hexagonal and roll flow patterns in temporally modulated Rayleigh-Bénard convection”, Phys. Rev. A **45**, 8583.
- Meyer, C. W., D. S. Cannell, G. Ahlers, J. B. Swift, and P. C. Hohenberg, 1988, “Pattern competition in temporally modu-

- lated Rayleigh-Bénard convection”, Phys. Rev. Lett. **61**, 947.
- Meyer-Spasche, R., and H. B. Keller, 1985, “Some bifurcation diagrams for Taylor-vortex flows”, Phys. Fluids **28**, 1248.
- Migler, K. B., and R. B. Meyer, 1991, “Solitons and pattern formation in liquid crystals in a rotating magnetic field”, Phys. Rev. Lett. **66**, 1485.
- Mikhailov, A. S., 1991, *Foundations of Synergetics. I: Distributed Active Systems* (Springer-Verlag, Berlin).
- Mikhailov, A. S., and A. Y. Loskutov, 1991, *Foundations of Synergetics II, Complex Patterns* (Springer-Verlag, Berlin).
- Mikhailov, A. S., and I. V. Uporov, 1984, “Critical phenomena in media with breeding, decay, and diffusion”, Usp. Fiz. Nauk. **144**, 79 [Sov. Phys. Usp. **27**, 695].
- Mikhailov, A. S., and V. S. Zykov, 1991, “Kinematical theory of spiral waves in excitable media: comparison with numerical simulations”, Physica D **52**, 379.
- Miles, J. W., 1967, “Surface-wave damping in closed basins”, Proc. R. Soc. London **297**, 459.
- Miles, J. W., 1984a, “Nonlinear Faraday resonance,” J. Fluid Mech. **146**, 285.
- Miles, J. W., 1984b, “Parametrically excited solitary waves”, J. Fluid Mech. **148**, 451.
- Miles, J. W., 1984c, “Strange attractors in hydrodynamics”, Adv. Appl. Mech. **24**, 189.
- Miles, J., and D. Henderson, 1990, “Parametrically forced surface waves”, Annu. Rev. Fluid Mech. **22**, 143.
- Miller, J., and D. A. Huse, 1993, “Hydrodynamics of extended chaotic systems with Ising symmetry”, Phys. Rev. E (to be published).
- Miller, P. L., and P. E. Dimotakis, 1991, “Stochastic geometric properties of scalar interfaces in turbulent jets”, Phys. Fluids A **3**, 168.
- Milner, S. T., 1991, “Square patterns and secondary instabilities in driven capillary waves”, J. Fluid Mech. **225**, 81.
- Mitais, J. C., P. Haldenwang, and G. Labrosse, 1986, “Selection of 2-D patterns near the threshold of the Rayleigh-Bénard convection”, in *Proceedings of the VIIIf International Heat Transfer Conference*, edited by C. L. Tien, V. P. Carey, and J. K. Ferrell (Harper and Row, New York).
- Mollenauer, L. F., J. P. Gordon, and M. N. Islam, 1986, “Soliton propagation in long fibres with periodically compensated loss”, IEEE J. Quantum Electron **22**, 157.
- Moloney, J. V., and A. C. Newell, 1990, “Nonlinear optics”, Physica D **44**, 1.
- Moloney, J. V., and A. C. Newell, 1992, *Nonlinear Optics* (Addison Wesley, Reading, MA).
- Monin, A. S., 1978, “On the nature of turbulence”, Usp. Fiz. Nauk. **125**, 97 [Soviet Physics Usp. **21**, 429].
- Monin, A. S., and A. M. Yaglom, 1975, *Statistical Fluid Mechanics: Mechanics of Turbulence*, Vol. II (MIT Press, Cambridge, MA).
- Moon, H. T., P. Huerre, and L. G. Redekopp, 1983, “Transitions to chaos in the Ginzburg-Landau equation”, Physica **7D**, 135.
- Morgenthaler, F. R., 1960, “Survey of ferromagnetic resonance in small ferrimagnetic ellipsoids”, J. Appl. Phys. **31**, 955.
- Mori, H., H. Hata, T. Horita, and T. Kobayashi, 1989, “Statistical mechanics of dynamical systems”, Prog. Theor. Phys. Suppl. **99**, 1.
- Mornev, O. A., 1984, “Elements of the ‘optics’ of autowaves”, in *Self-organization, Autowaves and Structures Far from Equilibrium*, edited by V. I. Krinsky (Springer-Verlag, Berlin), p. 111.
- Moses, E., J. Fineberg, and V. Steinberg, 1987, “Multistability and confined traveling-wave patterns in a convecting binary mixture”, Phys. Rev. A **35**, 2757.
- Moses, E., and V. Steinberg, 1986a, “Flow patterns and nonlinear behavior of traveling waves in a convective binary mixture”, Phys. Rev. A **34**, 693.
- Moses, E., and V. Steinberg, 1986b, “Competing patterns in a convective binary mixture”, Phys. Rev. Lett. **57**, 2018.
- Moses, E., and V. Steinberg, 1991, “Stationary convection in a binary mixture”, Phys. Rev. A **43**, 707.
- Moss, F., and P. V. E. McClintock, 1989, Eds., *Noise in Nonlinear Dynamical Systems, Volume 1, Theory of Continuous Fokker-Planck Systems* (Cambridge University Press, Cambridge, U.K.).
- Motsay, R. W., K. E. Anderson, and R. P. Behringer, 1988, “The onset of convection and turbulence in rectangular layer of normal liquid ⁴He”, J. Fluid Mech. **189**, 263.
- Müller, H. W., and M. Lücke, 1988, “Competition between roll and square convection patterns in binary mixtures”, Phys. Rev. A **38**, 2965.
- Müller, H. W., M. Lücke, and M. Kamps, 1989, “Convective patterns in horizontal flow”, Europhys. Lett. **10**, 451.
- Müller, H. W., M. Lücke, and M. Kamps, 1992, “The effect of throughflow on Rayleigh-Bénard convective rolls”, in *Ordered and Turbulent Patterns in Taylor-Couette Flow*, edited by C. D. Andereck and F. Hayot (Plenum, New York).
- Müller, S. C., T. Plessner, and B. Hess, 1987, “Two-dimensional spectrophotometry of spiral wave propagation in the Belousov-Zhabotinskii reaction, I. Experiments and digital data representation; II. Geometric and kinematic parameters”, Physica **24D**, 71, 87.
- Mullin, T., and K. A. Cliffe, 1986, “Symmetry breaking and the onset of time dependence in fluid mechanical systems”, in *Nonlinear Phenomena and Chaos*, edited by S. Sarkar (Adam Hilger, Bristol), p. 96.
- Mullins, W. W., and R. F. Sekerka, 1964, “Stability of a planar interface during solidification of a dilute binary alloy”, J. Appl. Phys. **35**, 444.
- Murray, J. D., 1977, *Nonlinear Differential Equation Models in Biology* (Clarendon, Oxford).
- Murray, J. D., 1981a, “On pattern formation mechanisms for lepidopteran wing patterns and mammalian coat markings”, Phil. Trans. R. Soc. London B **295**, 473.
- Murray, J. D., 1981b, “A pre-pattern formation mechanism for animal coat markings”, J. Theor. Biol. **88**, 161.
- Murray, J. D., 1989, *Mathematical Biology* (Springer-Verlag, Berlin).
- Muschol, M., D. Liu, and H. Z. Cummins, 1992, “Surfacetension-anisotropy measurements of succinonitrile and pivalic acid: comparison with microscopic solvability theory”, Phys. Rev. A **46**, 1038.
- Mutabazi, I., J. J. Hegseth, C. D. Andereck, and J. E. Wesfreid, 1988, “Pattern formation in the flow between two horizontal coaxial cylinders with a partially filled gap”, Phys. Rev. A **38**, 4752.
- Mutabazi, I., J. J. Hegseth, C. D. Andereck, and J. E. Wesfreid, 1990, “Spatiotemporal pattern modulations in the Taylor-Dean system”, Phys. Rev. Lett. **64**, 1729.
- Nagel, S. R., 1992, “Instabilities in a sandpile”, Rev. Mod. Phys. **64**, 321.
- Nagumo, J. S., S. Arimoto, and S. Yoshizawa, 1962, “An active pulse transmission line simulating nerve axon”, Proc. IRE **50**, 2061.
- Nandapurkar, P. J., and A. T. Winfree, 1989, “Dynamical stability of untwisted scroll rings in excitable media”, Physica D

- 35**, 277.
- Nasuno, S., M. Sano, and Y. Sawada, 1988, "Spatial instabilities and onset of chaos in Rayleigh-Bénard system with intermediate aspect-ratio", *J. Phys. Soc. Jpn.* **57**, 3357.
- Nasuno, S., M. Sano, and Y. Sawada, 1989a, "Phase wave propagation in a rectangular convective structure of nematic liquid crystal", *J. Phys. Soc. Jpn.* **58**, 1875.
- Nasuno, S., and Y. Sawada, 1989, "A new scheme of spatiotemporal chaos created by the interaction between the phase waves and the topological defects", *Prog. Theor. Phys. Suppl.* **99**, 450.
- Nasuno, S., S. Takeuchi, and Y. Sawada, 1989b, "Motion and interaction of dislocations in electrohydrodynamic convection of nematic liquid crystals", *Phys. Rev. A* **40**, 3457.
- Nelkin, M., 1992, "In what sense is turbulence an unsolved problem?", *Science* **255**, 566.
- Nelkin, M., and M. Tabor, 1990, "Time correlations and random sweeping in isotropic turbulence", *Phys. Fluids A* **2**, 81.
- Neu, J. C., 1990, "Vortices in complex scalar fields", *Physica D* **43**, 385.
- Newell, A. C., 1974, "Envelope equations," in *Lectures in Applied Mathematics* (American Mathematical Society, Providence, RI), Vol. 15, p. 157.
- Newell, A. C., 1978, "The inverse scattering transform, nonlinear waves, singular perturbations and synchronized solitons", *Rocky Mountain J. Mathematics* **8**, 25.
- Newell, A. C., 1986, "Chaos and turbulence: is there a connection?", in *Perspective in Nonlinear Dynamics*, edited by M. F. Shlesinger et al. (World Scientific, Singapore), p. 38.
- Newell, A. C., 1988, "The dynamics of patterns: a survey", in *Propagation in Systems Far from Equilibrium*, edited by J. E. Wesfreid, H. R. Brand, P. Manneville, G. Albinet, and N. Bocca (Springer-Verlag, Berlin), p. 122.
- Newell, A. C., C. G. Lange, and P. J. Aucoin, 1970, "Random convection", *J. Fluid. Mech.* **40**, 513.
- Newell, A. C., T. Passot, and J. Lega, 1993, "Order parameter equations for patterns", *Annu. Rev. Fluid Mech.* **25**, 399.
- Newell, A. C., T. Passot, and M. Souli, 1990a, "Convection at finite Rayleigh numbers in large-aspect-ratio containers", *Phys. Rev. Lett.* **64**, 2378.
- Newell, A. C., T. Passot, and M. Souli, 1990b, "The phase diffusion and mean drift equations for convection at finite Rayleigh numbers in large containers", *J. Fluid Mech.* **220**, 187.
- Newell, A. C., T. Passot, and M. Souli, 1991, "Focus instability in axisymmetrical Rayleigh-Bénard convection", *Eur. J. Mec. B* **10**, 151.
- Newell, A. C., D. A. Rand, and D. Russell, 1988, "Turbulent transport and the random occurrence of coherent events", *Physica D* **33**, 281.
- Newell, A. C., and J. A. Whitehead, 1969, "Finite bandwidth, finite amplitude convection," *J. Fluid Mech.* **38**, 279.
- Newell, P. C., 1983, "Attraction and adhesion in the slime mold *Dyctyostelium*", in *Fungal Differentiation: A contemporary Synthesis*, edited by J. E. Smith, Micology Series 43 (Marcel Dekker, New York), p. 43.
- Nicolis, G., and I. Prigogine, 1977, *Self-organization in Nonequilibrium Systems, from Dissipative Structures to Order through Fluctuations* (Wiley, New York).
- Nield, D. A., 1964, "Surface tension and buoyancy effects in cellular convection", *J. Fluid Mech.* **19**, 341.
- Niemela, J. J., G. Ahlers, and D. S. Cannell, 1990, "Localized traveling-wave states in binary-fluid convection", *Phys. Rev. Lett.* **64**, 1365.
- Niemela, J. J., and R. J. Donnelly, 1986, "Direct transition to turbulence in rotating Bénard convection", *Phys. Rev. Lett.* **57**, 2524.
- Niemela, J. J., and R. J. Donnelly, 1987, "External modulation of Rayleigh-Bénard convection", *Phys. Rev. Lett.* **59**, 2431.
- Niemela, J. J., M. R. Smith, and R. J. Donnelly, 1991, "Convective instability with time-varying rotation", *Phys. Rev. A* **44**, 8406.
- Niklas, M., M. Lücke, and H. Müller-Krumbhaar, 1989a, "Propagating front of a propagating pattern: influence of group velocity", *Europhys. Lett.* **9**, 237.
- Niklas, M., M. Lücke, and H. Müller-Krumbhaar, 1989b, "Velocity of a propagating Taylor-vortex front", *Phys. Rev. A* **40**, 493.
- Ning, L., G. Ahlers, and D. S. Cannell, 1990, "Wave-number selection and traveling vortex waves in spatially ramped Taylor-Couette flow", *Phys. Rev. Lett.* **64**, 1235.
- Nishioka, M., S. Iida, and Y. Ichikawa, 1975, "An experimental investigation of plane Poiseuille flow", *J. Fluid Mech.* **72**, 731.
- Normand, C., Y. Pomeau, and M. G. Velarde, 1977, "Convective instability: a physicist's approach", *Rev. Mod. Phys.* **49**, 581.
- Noszticzius, Z., W. Horsthemke, W. D. McDornick, H. L. Swinney, and W. Y. Tam, 1987, "Sustained chemical waves in an annular gel reactor: a chemical pinwheel", *Nature* **329**, 619.
- Nozaki, K., and N. Bekki, 1983, "Pattern selection and spatiotemporal transition to chaos in the Ginzburg-Landau equation", *Phys. Rev. Lett.* **51**, 2171.
- Nozaki, K., and N. Bekki, 1984, "Exact solutions of the generalized Ginzburg-Landau equation", *J. Phys. Soc. Jpn.* **53**, 1581.
- Obukhov, A. M., 1959, "Effect of Archimedean forces on the structure of the temperature field in a turbulent flow", *Dokl. Akad. Nauk SSSR* **125**, 1246 [Soviet Physics Dokl. **3**, 61].
- Obukhov, S. P., 1990, "Self-organized criticality: Goldstone modes and their interactions", *Phys. Rev. Lett.* **65**, 1395.
- Occelli, R., E. Guazzelli, and J. Pantaloni, 1983, "Order in convective structures", *J. Phys. Lett.* **44**, 567.
- Ohlsen, D. R., S. Y. Yamamoto, C. M. Surko, and P. Kolodner, 1990, "Transition from traveling-wave to stationary convection in fluid mixtures", *Phys. Rev. Lett.* **65**, 1431.
- Ohta, T., 1985, "Euclidian invariant formulation of phase dynamics, 1. nonpropagating periodic patterns," *Prog. Theor. Phys.* **73**, 1377.
- Ohta, T., and K. Kawasaki, 1987, "Euclidean invariant phase dynamics for propagating pattern", *Physica* **27D**, 21.
- Ohta, T., and M. Mimura, 1990, "Pattern dynamics in excitable reaction-diffusion media", in *Formation, Dynamics and Statistics of Patterns*, edited by K. Kawasaki, M. Suzuki, and A. Onuki (World Scientific, Singapore), p. 55.
- Ohta, T., M. Mimura, and R. Kobayashi, 1989, "Higher-dimensional localized patterns in excitable media", *Physica D* **34**, 115.
- Olami, Z., H. J. S. Feder, and K. Christensen, 1992, "Self-organized criticality in a continuous, nonconservative cellular automaton modeling earthquakes", *Phys. Rev. Lett.* **68**, 1244.
- Oono, Y., and C. Yeung, 1987, "A cell dynamical system model of chemical turbulence", *J. Stat. Phys.* **48**, 593.
- Oppo, G. L., and R. Kapral, 1986, "Discrete models for the formation and evolution of spatial structure in dissipative systems", *Phys. Rev. A* **33**, 4219.
- Orszag, S. A., and A. T. Patera, 1980, "Subcritical transition to turbulence in plane channel flows", *Phys. Rev. Lett.* **45**, 989.
- Ortoleva, P., and J. Ross, 1973, "Phase waves in oscillatory chemical reactions", *J. Chem. Phys.* **58**, 5673.

- Ortoleva, P., and J. Ross, 1974, "On a variety of wave phenomena in chemical reactions", *J. Chem. Phys.* **60**, 5090.
- Ortoleva, P., and J. Ross, 1975, "Theory of propagation of discontinuities in kinetic systems with multiple time scales: Fronts, front multiplicity, and pulses", *J. Chem. Phys.* **63**, 3398.
- Oster, G. F., 1988, "Lateral inhibition models of developmental processes", *Math. Biosciences* **90**, 265.
- Oswald, P., J. Bechhoefer, and A. Libchaber, 1987, "Instabilities of a moving nematic-isotropic interface", *Phys. Rev. Lett.* **58**, 2318.
- Othmer, H. G., 1987, "Current problems in pattern formation", *Lectures on Mathematics in the Life Sciences* **9**, 57.
- Othmer, H. G., and E. Pate, 1980, "Scale-invariance in reaction-diffusion models of spatial pattern formation", *Proc. Nat. Acad. Sci.* **77**, 4180.
- Ouyang, Q., J. Boissonade, J. C. Roux, and P. de Kepper, 1989, "Sustained reaction-diffusion structures in an open reactor", *Phys. Rev. A* **134**, 282.
- Ouyang, Q., V. Castets, J. Boissonade, J. C. Roux, P. DeKepper, and H. L. Swinney, 1991, "Sustained patterns in chlorite-iodide reactions in a one-dimensional reactor", *J. Chem. Phys.* **95**, 351.
- Ouyang, Q., and H. L. Swinney, 1991a, "Transition from a uniform state to hexagonal and striped Turing patterns", *Nature* **352**, 610.
- Ouyang, Q., and H. L. Swinney, 1991b, "Transition to chemical turbulence", *Chaos* **1**, 411.
- Paap, H. G., and H. Riecke, 1990, "Wave-number restriction and mode interaction in Taylor-vortex flow: appearance of a short-wavelength instability", *Phys. Rev. A* **41**, 1943.
- Paap, H. G., and H. Riecke, 1991, "Drifting vortices in ramped Taylor vortex flow: quantitative results from phase equation", *Phys. Fluids A* **3**, 1519.
- Pacault, A., and C. Vidal, 1979, Eds., *Synergetics - Far from Equilibrium: Proceedings of the Conference Far from Equilibrium, Instabilities and Structures* (Springer-Verlag, Berlin).
- Packard, N. H., J. P. Crutchfield, J. D. Farmer, and R. S. Shaw, 1980, "Geometry from a time series", *Phys. Rev. Lett.* **45**, 712.
- Pagola, A., J. Ross, and C. Vidal, 1988, "Measurement of dispersion relation of chemical waves in an oscillatory reacting medium", *J. Phys. Chem.* **92**, 163.
- Pagola, A., and C. Vidal, 1987, "Wave profile and speed near the core of a target pattern in the Belousov-Zhabotinsky reaction", *J. Phys. Chem.* **91**, 501.
- Pak, H. K., W. I. Goldburg, and A. Sirivat, 1991, "An experimental study of weak turbulence", *Fluid Dynamics Research* **8**, 19.
- Palm, E., 1960, "On the tendency towards hexagonal cells in steady convection", *J. Fluid Mech.* **8**, 183.
- Palm, E., 1975, "Nonlinear thermal convection", *Annu. Rev. Fluid Mech.* **7**, 39.
- Pan, L., and J. R. de Bruyn, 1993, "Broken-parity waves at a driven fluid-air interface", *Phys. Rev. Lett.* **70**, 1791.
- Panfilov, A. V., R. R. Aliev, and A. V. Moshinsky, 1989, "An integral invariant for scroll rings in a reaction-diffusion system", *Physica D* **36**, 181.
- Panfilov, A. V., and A. T. Winfree, 1985, "Dynamical simulations of twisted scroll rings in three-dimensional excitable media", *Physica D* **17 D**, 323.
- Pearson, J. E., 1992, "Pattern formation in a (2+1)-species activator-inhibitor-immobilizer system", *Physica A* **18**, 178.
- Pearson, J. E., and W. J. Bruno, 1993, "Pattern formation in an $N + Q$ component reaction-diffusion system", *Chaos* **2**.
- Pearson, J. E., and W. Hortschmke, 1989, "Turing instabilities with nearly equal diffusion coefficients", *J. Chem. Phys.* **90**, 1588.
- Pearson, J. R. A., 1958, "On convection cells induced by surface tension", *J. Fluid Mech.* **4**, 489. Pelc , P., 1988, *Dynamics of Curved Fronts* (Academic, San Diego, CA).
- Pelc , P., 1988, *Dynamics of Curved Fronts* (Academic, San Diego, CA).
- Pellew, A., and R. V. Southwell, 1940, "On maintained convective motion in a fluid heated from below", *Proc. R. Soc. Lond. A* **176**, 312.
- Pereira, N. R., and L. Stenflo, 1977, "Nonlinear Schr dinger equation including growth and damping", *Phys. Fluids* **20**, 1733.
- Perelson, A. S., B. Goldstein, M. Dembo, and J. A. Jacquez, 1988, Eds., *Nonlinearity in Biology and Medicine* (Elsevier, Amsterdam) [reprinted from *Math. Bioscience* **90** (1-2)].
- Perelson, A. S., P. K. Maini, J. D. Murray, J. M. Hyman, and G. F. Oster, 1986, "Nonlinear pattern selection in a mechanical model for morphogenesis", *J. Math. Biol.* **24**, 525.
- Perez-Garcia, C., 1992, Ed., "New trends in nonlinear dynamics: Nonvariational aspects", *Physica D* **61**, 1.
- Perez-Garcia, C., P. Cerd , and R. Occelli, 1988, "Pattern selection in the B nard-Marangoni instability", in *Propagation in Systems far from Equilibrium*, edited by J. E. Wesfreid, H. R. Brand, P. Manneville, G. Albinet, and N. Boccara (Springer-Verlag, Berlin), p. 232.
- Pertsov, A. M., E. A. Ermakova, and A. V. Panfilov, 1984, "Rotating spiral waves in a modified Fitz-Hugh-Nagumo model", *Physica* **14D**, 117.
- Pesch, W., and Kramer, L., 1986, "Nonlinear analysis of spatial structures in two-dimensional anisotropic pattern forming systems", *Z. Phys.* **63**, 121.
- Pfister, G., and I. Rehberg, 1981, "Couette flow transitions", *Phys. Lett.* **83 A**, 19.
- Pismen, L. M., 1980, "Pattern selection at the bifurcation point", *J. Chem. Phys.* **72**, 1900.
- Pismen, L. M., 1986, "Inertial effects in long-scale thermal convection", *Phys. Lett. A* **116**, 241.
- Pismen, L. M., 1987, "Bifurcation of quasiperiodic and nonstationary patterns under external forcing", *Phys. Rev. Lett.* **59**, 2740.
- Pismen, L. M., 1989, "Phase dynamics in aligned coordinate frame", *Physica D* **36**, 1.
- Pismen, L. M., and A. A. Nepomnyashchy, 1991, "Mobility of spiral waves", *Phys. Rev. A* **44**, R2243.
- Pismen, L. M., and A. A. Nepomnyashchy, 1992, "On interaction of spiral waves", *Physica D* **54**, 183.
- Pismen, L. M., and J. D. Rodriguez, 1990, "Mobility of singularities in the dissipative Ginzburg-Landau equation", *Phys. Rev. A* **42**, 2471.
- Pismen, L. M., and J. Rubinstein, 1991, "Motion of vortex lines in the Ginzburg-Landau model", *Physica D* **47**, 353.
- Platten, J. K., and J. C. Legros, 1984, *Convection in Liquids* (Springer-Verlag, Berlin).
- Pocheau, A., 1988, "Transition to turbulence of convective flows in a cylindrical container", *J. Phys. (Paris)* **49**, 1127.
- Pocheau, A., 1989, "Phase dynamics attractors in an extended cylindrical convective layer", *J. Phys. (Paris)* **50**, 2059.
- Pocheau, A., and V. Croquette, 1984, "Dislocation motion: a wavenumber selection mechanism in Rayleigh-B nard convection", *J. Phys. (Paris)* **45**, 35.
- Pocheau, A., V. Croquette, and P. Le Gal, 1985, "Turbulence in a cylindrical container of argon near threshold of convection,"

- Phys. Rev. Lett. **55**, 1094.
- Pocheau, A., V. Croquette, P. Le Gal, and C. Poitou, 1987, "Convective pattern deformations under mean flow-stress", *Europhys. Lett.* **3**, 915.
- Pogwizd, S. M., and P. B. Corr, 1990, "Mechanisms underlying ventricular tachycardia and fibrillation in the ischemic heart: relation to nonlinear dynamics", in *Mathematical Approaches to Cardiac Arrhythmias*, edited by J. Jalife (Ann. New York, Acad. Sci. **591**, 278).
- Pokrovsky, V. L., and A. L. Talapov, 1984, *Theory of Incommensurate Crystals* (Hardwood-Academic, New York).
- Pomeau, Y., 1984, "Nonadiabatic phenomena in cellular structures", in *Cellular Structures in Instabilities*, edited by J. E. Wesfreid and S. Zaleski (Springer-Verlag, New York), p. 207.
- Pomeau, Y., 1985, "Measurement of the information density in turbulence", *C. R. Acad. Sci. Paris* **300**, Ser. II, 239.
- Pomeau, Y., 1986, "Front motion, metastability and subcritical bifurcations in hydrodynamics", *Physica* **23D**, 3.
- Pomeau, Y., and P. Manneville, 1979, "Stability and fluctuations of a spatially periodic convective flow," *J. Phys. Lett.* **40**, L-609.
- Pomeau, Y., and P. Manneville, 1980, "Wavelength selection in cellular flows," *Phys. Lett.* **75A**, 296.
- Pomeau, Y., and P. Manneville, 1981, "Wavelength selection in axisymmetric cellular structures", *J. Phys. (Paris)* **42**, 1067.
- Pomeau, Y., P. Manneville, and S. Zaleski, 1983, "Dislocation motion in cellular structures", *Phys. Rev. A* **27**, 2710.
- Pomeau, Y., A. Pumir, and P. Pelcé, 1984, "Intrinsic stochasticity with many degrees of freedom", *J. Stat. Phys.* **37**, 39.
- Pomeau, Y., and S. Zaleski, 1980, "Selection du nombre d'onde dans les structures cellulaires convectives", *C. R. Acad. Sci. Paris* **290**, Série B, 505.
- Pomeau, Y., and S. Zaleski, 1981, "Wavelength selection in one-dimensional cellular structures", *J. Phys. (Paris)* **42**, 515.
- Pomeau, Y., and S. Zaleski, 1983, "Pattern selection in a slowly varying environment", *J. Phys. Lett.* **44**, L135.
- Pomeau, Y., S. Zaleski, and P. Manneville, 1985, "Axisymmetric cellular structures revisited", *J. Appl. Math. Phys. (ZAMP)* **36**, 367.
- Powell, J. A., A. C. Newell, and C. K. R. T. Jones, 1991, "Competition between generic and nongeneric fronts in envelope equations", *Phys. Rev. A* **44**, 3636.
- Priestley, C. H. B., 1954, "Convection from a large horizontal surface", *Austral. J. Phys.* **7**, 176.
- Privman, V., P. C. Hohenberg, and A. Aharony, 1991, "Universal critical-point amplitude relations", in *Phase Transitions and Critical Phenomena*, edited by C. Domb and J. L. Lebowitz (Academic, London), Vol. 14.
- Procaccia, I., and R. Zeitak, 1989, "Scaling exponents in non-isotropic convective turbulence", *Phys. Rev. Lett.* **62**, 2128.
- Proctor, M. R. E., 1977, "Inertial convection at low Prandtl number", *J. Fluid. Mech.* **82**, 97.
- Proctor, M. R. E., 1981, "Planform selection by finite-amplitude thermal convection between poorly conducting slabs", *J. Fluid Mech.* **113**, 469.
- Provansal, M., C. Mathis, and L. Boyer, 1987, "Bénard von Karman instability. Transient and forced regimes", *J. Fluid Mech.* **182**, 1.
- Pumir, A., 1985, "Statistical properties of an equation describing fluid interfaces", *J. Phys. (Paris)* **46**, 511.
- Pumir, A., B. Shraiman, and E. D. Siggia, 1991, "Exponential tails and random advection", *Phys. Rev. Lett.* **66**, 2984.
- Rabaud, M., Y. Couder, and S. Michalland, 1991, "Wavelength selection and transients in the one-dimensional array of cells of the printer instability", *Eur. J. Mec. B* **10**, 253.
- Rabaud, M., S. Michalland, and Y. Couder, 1989, "Dynamical regimes of directional viscous fingering: spatiotemporal chaos and wave propagation", *Phys. Rev. Lett.* **64**, 184.
- Rabinovich, M. I., and M. M. Sushchik, 1990, "The regular and chaotic dynamics of structures in fluid flows", *Usp. Fiz. Nauk* **160**, 3 [Sov. Phys. Usp. **33**, 1].
- Rand, D., 1982, "Dynamics and symmetry: predictions for modulated waves in rotating fluid", *Arch. Rational Mech. Anal.* **79**, 1.
- Rappel, W. J., and H. Riecke, 1992, "Parity breaking in directional solidification: numerics versus amplitude equations", *Phys. Rev. A* **45**, 846.
- Rasenat, S., E. Braun, and V. Steinberg, 1991, "Eckhaus instability and defect nucleation in two-dimensional anisotropic systems", *Phys. Rev. A* **43**, 5728.
- Rasenat, S., F. H. Busse, and I. Rehberg, 1989, "A theoretical and experimental study of double-layer convection", *J. Fluid Mech.* **199**, 519.
- Rasenat, S., V. Steinberg, and I. Rehberg, 1990, "Experimental studies of defect dynamics and interaction in electrohydrodynamic convection", *Phys. Rev. A* **42**, 5998.
- Rasmussen, D. R., and T. Bohr, 1987, "Temporal chaos and spatial disorder", *Phys. Lett. A* **125**, 107.
- Rasmussen, J. J., and K. Rypdal, 1986, "Blow-up in nonlinear Schrödinger equations-1.A general review", *Physica Scripta* **33**, 481.
- Rayleigh, Lord, 1916, "On the dynamics of revolving fluids", *Proc. R. Soc. London Ser. A* **93**, 148.
- Rehberg, I., and G. Ahlers, 1985, "Experimental observation of a codimension-two bifurcation in a binary-fluid mixture", *Phys. Rev. Lett.* **55**, 500.
- Rehberg, I., E. Bodenschatz, B. Winkler, and F. H. Busse, 1987, "Forced phase diffusion in a convection experiment", *Phys. Rev. Lett.* **59**, 282.
- Rehberg, I., S. Rasenat, M. de la Torre Juárez, W. Schöpf, F. Hörner, G. Ahlers, and H. R. Brand, 1991, "Thermally induced hydrodynamic fluctuations below the onset of electroconvection", *Phys. Rev. Lett.* **67**, 596.
- Rehberg, I., S. Rasenat, J. Fineberg, M. de la Torre Juárez, and V. Steinberg, 1988, "Temporal modulation of traveling waves", *Phys. Rev. Lett.* **61**, 2449.
- Rehberg, I., S. Rasenat, and V. Steinberg, 1989a, "Traveling waves and defect-initiated turbulence in electroconvection nematics", *Phys. Rev. Lett.* **62**, 756.
- Rehberg, I., B. L. Winkler, M. de la Torre Juárez, S. Rasenat, and W. Schöpf, 1989b, "Pattern formation in a liquid crystal", *Festkörperprobleme* **29**, 35.
- Reusser, E. J., and R. J. Field, 1979, "The transition from phase waves to trigger waves in a model of the Zhabotinskii reaction", *J. Am. Chem. Soc.* **101**, 1063.
- Rezende, S. M., and F. M. de Aguiar, 1986, "Nonlinear dynamics and chaotic behavior of spin wave instabilities", *Rev. Bras. Fis.* **16**, 324.
- Ribotta, R., A. Joets, and L. Lei, 1986, "Oblique roll instability in an electroconvective anisotropic fluid", *Phys. Rev. Lett.* **56**, 1595.
- Rica, S., and E. Tirapegui, 1990, "Interaction of defects in two dimensional systems", *Phys. Rev. Lett.* **64**, 878.
- Rica, S., and E. Tirapegui, 1991a, "Interaction of spirals in oscillatory media. Rica and Tirapegui reply", *Phys. Rev. Lett.* **67**, 405.
- Rica, S., and E. Tirapegui, 1991b, "Dynamics of vortices in the Ginzburg-Landau equation", *Phys. Lett. A* **161**, 53.

- Richetti, P., J. C. Roux, F. Argoul, and A. Arneodo, 1987, "From quasiperiodicity to chaos in the Belousov-Zhabotinskii reaction. 2. Modeling and Theory", *J. Chem. Phys.* **86**, 3339.
- Riecke, H., 1986, "Pattern selection by weakly pinning ramps", *Europhys. Lett.* **2**, 1.
- Riecke, H., 1988, "Imperfect wave-number selection by ramps in a model for Taylor-vortex flow", *Phys. Rev. A* **37**, 636.
- Riecke, H., 1990, "Stable wave-number kinks in parametrically excited standing waves", *Europhys. Lett.* **11**, 213.
- Riecke, H., 1992, "Self-trapping of traveling-wave pulses in binary mixture convection", *Phys. Rev. Lett.* **68**, 301.
- Riecke, H., J. D. Crawford, and E. Knobloch, 1988, "Time-modulated oscillatory convection", *Phys. Rev. Lett.* **61**, 1942.
- Riecke, H., and L. Kramer, 1985, "Surface-induced chemical oscillations and their influence on space-time periodic patterns", *J. Chem. Phys.* **83**, 3941.
- Riecke, H., and H. G. Paap, 1986, "Stability and wave-vector restriction of axisymmetric Taylor vortex flow", *Phys. Rev. A* **33**, 547.
- Riecke, H., and H. G. Paap, 1987, "Perfect wave-number selection and drifting patterns in ramped Taylor vortex flow", *Phys. Rev. Lett.* **59**, 2570.
- Riecke, H., and H. G. Paap, 1991, "Spatio-temporal chaos through ramp-induced Eckhaus instability", *Europhys. Lett.* **14**, 433.
- Riecke, H., and H. G. Paap, 1992, "Parity breaking and Hopf bifurcation in axisymmetric Taylor-vortex flow", *Phys. Rev. A* **45**, 8605.
- Rinzel, J., and D. Terman, 1982, "Propagation phenomena in a bistable reaction-diffusion system", *SIAM J. Appl. Math.* **42**, 1111.
- Rodriguez, J. D., L. M. Pismen, and L. Sirovich, 1991, "Motion of interacting defects in the Ginzburg-Landau model", *Phys. Rev. A* **44**, 7980.
- Rodriguez, J. D., and L. Sirovich, 1990, "Low-dimensional dynamics for the complex Ginzburg-Landau equation", *Physica D* **43**, 77.
- Roppo, M. N., S. H. Davis, and S. Rosenblatt, 1984, "Bénard convection with time-periodic heating", *Phys. Fluids* **27**, 796.
- Rosenblat, S., S. H. Davis, and G. M. Homsy, 1982a, "Nonlinear Marangoni convection in bounded layers. Part I. Circular cylindrical containers", *J. Fluid Mech.* **120**, 91.
- Rosenblat, S., G. M. Homsy, and S. H. Davis, 1982b, "Nonlinear Marangoni convection in bounded layers. Part 2. Rectangular cylindrical containers", *J. Fluid Mech.* **120**, 123.
- Ross, J., K. L. C. Hunt, and P. M. Hunt, 1988a, "Thermodynamics far from equilibrium: Reactions with multiple stationary states", *J. Chem. Phys.* **88**, 2719.
- Ross, J., K. L. C. Hunt, and P. M. Hunt, 1992, "Thermodynamic and stochastic theory for nonequilibrium systems with multiple reactive intermediates: The concept and role of excess work", *J. Chem. Phys.* **96**, 618 (1992).
- Ross, J., S. C. Muller, and C. Vidal, 1988b, "Chemical waves", *Science* **240**, 460.
- Roth, D., M. Lücke, M. Kamps, and R. Schmitz, 1992, "Structure of Taylor vortex flow and the influence of spatial amplitude variations on phase dynamics", in *Ordered and Turbulent Patterns in Taylor-Couette Flow*, edited by C. D. Andereck and F. Hayot (Plenum, New York).
- Ruelle, D., 1980, "Strange attractors", *Math. Intelligencer* **2**, 126 (French orig: *La Recherche* **108**, 132).
- Ruelle, D., 1982, "Large volume limit of the distribution of characteristic exponents in turbulence," *Commun. Math. Phys.* **87**, 287.
- Ruelle, D., 1990, "The Claude Bernard Lecture. Deterministic chaos — the science and the fiction", *Proc. R. Soc. London A* **427**, 241.
- Ruelle, D., and F. Takens, 1971, "On the nature of turbulence," *Commun. Math. Phys.* **20**, 167.
- Sakaguchi, H., 1989, "Numerical study of vortex motion in the two dimensional Ginzburg-Landau equation", *Prog. Theor. Phys.* **82**, 7.
- Sakaguchi, H., 1990a, "Breakdown of the phase dynamics", *Prog. Theor. Phys.* **84**, 792.
- Sakaguchi, H., 1990b, "Instability of the hole solution in the complex Ginzburg-Landau equation", *Prog. Theor. Phys.* **85**, 417.
- Sakaguchi, H., 1991a, "Defect creation by the Eckhaus instability", *Prog. Theor. Phys.* **85**, 927.
- Sakaguchi, H., 1991b, "Zigzag instability and reorientation of roll pattern in the Newell-Whitehead equation", *Prog. Theor. Phys.* **86**, 759.
- Sakaguchi, H., S. Shinomoto, and Y. Kuramoto, 1988, "Mutual entrainment in oscillator lattices with nonvariational type interaction", *Prog. Theor. Phys.* **79**, 1069.
- Sano, M., X.-Z. Wu, and A. Libchaber, 1989, "Turbulence in helium gas free convection", *Phys. Rev. A* **40**, 6421.
- Sasa, S., 1990, "The dynamics near zig-zag instability", *Prog. Theor. Phys.* **84**, 1009.
- Sato, S., M. Sano, and Y. Sawada, 1987, "Practical methods of measuring the generalized dimension and the largest Lyapunov exponent in high dimensional chaotic systems", *Prog. Theor. Phys.* **77**, 1.
- Schaeffer, D. G., 1980, "Qualitative analysis of a model for boundary effects in the Taylor problem", *Math. Proc. Camb. Phil. Soc.* **87**, 307.
- Schatz, M. F., R. P. Tagg, H. L. Swinney, P. F. Fisher, and A. T. Patera, 1991, "Supercritical transition in plane channel flow with spatially periodic perturbations", *Phys. Rev. Lett.* **66**, 1579.
- Schlömann, E., J. Green, and U. Milano, 1960, "Recent developments in ferromagnetic resonance at high power levels", *J. Appl. Phys.* **31**, 3855.
- Schlüter, A., D. Lortz, and F. H. Busse, 1965, "On the stability of steady finite amplitude convection", *J. Fluid Mech.* **23**, 129.
- Schmitt, S., and M. Lücke, 1991, "Amplitude equation for modulated Rayleigh-Bénard convection", *Phys. Rev. A* **44**, 4986.
- Schnaubelt, M., and F. H. Busse, 1989, "On the stability of two-dimensional convection rolls in an infinite Prandtl number fluid with stress-free boundaries", *J. Appl. Math. Phys. (ZAMP)* **40**, 153.
- Schnaufer, B., and H. Haken, 1985, "A theoretical derivation of cellular structures of flames", *Z. Phys. B* **59**, 349.
- Schober, H. R., E. Alroth, K. Schroeder, and H. Müller-Krumbhaar, 1986, "Dynamics of periodic pattern formation", *Phys. Rev. A* **33**, 567.
- Schöpf, W., and L. Kramer, 1991, "Small amplitude periodic and chaotic solutions of the complex Ginzburg-Landau equation for a subcritical bifurcation", *Phys. Rev. Lett.* **66**, 2316.
- Schöpf, W., and I. Rehberg, 1992, "Amplification of thermal noise via convective instability in binary fluid mixtures", *Europhys. Lett.* **17**, 321.
- Schöpf, W., and W. Zimmerman, 1989, "Multicritical behavior in binary fluid convection", *Europhys. Lett.* **8**, 41.
- Schöpf, W., and W. Zimmerman, 1990, "Results on wave patterns in binary-fluid convection", *Phys. Rev. A* **41**, 1145.
- Schöpf, W., and W. Zimmerman, 1993, "Convection in binary

- fluids: amplitude equations, codimension-2 bifurcation and thermal fluctuations" *Phys. Rev. E* **47**, 1739.
- Schuster, H. G., 1984, *Deterministic Chaos. An Introduction* (Physik-Verlag, Weinheim).
- Scott, A. C., 1975, "The electrophysics of a nerve fiber", *Rev. Mod. Phys.* **47**, 487.
- Segel, L. A., 1969, "Distant side-walls cause slow amplitude modulation of cellular convection," *J. Fluid Mech.* **38**, 203.
- Segel, L. A., 1984, *Modelling Dynamic Phenomena in Molecular and Cellular Biology* (Cambridge University Press, Cambridge, U.K.).
- Segur, H., S. Tanveer, and H. Levine, 1991, *Asymptotics Beyond All Orders* (Plenum, New York).
- Shen, Y. R., 1984, *The Principles of Nonlinear Optics* (Wiley, New York).
- Shlang, T., and G. I. Sivashinsky, 1982, "Irregular flow of a liquid film down a vertical column", *J. Phys. (Paris)* **43**, 459.
- Showalter, K., R. M. Noyes, and H. Turner, 1979, "Detailed studies of trigger wave initiation and detection", *J. Am. Chem. Soc.* **101**, 7463.
- Shraiman, B. I., 1987, "Order, disorder and phase turbulence", *Phys. Rev. Lett.* **57**, 325.
- Shraiman, B. I., A. Pumir, W. Van Saarloos, P. C. Hohenberg, H. Chaté, and M. Holen, 1992, "Spatiotemporal chaos in the one-dimensional complex Ginzburg-Landau equation", *Physica D* **57**, 241.
- Shraiman, B. I., and E. D. Siggia, 1990, "Heat transport in high-Rayleigh-number convection", *Phys. Rev. A* **42**, 3650.
- Shraiman, B., C. E. Wayne, and P. C. Martin, 1981, "Scaling theory for noisy period-doubling transitions to chaos", *Phys. Rev. Lett.* **46**, 935.
- Shtilman, L., and G. Sivashinsky, 1991, "Hexagonal structure of large-scale Marangoni convection", *Physica D* **52**, 477.
- Shydkrot, H., and J. Ross, 1985, "Propagating and stationary structures in chemical reaction-diffusion systems", *J. Chem. Phys.* **82**, 113.
- Siggia, E. D., 1994, "High Rayleigh number convection", *Annu. Rev. Fluid Mech.* (to be published).
- Siggia, E. D., and A. Zippelius, 1981a, "Dynamics of defects in Rayleigh-Bénard convection", *Phys. Rev. A* **24**, 1036.
- Siggia, E. D., and A. Zippelius, 1981b, "Pattern selection in Rayleigh-Bénard convection near threshold", *Phys. Rev. Lett.* **47**, 835.
- Silber, M., and E. Knobloch, 1988, "Pattern selection in ferrofluids", *Physica D* **30**, 83.
- Simon, A. J., J. Bechhoefer, and A. Libchaber, 1988, "Solitary modes and the Eckhaus instability in directional solidification", *Phys. Rev. Lett.* **61**, 2574.
- Simon, A. J., and A. Libchaber, 1990, "Moving interface — The stability tongue and phenomena within", *Phys. Rev. A* **41**, 7090.
- Simonelli, F., and J. P. Gollub, 1987, "Surface wave mode interactions: effects of symmetry and degeneracy", *J. Fluid Mech.* **199**, 471.
- Sirovich, L., 1989, "Chaotic dynamics of coherent structures", *Physica D* **37**, 126.
- Sirovich, L., 1991, Ed., *New Perspectives in Turbulence* (Springer-Verlag, New York).
- Sirovich, L., J. D. Rodriguez, and B. Knight, 1990, "Two boundary value problems for the Ginzburg-Landau equation", *Physica D* **43**, 63.
- Sivashinsky, G. I., 1977, "Nonlinear analysis of hydrodynamical instability in laminar flames. Part I. Derivation of basic equations," *Acta Astronautica* **4**, 1177.
- Sivashinsky, G. I., 1983, "Instabilities, pattern formation, and turbulence in flames", *Annu. Rev. Fluid Mech.* **15**, 179.
- Skinner, G. S., and H. L. Swinney, 1990, "Periodic to quasi-periodic transition of chemical spiral rotation", *Physica D* **48**, 1.
- Snoeys, M. L., 1980, "Chemical waves in the oscillatory Zhabotinskii system: a transition from temporal to spatiotemporal organization", in *Dynamics of Synergetic Systems*, edited by H. Haken (Springer-Verlag, Berlin), p. 80.
- Sneddon, L., and M. C. Cross, 1982, "Pattern forming tendencies in parametric wave instabilities and dissipative systems" (unpublished).
- Solomon, T. H., and J. P. Gollub, 1991, "Thermal boundary layers and heat flux in turbulent convection: the role of recirculating flows", *Phys. Rev. A* **43**, 6683.
- Sompolinsky, H., A. Crisanti, and H. J. Sommers, 1988, "Chaos in random neural networks", *Phys. Rev. Lett.* **61**, 259.
- Sompolinsky, H., D. Golomb, and D. Kleinfeld, 1991, "Cooperative dynamics in visual processing", *Phys. Rev. A* **43**, 6990.
- Sparrow, E. M., R. J. Goldstein, and V. K. Jonsson, 1964, "Thermal instability in a horizontal fluid layer: effect of boundary conditions and nonlinear temperature profile", *J. Fluid Mech.* **18**, 513.
- Sreenivasan, K. R., 1991, "Fractals and multifractals in fluid turbulence", *Annu. Rev. Fluid Mech.* **23**, 539.
- Stakgold, I., 1979, *Green's Functions and Boundary Value Problems* (Wiley, New York).
- Stassinopoulos, D., and P. Alström, 1992, "Coupled maps: An approach to spatiotemporal chaos", *Phys. Rev. A* **45**, 675.
- Stassinopoulos, D., G. Huber, and P. Alström, 1990, "Measuring the onset of spatiotemporal intermittency", *Phys. Rev. Lett.* **64**, 3007.
- Stavans, J., E. Domany, and D. Mukamel, 1991, "Universality and pattern selection in two-dimensional cellular structures", *Europhys. Lett.* **15**, 479.
- Stein, D. L., 1980, "Dissipative structures, broken symmetry, and the theory of equilibrium phase transitions", *J. Chem. Phys.* **72**, 2869.
- Stein, D. L., 1989, Ed., *Complex Systems, SFI Studies in the Science of Complexity* (Addison-Wesley, New York).
- Steinberg, V., G. Ahlers, and D. S. Cannell, 1985, "Pattern formation and wave-number selection by Rayleigh-Bénard convection in a cylindrical container", *Physica Scripta* **32**, 534.
- Steinberg, V., J. Fineberg, E. Moses, and I. Rehberg, 1989, "Pattern selection and transition to turbulence in propagating waves", *Physica D* **37**, 359.
- Steinberg, V., and E. Kaplan, 1991, "Localized and 'blinking' traveling wave patterns in a convective binary mixture", in *Spontaneous Formation of Space-time Structures and Criticality*, edited by T. Riste and D. Sherrington (Plenum, New York), p. 207.
- Steinberg, V., E. Moses, and J. Fineberg, 1987, "Spatiotemporal complexity at the onset of convection in a binary fluid", *Nucl. Phys. B* **2**, 109.
- Stewartson, K., and J. T. Stuart, 1971, "A nonlinear instability theory for a wave system in plane Poiseuille flow," *J. Fluid Mech.* **48**, 529.
- Strogatz, S. H., C. M. Marcus, R. M. Westervelt, and R. E. Mirollo, 1989, "Collective dynamics of coupled oscillators with random pinning", *Physica D* **36**, 23.
- Strogatz, S. H., and R. E. Mirollo, 1988, "Phase locking and critical phenomena in lattices of coupled nonlinear oscillators with random intrinsic frequencies", *Physica D* **31**, 143.

- Strykowski, P. J., and K. R. Sreenivasan, 1990, "On the formation and suppression of vortex shedding at low Reynolds numbers", *J. Fluid Mech.* **218**, 71.
- Stuart, J. T., 1958, "On the nonlinear mechanics of hydrodynamic stability", *J. Fluid. Mech.* **4**, 1.
- Stuart, J. T., 1960, "On the nonlinear mechanics of wave disturbances in stable and unstable parallel flows. Part I: the basic behavior in plane Poiseuille flow", *J. Fluid Mech.* **9**, 353.
- Stuart, J. T., and R. C. DiPrima, 1978, "The Eckhaus and Benjamin-Feir resonance mechanisms", *Proc. R. Soc. Lond. A* **362**, 27.
- Suhl, H., 1957, "The theory of ferromagnetic resonance at high signal powers", *J. Phys. Chem. Solids* **1**, 209.
- Sullivan, T. S., and G. Ahlers, 1988a, "Hopf bifurcation to convection near the codimension-two point in a ${}^3\text{He}-{}^4\text{He}$ mixture", *Phys. Rev. Lett.* **61**, 78.
- Sullivan, T. S., and G. Ahlers, 1988b, "Nonperiodic time dependence of the onset of convection in a binary-fluid mixture", *Phys. Rev. A* **38**, 3143.
- Sullivan, T. S., and R. J. Deissler, 1989, "Elimination of hysteresis in a system of coupled Ginzburg-Landau equations", *Phys. Rev. A* **40**, 6748.
- Surko, C. M., P. Kolodner, A. Passner, and R. W. Walden, 1986, "Finite-amplitude traveling-wave convection in binary fluid mixtures", *Physica D* **23**, 220.
- Surko, C. M., D. R. Ohlsen, S. Y. Yamamoto, and P. Kolodner, 1991, "Confined states of traveling-wave convection", *Phys. Rev. A* **43**, 7101.
- Suzuki, M., 1978a, "Theory of instability, nonlinear Brownian motion and formation of macroscopic order", *Phys. Lett. A* **67**, 339.
- Suzuki, M., 1978b, "Scaling theory of transient nonlinear fluctuations and formation of macroscopic order", *Prog. Theor. Phys. Suppl.* **64**, 402.
- Swift, J. B., and P. C. Hohenberg, 1977, "Hydrodynamic fluctuations at the convective instability", *Phys. Rev. A* **15**, 319.
- Swift, J. B., and P. C. Hohenberg, 1988, "Comment on initial stages of pattern formation in Rayleigh-Bénard convection", *Phys. Rev. Lett.* **60**, 75.
- Swift, J. B., and P. C. Hohenberg, 1989, "Rayleigh-Bénard convection with time-dependent boundary conditions", *Phys. Rev. A* **39**, 4132.
- Swift, J. B., P. C. Hohenberg, and G. Ahlers, 1991, "Stochastic Landau equation with time-dependent drift", *Phys. Rev. A* **43**, 6572.
- Swinney, H. L., and J. P. Gollub, 1981, Eds., *Hydrodynamic Instabilities and the Transition to Turbulence*, Topics in Applied Physics (Springer-Verlag, Berlin), Vol. 45.
- Swinney, H. L., and V. I. Krinsky, 1991, Eds., *Waves and Patterns in Chemical and Biological Media*, (MIT/North-Holland); [also in *Physica D* **49**, 1].
- Tagg, R., 1992, "A guide to literature related to the Taylor-Couette problem", in *Ordered and Turbulent Patterns in Taylor-Couette Flow*, edited by C. D. Andereck and F. Hayot (Plenum, New York).
- Tagg, R., W. S. Edwards, and H. L. Swinney, 1990, "Convective versus absolute instability in flow between counterrotating cylinders", *Phys. Rev. A* **42**, 831.
- Tagg, R., W. S. Edwards, H. L. Swinney, and P. S. Marcus, 1989, "Nonlinear standing waves in Couette-Taylor flow", *Phys. Rev. A* **39**, 3734.
- Tainaka, K., 1989, "Stationary pattern of vortices or strings in biological systems: Lattice version of the Lotka-Volterra model", *Phys. Rev. Lett.* **63**, 2688.
- Takens, F., 1981, "Detecting strange attractors in turbulence", in *Dynamical Systems and Turbulence*, edited by D. A. Rand and L. S. Young, Lecture Notes in Mathematics (Springer-Verlag, Berlin), Vol. 898, p. 366.
- Takens, F., 1985, "On the numerical determination of the dimension of an attractor", in *Dynamical Systems and Bifurcations*, edited by B. L. J. Braaksma, H. W. Broer, and F. Takens, Lecture Notes in Mathematics (Springer-Verlag, New York), Vol. 1125, p. 99.
- Tam, W. Y., W. Horsthemke, Z. Noszticzius, and H. L. Swinney, 1988, "Sustained spiral waves in a continuously fed un-stirred chemical reactor", *J. Chem. Phys.* **88**, 3395.
- Tam, W. Y., and H. L. Swinney, 1990, "Spatiotemporal patterns in a one-dimensional open reaction-diffusion system", *Physica D* **46**, 10.
- Tang, C., K. Wiesenfeld, P. Bak, S. N. Coppersmith, and P. B. Littlewood, 1987, "Phase organization", *Phys. Rev. Lett.* **58**, 1161.
- Tavener, S. J., T. Mullin, and K. A. Cliffe, 1991, "Novel bifurcation phenomena in a rotating annulus", *J. Fluid Mech.* **229**, 483.
- Temam, R., 1988, *Infinite Dimensional Dynamical Systems in Mechanics and Physics*, Lecture Notes in Mathematics (Springer-Verlag, New York), Vol. **68**, p. 475.
- Temam, R., 1989, "Do inertial manifolds apply to turbulence?", *Physica D* **37**, 146.
- Teman, R., 1990, "Inertial manifolds", *Mathematical Intelligencer* **12**, 68.
- Tesauro, G., and M. C. Cross, 1986, "Climbing of dislocations in nonequilibrium patterns", *Phys. Rev. A* **34**, 1363.
- Tesauro, G., and M. C. Cross, 1987, "Grain boundaries in models of convective patterns", *Phil. Mag. A* **56**, 703.
- Threlfall, D. C., 1975, "Free convection in low-temperature gaseous helium", *J. Fluid Mech.* **67**, 17.
- Thual, O., S. Douady, and S. Fauve, 1989, "Parametric instabilities", in *Instabilities and Nonequilibrium Structures II*, edited by E. Tirapegui and D. Villarroel (Kluwer, Dordrecht), p. 227.
- Thual, O., and S. Fauve, 1988, "Localized structures generated by subcritical instabilities", *J. Phys. (Paris)* **49**, 1829.
- Tirapegui, E., and D. Villarroel, 1987, Eds., *Instabilities and Nonequilibrium Structures I* (Kluwer, Dordrecht).
- Tirapegui, E., and D. Villarroel, 1989, Eds., *Instabilities and Nonequilibrium Structures II. Dynamical Systems and Instabilities* (Kluwer, Dordrecht).
- Tirapegui, E., and W. Zeller, 1991, Eds., *Instabilities and Nonequilibrium Structures III* (Kluwer, Dordrecht).
- Toh, S., 1987, "Statistical model with localized structures describing the spatio-temporal chaos of Kuramoto-Sivashinsky equation", *J. Phys. Soc. Jpn.* **36**, 949.
- Torcini, A., A. Politi, G. P. Puccioni, and G. D'Alessandro, 1991, "Fractal dimension of spatially extended systems", *Physica D* **53**, 85.
- Tritton, D. J., 1988, *Physical Fluid Dynamics* (Oxford University Press, Oxford, U.K.).
- Tsameret, A., and V. Steinberg, 1991a, "Noise-modulated propagating pattern in a convectively unstable system", *Phys. Rev. Lett.* **67**, 3392.
- Tsameret, A., and V. Steinberg, 1991b, "Convective vs. absolute instability in Couette-Taylor flow with an axial flow", *Europhys. Lett.* **14**, 331.
- Tu, Y., and M. C. Cross, 1992, "Chaotic domain structure in rotating convection", *Phys. Rev. Lett.* **69**, 2515.
- Tuckerman, L. S., and D. Barkley, 1988, "Global bifurcation to traveling waves in axisymmetric convection", *Phys. Rev. Lett.*

- 61, 408.
- Tuckerman, L. S., and D. Barkley, 1990, "Bifurcation analysis of the Eckhaus instability", *Physica D* **46**, 57.
- Tufillaro, N. B., R. Ramshankar, and J. P. Gollub, 1989, "Order-disorder transition in capillary ripples", *Phys. Rev. Lett.* **62**, 422.
- Turing, A. M., 1952, "The chemical basis of morphogenesis", *Phil. Trans. R. Soc. London B* **237**, 37.
- Tyson, J. J., 1985, "A quantitative account of oscillations, bistability, and traveling waves in the Belousov-Zhabotinskii reaction", in *Oscillations and Traveling Waves in Chemical Systems*, edited by R. J. Field and M. Burger (Wiley, New York), p. 93.
- Tyson, J. J., 1987, "Singular perturbation theory of target patterns in the Belousov-Zhabotinskii reaction", *J. Chim. Phys.* **84**, 1359.
- Tyson, J. J., K. A. Alexander, V. S. Manoranjan, and J. D. Murray, 1989, "Spiral waves of cyclic AMP in a model of slime mold aggregation", *Physica D* **34**, 193.
- Tyson, J. J., and P. C. Fife, 1980, "Target patterns in a realistic model of the Belousov-Zhabotinskii reaction", *J. Chem. Phys.* **73**, 2224.
- Tyson, J. J., and J. P. Keener, 1987, "Spiral waves in a model of myocardium", *Physica D* **29**, 215.
- Tyson, J. J., and J. P. Keener, 1988, "Singular perturbation theory of traveling waves in excitable media (a review)", *Physica D* **32**, 327.
- van Beijeren, H., and E. G. D. Cohen, 1988, "The effects of thermal noise in a Rayleigh-Bénard cell near its first convective instability", *J. Stat. Phys.* **53**, 77.
- Van Dyke, M., 1982, *An Album of Fluid Motion* (Parabolic, Stanford, CA).
- Van Kampen, N., 1981, *Stochastic Processes in Physics and Chemistry* (North-Holland, Amsterdam).
- van Saarloos, W., 1988, "Front propagation into unstable states: marginal stability as a dynamical mechanism for velocity selection", *Phys. Rev. A* **37**, 211.
- van Saarloos, W., 1989, "Front propagation into unstable states. II. linear versus nonlinear marginal stability and rate of convergence", *Phys. Rev. A* **39**, 6367.
- van Saarloos, W., 1990, "Front propagation into unstable states: some recent developments and surprises", in *Nonlinear Evolution of Spatio-Temporal Structures in Dissipative Continuous Systems*, edited by F. H. Busse and L. Kramer (Plenum, New York), p. 499.
- van Saarloos, W., and P. C. Hohenberg, 1990, "Pulses and fronts in the complex Ginzburg-Landau equation near a subcritical bifurcation", *Phys. Rev. Lett.* **64**, 749.
- van Saarloos, W., and P. C. Hohenberg, 1992, "Fronts, pulses, sources and sinks in generalized Ginzburg-Landau equations", *Physica D* **56**, 303.
- Vasiliev, V. A., Y. M. Romanovskii, D. S. Chernavskii, and V. G. Yakhno, 1987, *Autowave Processes in Kinetic Systems* (Reidel, Dordrecht).
- Vasiliev, V. A., Y. M. Romanovskii, and V. G. Yakhno, 1979, "Autowave processes in distributed kinetic systems", *Usp. Fiz. Nauk.* **128**, 625 [Sov. Phys. Usp. **22**, 615].
- Vastano, J. A., T. Russo, and H. L. Swinney, 1990, "Bifurcation to spatially induced chaos in a reaction-diffusion system", *Physica D* **46**, 23.
- Vastano, J. A., and H. L. Swinney, 1988, "Information transport in spatiotemporal systems", *Phys. Rev. Lett.* **60**, 1773.
- Veronis, G., 1958, "Cellular convection with finite amplitude in a rotating fluid", *J. Fluid Mech.* **5**, 401.
- Vicsek, T., 1989, *Fractal Growth Phenomena* (World Scientific, Singapore).
- Vidal, C., 1987, "Experimental study of traveling waves and target patterns in oscillatory reacting media", *J. Stat. Phys.* **48**, 1017.
- Vidal, C., and A. Pagola, 1989, "Observed properties of trigger waves close to the center of target patterns in an oscillating Belousov-Zhabotinsky reagent", *J. Phys. Chem.* **93**, 2711.
- Vidal, C., A. Pagola, J. M. Bodet, P. Hanusse, and E. Bastardie, 1986, "Etude experimentale statistique des structures cibles de la réaction de Belousov-Zhabotinsky en régime oscillant", *J. Phys. (Paris)* **47**, 1999.
- Viñals, J., E. Hernandez-Garcia, M. San-Miguel, and R. Toral, 1991, "Numerical study of the dynamical aspects of pattern selection in the stochastic Swift-Hohenberg equation in one dimension", *Phys. Rev. A* **44**, 1123.
- Viñals, J., H. W. Xi, and J. D. Gunton, 1992, "Numerical study of the influence of forcing terms and fluctuations near onset on roll patterns in Rayleigh-Bénard convection in a simple fluid", *Phys. Rev. A* **46**, 918.
- Walden, R. W., and G. Ahlers, 1981, "Non-Boussinesq and penetrative convection in a cylindrical cell", *J. Fluid Mech.* **109**, 89.
- Walden, R. W., P. Kolodner, A. Passner, and C. M. Surko, 1985, "Traveling waves and chaos in convection in binary fluid mixtures", *Phys. Rev. Lett.* **55**, 496.
- Walgraef, D., 1987, Ed., *Patterns, Defects and Microstructures in Nonequilibrium Systems: Applications in Materials Science* (M. Nijhoff).
- Walgraef, D., 1988a, "Instabilities and patterns in reaction-diffusion dynamics", *Solid State Phenomena* **3&4**, 77.
- Walgraef, D., 1988b, "External forcing of spatio-temporal patterns", *Europhys. Lett.* **7**, 485.
- Walgraef, D., 1991, "Transitions between patterns of different symmetries", in *Instabilities and Nonequilibrium Structures, III*, edited by E. Tirapegui and W. Zeller (Kluwer, Dordrecht), p. 269.
- Walgraef, D., G. Dewel, and P. Borckmans, 1981, "Dissipative structures and broken symmetry", *J. Chem. Phys.* **74**, 755.
- Walgraef, D., G. Dewel, and P. Borckmans, 1983, "Chemical waves in a two-dimensional oscillating system", *J. Chem. Phys.* **78**, 3043.
- Walgraef, D., and N. M. Ghoniem, 1990, Eds., *Patterns, Defects and Materials Instabilities* (Kluwer, Dordrecht).
- Weber, A., E. Bodenschatz, and L. Kramer, 1991, "Defects in continuous media", *Advan. Mater.* **3**, 191.
- Weber, A., L. Kramer, I. S. Aranson, and L. B. Aranson, "Stability limits of traveling waves and the transition to spatiotemporal chaos in the complex Ginzburg-Landau equation", *Physica D* **61**, 279.
- Wegner, F., 1980, "Inverse participation ratio in $2 + \epsilon$ dimensions", *Z. Phys. B* **36**, 209.
- Weiss, J., M. Tabor, and G. Carnevale, 1983, "The Painlevé property for partial differential equations", *J. Math. Phys.* **24**, 522.
- Wesfreid, J. E., H. R. Brand, P. Manneville, G. Albinet and N. Boccara, 1988, Eds., *Propagation in Systems Far from Equilibrium*, Springer Series in Synergetics (Springer-Verlag, Berlin), Vol. 41.
- Wesfreid, J., and V. Croquette, 1980, "Forced phase diffusion in Rayleigh-Bénard convection", *Phys. Rev. Lett.* **45**, 634.
- Wesfreid, J., Y. Pomeau, M. Dubois, C. Normand, and P. Bergé, 1978, "Critical effects in Rayleigh-Bénard convection", *J. Phys. (Paris)* **39**, 725.

- Wesfreid, J. E., and S. Zaleski, 1984, Eds., *Cellular Structures in Instabilities*, Lecture Notes in Physics (Springer-Verlag, Berlin), Vol. 210.
- Whitham, G. B., 1974, *Linear and Nonlinear Waves* (Wiley, New York).
- Wiener, R. J., P. W. Hammer, and R. Tagg, 1991, "Perturbation analysis of the primary instability in Taylor-Couette flow subjected to a Coriolis force", *Phys. Rev. A* **44**, 3653.
- Wiener, N., and A. Rosenblueth, 1946, "The mathematical formulation of the problem of conduction of impulses in a network of connected excitable elements, specifically in cardiac muscle", *Arch. Inst. Cardiol. Mexico* **16**, 202.
- Willaime, H., O. Cardoso, and P. Tabeling, 1991, "Frustration in a linear array of vortices", *Phys. Rev. Lett.* **67**, 3247.
- Winfree, A. T., 1974, "Rotating chemical reactions," *Sci. Am.* **230**, June, p. 82.
- Winfree, A. T., 1984a, "Wavefront geometry in excitable media", *Physica* **12D**, 321.
- Winfree, A. T., 1984b, "The prehistory of the Belousov-Zhabotinsky oscillator", *J. Chem. Educ.* **61**, 661.
- Winfree, A. T., 1985, "Organizing centers for chemical waves in two and three dimensions", in *Oscillations and Traveling Waves in Chemical Systems*, edited by R. J. Field and M. Burger (Wiley, New York), p. 441.
- Winfree, A. T., 1987, *When Time Breaks Down* (Princeton University Press, Princeton).
- Winfree, A. T., 1990, "Vortex action potentials in normal ventricular muscle", in *Mathematical Approaches to Cardiac Arrhythmias*, edited by J. Jalife (Ann. New York, Acad. Sci. **591**, 190).
- Winfree, A. T., 1991, "Varieties of spiral wave behavior: An experimentalist's approach to the theory of excitable media", *Chaos* **1**, 303.
- Winfree, A. T., and S. H. Strogatz, 1983, "Singular filaments organize chemical waves in three dimensions", *Physica* **8D**, 35.
- Winfree, A. T., and S. H. Strogatz, 1984, "Organizing centres for three-dimensional chemical waves", *Nature* **311**, 611.
- Wolf, A., J. B. Swift, H. L. Swinney, and J. A. Vastano, 1985, "Determining Lyapunov exponents from a time series," *Physica* **16D**, 285.
- Wolfram, S., 1986, Ed., *Theory and Applications of Cellular Automata* (World Scientific, Singapore).
- Wollkind, D., and L. Segel, 1970, "A nonlinear stability analysis of the freezing of a dilute binary alloy", *Phil. Trans. Roy. Soc. (Lond)* **268**, 351.
- Wood, P. M., and J. Ross, 1985, "A quantitative study of chemical waves in the Belousov-Zhabotinsky reaction", *J. Chem. Phys.* **82**, 1924.
- Wu, M., and C. D. Andereck, 1991, "Phase dynamics of wavy vortex flow", *Phys. Rev. Lett.* **67**, 1258.
- Wu, X.-Z., M.-N. Chee, and R. Kapral, 1991, "Vortex dynamics in oscillatory chemical systems", *Chaos* **1**, 421.
- Wu, X.-Z., L. Kadanoff, A. Libchaber, and M. Sano, 1990, "Frequency power spectrum of temperature fluctuations in free convection", *Phys. Rev. Lett.* **64**, 2140.
- Wu, J., R. Keolian, and I. Rudnick, 1984, "Observation of a nonpropagating hydrodynamic soliton", *Phys. Rev. Lett.* **52**, 1421.
- Wu, X.-Z., and A. Libchaber, 1992, "Scaling relations in thermal turbulence: The aspect-ratio dependence", *Phys. Rev. A* **45**, 842.
- Xi, H.-W., J. Viñals, and J. D. Gunton, 1991, "Numerical solution of the Swift-Hohenberg equation in two dimensions", *Physica A* **177**, 356.
- Yahata, H., 1989, "Dynamics of convection in binary fluid mixtures", *Prog. Theor. Phys. Suppl.* **99**, 493.
- Yahata, H., 1991, "Traveling convection rolls in a binary fluid mixture", *Prog. Theor. Phys.* **85**, 933.
- Yakhot, V., 1981, "Large-scale properties of unstable systems governed by the Kuramoto-Sivashinsky equation", *Phys. Rev. A* **24**, 642.
- Yakhot, V., and S. A. Orszag, 1986, "Renormalization group analysis of turbulence", *Phys. Rev. Lett.* **57**, 1722.
- Yakhot, V., and Z.-S. She, 1988, "Long-time, large-scale properties of the random-force-driven Burgers equation", *Phys. Rev. Lett.* **60**, 1840.
- Zaikin, A. N., and A. M. Zhabotinskii, 1970, "Concentration wave propagation in a two-dimensional liquid-phase self-oscillating system", *Nature* **225**, 535.
- Zaitsev, V. M., and M. I. Shliomis, 1970, "Hydrodynamic fluctuations near the convection threshold", *Zh. Eksp. Teor. Fiz.* **59**, 1583 [Sov. Phys. JETP **32**, 866, (1971)].
- Zakharov, V. E., 1984, "Kolmogorov spectra in weak turbulence problem", in *Basic Plasma Physics*, Vol. 2, edited by A. Galeev and R. N. Sudan (North-Holland, Amsterdam), p. 3.
- Zakharov, V. E., 1991, Ed., "Wave collapses. Proceedings of the international workshop on wave collapse physics", *Physica D* **52**.
- Zakharov, V. E., V. S. L'vov, and S. S. Starobinets, 1975, "Spin-wave turbulence beyond the parametric excitation threshold", *Usp. Fiz. Nauk.* **114**, 609 [Sov. Phys. Usp. **17**, 896].
- Zaleski, S., 1989a, "A stochastic model for the large scale dynamics of some fluctuating interfaces", *Physica D* **34**, 427.
- Zaleski, S., 1989b, "Low frequency noise from random dislocation noise in large convective systems", *Phys. Rev. A* **39**, 3088.
- Zaleski, S., Y. Pomeau, and A. Pumir, 1984, "Optimal merging of rolls near a plane boundary", *Phys. Rev. A* **29**, 366.
- Zaleski, S., P. Tabeling, and P. Lallemand, 1985, "Flow structures and wave-number selection in spiraling vortex flows", *Phys. Rev. A* **32**, 655.
- Zel'dovich, Ya. B., 1985, *Mathematical Theory of Combustion and Explosions* (Consultants Bureau, New York).
- Zhang, S.-Y., 1991, *Bibliography on Chaos*, Directions in Chaos (World Scientific, Singapore), Vol. 5.
- Zhong, F., R. Ecke, and V. Steinberg, 1991a, "Asymmetric modes and the transition to vortex structures in rotating Rayleigh-Bénard convection", *Phys. Rev. Lett.* **67**, 2473.
- Zhong, F., R. Ecke, and V. Steinberg, 1991b, "Rotating Rayleigh-Bénard convection: The Küppers-Lortz transition", *Physica D* **51**, 596.
- Zielinska, B. J. A., and H. R. Brand, 1987, "Exact solution of the linear stability problem for the onset of convection in binary fluid mixtures", *Phys. Rev. A* **35**, 4349.
- Zimmermann, W., 1991, "Pattern formation in electrohydrodynamic convection", *Mat. Res. Soc. Bull.* **16**, 46.
- Zimmerman, W., D. Armbruster, L. Kramer, and W. Kuang, 1988, "The effect of spatial modulations on codimension-2 bifurcations", *Europhys. Lett.* **6**, 505.
- Zykov, V. S., 1987, *Simulation of Wave Processes in Excitable Media* (Manchester University Press, Manchester, U.K.).
- Zykov, V. S., 1990, "Spiral waves in two-dimensional excitable media", in *Mathematical Approaches to Cardiac Arrhythmias*, edited by J. Jalife (Ann. N.Y. Acad. Sci. **591**, 75).
- Zykov, V. S., and O. L. Morozova, 1991, *J. Nonlin. Biol.* **1**, 127.

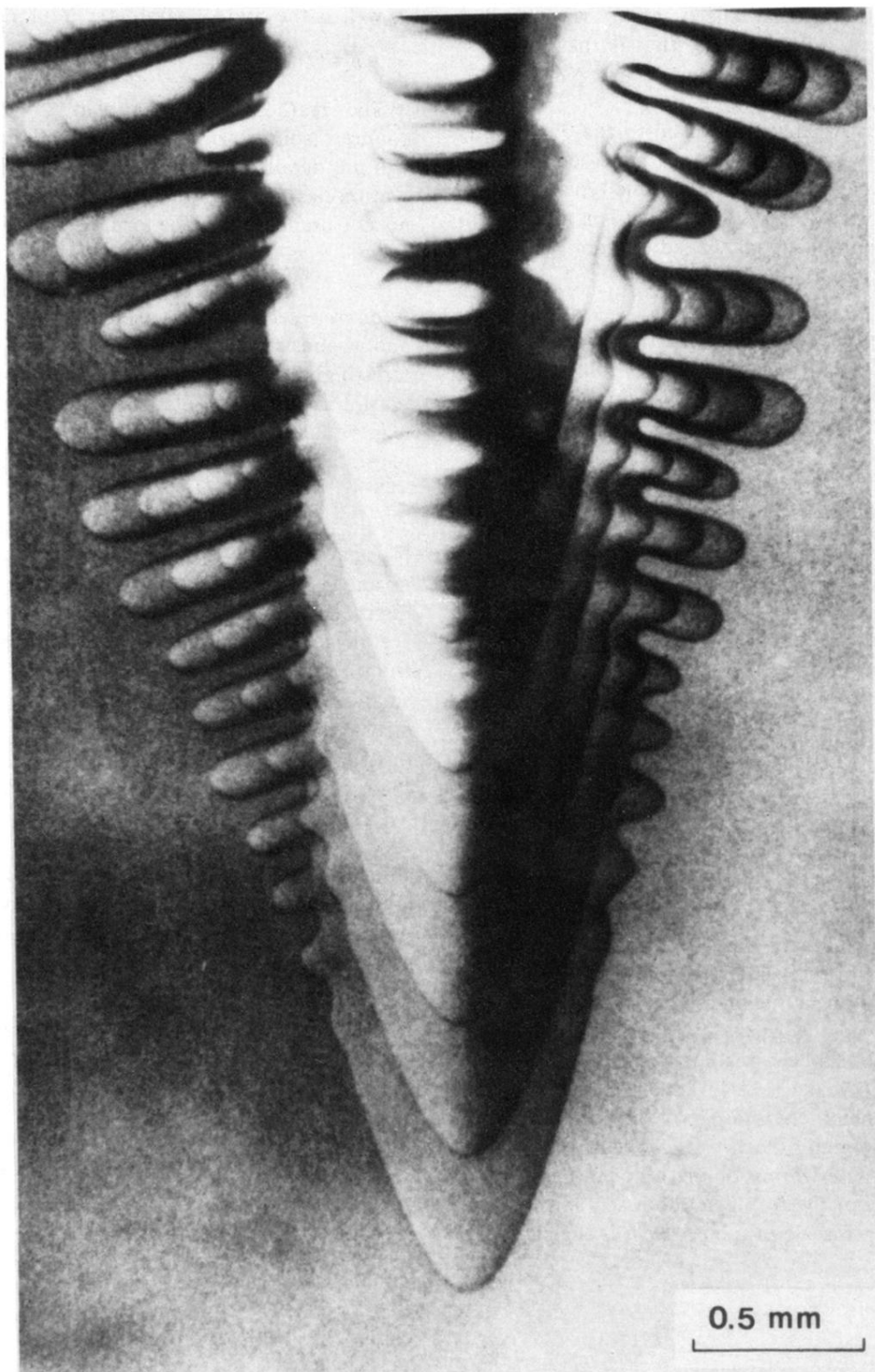


FIG. 101. Multiple-exposure photograph of a succinonitrile dendrite advancing downward. (From Huang and Glicksman, 1981; Copyright 1981 with permission from Pergamon Press Ltd., Headington Hill Hall, Oxford OX3 0BW, United Kingdom.)

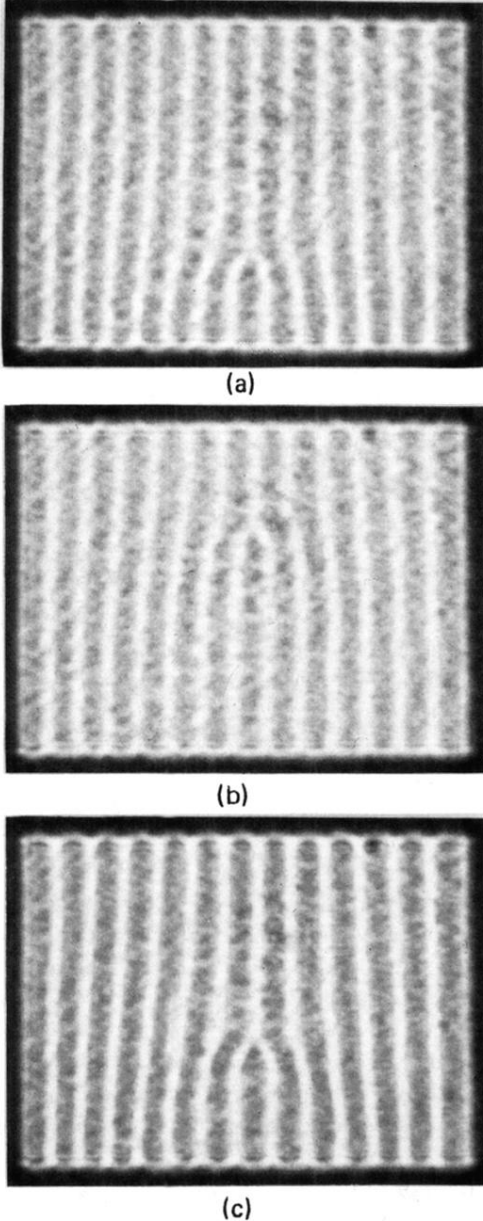


FIG. 19. Dislocation defects in a type I_s system. Photographs are flow visualizations of a Rayleigh-Bénard convection experiment showing a pattern of 14 wavelengths in the lower portion of the cell and 13 in the upper portion. Panels show climb motion of the defect induced by changing the Rayleigh number. (a) $R = 1.2 R_c$: the dislocation is moving towards the bottom of the picture. (b) Lowering the Rayleigh number to $R = 1.15 R_c$ reverses the motion. (c) The Rayleigh number has increased again. (From Croquette, 1989.)

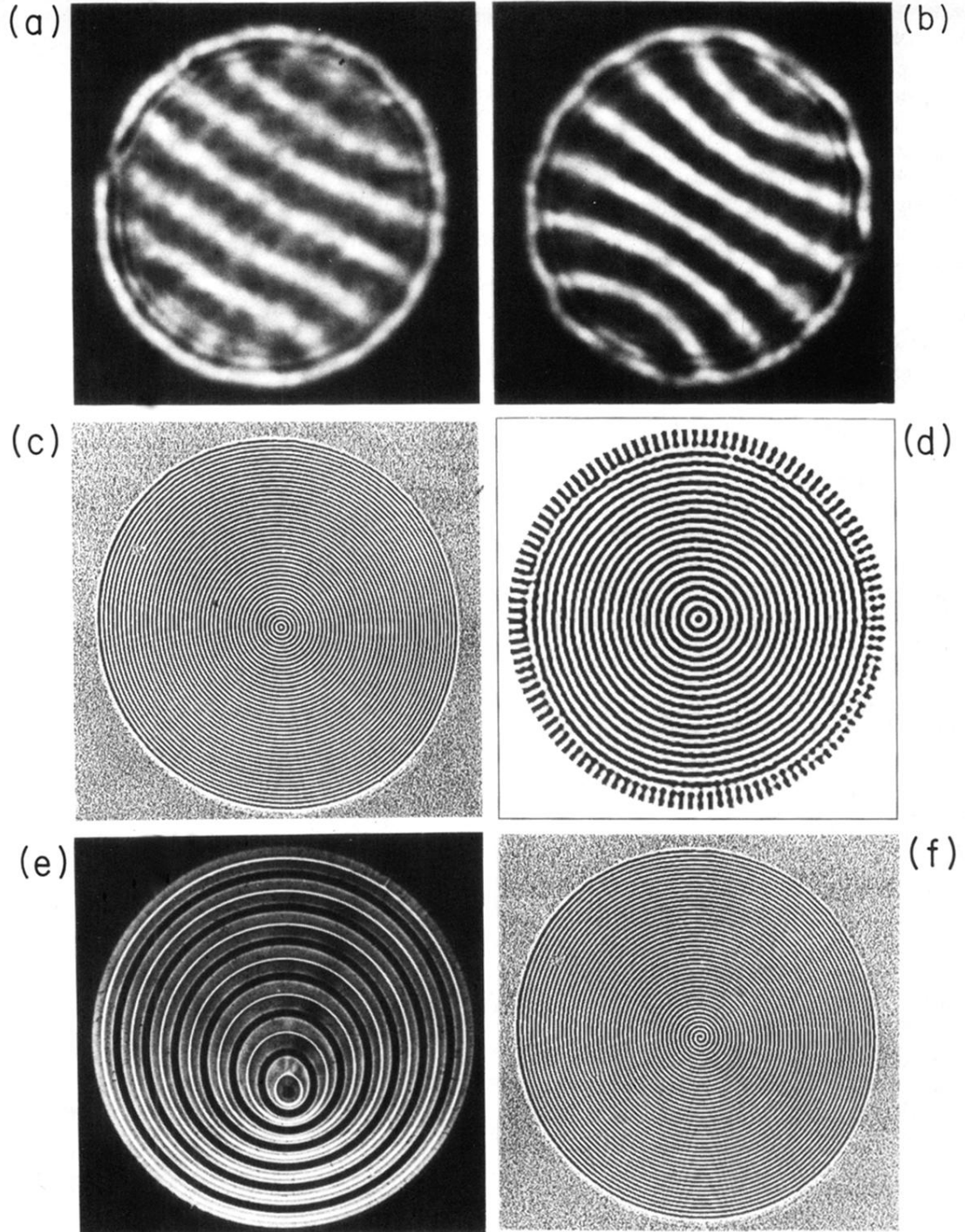


FIG. 39. Simple two-dimensional patterns in a cylindrical geometry obtained for different values of Prandtl number σ , Rayleigh number R , aspect ratio L and different sidewall conditions, showing (a) nearly straight rolls in argon gas with $\sigma=0.7$, $L=7.66$, $R/R_c=1.05$ (with R_c the critical Rayleigh number in the actual geometry); (b) more curved rolls in the same system (Pan-Am texture) at a larger Rayleigh number ($R/R_c=1.12$); (c) concentric rolls in CO_2 gas for $L=86$ with sidewall forcing; (d) convection in CO_2 gas for $L=41$ with very little or no sidewall forcing; (e) off-center pattern (convection in methanol, $\sigma=7$, $R/R_c=7.3$); (f) spiral pattern (convection in CO_2 gas, $R/R_c=1.15$, $L=86$). Both (e) and (f) are stabilized by sidewall forcing. [(a), (b), and (e) from Croquette (1989); (c) and (f) from Bodenschatz *et al.* (1991, and unpublished); (d) from Hu *et al.* (1992).]

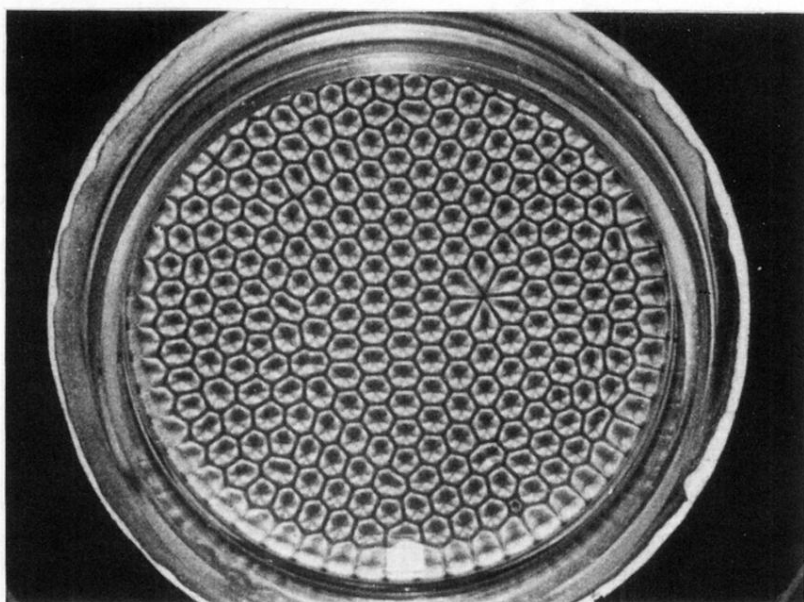


FIG. 4. Early experiment showing convection cells in silicone oil under an air surface. Visualization with aluminum powder. Dark lines indicate vertical motion. Bright areas indicate predominantly horizontal motion. (Koschmieder, 1974).

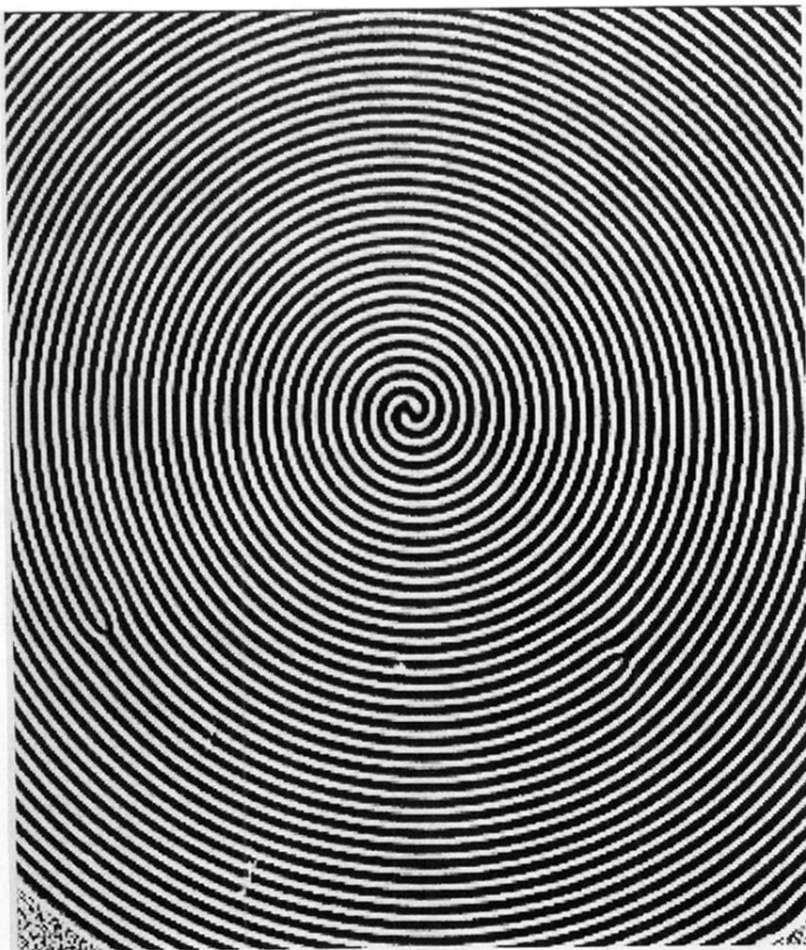
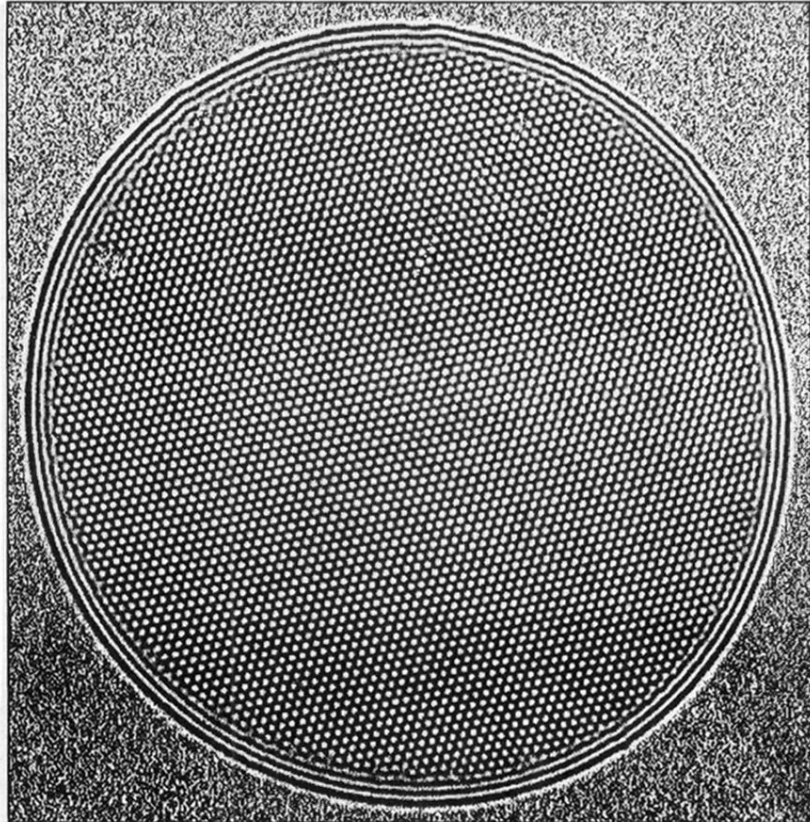


FIG. 49. Patterns in non-Boussinesq convection in an aspect ratio 86 cylindrical cell of gaseous CO₂. (a) Hexagonal pattern seen near threshold, $\epsilon = 0.06$: notice the remarkably regular hexagonal cells except in a thin layer near the boundary where the cylindrical walls induce circular rolls. (b) Roll state for slightly larger $\epsilon = 0.15$: the rolls here form a two-armed spiral which slowly rotates with a period of 2400 vertical diffusion times. Note that only a portion of the pattern is shown. (From Bodenschatz *et al.*, 1991.)

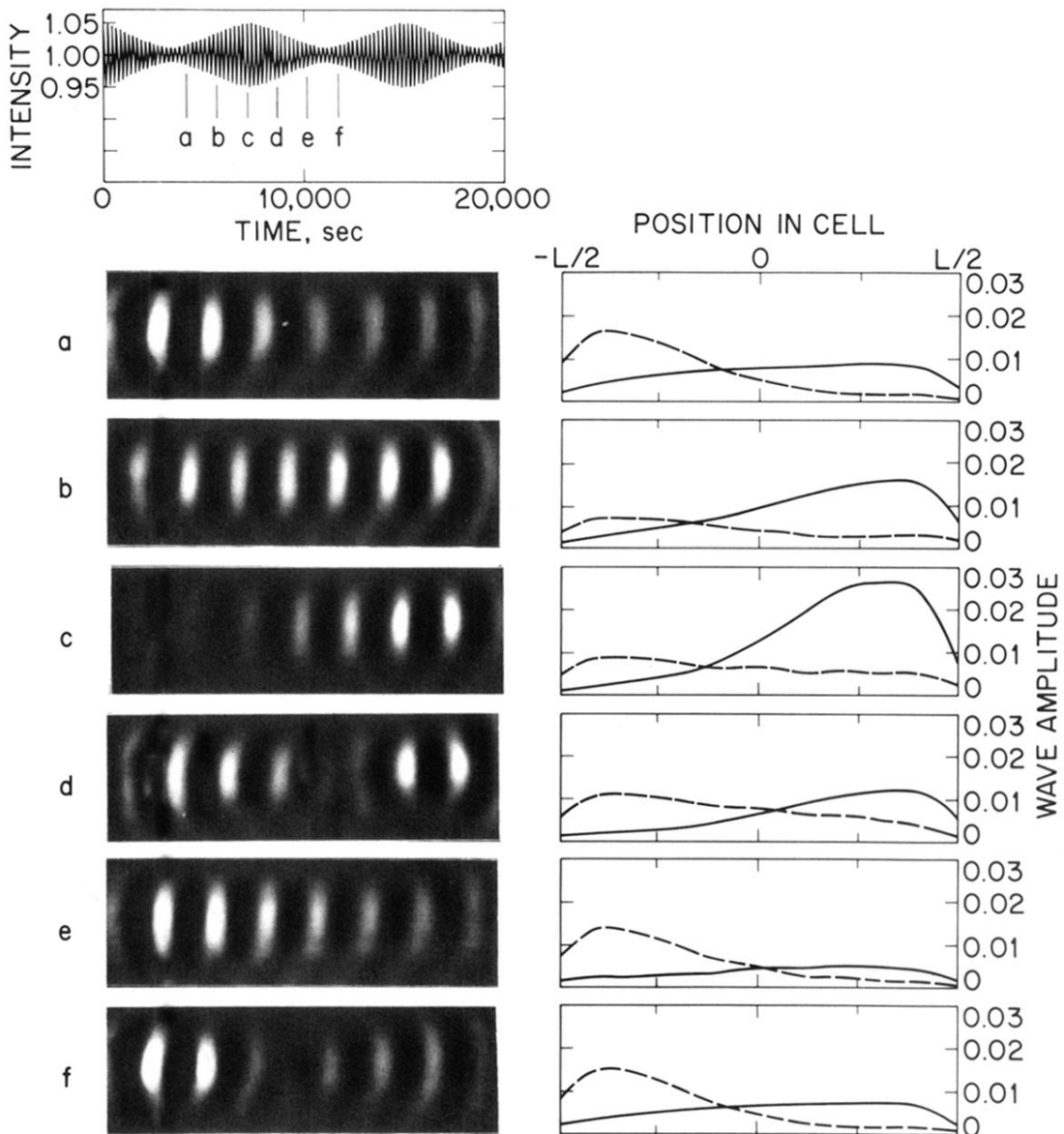


FIG. 55. "Sloshing" or "blinking" state in experimental binary fluid convection. The top trace is the intensity of an optical signal measuring the flow at a single point. The column of pictures on the left is a sequence of shadowgraph images taken at times indicated in the top trace. To the right of each image is the corresponding amplitude computed by demodulation of the optical signal. Full lines, right-moving waves; dashed lines, left-moving waves. Note the similarity with patterns observed in numerical simulations of the amplitude equations shown in Fig. 25(d). (From Kolodner *et al.*, 1989.)

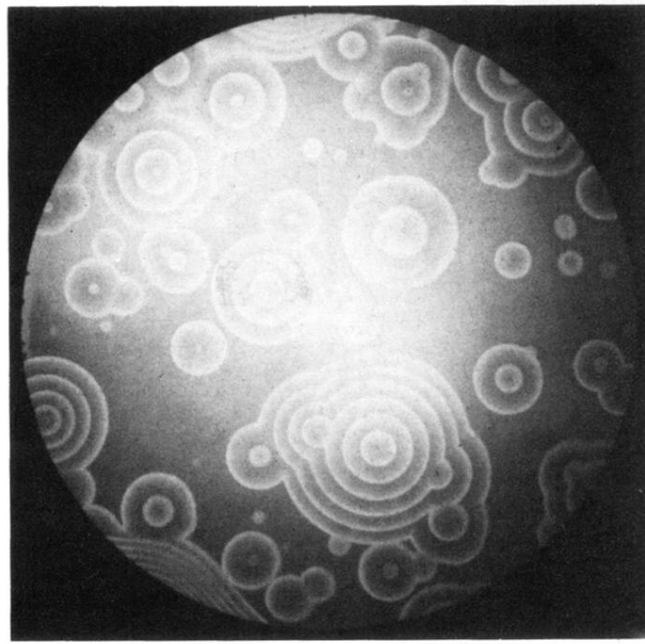


FIG. 75. Target pattern observed in a thin layer of an oscillating Belousov-Zhabotinsky reaction. (From Vidal *et al.*, 1986.)

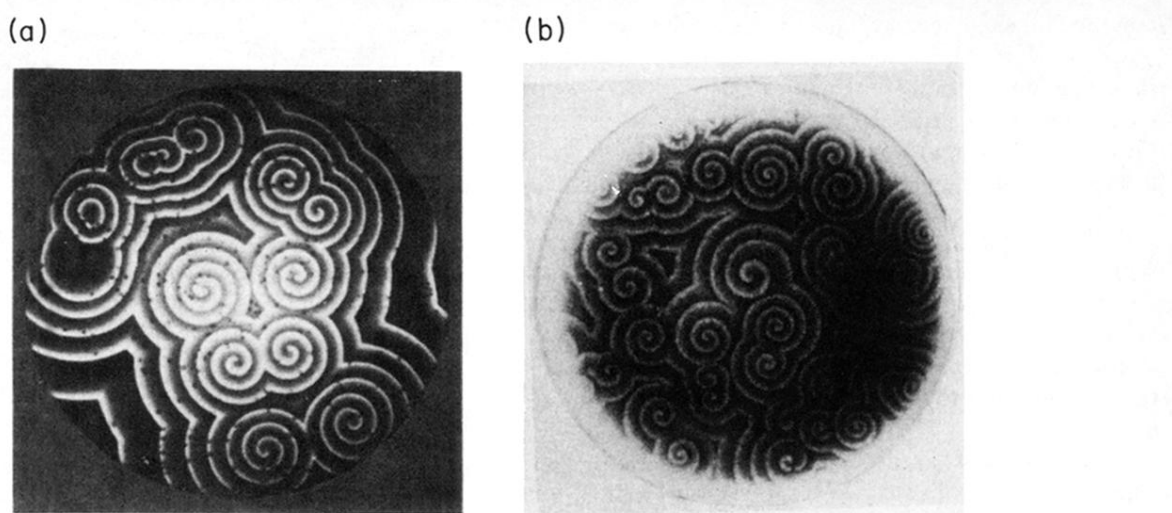


FIG. 76. Spiral patterns in excitable media. (a) Belousov-Zhabotinsky reaction photographed in blue light. Regions of maximum concentration of the blue indicator ferroin appear white. The spirals rotate with a period of about one minute. The dish is 90 mm in diameter with 1 mm depth of reageant. (From Winfree and Strogatz, 1983.) (b) Dark field photograph of a monolayer of slime mold *Dictyostelium discoideum* cells. The contrast is produced by the different refractive properties of the cells responding to a pulse of the diffusing chemical adenosine monophosphate (cAMP). Spirals are evident. They rotate every 5 minutes. The dish is 90 mm in diameter. (From Newell, 1983.)

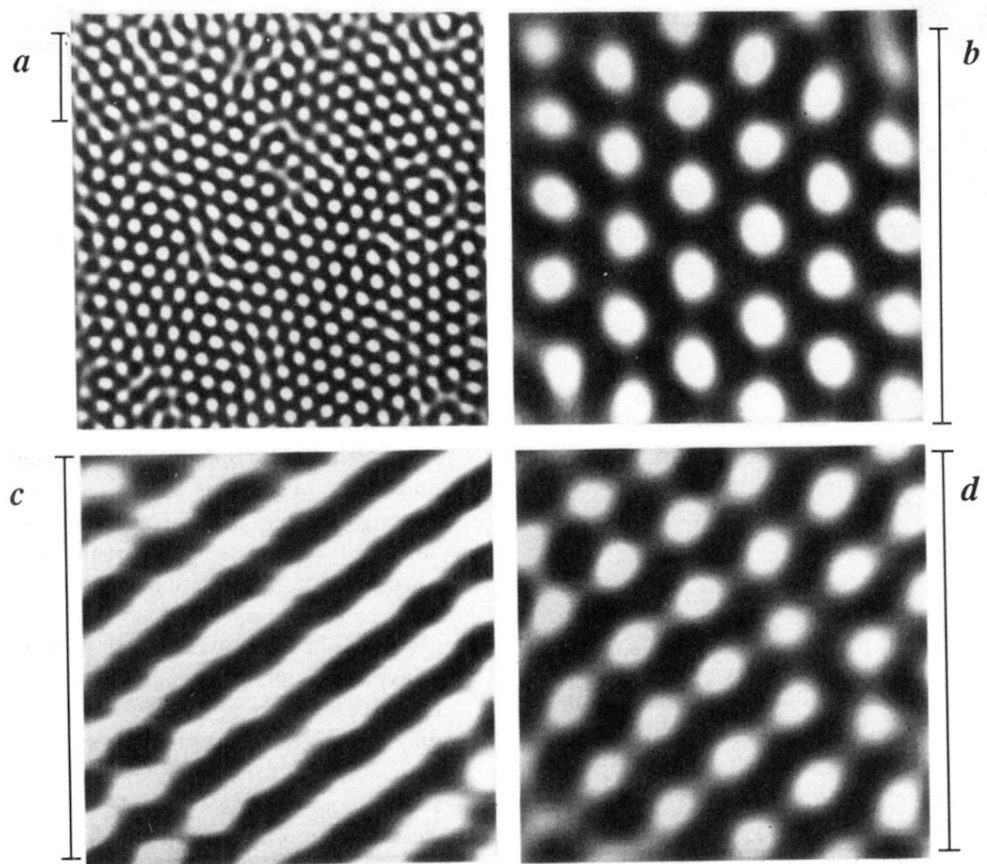
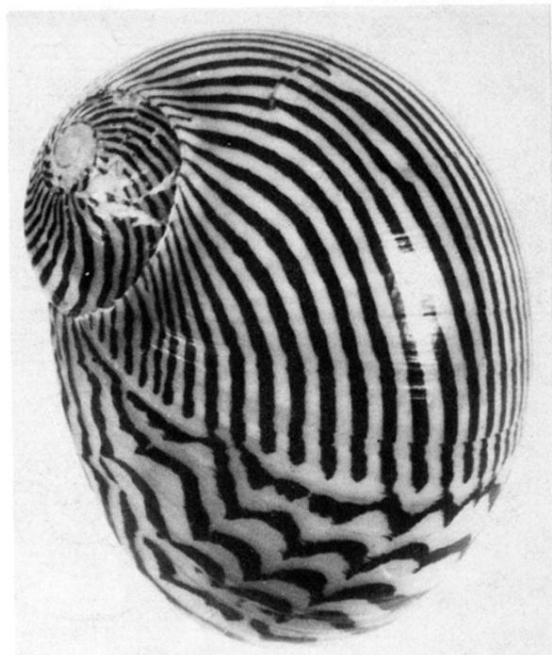


FIG. 87. Stationary Turing patterns in a continuously fed reactor. (a) and (b) hexagons; (c) stripes; (d) mixed state. Light and dark represent the yellow and blue colors of an indicator for the I_3^- concentration in a chlorite-iodide-malonic acid reaction. Patterns (a) and (d) coexist for the same parameter values, whereas (b) and (c) are given by different reactant concentrations. (From Ouyang and Swinney, 1991a; reprinted with permission from Nature, Copyright 1991 Macmillan Magazines Limited.)

(a)



(b)



FIG. 97. Patterns on natural mollusks. (a) *Nerita turrita*; (b) *Bankivia fasciata*. (Photos provided by J. Campbell.)

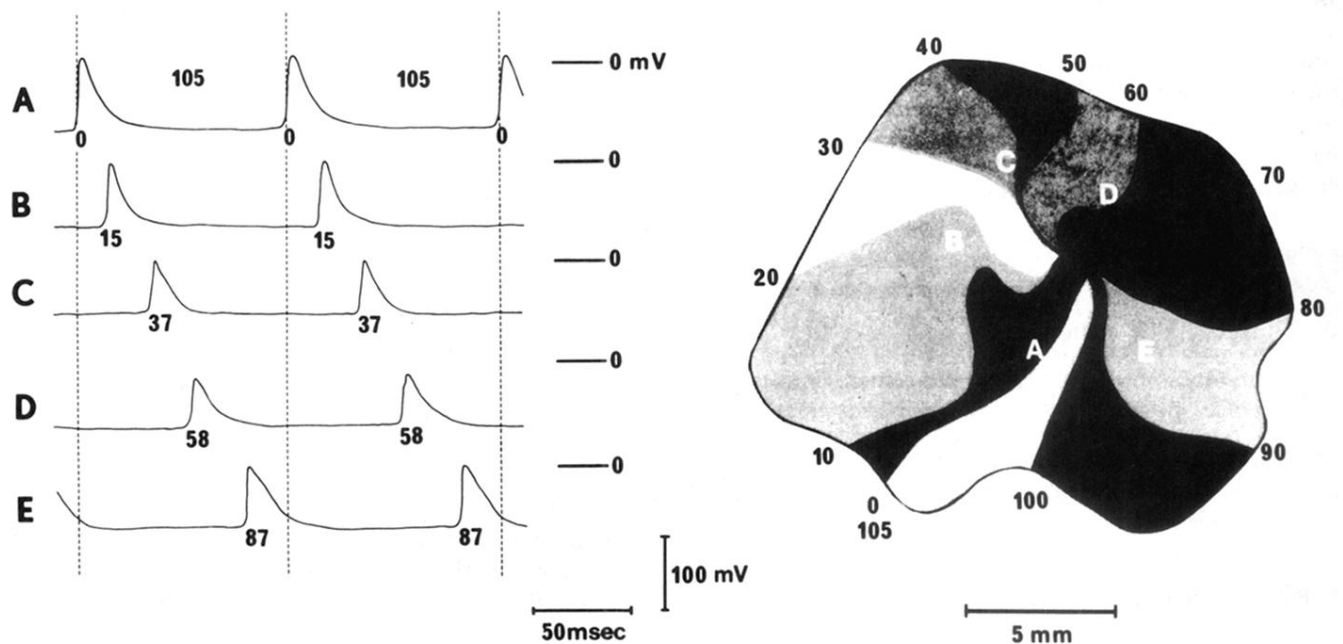


FIG. 99. Rotating spiral waves experimentally induced in a rabbit heart (left atria) muscle: the numbers represent times in milliseconds. Each region was traversed in 10 ms with a complete rotation in 105 ms. On the left panel the transmembrane potentials are shown with the lettering corresponding to the points in the heart muscle on the right. The lines separating different shaded regions in the right-hand panel correspond to the position of the pulse at the times indicated on the periphery. (From Allessie *et al.*, 1977; Copyright 1977 American Heart Association.)